Advanced Structured Materials

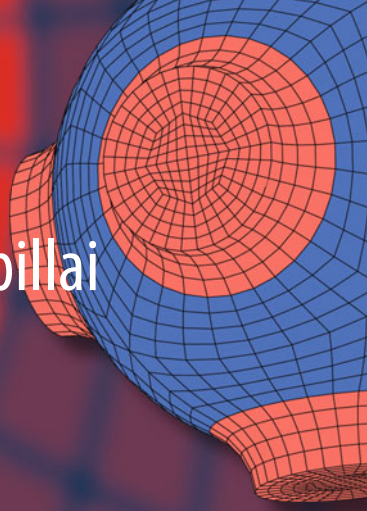

Jyotishkumar Parameswaranpillai
Suchart Siengchin
Jinu Jacob George
Seno Jose *Editors*

Shape Memory Polymers, Blends and Composites

Advances and Applications

Springer

Advanced Structured Materials

Volume 115

Common engineering materials reach in many applications their limits and new developments are required to fulfil increasing demands on engineering materials. The performance of materials can be increased by combining different materials to achieve better properties than a single constituent or by shaping the material or constituents in a specific structure. The interaction between material and structure may arise on different length scales, such as micro-, meso- or macroscale, and offers possible applications in quite diverse fields.

This book series addresses the fundamental relationship between materials and their structure on the overall properties (e.g. mechanical, thermal, chemical or magnetic etc) and applications.

The topics of *Advanced Structured Materials* include but are not limited to

- classical fibre-reinforced composites (e.g. glass, carbon or Aramid reinforced plastics)
- metal matrix composites (MMCs)
- micro porous composites
- micro channel materials
- multilayered materials
- cellular materials (e.g., metallic or polymer foams, sponges, hollow sphere structures)
- porous materials
- truss structures
- nanocomposite materials
- biomaterials
- nanoporous metals
- concrete
- coated materials
- smart materials

Advanced Structured Materials is indexed in Google Scholar and Scopus.

More information about this series at http://www.springer.com/series/8611

Jyotishkumar Parameswaranpillai ·
Suchart Siengchin · Jinu Jacob George ·
Seno Jose
Editors

Shape Memory Polymers, Blends and Composites

Advances and Applications

Springer

Editors
Jyotishkumar Parameswaranpillai
Center of Innovation in Design and Engineering for Manufacturing
King Mongkut's University of Technology North Bangkok (KMUTNB)
Bangkok, Thailand

Suchart Siengchin
Department of Mechanical and Process Engineering, The Sirindhorn International Thai-German Graduate School of Engineering (TGGS)
King Mongkut's University of Technology North Bangkok (KMUTNB)
Bangkok, Thailand

Jinu Jacob George
Department of Polymer Science and Rubber Technology
Cochin University of Science and Technology
Kochi, Kerala, India

Seno Jose
Department of Chemistry
Government College Kottayam
Kottayam, Kerala, India

ISSN 1869-8433 ISSN 1869-8441 (electronic)
Advanced Structured Materials
ISBN 978-981-13-8573-5 ISBN 978-981-13-8574-2 (eBook)
https://doi.org/10.1007/978-981-13-8574-2

This Springer imprint is published by the registered company Springer Nature Singapore Pte Ltd.
The registered company address is: 152 Beach Road, #21-01/04 Gateway East, Singapore 189721, Singapore

Preface

The desire of scientists to fabricate next-generation functional materials with fascinating properties has led to the development of one of the most exciting class of materials called shape memory polymers (SMPs). In recent years, SMPs including blends and composites have generated great interest among researchers on account of the ease of manufacture and the tremendous potential for application. In this technology, polymeric materials with desired polymer architecture can be designed, and those with increasingly sophisticated properties can be fabricated too by tuning the thermo-mechanical programming conditions. Moreover, these materials could meet the needs of extremely demanding forms of application. Over the past several years, academic and industrial research in this field is burgeoning and there is an exponential upsurge in the number of patents, papers and reviews.

Although the research in this field is flourishing steadily at an extremely rapid pace, only a few books have been published to provide a comprehensive account of the whole field. Moreover, a book which encompasses an integrated and contemporary overview of the pertinent developments of current research in this field is much desired. In the light of recent developments, we perceive that it is befitting to judiciously edit the dedicated efforts of researchers all over the world to assemble a reliable and accessible source of information for both beginners and practitioners in academia and industry. The principal objective of the present book is not only to provide an insight into the recent developments in this area of interest but also to indicate the right directions of future research.

This book comprises 13 chapters that throw a great deal of light on the field of SMPs, their blends and composites in a reasonably succinct way. Chapter "Introduction to Shape-Memory Polymers, Polymer Blends and Composites: State of the Art, Opportunities, New Challenges and Future Outlook", an introductory chapter on SMPs, provides a bird's-eye view of the current state of research, opportunities, new challenges and future prospects in this area. Chapter "Classification of Shape-Memory Polymers, Polymer Blends, and Composites" focuses on the classification of SMPs, their blends and composites based on polymer type, structural variety and external stimulus. Further, this chapter presents a compendious description of the chemical architecture requirements for the shape

memory effects, the shape memory enabling mechanisms and the structure–property correlations. Chapter "Novel Techniques for the Preparation of Shape-Memory Polymers, Polymer Blends, and Composites at Micro and Nanoscales" outlines the novel techniques including the design strategies for the preparation of SMPs, their blends and composites, while Chapter "Rheology of Shape-Memory Polymers, Polymer Blends, and Composites" zooms in on their rheological properties.

Chapter "Microscopy of Shape Memory Polymers, Polymer Blends, and Composites" seeks to elucidate the micro- and nanostructures of different SMPs, their blends and composites in terms of important microscopic techniques such as SEM, TEM, cryo-TEM, AFM and LCAM. Chapters "Dynamical Mechanical Thermal Analysis of Shape-Memory Polymers" and "Differential Scanning Thermal Analysis of Shape-Memory Polymers, Polymer Blends, and Composites", respectively, discuss the relevance of dynamic mechanical analysis and differential scanning calorimetry to understand the thermodynamic aspects, the molecular mechanisms and the multi-shape memory effect of SMPs. Chapter "Thermal Stability of Shape Memory Polymers, Polymer Blends, and Composites" throws ample light on the thermal stability and degradation behaviour of SMPs. Chapter "Mechanical Properties of Shape-Memory Polymers, Polymer Blends, and Composites" is an overview of mechanical properties of SMPs, blends and composites in terms of the conventional mechanical testing procedures, the cyclic mechanical testing methods and the nanoindentation technique. Chapter "Biodegradable Shape-Memory Polymers" summarizes the recent developments in the design and fabrication of completely biocompatible and biodegradable SMPs, and Chapter "Optical, Electrical, and Magnetic Properties of Shape-Memory Polymers, Polymer Blends, and Composites" illuminates the optical, the electrical and the magnetic properties of SMPs, blends and composites. Chapter "Scattering and Other Miscellanies Techniques for the Characterization of Shape Memory Polymers" reviews the applicability of X-ray scattering, light scattering and optical microscopic techniques to investigate the molecular-level mechanism in SMPs. Chapter "Applications of Shape-Memory Polymers, and Their Blends and Composites", the last chapter of this book, directs the readers right into the broad spectrum of applications of SMPs, which range from domestic to engineering, from automobiles to aerospace, from smart textiles to intelligent packaging and from switches to sensors, and a wide range of biomedical applications.

Science is important not just to researchers, but to the public. This book is so structured that each chapter is self-contained. We hope that all classes of readers will enjoy using this book and will find it informative and instructive. Finally, we express our deepest gratitude to our publisher and staff for their guidance, encouragement and support at every stage of the project.

Bangkok, Thailand — Dr. Jyotishkumar Parameswaranpillai
Bangkok, Thailand — Dr. Suchart Siengchin
Kochi, India — Dr. Jinu Jacob George
Kottayam, India — Dr. Seno Jose

Contents

About the Editors

Dr. Jyotishkumar Parameswaranpillai is a Professor at the Center of Innovation in Design and Engineering for Manufacturing, King Mongkut's University of Technology North Bangkok. He received his Ph.D. in polymer science and technology from Mahatma Gandhi University, Kerala, India. He is a former INSPIRE Faculty at the Department of Polymer Science and Rubber Technology of Cochin University of Science and Technology (India) from 2012 to 2017. He has authored around 100 papers and book chapters in reputed international journals on polymer nanocomposites, polymer blends and alloys, and biopolymers, and has edited four books. Dr. Jyotishkumar received the prestigious Kerala State Young Scientist Award in 2016 for his outstanding contributions to the field.

Prof. Dr.-Ing. habil. Suchart Siengchin is a Professor and the President of King Mongkut's University of Technology North Bangkok (KMUTNB), Thailand. He received his Dipl.-Ing. in Mechanical Engineering from University of Applied Sciences Giessen/Friedberg, Hessen, Germany in 1999, M.Sc. in Polymer Technology from University of Applied Sciences Aalen, Baden-Wuerttemberg, Germany in 2002, M.Sc. in Material Science at the Erlangen-Nürnberg University, Bayern, Germany in 2004, Doctor of Philosophy in Engineering (Dr.-Ing.) from Institute for Composite Materials, University of Kaiserslautern, Rheinland-Pfalz, Germany in 2008 and Postdoctoral Research from Kaiserslautern University and School of Materials Engineering, Purdue University, USA. In 2016 he received the habilitation at the Chemnitz University in Sachen, Germany. He worked as a Lecturer for Production and Material Engineering Department at the Sirindhorn International Thai-German Graduate School of Engineering (TGGS), KMUTNB. His research interests are in polymer processing and composite materials, and he has won the Outstanding Researcher Award in 2010, 2012 and 2013 at KMUTNB. He serves as the Editor-in-Chief of KMUTNB International Journal of Applied Science and Technology and has authored 100 peer reviewed journal articles. He has participated with presentations in more than 39 International and National Conferences with respect to Materials Science and Engineering topics.

Dr. Jinu Jacob George received his Ph.D. degree from the Indian Institute of Technology Kharagpur, India in 2009. He completed his B.Tech. from M G University, Kottayam and M.Tech. from Cochin University of Science and Technology, Kochi, India. After pursuing Ph.D. he moved to Leibniz Institute for Polymer Research (IPF), Dresden, Germany for his Post Doctoral Research. In 2011 he joined the Rubber Research Institute of India, Kottayam, as a Scientist. In 2015 he joined the Department of Polymer Science and Rubber Technology, CUSAT as a faculty member. At present, he is actively involved in research in the various advance fields of Polymer Science and Rubber Technology. He has a general research interest in the fields of Polymer micro/nano composites, Thermoplastic elastomers, Functional additives, and Shape memory polymers.

Dr. Seno Jose a native of Kerala, India, is an assistant Professor of Chemistry at Government College Kottayam. He did his masters in Chemistry in Mahatma Gandhi University. He has availed DST/DAAD fellowship and worked as a visiting researcher at Institute for Composite Materials Ltd., Germany. He received his Ph.D. in Chemistry from Mahatma Gandhi University in 2007. He has co-authored over 30 peer-reviewed publications. His research interests include polymer blends, polymer nanocomposites and shape memory polymeric materials.

Introduction to Shape-Memory Polymers, Polymer Blends and Composites: State of the Art, Opportunities, New Challenges and Future Outlook

Seno Jose, Jinu Jacob George, Suchart Siengchin and Jyotishkumar Parameswaranpillai

Abstract This chapter provides an overview of shape-memory polymers and their blends and composites. The history of shape-memory polymers, their advantages, shape-memory cycles, classification and the molecular mechanism of the shape-memory effect are briefly discussed. The characterisation techniques such as dynamic mechanical thermal analysis (DMTA), differential scanning calorimetry (DSC), scanning electron microscopy (SEM), transmission electron microscopy (TEM), optical and polarized optical microscopy (OM and POM), atomic force microscopy (AFM), laser scanning confocal microscopy (LSCM), universal testing machine (UTM), nanoindentation technique, etc., are powerful techniques to investigate the shape-memory mechanism and shape-memory performance. Shape-memory polymers have myriad of potential applications in automobile, sports products and textile, aerospace and medical fields.

S. Jose
Department of Chemistry, Government College Kottayam, Kottayam 686013, Kerala, India

J. J. George
Department of Polymer Science and Rubber Technology, Cochin University of Science and Technology, Kochi 682 022, Kerala, India

S. Siengchin
Department of Mechanical and Process Engineering, The Sirindhorn International Thai-German Graduate School of Engineering (TGGS), King Mongkut's University of Technology North Bangkok, 1518 Pracharaj 1, Wongsawang Road, Bangsue, Bangkok 10800, Thailand

J. Parameswaranpillai (✉)
Center of Innovation in Design and Engineering for Manufacturing, King Mongkut's University of Technology North Bangkok, 1518 Pracharaj 1, Wongsawang Road, Bangsue, Bangkok 10800, Thailand
e-mail: jyotishkumarp@gmail.com

J. Parameswaranpillai et al. (eds.), *Shape Memory Polymers, Blends and Composites*, Advanced Structured Materials 115,
https://doi.org/10.1007/978-981-13-8574-2_1

1 Introduction

The desire of scientists to fabricate next-generation functional materials with fascinating properties has led to the development of one of the most exciting class of materials called shape-memory polymers (SMPs). Recently, SMPs including blends and composites have generated great interest among researchers due to the ease of manufacture and the possibility of tremendous potential applications [1–5]. In this technology, polymeric materials with desired polymer architecture can be designed and by tuning the thermo-mechanical programming conditions, high-performance polymeric materials with increasingly sophisticated properties suitable for demanding applications can be fabricated. Over the past several years, academic and industrial research in this field is burgeoning, and there is an exponential upsurge in the number of patents, books, papers and reviews [6–18].

SMPs are active polymers that can transform from a temporary shape to their original permanent shape upon exposure to an external stimulus. This dual-shape or multi-shape capability—the shape-memory effect (SME)—makes them promising materials in numerous demanding applications such as smart fabrics, self-assembling mobile phones, intelligent medical devices, self-deployable space structures, drug carriers, etc. The external stimulus may be direct heating or indirect heating (where electric, magnetic, optical, acoustic or chemical energy can be converted to thermal energy), light, change in PH or solvent exposure. SME is originated from a combination of polymer morphology and careful thermo-mechanical programming.

2 A Brief History of Shape-Memory Materials

Chang and Read [19] discovered the first shape-memory material in 1951, when they observed the SME in a gold–cadmium alloy. Even before that, in 1941, in a United States Patent, L B Vernon mentioned a type of shape-memory effect in a dental material made of methacrylic acid resin [20]. In 1963, Buehler et al. [21] reported the shape-memory properties of nitinol, an equimolar mixture of nickel and titanium. Thereafter, researchers observed the SME in a number of metallic alloys and ceramics [22–24]. In metallic alloys, the alloy undergoes reversible thermal transitions between the two crystalline phases: low-temperature martensitic phase and high-temperature austenitic phase [24]. Although a wide range of shape-memory alloys (SMA's) are available, NiTi, CuZnAl and CuAlNi are the most popular in terms of their performance indexes [25].

Shape-memory polymers (SMPs) are superior to SMA's in many respects. For instance, they are easily processable, cost-effective and lighter, and possess greater recoverable strain. Moreover, they are various stimuli-responsive and their material properties can easily be tuned. In 1980s, covalently cross-linked polyethylene (PE), a heat shrinkable material, was developed, which exhibits properties similar to SME, where the permanent shape and the switching process are due to covalent

cross-links and melting of PE crystallites, respectively [26]. In 1984, CDF Chimie Company developed polynorbornene, shape-memory polymer [7, 27]. In this linear, amorphous thermoplastic, the SME is due to the formation of a physically cross-linked network resulting from the entanglements of the high molecular weight linear chains on cooling, and the recovery of permanent shape on heating above the glass transition temperature (T_g). Later, in 1990s researchers observed thermally induced shape-memory effects in hydrogels of poly(vinyl alcohol) [28, 29] and in phase segregated multiphase copolymers like polyurethanes [30–34]. In the former, temporary shapes are fixed by deswelling and by the formation of physical cross-links while the permanent shape could be achieved by immersing in boiling water. In the latter, the phase showing the highest thermal transition fixes the permanent shape and the T_g or T_m serves as molecular switch. An example of shape-memory effect in hydrogel is shown in Fig. 1 [35].

3 The Shape-Memory Cycle

The SM cycle to evaluate the SM property of an SMP, in general, involves four successive steps: deformation, cooling, fixing and recovery [3, 36–38]. In the first step, the sample is deformed at a deformation temperature (T_d), to a predetermined stress or strain. Opening of molecular switches is realized in this step because the material is heated to T_d, which is above the transition temperature or 'switching temperature', T_{trans}, at which the shape can be deformed. It is followed by cooling under pre-strain constraint from T_d to a set temperature, T_s, below the T_{trans}. During cooling, which is a strain storage process, the deformation history is stored. This step ensures the closing of 'switches' and fixation of a temporary shape. In the next step, the initial deformation constraint is released at T_s and a stress-free condition is achieved. In this state, the sample may be considered as a pre-deformed SMP. The final step is the unconstrained recovery in which the molecular switches are opened by heating back to a temperature above T_{trans}, under stress-free condition, where the test specimen regained its permanent shape. The SM cycle time, the overall time required to carry out steps 1–4, depends on material properties, geometric consideration and experimental condition. Figure 2 shows a typical stress–strain–temperature diagram representing the SM cycle.

4 Molecular Mechanism of Shape-Memory Effect

SMPs may be considered as elastic networks that are equipped with suitable stimuli-responsive molecular switches that fix the temporary shape by forming physical cross-links below a certain critical temperature, and netpoints of either physical (e.g. crystallites) or chemical (e.g. covalent bonds) nature that link chain segments determine the permanent shape. The shape-memory effect may be considered as an

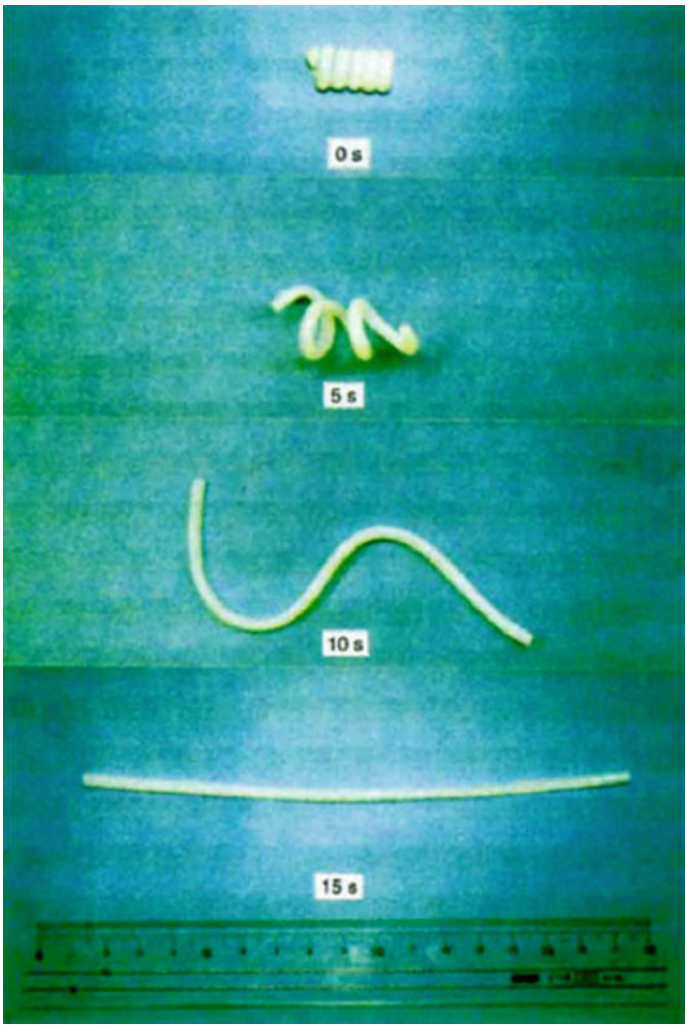

Fig. 1 An example of shape-memory effect in hydrogel [35]. Reproduced with permission from Springer Nature, License Number-4503380181682

entropic phenomenon [3, 37, 38]. The molecular chains of a shape-memory material, in a permanent macroscopic shape, are in a thermodynamically stable state with the highest entropy. When the material undergoes a macroscopic deformation the molecular chain conformation changes to a less stable low entropic state. When the material is cooled below the shape-memory transition temperature, at the molecular level, this low entropic state is kinetically trapped due to the freezing of the molecular chains and the deformed chain conformation is fixed. When the material is heated above its T_{trans}, at the molecular scale, heating activates the molecular mobility, and

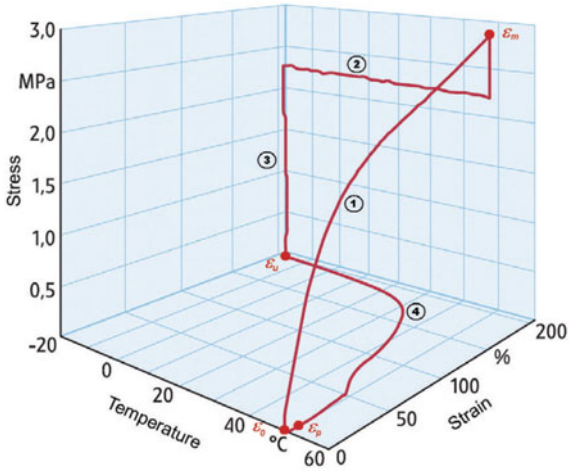

Fig. 2 A typical shape-memory cycle [3]. Reproduced with permission from Elsevier, License Number- 4503380473895

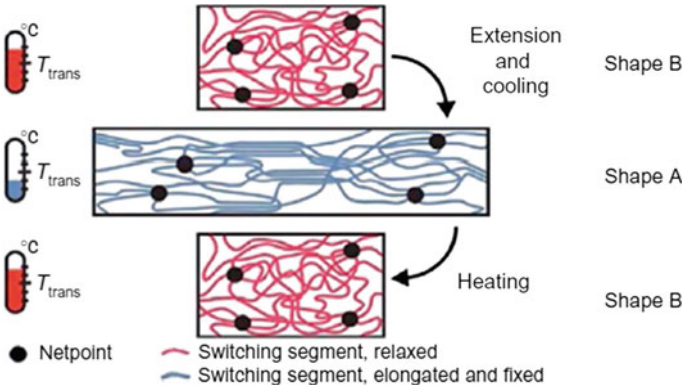

Fig. 3 Schematic representation of a thermally induced shape-memory effect for a polymer network with $T_{trans} = T_g$ [3]. Reproduced with permission from Elsevier, License Number- 4503380473895

the strain energy released acts as the driving force for the molecular chains to regain the lowest energy (highest entropy) state, and thus recover the original shape (Fig. 3). Thus, typically in an SMP, switch segments enable the fixation of temporary shape.

It is worth noting that the segmental switching alone is not sufficient for polymer shape-memory effect. The complete interdiction of long-range chain slippage that would lead to macroscopic deformation is a precondition for an ideal shape recovery process. Therefore, complete recovery is not realized if the netpoints are not sufficiently stable to withstand the thermo-mechanical conditions experienced by the material. The netpoints can be made up of either covalent bonds (chemical cross-links) or physical interactions (crystallites, glassy hard domains, hydrogen bonding,

ionic clusters or chain entanglements). Although physical interactions ensure reprocessability, they are not strong enough to offer a complete recovery. In contrary, chemical cross-links are robust enough to secure almost complete recovery, but repel reprocessability.

5 Classification of Shape-Memory Polymers

SMPs may be classified in terms of structure, composition and type of stimulus. Based on the polymer structure, there are four types of SMPs, viz. chemically cross-linked amorphous SMPs (class I), chemically cross-linked semi-crystalline SMPs (class II), physically cross-linked amorphous SMPs (class III) and physically cross-linked semi-crystalline SMPs (class IV). Table 1 summarizes their important features.

6 Shape-Memory Trigger Methods Other Than Heating

Indirect heating, where thermal energy is generated from light or electric or magnetic energies, is extensively used as alternate methods for developing SMPs. For instance, since the pioneering work by Lendlein et al. [106] to develop photoresponsive SMPs in which cinnamic acid type molecules when exposed to light undergo photoreversible cycloaddition reactions, researchers use photoresponsive materials that effectively absorb and convert light into heat to actualize shape-memory effect in polymers [107–112]. Here, the temporary shape is achieved by thermo-mechanical programming and the original shape is recovered by photoheating. Researchers also showed that incorporation of conductive materials like carbon nanotubes (CNTs), graphene, etc., into SMPs would act as an ideal heating source for stimulating SME. This could be achieved by a number of approaches like the dispersion of conductive fillers in SMP matrix through the formation of double percolation conductive network by confining the dispersion of conductive fillers in a co-continuous shape-memory polymer blend, assembly of conductive channels in shape-memory polymer composites, etc. [113–116]. Similarly, the incorporation of magnetic nanoparticles in SMPs enables them to generate heat to induce shape recovery process [117–121]. Likewise, solvent-driven shape-memory effect in which solvent molecules disrupt the secondary bonding in the SMP and depress the T_g below the operating conditions has attracted many researchers to develop SMPs, especially for shape-memory applications [122–126].

Table 1 Classification of shape-memory polymers based on their structure

Type	Important features	Examples	References
Class I	Sharp T_g is the shape transition temperature Permanent shape is fixed by chemical cross-linking while the secondary shape by vitrification Excellent degree of shape recovery Difficult to reprocess	Polynorbornene	[39, 40]
		Thermosetting PU	[41–45]
		Epoxy	[46–50]
		Styrene copolymers	[51]
		PET-PEG copolymer	[52]
		PMMA-PBMA copolymers	[53]
		Methacrylates	[54]
Class II	T_m is the shape transition temperature Permanent shape is fixed by chemical cross-linking while secondary shape by crystallization Fast shape recovery	PCL-BA copolymer	[55]
		Polycyclooctene	[56, 57]
		PE	[58]
		PE/PP blends	[59]
		Poly(ε-caprolactone) based systems	[60–70]
		Acrylates	[71]
		Poly(propylene sebacate)	[72]
Class III	T_g or T_m is the shape transition temperature Better processability Rigid amorphous domains or crystals or hydrogen bonding or ionic clusters that serve as physical cross-links fix the permanent shape, while soft segments with lower T_g or T_m fix the secondary shape on cooling Relatively low shape recovery	POSS-PN block	[41]
			[73, 74]
		Copolymer	[75–77]
		Styrene block copolymer	[78]
		PET-co-PEO	[79]
		PE-co-nylon 6	[80]
		PE-co-PMCP	[81, 82]
		PCL-b-ODX	[83]
		POSS telechelic	[84–87]
		PVDF/PMMA blend	[88]
		Polylactide-based systems oligo(ε-caprolactone)	
Class IV	T_g or T_m is the shape transition temperature Physical cross-links (polar interaction, hydrogen bonding or crystallization with such cross-links) fix permanent shape, while the crystallization of soft segments governs the secondary shape	Styrene–trans-butadiene–styrene TBCP	[89]
		Polyurethane copolymers with different soft segments	[90–99]
		PCL-based systems	[100–104
		Copolyesters	[105]

7 Characterization of Shape-Memory Polymers

A macroscopic level and molecular level characterization is essential to explore a comprehensive idea of shape-memory effect. Various sophisticated characterization techniques can be used to explore the micro- and nano-level features of thermo-mechanical programming and shape-memory characteristics, and visualize the shape recovery mechanism. Characterization of molecular level hierarchal organization of polymer structure and chemical net points in terms of cross-link density and functionality can be investigated by nuclear magnetic spectroscopy [127–130].

Thermal characterization techniques such as DMTA and DSC are extensively used to study the thermal properties including the crystallinity, phase transitions and glass transition behaviour of SMPs [131–136]. Figure 4 shows the various types of shape-memory properties exhibited by polymeric materials measured using differential scanning calorimetry. The static mechanical properties of SMPs can be evaluated by conventional mechanical testing [137, 138] while shape-memory parameters like shape fixity, shape recovery, etc., can be investigated by dynamic mechanical testing [107, 139, 140]. High-temperature nanoindentation technique is a powerful technique to analyse the shape-memory process at nanoscale dimensions [141, 142].

Microscopic techniques such as scanning electron microscopy (SEM) [143–151], transmission electron microscopy (TEM) [152–154], optical and polarized optical microscopy (OM and POM) [134, 155, 156], atomic force microscopy (AFM) [157–161], laser scanning confocal microscopy (LSCM) [162–164], etc., are widely used to determine the morphological features of shape-memory polymers. SEM can be made use to analyse micro-scale surface pattern, micro- and nano-level structural features, evolution and population of nanowrinkles, dispersion of nanomaterials in SMP matrix, etc. A better insight into the nano-level structural features could be obtained from TEM investigation. The structural organization and morphology evolution of SMPs can be visualized by OM and POM, while AFM, in addition to surface topography, provides information about the shape recovery process. LSCM is a powerful technique for the 3D visualization of structural features of biological samples. X-ray scattering technique is another powerful method to investigate the shape-memory behaviour through analysing the micro- and nano-state structural features of the material [165–167]. This method has flexibility in terms of sample preparation.

8 Applications of Shape-Memory Polymers

Researchers consider the field of SMPs as one of the most fascinating research subjects, mainly because of the myriad of potential applications of these materials in textile, space, electronic and medical fields. SMPs, due to the ease of designing lightweight, cost-effective and reliable space structures, are potential materials for developing deployable space structures such as panels, ground-based mirrors, solar

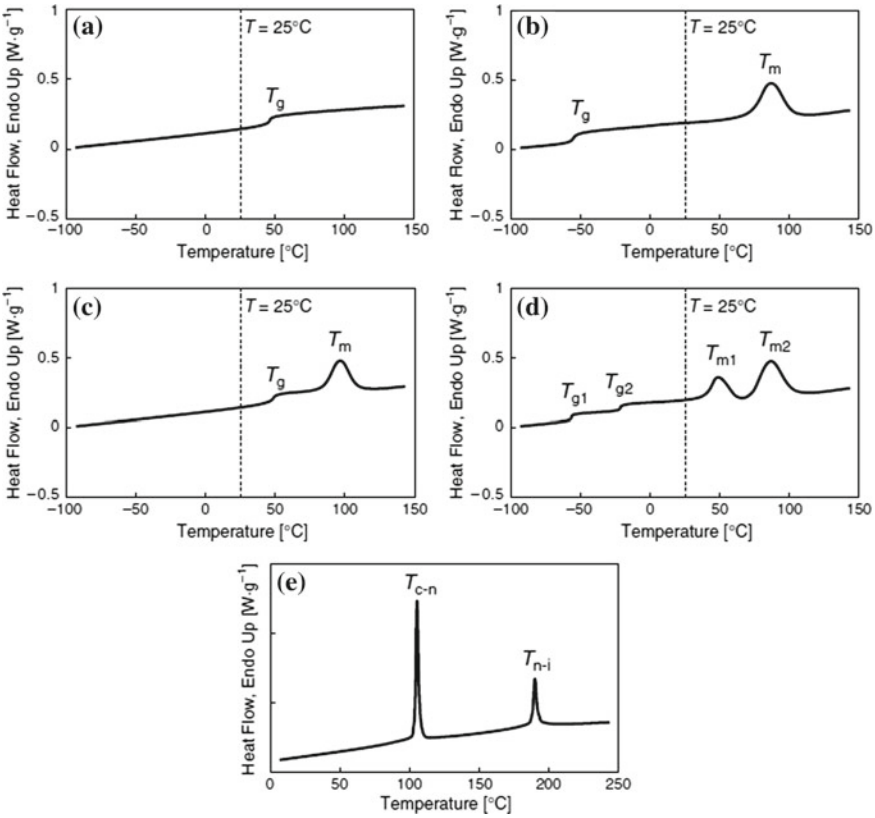

Fig. 4 Various types of shape-memory properties exhibited by polymeric materials measured using differential scanning calorimetry [131]. Reproduced with permission from Springer Nature, License Number- 4552351325096

arrays, booms, reflectors, hinges and morphing wings [168–174]. Biocompatibility, hydrolytic degradability, specific shape-memory functionality, low toxicity, etc. make biodegradable SMPs potential candidates for several biomedical applications. These include polymeric network systems for controlled drug delivery, microactuators for clot removal, foam for aneurysm occlusion, filaments for sutures, intravascular stents, tissue engineering scaffolds, dialysis needle adapters, annuloplasty rings, bone fillers and bone fracture fixation devices, etc. [1, 91, 175–177].

Several automobile applications such as tunable automotive brackets, self-repairing tyres, energy absorbing assemblies, automobile actuators, releasable fastener systems, airflow control devices, morphable automotive body moulding, etc., are proposed for SMPs [178–184]. Smart textiles, clothing and related products can be developed using shape-memory fibres, shape-memory yarns and shape-memory fabrics [185–191]. Other potential applications of SMPs include shape-memory packaging, food equipment, toys, sports products, etc. Since there is huge scope for the

successful commercialization of SMPs in domestic, industrial, automobile, aerospace and biomedical fields by making use of novel approaches such as 3D printing, SMPs and their composites would become next-generation materials in near future.

Challenges and Prospects

The exponential explosion in the number of patents, papers and reviews authenticate the glorious future of SMPs. Though extensive investigations on various aspects of SMEs in SMPs have been done by researchers, quite a number of issues still remain unresolved and unsettled. SMPs have unlimited application potential, but several factors restrict their practical applicability. As far as their end application is concerned, a consensus is necessary among several factors such as thermo-mechanical properties, multifunctionality, processability, durability, biocompatibility, etc. Compromise in any of these aspects may limit the practical applicability of the product. The relatively poor mechanical properties, low recovery stress, long response time, lower cyclic life, weak material stability, etc., of SMPs are some of the serious obstacles for their broad application. Further, the reliability, durability, precise predictability, controllable strain and deformation speed, etc., are prerequisites for utilizing SMPs for the development of devices for advanced applications. The end application of high molecular weight amorphous polymers is limited because of their intrinsic tendency to flow and therefore, high precision in programming and recovery processes is a precondition for the long-term storage of these materials in their temporary shape. Another important area of concern is the control of SME in biological systems, where simultaneous occurrences of several complex issues—flexible mechanical constraints, metabolic activities, complex chemical environment, etc.—should be properly addressed. Besides, stringent requirements and lengthy regulatory approval procedures pause constraints for the commercialization of SMPs for biomedical applications.

To realize the broad spectrum of end applications, development of new SMPs with novel structure and diversified functionalities are essential. For example, there is great interest among material researchers to fabricate multifunctional, multi-sensitive, two-way SMPs having multiple SMEs. Hence, the integration of several functions in a single system is a fascinating area of future research. Design of SMPs by combining non-SM materials, development of conducting elastomeric SMPs, enhancing the effectiveness of triggering mechanisms, optimizing the triggering conditions, inventing wireless and remote controllable shape-memory behaviour, implementing novel programming protocol, solar and electrochemical energy harvesting, etc., may result in the broadening and diversifying the commercialization and practical applications of SMPs. Generalized and advanced numerical modelling by unifying various structural features of the material and other parameters like stress, strain, time, external stimulus parameters, reinforcement content, etc., may contribute towards the accurate engineering and practical design of devices and may play a prominent role in future developments.

Completely non-thermal trigger mechanism such as photoisomerization of constituent molecules or solvent induced plasticization is another attractive area of research. Design of novel SMPs which utilize special molecular switches other than

conventional glass transition and melting may result in fortuitous properties and new functionalities. For example, acoustically or electrically sensitive non-thermal switches with short, accurate and controlled responsiveness to stimulation can avoid cold drawing and reversible plasticity of conventional SMPs.

Another promising area of interest is the fabrication of self-actuating biomedical devices with material which satisfies multidimensional requirements such as triggering condition, stiffness, degree of fixing/recovery, biocompatibility/biodegradability, etc. Shape-memory material could be effectively employed in minimally invasive surgery. Shape-memory implant materials would have a decisive influence in designing the medicinal products, in the future. Bio-inspired SMPs that mimic intelligent nature materials is another potential area of future research.

Fabrication of lightweight deployable structures for spacecraft such as hinges of satellite structure bearing photovoltaic arrays having stable and well-controlled recovery property, trusses, reflectors, SMP skins used for morphing aircraft wings, tuneable automotive brackets and automobile actuators, self-disassembling mobile phones, smart textiles, etc., are of great technological interest and some of the important prospective applications in this fascinating area of research. Finally, progress by protecting the environment is of great importance, and it is the responsibility of researchers to invent 'green methods' for the synthesis and fabrication of shape SM materials for the sustainable development.

References

1. Lendlein A, Langer R (2002) Biodegradable, elastic shape-memory polymers for potential biomedical applications. Science 296:1673–1676
2. Lendlein A, Kelc S (2002) Shape-memory polymer. Angew Chem 41:2034–2057
3. Behl M, Lendlein A (2007) Shape-memory polymers. Mater Today 10:20–28
4. Mather PT, Luo X, Rousseau IA (2009) Shape memory polymer research. Annu Rev Mater Res 39:445–471
5. Huang WM, Ding Z, Wang CC, Wei J, Zhao Y, Purnawali H (2010) Shape memory materials. Mater Today 13:54–61
6. Roussea IA (2008) Challenges of shape memory polymers: A review of the progress toward overcoming SMP's limitations. Polym Eng Sci 48:2075–2089
7. Ratna D, Karger-Kocsis J (2008) Recent advances in shape memory polymers and composites: a review. J Mater Sci 43:254–269
8. Pretsch T (2010) Review on the functional determinants and durability of shape memory polymers. Polymers 2:120–158
9. Behl M, Razzaq MY, Lendlein A (2010) Multifunctional shape-memory polymers. Adv Mater 22:3388–3410
10. Xie T (2011) Recent advances in polymer shape memory. Polymer 52:4985–5000
11. Leng J, Lan X, Liu Y, Du S (2011) Shape-memory polymers and their composites: stimulus methods and applications. Prog Mater Sci 56:1077–1135
12. Hu J, Zhu Y, Huang H, Lu J (2012) Recent advances in shape–memory polymers: structure, mechanism, functionality, modeling and applications. Prog Polym Sci 37:1720–1763
13. Serrano MC, Ameer GA (2012) Recent insights into the biomedical applications of shape-memory polymers. Macromol Biosci 12:1156–1171

14. Zhao Q, Qi HJ, Xie T (2015) Recent progress in shape memory polymer: New behavior, enabling materials, and mechanistic understanding. Prog Polym Sci 49–50:79–120
15. Hager MD, Bode S, Weber C, Schubert US (2015) Shape memory polymers: past, present and future developments. Prog Polym Sci 49–50:3–33
16. Yahia L (2015) Shape memory polymers for biomedical applications. Elsevier. https://doi.org/10.1016/C2013-0-16350-7
17. Safranski DL, Griffis JC (2017) Shape-memory polymer device design. Elsevier
18. Pilate F, Toncheva A, Dubois P, Raquez JM (2016) Shape-memory polymers for multiple applications in the materials world. Eur Polym J 80:268–294
19. Chang LC, Read TA (1951) Plastic deformation and diffusionless phase changes in metals—the gold-cadmium beta phase. JOM 3:47–52. https://doi.org/10.1007/BF03398954
20. Lester B, Vernon B, Vernon HM (1941) Process of manufacturing articles of thermoplastic synthetic resins. US 2234993
21. Buehler WJ, Gilfrich JV, Wiley RC (1963) Effect of low-temperature phase changes on the mechanical properties of alloys near composition TiNi. J Appl Phys 34:1475–1477
22. Duerig TW, Richter DF, Albrecht J (1982) Shape memory in Ti-10V-2Fe-3AI. Scr Metall 16:957–961
23. Swain MV (1986) Shape memory behaviour in partially stabilized zirconia ceramics. Nature 322:234–236
24. Duerig TW, Albrecht J, Gessinger GH (1982) A shape-memory alloy for high-temperature applications. JOM 34:14–20
25. Huang W (2002) On the selection of shape memory alloys for actuators. Mater Des 23:11–19
26. Ota S (1981) Current status of irradiated heat-shrinkable tubing in Japan. Radiat Phys Chem 18:81–87
27. Parameswaranpillai J, Siengchin S (2017) Shape memory polymers, KMUTNB. Int J Appl Sci Technol 10(2):77
28. Hirai T, Maruyama H, Suzuki T, Hayashi S (1992) Shape memorizing properties of a hydrogel of poly (vinyl alcohol). J Appl Polym Sci 45:1849–1855
29. Hirai T, Maruyama H, Suzuki T, Hayashi S (1992) Effect of chemical cross-linking under elongation on shape restoring of poly(vinyl alcohol) hydrogel. J Appl Polym Sci 46:1449–1451
30. Kim BK, Lee SY, Xu M (1996) Polyurethanes having shape memory effects. Polymer 37:5781–5793
31. Takahashi T, Hayashi N, Hayashi S (1996) Structure and properties of shape-memory polyurethane block copolymer. J Appl Polym Sci 60:1061–1069
32. Li F, Zhang X, Hou J, Xu M, Luo X, Ma D, Kim BK (1997) Studies on thermally stimulated shape memory effect of segmented polyurethanes. J Appl Polym Sci 64:1511–1516
33. Lin JR, Chen LW (1998) Study on shape-memory behavior of polyether-based polyurethanes. I. Influence of the hard-segment content. J Appl Polym Sci 69:1563–1574
34. Lin JR, Chen LW (1998) Study on shape-memory behavior of polyether-based polyurethanes. II. Influence of soft-segment molecular weight. J Appl Polym Sci 69:1575–1586
35. Osada Y, Matsuda A (1995) Shape memory in hydrogels. Nature 376:219–220
36. Liu Y, Gall K, Dunn ML, Greenberg AR, Diani J (2006) Thermomechanics of shape memory polymers: uniaxial experiments and constitutive modelling. Int J Plasticity 22:279–313
37. Parameswaranpillai J, Sreekanth PM, Jose S, Siengchin S, Magueresse A, Janke A, Pionteck J (2017) Shape memory properties of epoxy/PPO-PEO-PPO triblock copolymer blends with tunable thermal transitions and mechanical characteristics. Ind Eng Chem Res 56(47):14069–14077
38. Parameswaranpillai J, Ramanan SP, George JJ, Jose S, Zachariah AK, Siengchin S, Yorseng K, Janke A, Pionteck J (2018) PEG-ran-PPG modified epoxy thermosets: a simple approach to develop tough shape memory polymers. Ind Eng Chem Res 57(10):3583–3590
39. Nagata N (1990) Development of polynorbornene-based shape- memory resins. Kagaku (Kyoto) 45:554–557
40. Jeon HG, Mather PT, Haddad TS (2000) Shape memory and nanostructure in poly(norbornyl-POSS) copolymers. Polym Int 49:453–457

41. Lin JR, Chen LW (1999) Shape-memorized crosslinked ester-type polyurethane and its mechanical viscoelastic model. J Appl Polym Sci 73:1305–1319
42. Chen W, Zhu C, Gu X (2002) Thermosetting polyurethanes with water-swollen and shape memory properties. J Appl Polym Sci 84:1504–1512
43. Alteheld A, Feng Y, Kelch S, Lendlein A (2005) Biodegradable, amorphous copolyester urethane networks having shape-memory properties. Angew Chem Int Ed 44:1188–1192
44. Lendlein A, Zotzmann J, Feng Y, Alteheld A, Kelch S (2009) Controlling the switching temperature of biodegradable, amorphous, shape-memory poly(rac-lactide)urethane networks by incorporation of different comonomers. Biomacromolecules 10:975–982
45. Zotzmann J, Alteheld A, Behl M, Lendlein A (2009) Amorphous phase – segregated copoly(ether) esterurethane thermoset networks with oligo(propylene glycol) and oligo[(rac-lactide)-co-glycolide] segments: synthesis and characterization. J Mater Sci Mater Med 20:1815–1824
46. Gall K, Dunn ML, Liu Y, Finch D, Lake M, Munshi NA (2002) Shape memory polymer nanocomposites. Acta Mater 50:5115–5126
47. Beloshenko VA, Beygelzimer YE, Borzenko AP, Varyukhin VN (2002) Shape memory effect in the epoxy polymer–thermo expanded graphite system. Compos Part A Appl Sci Manuf 33:1001–1006
48. Beloshenko VA, Beigelzimer YE, Borzenko AP, Varyukhin VN (2003) Shape-memory effect in polymer composites with a compactible filler. Mech Compos Mater 39:255–264
49. Ken GL, Martin LD, McCluskey P (2003) Thermomechanical recovery couplings of shape memory polymers in flexure. Smart Mater Struct 12:947
50. Zhu J, Fang G, Cao Z, Meng X, Ren H (2018) A self-folding dynamic covalent shape memory epoxy and its continuous glass fiber composite. Ind Eng Chem Res 57(15):5276–5281
51. Tong TH (2004) Shape memory styrene copolymer. US Patent Grant US6759481B2
52. Shim YS, Chun BC, Chung Y-C (2006) Thermomechanical properties and shape memory effect of PET-PEG copolymers cross-linked with pentaerythritol. Fiber Polym 7:328–332
53. Mather PT, Liu C (2003) Castable shape memory polymers, World Patent WO2003093341
54. Bertmer M, Buda A, Hofges IB, Kelch S, Lendlein A (2005) Biodegradable shape-memory polymer networks: characterization with solid-state NMR. Macromolecules 38:3793–3799
55. Lendlein A, Schmidt AM, Langer R (2001) AB-polymer networks based on oligo(ε-caprolactone) segments showing shape-memory properties. Proc Natl Acad Sci USA 98:842–847
56. Liu C, Chun SB, Mather PT, Zheng L, Haley EH, Coughlin EB (2002) Chemically cross-linked polycyclooctene: synthesis, characterization, and shape memory behavior. Macromolecules 35:9868–9874
57. Mather PT, Liu C, Coughlin EB, Chun SB (2004) Crosslinked polycyclooctene, US Patent US7173096B2
58. Rezanejad S, Kokabi M (2007) Shape memory and mechanical properties of cross-linked polyethylene/clay nanocomposites. Eur Polym J 43:2856–2865
59. Zhao J, Chen M, Wang X, Zhao X, Wang Z, Dang Z, Ma L, Hu G, Chen F (2013) Triple shape memory effects of cross-linked polyethylene/polypropylene blends with cocontinuous architecture. ACS Appl Mater Interfaces 5(12):5550–5556
60. Zhu G, Liang G, Xu Q, Yu Q (2003) Shape-memory effects of radiation crosslinked poly(ϵ-caprolactone). J Appl Polym Sci 90:1589–1595
61. Lendlein A, Schmidt AM, Schroeter M, Langer R (2005) Shape-memory polymer networks from oligo(epsilon-caprolactone)dimethacrylates. J Polym Sci 43:1369–1381
62. Lee KM, Knight PT, Chung T, Mather PT (2008) Polycaprolactone-POSS chemical/physical double networks. Macromolecules 41:4730–4738
63. Zotzmann J, Behl M, Hofmann D, Lendlein A (2010) Reversible triple-shape effect of polymer networks containing polypentadecalactone- and poly(-caprolactone)-segments. Adv Mater 22:3424–3429
64. Mya KY, Gose HB, Pretsch T, Bothe M, He C (2011) Star-shaped POSS-polycaprolactone polyurethanes and their shape memory performance. J Mater Chem 21:4827–4836

65. Defize T, Riva R, Raquez JM, Dubois P, Jerome C, Alexandre M (2011) Thermoreversibly crosslinked poly(ε-caprolactone) as recyclable shape-memory polymer network. Macromol Rapid Commun 32:1264–1269
66. Garle A, Kong S, Ojha U, Budhlall BM (2012) Thermoresponsive semicrystalline poly(ε-caprolactone) networks: exploiting cross-linking with cinnamoyl moieties to design polymers with tunable shape memory. Appl Mater Interfaces 4:645–657
67. Pandini S, Passera S, Messori M, Paderni K, Toselli M, Gianoncelli A, Bontempi E, Riccò T (2012) Two-way reversible shape memory behaviour of crosslinked poly(ε-caprolactone). Polymer 53:1915–1924
68. Pandini S, Baldi F, Paderni K, Messori M, Toselli M, Pilati F, Gianoncelli A, Brisotto M, Bontempi E, Riccò T (2015) One-way and two-way shape memory behaviour of semi-crystalline networks based on sol-gel cross-linked poly(ε-caprolactone). Polymer 54:4253–4265
69. Dureamae I, Nishida M, Hirabayashi TN, Matsumura K, Kitano H (2016) Biodegradable shape memory polymers functionalized with anti-biofouling interpenetrating polymer networks. J Mater Chem B 4:5394–5404
70. Tian G, Zhu G, Ren T, Liu Y, Wei K, Liu YX (2019) The effects of PCL diol molecular weight on properties of shape memory poly(ε-caprolactone) networks. J Appl Polym Sci 136:47055
71. Kelch S, Steuer S, Schmidt AM, Lendlein A (2007) Shape–memory polymer networks from oligo[(ε-hydroxycaproate)-co-glycolate] dimethacrylates and butyl acrylate with adjustable hydrolytic degradation rate. Biomacromol 8:1018–1027
72. Guo B, Chen Y, Lei Y, Zhang L, Zhou WY, Rabie ABM, Zhao J (2011) Biobased poly(propylene sebacate) as shape memory polymer with tunable switching temperature for potential biomedical applications. Biomacromol 12:1312–1321
73. Ikematsu TK, Kishimoto Y, Miyamoto K (1990) Shape memory polymer resin, resin composition and shape-memorizing molded product therefrom. Europe Patent EP374961A2
74. Kitahara SN, Nigata N (1991) Novel crosslinked polymer having shape memorizing property, method of its use, and molded article having shape memory. US Patent, US, p 5043396A
75. Luo X, Zhang X, Wang M, Ma D, Xu M, Li F (1997) Thermally stimulated shape-memory behavior of ethylene oxide-ethylene terephthalate segmented copolymer. J Appl Polym Sci 64:2433–2440
76. Wang M, Luo X, Ma D (1998) Dynamic mechanical behavior in the ethylene terephthalate-ethylene oxide copolymer with long soft segment as a shape memory material. Eur Polym J 34:1–5
77. Wang M, Zhang L (1999) Recovery as a measure of oriented crystalline structure in poly(ether ester)s based on poly(ethylene oxide) and poly(ethylene terephthalate) used as shape memory polymers. J Polym Sci Part B Polym Phys 37:101–112
78. Li F, Chen Y, Zhu W, Zhang X, Xu M (1998) Shape memory effect of polyethylene/nylon 6 graft copolymers. Polymer 39:6929–6934
79. Jeong HM, Song JH, Chi KW, Kim I, Kim KT (2002) Shape memory effect of poly(methylene-1,3-cyclopentane) and its copolymer with polyethylene. Polym Int 51:275–280
80. Langer RS, Lendlein A (2003) Biodegradable Shape Memory Polymeric Sutures. World Patent WO 2003088818 A2
81. Mather PT, Kim BS, Ge Q, Liu C (2004) Synthesis of nonionic telechelic polymers incorporating polyhedral oligosilsesquioxane and uses thereof. US Patent 2004024098
82. Mather PT, Kim BS, Ge Q, Liu C (2004) Preparation and Uses of Nonionic Telechelic Polymers Incorporating Polyhedral Oligosilsesquioxane (POSS). World Patent 2004011525
83. Campo CJ, Mather PT (2005) PVDF: PMMA shape memory blends: effect of short carbon fiber addition. Polym Mater Sci Eng 93:933–934
84. Zheng XT, Zhou SB, Li XH, Weng H (2006) Shape memory properties of poly(D, L-lactide)/hydroxyapatite composites. Biomaterials 27:4288–4295
85. Zheng X, Zhou S, Yu X, Li X, Feng B, Qu S, Wenig J (2008) Effect of in vitro degradation of poly(D, L – lactide)/ β – tricalcium composite on its shape memory properties. J Biomed Mater Res B 86B:170–180

86. Radjabian M, Kish MH, Mohammadi N (2012) Structure–property relationship for poly(lactic acid) (PLA) filaments: physical, thermomechanical and shape memory characterization. J Polym Res 19:9870
87. Ferreroa SP, Fernandez J, Martın MMFS, barburu PAS, Oiz JRS (2016) The relevance of molecular weight in the design of amorphous biodegradable polymers with optimized shape memory effect. J Mech Behav Biomed Mater 61:541–553
88. Nagahama K, Ueda Y, Ouchi T, Ohya Y (2009) Biodegradable shape-memory polymers exhibiting sharp thermal transitions and controlled drug release. Biomacromol 10:1789–1794
89. Ikematsu T, Kishimoto Y, Karaushi M (1990) Block copolymer bumpers with good shape memory. Japan Patent 02022355
90. Kim BK, Lee SY, Lee JS, Baek SH, Choi YJ, Lee JO, Xu M (1998) Polyurethane ionomers having shape memory effects. Polymer 39:2803–2808
91. Jeong HM, Kim BK, Choi YJ (1999) Synthesis and properties of thermotropic liquid crystalline polyurethane elastomers. Polymer 41:1849–1855
92. Li F, Qi L, Yang J, Xu M, Luo X, Ma D (2000) Polyurethane/conducting carbon black composites: structure, electric conductivity, strain recovery behavior, and their relationships. J Appl Polym Sci 75:68–77
93. Kim BKS, Shin YJ, Cho SM, Jeong HM (2000) Shape-memory behavior of segmented polyurethanes with an amorphous reversible phase: the effect of block length and content. J Polym Sci Part B Polym Phys 38:2652–2657
94. Lee BS, Chun BC, Chung YC, Sul KI, Cho JW (2001) Structure and thermomechanical properties of polyurethane block copolymers with shape memory effect. Macromolecules 34:6431–6437
95. Ping P, Wang WS, Chen XS, Jing XB (2005) Poly(epsilon-caprolactone) polyurethane and its shape-memory property. Biomacromol 6:587–592
96. Knight PT, Lee KM, Qin H, Mather PT (2008) Biodegradable thermoplastic polyurethanes incorporating polyhedral oligosilsesquioxane. Biomacromol 9:2458–2467
97. Pretsch T, Jakob I, Müller W (2009) Hydrolytic degradation and functional stability of a segmented shape memory poly(ester urethane). Polym Degrad Stab 94:61–73
98. Bothe M, Pretsch T (2012) Two-way shape changes of a shape-memory poly(ester urethane). Macromol Chem Phys 213:2378–2385
99. Bothe M, Emmerling F, Pretsch T (2013) Poly(ester urethane) with varying polyester chain length: polymorphism and shape-memory behavior. Macromol Chem Phys 214:2683–2693
100. Luo H, Liu Y, Yu Z, Zhang S, Li B (2008) Novel biodegradable shape memory material based on partial inclusion complex formation between r-Cyclodextrin and poly(E-caprolactone). Biomacromolecules 9:2573–2577
101. Feng Y, Behl M, Kelch S, Lendlein A (2009) Biodegradable multiblock copolymers based on oligodepsipeptides with shape-memory properties. Macromol Biosci 9:45–54
102. Zhang W, Chen L, Zhang Y (2009) Surprising shape-memory effect of polylactide resulted from toughening by polyamide elastomer. Polymer 50:1311–1315
103. Xue L, Dai S, Li Z (2010) Biodegradable shape-memory block co-polymers for fast self-expandable stents. Biomaterials 31:8132–8140
104. Momtaz M, Nouri MR, Barikani M (2014) Effect of block ratio and strain amplitude on thermal, structural, and shape memory properties of segmented polycaprolactone based polyurethanes. J Mater Sci 49:7575–7584
105. Han S, Gu BH, Nam KH, Im SJ, Kim SC, Im SS (2007) Novel copolyester-based ionomer for a shape-memory biodegradable material. Polymer 48:1830–1834
106. Lendlein A, Jiang HY, Jünger O, Langer R (2005) Light-induced shape-memory polymers. Nature 434:879–882
107. Lee KM, Koerner H, Vaia RA, Bunning TJ, White TJ (2011) Light-activated shape memory of glassy, azobenzene liquid crystalline polymer networks. Soft Matter 7:4318–4324
108. Kumpfer JR, Rowan SJ (2011) Thermo-, photo-, and chemo-responsive shape-memory properties from photo-cross-linked metallo-supramolecular polymers. J Am Chem Soc 133:12866–12874

109. Zhang HJ, Zhao Y (2013) Polymers with dual light-triggered functions of shape memory and healing using gold nanoparticles. ACS Appl Mater Interfaces 5:13069–13075
110. Michal BT, McKenzie BM, Felder SE, Rowan SJ (2015) Metallo-, thermo-, and photoresponsive shape memory and actuating liquid crystalline elastomers. Macromolecules 48:3239–3246
111. Yu L, Wang Q, Sun J, Li CY, Zou C, He ZM, Wang ZD, Zhou L, Zhang LY, Yang H (2015) Multi-shape-memory effects in a wavelength-selective multicomposite. J Mater Chem A 3:13953–13961
112. Xie H, He MJ, Deng XY, Du L, Fan CJ, Yang KK, Wang YZ (2016) Design of poly(l-lactide)-poly(ethylene glycol) copolymer with light-induced shape-memory effect triggered by pendant anthracene groups. ACS Appl Mater Interfaces 8:9431–9439
113. Fei GX, Li G, Wu LS, Xia HS (2012) A spatially and temporally controlled shape memory process for electrically conductive polymer-carbon nanotube composites. Soft Matter 8:5123–5126
114. Raja M, Ryu SH, Shanmugharaj AM (2014) Influence of surface modified multiwalled carbon nanotubes on the mechanical and electroactive shape memory properties of polyurethane (PU)/poly(vinylidene diflouride) (PVDF) composites. Colloids Surf A 450:59–66
115. Zhang ZX, Wang WY, Yang JH, Zhang N, Huang T, Wang Y (2016) Excellent electroactive shape memory performance of EVA/PCL/CNT blend composites with selectively localized CNTs. J Phys Chem C 120:22793–22802
116. Qi XD, Xiu H, Wei Y, Zhou Y, Guo YL, Huang R, Bai HW, Fu Q (2017) Enhanced shape memory property of polylactide/thermoplastic poly(ether)urethane composites via carbon black self-networking induced co-continuous structure. Compos Sci Technol 139:8–16
117. Mohr R, Kratz K, Weigel T, Lucka-Gabor M, Moneke M, Lendlein A (2006) Initiation of shape-memory effect by inductive heating of magnetic nanoparticles in thermoplastic polymers. Proc Natl Acad Sci USA 103:3540–3545
118. Zheng XT, Zhou SB, Xiao Y, Yu XJ, Li XJ, Wu PZ (2009) Shape memory effect of poly(d, l-lactide)/Fe_3O_4 nanocomposites by inductive heating of magnetite particles. Colloids Surf B 71:67–72
119. Kumar UN, Kratz K, Wagermaier W, Behl M, Lendlein A (2010) Non-contact actuation of triple-shape effect in multiphase polymer network nanocomposites in alternating magnetic field. J Mater Chem 20:3404–3415
120. Zhang FH, Zhang ZC, Luo CJ, Lin IT, Liu YJ, Leng JS, Smoukov SK (2015) Remote, fast actuation of programmable multiple shape memory composites by magnetic fields. J Mater Chem C 3:11290–11293
121. Du L, Xu ZY, Fan CJ, Xiang G, Yang KK, Wang YZ (2018) A fascinating metallo-supramolecular polymer network with thermal/magnetic/light-responsive shape-memory effects anchored by Fe_3O_4 nanoparticles. Macromolecules 51:705–715
122. Chen S, Hu J, Yuen CW, Chan L (2009) Novel moisture-sensitive shape memory polyurethanes containing pyridine moieties. Polymer (Guildf) 50:4424–4428
123. Zhao Y, Wang CC, Huang MW, Purnawali H (2011) Buckling of poly(methyl methacrylate) in stimulus-responsive shape recovery. Appl Phys Lett 99: id.131911 (1–3)
124. Gu X, Mather PT (2013) Water-triggered shape memory of multiblock thermoplastic polyurethanes (TPUs). RSC Adv 3:15783–15791
125. Fang Y, Ni Y, Choi B, Leo SY, Gao J, Ge B, Taylor C, Basile V, Jiang P (2015) Chromogenic photonic crystals enabled by novel vapour-responsive shape-memory polymers. Adv Mater 27(24):3696–3704
126. Landsman TL, Bush RL, Glowczwski A, Horn J, Jessen SL, Ungchusri E, Diguette K, Smith HR, Hasan SM, Nash D, Clubb FJ Jr, Maitland DJ (2016) Design and verification of a shape memory polymer peripheral occlusion device. J Mech Behav Biomed Mater 63:195–206
127. Webb GA, Aliew AE (eds) (2006) Nuclear magnetic resonance. Chemical Society (UK), Royal Society of Chemistry, London
128. Bertmer M, Buda A, Blomenkamp-Hofges I, Kelch S, Lendlein A (2005) Solid-State NMR characterization of biodegradable shape-memory polymer networks. Macromol Symp 230:110–115

129. Powers DS, Vaia RA, Koerner H, Serres J, Mirau PA (2008) NMR characterization of low hard segment thermoplastic polyurethane/carbon nanofiber composites. Macromolecules 41:4290–4295
130. Behl M, Bellin I, Kelch S, Wagermaier W, Lendlein A (2009) One-step process for creating triple-shape capability of AB polymer networks. Adv Funct Mater 19:102–108
131. Wagermaier W, Kratz K, Heuchel M, Lendlein A (2010) Characterization methods for shape-memory polymers. In: Lendlein A. (eds) Shape-memory polymers. Adv Polym Sci, 226: 97–145, Springer, Berlin, Heidelberg
132. Zhu Y, Hu JL, Yeung KW, Liu YQ, Liem HM (2006) Influence of ionic groups on the crystallization and melting behavior of segmented polyurethane ionomers. J Appl Polym Sci 100:4603–4613
133. Fu S, Ren H, Ge Z, Zhuo H, Chen S (2017) Shape memory polyurethanes based on zwitterionic hard segments. Polymers 9(10):465–480
134. Ansari M, Golzar M, Baghani M, Soleimani M (2018) Shape memory characterization of poly (ε-caprolactone)(PCL)/polyurethane (PU) in combined torsion-tension loading with potential applications in cardiovascular stent. Polym Testing 68:424–432
135. Romo-Uribe A, Albanil L (2018) Dynamics retardation in hybrid POSS-NIPAm nanocomposites. Thermoplastic and thermally-responsive hydrogel behaviour. Eur Polym J 99:350–360
136. Kong D, Xiao X (2016) High cycle-life shape memory polymer at high temperature. Sci Rep 6:33610. https://doi.org/10.1038/srep33610
137. Ni Q-Q, Zhang C-S, Fu Y, Dai GS, Kimura T (2007) Shape memory effect and mechanical properties of carbon nanotube/shape memory polymer nanocomposites. Compos Struct 81:176–184
138. Lützen H, Gesing TM, Kim BK, Hartwig A (2012) Novel cationically polymerized epoxy/poly(ε-caprolactone) polymers showing a shape memory effect. Polymer 53:6089–6095
139. Auad ML, Contos VS, Nutt S, Aranguren MI, Marcovich NE (2008) Characterization of nanocellulose reinforced shape memory polyurethanes. Polym Int 57:651–659
140. Di Prima MA, Gall K, McDowell DL, Guldberg R, Lin A, Sanderson T, Campbell D, Arzberger SC (2010) Cyclic compression behavior of epoxy shape memory polymer foam. Mech Mater 42:405–416
141. Wornyo E, Gall K, Yang F, King W (2007) Nanoindentation of shape memory polymer networks. Polymer 48:3213–3225
142. Fulcher JT, Lu YC, Tandon GP, Foster DC (2010) Thermomechanical characterization of shape memory polymers using high temperature nanoindentation. Polym Test 29:544–552
143. Cox LM, Killgore JP, Li Z, Long R, Sanders AW, Xiao J, Ding Y (2016) Influences of substrate adhesion and particle size on the shape memory effect of polystyrene particles. Langmuir 32(15):3691–3698
144. Cox LM, Killgore JP, Li Z, Zhang Z, Hurley DC, Xiao J, Ding Y (2014) Morphing metal–polymer janus particles. Adv Mater 26:899–904
145. Huang J, Lai L, Chen H, Chen S, Gao J (2018) Development of a new shape-memory polymer in the form of microspheres. Mater Lett 225:24–27
146. Liu R, Dai H, Zhou Q, Zhang Q, Zhang P (2016) Synthesis and characterization of shape-memory poly carbonate urethane microspheres for future vascular embolization. J Biomater Sci Polym Ed 27(12):1248–1261
147. Xiao X, Hu J (2016) Animal hairs as water-stimulated shape memory materials: mechanism and structural networks in molecular assemblies. Sci Rep 6:26393
148. Xiao X, Xie T, Cheng YT (2010) Self-healable graphene polymer composites. J Mater Chem 20:3508–3514
149. Xiao X, Hu J (2016) Influence of sodium bisulfite and lithium bromide solutions on the shape fixation of camel guard hairs in slenderization process. Int J Chem Eng 2016, Id: 4803254. http://dx.doi.org/10.1155/2016/4803254
150. Chen H, Xia H, Ni Q-Q (2018) Study on material performances of lead zirconate titanate/shape memory polyurethane composites combining shape memory and piezoelectric effect. Compos Part A Appl Sci Manuf 110:183–189

151. Yu K, Liu Y, Liu Y, Peng H-X, Leng J (2014) Mechanical and shape recovery properties of shape memory polymer composite embedded with cup-stacked carbon nanotubes. J Intell Mater Syst Struct 25:1264–1275
152. Gunes IS, Cao F, Jana SC (2008) Evaluation of nanoparticulate fillers for development of shape memory polyurethane nanocomposites. Polymer 49(9):2223–2234
153. Han J, Zhu Y, Hu J, Luo H, Yeung L-Y, Li W, Meng Q, Ye G, Zhang S, Fan Y (2012) Morphology, reversible phase crystallization, and thermal sensitive shape memory effect of cellulose whisker/SMPU nano-composites. J Appl Polym Sci 123:749–762
154. Yin Q, Wang D, Jia H, Ji Q, Wang L, Li G, Yin B (2018) Water-induced modulus changes of bio-based uncured nanocomposite film based on natural rubber and bacterial cellulose nanocrystals. Ind Crops and Prod 113:240–248
155. Guo Q, Bishop CJ, Meyer RA, Wilson DR, Olasov L, Schlesinger DE, Mather PT, Spicer JB, Elisseeff JH, Green JJ (2018) Entanglement-based thermoplastic shape memory polymeric particles with photothermal actuation for biomedical applications. ACS Appl Mater Interfaces 10(16):13333–13341
156. Espinha A, Guidetti G, Serrano MC, Frka-Petesic B, Dumanli AG, Hamad WY, Blanco A, López C, Vignolini S (2016) Shape memory cellulose-based photonic reflectors. ACS Appl Mater Interfaces 8(46):31935–31940
157. Mendez J, Annamalai PK, Eichhorn SJ, Rusli R, Rowan SJ, Foster EJ, Weder C (2011) Bioinspired mechanically adaptive polymer nanocomposites with water-activated shape-memory effect. Macromolecules 44(17):6827–6835
158. Chen S, Ban J, Mu L, Zhuo H (2018) Development of liquid crystalline polyurethane composites with stage-responsive shape memory effects. Polym Chem 9(5):576–583
159. Yang F, Wornyo E, Gall K, King WP (2007) Nanoscale indent formation in shape memory polymers using a heated probe tip. Nanotechnology 18:285302
160. Fang L, Gould OEC, Lysyakova L, Jiang Y, Sauter T, Frank O, Becker T, Schossig M, Kratz K, Lendlein A (2018) Implementing and quantifying the shape-memory effect of single polymeric micro/nanowires with an atomic force microscope. Chem Phys Chem 19:2078–2084
161. Meier T, Bur J, Reinhard M, Schneider M, Kolew A, Worgull M, Hölscher H (2015) Programmable and self-demolding microstructured molds fabricated from shape-memory polymers. J Micromech Microeng 25(6):065017
162. Weems AC, Raymond JE, Easley AD, Wierzbicki MA, Gustafson T, Monroe MBB, Maitland DJ (2017) Shape memory polymers with visible and near-infrared imaging modalities: synthesis, characterization and in vitro analysis. RSC Adv 7(32):19742–19753
163. Gong T, Zhao K, Wang W, Chen H, Wang L, Zhou S (2014) Thermally activated reversible shape switch of polymer particles. J Mater Chem B 2(39):6855–6866
164. Gong T, Zhao K, Yang G, Li J, Chen H, Chen Y, Zhou S (2014) The control of mesenchymal stem cell differentiation using dynamically tunable surface microgrooves. Adv Healthc Mater 3(10):1608–1619
165. Chung T, Romo-Uribe A, Mather PT (2008) Two-way reversible shape memory in a semicrystalline network. Macromolecules 41(1):184–192
166. Alvarado-Tenorio B, Romo-Uribe A, Mather PT (2011) Microstructure and phase behavior of POSS/PCL shape memory nanocomposites. Macromolecules 44:5682–5692
167. Alvarado-Tenorio B, Romo-Uribe A, Mather PT (2015) Nanoscale order and crystallization in POSS-PCL shape memory molecular networks. Macromolecules 48:5770–5779
168. Arzberger SC et al (2005) Elastic memory composites (EMC) for deployable industrial and commercial applications. Bellingham, WA: SPIE. https://doi.org/10.1117/12.600583
169. Lin JKH, Knoll CF, Willey CE (2006) Shape memory rigidizable inflatable (RI) structures for large space systems applications. In: 47th AIAA/ASME/ASCE/AHS/ASC structures, structural dynamics, and materials conference. AIAA, Newport, Rhode Island, pp 1–10
170. Sanderson T, and Gall K (2007) Shape memory polymer characterization for advanced air vehicle technologies, Raytheon Technol Today
171. Bashir M, Lee C F, Rajendran P (2017) Shape memory materials and their applications in aircraft morphing: an introspective study. ARPN J Eng Appl Sci 12, Article no 19

172. Yu K, Liu Y, Leng J (2011) Conductive shape memory polymer composite incorporated with hybrid fillers: electrical, mechanical, and shape memory properties. J Intell Mater Syst Struct 22:1–11
173. Liu Y, Du H, Liu Land Leng J (2014) Shape memory polymers and their composites in aerospace applications: a review. Smart Mater Struct 23:023001
174. Sun J, Guan Q, Liu Y, Leng J (2016) Morphing aircraft based on smart materials and structures: a state-of the-art review. J Intell Mater Syst Struct 27:2289–2312
175. Wischke C, Neffe AT, Steuer S, Lendlein A (2009) Evaluation of a degradable shape-memory polymer network as matrix for controlled drug release. J Control Release 138:243–250
176. Wischke C, Lendlein A (2010) Shape-memory polymers as drug carriers—a multifunctional system. Pharm Res 27:527–529
177. Serrano MC, Carbajal L, Ameer GA (2011) Novel biodegradable shape-memory elastomers with drug-releasing capabilities. Adv Mater 23:2211–2215
178. Buravalla V, Browne A, Johnson N (2010) Tunable vehicle structural members and methods for selectively changing the mechanical properties thereto. United States Patent Grant US7669918B2
179. Aase JH, Browne AL, Johnson NL, Ulicny JC (2006) Airflow control devices based on active materials. United States Patent Grant 7059664B2
180. Browne AL, Johnson NL (2007) Shape memory polymer seat assemblies. United States Patent Grant 7309104B2
181. Barvosa-carter W, Johnson NL, Browne AL. Herrera GA, Mc Knight GP, Massey C (2007) Reversibly expandable energy absorbing assembly utilizing shape memory foams for impact management and methods for operating the same. United States Patent Grant US7267367B2
182. Browne AL, Johnson NL, Cafeo JA, Mayer RR, Aase JH (2011) Reconfigurable storage bins having a structural component formed of a shape memory material. United States Patent Grant US8061550B2
183. Browne AL, Johnson NL (2011) Hood assembly utilizing active materials based mechanisms. United States Patent Grant, US7950488B2
184. Browne AL, Johnson NL (2015) Self-healing and self-cleaning tires utilizing active material actuation. United States Patent Grant, US9211687B2
185. Mondal S, Hu JL (2006) Temperature stimulating shape memory polyurethane for smart clothing. Indian J Fibre Text Res 31:66–71
186. Kobayashi K, Hayashi S (1992) Shape memory fibrous sheet and method of imparting shape memory property to fibrous sheet product. United States Patent Grant US5098776A
187. Kobayashi K, Hayashi S (1992) Woven fabric made of shape memory polymer. United States Patent Grant US5128197A
188. Chen S, Hu J, Liu Y, Liem H, Zhu Y, Liu Y (2007) Effect of SSL and HSC on morphology and properties of PHA based SMPU synthesized by bulk polymerization method. J Polym Sci Part B Polym Phys 45:444–454
189. Hu J (2007) Shape memory polymers and textiles. Woodhead, Cambridge
190. Meng Q, Hu J, Zhu Y, Lu J, Liu Y (2007) Morphology, phase separation, thermal and mechanical property differences of shape memory fibres prepared by different spinning methods. Smart Mater Struct 16(4):1192
191. Hu J, Chen S (2010) A review of actively moving polymers in textile applications. J Mater Chem 20:3346–3355

Classification of Shape-Memory Polymers, Polymer Blends, and Composites

Krzysztof Strzelec, Natalia Sienkiewicz and Tomasz Szmechtyk

Abstract Since the last three decades, international research interest into the shape-memory effect in polymers has been rapidly growing. The recent progresses made in the synthesis of different types of shape-memory polymers (SMPs) significantly expanded the practical potential of their applications in such fields like microelectromechanical systems, medical and biomimetic devices, sensors, actuators, self-healing systems, etc. The present chapter is focused on the classification of shape-memory polymeric materials (SMPs), as well as the current developments and most important concepts for these types of smart polymers. The recent progress in the development of shape-memory polymer composites (SMPCs) and shape-memory polymer blends (SMPBs) is also highlighted. In this chapter, different classification criteria of SMPs with a view to polymer type and structure and external stimulus are described. Particular emphasis is placed on the factors enabling shape-memory effects, especially structure–property correlations that influence shape-memory mechanisms.

1 Introduction

Shape-memory polymers (SMPs) are a kind of very important smart polymers that have multiple shape capacities. They can be deformed and subsequently fixed into a temporary shape, which would remain stable unless they are exposed to an appropriate external stimulus such as temperature, light, pH, electric or magnetic field, and specific ion or enzyme that triggers the polymers to recover to their original shape. Usually, preparation of SMPs is conducted by conventional processing methods, e.g., injection molding or extruding. During processing, the polymer is formed into its ini-

K. Strzelec · N. Sienkiewicz (✉) · T. Szmechtyk
Institute of Polymer and Dye Technology, Faculty of Chemistry, Lodz University of Technology, Stefanowskiego 12/16, 90-924 Lodz, Poland
e-mail: natalia.sienkiewicz@p.lodz.pl

K. Strzelec
e-mail: krzysztof.strzelec@p.lodz.pl

J. Parameswaranpillai et al. (eds.), *Shape Memory Polymers, Blends and Composites*, Advanced Structured Materials 115,
https://doi.org/10.1007/978-981-13-8574-2_2

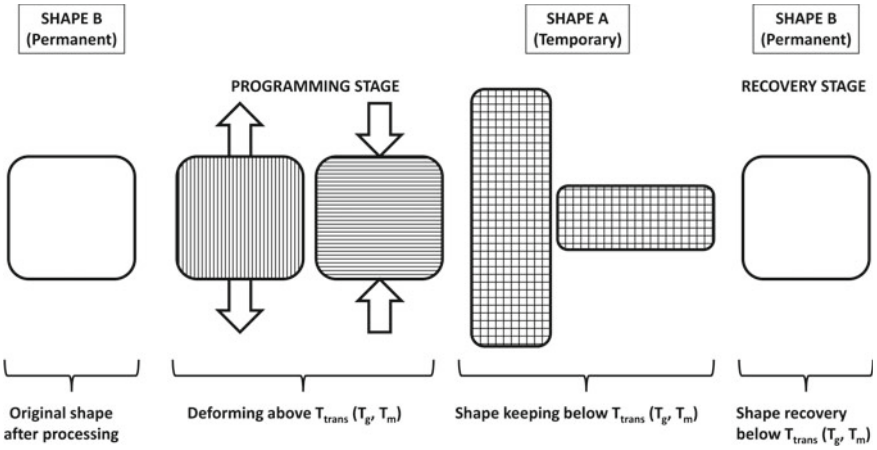

Fig. 1 Schematic representation of shape-memory effect for thermally induced process

tial permanent shape B. Afterward, the polymer specimen is deformed and fixed into the temporary shape A (Fig. 1). Polymer recovers its initial permanent shape B after application of an external stimulus [1]. In comparison with metallic shape-memory alloys, such cycle can be repeated several times in much shorter interval. Additionally, SMPs allow a much higher deformation rate between shapes A and B [2]. Apart from easy manufacturing and processing, for many applications, SMP materials are attractive substitutes to metals because of their flexibility, biocompatibility, low cost, and wide scope of modifications. Shape-memory polymer composites (SMPCs) and shape-memory polymer blends (SMPBs) have considerably enhanced the range of applications of shape-memory polymers.

The first shape-memory effect in polymers was described by Vernon et al. in the US patent on dental materials (methacrylic ester resin) [3, 4]. The first application of SMPs was heat-shrink tubing by Paul Cook at Raychem Company in the late 1950s [5]. The next important step in the development of SMPs was reported by Rainer et al. in [6], the utilization of heat-shrinkable polyethylenes [6]. This polymer was able to memorize its initial shape after irradiation with gamma rays. Also, George Odian with coworkers at Radiation Applications, Inc. in early 1960s, developed for NASA deployable space structures from polyethylene with radiation-induced memory. Besides these, only a few other studies were performed in the 1960s; however, industrial application was being widely explored as evidenced by patent literature on "heat-shrinkable" or "heat-recoverable" materials used in electrical engineering and packaging industry (Fig. 2) [5]. Starting in the mid-1990s, academic interest in the field of shape-memory polymers dramatically grew. Since then the research in SMPs has increased due to their possible and promising application in several fields such as smart textiles and apparels, medical devices, sensors and actuators, flexible electronic devices, high-performance water vapor permeability membranes, aerospace applications, and many others [7]. In recent years, a wide variety of polymers has been

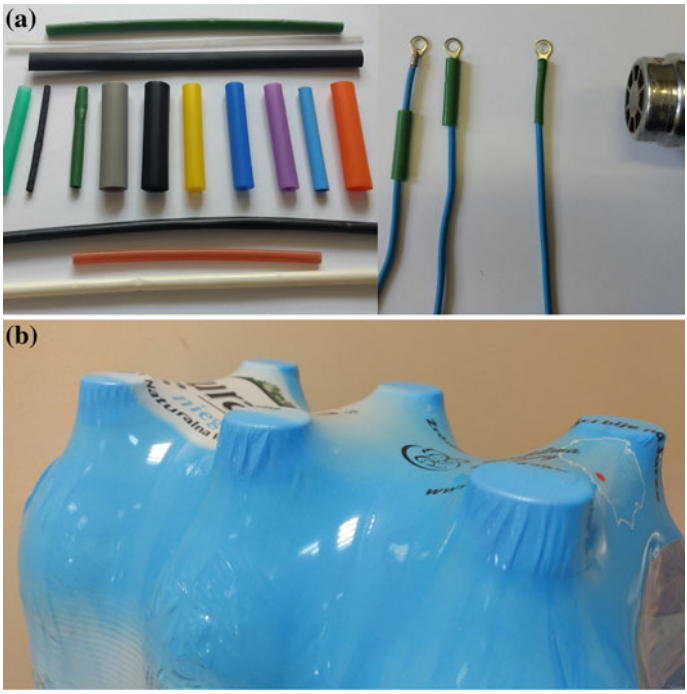

Fig. 2 **a** Heat-shrinkable plastic tubes used to insulate wires; **b** Packaging shrink-wrap foil

synthesized with shape-memory effects. A number of unique properties have been developed in different types of polymers like thermoplastics, elastomers, thermosets, polymeric blends and composites, hydrogels, and liquid crystals.

2 Classification of SMPs

With the emergence of new types of shape-memory polymers, the basic criteria for their classification were defined. The most commonly used classification of SMPs (discussed in this review) includes the three criteria: composition and structure of polymers, the type of stimulus which triggers the shaping back to the permanent phase, and the character of shape-memory function. Such integrated insight into the classification of SMPs was proposed by Hu et al. [8]. Another division into physically and chemically cross-linked SMPs, according to the nature of their netpoints, was introduced by Liu and coworkers [9]. The combined scheme of the two above classifications is presented in Fig. 3. The chemical structure of SMPs and a type of activation trigger were the main criteria for classification showed by Mather [5]. This division includes four categories. Category I and Category II are chemically cross-

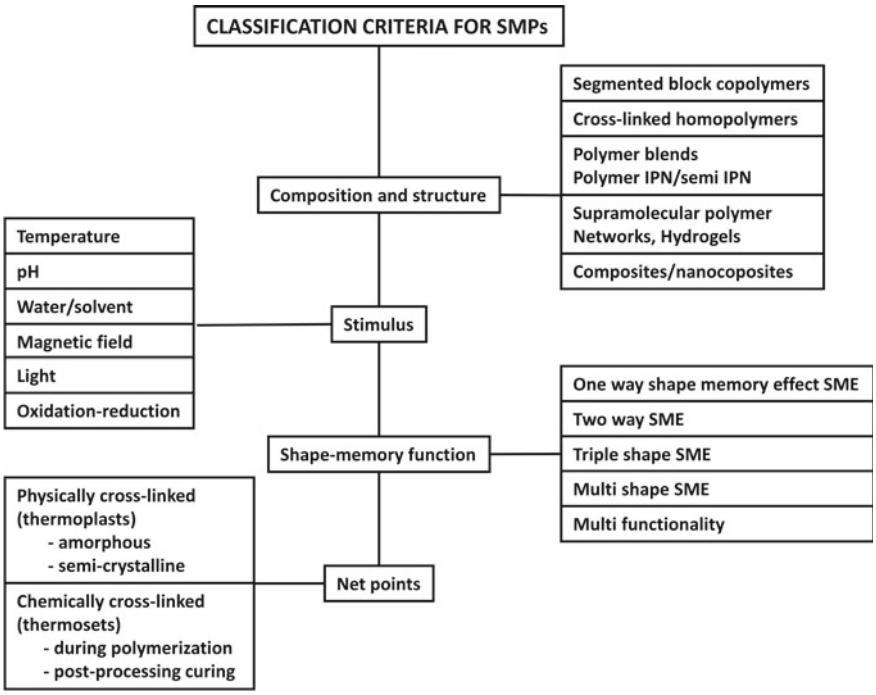

Fig. 3 Schematic view over classification criteria of shape-memory polymers

linked networks that utilize, respectively, a glass transition and melting transition for their activation. Category III and Category IV represent physically cross-linked polymers activated accordingly, with a glass transition and melting transitions.

2.1 Classification by Polymer Structure

Almost, all polymerization methods can be used to synthesize SMPs, including addition, condensation, free-radical and photochemical polymerization, and radiation reaction [9]. The shape-memory effect of the polymer can be achieved through the generation of strong interaction among the polymer chains. Usually, elastic entropic forces result from the presence of physical or chemical netpoints, which can be achieved by covalent bonds or intermolecular interactions. This kind of polymeric materials must present an adequate morphology in order to show this behavior [10]. Taking into account the cross-linking characteristics, composition, structure, morphology, and type of polymer materials, SMPs are often classified into four different polymer structures: chemically cross-linked, physically cross-linked, polymer blends, and polymer composites [11].

Generally, the molecular structure of SMPs consists of two practical parts, cross-links with chemical or physical nodes (hard segments), and switching segments. The cross-linked elements of structure allow for the memorization of the original permanent shape. The hard segments may be of physical or chemical nature, such as chemical cross-links, crystals, glassy domains, or chain entanglements [12]. The switching segments are the polymer chains between network nodes that undergo the reversible shape change (Fig. 4) [5]. The soft segments work as reversible molecular switch at transition temperatures. These segments can be either amorphous or crystalline, and therefore the transition temperature (T_{trans}) is glass transition temperature (T_g) and a melting point temperature (T_m), respectively. Chemically cross-linked SMPs can be obtained by a suitable cross-linking chemistry, which are referred to as thermosets. Physically cross-linked ones require a polymer morphology consisting of segregated domains, which is typical for thermoplastics [10].

2.1.1 Chemically Cross-Linked Polymers

For the chemically cross-linked polymers (thermosets), the polymer network is built from the polymer chains connected by covalent bonds, which are more stable than the physical cross-linking network and show an irreversible nature [13, 14]. When the covalent bonds are introduced into polymer matrix, the programmed shape of polymer cannot be further changed. Covalent netpoints can be obtained during polymerization by the cross-linking of linear or branched polymers as well as (co)polymerization/(co)polycondensation of one or several monomers, in which one has at least trifunctional. The other methods rely on postprocessing cross-linking of polymer chains. The physicochemical properties of the network can be adjusted by the choice of monomers, their ratio and functionality, and the cross-link content. Additionally, these properties can be controlled by the curing conditions and curing time. Several types of SMPs are also synthesized by synthesis route, which involve copolymerization of monofunctional monomers with oligomeric difunctional cross-linkers [10]. Such AB copolymer networks possess increased toughness and elasticity at room temperature. AB copolymer network with T_{trans} based on T_g was obtained by copolymerization of various acrylates with poly[(l-lactide-*ran*-glycolide)]dimethacrylate [13]. Similar covalently SMP AB copolymer network with melting transition T_m used as switching transition for the shape-memory effect was prepared by copolymerization of *n*-butyl acrylate with semicrystalline oligo[(ε-hydroxycaproate)-*co*-glycolate]dimethacrylates [15].

Typical examples of SMP networks prepared during polymerization processes are styrene copolymers, thermosetting polyurethanes, polyacrylates and polymethacrylates, PE/poly(vinyl acetate) copolymer, and epoxides. The thermosetting SMPs, like for example cross-linked styrene-based SMP and epoxy SMP, in contrast to thermoplastic SMPs with poor thermal and mechanical properties, are generally used for large-scale structural materials. Copolymerization of styrene with various co-monomers is the key to obtaining shape-memory materials with enhanced flexibility and a huge variety of network architectures [16]. For example, shape-

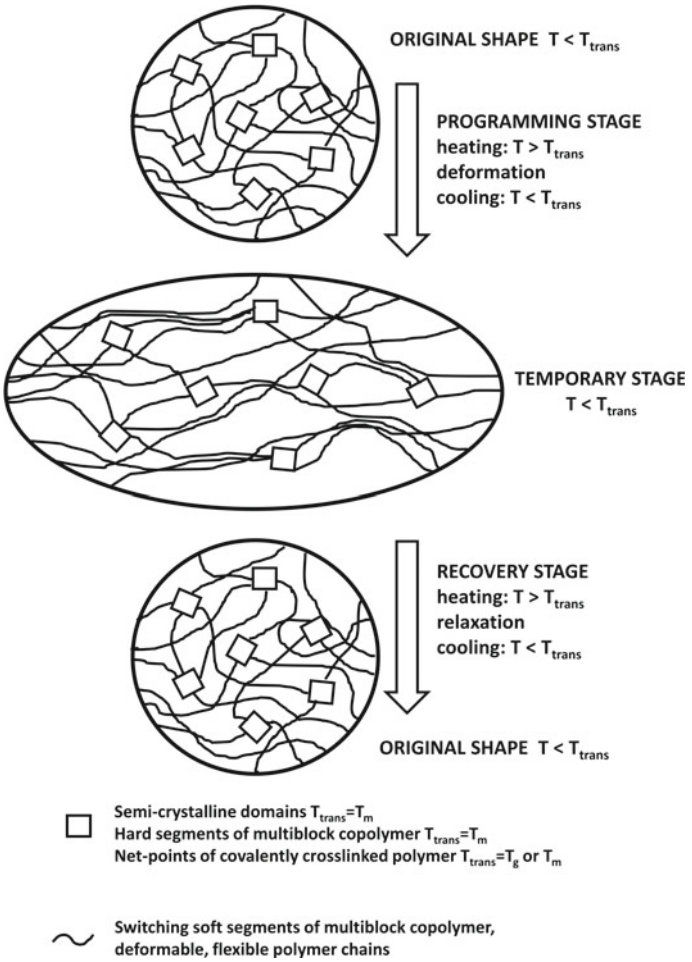

Fig. 4 Molecular mechanism of thermally induced shape-memory effect for different types of SMPs

memory effect has been reported for copolymer of styrene, corn oil and divinylbenzene [17], and *trans*-poly(1,4-butadiene)-polystyrene copolymer [18]. Also, polyacrylates and polymethacrylates are of interest as shape-memory materials due to their ease of preparation, their simple phase behavior, and the possibility of easily tuning their key characteristics. (Meth)acrylates with a wide variety of ester functionalities are commercially available, and many of them can be copolymerized by radical polymerization in bulk or in solution [13]. The acrylic monomers which are predominantly used for synthesis of SMP networks may have (1) network segments, (2) a switching segment, and (3) a cross-linker. For example, SMP networks were synthesized from poly(methyl methacrylate-*co*-butyl methacrylate)

copolymer cross-linked with tetra(ethylene glycol) dimethacrylate [19]. Apart from being built up by the main chain of poly((meth)acrylates), the switching segment can also be introduced as side chains or as long-chain cross-linkers by the use of (meth)acrylic ester macromonomers based on oligo(ε-caprolactone), PEG, and poly(lactide-*co*-glycolide) [13]. As cross-linkers, multifunctional (meth)acrylates include (meth)acrylates of polyols (ethylene glycol, butylene glycol, glycerol), trimethylolpropane, and acrylamides which are often employed. There are several reports on the SMPs based on the polyethylene oxide (PEO), cross-linked with maleic anhydride, glycerin or dimethyl 5-isophthalates [17]. Also, interpenetrating polymer network (IPN) of polyethylene oxide/poly(methyl methacrylate) (PMMA) was reported [20]. PEO/PMMA IPN systems show shape-memory properties with two transition temperatures: T_m of PEO and T_g of IPN.

Chemically cross-linked SMPs can be also synthesized by polyaddition and polycondensation reaction. Shape-memory behaviors were observed for thermosetting polyurethanes. Hu et al. reported the influence of the molecular weight on shape-memory behavior in polyurethane films [21]. Glycerin and 1,1,1-trimethylolpropane were applied as cross-linker for polyurethanes [12, 22, 23]. A clear improvement in creep and increase in recovery temperature have been observed due to the application of cross-linking [24]. Hybrid polyurethanes, cross-linked with Si–O–Si linkages, were made by Xu and coworkers [25]. Thermosetting polyurethanes were prepared by grafting of polyacrylamides and polyacrylates or by introducing hydrophilic groups into the cross-linked polyurethane backbone. Such networks showed both shape-memory and hydrogel properties [17].

SMPs based on epoxy polymers are a high-performance thermosetting resin possessing a unique thermomechanical property together with excellent shape-memory effect [10]. The epoxy SMP was synthesized from an epoxy resin, hardener, and additional linear epoxy monomer, by Leng et al. [26]. With the increase of active linear epoxy monomer, the T_g of such tailored network ranges from 37 to 96 °C. Shape-memory network was enabled by reaction of 3-amino-1,2,4-triazole with epoxidized natural rubber catalyzed by bisphenol-A [13]. The transition temperature of this network is the T_g, which could be controlled by the 3-amino-1,2,4-triazole content in the range between 29 and 64 °C [27]. The shape-memory IPN networks can be also prepared through successive polyaddition and polymerization. The example of such IPN is a system obtained from polyethyleneglycol dimethacrylate blended with star-shaped poly[(rac-lactide)-*co*-glycolide], which is first photopolymerized and later, the polyesterurethane network is formed using isophorone diisocyanate [13]. T_{trans} can be adjusted between −23 and 63 °C [28].

Another method of preparation of chemically cross-linked SMPs is a subsequent cross-linking of a linear or a branched polymer [14, 17, 29]. The SMPs created by postprocessing can be divided into two groups: cross-linked by means of cross-linking agent and cross-linked by electromagnetic radiation. An example of the first method is the application of peroxide to cross-link the linear polymers [11, 29–31]. Liu and coworkers used a dicumyl peroxide to cross-link semicrystalline polycyclooctene obtained by ring-opening metathesis polymerization containing unsaturated carbon bonds [32, 33]. The electromagnetic radiation with different wave-

lengths (γ-radiation, UV, neutrons, e-beam) is often used to cross-link polymers during postprocessing processes. The abovementioned polyethylene cured with gamma rays obtained by Rainer in 1964 was one of the first SMPs [6]. The γ-radiation has been also used to generate SMPs based on poly(ε-caprolactone) and its blends with poly(methyl vinyl siloxane) [11, 34]. Application of UV radiation to cross-linking SMPs requires incorporation of photo-initiators or light-sensitive monomers. For example, a covalent network with shape-memory properties was synthesized from poly(lactide-*co*-glycolide) and polyhedral oligomeric silsesquioxanes (POSS) using tetrathiol as cross-linking agent and 2,2-dimethoxy-2-phenylacetophenone as radical photo-initiator [35]. The use of functional, light-sensitive monomers, for example, monomers with acrylic groups, allows easy control of the initial shape and degree of cross-linking of the network formed by photo-curing [36, 37].

2.1.2 Physically Cross-Linked Polymers

For the physically cross-linked SMPs, the formation of phase segregate morphology is the fundamental mechanism behind the thermal-induced shape-memory behavior of these thermoplastic materials [10]. The molecular switch and physical cross-link are provided by separate phases of the polymer. A notable difference between physical and chemical cross-linking is that in the physically cross-linked polymers it is possible to remold the fixity phase after reaching the temperature at which the physical bonds disappear [11]. Physically cross-linked polymers can be further classified into linear polymers (block copolymers and high-molecular-weight polymers), branched polymers, and polymer complex [10]. Another classification takes into account the presence of the SMP amorphous or crystalline switching segments.

In glassy SMPs with amorphous switching segments, the hard amorphous domains act as physical cross-link via van der Waals forces, polar–polar interactions, hydrogen bonding, and other weak interactions. The T_g of the soft segments represents the transition temperature T_{trans} and is responsible for SME [38]. The shape-memory behaviors of this type SMPs depend on the chain length, structure, and arrangements of soft segment. Segmented amorphous shape-memory polyurethanes (PU) are the most important class of this type of SMPs. The hard segments of linear PU are formed either from a long-chain macro-diol with a higher thermal transition temperature or from diisocyanates and chain extenders [13]. The T_g of thermoplastic polyurethanes can be controlled in a wide range by using different kinds of monomers (aromatic or aliphatic diisocyanates) and chain extenders (low-molecular-weight diols or diamines) and by adjusting their amounts [17]. Precise control of PU composition and structure of soft and hard segments are necessary for effective shape-memory effect. The glassy hard segments, except physical cross-linking, should maintain the shape of material through hydrogen bridges or polar interaction. The soft segments could freely absorb external stress by unfolding and extending PU chains in these domains. The synthetic route for long polymer polyurethane chains (soft segments) and highly polar (hard) segments is based on the two-step procedure. In the first step, a polymeric diol reacts with diisocyanate to form the

prepolymer. Next, this prepolymer reacts with low-molecular-weight chain extenders, like diols or diamines [39–42]. Another method of obtaining shape-memory polyurethanes based on joining block copolymers was proposed by Lendlein et al. [43]. He prepared SMPs with tunable T_{trans} between 14 and 56 °C, from copolymers of lactic acid with other monomers. Besides polyurethanes, many other SMPs with amorphous switching segments have been reported. Both homopolymers and their blends, like poly(methyl methacrylate), polynorbornene, poly(methylene-1,3-cyclopentane), poly(vinyl chloride) [17], as well as, numerous block copolymers like, for instance, poly(lactic-*co*-glycolic acid), allow to obtain separated phase systems [44, 45]. In the case of copolymer SMPs, the blocks from co-monomer with the highest transition temperature act as the hard segments (fixity phase), while the other ones are the soft segments (switching phase). In the case of SMPs prepared by copolymerization, the appropriate selection of monomers allows improvement in other properties like biodegradability, hydrophilicity, solvent absorption and diffusion, toughness, transition temperature, or activation shape-memory time [11].

The second group of physically cross-linked SMPs comprises polymers with crystalline switching segments. The temporary shape of these materials is fixed by crystallization of the soft domains, which occurs below T_g. The transition temperature region corresponding to T_m (melting of crystalline domains) is narrow, in contrast to the SMPs, with amorphous switching segments, which often show broad transition temperature range and usually requires difficult to achieve precise combination of soft segments [17]. Various physically cross-linked semicrystalline SMPs were reported. Typical examples are biodegradable poly(L-lactide-*co*-ε-caprolactone) [46], poly(ethylene oxide-*co*-butylene terephthalate) [47], and polystyrene-*co*-poly(butadiene) [38]. However, the largest group in this category are the thermoplastic segmented shape-memory semicrystalline polyurethanes. Polycaprolactone-diol (PCL-diol) has been extensively used for the synthesis of PU with crystalline soft phase [48]. The hard segments were incorporated in 4,4′-diphenylmethane diisocyanate (MDI)-based PU by application of such monomers as 1,4-butanediol [49], 4,4′-bis(2-hydroxyethoxy)biphenyl (BEBP) or 4,4′-bis(2-hydroxyhexoxy)biphenyl (BHPP) [50], and 1-octadecanol [51, 52].

2.1.3 Segmented Block Copolymers

Shape-memory effect in segmented block copolymers is based on different transition temperatures (T_g or T_m) of co-monomers [11]. The transition temperatures determine, which co-monomer will be switching phase (lower temperature) and which one will be fixity phase (higher temperature). Well-known example of switching phase co-monomer is lactic acid as PLA, but it cannot provide optimal SME without appropriate fixity phase. Only combined with ε-caprolactone as poly(l-lactide-*co*-ε-caprolactone) (PCLA) [46] or with glycolic acid as poly(lactic-*co*-glycolic acid) (PLGA) [44] shows superb SME. Similar relation between phases is also observed in polyurethanes, where reaction between diisocyanate and diol allows to obtain fixity phase with urethane groups and switching phase of oligoester [39–43]. Strong inter-

actions between dipoles and hydrogen bonds ensure polarity of fixity phase, high enough to use PLA, or even polycaprolactone (PCL) as switching phase. Another example of segmented block copolymer with shape-memory effect is poly(ethylene terephthalate) (PET) as fixity phase with poly(ethylene dioxide) (PEO) as switching phase [47].

2.1.4 Cross-Linked Homopolymers

Shape-memory homopolymers have fixity phase and switching phase as block copolymers, but the difference lies in the presence of both amorphous and crystalline regions in one polymer. While crystals act as fixity phase and provide shape, physical bonds of amorphous chains (switching phase) react to appropriate temperature and reshaping occurs. Example of shape-memory homopolymer is semicrystalline PLA, which in addition to being SMP also is biocompatible and biodegradable [46, 53–55]. Unfortunately, shape-memory effect of PLA is limited to narrow temperature range. Also compared with the performance of polymer blends, block copolymers, and interpenetrating polymer networks, shape-memory effect of PLA homopolymer is limited.

2.1.5 Polymer Blends, Polymer IPN/Semi-iPN

There are two types of polymer blends with shape-memory effect: miscible and immiscible. Both of them are interesting for industrial applications, due to the fact that blending is easily implementable and can provide enhancement of mechanical and thermal properties. Miscible blends can be made from semicrystalline polymers like PCL and polydioxanone [56] or from semicrystalline and amorphous polymers like polyurethanes based on PCL with poly(vinyl chloride) [57] or phenolic resin [58]. Although miscibility theoretically causes one T_g of blend, different concentrations of each polymer in various regions differentiate local T_g. Immiscible blends like PCL matrix with poly(styrene-*b*-butadiene-*b*-styrene) (SBS) [59] or PLCA with PLGA [25] also represent shape-memory polymers.

Specific blends of miscible polymers with interlaced networks are known as interpenetrating polymer networks (IPNs). They can also exhibit shape-memory properties if aforementioned T_g issue is solved in similar way as for other miscible polymers. IPNs based on PLGA polyurethanes with poly(ethylene glycol) (PEG) dimethacrylates were proposed by Zhang et al. [28]. Other IPNs with acrylates were made of PMMA with PEO, where shape-memory effect was based on melting of PEO crystals, and poly(methyl methacrylate-*N*-vinyl-2-pyrrolidone) with PEG, where shape-memory effect was provided by hydrogen bonds [60, 61].

2.1.6 Supramolecular Polymer Networks, Hydrogels

SMPs obtained via supramolecular chemistry are based on non-covalent interactions such as hydrogen bonds, dipole–dipole bonds, or van der Waals forces. Great numbers of these interactions can provide better stability of polymer structure and act as fixity phase [62]. Despite this, thermal-induced dissociation of hydrogen bonds also provides shape recovery of the structure [63]. Also, supramolecular SMPs have distinctive dynamics of shape change response. Most notable studies on supramolecular SMPs include solutions with ureidopyrimidinone (UPy) in polyurethane elastomers [64] or polyacrylate copolymers [63]; α-cyclodextrin (α-CD) and polyethylene glycol (PEG) in PEG-α-CD [65]; PEG and acrylates in PEG-PMMA-*co*-(*N*-vinyl-2-pyrrolidone) [60, 61], PEG–PMMA-*co*-acrylic acid [66], and PEG–polymethyl acrylate [20]; and pyridine in polyurethanes [21].

Hydrogels, as polymers with hydrophilic groups, are able to change their structure, thanks to ability of absorbing significant amounts of water. Temperature is a stimulus, which has important role in mechanism of shape change. There are two types of hydrogels behaving conversely: lower solution critical temperature (LSCT) hydrogels and higher solution critical temperature (HSCT) hydrogels. While LSCT hydrogels are swollen at temperatures lower than LSCT and shrunken at temperatures higher than LSCT, HSCT hydrogels have inverted characteristic (swell above HSCT and shrink below HSCT) (Fig. 5).

First shape-memory hydrogels were obtained from stearyl acrylate [67], but shape-memory effect was not obtained immediately in both states. After achieving SMP

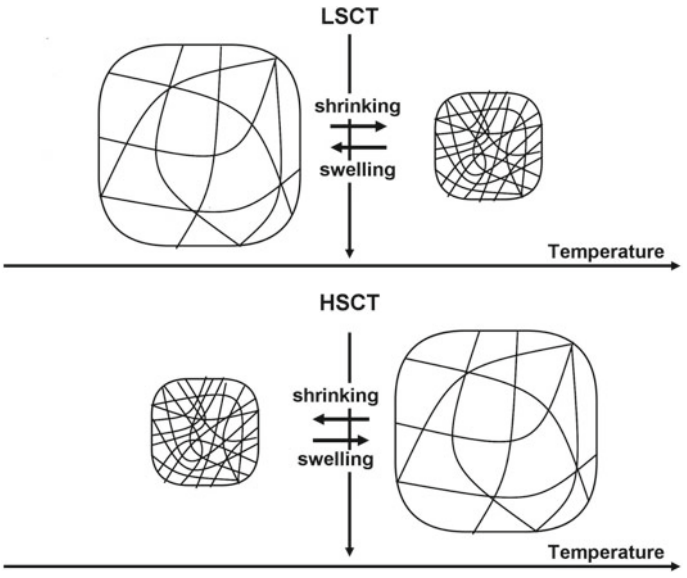

Fig. 5 Swelling/shrinking mechanism of shape-memory hydrogels

as swollen hydrogel, exchange of stearyl acrylate to methyl acrylate was necessary to create hydrogel with shape-memory effect in both (shrunken and swollen) states [68]. Other polymers common in hydrogel synthesis are polyacrylamide (PAAm) and poly(vinyl alcohol) (PVA). While PAAm is very useful in drug delivery, shape-memory effect of PVA is hindered by cleavage of hydrogen bond above 60 °C and in consequence, unstable structure of PVA [69, 70]. Success of PAAm results from its LSCT, which is close to temperature of human body, and from modulated gel technology technique [53] using interpenetrating networks of PAAm with *N*-isopropylacrylamide (NIPAAm), which provides shrinkage of hydrogel at elevated temperature.

2.1.7 Composites/Nanocomposites

Shape-memory polymer composites (SMPCs) differ from other structures because of fillers and nanofillers influence on shape-memory effect. SMPs have intrinsic low mechanical strength and shape recovery stress, which have largely restricted their applications [71]. A small amount of micro/nano-sized fillers can significantly improve these properties of SMPs. SMPCs not only exhibit improved mechanical properties and shape-memory properties but also possess novel properties like multi-shape-memory effect, indirect SME, gradient SME, two-way SME, and complicated movement SME, indirectly triggering SME [71]. SMPCs can also enable or enhance thermal stimuli-active effects, include electroactive effect, magnetic-active effect, water-active effect, and photoactive effect. Zheng et al. [72] reported poly(l-lactic acid fillers) (PLLA) matrix with shape-memory effect improved by β-tricalcium. Another PLLA composites with hydroxyapatite [73] and chitosan [44] also exhibit better shape-memory effect than PLLA homopolymer. Increased stiffness and decreased recoverable strain were observed for SMPs reinforced with glass and Kevlar [17]. Conducting SMPCs were prepared by blending carbon black or a conducting polymer with the SMP [74–76]. Incorporation of 3.3% of carbon nanofibers resulted in 200% increase in recovery stress of the SMPCs [77]. Application of carbon nanotubes or carbon black of similar size for reinforcement of polyurethanes gave the nanocomposites with increased shape fixity [78]. SMPCs with shape-memory effect triggered by magnetic field were obtained using magnetic nanofiller like Fe_2O_3 with a shell of oligo(ε-caprolactone) or Ni–Zn ferrite particles [79, 126] .

2.2 Classification of Shape-Memory Function

Shape-memory polymers may have different kinds of shape-memory effect. The most common memory effects are the one-way and two-way shape-memory, multi-shape, and multifunctionality.

2.2.1 One-Way Shape-Memory Effect SMP

The procedures in one-way shape-memory effect (1W-SMPs) consist of programming and recovery of a shape. Depending on chemical structure of polymer, its behavior can differ significantly. In Fig. 6, the process of programming and recovery of a shape is shown in a schematic way. In the beginning, a programming process is carried out during which the shape-memory polymer is subjected to such action to obtain its permanent shape. In the next stage, the SMP is distorted and the intentional temporary shape is fixed. The whole this process is based on heating up the sample, deforming, and cooling the sample, or as it is possible drawing the sample at a low temperature. Shape-memory effect is inducted by heating up the sample above a transition temperature (T_{trans}), and the recovery of SMP is observed. Solidification of the material is possible during cooling down the polymer below transition temperature; however, no recovery of the temporary shape is observed—what is called a one-way shape-memory effect. During next programming, including mechanical deformation, the polymer can obtain a temporary shape again but this new temporary shape is not identical as the first temporary shape. The best example of materials which have a thermo-responsive one-way shape-memory effect are hydrogels with hydrophobic, crystallizable side chains, and cross-linked poly(vinyl alcohols) [80, 81]. Hydrogels prepared from copolymerized acrylic acid and stearyl acrylate cross-linked with methylenebisacrylamide have a really strong temperature dependence in their mechanical properties. Polymers obtained in this reaction behave like tough polymers in temperature below 25 °C, but above 50 °C softening enables the materials to be extended up to 50%. 1W-SMPs behavior of poly(cyclooctene) that was cross-linked through a free-radical reaction using dicumyl peroxide was reported [32, 33]. What is important is the establishment of a provisional shape on cooling as well as quick improvement to the basic form upon heating. Besides, it was also proposed that cross-linked poly(cyclooctene) reveals crystallization-induced elongation and melting-induced contraction on heating, which can be explained by thermo-reversible actuation. The melting temperature of sample (T_m) can be customized by change of the quantity of dicumyl peroxide used for the cross-linking stage. Poly(cyclooctene) has a stable molten–rubbery plateau above the T_m, which provides effortless deformation and reacts as the transition temperature for shape-memory step, as well as a crystallization temperature (T_c) close to room temperature that lets fast crystallization process and efficient fixing of a temporary shape [82].

2.2.2 Two-Way Shape-Memory Effect SMP

Recently, two-way convertible shape-memory polymer materials (2W-SMPs) are greatly advisable for many applications [83–85]. Nowadays, some polymers have been investigated for two-way shape-memory properties, such as liquid crystal elastomers and photo-deformation polymers. Variety from the mechanism of 1W-SMPs, the 2W-SMPs process in liquid crystal elastomers and photo-deformation materials is imputed to the conversion of anisotropic polymer chain conformation and

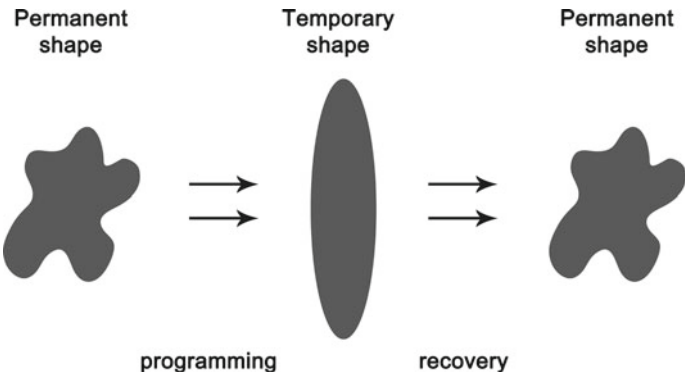

Fig. 6 Schematic picture of the thermally induced one-way shape-memory effect

light-stimulated phase transitions (Fig. 7) [86–89]. Shape change gel layer is one of the samples with a thermally caused two-way shape-memory effect. Discussed gels include two types of layers: a thermosensitive control layer and a substrate layer which is not sensitive to changes in variables temperature. The first one consists of an ionic gel prepared from the *N*-isopropylacrylamide and sodium acrylate cross-linked with *N, N′*-methylenebisacrylamide. During the temperature exceed of 37 °C, the control layer shrinks while the substrate layer does not change. For connecting both varied layers, one part of the control layer includes cross-linked copolymer which is exposed to an aqueous solution of acrylamide. Next, the acrylamide is polymerized by the use of a radical initiator to form diffuse chains. The pronounced variation in shape of gels is convertible, and the system can reverse between two defined shapes depending on the reaction conditions (below or above the transition temperature) [90] (Fig. 8).

Wang et al. reported the application of homopolymers and copolymers of ε-caprolactone and ω-pentadecalactone with cocrystallizable monomeric units for the composition of 2W-SMPs. The thiol–ene cross-linking system exposed two-way reversible 2W-effects under stress-free and stress conditions. The propulsion temperature of the two-way shape-memory effect under stress-free condition can be adapted in an extensive scope using suggested prepolymers by photo-cross-linking with a multifunctional cross-linker [91].

The shape-memory elastomer with a pre-stretched in stencil is checked. Designed material shows 2W-SM effect in reply to alterations in temperature without the need of an unchanged permanent exterior load [92]. Chen et al. prepared laminated composites with SMPs membrane and elastic polymers membrane. It is 2W-SM behavior in which the mechanism of shape-memory is ascribed to the release of elastic strain of SMP layer upon heating, and the recovery of elastic strain caused by the bending force of substratum membrane upon cooling [93].

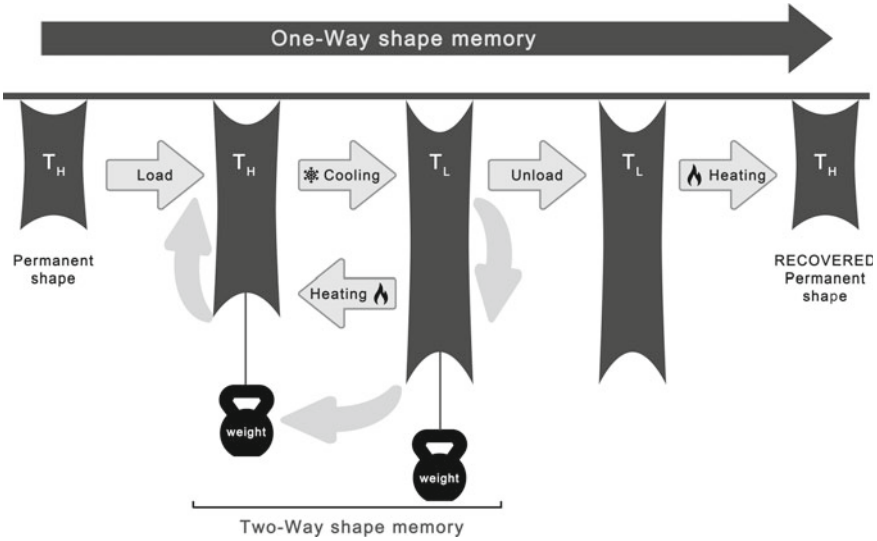

Fig. 7 Schematic showing the difference between the one-way and two-way shape-memory effects

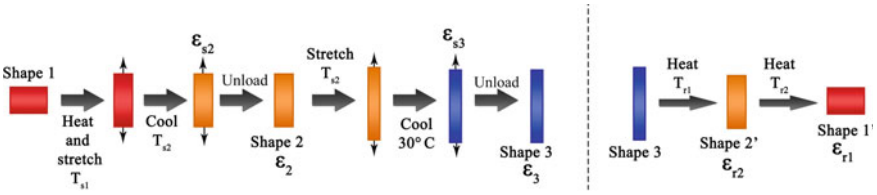

Fig. 8 Schematic of multi-shape-memory effect

2.2.3 Triple-Way Shape-Memory Effect SMP

Triple-way shape-memory polymers (3W-SMPs) can change forms twice and can fix two shapes compared to its permanent and initial shape. The 3W-SMPs comprise a cross-linking phase and two independent phases related to two different conversions which contain programming and recovery cycles. The programming stage of 3W-SMPs commences with heating the sample above both transitions and inducing distortion. Next, maintain the deformation while cooling the polymer to fix form at a temperature between the two conversions. Ware et al. reported a novel 3W-SM system contained both permanent covalent cross-links and supramolecular hydrogen bonding cross-links. The described effect comes into being from the connection of the glass transition of methacrylate copolymers and the dissociation of self-complementary hydrogen bonding moieties providing easy control of both glass transition temperature (T_g) and cross-link density [94]. Bellin et al. have shown the 3W-SM effect in systems containing two crystalline switching phases, while others have linked an amorphous phase with a crystalline switching phase [95]. Recently, Xie and cowork-

ers have shown quadruple shape-memory utilizing the broad transition of perfluorosulfonic acid ionomers [96]. The composites capable of being the 3W-SMPs stand to increase the complexity of appliances utilizing the shape-memory effect by enabling multistage complex recovery profiles were prepared [97, 98]. Recently, the 3W-SM epoxy composites consisting of two layers of well-separated glass transition temperatures have been successfully synthesized. The various amounts of nanosilica particles entered into the matrix are able to cause different glass transition temperatures of the epoxy composites [99–101]. The application of 3-aminopropyltriethoxysilane as a chemical modifier for graphene oxide into silanized polyurethanes gives two different molecular weights and chemical compositions by sol–gel reactions. The research has proven that the materials act as multifunctional cross-links as well as supporting fillers and significantly enhanced the glassy and rubbery state moduli, glass transition temperature, and 3W-SM properties [102].

2.2.4 Multi-Way Shape-Memory Effect SMP

In last time, it has been shown that polymers with a wide thermomechanical transition temperature range can have a multi-shape-memory effect what is related to a shape recovery process with one or more intermediate shapes between the temporary shape and permanent shape. Actually, such a condition for the multiple SME is not necessary, the use only one single transition to gain that as well. It is possible because one single transition should be considered as a combination of many small transition steps, so in fact, the multi-SME is a common property of polymers [95, 96, 103, 104].

Prathumrat and coworkers prepared benzoxazine–urethane copolymers with multiple shape-memory behaviors. These polymers exhibited great shape fixity values of 70–96% for the first temporary shape and 83–99% for the second temporary shape. Regarding shape recovery, synthesized copolymers also had significant values of 88%–96% for the first temporary shape and 97–99% for the original shape. What is important is that the proper curing conversion influences the multiple shape-memory behaviors of copolymers—curing conversion at roughly 70% was adequate for this sample to demonstrate a multi-shape-memory effect [105].

Poly(*l*-lactide) (PLLA)/poly(methyl methacrylate) (PMMA) blends with wide glass transitions are known as an optional matrix to design multiple shape-memory polymers. The temperature range of the symmetric 50% PLLA/50% PMMA blend softly moved from 70 to 90 °C for stretching temperatures increasing from 65 to 94 °C, and certify for a meaningful temperature memory effect. In the case of asymmetric compositions with 30 and 80% PMMA, polymer also presented a “temperature memory effect”; however, the symmetric blend greatly was revealed as the most effective composition for multiple shape-memory applications. The symmetric blend can be a really interesting material for future developments because its programming step designed with two successive stretchings within the wide glass transition provided high multi-shape-memory effect with tunable intermediate shapes [106].

2.3 *Classification of Shape-Memory Polymers by Type of Stimulus*

Shape-memory polymers (SMPs) as a type of significant stimuli-responsive materials can receive their original and initial shape upon exposure to external stimuli. The SMPs are stimuli-sensitive polymers with the ability to transmit a large recoverable deformation upon the application of external impulses. So far, known methods of stimulus can be generally divided into heat, electricity, light, magnetism, moisture, etc. Nowadays, SMPs are attracting increasing international research attention and there is huge progress in developing stimuli-responsive shape-memory polymers with potential applications in many fields such as biomedical devices, aerospace, textiles, bionics engineering, and energy, electronic engineering.

2.3.1 Stimulation by Temperature

The characteristic thermo-responsive SMPs are really universal, frequent, and occurring for polymers [32, 33, 107, 108, 109], in which vitrification or crystallization of polymer chains is adapted as a momentary cross-link to stabilize the change in the dimension of forms and the shape recovery is induced by heat [110]. Thermo-responsive SMPs can gain their original and initial figure and form when they are warmed above T_g for amorphous polymer and above T_m for crystalline polymers. The characteristic thermomechanical cycle of SMPs is illustrated in the following steps in Fig. 9 [60, 61, 111]. The whole process consists of formation of the SMPs into an original shape, and next stage should be heating the SMPs above the thermal transition temperature (T_{trans}) (depending on the type of polymer it is a glass transition temperature (T_g), or a melting temperature (T_m)), and change of shape of the SMPs using an external force and finally cooling under T_{trans}.

French CdF Chimie Company first developed polynorbornene with a T_g range of 35–40 °C what next was introduced to the industry by the Japan Nippon Zeon Company [13, 112]. Styrene-butadiene SMPs with T_g of about 60–90 °C were synthesized by the Asahi Company [113]. Furthermore, the Cornerstone Research Group (CRG), Inc. has expanded some thermosetting SMPs [114], which comprising a one-part epoxy SMP with a T_g of about 90 °C, a two-part epoxy SMP with a T_g

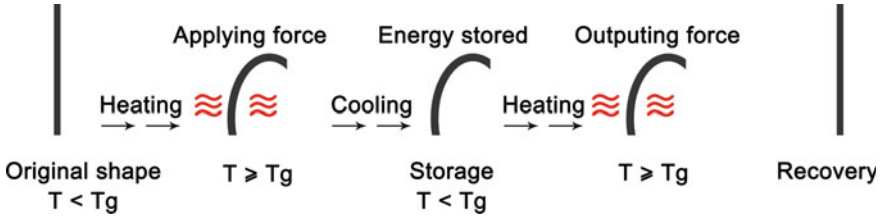

Fig. 9 Schematic of shape-memory effect during a typical thermomechanical cycle

of about 104 °C, and also a cyanate ester SMP with a high T_g range from 135 to 230 °C. Moreover, Composite Technology Development (CTD), Inc. has proceeded a thermosetting epoxy SMP with a T_g of about 113 °C. In addition, it is known that a series of thermoplastic polyurethane SMPs is commercially available from Mitsubishi Heavy Industry, with the T_g ranging from 40 to 55 °C. Lamm et al. prepared sustainable epoxy resins derived from plant oils with thermo- and chemo-responsive SM maintenance which were obtained using plant oils and cellulose nanocrystals (CNCs). Epoxidized soybean polymers (PESBMA) were grafted from CNCs using surface-initiated atom transfer radical polymerization (SI-ATRP) where the polymer was combined with P(ESBMA-co-SBMA) copolymer. P(ESBMA-co-SBMA) has a T_g of 13 °C, versus 20 °C for CNC-g-PESBMA [115]. Truong et al. [116] prepared thermo-responsive SM poly(ε-caprolactone) (PCL) networks with multiple pendant double chains at both link ends which are used to cross-link with multi-thiol compounds via photo-initiated thiol–ene reactions. SM features can be also changed through modification in the number of alkene side groups at the poly(ε-caprolactone) and thiol cross-linker structure. The developed thermoset materials exhibit great thermo-responsive shape-memory efficiency by changing the operating temperature below or above the melting temperature of crystalline poly(ε-caprolactone) segments, which changes in the range of 34–40 °C, and the highest shape retention and recovery factors can get 98–100% [117].

2.3.2 Stimulation by PH Changes

In this section, shape-memory material-stimulated pH change will be shown. The change of polymer properties occurs when in present ionizable functional groups' material gets ionized and obtains charge in certain pH. The shape-memory polymer chains between like-charged groups lead to repulsion force and from here widen their dimension and finally at the moment when the pH changed, the repulsion disappears and the materials come to the original shape and position. The reversibility and changes to this material can be treated as a disadvantage that comes into being with the use of pH-responsive materials because it commonly needs solvent replacement, which is not good for the environment. Despite these restrictions, pH-responsive polymers have shown promise in many areas such as drug delivery and microprocessing [82]. pH-sensitive SMPs were prepared by cross-linking the β-cyclodextrin-modified alginate (β-CD-Alg) and diethylenetriamine-modified alginate (DETA-Alg). The pH reversible β-CD-DETA inclusion complexes operate as a convertible phase, and the cross-linked alginate serves as a fixing phase. It is shown that this material can be processed into temporary shape at pH 11.5 and recover to its initial shape at pH 7. The recovery relation and the fixity ratio were accordingly $95.7 \pm 0.9\%$ and $94.8 \pm 1.1\%$ [118]. Han et al. proposed to use pH as a stimulus for SMPs for its convenience and safety in medical applications because the shape transition pH value is almost to that of our body fluid and this pH-triggered shape-memory effect is convenient and safe to use. It is also indicated a polyurethane with a pH-sensitive SM effect. First, a series of polyurethanes were

successfully synthesized through solution polymerization of polyethylene glycol, dimethylolpropionic acid (DMPA), and 4,4′-diphenylmethane diisocyanate (MDI). These polymers PEG-*i*-MDI-DMPA ($i = 20$, 30, 40%) and i represent the weight content of PEG in the polymers. The results of SM testing showed that the PEG-30%-MDI-DMPA has both the 3-SM effects. In PEG-30%-MDI-DMPA, the glass transition of PEG and the association and disassociation of carboxylic dimers act as two switches to control the 3-SM conversion, while the carboxylic dimer is affected by pH values to associate in acidic solutions (at pH 2) and dissociate in alkaline solutions (at pH 9) to induce the pH-sensitive shape-memory [119], which developed pH-responsive SMPs by blending poly(ethylene glycol)-poly(ε-caprolactone)-based polyurethane (PECU) with functionalized cellulose nanocrystals (CNCs). CNCs were functionalized with pyridine (CNC-$C_6H_4NO_2$) through hydroxyl substitution of CNCs with pyridine-4-carbonyl chloride and with carboxyl groups (CNC-CO_2H) via 2,2,6,6-tetramethyl-1-piperidinyloxy (TEMPO) conjunctived surface oxidation. At a high pH, the CNC–$C_6H_4NO_2$ had inviting interactions from the hydrogen bonding between pyridine groups and hydroxyl moieties at a low pH, the interplays reduced, or disappeared due to the protonation of pyridine groups, which are a Lewis base. The shape-memory function of the nanocomposite network was only dependent on the pH variation of the environment [99–101]. Xiao et al. reported novel multi-responsive polyacrylamide-(PAAm)-based cross-linked copolymer (PAAm-TSMP) hydrogel which is characterized by pH-sensitive and photo-sensitive at the same time. pH-sensitive of hydrogel is possible by adding active group in the structure (positively and negatively ionized). Polyacids and polybases are the only available groups because the first ones accept protons at low pH, producing gel shrinkage, while polybases donate protons at high pH (Fig. 10) [120].

2.3.3 Stimulation by Water/Solvent

Yang et al. discovered this particular effect. The glass transition temperature (equal to 35 °C) of an ether-based polyurethane shape-memory polymer (SMP) has been found to decrease significantly after immersion in water. The results reveal that the hydrogen bonding between N–H and CO groups is weakened by the absorbed water. Moreover, the H_2O absorbed into the SMP can be in two forms (free water and the bound water). Bound water notably reduces the T_g in a linear way and has an influence on the uniaxial tensile behavior, while the effect of free water is negligible [121]. Also, Du and coworkers studied recovery time of poly(vinyl alcohol) in different solvents, and the results presented that the best recovery time for water is immersed. This kind of stimulation of shape-memory polymers is very interesting because it does not need to apply heat to obtain shape-memory conversion [122]. Diffusion of water, acetone, and ethanol into a polyether urethane matrix has been studied by Ghobadi et al. It was revealed that even after 1 week, putting the samples in the corresponding solvent baths, neither enthalpy relaxation nor monomer release could occur because of the lack of hydrophilic groups. Dry and physically (hydrolytically) aged samples have been conducted to different maximum strains and different holding times. It could be

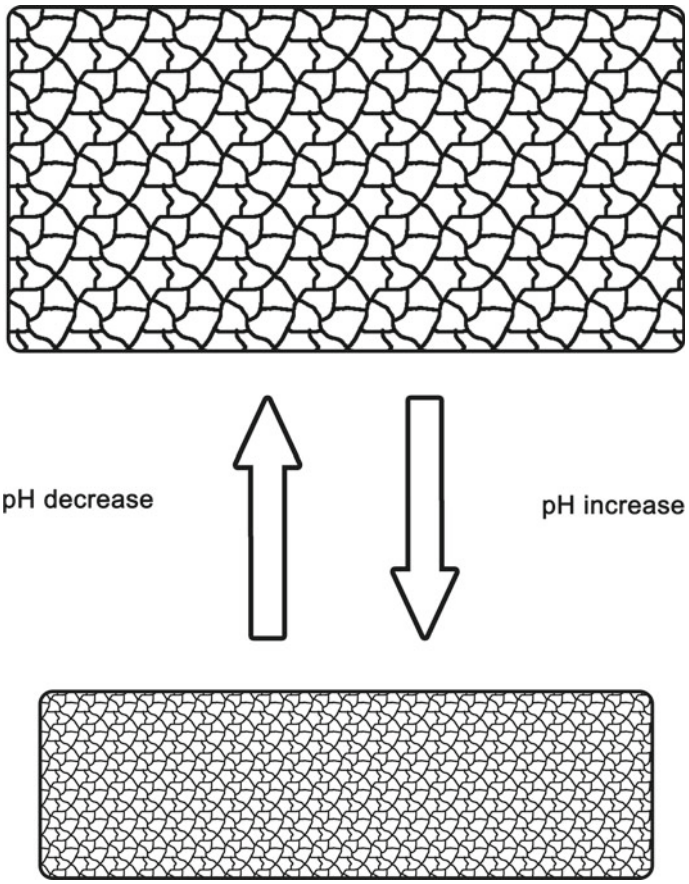

Fig. 10 Swelling and shrinkage properties in ionic-based hydrogel by change in pH

indicated that the shape fixation of physically (hydrolytically) aged polymers do not differ from dry samples. However, physical (hydrolytic) aging resulted in an obvious better and faster shape recovery ratio as a result of additional physical cross-links [123].

2.3.4 Stimulation by Magnetic Field

Magnetic field-sensitive polymer can be achieved by preparing nanocomposites loaded with specific magnetic nanoparticles. The magnetic nanofillers produce heat when they are subjected to magnetic field. The shape of nanocomposites is obtained in the same way as that in the thermally inducted one. Recovery of shape is fixed by the Joule effect at a time when the sample is exposed to exterior magnetic field.

Via magnetic fields can induce internal heating within SMP composites containing magnetic nanoparticles (Fe_2O_3, Fe_3O_4, Ni, etc.) [47, 79, 124] which are known as ferromagnetic shape-memory polymers. This type of composites can actuate at higher frequencies (up to 1 kHz) because the actuation energy is transmitted via magnetic fields and is not hindered by the relatively slow heat transfer mechanism [125]. Iron oxide (Fe_3O_4) particles are known as magnetic fillers which induce heating when exposed to a magnetic field. Incorporating them into an SMP is a known practice to fabricate a shape-memory composite for which the shape recovery can be actuated remotely via magnetic field. Leng et al. analyzed that the micro-sized Ni powder formed chains under a weak external magnetic field, which can strengthen significantly the electrical conductivity in the chain direction. Schmidt et al. and Zrinyi et al. added magnetite to poly(butyl acrylate), polylactide, and polycaprolactone matrixes [126–128]. For instance, Fuhrer and coworkers used magnetosensitive particles in shape-memory hydrogels [129]. One class of biodegradable polymer composite was elaborated with an electrospinning process using poly(ε-caprolactone) (c-PCL) as the basis and carbon nanotubes as the supplement coated with Fe_3O_4. The fibers showed an excellent SM behavior stimuli by hot water and by an alternating magnetic field [130].

2.3.5 Stimulation by Light

Light stimuli shape-memory polymer has meaningful advantage in comparison with the thermal stimuli shape-memory polymer which results from the fact that photoactivation does not produce tissue damage as could be produced by heat treatments. Thanks to this behavior, light activation is very attractive for biomedical application. Jiang et al. reported that there are three kinds of photoresponsive molecules [131]. The division created by them is as follows: molecules which have ability to change their configuration from *trans* to *cis* and contrariwise at the time when they are exposed to UV light, and molecules obtained by cationic inducted polymerization and photoresponsive molecules. The configuration capable of producing shape-memory effect with photo-reactive molecules is presented in Fig. 11. Black dots in Fig. 11 mean molecules which are the switch phase and the covalent bonds between polymer chains are the fixity phase. When the sample is in the presence of electromagnetic radiation $\lambda > \lambda_{trans}$, the photo-reactive molecules form dimers that are accountable to fix the temporary shape and dimension. At the moment when the shape-memory polymer is exposed to another radiation $\lambda < \lambda_{trans}$, it can recover its original shape (Fig. 12). Lu et al. developed a photoactive SMP by incorporating boron nitride and carbon nanotube, which reportedly have a synergistic effect, into an epoxy-based SMP. The use of these additives improves the thermal conductivity of the material and its infrared light absorption, while the transferred nitrides aided in the heat transfer to the SMP matrix, resulting in faster shape-memory recovery [132]. Inam and coworkers reported that infrared light can be used to produce indirect shape-memory polymer matrix with addition of carbon black or carbon nanotubes. These reinforced nanofillers increase the thermal conductivity of the polymer. The behavior of these

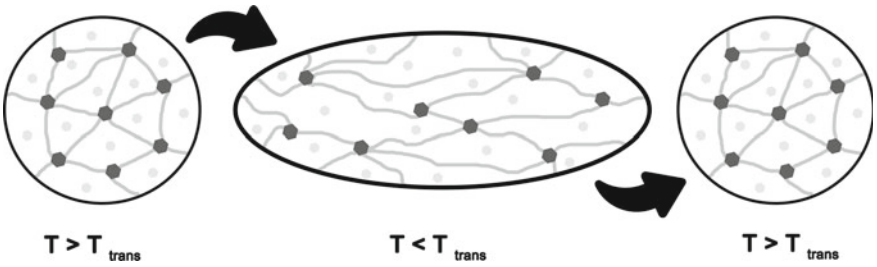

Fig. 11 Occurring processes in shape-memory polymer stimulated by magnetic field

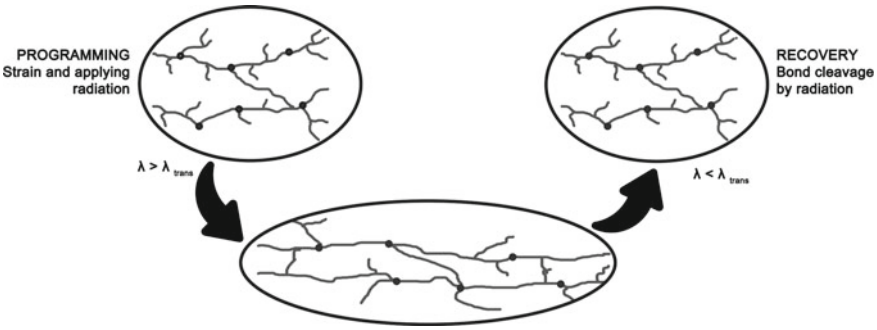

Fig. 12 Molecular mechanism of photoinduced shape-memory effect at various states

polymers is analogous to the thermal-induced shape-memory mechanism but the recovery appears when the polymer is irradiated with infrared light [133]. Shou et al. also developed near-infrared (near-IR) light-responsive SMPs by incorporating gold nanorods (AuNRs) into a poly(ε-caprolactone) matrix [134]. The second method, as reported by Lendlein et al., involves the introduction of cinnamic groups, which can be set in motion by ultraviolet light (UV). In research applied, two other configurations of cinnamic acid in polymer matrix permitted obtained SM network stimulated by light [135].

2.3.6 Stimulation by Oxidation/Reduction

SM effect in hydrogels is mostly stimulated with use of a redox reaction [136]. Aoki et al. prepared cellulose derivatives by esterification of cellulose acetate (CA) with mercaptoacetic acid (MA). The CA-MA samples thus synthesized showed a sol–gel transition in solution and a shape-memory behavior formed through adequate redox treatments due to the reversible, cross-linking association and dissociation between mercapto groups [137]. Studies showed that host (poly(acrylic acid) (pAA) modified with beta-cyclodextrins (pAA-β-CDs))—guest (ferrocene (pAA-Fc)) are complementarity and multipoint cross-links have cooperative roles in forming the

supramolecular polymer hydrogel. The reversible gel–sol transitions were achieved by adding an oxidant (NaClO aq.) and then a reductant (glutathione, GSH). What is more interesting is that the self-healing property of the hydrogel can be controlled by redox reactions. This study represents the first example of self-healing of supramolecular polymeric materials based on host–guest interactions and will further prompt the applications of host–guest recognition motifs in advanced supramolecular polymeric materials [138]. Moreover, redox-stimuli shape-memory matrix was obtained by cross-linking β-cyclodextrin-modified chitosan (β-CD-CS) and ferrocene-modified ethyleneimine polymer (Fc-PEI). The obtained β-CD-CS/Fc-PEI has two cross-links: convertible redox-sensitive β-CD-Fc complexes and covalent cross-links as fixing stages. The analyses showed that studied system can be processed into interim forms as needed in the reduced state and recovers its initial shape after oxidation reaction. In both cases, the recovery ratio and the fixity relation are more than 70% [139].

2.3.7 Multifunctionality

Multifunctionality is a set of material properties, which contains shape-memory effect and at least one other functionality (e.g., optical, permeable, thermal chromic, biodegradable) non-linked with SME [140]. Combining SME with phase-changing materials (PCM) can result in wrinkle-free textiles. Addition of active fillers like carbon black or carbon nanotubes to SMP will provide actuation through electric field [75, 76]. Similar actuation in magnetic field can be obtained with magnetically active fillers like iron oxide [79, 107]. Also, drug delivery systems made of SMP and drug are examples of multifunctionality. Radio-opacity of medical can be obtained via adding barium sulfate or zirconium oxide [141]. All types of modifications can provide attractive multifunctional SMP. The variety of multifunctional SMPs results from unique requirements, which are designed for certain applications.

3 Main Applications of SMP

Shape-memory polymers possess great functionality in shape-memory effect, and natural consequence is their wide range of possible applications. Most notable of them are in four fields: spacecraft, medical, textile, and engineering. Medical applications benefit from functions of SMP such as deployment, fixation, and actuation.

Deployment function plays an important role in SMP foams, which can be useful in treatment of aneurysms, especially embolic treatment [142]. Idea of SMP foam usage as device is still in the test phase, but delivery of compressed foam and its size increase after laser stimulation are still interesting solutions. Another application of deployment function in medicine is SMPs as cardiovascular stents [143]. They provide protection of small blood vessels from collapse, thanks to SME triggered by temperature change or polymer's hydration [144, 145]. On the other hand, intracranial

aneurysms can be treated with special SMP coils as blood flow reducers, which are able to help in formation of thrombus [146].

Fixation function of SMPs is useful in SMPU-PCL orthodontic wires, which are competitive alternative for traditional, metallic wires [147]. Their main advantage is better aesthetic appearance in comparison with metallic ones. SMP wires also provide low density, transparency, easy processing and, of course, high shape recovery. Another application, which benefits from fixation function of SMPs, is medical casts. Rousseau et al. proposed SMP medical cast with adjustable diameter and ability to fit the shape to broken limbs. These casts also provide easy and low-cost processing, recyclability, permeability, and lightweight [148]. Actuation function is usually related to artificial muscles, which in case of SMPs can be used in endovascular thrombectomy. Takashima and coworkers [149] obtained nitinol-core/SMP-shell artificial muscle with preprogrammed and thermally activated corkscrew form. This kind of micro-actuator can be very promising for clot and thrombus removal. SMPs with actuation function are versatile solutions, similarly attractive for spacecraft and engineering fields. Harris et al. reported liquid crystal elastomers (LCE) with shape-memory effect allowing to obtain mechanical energy from light energy [150]. These SMP actuator devices are obtained from azobenzene units in twisted and densely cross-linked structure, which results in high elastic modulus ($\approx$1 GPa) at room temperature. Other possible applications attractive for spacecraft and other engineering fields are systems like micro-valves and micro-transducers [151, 152] which are microelectromechanical systems (MEMS) providing temperature-adjustable flow through the tube. Also, stimuli-responsive SMPs can be suitable in applications such as antennas in spacecraft, morphing wing structures, or wrinkle-free fabrics [153].

Self-healing is another SMPs function, which can be widely applicable. Self-healing mechanism of SMPs can be based on reverse plasticity [154] or combination of different shape-memory effects in two-component blends called SMASH (shape-memory assisted self-healing) [155].

Group of SMPs dedicated for textile industry is based on special fibers—shape-memory fibers (SMFs). The SMFs can be obtained via different spinning methods (melt, dry, and wet) and their uniqueness results from outstanding temperature-response performance in their elastic modulus and recovery parameters [51, 52]. These properties allow to use SMFs in many textile applications, which are presented in Fig. 13.

4 Conclusion

Shape-memory polymers are one of the most intensively developing areas of materials science and technology providing excellent opportunities for scientific discoveries in the field of molecular design, polymer synthesis, functionalization and processing of polymer blends, copolymers, composites, and nanocomposites. The properties of SMPs, such as easy processing, large recoverable strains, tunability, low weight, different types of external switching stimulus, easy to control a wide range of transi-

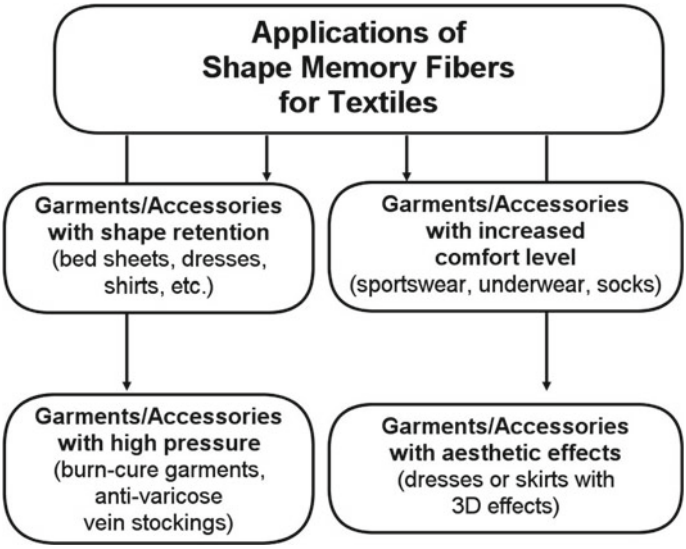

Fig. 13 Classification of shape-memory fibers' applications with examples

tion temperatures, switching at body temperature, biocompatibility, and biodegradability, makes them superior in comparison to shape-memory alloys. Due to these excellent properties and the low-cost and commercial availability of most of the polymers used as shape-memory materials, the applications of SMPs will increase in near future, within the numerous, new fields, like, for example, biomedical smart materials, advanced mechanical sectors, mechatronic, and power generation. However, great research efforts are still required to obtain SMPs with precisely controlled response and better durability and reliability over those offered by currently available technologies. In order to increase the versatility of SMPs, it is necessary to solve the major drawbacks of SMPs, which are associated with their relatively lower recovery stress/forces, long response time, lower cycle life, and weak material stability.

In this chapter, the literature reports on shape-memory polymers have been reviewed highlighting the classification of shape-memory polymeric materials and most important concepts for these types of smart materials. The main emphasis was put on the development of many types of SMPs categorized by the different classification criteria, with particular regard to polymer type and structure, shape-memory function, and external stimulus.

References

1. Behl M, Lendlein A (2007) Shape-memory polymers. Mater Today 10(4):20–28
2. Hornbogen E (2006) Comparison of shape memory metals and polymers. Adv Eng Mat 14:101–106
3. Hager MD, Bode S, Weber C, Schubert US (2015) Shape memory polymers: past, present and future developments. Prog Polym Sci 45–50:3–33
4. Lester B, Vernon B, Vernon HM (1941) Process of manufacturing articles of thermoplastic synthetic resins. US 2234993
5. Safranski DL, Griffis JC (2017) Shape-memory polymer device design. Elsevier, Oxford
6. Rainer WC, Redding EM, Hitov JJ, Sloan AW, Steward WD (1964) Heat-shrinkable polyethylene. US 3144398
7. Pilate F, Toncheva A, Dubois P, Raquez J-M (2016) Shape-memory polymers for multiple applications in the material world. Europ Polym J 80:268–294
8. Hu J, Zhu Y, Huang H, Lu J (2012) Recent advances in shape-memory polymers: Structure, mechanism, functionality, modeling and applications. Prog Polym Sci 37:1720–1763
9. Liu C, Qin H, Mather PT (2007) Review of progress in shape-memory polymers. J Mat Chem 17:1543–1558
10. Leng J, Lan X, Liu Y, Du S (2011) Shape-memory polymers and their composites: Stimulus methods and applications. Prog Mater Sci 56:1077–1135
11. Aguilar MR, Roman JS (2014) Smart polymers and their applications. Woodhead Publishing, Cambridge
12. Lee SH, Kim JW, Kim BK (2004) Shape memory polyurethanes having crosslinks in soft and hard segments. Smart Mater Struc 13:1345–1350
13. Leng JS, Du SY (2010) Shape memory polymer and multifunctional composite. CRC Press, Taylor & Francis Group, New York
14. Naga N, Tsuchiya Toyata A (2006) Synthesis and properties of polyethylene and polypropylene containing hydroxylated cyclic units in the main chain. Polymer 47:520–526
15. Kelch S, Steuer S, Schmidt AM, Lendlein A (2007) Shape-memory polymer networks from oligo[(epsilon-hydroxycaproate)-co-glycolate]dimethacrylates and butyl acrylate with adjustable hydrolytic degradation rate. Biomacromol 8:1018–1027
16. Meng Q, Hu J (2009) A review of shape memory polymer composites and blends. Composites:Part A 40:1661–1672
17. Ratna D, Karger-Kocsis (2008) Recent advances in shape memory polymers and composites:a review. J Mater Sci 43:254–269
18. Sakurai K, Shirakawa Y, Kashiwagi T, Takahashi T (1994) Crystal transformation of styrene–butadiene block-copolymer. Polymer 35:4238–4239
19. Lui C, Mather PT (2002) Thermomechanical characterization of a tailored series of shape memory polymers. J Appl Med Polym 6:47–52
20. Liu G, Ding X, Cao Y, Zheng Z, Peng Y (2005) Novel shape-memory polymer with two transition temperatures. Macromol Rapid Commun 26(8):649–652
21. Chen SJ, Hu JL, Liu YQ, Liem HM, Zhu Y, Meng QH (2007) Effect of molecular weight on shape memory behavior in polyurethane films. Polym Int 56:1128–1134
22. Hu J, Yang Z, Yeung L, Ji F, Liu Y (2005) Dependency of the shape memory properties of a polyurethane upon thermomechanical cyclic conditions. Polym Int 54:600–605
23. Zouohong Y, Jinlian H, Yeqiu L, Lapyan Y (2006) The study of crosslinked shape memory polyurethanes. Mater Chem Phys 98:368–372
24. Buckley CP, Prisacariu C, Caraculacu A (2007) Novel triol-crosslinked polyurethanes and their thermorheological characterization as shape-memory materials. Polymer 48:1388–1396
25. Xu J, Shi W, Pang W (2006) Synthesis and shape memory effects of Si–O–Si cross-linked hybrid polyurethanes. Polymer 47:457–465
26. Leng JS, Wu XL, Liu YJ (2009) Effect of linear monomer on thermomechanical properties of epoxy shape-memory polymer. Smart Mater Struct 18(095031):1–6

27. Chang YW, Mishra JK, Cheong JH, Kim DK (2007) Thermomechanical properties and shape memory effect of epoxidized natural rubber crosslinked by 3-amino-1,2,4-triazole. Polym Int 56:694–698
28. Zhang SF, Feng YK, Zhang L, Sun JF, Xu XK, Xu YS (2007) Novel interpenetrating networks with shape-memory properties. J Polym Sci Part A Polym Chem 45:768–775
29. Li F, Zhu W, Zhang X, Zhao C, Xu M (1999) Shape memory effect of ethylene–vinyl acetate copolymers. J Appl Polym Sci 71:1063–1070
30. Helminen AO, Korhonen H, Seppala JV (2002) Cross-linked poly(epsiloncaprolactone/D, L-lactide) copolymers with elastic properties. Macromol Chem Phys 203:2630–2639
31. Morshedian J, Khonakdar HA, Mehrabzadeh M, Eslami H (2003) Preparation and properties of heat-shrinkable cross-linked low-density polyethylene. Adv in Polym Tech 22:112–119
32. Liu C, Chun S, Mather P, Zheng L, Haley E, Coughlin B (2002) Chemically cross-linked polycyclooctene: synthesis, characterization, and shape memory behavior. Macromol 35:9868–9874
33. Liu C, Chun SB, Mather PT, Zheng L, Haley EH, Coughlin EB (2002) Chemically cross-linked polycyclooctene: synthesis, characterization, and shape memory behavior. Macromol 35:9868–9874
34. Zhu G, Liang G, Xu Q, Yu Q (2003) Shape-memory effects of radiation crosslinked poly(epsilon-caprolactone). J Appl Polym Sci 90:1589–1595
35. Knight PT, Lee KM, Chung T, Mather PT (2009) PLGA-POSS end-linked networks with tailored degradation and shape memory behavior. Macromol 42:6596–6605
36. Schoener CA, Weyand CB, Murthy R, Grunlan MA (2010) Shape memory polymers with silicon-containing segments. J Mater Chem 20:1787–1793
37. Wischke C, Lendlein A (2010) Shape-memory polymers as drug carriers - a multifunctional system. Pharma Research 27:527–529
38. Kalita H (2018) Shape memory polymers. De Gruyter, Berlin
39. Cao Q, Liu PS (2006) Structure and mechanical properties of shape memory polyurethane based on hyperbranched polyesters. Polymer Bull 57:889–899
40. Nagahama K, Ueda Y, Ouchi T, Ohya Y (2009) Biodegradable shape-memory polymers exhibiting sharp thermal transitions and controlled drug release. Biomacromol 10:1789–1794
41. Wang WS, Ping P, Chen X, Jing X (2006) Polylactide-based polyurethane and its shape-memory behavior. Eur Polymer J 42:1240–1249
42. Xue LA, Dai SY, Li Z (2010) Biodegradable shape-memory block co-polymers for fast self-expandable stents. Biomaterials 31:8132–8140
43. Lendlein A, Zotzmann J, Feng Y, Altheld A, Kelch S (2009) Controlling the switching temperature of biodegradable, amorphous, shape-memory poly(rac-lactide)urethane networks by incorporation of different comonomers. Biomacromol 10:975–982
44. Meng QH, Hu J, Ho KC, Ji F, Chen S (2009) The shape memory properties of biodegradable chitosan/poly(l-lactide) composites. J Poly and Envi 17:212–224
45. Min CC, Cui W, Bei J, Wang S (2005) Biodegradable shape-memory polymer polylactide-co-poly(glycolide-co-caprolactone) multiblock copolymer. Polym for Advan Tech 16:608–615
46. Lu XL, Sun ZJ, Cai W, Gao ZY (2008) Study on the shape memory effects of poly(L-lactide-co-epsilon-caprolactone) biodegradable polymers. J Mat Sci Mat Med 19:395–399
47. Luo XL, Zhao MC, Wang MZ, Ding LN, Ma DZ (2000) Thermally stimulated shape memory behavior of (ethylene oxide-butylene terephthalate) segmented copolymer. Chin J Polym Sci 18:357–361
48. Xu M, Li F (1999) Thermally stimulated shape memory behavior of polymers with physical crosslinks. Chin J Polym Sci 17:203–213
49. Lendlein A, Kelch S, Kratz K (2006) Kunststoffe mit programmiertem Gedächtnis. Kunstoffe 2:54–59
50. Jeong HM, Kim BK, Choi YJ (2000) Synthesis and properties of thermotropic liquid crystalline polyurethane elastomers. Polymer 41:1849–1855
51. Zhu Y, Hu JL, Yeung KW, Liu YQ, Lien HM (2006) Influence of ionic groups on the crystallization and melting behavior of segmented polyurethane ionomers. J Appl Polym Sci 100:4603–4613

52. Zhu Y, Hu JL, Yeung LY, Liu Y, Ji FL, Yeung KW (2006) Development of shape memory polyurethane fiber with complete shape recoverability. Smart Mater Struct 15:1385–1394
53. Li Y, Hu ZB, Chen YY (1997) Shape memory gels made by the modulated gel technology. J Appl Polym Sci 63(9):1173–1178
54. Lu XL, Cai W, Gao Z, Tang WJ (2007) Shape memory effects of poly(Llactide) and its copolymer with poly(epsilon-caprolactone). Polym Bull 58(2):381–391
55. Wong YS, Venkatraman SS (2010) Recovery as a measure of oriented crystalline structure in poly(L-lactide) used as shape memory polymer. Acta Mater 58(1):49–58
56. Behl M, Bellin I, Kelch S, Wagermaier W, Lendlein A (2009) One-step process for creating triple-shape capability of AB polymer networks. Adv Funct Mat 19(1):102–108
57. Jeong HM, Song JH (2001) Miscibility and shape memory property of poly(vinyl chloride)/thermoplastic polyurethane blends. J Mater Sci 36(22):5457–5463
58. Jeong HM, Ahn BK, Kim BK (2001) Miscibility and shape memory effect of thermoplastic polyurethane blends with phenoxy resin. Eur Polym J 37(11):2245–2252
59. Zhang H, Wang H, Zhong W, Du Q (2009) A novel type of shape memory polymer blend and the shape memory mechanism. Polymer 50(6):1596–1601
60. Liu GQ, Guan CL, Xia H, Guo F, Ding X, Peng Y (2006) Novel shape-memory polymer based on hydrogen bonding. Macromol Rapid Comm 27(14):1100–1104
61. Liu YP, Gall K, Dunn ML, Greenberg AR, Diani J (2006) Thermomechanics of shape memory polymers: uniaxial experiments and constitutive modeling. Int J Plast 22:279–313
62. Hu J (2014) Shape memory polymers: fundamentals, advances and applications. Smithers Rapra, Shawbury
63. Li J, Viveros JA, Wrue MH, Anthamatten M (2007) Shape memory effects in polymer networks containing reversibly associating side-groups. Adv Mater 19(19):2851–2855
64. Zhu Y, Hu J, Liu Y (2009) Shape memory effect of thermoplastic segmented polyurethanes with self-complementary quadruple hydrogen bonding in soft segments. Eur Phys J E 28(1):3–10
65. Zhang S, Yu Z, Govender T, Luo H, Li B (2008) A novel supramolecular shape memory material based on partial α-CD–PEG inclusion complex. Polymer 49(15):3205–3210
66. Liu G, Ding X, Cao Y, Zheng Z, Peng Y (2004) Shape memory of hydrogen-bonded polymer network/poly (ethylene glycol) complexes. Macromol 37(6):2228–2232
67. Osada Y, Matsuda A (1995) Shape memory in hydrogels. Nat 376:219–220
68. Kagami Y, Gong JP, Osada Y (1996) Shape memory behaviors of crosslinked copolymers containing stearyl acrylate. Macromol Rapid Comm 17(8):539–543
69. Hirai T, Matuyama H, Suzuki T, Hayashi S (1992) Effect of chemical crosslinking under elongation on shape restoring of poly(vinyl alcohol) hydrogel. J Appl Polym Sci 46(8):1449–1451
70. Hirai T, Matuyama H, Suzuki T, Hayashi S (1992) Shape memorizing properties of a hydrogel of poly(vinyl alcohol). J Appl Polym Sci 45(10):1849–1855
71. Meng H, Li G (2013) A review of stimuli-responsive shape memory polymer composites. Polymer 54:2199–2221
72. Zheng XT, Zhou S, Yu X, Li X, Feng B, Qu S, Weng J (2008) Effect of in vitro degradation of poly(D, L-lactide)/beta-tricalcium composite on its shape memory properties. J Biomed Mater Res B 86B(1):170–180
73. Zhou SB, Zheng X, Yu X, Wang J, Weng J, Li X, Feng B, Yin M (2007) Hydrogen bonding interaction of poly(D, L-lactide)/hydroxyapatite nanocomposites. Chem Mater 19(2):247–253
74. Ni QQ, Zhang CS, Fu Y, Dai G, Kimura T (2007) Shape memory effect and mechanical properties of carbon nanotube/shape memory polymer nanocomposites. Compos Struct 81:176–184
75. Cho JW, Kim JW, Jung YC, Goo NS (2005) Electroactive shape-memory polyurethane composites incorporating Carbon Nanotubes. Macromol Rapid Commun 26:412–416
76. Cho JW, Kim JW, Jung YC, Goo NS (2005) Electroactive shape-memory polyurethane composites incorporating carbon nanotubes. Macromol Rapid Comm 26:412–416
77. Sahoo NG, Jung YC, Goo NS, Cho JW (2005) Conducting shape memory polyurethane-polypyrrole composites for an electroactive actuator. Macromol Mater Eng 290:1049–1055

78. Koerner H, Price G, Pearce NA, Alexander M, Vaia R (2004) Remotely actuated polymer nanocomposites - stress-recovery of carbon-nanotube-filled thermoplastic elastomers. Nature Mater 3:115–120
79. Mohr R, Kratz K, Weigel T, Lucka-Gabor M, Moneke M, Lendlein A (2006) Initiation of shape-memory effect by inductive heating of magnetic nanoparticles in thermoplastic polymers. Proc Natl Acad Sci 103:3540–3545
80. Bilici C, Can V, Nöchel U, Behl M, Lendlein A, Okay O (2016) Melt-processable shape-memory hydrogels with self-healing ability of high mechanical strength. Macromol 49(19):7442–7449
81. Lee YM, Kim SH, Cho CS (1996) Synthesis and swelling characteristics of pH and thermoresponsive interpenetrating polymer network hydrogel composed of poly(vinyl alcohol) and poly(acrylic acid). J Appl Polym Sci 62:301–311
82. Chung T, Romo-Uribe A, Mather PT (2008) Two-way reversible shape memory in a semicrystalline network. Macromol 41:184–192
83. Huang W, Toh W (2000) Training two-way shape memory alloy by reheat treatment. J Mater Sci Lett 19:1549–1550
84. Liu Y, Liu Y, Humbeeck JV (1999) Two-way shape memory effect developed by martensite deformation in NiTi. Acta Mater 47(1):199–209
85. Tokuda M, Sugino S, Inaba T (2001) Two-way shape memory behavior obtained by combined loading training. J Intell Mater Syst Struct 12:289–292
86. Ahir SV, Tajbakhsh AR, Terentjev EM (2006) Self-assembled shape-memory fibers of triblock liquid-crystal polymers. Adv Funct Mater 16:556–560
87. Li MH, Keller P, Li B, Wang X, Brunet M (2003) Light-driven side on nematic elastomer actuators. Adv Mater 15:569–572
88. Naciri J, Srinivasan A, Jeon H, Nikolov N, Keller P, Ratna BR (2003) Nematic elastomer fiber actuator. Macromol 36(2003):8499–8505
89. Yu Y, Nakano M, Ikeda T (2003) Photomechanics: directed bending of a polymer film by light. Nat 425:145–145
90. Hu Z, Zhang X, Li Y (1995) Synthesis and application of modulated polymer gels. Science 269:525–526
91. Wang K, Jia YG, ZhuXX (2017) Two-way reversible shape memory polymers made of crosslinked cocrystallizable random copolymers with tunable actuation temperatures. Macromol 50(21):8570–8579
92. Westbrook K, Mather PT, Parakh V, Dunn ML, Ge Q, Lee BM, Qi HJ (2011) Two-way reversible shape memory effects in a free-standing polymer composite. Smart Mat and Struct 20(6):1–9
93. Chen SJ, Hu JL, Zhuo H, Zhu Y (2008) Two-way shape memory effect in polymer laminates. Mat Let 62:4088–4090
94. Ware T, Hearon K, Lonnecker A, Wooley KL, Maitland DJ, Voit W (2012) Triple-shape memory polymers based on self-complementary hydrogen bonding. Macromol 45(2):1062–1069
95. Bellin I, Kelch S, Langer R, Lendlein A (2006) Polymeric triple-shape materials. Proc Natl Acad Sci USA 103(48):18043–18047
96. Xie T (2010) Tunable polymer multi-shape memory effect. Nat 464(7286):267–270
97. Luo X, Mather P (2010) Conductive shape memory nanocomposites for high speed electrical actuation. Soft Matter 6:2146–2149
98. Luo X, Mather PT (2010) Triple-Shape Polymeric Composites (TSPCs). Adv Funct Mater 20(16):2649–2656
99. Li G, Zhang H, Fortin D, Xia H, Zhao Y (2015) Poly(vinyl alcohol)-poly(ethylene glycol) double-network hydrogel: a general approach to shape memory and self-healing functionalities. Langmuir 27,31(42):11709–11716
100. Li Y, Chen H, Liu D, Wang W, Liu Y, Zhou S (2015) pH-responsive shape memory poly(ethylene glycol)-poly(ε-caprolactone)-based polyurethane/cellulose nanocrystals nanocomposite. ACS Appl Mater Interfaces 17:7(23):12988-12999

101. Li Xixi, Zhu Yaofeng, Dong Yubing, Liu Meng, Ni Qingqing, Yaqin Fu (2015) Epoxy resin composite bilayers with triple-shape memory effect. J Nanomat 475316:1–8
102. Kim YJ, Park HC, Kim BK (2015) Triple shape-memory effect by silanized polyurethane/silane-functionalized graphene oxide nanocomposites bilayer. High Perform Polym 27(7):886–897
103. Behl M, Ridder U, Feng Y, Kelch S, Lendlein A (2009) Shape-memory capability of binary multiblock copolymer blends with hard and switching domains provided by different components. Soft Matter 5(3):676–684
104. Sun L, Huang WM (2010) Mechanisms of the multi-shape memory effect and temperature memory effect in shape memory polymers. Soft Matter 6(18):4403–4406
105. Prathumrat P, Tiptipakorn S, Rimdusit S (2017) Multiple-shape memory polymers from benzoxazine–urethane copolymers. Smart Mater Struct 26(9):1–9
106. Samuel C, Barrau S, Lefebvre JM, Raquez JM, Dubois P (2014) Designing multiple-shape memory polymers with miscible polymer blends: evidence and origins of a triple-shape memory effect for miscible PLLA/PMMA blends.Macromol 47(19):6791–6803
107. Buckley PR, McKinley GH, Wilson T, Small W, Benett J, McElfresh M, Maitland D (2006) Inductively heated shape memory polymer for the magnetic actuation of medical devices. IEEE Trans Biomed Eng 53(10):2075–2083
108. Tobushi H, Hashimoto T, Hayashi S, Yamada E (1997) Thermomechanical constitutive modeling in shape memory polymer of polyurethane series. J Intell Mater Syst Struct 8:711–718
109. Tobushi H, Okumura K, Hayashi S, Ito N (2001) Thermomechanical constitutive model of shape memory polymer. Mech Mater 33(10):545–554
110. Lu W, Le X, Zhang J, Huang Y, Chen T (2017) Supramolecular shape memory hydrogels: a new bridge between stimuli-responsive polymers and supramolecular chemistry. Chem Soc Rev 46:1284–1294
111. Lan X, Wang XH, Liu YJ, Leng JS (2009) Fiber reinforced shape-memory polymer composite, its application in a deployable hinge. Smart Mater Struct 8(024002):1–6
112. Liang C, Rogers CA, Malafeew E (1997) Investigation of shape memory polymers and their hybrid composites. J Intell Mater Syst Struct 8:380–386
113. Wei ZG, Sandstroum R, Miyazaki S (1998) Shape memory materials and hybrid composites for smart systems: part II shape memory hybrid composites. J Mater Sci 33(15):3763–3783
114. Simkevitz S, Naguib HE (2008) Development of two part porous shape memory polymer nanocomposites. Proceedings of the ASME Conference on Smart Materials, Adaptive Structures and Intelligent Systems, SMASIS2008 1:453–460
115. Lamm M, Wang Z, Zhou J, Yuan L, Zhang X, Tang C (2018) Sustainable epoxy resins derived from plant oils with thermo- and chemo-responsive shape memory behavior. Polymer 111:121–127
116. Truong TT, Thai SH, Nguyen HT (2018) Poly(ε-caprolactone) networks with tunable thermoresponsive shape memory via a facile photo-initiated thiol–ene pathway. J Mater Sci 53:2236–2252
117. Kalita H, Karak N (2014) Biobased hyperbranched shape-memory polyurethanes: effect of different vegetable oils. J Appl Polym 131:1–8
118. Han XJ, Dong ZQ, Fan MM, Liu Y, li JH, Wang YF, Yuan QJ, Li BJ, Zhang S (2012) pH-induced shape-memory polymers. Macromol Rapid Commun 27:33(12):1055–1060
119. Song Q, Chen H, Zhou S, Zhao K, Wang B, Hu P (2016) Thermo- and pH-sensitive shape memory polyurethane containing carboxyl groups. Polym Chem 7:1739–1746
120. Xiao Y, Gong X, Kang Y, Jiang Z, Zhang S, Li B (2016) Light-, pH- and thermal-responsive hydrogels with the triple-shape memory effect. Chem Commun 52:10609–10612
121. Yang B, Huang W, Li C, Li L (2006) Effects of moisture on the thermomechanical properties of a polyurethane shape memory polymer. Polymer 47(4):1348–1356
122. Du H, Zhang J (2010) Shape memory polymer based on chemically cross-linked poly(vinyl alcohol) containing a small number of water molecules. J Colloid Polym Sci 288:15–24
123. Ghobadi E, Marquardt A, Zirdehi E, Neuking K, Varnik F, Eggeler G, Steeb H (2018) The influence of water and solvent uptake on functional properties of shape-memory polymers. Inter J Poly Sci 7819353:15–30

124. Leng JS, Lv H, Liu Y, Du SY (2007) Electroactivate shape-memory polymer filled with nanocarbon particles and short carbon fibers. Appl Phys Lett 91(144105):1–3
125. Leng J, Lan X, Liu Y, Du S, Huang W, Liu N, Phee S, Yuan Q (2008) Electrical conductivity of thermoresponsive shape-memory polymer with embedded micron sized Ni powder chains. Appl Phys Lett 92(014104):1–2
126. Schmidt AM (2006) Electromagnetic activation of shape memory polymer networks containing magnetic nanoparticles. Macromol Rapid Commun 27:1168–1172
127. Schmidt AM (2006) Electromagnetic activation of shape memory polymer networks containing magnetic nanoparticles. Macromol Rapid Commun 27(14):1168–1172
128. Zrínyi M (2000) Intelligent polymer gels controlled by magnetic fields. Colloid Polym Sci 278(2):98–103
129. Fuhrer R, Athanassiou EK, Luechinger NA, Stark WJ (2009) Crosslinking metal nanoparticles into the polymer backbone of hydrogels enables preparation of soft, magnetic field-driven actuators with muscle-like flexibility. Small 5(3):383–388
130. Gong T, Li W, Chen H, Wang L, Shao S, Zhou S (2012) Remotely actuated shape memory effect of electrospun composite nanofibers. Acta Biomater 8(3):1248–1259
131. Jiang H, Kelch S, Lendlein A (2006) Polymers move in response to light. Ad Mat 18(11):1471–1475
132. Lu H, Yao Y, Huang WM, Leng J, Hui D (2014) Significantly improving infrared light-induced shape recovery behavior of shape memory polymeric nanocomposite via a synergistic effect of carbon nanotube and boron nitride. Compos Part B 62:256–261
133. Inam F, Wong D, Kuwata M, Peijs T (2010) Multiscale hybrid micro-nanocomposites based on carbon nanotubes and carbon fibers. J of Nanomat 453420:12–24
134. Shou Q, Uto K, Iwanaga M, Ebara M, Aoyagi T (2014) Nearinfrared light-responsive shape-memory poly([epsiv]-caprolactone) films that actuate in physiological temperature range. Polym J 46(8):492–498
135. Lendlein A, Jiang H, Junger O, Langer R (2005) Light-induced shape-memory polymers. Nat 434(7035):879–882
136. Miyamae K, Nakahata M, Takashima Y, Harada A (2015) Self-healing, expansion − contraction, and shape memory properties of a preorganized supramolecular hydrogel through host guest interactions. Angew Chem 127(31):9112–9115
137. Aoki D, Teramoto Y, Nishio Y (2007) SH-containing cellulose acetate derivatives: preparation and characterization as a shape memory-recovery material. Biomacromol 8(12):3749–3757
138. Xuzhou Y, Feng W, Bo Z, Feihe H (2012) Stimuli-responsive supramolecular polymeric materials. Chem Soc Rev 41:6042–6065
139. Dong Z, Cao Y, Yuan Q, Wang Y, Li J, Li B, Zhang S (2013) Redox and glucose induced shape memory polymers. Macromol Rapid Comm 34(10):867–872
140. Behl M, Razzaq MY, Lendlein A (2010) Multifunctional shape-memory polymers. Adv Mater 22(31):3388–3410
141. Kruft MAB, Benzina A, Blezer R, Koole LH (1996) Studies on radio-opaque polymeric biomaterials with potential applications to endovascular prostheses. Biomat 17:1803–1812
142. Small W, Buckley PR, Wilson TS, Benett WJ, Hartman J, Saloner D, Maitland DJ (2007) Shape memory polymer stent with expandable foam: a new concept for endovascular embolization of fusiform aneurysms. IEEE T Bio-Med Eng 54(6):1157–1160
143. Yakacki CM, Shandas R, Lanning C, Rech B, Eckstein A, Gall K (2007) Unconstrained recovery characterization of shape-memory polymer networks for cardiovascular applications. Biomat 28(14):2255–2263
144. Baer GM, Wilson TS, Small W, Hartman J, Benett WJ, Matthews DL, Maitland DJ (2009) Thermomechanical properties, collapse pressure, and expansion of shape memory polymer neurovascular stent prototypes. J Biomed Mater Res B Appl Biomater 90(1):421–429
145. Wache HM, Tartakowska DJ, Hentrich A, Wagner MH (2003) Development of a polymer stent with shape memory effect as a drug delivery system. J Mater Sci-Mater Med 14(2):109–112
146. Hampikian JM, Heaton BC, Tong FC, Zhang ZQ, Wong CP (2006) Mat Sci Eng C Mater 26(8):1373–1379

147. Jung YC, Cho JW (2010) Application of shape memory polyurethane in orthodontic. J Mater Sci Mater Med 21(10):2881–2886
148. Rousseau LA, Berger E, Owens J, Kia H (2012) Shape memory polymer medical cast. US 8100843B2
149. Takashima K, Rossiter J, Mukai T (2010) McKibben artificial muscle using shape-memory polymer. Sensor Actuat A-Phys 164(1–2):116–124
150. Harris KD, Cuypers R, Scheibe P, van Oosten CL, Bastiaansen CWM, Lub J, Broer DJ (2005) Large amplitude light-induced motion in high elastic modulus polymer actuators. J Mater Chem 15(47):5043–5048
151. Gall K, Dunn ML, Liu Y, Finch D, Lake M, Munshi NA (2002) Shape memory polymer nanocomposites. Acta Mater 50(20):5115–5126
152. Gall K, Kreiner P, Turner D, Hulse M (2004) Shape-memory polymers for microelectromechanical systems. J Microelectromech S 13(3):472–483
153. Serrano MC, Ameer GA (2012) Recent insights into the biomedical applications of shape-memory polymers. Macromol Biosci 12(9):1156–1171
154. Xiao XC, Xie T, Cheng YT (2010) Self-healable graphene polymer composites. J Mater Chem 20(17):3508–3514
155. Rodriguez ED, Luo XF, Mather PT (2011) Linear/network poly(ε-caprolactone) blends exhibiting shape memory assisted self-healing (SMASH). ACS Appl Mater Inter 3(2):152–161

Novel Techniques for the Preparation of Shape-Memory Polymers, Polymer Blends and Composites at Micro and Nanoscales

Xiao-dong Qi and Yong Wang

Abstract Shape-memory polymers (SMPs) are one type of smart materials that are capable to recover from a "fixed" temporary shape to a "memorized" original shape under external stimulus. This chapter provides a comprehensive overview about the preparation methods of shape-memory polymers, polymer blends, and composites. Following a brief introduction of SMPs, the strategies for the preparation of conventional SMPs such as chemical cross-linking of thermoplastic polymers, single-step polymerization of monomers/prepolymers with cross-linkers, one-step synthesis of phase-segregated block copolymers are reviewed. Next, the notable recent progress in SMP blends are systemically studied including direct blending of different polymers, addition of a third component into blends, novel processing methods, etc. Third, the researches in SMP composites including reinforcement effect, indirect thermal stimuli-responsive effects, novel shape-memory effect, and functional applications are discussed. Finally, the current challenges and future advancements of SMP blends and composites are proposed.

1 Introduction of Shape-Memory Polymers

Shape-memory polymers (SMPs) are one kind of intelligent materials that are capable to recover from a temporary shape to a permanent (original) shape under external stimulus [1–3]. Due to their unique memory function, SMPs have attracted wide attention of researchers, and show great application prospects in many fields such as biomedical science and aerospace industry. Thermal-actuated SMPs are the most widely studied SMPs. The glass transition temperature (T_g) or melting temperature (T_m) is often used as the shape transition temperature (T_{trans}) of SMPs [4]. The conventional dual-shape-memory cycle mainly contains five steps. First (step 1), the sample is heated above T_{trans} and thus, the molecular chain mobility is activated.

X. Qi · Y. Wang (✉)
Key Laboratory of Advanced Technologies of Materials (Ministry of Education), School of Materials Science & Engineering, Southwest Jiaotong University, Chengdu, China
e-mail: yongwang1976@163.com

J. Parameswaranpillai et al. (eds.), *Shape Memory Polymers, Blends and Composites*, Advanced Structured Materials 115,
https://doi.org/10.1007/978-981-13-8574-2_3

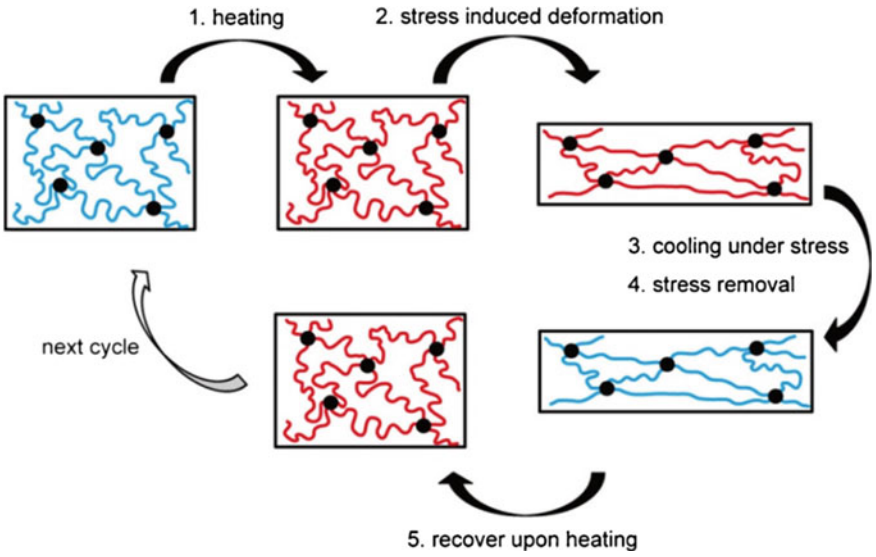

Fig. 1 The molecular mechanism of the polymeric shape-memory effect. Black dots: cross-linked netpoints; blue lines: the frozen polymer chains below T_{trans}; red lines: the active polymer chains above T_{trans} [4]. Copyright 2011, Elsevier Science Ltd., UK

Then, an external force is applied (step 2), the chain conformations are changed, resulting in the macroscopic shape deformation and entropy reduction. After cooling below T_{trans} and holding the deformation force, the chain mobility is frozen (step 3) and the temporary shape is fixed after the removal of deformation force (step 4). Finally, upon reheating above T_{trans} (step 5), the chain mobility is reactivated, allowing the chains to return to its entropically favored state. As a result, the material transforms from the temporary shape to the original shape under a stress-free condition. Therefore, the shape-memory effect (SME) of polymers is essentially regarded as an entropic phenomenon. Figure 1 illustrates the typical macroscopic shape change and molecular mechanism of SMPs.

From the point of molecular mechanism, the efficient prohibition of molecular chain slippage during the deformation process is necessary for ideal SME. Therefore, SMPs usually contain two structural components: the cross-linked netpoints and the reversible switching phase. The chemically or physically cross-linked netpoints that prohibit the chain slippage are responsible for the permanent (initial) shape. The reversible switching phase that sets the shape-memory transition is responsible for the fixing or unfixing of temporary shape. The glass–rubber transition and the crystallization–melting transition are the two most commonly used shape-memory transitions. According to the nature of the cross-linked netpoints and the shape-memory transition, SMPs can be divided into four types: (1) chemically cross-linked amorphous polymers, (2) chemically cross-linked semi-crystalline polymers, (3) physically cross-linked amorphous polymers, and (4) physically cross-linked semi-

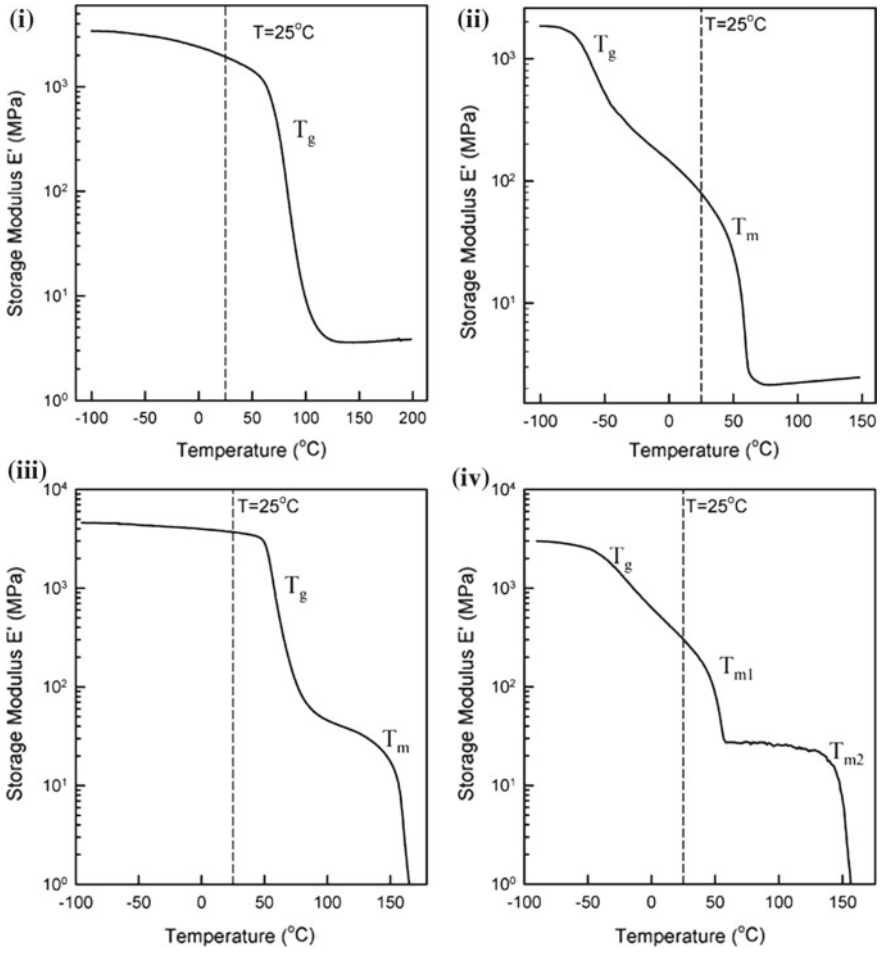

Fig. 2 Four types of SMPs based on their dynamic mechanical behavior. (I) Chemically cross-linked amorphous polymers, (II) chemically cross-linked semi-crystalline polymers, (III) physically cross-linked amorphous polymers, and (IV) physically cross-linked semi-crystalline polymers [5]. Copyright 2007, The Royal Society of Chemistry, UK

crystalline polymers [5, 6]. Compared with physically cross-linked SMPs, chemically cross-linked SMPs are considered to have better shape-memory properties and cyclic stability. The illustration of four types of SMPs based on their dynamic mechanical behavior is shown in Fig. 2.

2 Strategies for the Preparation of Shape-Memory Polymers

2.1 Chemical Cross-linking of Thermoplastic Polymers

In theory, the most direct method for the preparation of SMPs is chemical cross-linking of thermoplastic polymer with high molecular weight. Chemical cross-linking will introduce a network that prohibits the chain slippage and determines the permanent shape [7]. High energy radiation and addition of organic peroxides are the two common methods to fabricate chemically cross-linked thermoplastic polymers. The early application of SMPs, the "heat-shrinkable" films, were prepared through radiation cross-linking of polyethylene (PE). For example, Mather et al. used dicumyl peroxide (DCP) to prepare a chemically cross-linked SMP based on semi-crystalline polycyclooctene (PCO) [8]. The chemically cross-linked PCO presented the rubbery state above the T_m of PCO crystalline phase, and thus, the sample was easily stretched to a temporary shape. Figure 3a illustrates the microstructural transformations of cross-linked PCO during a dual-shape-memory cycle. The crystallization–melting transition of PCO crystals was used as the shape-memory transition. As shown in Fig. 3b, when the sample was immersed in hot water, accompanying with the rapid melting of PCO crystals, the temporary ("U" shape) was quickly transformed into its permanent shape (linear shape) within 0.7 s.

This approach of chemical cross-linking of thermoplastic polymers is appropriate for both amorphous and semi-crystalline polymers, and can be applied to conventional processing techniques such as extrusion, hot pressing, and injection molding. However, the chemical cross-linking would inevitably change the transition temperature (either T_m or T_g) of bulk polymers [9].

2.2 Single-Step Polymerization of Monomers/Prepolymers and Cross-linkers

The second strategy to prepare SMPs is the polymerization of monomers or prepolymers with chemical cross-linking agents in one step. The most notable example is epoxy, a common thermosetting resin. Xie et al. reported a shape-memory epoxy with tunable thermal transition temperatures [10]. Figure 4a shows the chemical structures of the reactants used in this amine cured aromatic epoxy system. The epoxy system mainly included an aromatic diepoxide (EPON 826) and an aliphatic diamine cross-linking agent (Jeffamine D230). Starting with the rigid aromatic diepoxide, a flexible cross-linking agent was introduced to obtain a chemically cross-linked epoxy system. This system would undergo a sol–gel transition which was similar to other thermosetting resins. As shown in Fig. 4b, starting from the original rectangular shape, the epoxy sample was deformed to various shapes by bending and twisting.

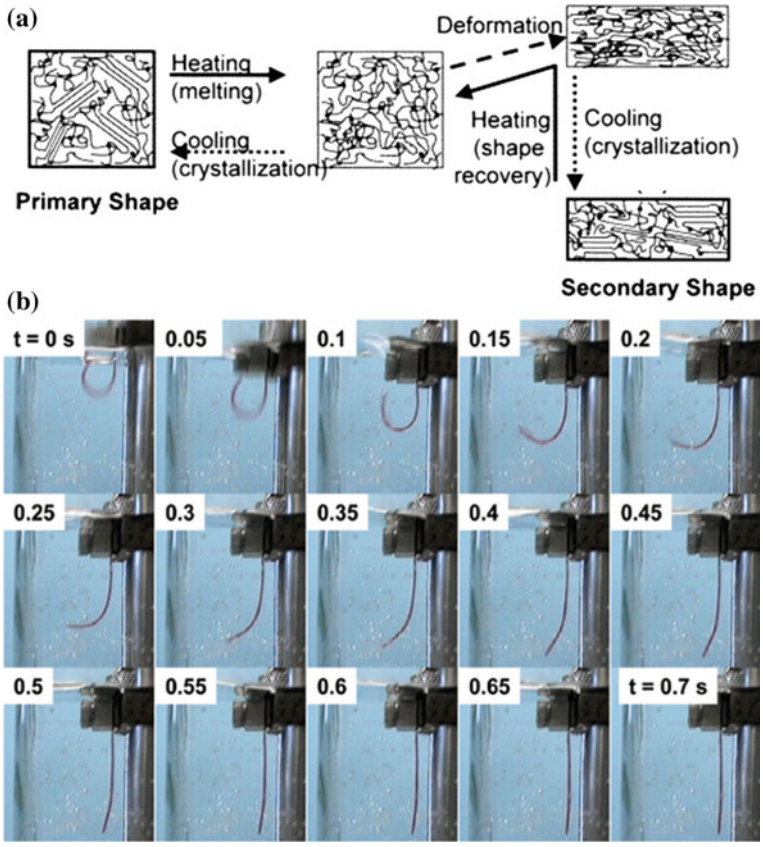

Fig. 3 **a** Schematic depiction of the microstructural transformations during a dual-shape-memory cycle of chemically cross-linked PCO. **b** Shape-memory behavior of cross-linked PCO following rapid immersion in water at 70 °C [8]. Copyright 2002, American Chemical Society, USA

These deformed temporary shapes could be well fixed upon quenching under load. When heating to 70 °C, within 6 s, these temporary shapes quickly transformed into the original rectangular shapes. The excellent shape fixation and recovery performance of the epoxy system were ascribed to its chemically cross-linked character. In addition, the T_g of epoxy could be tailored by changing the cross-link density or aliphatic chain flexibility, thus the T_{trans} could be varied over a wide range.

Generally speaking, this strategy can realize the efficient control of shape-memory properties by adjusting variables such as the concentration of cross-linking agent, molecular weight of prepolymers, and monomer composition [11]. Because of the thermoset nature (permanent network), the SMPs prepared by this strategy show good shape-memory performance and cycle stability [12]. Nevertheless, the constraints of processing (high viscosity of thermosetting resin) and the narrow processing windows (before the gel time) are two disadvantages of this strategy.

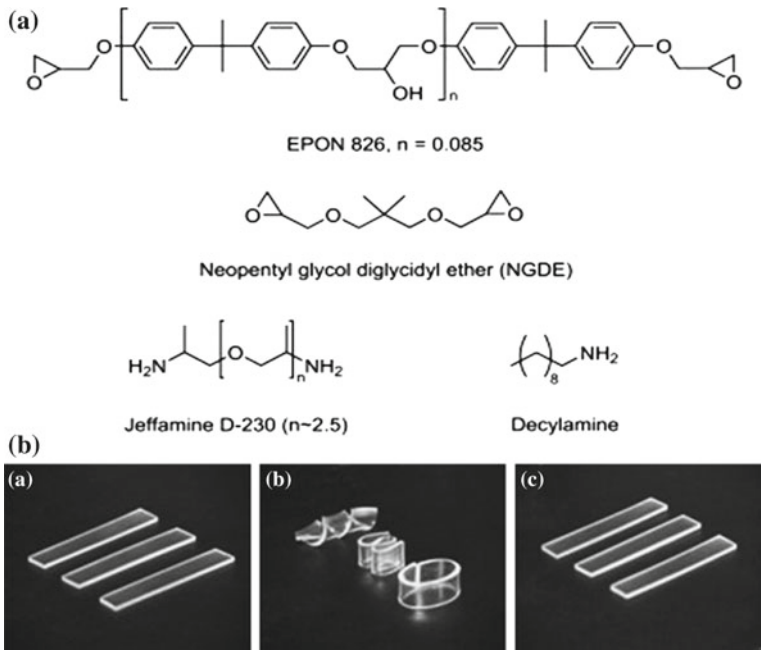

Fig. 4 **a** Chemical structures of the epoxy components, **b** photographs of shape-memory behavior (a: original shape, b: fixed temporary shape, c: recovered shape) [10]. Copyright 2009, Elsevier Science Ltd., UK

2.3 One-Step Synthesis of Phase-Segregated Block Copolymers

Different from the previous thermoset SMPs, the target of this strategy is to obtain a thermoplastic polymer which can be processed via more conventional polymer processing techniques. The SMPs prepared by this method are often phase-segregated block copolymers, having two blocks showing different thermal transition temperatures. Polyurethane (PU), having a multi-block structure with hard and soft segments, is the most extensively studied SMP fabricated by this method [13]. The hard segments play the role of physical cross-linkers that determine the permanent shape, and the soft segments serve as the switching phases that realize the fixing or unfixing of temporary shape [14]. Both type (3) and type (4) SMPs can be fabricated based on the category of soft segment (glassy or semi-crystalline). For example, Lendlein et al. prepared a multi-block co-polyesterurethane SMP containing poly(p-dioxanone) (PPDO) hard segment and poly(ε-caprolactone) (PCL) soft segment [15]. The thermal properties of multi-block copolymers can be flexibly adjusted in a wide range by varying the weight ratio of hard segments to soft segments. Moreover, this biodegradable shape-memory PU has several biomedical applications. The fiber

(elongated by 200%) can recover its original shape while temperature increases, thus the SMP fiber is expected to be used as the degradable suture for wound closure.

In short, the above-discussed methods are the most widely used methods to prepare SMPs. However, it should be noted that any new combination of materials in the above methods require complicate chemical synthesis. An efficient method to tailor the properties of SMPs is the blending two polymers through a physical process.

3 Shape-Memory Polymer Blends

3.1 Direct Blending of Different Polymers

Physical blending of two polymers provides an easier approach to prepare SMPs because of its good processability and mass production [16]. As mentioned before, many conventional polymers contain at least one thermal transition. An effective network is necessary for them to prohibit the chain slippage when the temperature is above T_{trans}. Based on the structural concept, SMP blends usually contain one polymer playing the role of permanent phase and the other polymer serving as switching phase.

According to this approach, the first step is to blend one polymer with another polymer which has a higher thermal transition temperature (T_g or T_m). In a pioneering work in this field, Mather et al. reported a thermal-actuated SMP blend based on poly(vinyl acetate) (PVAc) and poly(lactic acid) (PLA) [17]. PVAc with a relatively lower T_g (40 °C), acted as the switching phase and PLA with a higher T_m (165 °C), played the role of physical cross-linker to form a deformable elastic network. A well-defined rubbery plateau was observed when the temperature was between the T_g of PVAc and the T_m of PLA. Therefore, the blend was able to be deformed, and the deformed shape could be well recovered when the temperature was increased. Similarly, Behl et al. prepared a binary immiscible SMP blend consisting of poly(p-dioxanone) (PPDO) hard segment and poly(ε-caprolactone) (PCL) switching segment. In this approach, the complicate synthesis of SMPs can be avoided [18].

The structure of SMPs mainly contains two key components, one is the chemically or physically cross-linked network determining the permanent shape, the other is the switching phase determining the fixation of temporary shape. For conventional SMPs, the cross-linked network and switching phase are usually combined in one macromolecule. Li et al. prepared a miscible SMP blend composed of poly(vinylidene fluoride) (PVDF) and acrylic copolymer (ACP) through melt blending [19]. In this miscible crystalline/amorphous system, the tiny PVDF crystals bridge the adjacent amorphous ACP molecular chains. As shown in Fig. 5, the tiny PVDF crystals could act as the physical cross-linkers to efficiently prevent the ACP chains slippage during the deformation process. These blends exhibited excellent shape fixing and recovery performance when the composition ratio was well controlled. When the amount of PVDF crystals was too low or too high, the slippage of the amorphous ACP chains or

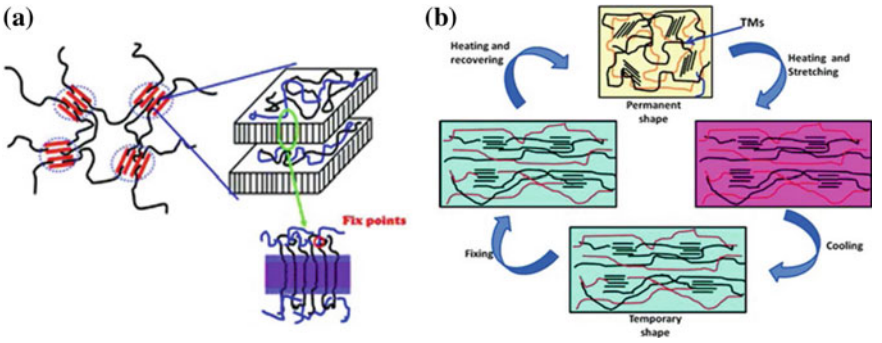

Fig. 5 Schematic diagrams for **a** molecular mechanism, **b** the shape-memory properties of PVDF/ACP blends [19]. Copyright 2012, American Chemical Society, USA

the breakage of large fibrillar PVDF crystals occurred, resulting in the deteriorated shape recovery property. The PVDF/ACP blend (50/50, wt%) showed the optimal shape recovery performance. Furthermore, they found that the crystal morphologies had a significant effect on the shape-memory properties [20]. The PVDF/ACP blend (50/50, wt%) was annealed at different temperatures, inducing the crystallization of PVDF from the miscible crystalline/amorphous blend. Large PVDF spherulites were observed at higher annealing temperature, while tiny PVDF crystals were formed at lower annealing temperature. The large PVDF spherulites were easily broken during the deformation process, giving rise to the bad shape recovery property. However, the tiny PVDF crystals could well act as the physical cross-linkers, prohibiting the slippage of amorphous ACP chains. Therefore, the blends with tiny PVDF crystals exhibited good shape fixing and recovery properties.

Miscible polymer blends also exhibit multi-SME. For example, Samuel et al. designed a miscible PLLA/poly(methyl methacrylate) (PMMA) SMP blend, in which the chain entanglements served as physical cross-linkers [21]. The miscible PLLA/PMMA (50/50) blend showed a broad T_g ranging from 60 to 100 °C. More interestingly, because of the broad T_g, the PLLA/PMMA blend not only exhibited the dual SME, but also exhibited multiple SME, such as triple SME and temperature memory effect.

The second method is to blend an amorphous or a crystalline plastic with an elastomer. Elastomers usually contain cross-linked networks and have the ability to remember their permanent shape by entropic elasticity. However, elastomers are often in a rubbery state at room temperature, and they could not fix the deformed shape. An efficient approach is blending an elastomer with another polymer of desired T_g or T_m [22]. For example, Zhang et al. prepared an immiscible SMP blend of styrene-butadiene-styrene (SBS) thermoplastic elastomer and PCL [23]. Kurahashi et al. found that the PU/poly(oxyethylene) (POE) blend with co-continuous structure exhibited good shape fixing and recovery behavior [24]. Similarly, Fu et al. designed an optimal shape-memory thermoplastic polyurethane/polylactide (TPU/PLA) blend through morphology control [25]. As shown in Fig. 6, the phase morphology was

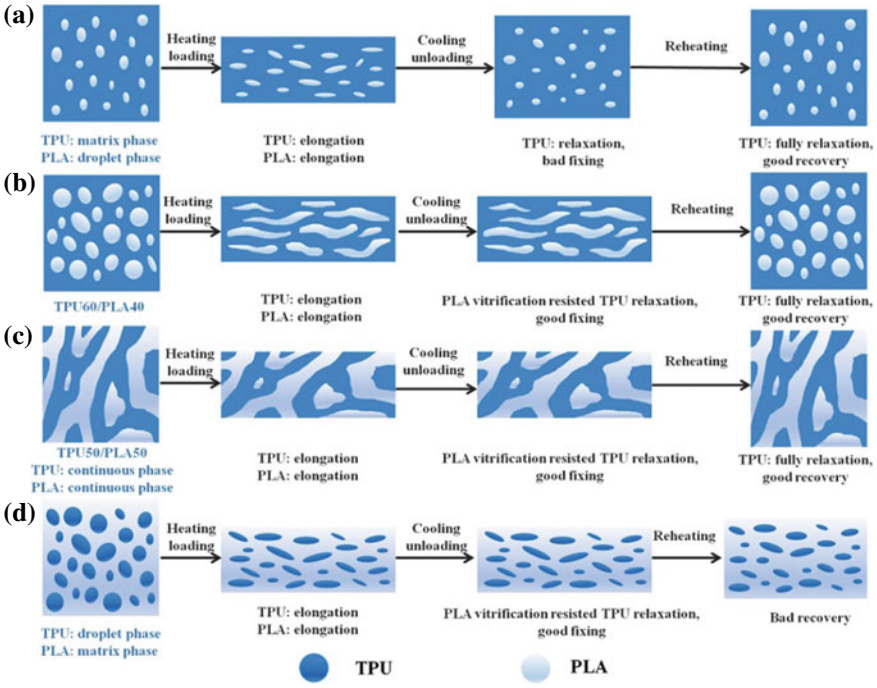

Fig. 6 Schematic images of the shape-memory mechanism of binary TPU/PLA blends with various composition ratios [25]. Copyright 2016, Elsevier Science Ltd., UK

changed with respect to varying the composition ratio. In this blend, the elastic TPU served as the permanent phase which provided the recovery performance, and PLA acted as the switching phase which was responsible for the fixing or unfixing of temporary shape. When the TPU content was 50–60 wt%, the TPU/PLA blend with the co-continuous phase morphology exhibited an optimal shape fixing and recovery effect.

Apart from blending the elastomers with thermoplastics, Weiss et al. and Feng et al. mixed elastomers with small crystalline molecules such as fatty acid and paraffin respectively to fabricate SMP blends [26, 27]. For example, Feng et al. reported a hydrogenated styrene-butadiene block copolymer (SEBS)/paraffin blend with a wide melting transition, showing the triple and quadruple shape-memory effect [28].

From the perspective of stress transfer in SMP blends, the continuous degree of each phase plays an important role in determining the shape fixing and recovery performances. It is widely accepted that the elastomer/plastic blends with co-continuous structure have balanced shape fixing and recovery properties. However, the co-continuous structure is often achieved within a relatively narrow range of composition. Besides, to obtain the co-continuous structure, high content of elastomer is needed, resulting in the decline of the modulus and strength. Therefore, the application of elastomer/plastic SMP blends is greatly limited. To address these

problems, Chen et al. utilized peroxide-induced dynamic vulcanization to fabricate SMP blends based on natural rubber (NR)/PLA thermoplastic vulcanizates (TPVs) [29]. Differing from the conventional TPVs in which spherical rubber particles were formed after dynamic vulcanization, the NR phase (40 wt%) was formed a continuous structure in PLA matrix. This novel structure imparted the NR/PLA TPV with excellent shape-memory performances (shape fixing ratio ~100%, shape recovery ratio >95%). In addition, the NR/PLA TPV showed balanced strength and toughness. The impact strength of NR/PLA (40/60, wt%) TPV was 42.5 kJ/m^2, which was 15 times higher than that of pure PLA (2.75 kJ/m^2). The NR/PLA TPV with good shape-memory properties and stiffness–toughness balance exhibited exciting perspective in intelligent devices.

3.2 Addition of a Third Component into Binary Polymer Blends

Introducing a third component (such as cross-linking agent, compatibilizer, etc.) into a polymer blend is also considered to be an efficient method to prepare SMP blends. For example, Cuevas et al. prepared a chemically cross-linked polyethylene (PE)/PCO blend by adding DCP [30]. As shown in Fig. 7, the cross-linked PE/PCO blend showed two thermal transitions, originated from its two distinct crystalline domains. By applying a two-step programming process, the cross-linked PE/PCO blend with two switching domains could recover from one temporary shape (C) to an intermediate shape (B), and to the original shape (A) on sequential reheating to the T_m of PCO and PE. This chemically cross-linked strategy can be applied to other binary immiscible blends. The triple SME is also found in the chemically cross-linked poly(ethylene vinyl acetate) (EVA)/PCL blend and polypropylene (PP)/PE blend with the addition of DCP [31, 32].

Addition of compatibilizer is an efficient method to improve the compatibility and interfacial adhesions of polymer blends. The compatibilizers not only keep each component's characteristic, but also have a promoting effect in the shape-memory properties. For example, Xu et al. observed shape-memory properties in maleated-polyethylene (MA-PE)/nylon 6 (PA6) blend, where the in situ generated PE-g-PA6 graft copolymers by the reaction between MA-PE and PA6 acted as compatibilizer [33]. In this system, the PE segments served as switching phase and the nylon domains acted as physical cross-linkers. The reactive blending, which enhanced the interfacial adhesions of two phases, was considered to be necessary for the good shape-memory properties. Similarly, in situ compatibilized maleated-polystyrene-b-poly(ethylene-co-butylene)-b-polystyrene (MA-SEBS) block copolymer (MA-SEBS)/polybutylene succinate (PBS) blend showed triple SME based on the T_m of poly(ethylene-co-butylene) (at 55–65 °C) and PBS (at 105–115 °C) [34]. Chen et al. introduced zinc dimethacrylate (ZDMA) to enhance the interfacial adhesions and shape-memory properties of ethylenepropylenediene rub-

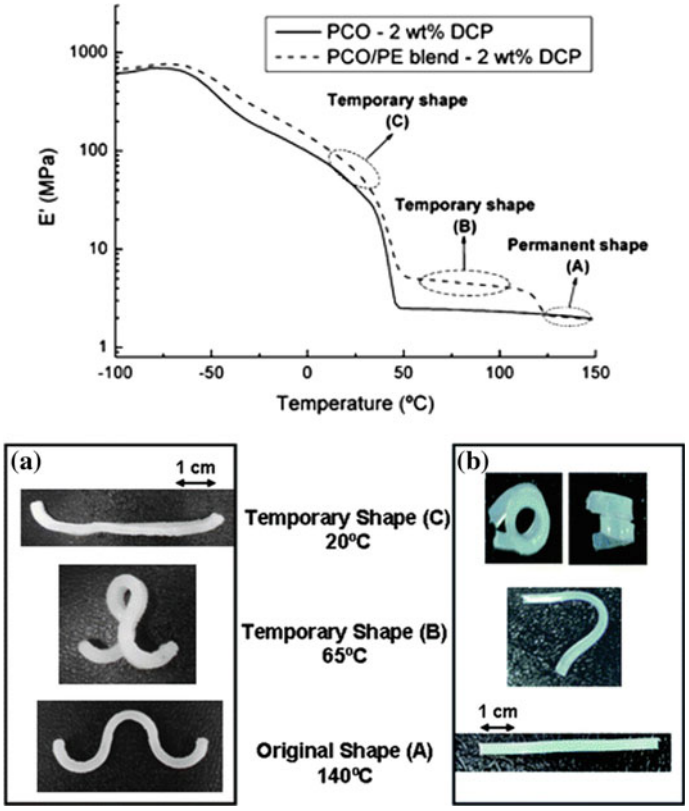

Fig. 7 Comparison of the evolution of storage modulus (E') with temperature for a PCO homopolymer and PCO/PE blend cross-linked with DCP. Photographs illustrate the triple SME of cross-linked PCO/PE blends for different temporary and permanent shapes [30]. Copyright 2012, The Royal Society of Chemistry, UK

ber/polypropylene (EPDM/PP) TPVs [35, 36]. As shown in Fig. 8a, b, the ZDMA-induced compatibilization greatly enhanced the interfacial adhesions between EPDM and PP, promoting the deformation of rubber particles in temporary shape and storing sufficient resilience to remember the permeant shape. However, the weak interfacial adhesion could not hold the deformed EPDM particles, and caused the retraction of prolonged EPDM particles (Fig. 8c). Both the shape fixing ratio and recovery ratio of EPDM/PP/ZDMA TPVs were above 90%. These studies indicated that the reactive processing induced by compatibilizers was a simple and promising strategy to develop SMP blends with good shape-memory properties.

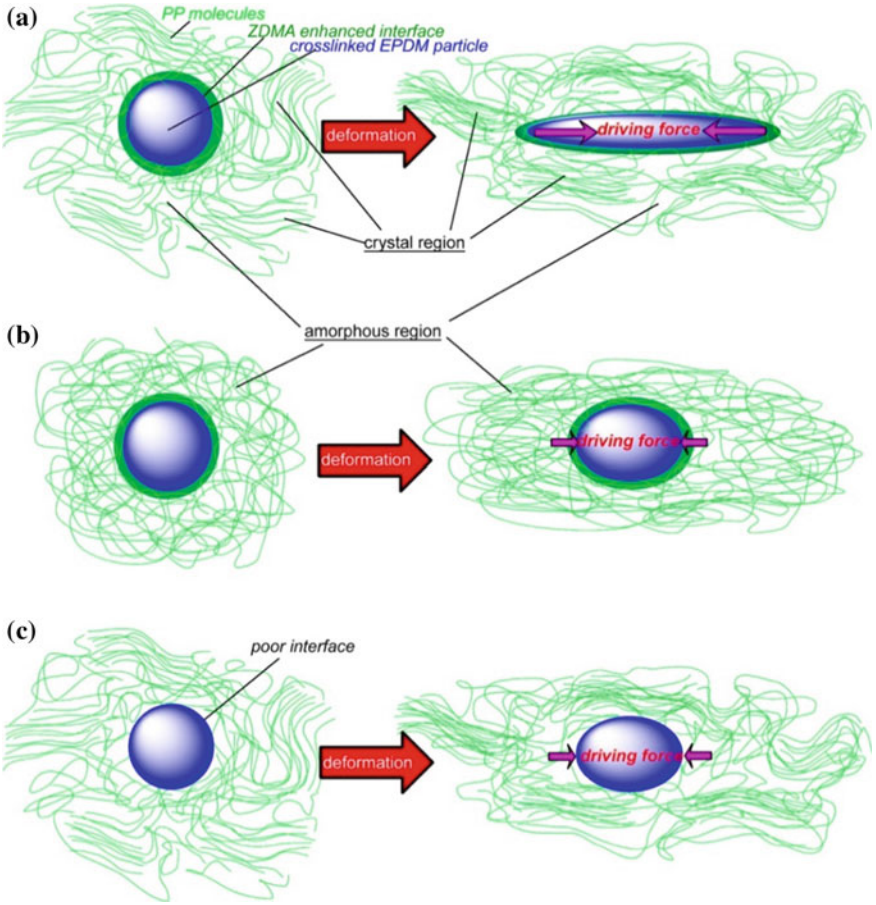

Fig. 8 Schematic representation for the detailed structure of a EPDM/PP/ZDMA TPV with an enhanced interface deformed **a** below and **b** above T_m. **c** EPDM/PP TPV with a poor interface deformed below T_m [36]. Copyright 2016, American Chemical Society, USA

3.3 Novel Processing Methods to Prepare Shape-Memory Polymer Blends

Recently, some novel processing methods were proposed to control the phase morphology and shape-memory properties of blends. Baer et al. designed PU/PCL multilayer SMP blends through forced assembly multilayer co-extrusion [37]. The elastic TPU layer provided strong resilience and the rigid PCL layer played the role of heat-control switch. PU layer and PCL layer maintained an alternatively arranged layer structure, which could generate a synergistic effect, thus endowing the multilayer PU/PCL blends with balanced shape fixing and recovery performance. The multilayer PU/PCL blends exhibited better shape-memory properties than conven-

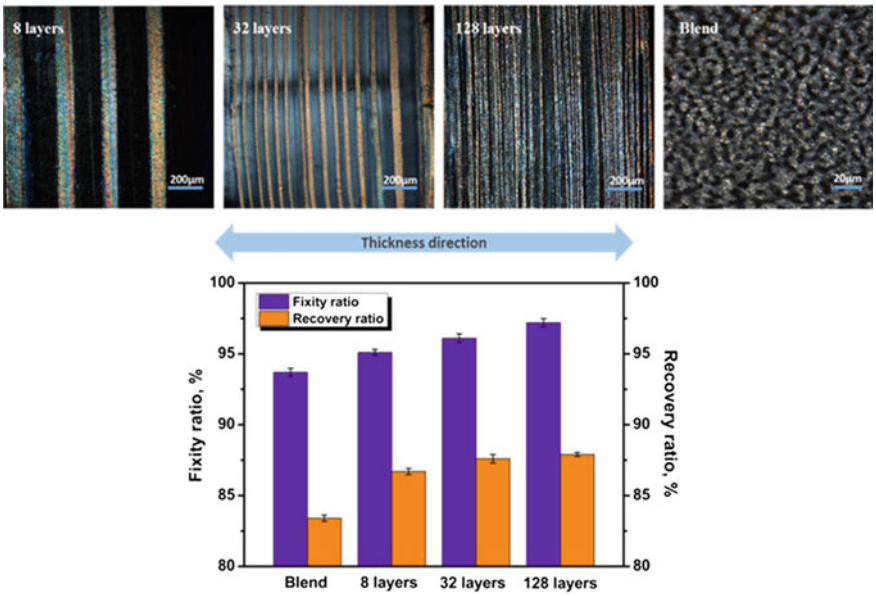

Fig. 9 Morphological observation, shape fixing and recovery ratios of TPU/PCL multilayer, and blend samples through polarized light microscopy [38]. Copyright 2016, American Chemical Society, USA

tional PU/PCL blends. At 75/25 and 25/75 compositions, these blends showed good shape fixing and recovery properties, while the conventional PU/PCL blends with sea-island structure showed deteriorated shape fixing or recovery properties. It can be seen that the phase morphology has a significant effect on the shape-memory properties of polymer blends. Similarly, Guo et al. prepared TPU/PCL SMP blends containing alternating layers via layer-multiplying extrusion [38]. As shown in Fig. 9, the well-defined layer spaces could be flexibly tailored by changing the layer numbers. The shape fixing and recovery ratios were increased with the increase of layer numbers, and these ratios were remarkably higher than those of the conventional TPU/PCL blend. The layer-multiplying extrusion opens a new window to adjust the shape-memory properties of polymer blends over a broad composition range.

Mather et al. reported a novel approach to prepare SMP blends through electrostatic spinning technology and vacuum impregnation [39]. As shown in Fig. 10, PCL nonwoven fabrics were first prepared via electrostatic spinning technology, and then they were vacuum infiltrated with silicone rubber. The blend exhibited a two-phase morphology in which PCL microfibers were well distributed in the silicone rubber matrix. The PCL phase acted as a T_m-based switching phase, and the silicone rubber provided the elasticity to recover its original shape. As the PCL fiber framework penetrated across the whole material, the blend showed excellent shape fixing and recovery properties. Differing from direct blending, the PCL nonwoven fabrics and silicone rubber were mixed below the T_m of PCL. Therefore, the blend

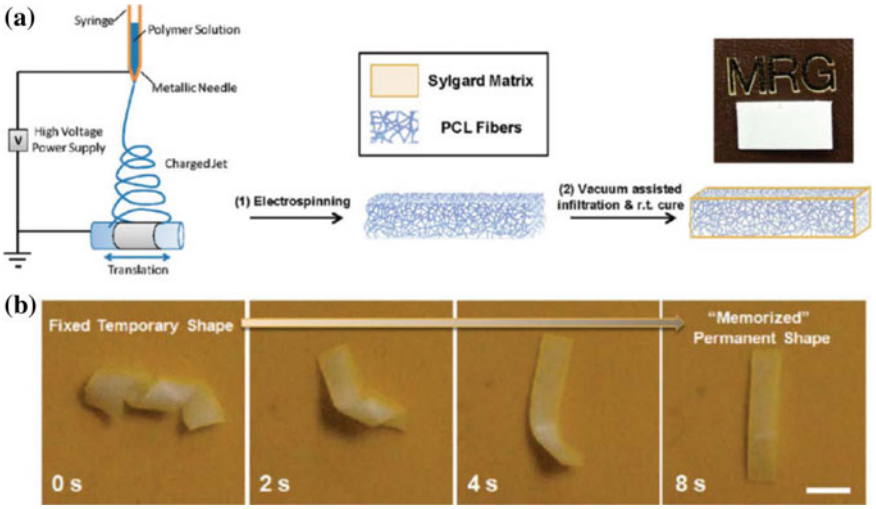

Fig. 10 **a** Two-step fabrication of Sylgard/PCL SMP blend; **b** photographs showing the recovery from a fixed temporary shape to its "memorized" permanent shape at 80 °C [39]. Copyright 2009, American Chemical Society, USA

was not mixed in a melt or solution state. The morphology was predetermined, which was not affected by the factors such as blending conditions, polymer compatibility, and thermal history. Furthermore, they replaced silicone rubber with an epoxy to fabricate a triple SMP blend [40]. The PCL/epoxy blend exhibited two thermal transitions, namely the T_g of epoxy matrix and the T_m of PCL nonwoven fabrics, and thus showed triple SME. The PCL/epoxy blend could well fix two temporary shapes and recover sequentially to the permanent shape on reheating to the T_m of PCL and the T_g of epoxy. This strategy makes the functional components (switching phase and memory phase) manipulate independently, and impart controllable shape-memory properties.

3.4 A Thermal Stimuli-Actuated Shape-Memory Polymer Blends

Despite the remarkable development of SMP blends, there still exist some limitations in their practical applications. The SMP blends are usually in a rubbery state above the T_{trans}, and show low shape recovery force. Besides, most SMP blends are stimulated by direct heating. It is necessary to increase the high-temperature recovery force and develop other stimuli (such as electricity, light, magnetic, humidity, etc.) for SMP blends. In order to solve these problems, some functional fillers are introduced to SMP blends. For instance, the electro-actuated SMPs have attracted great attention

because of their convenient operation and remote control [41]. Various conductive fillers like carbon black (CB), carbon nanofibers (CNFs), carbon nanotubes (CNTs), and graphene are added into SMP blends. According to Joule's law, the conductive fillers generate heat and transfer heat to trigger the shape recovery of SMP blends. However, to realize the electro-actuated SME, high loading of fillers is often needed, which will lead to the deterioration of shape recovery performance and is unfavorable for practical processing.

Recently, Wang et al. fabricated a rapid electro-actuated shape-memory EVA/PCL/CNT blend composites with low CNT loadings [42]. For the EVA/PCL binary blend, the elastic EVA phase provided the recovery performance, and the PCL phase was responsible for the fixing and removal of the temporary shape. When the composition of EVA/PCL was 60/40, the blend formed a co-continuous structure, exhibiting optimal shape fixing and recovery properties. Further addition CNTs into EVA/PCL (60/40) blend resulted in the selective localization of CNT in EVA phase, and thus formed the double percolation structure. The selective localization of CNTs not only improved the high-temperature mechanical properties of the blends, but also imparted excellent electrical conductivity. As shown in Fig. 11, The EVA/PCL/CNT system with 5 wt% CNTs could completely recover its permanent shape in 24 s under a voltage of 20 V. Similarly, Fu et al. also utilized the selective localization of CNTs in the co-continuous TPU/PLA and PPC/PLA blends to prepare rapid electro-actuated SMP blends [25, 43]. Based on the concept of double percolation, the selective localization of CNTs in one phase of binary immiscible blend could provide a percolating conductive network with low CNT content. Therefore, this strategy is significant in terms of processing and cost, and would be expected to achieve large-scale production in industry.

Most SMP blends are dual SMPs that can only store one temporary shape and remember one permanent shape. In contrast, the triple and multiple SMP blends which can store two or more temporary shapes show great application prospects in the intelligent devices. Dang et al. fabricated an electro-actuated triple SM material of chemically cross-linked PCO/PE/CNT blend composite [44]. To selectively localize CNT in PCO phase, they first mixed CNT with PCO and the resulting mixture is then mixed with PE. The cross-linked PCO/PE/CNT blend composites with two thermal transitions, namely the low-temperature $T_{m,PCO}$ and high-temperature $T_{m,PE}$, form ideal candidates for exhibiting triple SME. Under the electric actuation, the intermediate and original shapes could sequentially recover when the temperature was increased to 60 °C ($T_{m,PCO}$) and to 120 °C ($T_{m,PE}$). This work indicated that the rapid electro-actuated SME could be obtained by making CNTs selectively localize in one component of binary immiscible blends.

Developing remote controlled multi-SMP blends with complex deformation is also of great significance in industrial applications. Wang et al. fabricated an electro-actuated and infrared-actuated SMP blend composites by introducing graphene nanoplatelets (GNPs) into PCL/TPU blends [45]. Because of the good electrical conductivity and photo-thermal effect of GNP, the PCL/TPU/GNP blend composites exhibited excellent electro-actuated and infrared-actuated shape recovery behavior. Meanwhile, it is interesting to observe the PCL/TPU/GNP blend composites with

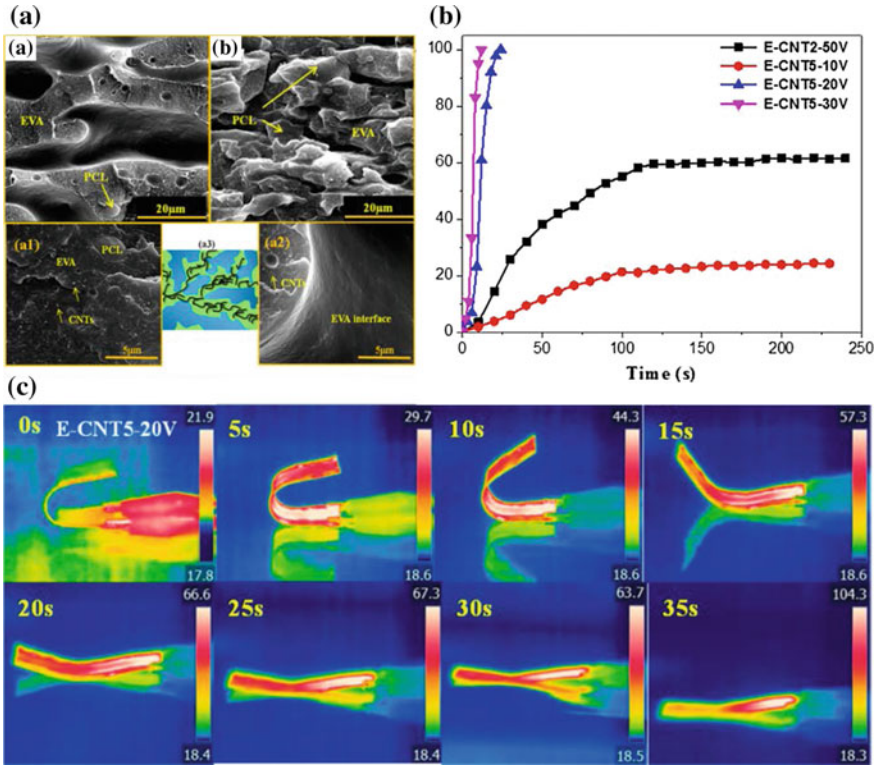

Fig. 11 **a** SEM images showing the phase morphologies of the EVA/PLA/CNT blend composites, **b** variation of the shape recovery ratio of the EVA/PLA/CNT2 and EVA/PLA/CNT5 at different triggering voltages, and **c** infrared photographs showing the shape recovery process and the temperature change of the EVA/PLA/CNT5 operated at the voltage of 20 V [42]. Copyright 2016, American Chemical Society, USA

oriented structure could show the complex shape-memory effect and self-driven behavior, as shown in Fig. 12. The PCL/TPU/GNP blend composites with dual-responsive (electric, infrared light) and self-driven properties exhibited enormous application potentiality in the field of robot hands and smart switches.

Concerning the blending strategy, there are still some questions that require further clarification. First, polymer blending provides an accessible route to realize the commercial applications of SMPs. There are many factors influencing the phase morphology of binary immiscible blends, such as mixing temperature, shear rate, composition ratio and viscosity ratio of two phases. Therefore, by controlling the processing parameters or with the aid of special processing equipment, we can investigate the evolution of phase morphology under different field (temperature, shear, etc.) and study the structure–property relationship of SMP blends.

Second, most polymer pairs are thermodynamically incompatible, resulting in the poor interfacial adhesion. Since the interfacial adhesion has an important effect

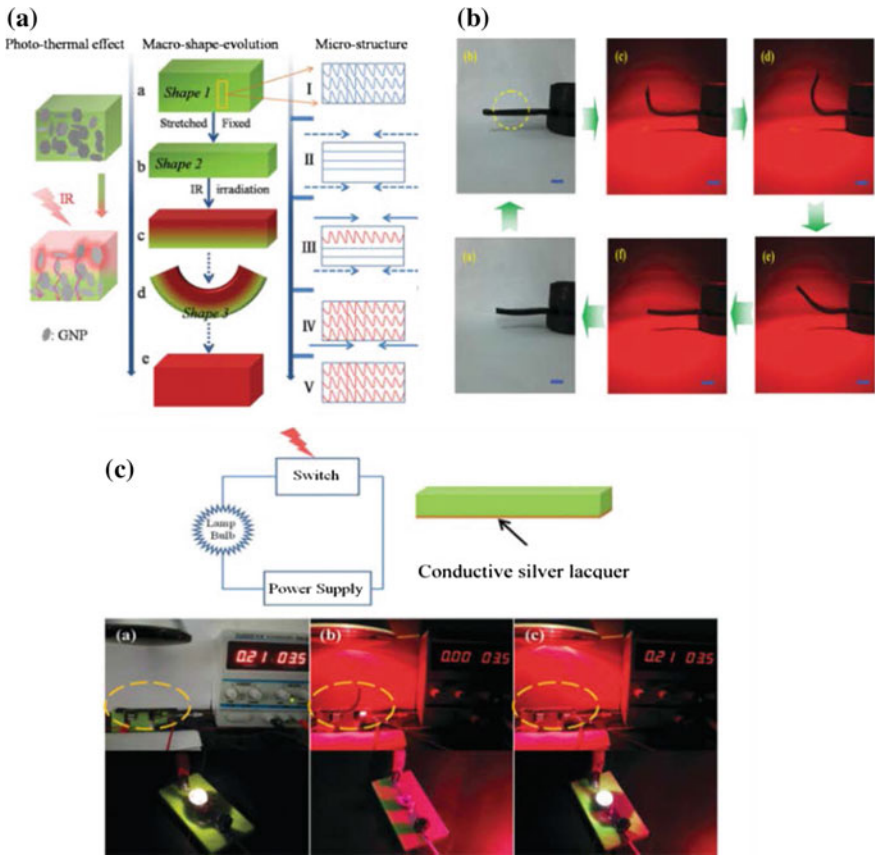

Fig. 12 **a** Schematic illustration of the deformation mechanism of PCL/TPU/GNP blend composites upon infrared light irradiation. **b** Typical images of the flexible anisotropic actuator upon infrared light irradiation from the flat to folded shapes, and the original shape. **c** A simple apparatus was designed to show the potential application of smart switch [45]. Copyright 2017, The Royal Society of Chemistry, UK

on the stress transfer during the deformation process, attention should be paid to improve the interfacial adhesion between the components of SMP blends.

Third, to prepare double percolated conductive polymer composites (CPCs), the high critical content (50 wt%) is usually needed to form the continuous filler-enriched polymer phase, otherwise, the formation of dispersed phase might bring about unconnected filler networks. Therefore, only two times in the effective filler concentration is obtained in the double percolated CPCs compared to single CPCs, giving rise to a relatively modest increment of electrical conductivity. In order to obtain highly conductive CPCs with a low CNT content, it's important to broaden the composition range for the co-continuity of binary immiscible blends. For example, Fu et al. introduced CB nanoparticles with self-networking ability to tailor the morphology

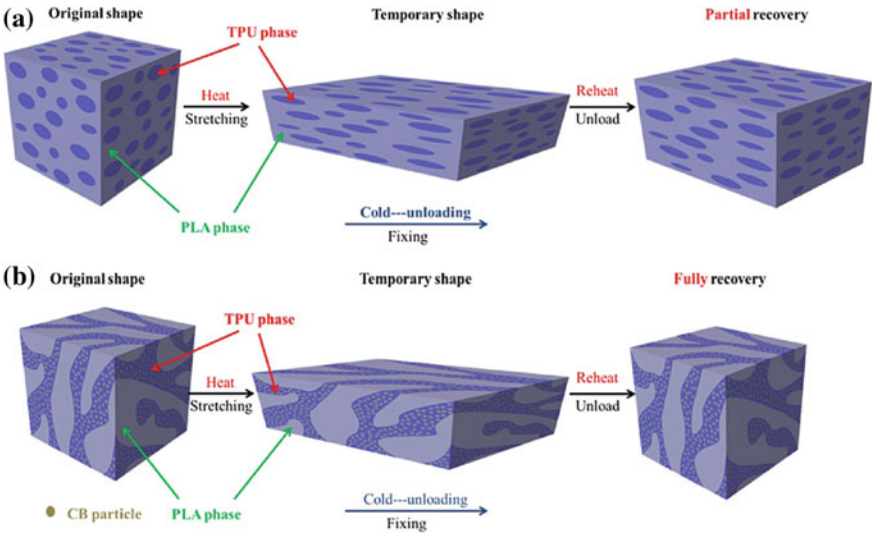

Fig. 13 Schematic illustration of the shape-memory mechanism for **a** PLA70/TPU30 binary blend and **b** PLA70/TPU30/CB5 ternary blend composites [46]. Copyright 2017, Elsevier Science Ltd., UK

of PLA/TPU (70/30, wt%) blend [46, 47]. As shown in Fig. 13, it was found that the CB selectively distributed in the TPU phase, and the CB network induced the TPU phase change from island structure to continuous structure. The continuous degree of TPU phase was increased with the increase of CB content, deriving from the self-networking ability of CB nanoparticles and the strong affinities between CB nanoparticles and TPU phase. When CB nanoparticles were selectively localized in the continuous TPU phase, a double percolated conductive network was formed, enabling a remarkable improvement of electrical conductivity. The PLA/TPU/CB blend composites could realize the good electro-actuated shape recovery performance at a voltage of 30 V. This work proves that introducing nanoparticles with self-networking ability into binary immiscible blends is an efficient method to control the phase morphology and shape-memory properties over a much larger composition range.

4 Shape-Memory Polymer Composites

SMPs have received extensive attention because of their memorizing property and potential application prospects in many fields, such as the medical, aerospace, textile, packaging and electronic engineering industries. However, the development of SMPs is greatly limited because of their poor mechanical properties (low recovery force, low strength, etc.). Incorporation of functional fillers to generate SMP

composite would be an efficient method to improve the mechanical properties and shape-memory properties of SMPs [48–50]. Therefore, the SMP composite is another important branch that needs more attention in the SMP's family. The first topic of SMP composites is about the reinforcement of SMPs. The incorporation of reinforcing fillers is beneficial for enhancing the mechanical properties and shape recovery forces of SMPs. Second, functional fillers could make SMP composites response under a thermal stimuli, such as electricity, magnetic field, light, solvent, etc. In addition to the reinforcement effect and a thermal stimuli, novel SME and functional applications could be created by adding fillers.

4.1 Reinforcement Effect of Shape-Memory Polymer Composites

Reinforcing fillers (such as glass fibers, carbon fibers, Kevlar fibers, CNTs, graphene, etc.) are capable to enhance the mechanical properties and shape recovery forces of SMPs by solution blending, melt blending, and in situ polymerization. Poulin et al. prepared PVA/CNT SM composites containing 20 wt% CNTs [51]. The maximal recovery stress of PVA/CNT fiber could reach nearly 150 MPa, which is about two orders of magnitude higher than that of pure PVA. Interestingly, the high content of CNTs (20 wt%) significantly changed the thermodynamic behavior of PVA molecular chains, enabling PVA/CNT fiber to have a wide range of T_g. The PVA/CNT fiber had the ability to remember the initial deformation temperature (T_d) under free load mode. That was a maximum instant recovery rate would occur near the initial T_d during the heating process.

It should be noted that the fillers that are physically blended with SMPs may not simultaneously improve the mechanical properties and shape-memory properties. Fillers that chemically bonded with SMP chains are beneficial in satisfactorily improving the shape-memory properties of SMPs. Wang et al. prepared PCL/SiO_2 SMP composites through in situ polymerization (Fig. 14) [52]. Due to the addition of SiO_2, the tensile strength and elastic modulus of PCL/SiO_2 composites could reach up to 90 MPa and 500 MPa, respectively. Besides, both the shape fixing and recovery ratio of PCL/SiO_2 composites were greater than 95%. Similarly, Archer et al. designed an inorganic–organic hybrid SMP with SiO_2 nanoparticles as chemically cross-linked points. SiO_2 nanoparticles were first modified by sulfonic acid, then connected with the polyethylene glycol (PEG) segments through static adsorption, forming a core–shell structure in which SiO_2 as the core and PEG as the shell [53]. The PEG/SiO_2 composites not only showed rapid shape recovery effect, but also exhibited high modulus (100 MPa) above the T_{trans}.

Polyhedral oligomeric silsesquioxane (POSS) nanoparticles are another kind of inorganic particles with well-defined cubic geometry and active functional groups, which can be used as ideal cross-linked points for SMPs. Song et al. used POSS with eight pendent organic groups to prepare a star-shaped POSS/PLA hybrid mate-

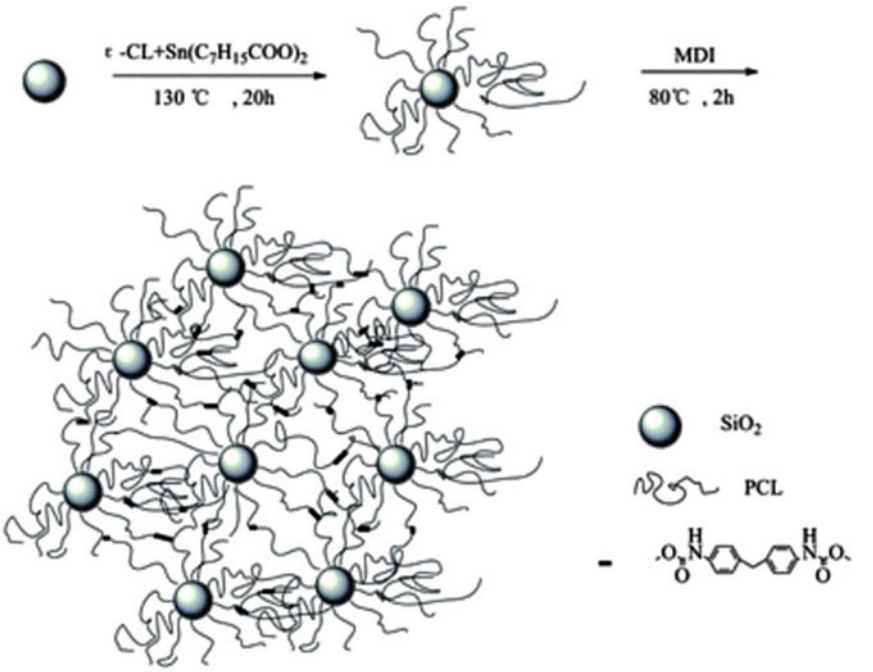

Fig. 14 Schematic illustration of SiO_2-SMP synthesis [52]. Copyright 2011, The Royal Society of Chemistry, UK

rial [54]. The POSS nanoparticles could act as chemically cross-linked netpoints, enabling the POSS/PLA hybrid material to recover its original shape in a very short period of time. Mya et al. also prepared PCL/POSS SMP composites by in situ polymerization. The shape fixing and recovery ratio of PCL/POSS composites were up to 98% [55].

For the SMP composites in which nanoparticles act as covalent cross-linkers, the nanoparticles not only bring about enhanced mechanical properties, but also give excellent shape-memory performance. The nanoparticles give rise to a remarkable increase in rubbery modulus (100 MPa), which is higher than that of conventional SMPs (1–10 MPa). These SMP composites with high mechanical strength have a great application prospect in the aerospace field. However, to effectively restrict the polymer chain relaxation in the deformation process, high content of nanoparticles as well as strong interactions between nanoparticles and polymer chains are often needed. Therefore, it's an important consideration to efficiently control the interactions among nanoparticles, and polymer matrix and nanoparticles.

4.2 Electro-actuated Shape-Memory Polymer Composites

Like other polymers, most SMPs are insulators. To achieve the electro-actuated SME, the conductive fillers such as CB, CF, CNTs, and graphene are usually added to SMPs. When imposing a certain voltage on the SMP composites, these conductive fillers can generate heat energy, making the temperature to increase [56]. Therefore, the electro-actuated SME could be regarded as an indirect thermal-actuated SME. Cho et al. introduced acidized CNTs into TPU matrix through solution blending, and found that the TPU/CNT composite containing 5 wt% CNTs could recover its original shape within 10 s at 40 V [57]. Tang et al. added carbon nanofibers (CNFs) into polyester SMP, and observed that the composite with 11.6 vol% CNF recovered its original shape within 90 s at 20 V [58]. Leng et al. made a series of achievements in the field of electro-actuated SMPs [41]. They introduced nickel (Ni) powders and CB nanoparticles which had a magnetic field response into PU [59]. By applying a magnetic field during the curing process of PU, the Ni powders were oriented to form Ni chains, so as to improve the electrical conductivity of composite and facilitate the heat transfer in the matrix. The composite (a) with chained Ni powders recovered faster than the composite (b) with randomly distributed Ni powders or the composite (c) with only CB (Fig. 15).

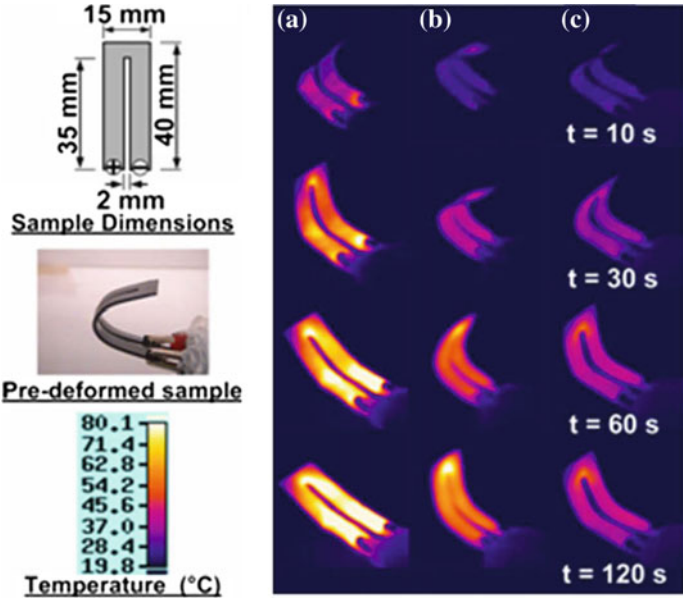

Fig. 15 Infrared thermal images showing the temperature distribution and shape recovery. Sample **a** with 10 vol% CB and 0.5 vol% chained Ni powders; sample **b** with 10 vol% CB and 0.5 vol% randomly distributed Ni powders; sample **c** with 10 vol% CB [59]. Copyright 2008, AIP Publishing, USA

There are some questions that need to be considered for electro-actuated SMP composites. First, high content of conductive fillers is usually required to realize electro-actuated SME, which may cause the aggregation of fillers and therefore is unfavorable to the shape deformation. It is important to design SMP composites with excellent conductivity at low concentration of conductive fillers. Second, during the shape deformation process, the change of shape and temperature will have a certain influence on the electrical conductivity of SMP composites, and this phenomenon is rarely reported. Therefore, when preparing electro-actuated SMP composites, it is necessary to consider factors such as filler type, filler content, deformation degree, temperature, etc.

4.3 Magnetic-Actuated Shape-Memory Polymer Composites

Magnetic-actuated SMP composites also belong to one kind of indirect thermal-actuated SMPs. The magnetic particles include Fe_2O_3, Fe_3O_4, and nickel (Ni) powder, among which Fe_3O_4 is the most commonly used filler because of its strong magnetism and low toxicity. Lendlein et al. reported that PU/Fe_3O_4 (10 wt%) composite could recover from the spiral shape to the initial flat shape in 22 s under the alternating magnetic field [60]. Zhou et al. prepared superparamagnetic Fe_3O_4 nanoparticles (with an average particle size of 10 nm) by chemical precipitation and added Fe_3O_4 nanoparticles into cross-linked PCL matrix [61]. The PCL/Fe_3O_4 composites containing 15 wt% Fe_3O_4 could recover its original shape in 130 s. The magnetic field frequency suitable for the human body is between 50 and 100 kHz. Magnetic-actuated SMP composites have potential applications in biomedical field due to their advantages of noncontact response and remote control. The thermal efficiency produced by magnetic particles, on the one hand is related to the properties of magnetic particles (such as particle size, magnetism, and surface properties), and on the other hand is related to the dispersion of magnetic particles in SMP matrix. Therefore, the preparation of superparamagnetic nanoparticles and the good dispersion of magnetic particles in SMPs are believed to be helpful in improving the magnetic-actuated shape recovery performance.

4.4 Light-Actuated Shape-Memory Polymer Composites

Because of the advantages of noncontact control, selective regional control, and efficient utilization of light, the light-actuated SMPs have received extensive attention of the researchers [62]. The light-actuated SMPs are divided into photo-sensitive SMPs and photo-thermal SMPs. Here, we mainly focus on the photo-thermal SMP composites. Photo-thermal SMP composites refer to adding fillers which are capable of photo-thermal conversion into SMP matrix. The fillers include carbon materials (such as CNTs, graphene), gold nanoparticles (AuNP), polydopamine (PDA), nanoparti-

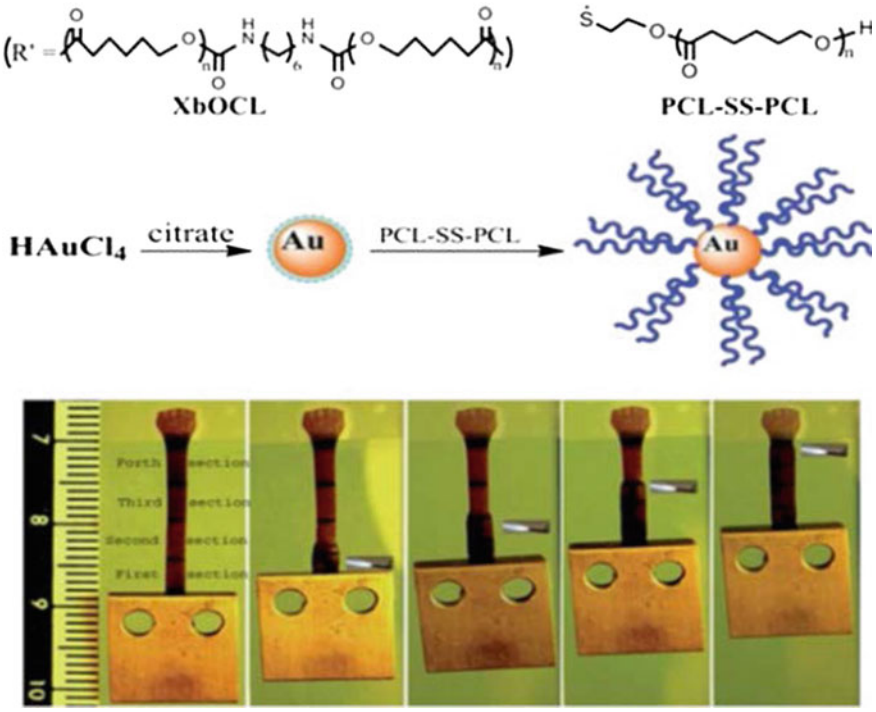

Fig. 16 Light-actuated shape-memory effect of the gold nanoparticles (AuNPs) filled SMP [65]. Copyright 2012, The Royal Society of Chemistry, UK

cles, etc. These fillers could absorb the light and convert it into heat, thus increasing the temperature and realize the light-actuated SME. For example, Koerner et al. introduced CNTs into TPU matrix [63]. The temporary shape could be fixed by the crystallization during the tensile deformation. Under the irradiation of infrared light, CNTs absorbed light and converted light energy into heat energy. When the temperature was higher than the T_m of strain-induced polymer crystallites, the TPU/CNT composite could quickly recover its original shape. Gold nanoparticle (AuNP) is regarded as an efficient photo-thermal reagent due to its surface plasma resonance [64]. Zhao et al. prepared a noncontacted light-actuated SMP composite by adding AuNPs into cross-linked poly(ε-caprolactone) [65]. Under the laser irradiation of 532 nm, AuNPs transferred light energy into heat energy, and drove the composite to recover to its original shape (Fig. 16). The shape recovery time could be well regulated via changing the intensity of the light source. In addition, the spatially controllable shape recovery behavior was achieved by irradiation to a specific area of the composite.

4.5 Solvent-Actuated Shape-Memory Polymer Composites

Thermal-actuated SMP is the most common used SMP, that is the shape recovery occurs under the thermal stimulation. However, the thermal-actuated SMP has certain limitations in the biomedical field, because excess heat may damage the surrounding biological tissues. The solvent-actuated SMP is able to solve this problem due to its mild condition and easy operation. Weder et al. and Hu et al. introduced hydrophilic cellulose nanowhisker (CNW) into PU matrix to achieve the water-actuated SME [66–68]. The elastic PU is responsible for the shape recovery performance, and the CNW network is responsible for the fixing and unfixing of temporary shape. As shown in Fig. 17, when the PU/CNW composite was immersed in water, water molecules decreased the hydrogen-bonding interactions of internal CNW network. Consequently, the PU/CNW composite became soft, and the water-actuated shape recovery behavior was then occurred. Fu et al. also reported a rapid water-actuated SMP composite based on polyvinyl alcohol (PVA) and graphene oxide (GO) [69]. When the PVA/GO composite was immersed in water, a rapid shape recovery behavior was observed at room temperature (25 °C), resulting from the decrease of T_g and storage modulus of PVA. The swelling plasticizing effect and the weakened hydrogen-bonding interactions between PVA and GO were the main reasons for the decrease.

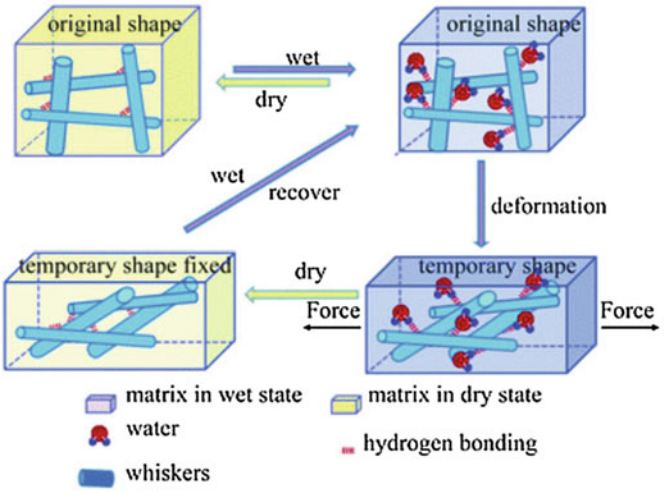

Fig. 17 Schematic illustration of water-actuated SME for PU/CNW nanocomposites containing a CNW percolation network [68]. Copyright 2012, The Royal Society of Chemistry, UK

4.6 Novel Shape-Memory Effect and Functional Applications

In addition to the reinforcing effect and a thermal stimuli, the strong confinement induced by fillers can also greatly change the thermodynamical behavior of polymers, thus imparting SMP composites with multi-SME (triple/quadrate/quintuple SME) and temperature memory effect (TME). For example, Fu et al. reported poly(propylene carbonate)/graphene oxide (PPC/GO) composites with multi-SME and TME (Fig. 18) [70]. GO formed strong hydrogen-bonding interactions with PPC chains, thus GO could be viewed as physical cross-linkers. As the content of GO increased, the topological structure of GO changed from "dotted structure" to "network structure" and "highly dense layered structure". The different GO topological structure induced different thermodynamical behavior of PPC. When the GO content was less than 10 wt%, the PPC/GO composite showed only one T_g, which was defined as a slightly confined system. Interestingly, when the GO content was higher than 10 wt%, two T_gs appeared in the PPC/GO composite, which was defined as a highly confined system. The slightly confined composites exhibited dual SME, while complex triple SME was observed in the highly confined composites. In addition, because of the broad T_g, the PPC/GO composites exhibited good TME, namely the composites could memory the initial deformation temperature. This work provides a new idea to utilize the physical confinement effect of fillers to obtain versatile SMEs, such as dual SME, triple SME and TME.

Xie et al. proposed that the utilization two different stimuli response of fillers was a flexible strategy to achieve triple SME, because the recovery of two temporary shapes would not affect each other [71]. They prepared epoxy-CNT/epoxy/epoxy-Fe_3O_4 multicomponent composites through layer by layer casting. CNTs and Fe_3O_4 could selectively generate heat at two different radiofrequency ranges (296 kHz and 13.56 MHz frequency). When the epoxy-CNT/epoxy/epoxy-Fe_3O_4 multicomponent composites were placed under two different radiofrequency fields, the multiple shape recovery behavior could be realized. This selective stimulation method enables SMPs with only a single transition temperature realize triple or multiple SME, fundamentally unshackles the dependence on multiphase structures that provide multiple transition temperatures. This approach of selective stimulation is widely applicable to other SMPs.

SMP composites with novel functions can also expand the applications of SMPs. Shape-memory-assisted self-healing is one of the functional applications of SMPs. Fu et al. reported a biodegradable SMP composite with self-healing property based on PPC/microfibrillated cellulose (MFC) [72, 73]. MFC could be viewed as reinforcing fillers, physical cross-linkers, and relaxation retarders, thus greatly improving the mechanical properties and shape-memory properties of PPC. Besides, the PPC/MFC composites showed excellent water-actuated SME upon exposure to water at 30 °C because of the hydrophilic MFC. More importantly, as shown in Fig. 19, the PPC/MFC composites exhibited much enhanced scratch resistance and scratch self-healing behavior, resulting from the reinforcement of MFC fibers and the assistance of shape-memory behavior. This composite approach opens a new way to adjust

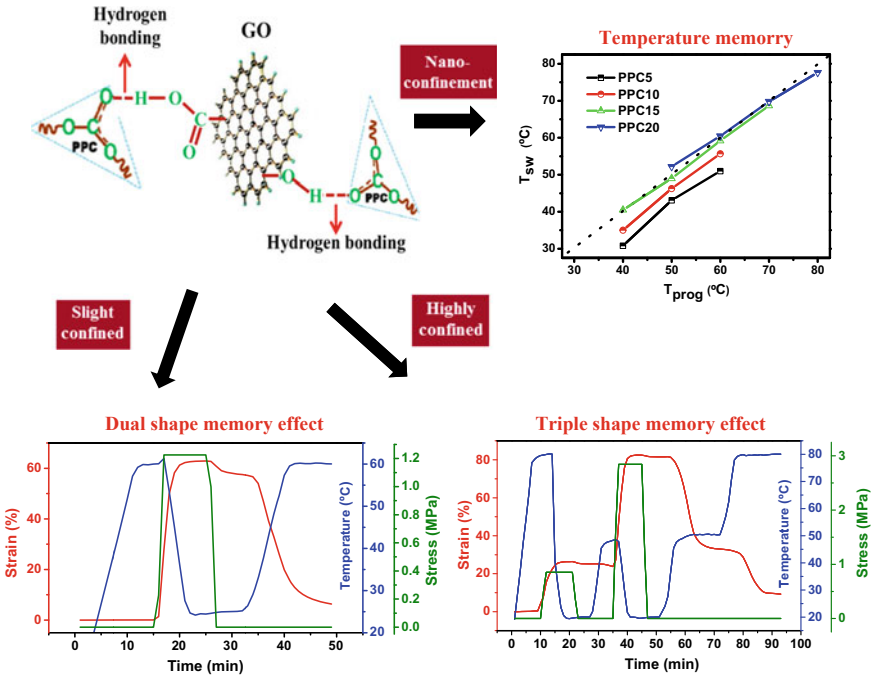

Fig. 18 Proposed hydrogen-bonding interactions between GO and PPC chains. Multi-shape-memory and temperature memory effects via strong physical confinement in PPC/GO composites [70]. Copyright 2016, American Chemical Society, USA

the shape-memory properties and promote the applications of SMPs in intelligent materials field.

5 Conclusions and Outlook

In general, SMP materials including SMP blends and composites are a kind of very significant smart materials, which not only show remarkably improved shape-memory properties, but also have novel properties such as indirect heating SME, multi (triple/quadrate/quintuple)-SME, TME, and complicated movement SME. These SMP materials show promising potential prospects in many applications including deployable space devices, remote control biomedical instruments, intelligent switches, and robot hands.

Although many studies have been done, more in-depth work still needs to be conducted. (1) First, the shape recovery force of SMPs is relatively low above T_{trans}. Though the recovery force can be increased by adding reinforcing fillers, the problems of low deformable strain and low shape recovery ratio are caused at the same

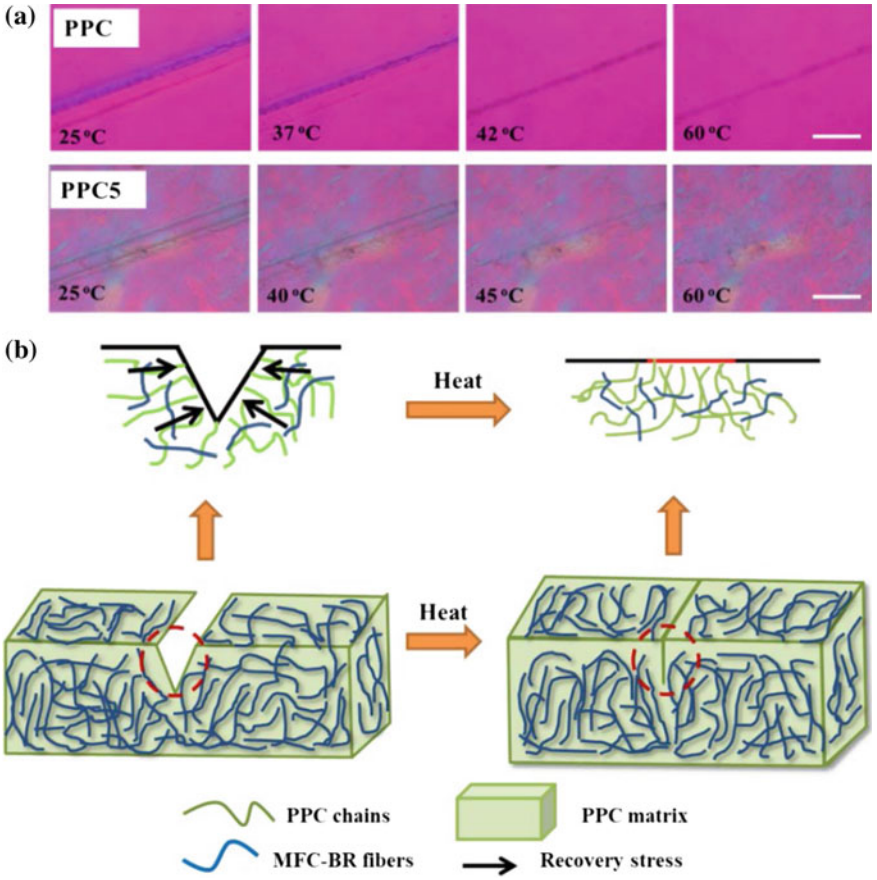

Fig. 19 **a** Polarizing optical microscopy (POM) images showing the evolution of the scratch on the surface of PPC and PPC/MFC5 (PPC5) after heating. Scale bar is 200 μm. **b** Schematic illustration of the shape-memory-assisted self-healing concept [72]. Copyright 2014, The Royal Society of Chemistry, UK

time. Thus, the mechanical properties, especially the shape recovery force of SMPs should be further improved without reducing other shape-memory properties. (2) Second, the structure–property relationship is needed to be extensively investigated. For instance, the interfacial adhesion strength of elastomer/plastic blend is important during the shape deformation and recovery process. Improving the compatibility and the interfacial adhesion strength is beneficial in improving the shape-memory properties of SMP blends. Nevertheless, little attention has been paid to this aspect at present. (3) Third, SMPs with controllable shape recovery properties (such as recovery temperature, recovery speed, recovery ratio, etc.) and complex shape-memory effect (such as multiple SME, two-way reversible SME, temperature memory effect, etc.) are preferred in more complicated applications. (4) Finally, most of the shape

recovery behaviors RE actuated through direct or indirect heating (electricity, magnetic field, light, solvent, etc.). Further studies are needed to design multi-sensitive SMPs, which can simultaneously respond to different stimuli.

References

1. Lendlein A, Kelch S (2002) Shape-memory polymers. Angew Chem Int Ed 41(12):2034
2. Hu J, Zhu Y, Huang H, Lu J (2012) Recent advances in shape-memory polymers: structure, mechanism, functionality, modeling and applications. Prog Polym Sci 37(12):1720
3. Zhao Q, Qi HJ, Xie T (2015) Recent progress in shape memory polymer: new behavior, enabling materials, and mechanistic understanding. Prog Polym Sci 49–50:79
4. Xie T (2011) Recent advances in polymer shape memory. Polymer 52(22):4985
5. Liu C, Qin H, Mather PT (2007) Review of progress in shape-memory polymers. J Mater Chem 17(16):1543
6. Wang W, Liu Y, Leng J (2016) Recent developments in shape memory polymer nanocomposites: actuation methods and mechanisms. Coord Chem Rev 320–321:38
7. Du H, Zhang J (2010) Solvent induced shape recovery of shape memory polymer based on chemically cross-linked poly(vinyl alcohol). Soft Matter 6(14):3370
8. Liu CD, Chun SB, Mather PT, Zheng L, Haley EH, Coughlin EB (2002) Chemically cross-linked polycyclooctene: synthesis, characterization, and shape memory behavior. Macromolecules 35(27):9868
9. Li J, Rodgers WR, Xie T (2011) Semi-crystalline two-way shape memory elastomer. Polymer 52(23):5320
10. Xie T, Rousseau IA (2009) Facile tailoring of thermal transition temperatures of epoxy shape memory polymers. Polymer 50(8):1852
11. Xie T, Xiao X, Cheng YT (2009) Revealing triple-shape memory effect by polymer bilayers. Macromol Rapid Commun 30(21):1823
12. Liu X, Li H, Zeng Q, Zhang Y, Kang H, Duan H, Guo Y, Liu H (2015) Electro-active shape memory composites enhanced by flexible carbon nanotube/graphene aerogels. J Mater Chem A 3(21):11641
13. Lee BS, Chun BC, Chung Y-C, Sul KI, Cho JW (2001) Structure and thermomechanical properties of polyurethane block copolymers with shape memory effect. Macromolecules 34(18):6431
14. Huang WM, Yang B, Zhao Y, Ding Z (2010) Thermo-moisture responsive polyurethane shape-memory polymer and composites: a review. J Mater Chem 20(17):3367
15. Lendlein A, Langer R (2002) Biodegradable, elastic shape-memory polymers for potential biomedical applications. Science 296(5573):1673
16. Meng Q, Hu J (2009) A review of shape memory polymer composites and blends. Compos A Appl Sci Manuf 40(11):1661
17. Liu C, Mather PT (2003) Thermomechanical characterization of blends of poly (vinyl acetate) with semicrystalline polymers for shape memory applications. In: Annual technical conference—ANTEC, conference proceedings, vol 2, pp 1962–1966
18. Behl M, Ridder U, Feng Y, Kelch S, Lendlein A (2009) Shape-memory capability of binary multiblock copolymer blends with hard and switching domains provided by different components. Soft Matter 5(3):676
19. You J, Dong W, Zhao L, Cao X, Qiu J, Sheng W, Li Y (2012) Crystal orientation behavior and shape-memory performance of poly(vinylidene fluoride)/acrylic copolymer blends. J Phys Chem B 116(4):1256
20. You J, Fu H, Dong W, Zhao L, Cao X, Li Y (2012) Shape memory performance of thermoplastic polyvinylidene fluoride/acrylic copolymer blends physically cross-linked by tiny crystals. ACS Appl Mater Interfaces 4(9):4825

21. Samuel C, Barrau S, Lefebvre J-M, Raquez J-M, Dubois P (2014) Designing multiple-shape memory polymers with miscible polymer blends: evidence and origins of a triple-shape memory effect for miscible PLLA/PMMA blends. Macromolecules 47(19):6791
22. Zhang Z-X, Qi X-D, Li S-T, Yang J-H, Zhang N, Huang T, Wang Y (2018) Water-actuated shape-memory and mechanically-adaptive poly(ethylene vinyl acetate) achieved by adding hydrophilic poly (vinyl alcohol). Eur Polymer J 98:237
23. Zhang H, Wang H, Zhong W, Du Q (2009) A novel type of shape memory polymer blend and the shape memory mechanism. Polymer 50(6):1596
24. Kurahashi E, Sugimoto H, Nakanishi E, Nagata K, Inomata K (2012) Shape memory properties of polyurethane/poly(oxyethylene) blends. Soft Matter 8(2):496
25. Liu T, Huang R, Qi X, Dong P, Fu Q (2017) Facile preparation of rapidly electro-active shape memory thermoplastic polyurethane/polylactide blends via phase morphology control and incorporation of conductive fillers. Polymer 114:28
26. Weiss RA, Izzo E, Mandelbaum S (2008) New design of shape memory polymers: mixtures of an elastomeric ionomer and low molar mass fatty acids and their salts. Macromolecules 41(9):2978
27. Song S, Feng J, Wu P (2011) A new strategy to prepare polymer-based shape memory elastomers. Macromol Rapid Commun 32:1569
28. Zhang Q, Song S, Feng J, Wu P (2012) A new strategy to prepare polymer composites with versatile shape memory properties. J Mater Chem 22(47):24776
29. Yuan D, Chen Z, Xu C, Chen K, Chen Y (2015) Fully biobased shape memory material based on novel cocontinuous structure in poly(lactic acid)/natural rubber TPVs fabricated via peroxide-induced dynamic vulcanization and in situ interfacial compatibilization. ACS Sustain Chem Eng 3(11):2856
30. Cuevas JM, Rubio R, Germán L, Laza JM, Vilas JL, Rodriguez M, León LM (2012) Triple-shape memory effect of covalently crosslinked polyalkenamer based semicrystalline polymer blends. Soft Matter 8(18):4928
31. Zhang Z-X, Wei X, Yang J-H, Zhang N, Huang T, Wang Y, Gao X-L (2016) Triple-shape memory materials based on cross-linked poly(ethylene vinyl acetate) and poly(ε-caprolactone). Ind Eng Chem Res 55(47):12232
32. Zhao J, Chen M, Wang X, Zhao X, Wang Z, Dang ZM, Ma L, Hu GH, Chen F (2013) Triple shape memory effects of cross-linked polyethylene/polypropylene blends with cocontinuous architecture. ACS Appl Mater Interfaces 5(12):5550
33. Li F, Chen Y, Zhu W, Zhang X, Xu M (1998) Shape memory effect of polyethylene/nylon 6 graft copolymers. Polymer 39(26):6929
34. Suchao-in K, Chirachanchai S (2013) "Grafting to" as a novel and simple approach for triple-shape memory polymers. ACS Appl Mater Interfaces 5(15):6850
35. Chen Y, Chen K, Wang Y, Xu C (2015) Biobased heat-triggered shape-memory polymers based on polylactide/epoxidized natural rubber blend system fabricated via peroxide-induced dynamic vulcanization: co-continuous phase structure, shape memory behavior, and interfacial compatibilization. Ind Eng Chem Res 54(35):8723
36. Xu C, Lin B, Liang X, Chen Y (2016) Zinc dimethacrylate induced in situ interfacial compatibilization turns EPDM/PP TPVs into a shape memory material. Ind Eng Chem Res 55(16):4539
37. Du J, Armstrong SR, Baer E (2013) Co-extruded multilayer shape memory materials: comparing layered and blend architectures. Polymer 54(20):5399
38. Zheng Y, Dong R, Shen J, Guo S (2016) Tunable shape memory performances via multilayer assembly of thermoplastic polyurethane and polycaprolactone. ACS Appl Mater Interfaces 8(2):1371
39. Luo X, Mather PT (2009) Preparation and characterization of shape memory elastomeric composites. Macromolecules 42(19):7251
40. Luo X, Mather PT (2010) Triple-shape polymeric composites (TSPCs). Adv Func Mater 20(16):2649
41. Liu Y, Lv H, Lan X, Leng J, Du S (2009) Review of electro-active shape-memory polymer composite. Compos Sci Technol 69(13):2064

42. Zhang Z-X, Wang W-Y, Yang J-H, Zhang N, Huang T, Wang Y (2016) Excellent electroactive shape memory performance of EVA/PCL/CNT blend composites with selectively localized CNTs. J Phys Chem C 120(40):22793
43. Qi X, Dong P, Liu Z, Liu T, Fu Q (2016) Selective localization of multi-walled carbon nanotubes in bi-component biodegradable polyester blend for rapid electroactive shape memory performance. Compos Sci Technol 125:38
44. Wang Z, Zhao J, Chen M, Yang M, Tang L, Dang ZM, Chen F, Huang M, Dong X (2014) Dually actuated triple shape memory polymers of cross-linked polycyclooctene-carbon nanotube/polyethylene nanocomposites. ACS Appl Mater Interfaces 6(22):20051
45. Zhang ZX, Dou JX, He JH, Xiao CX, Shen LY, Yang JH, Wang Y, Zhou ZW (2017) Electrically/infrared actuated shape memory composites based on a bio-based polyester blend and graphene nanoplatelets and their excellent self-driven ability. J Mater Chem C 5(17):4145
46. Qi X, Xiu H, Wei Y, Zhou Y, Guo Y, Huang R, Bai H, Fu Q (2017) Enhanced shape memory property of polylactide/thermoplastic poly(ether)urethane composites via carbon black self-networking induced co-continuous structure. Compos Sci Technol 139:8
47. Wei Y, Huang R, Dong P, Qi X-D, Fu Q (2018) Preparation of polylactide/poly(ether)urethane blends with excellent electro-actuated shape memory via incorporating carbon black and carbon nanotubes hybrids fillers. Chin J Polym Sci 36(10):1175
48. Leng J, Lan X, Liu Y, Du S (2011) Shape-memory polymers and their composites: stimulus methods and applications. Prog Mater Sci 56(7):1077
49. Mu T, Liu L, Lan X, Liu Y, Leng J (2018) Shape memory polymers for composites. Compos Sci Technol 160:169
50. Meng H, Li G (2013) A review of stimuli-responsive shape memory polymer composites. Polymer 54(9):2199
51. Miaudet P, Derre A, Maugey M, Zakri C, Piccione PM, Inoubli R, Poulin P (2007) Shape and temperature memory of nanocomposites with broadened glass transition. Science 318(5854):1294
52. Zhang Y, Wang Q, Wang C, Wang T (2011) High-strain shape memory polymer networks crosslinked by SiO_2. J Mater Chem 21(25):9073
53. Agarwal P, Chopra M, Archer LA (2011) Nanoparticle netpoints for shape-memory polymers. Angew Chem Int Ed 50(37):8670
54. Xu J, Song J (2010) High performance shape memory polymer networks based on rigid nanoparticle cores. Proc Natl Acad Sci USA 107(17):7652
55. Mya KY, Gose HB, Pretsch T, Bothe M, He C (2011) Star-shaped POSS-polycaprolactone polyurethanes and their shape memory performance. J Mater Chem 21(13):4827
56. Chen J, Zhang Z-X, Huang W-B, Li J-L, Yang J-H, Wang Y, Zhou Z-W, Zhang J-H (2015) Carbon nanotube network structure induced strain sensitivity and shape memory behavior changes of thermoplastic polyurethane. Mater Des 69:105
57. Cho JW, Kim JW, Jung YC, Goo NS (2005) Electroactive shape-memory polyurethane composites incorporating carbon nanotubes. Macromol Rapid Commun 26(5):412
58. Tang Z, Sun D, Yang D, Guo B, Zhang L, Jia D (2013) Vapor grown carbon nanofiber reinforced bio-based polyester for electroactive shape memory performance. Compos Sci Technol 75:15
59. Leng JS, Huang WM, Lan X, Liu YJ, Du SY (2008) Significantly reducing electrical resistivity by forming conductive Ni chains in a polyurethane shape-memory polymer/carbon-black composite. Appl Phys Lett 92(20):204101
60. Mohr R, Kratz K, Weigel T, Lucka-Gabor M, Moneke M, Lendlein A (2006) Initiation of shape-memory effect by inductive heating of magnetic nanoparticles in thermoplastic polymers. Proc Natl Acad Sci USA 103(10):3540
61. Yu X, Zhou S, Zheng X, Guo T, Xiao Y, Song B (2009) A biodegradable shape-memory nanocomposite with excellent magnetism sensitivity. Nanotechnology 20(23):235702
62. Habault D, Zhang H, Zhao Y (2013) Light-triggered self-healing and shape-memory polymers. Chem Soc Rev 42(17):7244
63. Koerner H, Price G, Pearce NA, Alexander M, Vaia RA (2004) Remotely actuated polymer nanocomposites–stress-recovery of carbon-nanotube-filled thermoplastic elastomers. Nat Mater 3(2):115

64. Ge F, Lu X, Xiang J, Tong X, Zhao Y (2017) An optical actuator based on gold-nanoparticle-containing temperature-memory semicrystalline polymers. Angew Chem Int Ed 56(22):6126
65. Zhang H, Xia H, Zhao Y (2012) Optically triggered and spatially controllable shape-memory polymer-gold nanoparticle composite materials. J Mater Chem 22(3):845
66. Capadona JR, Shanmuganathan K, Tyler DJ, Rowan SJ, Weder C (2008) Stimuli-responsive polymer nanocomposites inspired by the sea cucumber dermis. Science 319(5868):1370
67. Mendez J, Annamalai PK, Eichhorn SJ, Rusli R, Rowan SJ, Foster EJ, Weder C (2011) Bioinspired mechanically adaptive polymer nanocomposites with water-activated shape-memory effect. Macromolecules 44(17):6827
68. Zhu Y, Hu J, Luo H, Young RJ, Deng L, Zhang S, Fan Y, Ye G (2012) Rapidly switchable water-sensitive shape-memory cellulose/elastomer nano-composites. Soft Matter 8(8):2509
69. Qi X, Yao X, Deng S, Zhou T, Fu Q (2014) Water-induced shape memory effect of graphene oxide reinforced polyvinyl alcohol nanocomposites. J Mater Chem A 2(7):2240
70. Qi X, Guo Y, Wei Y, Dong P, Fu Q (2016) Multi-shape and temperature memory effects via strong physical confinement in poly(propylene carbonate)/graphene oxide nanocomposites. J Phys Chem B 120:11064
71. He Z, Satarkar N, Xie T, Cheng YT, Hilt JZ (2011) Remote controlled multishape polymer nanocomposites with selective radiofrequency actuations. Adv Mater 23(28):3192
72. Qi XD, Yang GH, Jing MF, Fu Q, Chiu FC (2014) Microfibrillated cellulose-reinforced bio-based poly(propylene carbonate) with dual shape memory and self-healing properties. J Mater Chem A 2(47):20393
73. Qi X, Jing M, Liu Z, Dong P, Liu T, Fu Q (2016) Microfibrillated cellulose reinforced bio-based poly(propylene carbonate) with dual-responsive shape memory properties. RSC Adv 6(9):7560

Rheology of Shape-Memory Polymers, Polymer Blends, and Composites

Sanjay Mavinkere Rangappa, Suchart Siengchin and Jyotishkumar Parameswaranpillai

Abstract Shape-memory polymers (SMPs) have attracted considerable attention in recent decades due to the characteristics of switching from permanent shape to temporary shape and vice versa by the application of an external stimulus. The significance and diverse applications of SMPs in the scientific and commercial scope generate researchers to have keen knowledge in the manufacturing of new shape-memory polymers and their blends and composites with improved thermomechanical and other desired properties. This chapter will provide a generalized view on the rheology of SMPs and their blends and composites that would give a holistic picture of this promising area of research.

1 Introduction

Shape-memory polymers (SMPs) are smart polymeric materials capable of returning from a deformed state to their original shape and vice versa induced by an external stimulus such as temperature, electricity, magnetic field, UV light, change in pH, etc. [1–5]. SMPs are materials with great potential for the use in intelligent materials and structures [6–9]. The advantages of SMPs over shape-memory alloy and ceramics are excellent elastic deformation, greater recoverable strain, low cost, and lightweight [10, 11]. Polynorbornene, epoxy resin, polyurethane, poly(ε-caprolactone), etc. are the generally used SMPs [12–17]. Owing to this, SMPs have found promising applications in fields as diverse as medicine (e.g., vascular stents and surgical sutures) [18], flexible electronics, actuators, deployable space structures, and transport (e.g.,

S. M. Rangappa · S. Siengchin
Department of Mechanical and Process Engineering, The Sirindhorn International Thai-German Graduate School of Engineering (TGGS), King Mongkut's University of Technology North Bangkok, Bangkok, Thailand

J. Parameswaranpillai (✉)
Center of Innovation in Design and Engineering for Manufacturing, King Mongkut's University of Technology North Bangkok, 1518 Pracharaj 1, Wongsawang Road, Bangsue, Bangkok 10800, Thailand
e-mail: jyotishkumarp@gmail.com

J. Parameswaranpillai et al. (eds.), *Shape Memory Polymers, Blends and Composites*, Advanced Structured Materials 115,
https://doi.org/10.1007/978-981-13-8574-2_4

automobiles fenders, wings morphing), aerospace applications [19–22], and new application areas such as repair of cracks and scratches in coatings [5, 23].

Polymers blends and composites are smart and economical materials for the development of new and improved polymeric materials that are difficult to obtain by direct polymerization process [24–27]. The advantages of manufacturing shape-memory polymer blends and composites are better shape recovery stress, simple technology, tuning of shape-memory transition temperature, and also SMPs sensitive to electricity, magnetic field, UV light, solvent, etc., could be developed [28, 29]. Several shape-memory polymer blends have been reported by several authors including polyethylene/nylon 6 [30], PVDF/PMMA [31], poly(D,L-lactide)/hydroxyapatite [32], etc. The SMP composites containing nanofillers, such as carbon black [33], carbon nanotube (CNTs) [34], carbon nanofiber (CNF)/SMP [35], etc., have been reported.

2 Rheology of Shape-Memory Polymers

Rheology studies of SMPs enable the understanding of the processing of the polymers. Since the rheological performance of polymers depends on a large extent on the molar mass, processing temperature, and shear rate [36], the parameters obtained from the rheological experiments are storage modulus, loss modulus, tan delta, complex viscosity, shear stress, etc. The variations of above-said parameters with respect to time, temperature, frequency, shear strain, etc., give an overview of the morphology, polymer structure, phase separation, progress in curing, gelation (crossover point), verification (the final plateau region in the rheological profile), etc. In thermosetting SMP's systems like epoxy, phenol formaldehyde, polyurethanes, etc., the rheology can be used to study the curing of thermosets (either by isothermal curing or by dynamic curing), the phase separation process, changes in phase morphology, extend of phase separation, etc. [37–41]. Figure 1 shows the rheological profile of neat epoxy and 10 wt% ABS-modified epoxy blends. For neat epoxy system, a typical rheological profile is observed (Fig. 1a). But for the 10 wt% ABS-modified epoxy blend system, the phase separation took place at ca 600 s, and this is confirmed by the drop in tan δ and the rise in G′ and G″ [37].

In thermoplastic SMPs, the rheology enables the understanding of polymer structure, molecular weight, branching in polymers, processing parameters, etc. [42]. In thermoplastic polymer blends, the phase separation, changes in phase morphology, extend of phase separation, etc. can be easily studied by rheological studies [43, 44]. For polymer composites, the filler dispersion, interactions between the filler and polymer, polymer–polymer interactions, and filler–filler interactions can be carefully analyzed using rheological studies [45–48].

The different stages of shape-memory cycles are the deformation of the permanent shape above T_g or T_m by the application of external stress, and this is followed by slow cooling to room temperature with the applied external stress for shape fixing. Once the stress is released, the temporary shape is fixed. Upon heating again, the

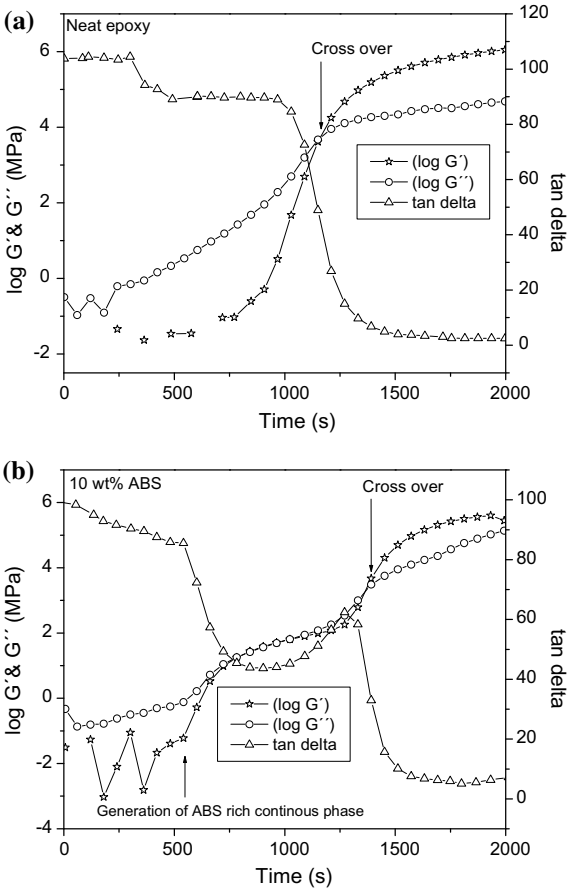

Fig. 1 Rheology of **a** neat epoxy, **b** 10 wt% ABS different ABS-modified epoxy blends at 180 °C [37]

SMPs regain its original permanent shape. The breaking of the cross-linking chains and their reforming during the shape-memory process are shown in Fig. 2 [10].

Different rheological models were introduced by the scientists for the study of the shape-memory process in SMPs. Some of the interesting works are mentioned as follows. Bhattacharyya et al. [49] derived the mechanical response of a four-element rheological model for shape-memory polyurethane under the conditions of constant stress (creep), constant strain (stress relaxation), constant stress rate, constant strain rate, and periodic strain for the better understanding of the performance of shape-memory polyurethane. They found that the shape-memory strain/damping could be considerably reduced by the application of frequency higher than the threshold frequency. The damping or shape-memory strain is maximum at the glass transition temperature. Recently, Hosseini et al. [50] introduced a rheological model for the understanding of the change in the size of the SMPs with respect to temperature. The developed nonlinear viscoelastic model allows the better understanding of the

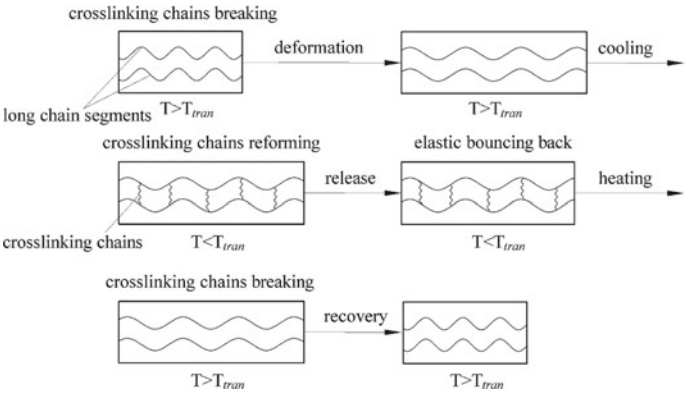

Fig. 2 Breaking of the cross-linking chains and reforming during the shape-memory process [10]. (Reproduced with permission from Elsevier, License Number-4502761431416)

production of heat-shrinkable SMPs. In another work, Liu et al. [51] developed a small-scale constitutive model for SMPs to study the strain and stress recovery at the molecular level during the shape-memory cycle. Inomata et al. [52] studied the shape-memory effect of poly (methyl methacrylate)-graft-poly (ethylene glycol) copolymers. Interestingly, the copolymer shows excellent shape-memory effect because of the physical cross-links formed due to the entanglements of the copolymer chains, confirmed by the stress relaxation studies of the SMPs.

3 Rheology of Polymer Blends and Composites

García-Huete et al. [5] studied the rheology of polycyclooctene (PCO)/poly(ethylene-co-methacrylic acid) (EMAA) zinc ionomer (Surlyn 9520) shape-memory blend for the study of self-healing. They observe a crossover for Surlyn 9520 in the range of 0.01–0.1 Hz, suitable for good healing, but PCO is a poor healing agent and shows a crossover at ca. 20 Hz. Three different blend systems were prepared 30/70, 50/50, and 70/30 with 3 wt% DCP. The authors claim that only 30/70 (PCO/Surlyn 9520) blend is suitable for self-healing, which shows a crossover at a lower frequency range. Ping et al. [53] prepared poly(ε-caprolactone)-segmented polyurethane-based shape-memory polymers. The phase separation of the hard segments in the PCL matrix was carefully analyzed by rheological measurements. The hard segments and the PCL crystals impart shape-memory properties for the PCL-segmented PU system. Sungsanit et al. [54] investigated the rheological properties of linear PLA (L-PLA) plasticized with varying content of poly(ethylene glycol) (PEG). The authors observed reduced viscosity and modulus with increasing PEG content. Feng et al. [55] successfully synthesized PLA/poly(ethylene glycol)-succinate copolymer (PES) and PLA/poly(ethylene glycol)-succinate-l-lactide copolymer (PESL) blends. They

observed a shear thinning behavior for both the blends and also the blends showed reduced viscosity and modulus with an increasing amount of PES and PESL. The rheological behaviors of PLA/PES and PLA/PESL are shown in Fig. 3.

Wei et al. [56] prepared hybrid composites containing both carbon black (CB) and carbon nanotubes (CNTs) in a 70/30 blend of polylactide (PLA)/thermoplastic poly(ether)urethane (TPU) for the making of an electrically actuated shape-memory polymer composites. The concentrations of the CB and CNTs used for making the composites are CB (3 phr, 5 phr) and CNTs (0, 0.25 phr, 0.5 phr, 0.75 phr, 1.0 phr, 2.0 phr). The rheology of the polymer composites was studied for the understanding of the filler–filler interaction and polymer–filler interaction. The authors observed a percolation threshold (filler network formation) for all the composites prepared. Similarly, the percolation threshold in multiwalled carbon nanotube/polycarbonate and multiwalled carbon nanotube/poly(methyl methacrylate) composites was reported by Pötschke et al. [57, 58].

In a more recent work, Chen et al. [59] studied the network formation of CNTs in thermoplastic polyurethane (TPU) by rheological measurements. From the rheological results, 2 wt% CNT provides a moderate level of network formation in the polymer matrix. On the other hand, a dense network of nanofillers is formed in the polymer composites at higher concentrations. The network formation by the CNTs affects the stress/strain curve (stress increases considerably at higher filler content). Similarly, storage modulus increases and the T_g shifted to higher temperatures due to the reduced mobility of the polymer chains because of the network formation with increasing filler content. The strain sensitivity and shape-memory performance of the composites can also be tuned with increasing filler content. In another work, Haghayegh et al. [60] studied the network formation in shape-memory polyurethane/clay nanocomposites using rheology. The best shape-memory properties were obtained for the composites containing 1 wt% clay.

Kim et al. [61] used rheology for the study of filler (Na-MMT intercalated with a PEG) dispersion and role of Na-MMT intercalated with a PEG as a physical cross-link in poly(ethyl methacrylate) (PEMA) nanocomposites. The authors observed a pseudo-solid behavior of the composites from the rheological results. This pseudo-solid behavior is due to the better dispersion of the Na-MMT fillers within the polymer matrix, also the nanofillers intercalated with a PEG acts as effective physical cross-links for the polymer composites even at 1.2 wt% filler content. In an interesting work, Meng et al. [62] developed shape-memory polyurethane/multiwalled carbon nanotube fibers. The fibers were spun by a single screw extruder. The authors observed that the spinnability is significantly reduced with increasing MWCNTs. In fact, at 8 wt% MWCNTs the spinnability of the composites is completely lost due to its poor rheological properties. Gelfer et al. [63] introduced organoclay in polystyrene (PS), poly(methyl methacrylate) (PMMA), and PS/PMMA blends by the melt blending process. The authors studied the rheology of the polymer composites for the understanding of the interactions of the filler with the polymer matrix. They found that the organoclay has no effect on the rheological properties of the polymers, which means the fillers have no interaction/weak interaction with the neat polymers or polymer blends.

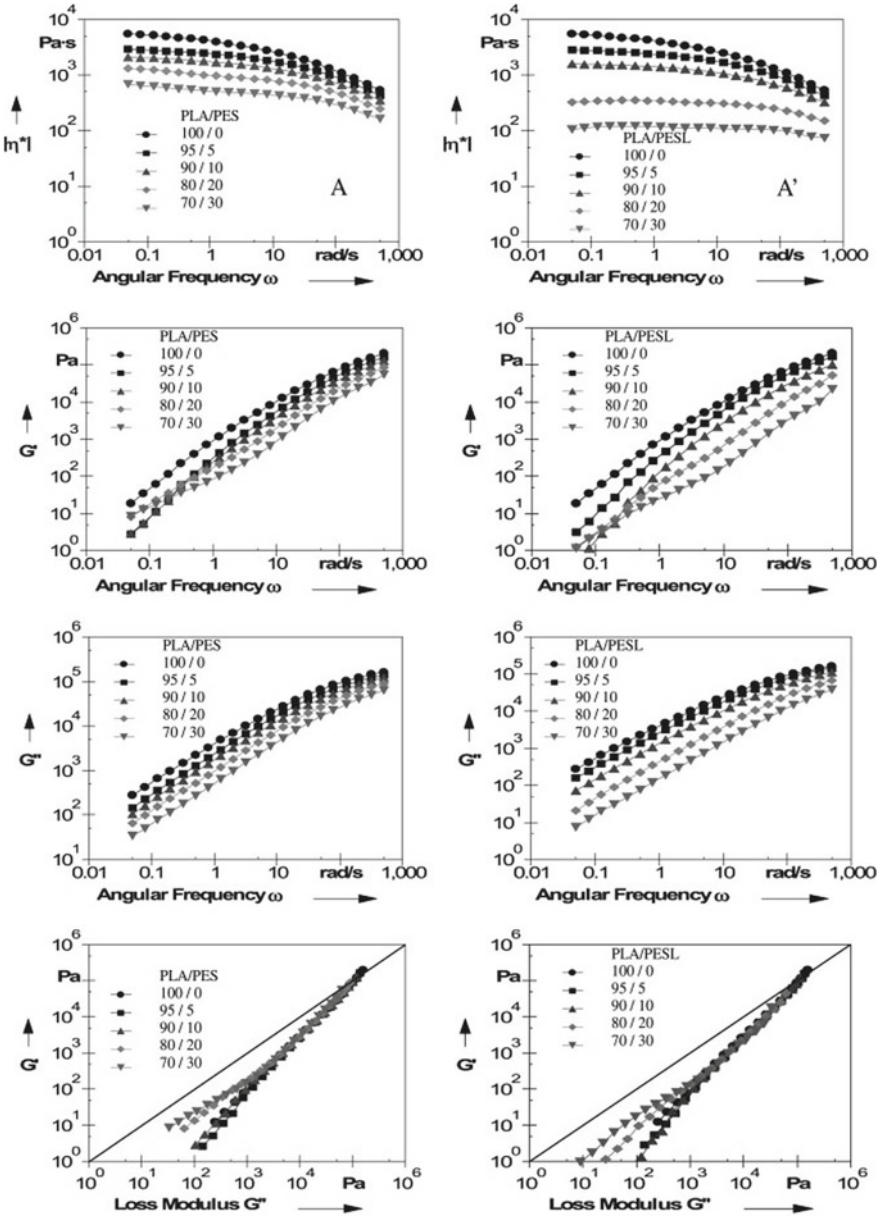

Fig. 3 The rheological behavior of PLA/PES and PLA/PESL blends [55]. (Reproduced with permission from Elsevier, License Number-4502771066270)

4 Conclusion

Rheological studies of polymers, polymer blends, and composites give an overview of polymer structure, phase morphology, phase separation, polymer–polymer interaction, polymer filler interactions, filler dispersion, etc. The processing and shape-memory performance of the polymer depends on all the above-said parameters, underlining the importance of rheological measurements of SMPs for advanced applications.

References

1. Lendlein A, Kelch S (2002) Shape-memory polymers. Angew Chem Int Edit 41(12):2034–2057
2. Hager MD, Bode S, Weber C, Schubert US (2015) Shape memory polymers: past, present and future developments. Prog Polym Sci 49–50:3–33
3. Safranski DL, Griffis JC (2017) Shape-memory polymer device design. Elsevier
4. Parameswaranpillai J, Ramanan SP, George JJ, Jose S, Zachariah AK, Siengchin S, Yorseng K, Janke A, Pionteck J (2018) PEG-ran-PPG modified epoxy thermosets: a simple approach to develop tough shape memory polymers. Ind Eng Chem Res 57:3583–3590
5. García-Huete N, Post W, Laza JM, Vilas JL, León LM, García SJ (2018) Effect of the blend ratio on the shape memory and self-healing behaviour of ionomer-polycyclooctene crosslinked polymer blends. Eur Polym J 98:154–161
6. Hu J, Zhu Y, Huang H, Lu J (2012) Recent advances in shape–memory polymers: structure, mechanism, functionality, modeling and applications. Prog Polym Sci 37:1720–1763
7. Berg GJ, McBride MK, Wang C, Bowman CN (2014) New directions in the chemistry of shape memory polymers. Polymer 55(23):5849–5872
8. Butaud P, Placet V, Klesa J, Ouisse M, Foltête E, Gabrion X (2015) Investigations on the frequency and temperature effects on mechanical properties of a shape memory polymer (veriflex). Mech Mater 87:50–60
9. Pilate F, Toncheva A, Dubois P, Raquez JM (2016) Shape-memory polymers for multiple applications in the materials world. Eur Polym J 80:268–294
10. Fan P, Chen W, Zhao B, Hu J, Gao J, Fang G, Peng F (2018) Formulation and numerical implementation of tensile shape memory process of shape memory polymers. Polymer 148:370–381
11. Liu C, Qin H, Mather PT (2007) Review of progress in shape-memory polymers. J Mater Chem 17(16):1543–1558
12. Nagata N (1990) Development of polynorbornene-based shape-memory resins. Kagaku (Kyoto) 45:554–557
13. Santo L, Quadrini F, Shape Memory Materials from Epoxy Matrix Composites, Smart Polymer Nanocomposites (2017) Springer International Publishing AG
14. Santo L, Quadrini F, Villadei W, Mascetti G, Zolesi V (2015) Shape memory epoxy foams and composites: Ribes_foam2 experiment on spacecraft "Bion-m1" and future perspective. Procedia Engineering 104:50–56
15. Jung YC, Cho JW (2010) Application of shape memory polyurethane in orthodontic". J Mater Sci Mater Med 21:2881–2886
16. Jing X, Mi HY, Huang HX, Turng LS (2016) Shape memory thermoplastic polyurethane (TPU)/poly(ε-caprolactone) (PCL) blends as self-knotting sutures". J Mech Behav Biomed Mater 64:94–103
17. Tian G, Zhu G, Ren T, Liu Y, Wei K, Liu YX (2019) The effects of PCL diol molecular weight on properties of shape memory poly (ε-caprolactone) networks. J Appl Polym Sci 136(6):47055

18. Buckley PR, McKinley GH, Wilson TS, Small W, Benett WJ, Bearinger JP, McElfresh MW, Maitland DJ (2006) Inductively heated shape memory polymer for the magnetic actuation of medical devices. IEEE Trans Biomed Eng 53(10):2075–2083
19. Liu Y, Du H, Liu L, Leng J (2014) Shape memory polymers and their composites in aerospace applications: a review. Smart Mater Struct 23(2):023001
20. Leng J, Lan X, Liu Y, Du S (2011) Shape-memory polymers and their composites: stimulus methods and applications. Prog Mater Sci 56(7):1077–1135
21. Cuevas JM, Laza JM, Rubio R, German L, Vilas JL, León LM (2011) Development and characterization of semi-crystalline polyalkenamer based shape memory polymers. Smart Mater Struct 20(3):035003
22. Tcharkhtchi A, Abdallah-Elhirtsi S, Ebrahimi K, Fitoussi J, Shirinbayan M, Farzaneh S (2014) Some new concepts of shape memory effect of polymers. Polymers 6(4):1144–1163
23. Luo XF, Mather PT (2013) Shape memory assisted self-healing coating. ACS Macro Lett 2:152–156
24. Chatterjee T, Dutta J, Naskar K (2018) Unique shape memory behavior of polyolefinic blends with special reference to creep behavior, stress relaxation, and melt rheological study. Polym Eng Sci 58(6):876–885
25. Cuevas JM, Rubio R, Germán L, Laza JM, Vilas JL, Rodriguez M, León LM (2012) Triple-shape memory effect of covalently crosslinked polyalkenamer based semicrystalline polymer blends. Soft Matter 8(18):4928–4935
26. Qi X, Dong P, Liu Z, Liu T, Fu Q (2016) Selective localization of multi-walled carbon nanotubes in bi-component biodegradable polyester blend for rapid electroactive shape memory performance. Compos Sci Technol 125:38–46
27. Qi X, Xiu H, Wei Y, Zhou Y, Guo Y, Huang R, Bai H, Fu Q (2017) Enhanced shape memory property of polylactide/thermoplastic poly(ether)urethane composites via carbon black self-networking induced co-continuous structure. Compos Sci Technol 139:8–16
28. Parameswaranpillai J, Sreekanth PM, Jose S, Siengchin S, Magueresse A, Janke A, Pionteck J (2017) Shape memory properties of epoxy/PPO-PEO-PPO triblock copolymer blends with tunable thermal transitions and mechanical characteristics. Ind Eng Chem Res 56(47):14069–14077
29. Meng Q, Hu J (2009) A review of shape memory polymer composites and blends. Compos Part A Appl Sci Manuf 40(11):1661–1672
30. Li F, Chen Y, Zhu W, Zhang X, Xu M (1998) Shape memory effect of polyethylene/nylon 6 graft copolymers. Polymer 39:6929–6934
31. Campo CJ, Mather PT (2005) PVDF: PMMA shape memory blends: effect of short carbon fiber addition. Polym Mater Sci Eng 93:933–934
32. Zheng XT, Zhou SB, Li XH, Weng H (2006) Shape memory properties of poly(D, L-lactide)/hydroxyapatite composites. Biomaterials 27:4288–4295
33. Li F, Qi L, Yang J, Xu M, Luo X, Ma D (2000) Polyurethane/conducting carbon black composites: structure, electric conductivity, strain recovery behavior, and their relationships. J Appl Polym Sci 75:68–77
34. Fei GX, Li G, Wu LS, Xia HS (2012) A spatially and temporally controlled shape memory process for electrically conductive polymer-carbon nanotube composites. Soft Matter 8:5123–5126
35. Powers DS, Vaia RA, Koerner H, Serres J, Mirau PA (2008) NMR characterization of low hard segment thermoplastic polyurethane/carbon nanofiber composites. Macromolecules 41:4290–4295
36. Lim LT, Auras R, Rubino M (2008) Processing technologies for poly (lactic acid). Prog Polym Sci 33(8):820–852
37. Jyotishkumar P, Pionteck J, Özdilek C, Moldenaers P, Cvelbar U, Mozetic M, Thomas S (2011) Rheology and pressure–volume–temperature behavior of the thermoplastic poly (acrylonitrile-butadiene-styrene)-modified epoxy-DDS system during reaction induced phase separation. Soft Matter 7(16):7248–7256
38. Jyotishkumar P, Moldenaers P, George SM, Thomas S (2012) Visco-elastic phase separation in thermoplastic poly (styrene -acrylonitrile)-modified epoxy-DDM system during reaction induced phase separation. Soft Matter 8:7452–7462

39. Parameswaranpillai J, Moldenaers P, Thomas S (2013) Rheological study of the SAN modified epoxy–DDM system: relationship between viscosity and viscoelastic phase separation. RSC Adv 3(46):23967–23971
40. Artmann A, Bianchi O, Soares MR, Nunes RC (2010) Rheokinetic investigations on the thermal cure of phenol-formaldehyde novolac resins. Mater Sci Eng C 30(8):1245–1251
41. Lucio B, de la Fuente JL (2016) Kinetic and thermodynamic analysis of the polymerization of polyurethanes by a rheological method. Thermochim Acta 625:28–35
42. Dorgan JR, Williams JS, Lewis DN (1999) Melt rheology of poly (lactic acid): entanglement and chain architecture effects. J Rheol 43(5):1141–1155
43. Van Puyvelde P, Velankar S, Moldenaers P (2001) Rheology and morphology of compatibilized polymer blends. Curr Opin Colloid Interface Sci 6(5–6):457–463
44. Han JH, Choi-Feng C, Li DJ, Han CD (1995). Effect of flow geometry on the rheology of dispersed two-phase blends of polystyrene and poly (methyl methacrylate). Polymer: 36(12):2451–2462
45. Bose S, Bhattacharyya AR, Kulkarni AR, Pötschke P (2009) Electrical, rheological and morphological studies in co-continuous blends of polyamide 6 and acrylonitrile–butadiene–styrene with multiwall carbon nanotubes prepared by melt blending. Compos Sci Technol 69(3–4):365–372
46. Bose S, Bhattacharyya AR, Kodgire PV, Misra A, Pötschke P (2007) Rheology, morphology, and crystallization behavior of melt-mixed blends of polyamide6 and acrylonitrile-butadiene-styrene: Influence of reactive compatibilizer premixed with multiwall carbon nanotubes. J Appl Polym Sci 106(5):3394–3408
47. Singh S, Ghosh AK, Maiti SN, Raha S, Gupta RK, Bhattacharya S (2012) Morphology and rheological behavior of polylactic acid/clay nanocomposites. Polym Eng Sci 52(1):225–232
48. Abraham TN, Ratna D, Siengchin S, Karger-Kocsis J (2008) Rheological and thermal properties of poly (ethylene oxide)/multiwall carbon nanotube composites. J Appl Polym Sci 110(4):2094–2101
49. Bhattacharyya A, Tobushi H (2000) Analysis of the isothermal mechanical response of a shape memory polymer rheological model. Polym Eng Sci 40(12):2498–2510
50. Hosseini H, Berdyshev BV, Iskopintsev I (2015) Rheological modeling for shape-memory thermoplastic polymers. World Acad Sci Eng Technol Int J Chem Mol Nucl Mater Metallurg Eng 9(8):980–983
51. Liu Y, Gall K, Dunn ML, Greenberg AR, Diani J (2006) Thermomechanics of shape memory polymers: uniaxial experiments and constitutive modeling. Int J Plasticity 22(2):279–313
52. Inomata K, Nakagawa K, Fukuda C, Nakada Y, Sugimoto H, Nakanishi E (2010) Shape memory behavior of poly (methyl methacrylate)-graft-poly (ethylene glycol) copolymers. Polymer 51(3):793–798
53. Ping P, Wang W, Chen X, Jing X (2007) The influence of hard-segments on two-phase structure and shape memory properties of PCL-based segmented polyurethanes. J Polym Sci B 45(5):557–570
54. Sungsanit K, Kao N, Bhattacharya SN (2012) Properties of linear poly (lactic acid)/polyethylene glycol blends. Polym Eng Sci 52(1):108–116
55. Feng L, Bian X, Chen Z, Li G, Chen X (2013) Mechanical, aging, optical and rheological properties of toughening polylactide by melt blending with poly (ethylene glycol) based copolymers. Polym Degrad Stab 98(9):1591–1600
56. Wei Y, Huang R, Dong P, Qi XD, Fu Q (2018) Preparation of polylactide/poly (ether) urethane blends with excellent electro-actuated shape memory via incorporating carbon black and carbon nanotubes hybrids fillers. Chin J Polym Sci 36(10):1175–1186
57. Pötschke P, Fornes TD, Paul DR (2002) Rheological behavior of multiwalled carbon nanotube/polycarbonate composites. Polymer 43(11):3247–3255
58. McClory C, McNally T, Baxendale M, Pötschke P, Blau W, Ruether M (2010) Electrical and rheological percolation of PMMA/MWCNT nanocomposites as a function of CNT geometry and functionality. Eur Polym J 46(5):854–868

59. Chen J, Zhang ZX, Huang WB, Yang JH, Wang Y, Zhou ZW, Zhang JH (2015) Carbon nanotube network structure induced strain sensitivity and shape memory behavior changes of thermoplastic polyurethane. Mater Des 69:105–113
60. Haghayegh M, Mir Mohamad Sadeghi G (2012) Synthesis of shape memory polyurethane/clay nanocomposites and analysis of shape memory, thermal, and mechanical properties. Polym Compos 33(6):843–849
61. Kim MS, Jun JK, Jeong HM (2008) Shape memory and physical properties of poly (ethyl methacrylate)/Na-MMT nanocomposites prepared by macroazoinitiator intercalated in Na-MMT. Compos Sci Technol 68(7–8):1919–1926
62. Meng Q, Hu J, Zhu Y (2007) Shape-memory polyurethane/multiwalled carbon nanotube fibers. J Appl Polym Sci 106(2):837–848
63. Gelfer MY, Song HH, Liu L, Hsiao BS, Chu B, Rafailovich M, Zaitsev V (2003) Effects of organoclays on morphology and thermal and rheological properties of polystyrene and poly (methyl methacrylate) blends. J Polym Sci B 41(1):44–54

Microscopy of Shape Memory Polymers, Polymer Blends, and Composites

Jinlian Hu and Shanshan Zhu

Abstract Contemporary microscopes can magnify almost everything that is invisible to the naked eye, down to the atomic level. Current classifications include optical microscopy, electron microscopy, and scanning probe microscopy, in which optical one focuses on microscale while electron and scanning probe ones focus on the nanoscale. Microscopy is an indispensable technique of characterization for shape memory polymers (SMPs), including optical microscopy (OM), scanning electron microscopy (SEM), transmission electron microscopy (TEM), atomic force microscopy (AFM), infrared microscopy, fluorescence microscopy, and laser scanning confocal microscopy (LSCM). In this chapter, the micro- and nanostructures of different shape memory polymers, blends, and composites will be discussed. The applications of these microscopical techniques will be outlined. A brief account of various types of morphologies and their impact on shape memory effects will be provided.

1 Introduction

Shape-memory polymer materials and their derivatives are one of the most promising smart materials available today. They are the kind of materials that can change shape with the sensitivity of temperature, light, electricity, humidity, and other stimuli, thus affecting performance. This characteristic makes them ideal materials for different application fields, such as biomedicine and aviation. Sometimes, pure SMPs cannot perform well in practical application especially where the high modulus, high recovery stress, or good electrical conductivity are needed. As a result, the shape memory composites (SMPC) filled with particles, fibers, nanotubes have been explored for various fields. The change in shape and other properties are closely related to the microstructure of the materials. Choosing proper microscopy methods

J. Hu (✉) · S. Zhu
Institute of Textiles and Clothing, The Hong Kong Polytechnic University, Kowloon, Hong Kong 999077, China
e-mail: jin-lian.hu@polyu.edu.hk

J. Parameswaranpillai et al. (eds.), *Shape Memory Polymers, Blends and Composites*, Advanced Structured Materials 115,
https://doi.org/10.1007/978-981-13-8574-2_5

should depend on the specific structure inside SMPs or composites. For instance, spherulites in crystal polymer domains should be determined by POM due to its characteristic cross-extinction phenomenon. Surface phase-segregated morphology with nanometer- or micrometer-scale and their distribution can be characterized by means of both SEM and TEM. And LSCM is always the best choice for investigating polymeric materials and cells growth in organisms. The specific applications of these microscopes are classified according to research objects. It is expected that this chapter can provide more inspirations to readers in the aspect of microscopy for study on SMPs.

2 Optical Microscopy (OM)

Optical microscopy (OM) is widely used in polymer materials because it is inexpensive, easy to operate, and can be used to study the structural morphology of both transparent and opaque materials. It is the most general and available microscopy in the laboratory using visible light and a system of lenses to visualize the microstructural features of polymeric materials, reflecting physical or chemical information.

From the aspect of phase structure, the morphology of soft and hard segments in SMPs is quite different under OM, making it is an easy way to follow degree of synthesis and phase separation. Figure 5.1 presents the microscopic image of PU/PCL solution at 25 °C in three conditions. Then two segments start to separate from each other with time as shown in Fig. 5.1c.

From the aspect of local or microscale shape memory effect (SME), OM becomes an easy method to investigate the recovery process of objects with small size which cannot be clearly distinguished by eyes. During processing, necking is a common phenomenon in stretching, especially in cold drawing. A direct proof of shape recovery process of the shoulder region in the fully necked specimen can be captured [66]. The thermally activated shape memory behavior of hydrogel was acquired by OM

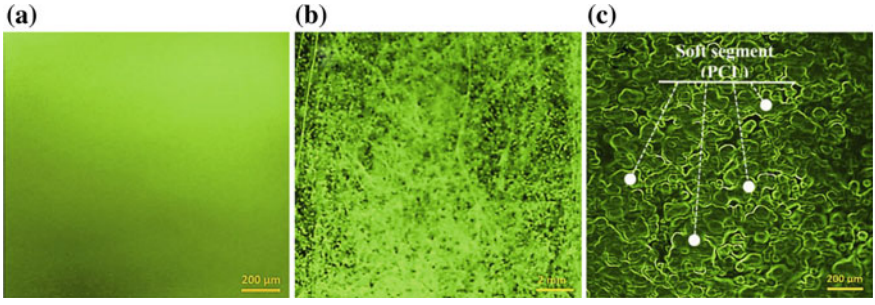

Fig. 5.1 PU/PCL solution at room temperature of 25 °C. **a** solution after 1 h (homogenous), **b** solution after a week (nonhomogeneous), **c** solution after three weeks (nonhomogeneous). [1]

combined with a heating unit. It has been clearly observed that during heating scans through a lower critical solution temperature, the hydrogel will collapse with the increase of temperature. However, the shape and size have large recovery in the cooling process, indicating the memory behaviors [62].

From the aspect of SMP composites, the morphologies and properties are largely influenced by fillers. Carbon fiber reinforced SMP matrix composites appeared and became one of the most popular SMP composites. Microstructural deformation must occur accompanying with macro-deformation of samples. So, the detailed exploration of inner structural variation during the shape memory process is highly required. Optical micrographs of the evolution of local out-of-plane buckling during bending of the satin weave composites were explored [24]. It was observed that buckles would occur and grow in satin weave composite during the bending process, which can lead to early delamination and subsequent damage on the inner surface. Although the buckles recover during heating, the optimum fabrication and processing methods or the weave architecture should also be explored. Another work on microbuckling in SMPC from a side view was also conducted through OM, where no failure or delamination appears before deformation, then the fiber microbuckling comes into sight together with large delamination gap. During heating, a large recovery of fiber microbuckling and a small recovery of delamination can be observed. It was proposed that the microbuckling is the primary mechanism in the bending deformation of SMPC, which provides a higher bending strain than that in a traditional structural composite [40]. These studies of microstructure provide guidance in designing the structure of SMPC and further developing better mechanical performance in bending or stretching.

3 Polarized Light Optical Microscopy (POM)

POM is specifically targeted at crystalline polymeric materials containing spherulite morphology, oriented crystals, etc. The characteristics of polarized light microscopy are to change an ordinary light to a polarized one for microscopic examination to identify whether a substance is monorefractive (isotropic) or birefringent (anisotropic). To yield polarized light, the ordinary light should go through a polarizing device which can filter all directions of light vibration except the regulated direction. The bulk morphology of the thin films can be studied with the help of POM.

3.1 Domains in SMP Structure

SMPs consists of at least two segregated domains, where one is in charge of temporary shape and the other is in charge of permanent shape [5, 34]. Crystalline domains appear responsible for either physical cross-linkers or reversible phase with specific transition temperature. By means of POM, two or more domains in structure can be

separated, the effect of each segment on the crystal structure as well as crystalline morphologies with characteristic cross-extinction patterns can be directly visualized, and crystallization capabilities can be judged [23, 92]. The overall process of crystallization can be well tracked if POM is equipped with a heating stage [23]. Luo et al. used POM to investigate ethylene oxide and ethylene terephthalate (EOET) SMP, where the crystal states of both soft and hard domains can be observed after annealing at 120 °C for 6 h and at 35 °C for 12 h. The micrograph captured from 70 °C illustrates the distinguishable cross-extinction of hard segments [52].

3.2 SME of Polymeric System with Small Scales

Polymeric particle has large potential in biomedical application due to its small scale, round shape, and large surface area that meet the requirements of interaction between materials and biological surfaces [84]. As a result, particles with shape memory functions and stimuli-responsive abilities have attracted a lot of attention. Guo et al. proposed a kind of thermoplastic shape memory polymeric particles through a modified film-stretching processing method, where SME is controlled by entropy elasticity of polymer chains through coil and alignment as well as entanglements [29]. First, chain alignment and existence of entanglements were characterized through POM due to its anisotropic shape and birefringence as shown in Fig. 5.2. The microparticle stretched at 65 °C illustrates strong birefringence under crossed polarizers at 40°, 135°, 315°, and 225°, respectively, indicating chain alignment exists inside the particles, that can serve as driving force to trigger SME. However, the microparticle stretched at 90 °C does not show a little sign of birefringence, demonstrating the random stated of molecular chains inside and disappearance of entanglement at high temperature. The prerequisite in achieving SME of microparticles was identified clearly through this technique.

In addition to this, morphology evolution with SME and arrangement of nanofillers should also be carefully examined where POM can provide such a chance and choice. For instance, fabrication steps of polydiolcitrate elastomer with cellulose nanocrystals (CNCs), known as hydroxyl-dominant poly(dodecanediol-co-citrate) (PDDC-HD), were well characterized by POM [19]. It was proved that CNCs can significantly affect the physical properties of SMP as well as improve the shape fixity and recovery ratio.

4 Scanning Electron Microscopy (SEM)

SEM is generally used to evaluate the morphology, microarchitectures of different regions, and composition of nanomaterials with magnification ranges from 20 to 100,000. Different from normal OM, SEM can control magnifying power through the size of scanning area but not lens, and it can produce an image with a depth of field

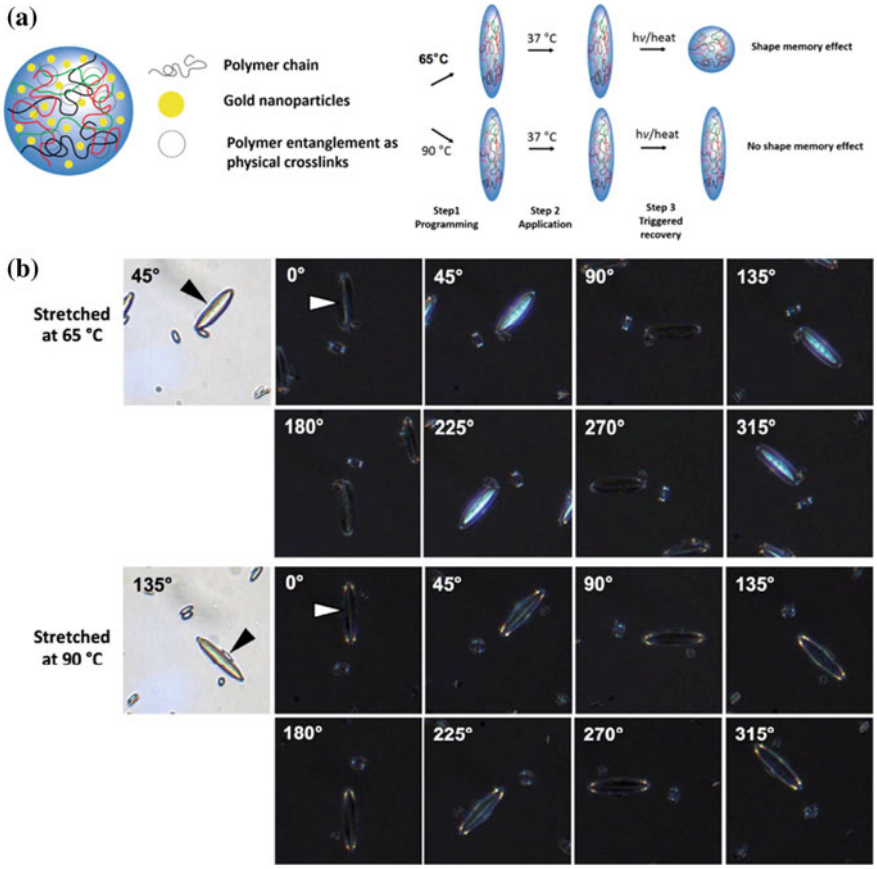

Fig. 5.2 **a** Poly(D,L-lactic acid) particles were fabricated encapsulating hydrophobic lipid stabilized gold nanoparticles. **b** Polymer alignment was observed in POM images of 65 °C stretched particles to a higher degree as opposed to 90 °C stretched particles. Copyright © 2018 American Chemical Society [29]

that is 300–600 times better than that of OM [67]. For SMPs whose microstructure and composition are of vital importance for their smart properties, SEM contributes a lot in investigation relationships between structure and function. In terms of natural materials, such as the collagen skin recently proposed by Hu et al., a water-sensitive SME exists because of its interlaced flexuous fiber bundles constructed a fibrous network with some interspace between the large fiber bundles which were observed by SEM, porosity allowing rapid permeation of vapors and solvents [31]. Another example is the shape memory performance of natural hairs [75, 77, 78]. In terms of composite materials, a kind of composite nanofibrous mats was fabricated with chitosan, gelatin, and shape memory polyurethane for smart wound healing [68, 70]. Or fabric coated with shape memory polyurethane has a water-resistant property

with good water vapor transmitting ability [36]. The specific application of SEM on shape memory polymeric materials can be divided into the following aspects.

4.1 Microscale Shape Memory Behaviors

Macroscopic shape memory phenomena must be accompanied by changes in microscopic properties. For instance, shape memory ability can facilitate recovery of microscopic damages such as scratch, of which the recovery and healing process can be easily followed by SEM [47, 76]. SMPs also appear a lot in the form of microsphere [44], micro-, nanoscale particles [12, 13], or nanofibers [93], which have the advantage of small size and high surface area, enabling microlevel SMP with broader application. For shape memory fibers (SMFs), the diameters of fibers can be directly measured and the cross-sectional area can be calculated accordingly [37]. Huang et al. characterized a cross-linked poly(St-DVB-BA) (Styrene (St), butylacrylate (BA), and divinylbenzene (DVB)) polymeric microsphere with size in the range of 30–100 μm [35]. Using SEM, the influence of DVB content on the surface roughness, the shape as well as the size of microsphere can be easily followed. Further, the shape memory ability including integrate shape deformation, fixation, and recovery with stimuli of thermal were visualized.

4.2 Microscale Surface Modification and Surface Pattern

In most cases, surface modification can help SMPs to be used in broader practical applications. It is well known that cell behaviors depend a lot on tissue scaffolds [41]. Therefore, the adjustable micropatterned surface stemmed from SMP has good potential in biomedical application. Plasma immersion ion implantation (PIII) uses energetic ions to yield radicals on the surfaces of SMP, improving the bioactivity of SMPs which can fit into the permanent implantable biomedical devices [10]. Zhou et al. proposed a thermal-induced SMP with adjustable surface topography where mechanical force can be produced spatiotemporally with surface shape change to effectively control cell morphology. The whole shape memory process with the relationship of temperature of the micropatterned surface with concentric circular microgrooves are observed by SEM [7]. Another common surface pattern is nanowrinkles on the surface of the polymer. As shown in Fig. 5.3, tunable nanowrinkles are successfully produced by spreading a metal layer on a pre-strained shape memory substrate through simple metal deposition and subsequent heating. Shape recovery of the substrate occurs during heating, inducing non-shrinkable metal to buckle. Doubtlessly, for study of nanowrinkles on SMP, SEM is one of the most appropriate techniques. For Fig. 5.3b, c with evenly distributed biaxial and uniaxial nanowrinkles, information of distribution, winkle wavelength, and dimension obtained by SEM can be the imperative indicators for a specific application such

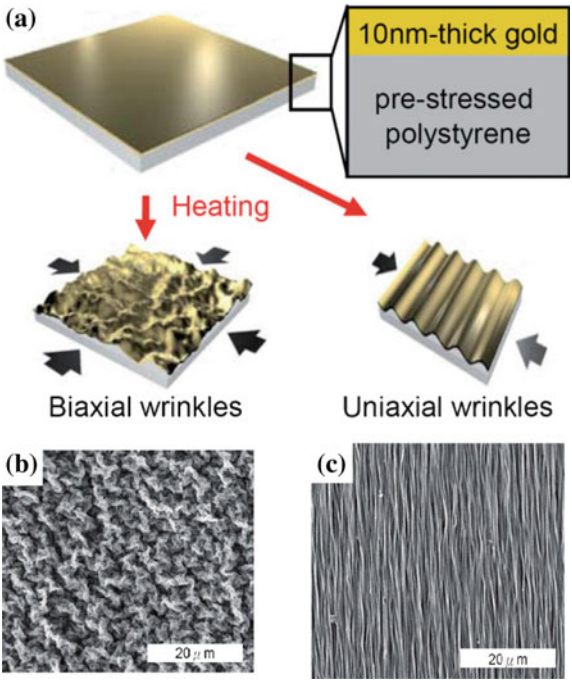

Fig. 5.3 Fabrication of nanowrinkles. **a** Scheme of fabrication of biaxial (left) and uniaxial (right) wrinkles. SEM images of biaxial (**b**) and uniaxial (**c**) wrinkles on shrunk polystyrene sheets covered with a 10 nm thick layer of gold. **d** SEM image of biaxial wrinkles with 10 nm thick gold. Copyright © 1999–2018 John Wiley & Sons, Inc. [22]

as sensors. Also, from the SEM analyses, the evolution, population, and states of wrinkles such as their durability, can be followed with the change in parameters. Take advantage of SMPs and proposed methods, wrinkles can be easily patterned even to a beautiful "wrinkled flowers" in their work [22].

4.3 Free Spaces/Microporous Structure

Free spaces or porous structure commonly appear in polymeric materials, especially in the condition of deformation. Structures like these provide more possibilities to polymers with broader applications even though sometimes they affect their physical properties. As a result, the porous polymer structures are preferred in specific applications such as absorbing, filtration, thermal management. For SMPs, it was newly demonstrated by SEM that the appearance of free spaces in lead zirconate titanate/SMPC could weaken the piezoelectric effect [8]. However, SMPs like poly(N-isopropylacrylamide) (PNIPAM) cryogel with microporous structure presents a lot of excellent properties, which could allow the gel to take in or release water speedily, improving the response rate with an external stimulus. The pore sized characterized by SEM is about 150–350 μm, which is of importance in smart responses [15]. The pore size ranges, information of pore distribution, and whether

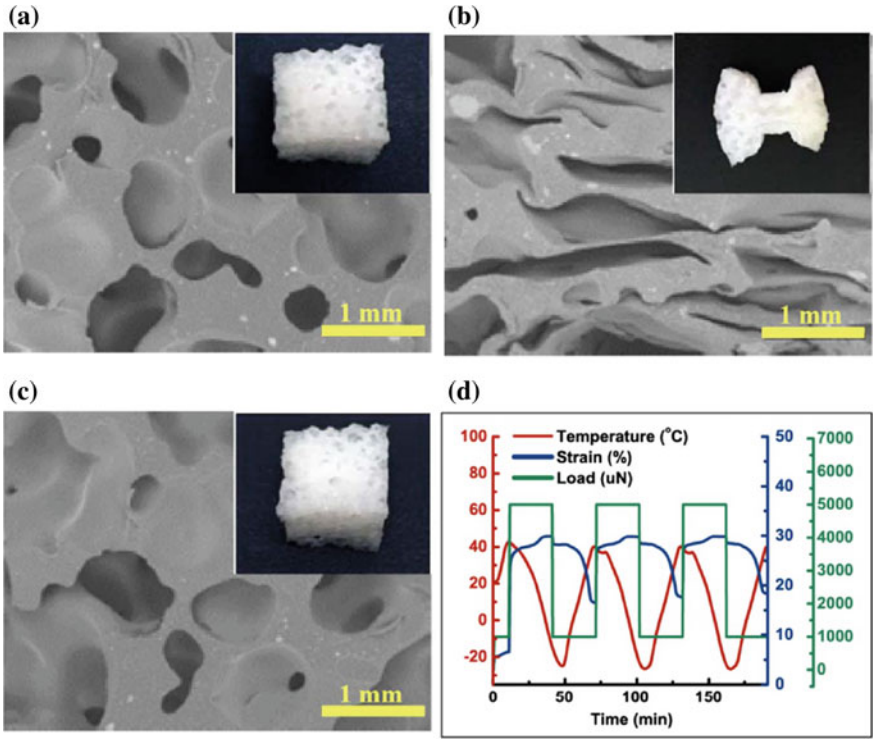

Fig. 5.4 Shape memory characteristics of the SMP foam. SEM micrographs of **a** original, **b** temporary and **c** recovery shape; and **d** shape memory cycles detected by DMA. 0304-4165/© 2018 Elsevier B.V. [79]

it is an interconnected porous network in SMPs or composites can all be investigated by SEM [20, 39] which are critical in analyze the smart function, overall stiffness, degree of crosslinking, etc. For shape memory foam, the pore architecture as well as size affected by SME can be effortlessly characterized by SEM. As shown in Fig. 5.4, the pore transfer between mean-size shape and collapsed ones during the shape recovery process [79].

4.4 Fillers in SMPC

Compared with shape memory alloy (SMA), the advantages of SMP such as easy fabrication, low costs, or conveniently controllable properties through common processing techniques are well known to us. Nevertheless, some instinctive obstacles of SMPs still exist such as low recovery stress or low thermal conductivity in inhibiting their application in more fields. Therefore, incorporation of nano fillers into SMPs

becomes necessary, first strengthening the mechanical properties and second enlarging the practical application fields. In general, the categories and characteristics of each nanofillers are listed below acquired from SEM studies [25, 86].

- Cellulose nanofiber (NFC): NFCs exhibit a highly entangled, web-like structure with diameters ranging from 50 to 200 nm
- Cellulose nanocrystal (CNC): CNCs present a needle-like structure with an average length of 150 nm and a diameter of 12 nm,
- Carbon nanotube (CNT), single-walled CNTs (SWCNTs), multi-walled CNTs (MWCNTs): The structure of SWCNTs is a cylindrical tube with a 3D structure and the diameters are about 0.7–2.0 nm. While MWCNTs contains several tubes in concentric cylinders with diameters of about 10–30 nm.
- Carbon nanofiber (CNF): CNF with rod-shaped structure and 150–200 nm in diameter. The length for both CNT and CNF is too long to characterize, including the effect of entanglement on measurement.
- Cup-stacked carbon nanotubes (CSCNT): CSCNTs have novel structural characteristics such as a larger hollow core and a larger portion of open ends than other CNTs, featuring with an average outer diameter of 100 nm, an average inner diameter of 70 nm, and an average aspect ratio of 50 [86].
- Nanolayered graphene (NLG): NLG with less than 10 layers of graphene single sheets stacked together and with a total thickness less than 5 nm [76]. The incorporation of NLG into SMP matrix imparts the composites both excellent in-plane fracture strength, scratch resistance as well as a thermal healing capability.
- Metal: Metal incorporated into SMP matrix mainly for electroactive SME.

The nanostructures and instinctive properties of fillers are of vital importance in affecting the function of the matrix. Figure 5.5 compared the basic structure of nanomaterials including natural ones CNC and NFC, as well as synthetic ones CNF and CNT through both SEM and TEM [25].

4.4.1 Carbon Fillers

Ordinary SMP materials are insulators, limiting their use in conductive applications. Carbon nanomaterials have high electrical conductivity, high tensile strength as well as low density, giving them high potential when they are incorporated into SMP matrix [11, 81]. MWCNTs are one of the most popular fillers appearing in SMPC, especially for electroactive shape memory effect [55, 57, 73]. The homogeneous dispersion of MWCNTs throughout the whole materials and the interfacial adhesion between fillers and the SMP matrix was investigated through SEM. It was proved that the situation of filler's distribution can be well observed through direction of cross section. However, the globular structure from the agglomerates formed by polypyrrole-coated MWCNTs will affect the mechanical capability of whole materials [63]. It was also proved from the same work that the SMP with 2.5% MWCNT presented better mechanical and thermal properties, illustrating that thermal conductivity should also be seriously considered. Heat transfer efficiency will undoubtedly

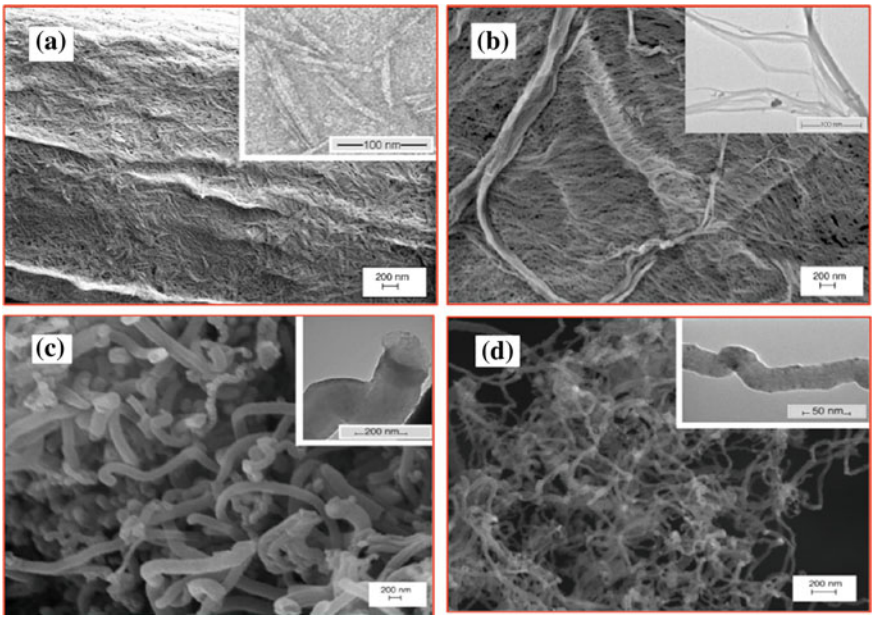

Fig. 5.5 SEM/TEM images of **a** CNC, **b** NFC, **c** CNF, and **d** CNT. © The Author(s). 2018 [25]

affect the response rate of these smart materials. Yu et al. found from SEM that, CSCNT can be better dispersed in SMP matrix compared with CNF [86] and it can remarkably improve the mechanical behaviors, rate of thermal–mechanical responses as well as thermal conductivity in styrene-based SMPs.

The use of hybrid fillers can make up for the defects of single fillers in nature, such as the combination of carbon nanotubes and short carbon fibers. In conductive SMPC where a styrene-based SMP is selected as the matrix resin, the separated carbon nanotubes (CNTs) aggregations can be bridged by short carbon fibers (SCFs) [85]. SEM study in Yu et al.'s work illustrated the existence of interpenetrated SCFs through the whole SMPC network, that can improve electrical conductivity with the implantation of separated conductive channels into the matrix. At the same time, CNTs aggregate as a cluster and act as conductive nodes among SCFs, facilitating the local conductive capability. The synergistic effect between SCFs and CNTs effectively increase the electric conductivity.

A another clever method utilized in incorporating CNT into SMPs was presented by Song et al. [65]. In their work, a helical composite yarn was fabricated by infiltrating CNT fiber with polyurethane resin. Then the composite was over-twisted as shown in Fig. 5.6. Figure 5.6a, c illustrates the hierarchical coil structure of CNT yarn and CNT/TPU composite yarn which is expected to offer high actuation. After infiltrating by TPU, the bundles in (c) and (d) are larger than the pristine ones. The cross-sectional surface of composite in (f) seems smoother than that in (e), and the holes almost disappear in composites yarn, demonstrating more uniform structure

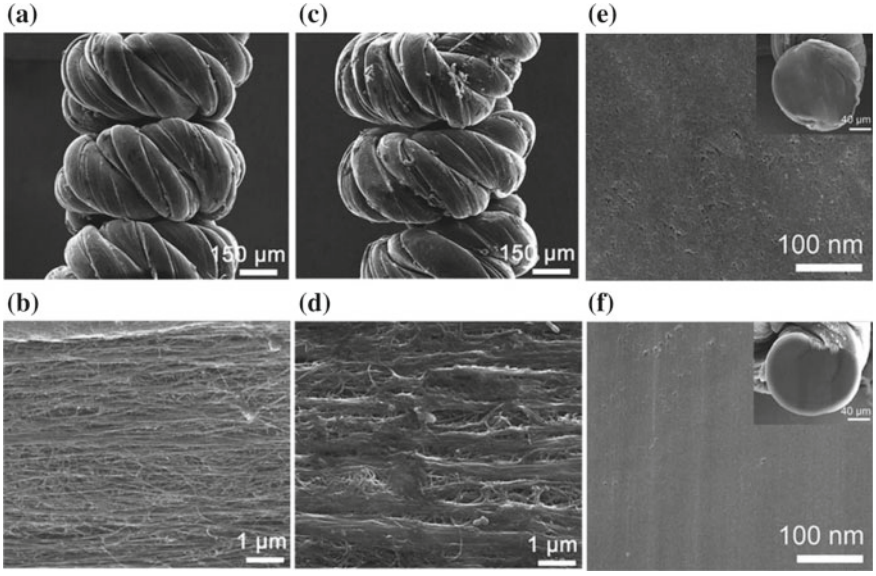

Fig. 5.6 **a**, **b** SEM images of coiled CNT yarns before the annealing treatment and contraction training, at different magnifications. **c**, **d** SEM images of coiled CNT/TPU composite yarn before the annealing treatment and contraction training, at different magnifications. The surface morphology has changed after TPU infiltration. **e** Cross-sectional view of the coiled CNT yarn. **f** Cross-sectional view of the coiled CNT/TPU composite yarn. © The Royal Society of Chemistry 2018 [66]

formed and more spaces in CNT are filled by TPU. As a result, coil composite yarn can perform better compared with pristine CNT yarn, with the combination of both SME of TPU and high actuation capability of CNT.

4.4.2 Cellulose Nanocrystal/Nano Fiber

Cellulose nanocrystals or nanofibers have been developed to be a perfect nanofiller in enhancing the mechanical properties of SMPs. In many cases, they are used in SMP to produce water-induced shape memory effect [51, 69, 92]. However, the degree of binding or the interaction between fillers and matrix decides the success rate. Well-dispersion of CNC can be characterized by SEM [12] representing a good compatibility between CNC and SMP matrix, which was explained by the covalent bonding between CNC and molecular chains of matrix [48]. Similarly, in a thermo-responsive photonic film with the combination of CNC and a SMP, hydroxyl-dominant poly(dodecanediol-co-citrate) (PDDC-HD), the cross section of hybrid materials was visualized by SEM as shown in Fig. 5.7 [19]. The architecture, distribution, and thickness of each layer can be straightforwardly acquired. It is shown that the CNC layer locates in the middle of two thick layers of PDDC-HD. The thickness of CNC layer increases from about 4.5 μm in a pristine state to

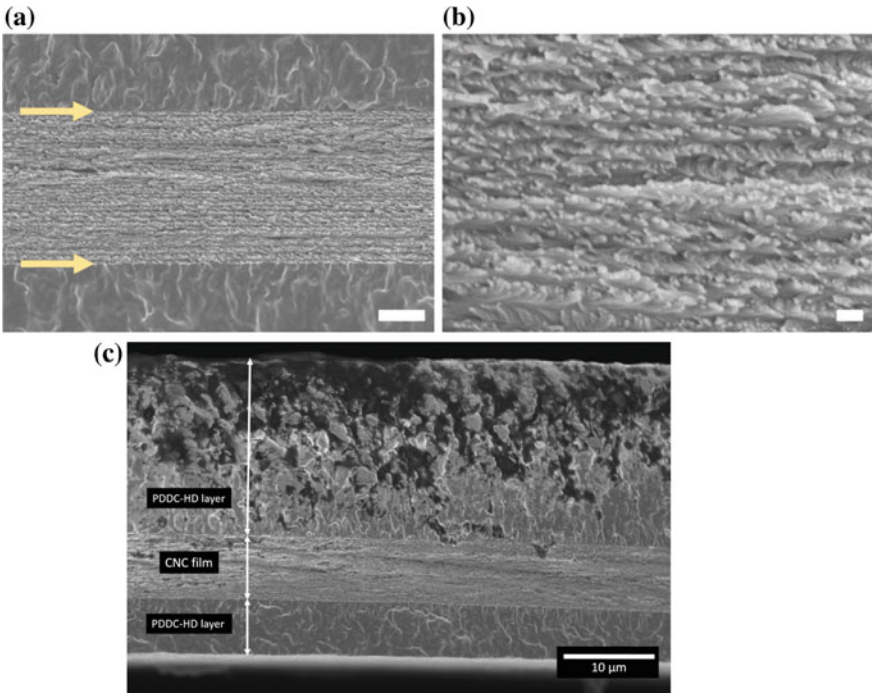

Fig. 5.7 Representative SEM cross-section images of a cellulose nanocrystals/hydroxyl-dominant poly(dodecanediol-co-citrate) (CNC/PDDC-HD) hybrid material after impregnation of the prepolymer and curing. **a** The elastomer layers surrounding both sides of the CNC film (the scale bar is 2 μm; interfaces are indicated by yellow arrows). **b** The arrangement of the cellulose nanocrystals into a chiral nematic structure (the scale bar is 200 nm). **c** The layered structure of the CNC/PDDC-HD hybrid material. Copyright © 2016 American Chemical Society [19]

about 6.5 μm in composite, illustrating the infiltration of PDDC-HD into CNC layer. Moreover, SEM with high magnification is able to distinguish the Bouligand arches, representing the cholesteric architecture in the cellulose film. The pattern periodicity of cholesteric pitch obtained from SEM increased in composites, illustrating the hybrid composites can be further stabilized by the formation of the ester bonds between prepolymer and CNC.

4.4.3 Metal

Deformable electronic devices are anticipated in many advanced applications. Compared with traditional filler single-walled nanotubes, silver nanowires (AgNW) have better performance due to lower sheet resistance. SMP with silver nanowire electrodes possess the ability in the application of organic light-emitting diodes (OLEDs). As obtained from the SEM image, AgNWs have an average diameter of approxi-

mately 60 nm and an average length of approximately 6 μm [87] and they can facilitate self-healing ability [50]. Ge et al. reported another conductive fillers composed of antimony-doped tin oxide (ATO) and TiO_2 whiskers in shape memory matrix. The specimens for morphology analysis in SEM were prepared by brittle fracturing in liquid nitrogen. Results show that the whiskers overlap with each other in a homogenous distribution without heavy aggregation and defected interface, which is of great importance for mechanical properties and SME of composites [45]. Metal nanoparticles or powder introduced to SMP matrix are also used to improve light or electric-sensitive responses without limiting the tension strain of materials, where the dispersion and morphologies of nanoparticles should be strictly characterized [74]. Figure 5.8 shows a kind of thermo-responsive SMP with embedded micron-sized Ni powder chains. SEM can be used to observe the details of Ni chains in shape memory condition. Figure 5.8a reveals that Ni chain can be developed and the bundles can be resulted with an increase of Ni content. (left column). After shape recovery cycles with five times stretching as presented in right column, Ni chains have not been destroyed, indicating the feasibility of Ni chains in SMP to produce electroactive SME [42].

5 Transmission Electron Microscopy (TEM)

Different from the raster scanning across the specimen surface in SEM, the electron beam in TEM is transmitted through the specimen. As a result, samples for TEM characterization should be thin enough (50–100 nm thick) to permit the electron beam to penetrate. The chiaroscuro on micrograph indicates the differences in the density of materials. In regular, denser packing of atoms or crystal orientation will lead to the darker areas where the electrons are limited to go through the sample [43]. Compared with SEM, the magnifications and resolution of TEM is higher, 50,000,000 × and below 0.5 Å, respectively. TEM has been used maturely for the study in the morphology of polymeric materials. For shape memory polymer, the crystal structure, composition or the information of fillers including nanoparticles, fibers, or graphene [76] can be well characterized. For example, the influence of morphology, dispersion of organoclay platelets in SMPU and the agglomerates of SiC particles on the properties of SMPU were analyzed by Jana et al. using TEM. It was found that SME was strongly and directly affected by nanofillers due to their interference on crystallization in soft segment [28]. TEM was also applied to observe cellulose whiskers and their relative uniform distribution in nanoscale after the hydrolysis treatment [30], or their dimensions with average length of 272 ± 87 nm and diameter of 18.5 ± 5.9 nm (average values ± one standard deviation) [89, 91].

The incorporation of nanoparticles into SMP matrix will bring new functions to them. For electromagnetic-responsive SMP, the magnetite nanoparticles which are able to transform electromagnetic energy to heat are always introduced into SMP matrix as nanofillers. Nanoparticles are always in core–shell structure for better incor-

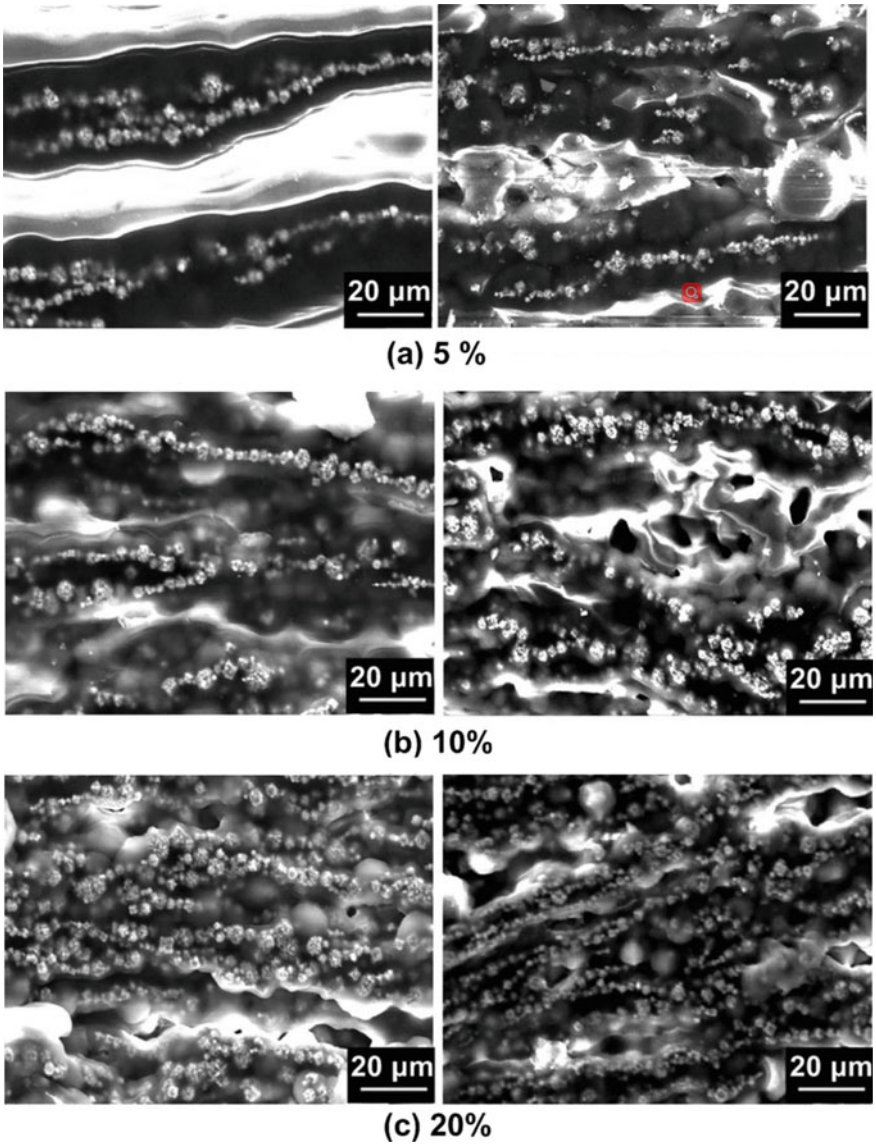

Fig. 5.8 Typical SEM images before (left column) and after (right column) five stretching (at 50% strain)-shape recovery cycles. © 2018 AIP Publishing LLC [42]

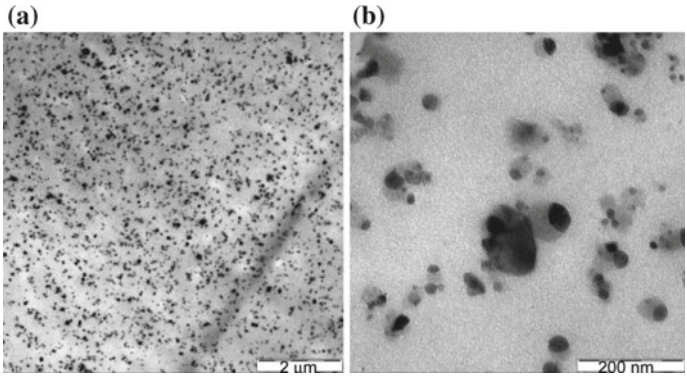

Fig. 5.9 Transmission electron microscopy pictures of TFX100 with 10 wt% particle contents. (Scale bars: **a** 2 m; **b** 200 nm.) Copyright (2006) National Academy of Sciences, U.S.A. [59]

poration with SMP matrix, like Fe_3O_4 nanoparticles warped by oligo(e-caprolactone) [64]. Another example is that the addition of nanoparticles consisting of an iron(iii) oxide core in a silica matrix into a polyetherurethane (TFX) makes the SMP become magnetic responsive. The homogenous distribution of nanoparticle in TFX100 matrix was firstly confirmed by TEM as shown in Fig. 5.9a. Then, the special structure of nanoparticle was well characterized with various scale. Both the mechanical properties and the shape memory function of composites are closely influenced by the distribution and the structure of nanoparticles [59].

In addition to nanoparticles, multi-walled carbon nanotubes (MWCNTs) modified by polypyrrole (PPy) as nanofillers were mixed in SMP matrix to enhance the conductivity of SMP composites. TEM was used to explore the structural evolution of carbon nanotubes after treatment. Figure 5.10a illustrates the tubular morphology of MWCNTs imaged by TEM. It was intuitive that the surface of MWCNTs are coated by PPy, of which the electroactive shape recovery is good due to the highest conductivity among other composites [63]. Acid-functionalized MWCNTs was also proposed in polylactic acid/epoxidized soybean oil (PLA/ESO) matrix with optimum mechanical and thermal performance and electroactive SME [61]. TEM is critical in qualitatively analyzing the distribution of MWCNTs and its interaction between matrix through carboxylic acid functionalization. An uncommon filler, bacterial cellulose whiskers (BCWs), proposed recently by Yin et al. were incorporated into natural rubber to produce water-induced modulus change nanocomposites, fabricating a new kind of SMP for biomedical application [83]. Figure 5.10b illustrates the slender rod-like shape of BCWs and their tendency to connect with each other due to the strong hydrogen bonds between hydroxyl groups.

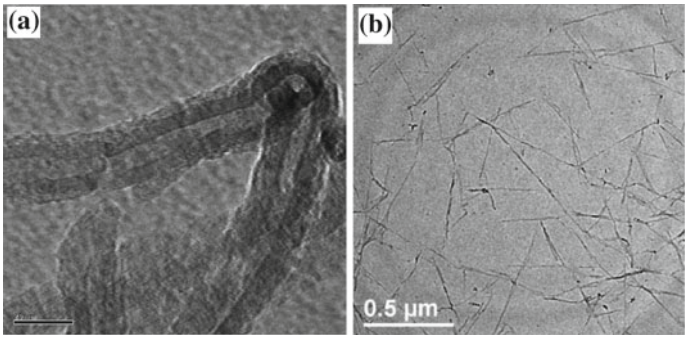

Fig. 5.10 **a** TEM photographs of polyurethane–polypyrrole-coated multi-walled carbon nanotubes [63]; **b** Morphological characterization of BCWs by TEM. Copyright © Taylor & Francis Group, LLC. © 2018 Elsevier B.V. [83]

6 Atomic Force Microscopy (AFM)

AFM is widely used in polymeric materials. It fixes one end of a micro-cantilever that is sensitive to force and has a tiny tip at the other end. A weak repulsive force between tip atom and surface of the sample can be sensed through optical detection or tunnel current detection. Three-dimensional information on the surface topography of samples can be obtained. In this way, the morphology in nanometer scale of SMP could be pictured using AFM.

6.1 Morphology and Nanofiller Characterization

A mature use of AFM in polymer materials is to observe the morphology and phase separation of surface [32, 56, 60, 90]. The micro-phase-separation morphology and phase size in a novel type SMP of styrene–butadiene–styrene triblock copolymer (SBS) and poly(3-caprolactone) (PCL) blend were characterized by AFM through observing the cross sections of samples those were fractured in liquid nitrogen. Combined with stress–strain test, SMP blend was confirmed with two-phase morphology [88]. In SMPC, AFM was generally carried out to identify the dispersion and nanoscale of liquid crystal and nanowhisker fillers as presented in Fig. 5.11 [9, 54, 83]. The comparison of AFM topographies of PU-MWCNTs composites with different preparation method provides direct proof on choosing the best composites preparation route [38].

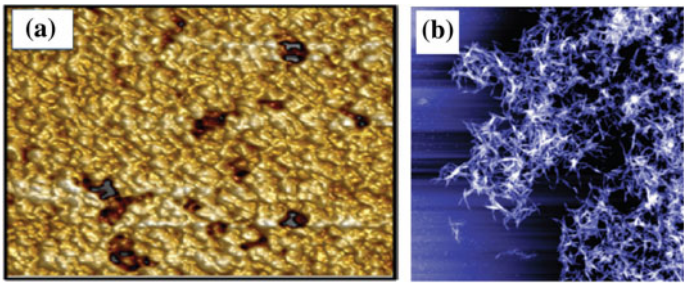

Fig. 5.11 **a** AFM image of typical PSMPU-Azom composites. (PCL-based SMPs matrix with a trans–cis photo-isomer of azobenzene mesogen (coded as Azo11) as the Liquid Crystal fillers) [9]. **b** AFM of cellulose nanowhiskers isolated from cotton on a mica surface (area = 3 * 3 μm). Copyright © 2011 American Chemical Society [54]

6.2 Adhesive Force

The reversible nature of SMP with external conditions makes it possible to develop into different fields. Dry adhesion belongs to one of them. Dry adhesives typically utilize non-covalent intermolecular forces to bond, where flexible adhesive materials are always preferred. However, compliant materials are vulnerable to failure under external force, leading to adhesive peeling in turn. Then Eisenhaure et al. proposed an SMP with microtip surface design through AFM that achieves an extremely reversible and strong dry adhesion to a glass substrate [18]. The SMP surface visualized by AFM during adhesion testing is shown in Fig. 5.12a. Using the data collected from AFM testing, the work of adhesion is estimated to be 46 mJ/m^2.

6.3 Nanoscale Indentation

Burnham et al. first proposed to directly measure the nanoscale mechanical properties of materials by AFM using nanoindentation technique in 1989 [6]. In studies of polymer materials, nanoindentation testing is becoming popular to a greater extent. It can not only quantify mechanical properties, but also allow researchers to observe morphologies of materials after indentation. For SMPs, understanding the variation of material surface information, small-scale deformation and thermally induced SME are of great significance for comprehensively investigating the performance of SMP. The surface of materials can be characterized by means of penetrating by an indenter tip of AFM with a penetration depth of the tip into the surface. The tapping mode in AFM topographic scans of the indents can follow the shape recovery process in heating [72]. As shown in Fig. 5.13, the nanoscale responses was investigated by AFM through the formation of nanoscale indentations using a heated AFM cantilever at the temperature above the transition temperature of SMP. The thermomechanical

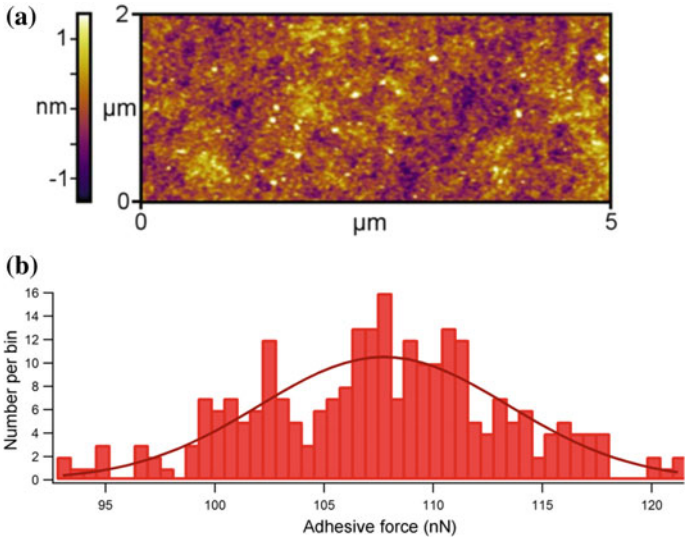

Fig. 5.12 **a** AFM measurement of SMP surface roughness, cured against polished silicon (root mean square roughness = 4.7 Å). **b** AFM adhesive force histogram of 256 individual tests in a grid pattern at 30 °C with a Gaussian curve-fit and mean of 108.7 nN. Copyright © 2013 American Chemical Society [18]

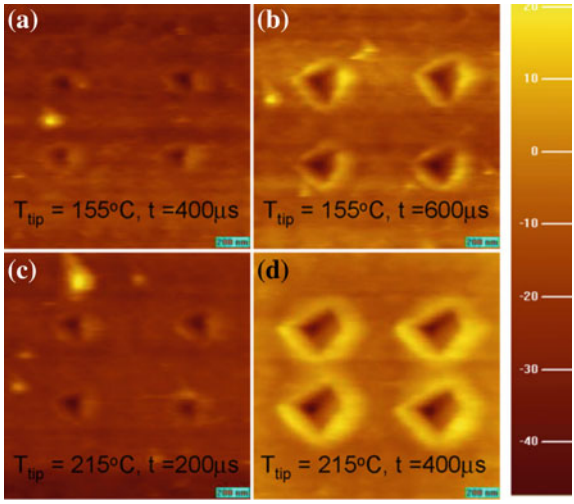

Fig. 5.13 AFM images of nanoscale indents made at different cantilever temperatures and heating durations of contact on a 10% DEGDMA polymer surface at a fixed load force of 0.11 μN. The length of the scale bars in the figures represents 200 nm. © 2007 IOP Publishing Ltd. [72]

behavior of nanoindentation can be directly studied, which will provide valuable information for the design of polymer actuators at small scales [82].

6.4 SME of Micro/Nanoscale Materials (Micro/Nanowires)

As mentioned earlier, if the function of SME is zoomed out to micro- or nanoscale, a great potential will appear in the application such as biomedical [16, 17] or microstructure [53]. OM, SEM have played a big role in characterizing microscale SME effect. However, Fang et al. not only used AFM to characterize SMP but also performed programming, which greatly improved the control effect and accuracy. Figure 5.14 illustrates shape memory effect and stress recovery of single polymeric micro/nanowires quantitatively on a structured silicon substrate [21].

7 Infrared Microscopy

Infrared thermal imager can quickly determine the temperature distribution of an object. The temperature of a coiled carbon nanotube SMC yarn is characterized by

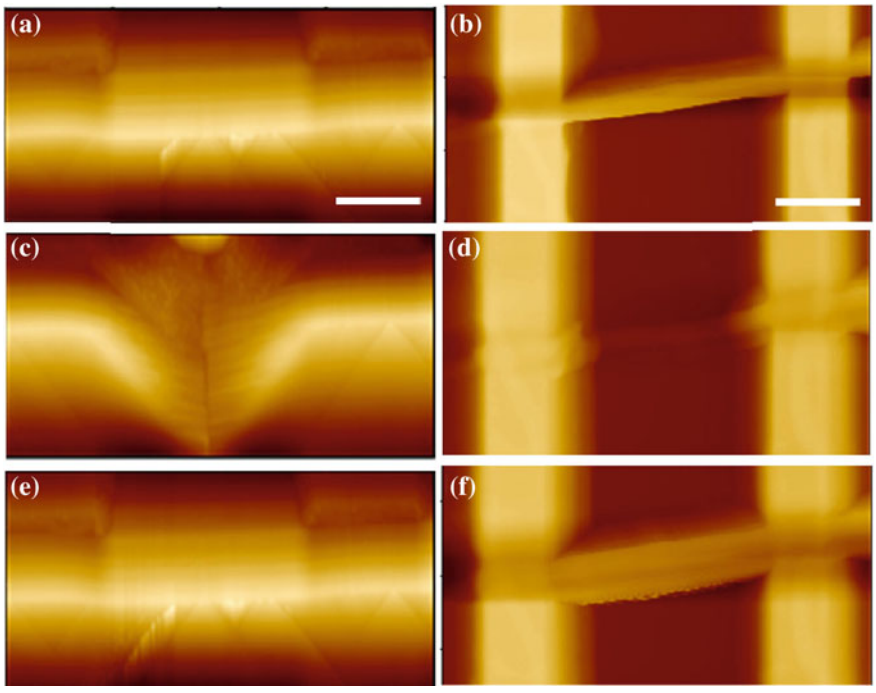

Fig. 5.14 **a**, **b** AFM height images of single, free-suspended **a** micro and **b** nanowires taken before the programming procedures at $T_{deform} = 40$ °C and 30 °C, respectively. **c** Micro and **d** nanowire in their temporary shape taken at $T_{low} = 10$ °C. **e** Micro and **f** nanowire after shape recovery. The scale bars for **a**, **c**, **e** microwire (**b**, **d**, **f**) nanowire are 8 and 1.2 mm, respectively. [21]

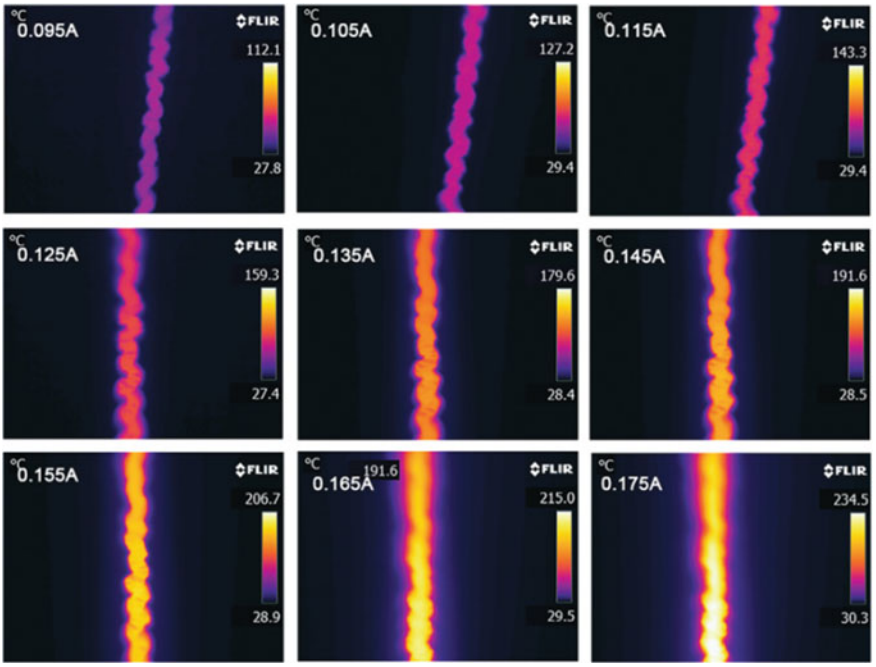

Fig. 5.15 Temperature distribution of coiled CNT/TPU composite yarn with the length of 3.5 cm after passing current (0.095A–0.175 A) through the yarn for 5 s, measured by an infrared microscope. © The Royal Society of Chemistry 2018. [66]

an infrared microscope with a current of 0.095 A to 0.175 A as shown in Fig. 5.15. It is visualized that the increase of current results in a brighter image because of the increase of temperature.

8 Fluorescence Microscopy

Only a few polymers can exhibit autofluorescence effect on excitation with visible light (488 nm), but polyurethanes will [33]. Other polymers should be strained by fluorescence dye such as Neocarmine, or Lumogen red 300, that can interact with objected materials. Fluorescence can improve the visibility of materials in blood and tissues, which can greatly enhance the application value of SMPs in areas such as biology and medicine.

8.1 Dynamic Memory Process—Molecular/Bond Switch

Dynamic memory process with breakage and recombination of molecular or bond switches have abilities to provide more information and opportunities on molecular design in novel memory polymers and enable more advanced as well as broader applications. However, this kind of dynamic memory process is not easy to follow and explore using the same method as used in common SMPs. For example, shape memory hydrogels (SMHs) have successfully found a large number of applications in smart soft materials like textiles and soft robotics. However, the detailed and in-depth exploration of the molecular-level dynamic change such as transition of cross-links is not easy enough. As a result, the fluorescence-assisted characterization method shows a great potential. As illustrated in Fig. 5.16, SME of chemically cross-linked poly- (dimethyl acrylamide) (PDMAA) network (permanent hard segment) −Alg hydrogel was directly visualized using Eu^{3+} ion solutions, where Eu^{3+} can spontaneously diffuse into the hydrogel and bind to alginate to fix the temporary shape. It is convenient that Eu^{3+}−Alg complexes have the ability to emit red light, at the same time, a quantitative study can be conducted [50].

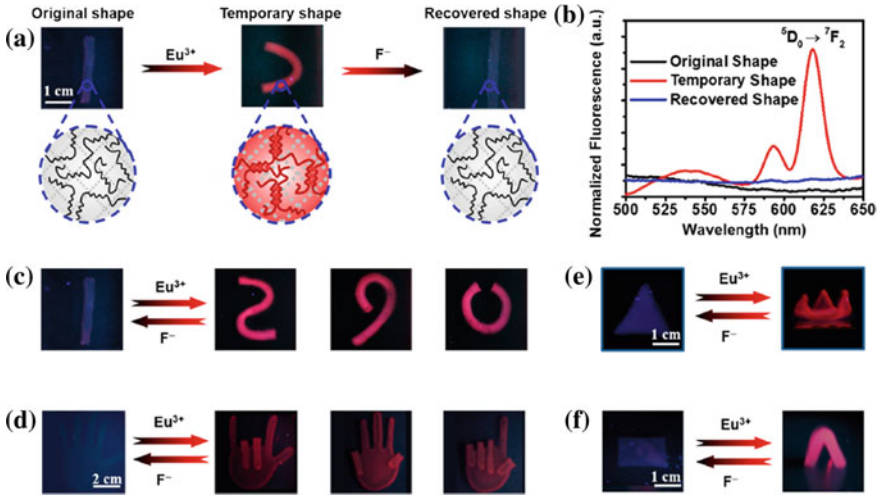

Fig. 5.16 **a** Demonstration of shape memory and recovery for PDMAA −Alg-17% hydrogel. **b** Recorded fluorescence spectra of original, temporary, and recovered shapes. **c** 1D → 2D shape memory and recovery. **d** 2D → 2D shape memory and recovery. **e**, **f** 2D → 3D shape memory and recovery. Copyright © 2018 American Chemical Society [49]

8.2 Biomaterial System

Polyurethane-based SMPs are well recognized as minimally invasive medical materials in the application of peripheral occlusion, vascular grafts, regenerated bones, tissue scaffolds, etc. However, due to the lack of visibility under clinical imaging, some of applications are limited. Therefore, fluorescent dyes are utilized to make SMP visible in clinical imaging and valuable in biomaterial system [71].

8.2.1 Cell/Bone Repair(Nanofiber/Foam)

Zhang's laboratory investigated the shape memory copolymer nanofibers, which are well capable of proliferating osteoblast as a scaffold for bone regeneration and possess good shape fixity and recovery effect. The morphology and proliferation of osteoblasts cultured onto the SMP scaffolds were directly observed by fluorescence microscopy [3]. In another research of bone generation, the cytotoxicity was evaluated through a live/dead viability assay qualitatively. As illustrated in Fig. 5.17, preosteoblast viability was not affected by addition and different contents of imHA into SMPU foams where the cell viability exhibited above 95%, illustrating no cytotoxicity of SMPU/imHA foams [80].

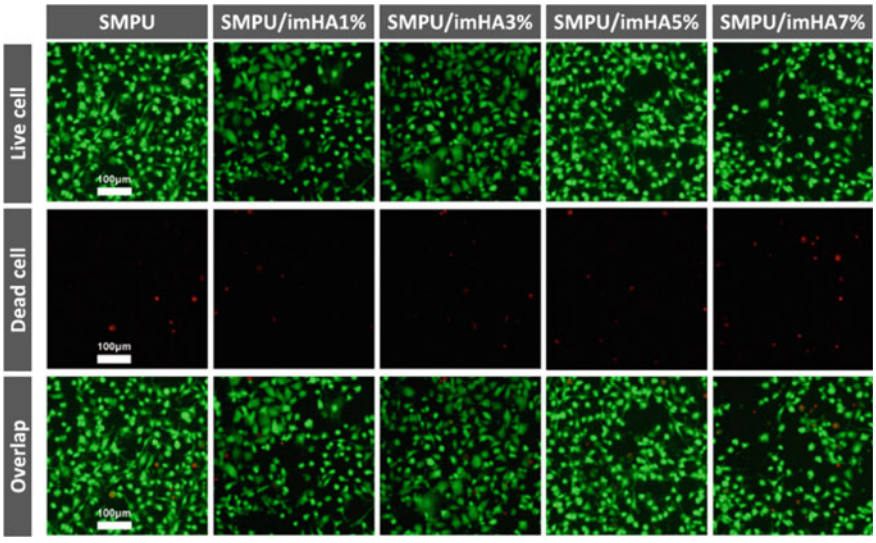

Fig. 5.17 Fluorescence images of the cells stained with calcein AM/PI. 0272-8842/© 2016 Elsevier Ltd. and Techna Group S.r.l. [80]

8.2.2 Carrier for Cell

Dynamically tunable surface microgrooves with SME were designed to regulate the differentiation of rat bone marrow mesenchymal stem cell (rBMSC). Figure 5.18 presents the cell arrangement in different surface microgrooves condition including non-patterned surface (Static-NP), 3-μm-wide microgroove surface (Static-3), and dynamic ones including compressed and stretched microgroove surfaces. The shape and arrangement of cells were better affected by dynamic surfaces compared with static ones. The cells distribute randomly on the surface of static non-patterned ones. This study proposed by Zhou et al. provided a facile strategy in mimicking natural cellular environment through a thermal-controlled surface microgrooves with memory effect to exactly regulate the cell differentiation [26, 27].

8.2.3 Carrier for Drug

SME of materials like particles which can change and recovery their shape with the stimuli of the environment have potential in drug carriers. The reversible shape switch of polymer particles was achieved through the tension of modified polyvinyl alcohol (PVA) film, of which the morphologies were directly observed by confocal laser scanning microscopy. Figure 5.19 shows spherical micrometer-sized particles with an average size of 5 μm. The particles can exist in a well-spherical shape and become a prolate ellipsoid when they are stretched and fixed. The microscopic

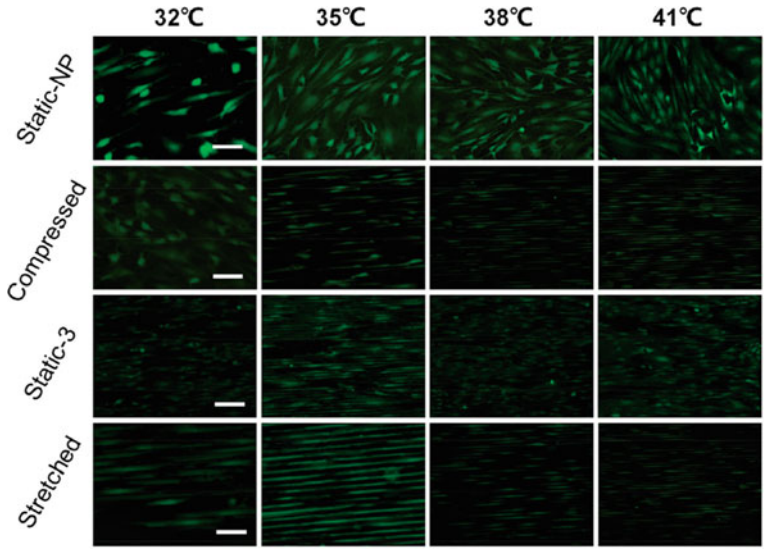

Fig. 5.18 Fluorescence images of rBMSCs stained with calcein AM (Scale bar: 20 μm) Copyright © 1999–2018 John Wiley & Sons, Inc. [26, 27]

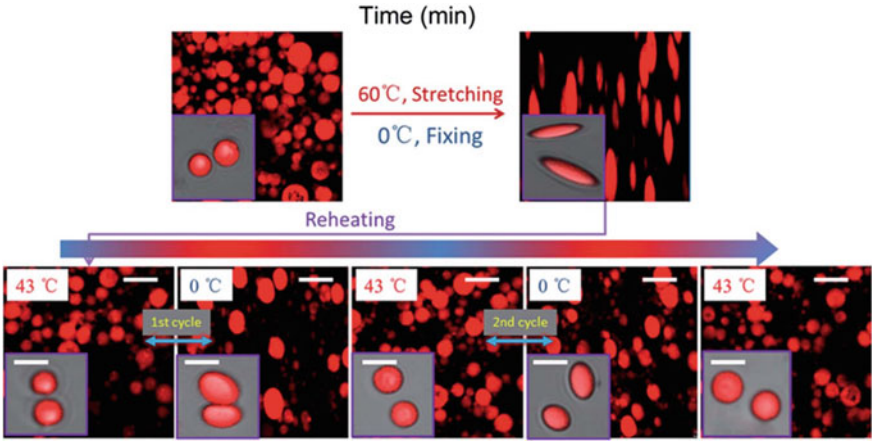

Fig. 5.19 Fluorescence images showing the deformation and fixation of the micro-sized particles (the stretching strain of PVA film is 200%) and microscopically reversible shape memory recovery process of the particles. The inset images are obtained by confocal laser scanning microscopy. (Scale bar: 10 mm). © The Royal Society of Chemistry 2014 [26, 27]

reversible SME from the shape of sphere to spheroidicity can be clearly observed in cyclic heating and cooling process.

9 Laser Scanning Confocal Microscopy (LSCM)

Materials with larger thickness than about 50 μm cannot be well recognized by common microscopies, especially the inner structure. As a modern technique, LSCM can achieve 3D imaging with high resolution without destroying the specimen. It has been used to investigate the structural information directly through the thickness of films, the biological cells or semiconductor devices. For conductive SMPs with conductive fillers, structural change of conductive fillers during tension can be monitored by an LSCM using carbon nanotube composite/natural rubber as a model compound [45, 46].

9.1 SMP Foam Structure

Owing to the existence of a large number of micropores, the polymeric foam has the characteristics of small density, shock absorption, insulation, etc., and thus has a wide range of uses. SMP foam has these advantages plus the ability to respond to external stimuli, expanding its application field to larger areas especially biomedical ones such as endovascular interventions [58], aneurysm treatment [2]. However,

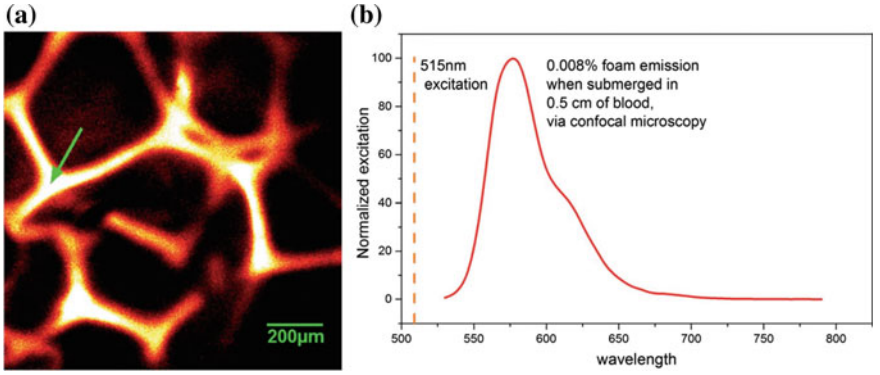

Fig. 5.20 **a** 0.01% fluorescent dyes (phloxine B (PhB) foam struts, taken by confocal microscopy through 0.5 cm of porcine blood. **b** Emission spectra taken at the arrow in A, using 515 nm light for excitation. © The Royal Society of Chemistry [71]

their invisibility under the clinic imaging limits these advantages. Consequently, the influence of fluorescent dyes (phloxine B (PhB) on SMP was studied systematically from thermomechanical behaviors to SME. Results show that the foam structure of SMP were clearly imaged by an Olympus Fluoview 1000 LSCM and were excited at 543 nm utilizing <1% maximum intensity as illustrated in Fig. 5.20. The homogenous emission from the foam struts can be distinctively visualized via blood. The fluorescent dyes (phloxine B (PhB) make SMP a promising materials in biomedical materials system [71].

9.2 SMP Foam as Carrier for Cell

The porous nature of the foam is well suited for use in cell scaffolds. In biological research, if the distribution of cells in a thick material is expected to be investigated, confocal micro scanning microscopy is the best choice. It is capable of providing 3D views of cells location in each depth of materials that cannot be achieved by common microscopy which can only focus on one layer. For example, before observing the MC3T3-E1 preosteoblasts infiltrating inside SMP foam through LSCM, the samples were firstly stained by calcein AM [79]. Figure 5.21 presents that labeled cells with green color could infiltrate deeper with an increase of cultivation period, illustrating the excellent biocompatibility of SMP foam for bone generation.

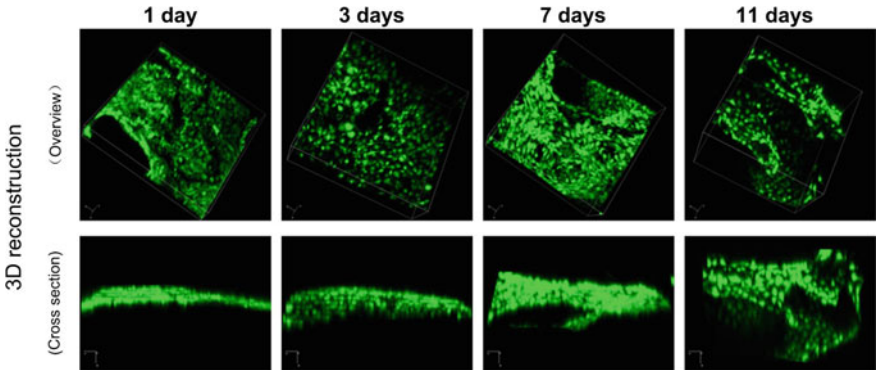

Fig. 5.21 In vitro cell infiltration and viability. **a** Reconstructed 3D confocal microscopic images of preosteoblasts infiltrating into the SMP foam (field of view, 653 × 653 μm) 0304-4165/© 2018 Elsevier B.V. [79]

9.3 SMP Substrates for Cell Activity

SMP have been proved to have a significant impact on macrophage activity. Usually, macrophages take hours to complete transformation from elliptical shape to circular one, so Guo et al. proposed a kind of photothermal actuation to influence macrophage where a laser was utilized to activate the light-induced shape recovery of shape memory microparticles [29]. They measured that the aspect ratio reversion was detected only within the 5 mm diameter of the laser spot, where the aspect ratio of the particle is almost 1, indicating a spherical form with irradiation. It was visualized that SME can be effectively triggered by laser in biocompatible temperature range and is restricted to the irradiated area. They also presented Macrophage Phagocytosis influenced by shape memory response of differentially stretched particles triggered by laser. It was proved that low temperature stretched particles (blue) can recovery to spherical form during heating compared to the high temperature stretched particles (magenta). As a result, low-temperature-stretched particles are easier to be phagocytosed, indicating the large influence of SME from nanoparticles on Macrophage Phagocytosis.

SMP was also used as actin cell culture substrates where substrate topography was studied to control cell behaviors as illustrated in Fig. 5.22 [14]. The SME of substrates were triggered after plating cells on it. As shown in Fig. 5.22a, cell actin cytoskeleton microfilaments align with groove direction in temporary shape before transition, while they begin to rearrange and become randomly oriented when substrate recovers to flat. Figure 5.22b presents randomly oriented microfilaments before and after transition in flat control. Figure 5.22c shows microfilaments align with groove direction in grooved control before and after temperature increase. It was also proved that SME of substrates has a comparable effect on cells.

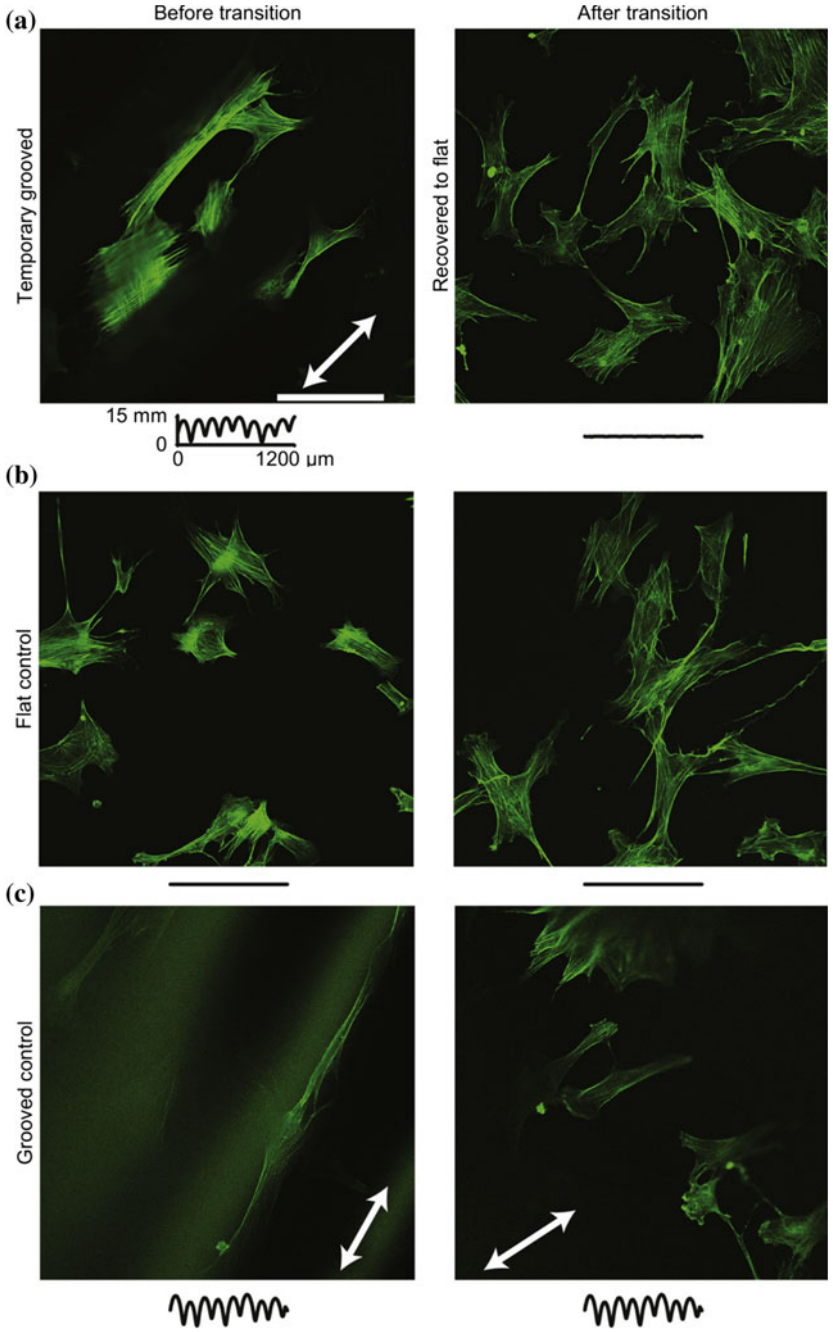

Fig. 5.22 Cell actin cytoskeleton rearranges following topographic transition. **a** Confocal images of cells stained with phalloidin on a temporary grooved topography. **b** Cells on flat control substrates. **c** Cells on grooved control substrates. Scale bar is 100 mm. Copyright © 2010 Elsevier Ltd. [14]

9.4 SMP Particles as Carrier for Drug

In biological research like drug delivery, the shape of particle has large influence on phagocytic internalization. It is shown in Fig. 5.23 that the spherical particle has been all taken up after 15 min while the ellipsoidal particle still stays on the surface. However, once the ellipsoidal particles enter the target cells, the shape can recover to spherical ones with mild stimulus as shown in Figure B. The advantage of this characteristic shape change of particles as drug carriers can prolong the blood circulation and enlarge the effectiveness of drug by escaping premature phagocytosis [26, 27].

10 Conclusions and Outlook

SMPs have great potential due to their structural characteristics. They can respond to different forms of external stimuli, possess flexible structural design and performance as well as large extensibility and volume-to-mass ratio. Research on shape memory polymeric materials including SMPC or blends has been greatly developed.

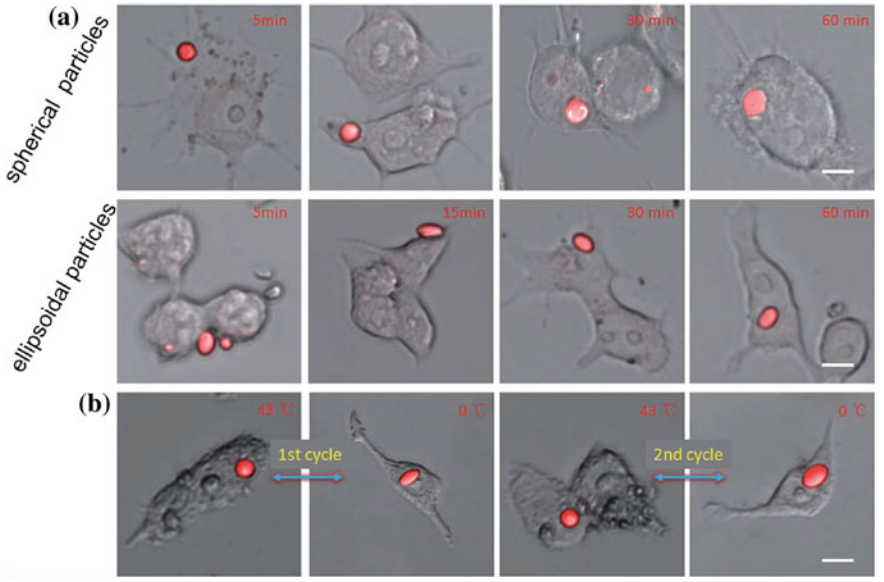

Fig. 5.23 Phagocytosis and intracellular shape memory recovery of the shape-switching particles. **a** The association process of both spherical and ellipsoidal particles with macrophages, observed with CLSM at 5, 15, 30, and 60 min. These particles are stained with a fluorescent dye, Nile red. **b** Intracellularly reversible shape memory recovery of the particles. (Scale bar: 10 mm). © The Royal Society of Chemistry 2014 [26, 27]

Most microscopy applications provide a characterization on the basic structure of materials in current research. For example, phase identification and separation can be characterized by OM, POM, SEM, TEM, and AFM. The size of the fillers in SMPC, the degree of fusion with the matrix, and their effect on the matrix are mostly characterized by SEM, TEM, AFM. SEM and AFM are the best tools for the investigation of surface treatment and surface pattern on SMP substrates. Fluorescence microscopy and LSCM are useful for studying SMP in biomedical fields, such as the effect of materials on cellular activity, or in drug delivery. There is also a class of SMEs that specialize in microlevel or nanolevel, where SEM, TEM, and AFM are good choices. However, there are more applications for SMP combined with microscopes waiting for us to dig. For example, cryo-electron microscopy is very rare in SMP studies. The cryo-electron microscope usually mounts a device for freezing the sample on a normal-temperature electron microscope. Freezing the sample can reduce the unexpected deformation of the sample due to electron beam, which is of great significance for protein research with flexible structures in biology [4]. The 2017 Nobel Prize in Chemistry was awarded to Dr. Jacques Dubochet, Dr. Joachim Frank and Richard Henderson who promoted the development of cryo-electron microscopy, which we should develop in area of SMPs. Besides, infrared microscopy with high time resolution is also expected in many thermal-induced SMPs, where the temperature change and distribution of materials can be precisely captured and evidently visualized.

References

1. Ansari M, Golzar M, Baghani M, Soleimani M (2018) Shape memory characterization of poly (ε-caprolactone)(PCL)/polyurethane (PU) in combined torsion-tension loading with potential applications in cardiovascular stent. Polym Test
2. Baer GM, Small W, Wilson TS, Benett WJ, Matthews DL, Hartman J, Maitland DJ (2007) Fabrication and in vitro deployment of a laser-activated shape memory polymer vascular stent. Biomed Eng Online 6(1):43
3. Bao M, Lou X, Zhou Q, Dong W, Yuan H, Zhang Y (2014) Electrospun biomimetic fibrous scaffold from shape memory polymer of PDLLA-co-TMC for bone tissue engineering. ACS Appl Mater Interfaces 6(4):2611–2621
4. Baretić D, Pollard HK, Fisher DI, Johnson CM, Santhanam B, Truman CM, Kouba T, Fersht AR, Phillips C, Williams RL (2017) Structures of closed and open conformations of dimeric human ATM. Sci Advanc 3(5)
5. Behl M, Lendlein A (2007) Shape-memory polymers. Mater Today 10(4):20–28
6. Burnham NA, Colton RJ (1989) Measuring the nanomechanical properties and surface forces of materials using an atomic force microscope. J Vacuum Sci Technol A Vacuum Surf Films 7(4):2906–2913
7. Chen HM, Wang L, Zhou SB (2018) Recent progress in shape memory polymers for biomedical applications. Chinese J Polym Sci: 1–13
8. Chen H, Xia H, Ni Q-Q (2018) Study on material performances of lead zirconate titanate/shape memory polyurethane composites combining shape memory and piezoelectric effect. Appl Sci Manufact, Compos Part A
9. Chen S, Ban J, Mu L, Zhuo H (2018) Development of liquid crystalline polyurethane composites with stage-responsive shape memory effects. Polym Chem 9(5):576–583

10. Cheng X, Kondyurin A, Bao S, Bilek MM, Ye L (2017) Plasma immersion ion implantation of polyurethane shape memory polymer: surface properties and protein immobilization. Appl Surf Sci 416:686–695
11. Cho JW, Kim JW, Jung YC, Goo NS (2005) Electroactive shape-memory polyurethane composites incorporating carbon nanotubes. Macromol Rapid Commun 26(5):412–416
12. Cox LM, Killgore JP, Li Z, Long R, Sanders AW, Xiao J, Ding Y (2016) Influences of substrate adhesion and particle size on the shape memory effect of polystyrene particles. Langmuir 32(15):3691–3698
13. Cox LM, Killgore JP, Li Z, Zhang Z, Hurley DC, Xiao J, Ding Y (2014) Morphing metal–polymer Janus particles. Adv Mater 26(6):899–904
14. Davis KA, Burke KA, Mather PT, Henderson JH (2011) Dynamic cell behavior on shape memory polymer substrates. Biomaterials 32(9):2285–2293
15. Deng Z, Guo Y, Ma PX, Guo B (2018) Rapid thermal responsive conductive hybrid cryogels with shape memory properties, photothermal properties and pressure dependent conductivity. J Colloid Interface Sci
16. Ebara M (2015) Shape-memory surfaces for cell mechanobiology. Sci Technol Adv Mater 16(1):014804
17. Ebara M, Uto K, Idota N, Hoffman JM, Aoyagi T (2012) Shape-memory surface with dynamically tunable nano-geometry activated by body heat. Adv Mater 24(2):273–278
18. Eisenhaure JD, Xie T, Varghese S, Kim S (2013) Microstructured shape memory polymer surfaces with reversible dry adhesion. ACS Appl Mater Interfaces 5(16):7714–7717
19. Espinha A, Guidetti G, Serrano MC, Frka-Petesic B, Dumanli AG, Hamad WY, Blanco A, López C, Vignolini S (2016) Shape memory cellulose-based photonic reflectors. ACS Appl Mater Interfaces 8(46): 31935–31940
20. Fadeev M, Davidson-Rozenfeld G, Biniuri Y, Yakobi R, Cazelles R, Aleman-Garcia MA, Willner I (2018) Redox-triggered hydrogels revealing switchable stiffness properties and shape-memory functions. Polym Chem
21. Fang L, Gould OE, Lysyakova L, Jiang Y, Sauter T, Frank O, Becker T, Schossig M, Kratz K, Lendlein A (2018) Implementing and quantifying the shape-memory effect of single polymeric micro/nanowires with an atomic force microscope. Chem Phys Chem
22. Fu CC, Grimes A, Long M, Ferri CG, Rich BD, Ghosh S, Ghosh S, Lee LP, Gopinathan A, Khine M (2009) Tunable nanowrinkles on shape memory polymer sheets. Adv Mater 21(44):4472–4476
23. Fu S, Ren H, Ge Z, Zhuo H, Chen S (2017) Shape memory polyurethanes based on zwitterionic hard segments. Polymers 9(10):465
24. Gall K, Mikulas M, Munshi NA, Beavers F, Tupper M (2000) Carbon fiber reinforced shape memory polymer composites. J Intell Mater Syst Struct 11(11):877–886
25. Ghaemi F, Abdullah LC, Kargarzadeh H, Abdi MM, Azli NFWM, Abbasian M (2018) Comparative study of the electrochemical, biomedical, and thermal properties of natural and synthetic nanomaterials. Nanoscale Res Lett 13(1):112
26. Gong T, Zhao K, Wang W, Chen H, Wang L, Zhou S (2014) Thermally activated reversible shape switch of polymer particles. J Mater Chem B 2(39):6855–6866
27. Gong T, Zhao K, Yang G, Li J, Chen H, Chen Y, Zhou S (2014) The control of mesenchymal stem cell differentiation using dynamically tunable surface microgrooves. Advanc Healthcare Mater 3(10):1608–1619
28. Gunes IS, Cao F, Jana SC (2008) Evaluation of nanoparticulate fillers for development of shape memory polyurethane nanocomposites. Polymer 49(9):2223–2234
29. Guo Q, Bishop CJ, Meyer RA, Wilson DR, Olasov L, Schlesinger DE, Mather PT, Spicer JB, Elisseeff JH, Green JJ (2018) Entanglement-Based thermoplastic shape memory polymeric particles with photothermal actuation for biomedical applications. ACS Appl Mater Interfaces 10(16):13333–13341
30. Han JP, Zhu Y, Hu JL, Luo HS, Yeung LY, Li WG, Meng QH, Ye GD, Zhang S, Fan Y (2012) Morphology, reversible phase crystallization, and thermal sensitive shape memory effect of cellulose Whisker/SMPU nano-composites. J Appl Polym Sci 123(2):749–762

31. Han Y, Hu J, Jiang L (2018) Collagen skin, a water-sensitive shape memory material. J Mater Chem B
32. Han Y, Hu J, Xin Z (2018) In-Situ incorporation of alkyl-grafted silica into waterborne polyurethane with high solid content for enhanced physical properties of coatings. Polymers 10(5):514
33. Heckmann W (2005) Characterization of polymer materials by fluorescence imaging. Microsc Microanal 11(S02):2036–2037
34. Hu J, Zhu Y, Huang H, Lu J (2012) Recent advances in shape–memory polymers: structure, mechanism, functionality, modeling and applications. Prog Polym Sci 37(12):1720–1763
35. Huang J, Lai L, Chen H, Chen S, Gao J (2018) Development of a new shape-memory polymer in the form of microspheres. Mater Lett 225:24–27
36. Jahid MA, Hu J, Wong K, Wu Y, Zhu Y, Sheng HL, Zhongmin D (2018) Fabric coated with shape memory polyurethane and its properties. Polymers (20734360) 10(6)
37. Ji F, Zhu Y, Hu J, Liu Y, Yeung L-Y, Ye G (2006) Smart polymer fibers with shape memory effect. Smart Mater Struct 15(6):1547
38. Jin Yoo H, Chae Jung Y, Gopal Sahoo N, Whan Cho J (2006) Polyurethane-Carbon nanotube nanocomposites prepared by in-situ polymerization with electroactive shape memory. J Macromol Sci Part B 45(4):441–451
39. Kashyap D, Kumar PK, Kanagaraj S (2018) 4D printed porous radiopaque shape memory polyurethane for endovascular embolization Additive Manufact
40. Lan X, Liu Y, Lv H, Wang X, Leng J, Du S (2009) Fiber reinforced shape-memory polymer composite and its application in a deployable hinge. Smart Mater Struct 18(2):024002
41. Lee SJ, Atala A (2013) Scaffold technologies for controlling cell behavior in tissue engineering. Biomed Mater 8(1):010201
42. Leng J, Lan X, Liu Y, Du S, Huang W, Liu N, Phee S, Yuan Q (2008) Electrical conductivity of thermoresponsive shape-memory polymer with embedded micron sized Ni powder chains. Appl Phys Lett 92(1):014104
43. Libera MR, Egerton RF (2010) Advances in the transmission electron microscopy of polymers. Polym Rev 50(3):321–339
44. Liu R, Dai H, Zhou Q, Zhang Q, Zhang P (2016) Synthesis and characterization of shape-memory poly carbonate urethane microspheres for future vascular embolization. J Biomater Sci Polym Edition 27(12):1248–1261
45. Liu W, Chen H, Ge M, Ni Q-Q, Gao Q (2018) Electroactive shape memory composites with TiO_2 whiskers for switching an electrical circuit. Mater Design 143:196–203
46. Liu X, Su G, Guo Q, Lu C, Zhou T, Zhou C, Zhang X (2018) Hierarchically structured self-healing sensors with tunable positive/negative piezoresistivity. Advanc Function Mater 28(15):1706658
47. Liu X, Su G, Guo Q, Lu C, Zhou T, Zhou C, Zhang X (2018) Hierarchically structured self-healing sensors with tunable positive/negative piezoresistivity. Advanc Function Mater: 1706658
48. Liu ZQ, Jiao D, Zhang ZF (2015) Remarkable shape memory effect of a natural biopolymer in aqueous environment. Biomaterials 65:13–21
49. Lu W, Ma C, Zhang D, Le X, Zhang J, Huang Y, Huang CF, Chen T (2018) Real-time and in-situ investigation of supramolecular shape memory process by fluorescence switching. J Phys Chem C
50. Luo H, Wang H, Zhou H, Zhou X, Hu J, Yi G, Hao Z, Lin W (2018) Shape memory-enhanced electrical self-healing of stretchable electrodes. Appl Sci 8(3):392
51. Luo HS, Hu JL, Zhu Y, Zhang S, Fan Y, Ye GD (2012) Achieving shape memory: reversible behaviors of cellulose-PU blends in wet-dry cycles. J Appl Polym Sci 125(1):657–665
52. Luo X, Zhang X, Wang M, Ma D, Xu M, Li F (1997) Thermally stimulated shape-memory behavior of ethylene oxide-ethylene terephthalate segmented copolymer. J Appl Polym Sci 64(12):2433–2440
53. Meier T, Bur J, Reinhard M, Schneider M, Kolew A, Worgull M, Hölscher H (2015) Programmable and self-demolding microstructured molds fabricated from shape-memory polymers. J Micromech Microeng 25(6):065017

54. Mendez J, Annamalai PK, Eichhorn SJ, Rusli R, Rowan SJ, Foster EJ, Weder C (2011) Bioinspired mechanically adaptive polymer nanocomposites with water-activated shape-memory effect. Macromolecules 44(17):6827–6835
55. Meng QH, Hu JL (2008) Self-organizing alignment of carbon nanotube in shape memory segmented fiber prepared by in situ polymerization and melt spinning. Compos Part A Appl Sci Manufact 39(2):314–321
56. Meng QH, Hu JL, Ho KC, Ji FL, Chen SJ (2009) The shape memory properties of biodegradable Chitosan/Poly(L-lactide) composites. J Polym Environ 17(3):212–224
57. Meng QH, Hu JL, Zhu Y (2007) Shape-memory polyurethane/multiwalled carbon nanotube fibers. J Appl Polym Sci 106(2):837–848
58. Metcalfe A, Desfaits A-C, Salazkin I, Yahia LH, Sokolowski WM, Raymond J (2003) Cold hibernated elastic memory foams for endovascular interventions. Biomaterials 24(3):491–497
59. Mohr R, Kratz K, Weigel T, Lucka-Gabor M, Moneke M, Lendlein A (2006) Initiation of shape-memory effect by inductive heating of magnetic nanoparticles in thermoplastic polymers. Proc Nat Acad Sci USA 103(10):3540–3545
60. Parameswaranpillai J, Ramanan SP, George JJ, Jose S, Zachariah AK, Siengchin S, Yorseng K, Janke A, Pionteck J (2018) PEG-ran-PPG modified epoxy thermosets: a simple approach to develop tough shape memory polymers. Indust Eng Chem Res 57(10): 3583–3590
61. Raghunath S, Kumar S, Samal SK, Mohanty S, Nayak SK (2018) PLA/ESO/MWCNT nanocomposite: a study on mechanical, thermal and electroactive shape memory properties. J Polym Res 25:1–12
62. Romo-Uribe A, Albanil L (2017) Dynamics retardation in hybrid POSS-NIPAm nanocomposites. Thermoplastic and thermally-responsive hydrogel behavior. Eur Polym J
63. Sahoo NG, Jung YC, Cho JW (2007) Electroactive shape memory effect of polyurethane composites filled with carbon nanotubes and conducting polymer. Mater Manufact Proc 22(4):419–423
64. Schmidt AM (2006) Electromagnetic activation of shape memory polymer networks containing magnetic nanoparticles. Macromol Rapid Commun 27(14):1168–1172
65. Song HB, Baranek A, Worrell BT, Cook WD, Bowman CN (2018) Photopolymerized Triazole-based glassy polymer networks with superior tensile toughness. Advanc Function Mater: 1801095
66. Song Y, Zhou S, Jin K, Qiao J, Li D, Xu C, Hu D, Di J, Li M, Zhang Z (2018) Hierarchical carbon nanotube composite yarn muscles. Nanoscale 10(8):4077–4084
67. Stuart BH (2008) Polymer analysis. Wiley
68. Tan L, Hu J, Huang H, Han J, Hu H (2015) Study of multi-functional electrospun composite nanofibrous mats for smart wound healing. Int J Biol Macromol 79:469–476
69. Tan L, Hu J, Ying Rena K, Zhu Y, Liu P (2017) Quick water-responsive shape memory hybrids with cellulose nanofibers. J Polym Sci Part A Polym Chem 55(4):767–775
70. Tan L, Hu J, Zhao H (2015) Design of bilayered nanofibrous mats for wound dressing using an electrospinning technique. Mater Lett 156:46–49
71. Weems A, Raymond J, Easley A, Wierzbicki M, Gustafson T, Monroe M, Maitland D (2017) Shape memory polymers with visible and near-infrared imaging modalities: synthesis, characterization and in vitro analysis. RSC Advanc 7(32):19742–19753
72. Wornyo E, Gall K, Yang F, King W (2007) Nanoindentation of shape memory polymer networks. Polymer 48(11):3213–3225
73. Wu Q, Hu J (2016) Waterborne polyurethane based thermoelectric composites and their application potential in wearable thermoelectric textiles. Compos Part B Eng 107:59–66
74. Wu Y, Hu J, Zhang C, Han J, Wang Y, Kumar B (2015) A facile approach to fabricate a UV/heat dual-responsive triple shape memory polymer. J Mater Chem A 3(1):97–100
75. Xiao X, Hu J (2016) Animal hairs as water-stimulated shape memory materials: mechanism and structural networks in molecular assemblies. Scientif Rep 6:26393
76. Xiao X, Xie T, Cheng Y-T (2010) Self-healable graphene polymer composites. J Mater Chem 20(17):3508–3514

77. Xiao XL, Hu JL (2016) Influence of sodium bisulfite and lithium bromide solutions on the shape fixation of camel guard hairs in slenderization process. Int J Chem Eng
78. Xiao XL, Hu JL, Hui D (2016) Tensile-relaxation study of camel hair fiber at elastic stretching region: Analytical model and experiment. Compos Part B-Eng 91:559–568
79. Xie R, Hu J, Hoffmann O, Zhang Y, Ng F, Qin T, Guo X (2018) Self-fitting shape memory polymer foam inducing bone regeneration: a rabbit femoral defect study. Biochimica et Biophysica Acta (BBA)-General Subjects 1862(4): 936–945
80. Xie R, Hu J, Ng F, Tan L, Qin T, Zhang M, Guo X (2017) High performance shape memory foams with isocyanate-modified hydroxyapatite nanoparticles for minimally invasive bone regeneration. Ceramics Int 43(6):4794–4802
81. Yang B, Huang WM, Li C, Chor JH (2005) Effects of moisture on the glass transition temperature of polyurethane shape memory polymer filled with nano-carbon powder. Eur Polym J 41(5):1123–1128
82. Yang F, Wornyo E, Gall K, King W (2007) Nanoscale indent formation in shape memory polymers using a heated probe tip. Nanotechnology 18(28):285302
83. Yin Q, Wang D, Jia H, Ji Q, Wang L, Li G, Yin B (2018) Water-induced modulus changes of bio-based uncured nanocomposite film based on natural rubber and bacterial cellulose nanocrystals. Indust Crops Products 113:240–248
84. Yoo J-W, Mitragotri S (2010) Polymer particles that switch shape in response to a stimulus. Proc Nat Acad Sci 107(25):11205–11210
85. Yu K, Liu Y, Leng J (2011) Conductive shape memory polymer composite incorporated with hybrid fillers: electrical, mechanical, and shape memory properties. J Intell Mater Syst Struct 22(4):369–379
86. Yu K, Liu Y, Liu Y, Peng H-X, Leng J (2014) Mechanical and shape recovery properties of shape memory polymer composite embedded with cup-stacked carbon nanotubes. J Intell Mater Syst Struct 25(10):1264–1275
87. Yu Z, Zhang Q, Li L, Chen Q, Niu X, Liu J, Pei Q (2011) Highly flexible silver nanowire electrodes for shape-memory polymer light-emitting diodes. Advanc Mater 23(5):664–668
88. Zhang H, Wang H, Zhong W, Du Q (2009) A novel type of shape memory polymer blend and the shape memory mechanism. Polymer 50(6):1596–1601
89. Zhu Y, Hu J, Luo H, Young RJ, Deng L, Zhang S, Fan Y, Ye G (2012) Rapidly switchable water-sensitive shape-memory cellulose/elastomer nano-composites. Soft Matter 8(8):2509–2517
90. Zhu Y, Hu JL, Liu YJ (2009) Shape memory effect of thermoplastic segmented polyurethanes with self-complementary quadruple hydrogen bonding in soft segments. Eur Phys J E 28(1):3–10
91. Zhu Y, Hu JL, Luo HS, Young RJ, Deng LB, Zhang S, Fan Y, Ye GD (2012) Rapidly switchable water-sensitive shape-memory cellulose/elastomer nano-composites. Soft Matter 8(8):2509–2517
92. Zhu Y, Hu JL, Yeung KW, Liu YQ, Liem HM (2006) Influence of ionic groups on the crystallization and melting behavior of segmented polyurethane ionomers. J Appl Polym Sci 100(6):4603–4613
93. Zhuo HT, Hu JL, Chen SJ (2008) Electrospun polyurethane nanofibres having shape memory effect. Mater Lett 62(14):2074–2076

Dynamical Mechanical Thermal Analysis of Shape-Memory Polymers

Pauline Butaud, Morvan Ouisse, Kévin Jaboviste, Vincent Placet and Emmanuel Foltête

Abstract This chapter is dedicated to the dynamical mechanical thermal analysis of shape-memory polymers. Temperature obviously plays a major role in the mechanical properties of these materials; hence, the understanding of the physical phenomena driving the shape-memory effect is of first importance for the design of practical applications in which shape-memory polymers are used. The shape-memory effect being closely related to the viscoelastic behavior of the polymer, it is important to properly describe it with appropriate tools. The objective of this chapter is to describe characterization methods, models, and parameters identification techniques that can be easily used for the description of the thermomechanical behavior of SMPs. The associated models can easily be implemented in finite element codes for time- or frequency-domain simulations. The experimental results and all numerical values of the models are provided for three shape-memory polymers: the tBA/PEGDMA and a vitrimer, which can easily be manufactured according to the data provided in open literature, and a shape-memory polymer filament for 3D printing, which is available on the shelf.

1 Introduction

As all polymers, shape-memory polymers (SMPs) exhibit a strong viscoelastic behavior. The stable rubbery and glassy states play a major role in the shape-memory effect, which is associated with fast transitions between these states with a large elasticity gap, inducing high loss factor values at glass transition [1, 2]. The typical values of the loss factor which are reported in SMP-related open literature typically vary between 0.5 [3] and more than 2.5 [4, 5], most of them being between 1 and 2 [6–9]. These qualitatively high values of loss factor must be considered for practical applications since they can have a strong impact on the efficiency and the behav-

P. Butaud · M. Ouisse (✉) · K. Jaboviste · V. Placet · E. Foltête
FEMTO-ST Department of Applied Mechanics, University of Bourgogne Franche-Comté, 24 rue de l'Epitaphe, 25000 Besançon, France
e-mail: morvan.ouisse@femto-st.fr

J. Parameswaranpillai et al. (eds.), *Shape Memory Polymers, Blends and Composites*, Advanced Structured Materials 115,
https://doi.org/10.1007/978-981-13-8574-2_6

ior of the SMP-based devices. For applications in which only static phenomena are involved, the intrinsic losses may be neglected but as soon as dynamical phenomena contribute to the mechanical response, viscoelastic effects must be considered. This has been highlighted for years now, and numerous works can be found in the literature that present models of the shape-memory effect based on rate-dependent viscoelastic models [10–16]. Recently, these materials have been identified as able to play a major role in damping-related applications, thanks to the high damping capacities associated with the glass transition [17]. In these applications, the shape-memory material acts as a classical passive damping treatment, which is known to be a reliable, low cost, and robust solution for vibration control [18, 19], whose damping and stiffness can be tuned by a temperature control [20]. The polymer layer is classically used as a core in a multilayered composite, in order to enhance the shear effects in the material, leading to high damping performance. Many articles have been published on composite structures embedding viscoelastic materials to damp vibrations [21, 22]. The design optimization of multilayers structures has particularly been investigated [23–26] by varying the thickness of the viscoelastic layer, the fiber orientation, or the aspect ratio of the structure. When dealing with these materials, it is important to precisely describe the behavior of interest with adequate models based on confident parameters. The most usual way to obtain the viscoelastic mechanical properties of a polymer is the Dynamic Mechanical Analysis (DMA), also called Dynamical Mechanical Thermal Analysis (DMTA), which consists in conducting mechanical tests on a small frequency band and a large temperature range [27–29]. Using laws such as Williams–Landel–Ferry (WLF) law [30] or Arrhenius law [31], in a Time–Temperature Superposition (TTS) model, DMA measurements are used in order to obtain the mechanical behavior of the polymer on a large band of frequencies and temperatures. The extrapolated properties obtained can then be used to design composite structures. Even if some limitations of this apparatus have been reported (effect of the instrument compliance [32], of the specimen dimensions [33] or even of the chosen TTS model [6]), and despite the fact that viscoelastic properties are often obtained only for a specific loading mode, DMA remains a confident way to obtain a description of the behavior which is valid for different loading modes, for different scales, on wide temperature, and frequency ranges, even for shape-memory polymers [4]. Among others, these materials are very good candidates for temperature-controlled damping devices [20, 34].

In this chapter, original results are presented for three shape-memory polymers: the tBA/PEGDMA and the vitrimer, which can easily be manufactured according to the data provided in the open literature, and a shape-memory polymer filament for 3D printer, which is available on the shelf. For each of these materials, DMA results are performed by varying frequency and temperature, the TTS is checked, and a corresponding model is described. Finally, a viscoelastic model (Generalized Maxwell model) is identified in order to describe the behavior of the material on a wide frequency and temperature ranges. All numerical values of the models are provided in order that readers can use the data in their work.

The chapter is organized as follows: Sect. 2 describes the three materials used in this work, Sect. 3 presents the DMA apparatus and protocol, Sect. 4 describes the viscoelastic and TTS models, and Sect. 5 provides all the results.

2 Materials

In this section, the three materials considered in this chapter are presented.

2.1 tBA/PEGDMA

Srivastava et al. [35] introduced the tBA/PEGDMA as shape-memory polymer in 2010. This material is used here, following the procedure described in Yakacki et al. [36] to elaborate the samples. The chemical components were obtained from Sigma-Aldrich and used as received. The SMP is obtained by mixing 95 wt% of tert-butyl acrylate (tBA) with 5 wt% of poly(ethylene glycol) dimethacrylate (PEGDMA) which is a cross-linking agent with a molecular weight of Mn = 550 g/mol. 2.2-dimethoxy-2-phenylacetophenone (DMPA), and is added to the solution as photo-initiator (0.5 wt%). A mold constituted by two glass plates is used for the curing: 10 min UV exposure followed by 1 h heating (90 °C). The plates are machined for obtaining the shapes required for the mechanical tests.

The tBA/PEGDMA is thermo-rheologically simple [4], thermoset amorphous polymer. No crystallite and full cross-linking of the polymer was observed from DSC analysis. The density of the material is $\rho = 1000$ kg/m^3. The Poisson's ratio of the tBA/PEGDMA, determined during quasi-static tests (10^{-4} Hz) at room temperature [4], has been measured at $\nu = 0.37$.

2.2 SMP Filament

The shape-memory polymer filament is provided from SMP Technologies Inc. This polymer is available on the shelf for 3D printing. The filament is used as received and without any printing to avoid structural aspects in the evaluation of the mechanical properties. The SMP filament is a thermoplastic polymer with a density of 1260 kg/m^3 (determined by measuring the sample's mass and volume). This material may be used in most of FDM-based 3D printers to obtain the shapes of interest.

2.3 Vitrimer

The third shape-memory polymer studied in this paper is a vitrimer. It has been proposed by Ludwik Leibler [37]. In this work, the hard network of vitrimer is considered. It has been elaborated at FEMTO-ST Institute following the procedure described by Montarnal et al. [38]. The components were obtained from Sigma-Aldrich and used as received. The reaction of the diglycidyl ether of bisphenol A (DGEBA) with glutaric anhydride with epoxy/acyl 1:1 in the presence of 5 mol% zinc acetylacetonate [Zn(acac)2] provides the mixture, which is homogenized at 140 °C until phase miscibility. A mold is then used to cure the plates ($210 \times 300 \times 20$ mm^3) at 140 °C during 12 h. The produced plates were machined whenever necessary. The density of this polymer is 1290 kg/m^3.

3 Dynamical Mechanical Thermal Analysis

3.1 tBA/PEGDMA

A Metravib DMA50 apparatus is used with $29 \times 6 \times 3$ mm samples. The temperatures are changed by 5 °C or 10 °C steps between 30 °C and 90 °C with a heating rate of 2 °C/min. A sinusoidal tensile displacement varying from 0.1 Hz to 180 Hz is applied to the sample with an amplitude of 10 μm.

3.2 SMP Filament

A Metravib DMA300+ apparatus is used at temperatures varying by 5 °C steps at heating rate of 2 °C/min, between 33 °C and 83 °C. The temperature is stabilized for 1 min before each measurement to ensure a homogeneous temperature inside the specimen. Specimen's shape is cylindrical, with a diameter of 1.75 mm. The length is cut to 6 mm between the jaws. The frequency of the excitation varies from 0.1 Hz to 180 Hz. A sinusoidal tensile displacement is applied to the sample with a peak-to-peak amplitude of 5 μm allowing to ensure a linear viscoelastic behavior.

3.3 Vitrimer

A Bose Electroforce 3200 apparatus is used with $80 \times 2 \times 2$ mm samples, at temperatures varying by 5 °C steps at heating rate of 3 °C/min, between 36 °C and 102 °C. In order to ensure a homogeneous temperature inside the specimen, the temperature is stabilized for 2 min before each measurement. Inside the heating chamber, a ref-

erence sample including a thermocouple is used to measure the temperature. The range of frequencies is from 0.01 Hz to 10 Hz, with a mean amplitude of 4 N and a peak-to-peak amplitude of 6 N.

4 Models for Linear Viscoelasticity

Linear viscoelasticity has been studied by many authors in the context of continuous mechanics. Historically, Caputo [39] proposed in 1971 a linear modeling of the dissipation taking into account the history of the solicitations applied to the material. Later, Ferry [18] and Lakes [40] proposed a framework on the basics of modeling viscoelastic behavior. This work has been enhanced by many contributions such as that of Lesieutre [41] in which the constitutive equations of viscoelasticity are formulated in the time domain based on a method called *"Anelastic Displacement Fields"* (ADF). A general objective of these works was to understand and model the physical phenomena before adapting the formulations to numerical simulation tools. Among others, Salençon [42] and Chevalier [43] propose some syntheses of the mechanical phenomena linked to viscoelasticity.

A viscoelastic material has a response that varies over time even if the loading it undergoes is constant over time. If the loading is carried out in stress and the response is observed in strain, one speaks of creep test. The reciprocal is called as relaxation test. In addition, if a succession of loadings (in stress or strain) is applied to the material, then its final state corresponds to the sum of the modifications brought by each loading. The history of the loads applied to the viscoelastic material over time plays a major role in the behavior of the material, and hence on the associated models required to describe it. The following constitutive law, which relates the stress tensor σ_{ij} to the strain tensor ε_{kl}, includes this dependency:

$$\sigma_{ij}(t) = C^{\infty}_{ijkl}\varepsilon_{kl}(t) + \int_0^t C^{*}_{ijkl}(t-\tau)\dot{\varepsilon}_{kl}(\tau)d\tau + C_{ijkl}(t)\varepsilon_{kl}(0), \tag{1}$$

where $\sigma_{ij}(t) = C^{\infty}_{ijkl}\varepsilon_{kl}(t)$ corresponds to the elastic part of the constitutive law, C^{∞}_{ijkl} being the long-term elasticity tensor. The tensor $C^{*}_{ijkl}(t)$ is called relaxation function and can be determined by measuring the evolution of the stress as a function of time when the material is subjected to a constant displacement. The rheological models used in viscoelasticity are typically built according to the assumptions made on the kernel of the relaxation function C^{*}_{ijkl}. The Fourier transform of this viscoelastic law is

$$\hat{\sigma}_{ij}(\omega) = C^{\infty}_{ijkl}\hat{\varepsilon}_{kl}(\omega) + j\omega\hat{C}^{*}_{ijkl}(\omega)\hat{\varepsilon}_{kl}(\omega), \tag{2}$$

where $\hat{\cdot}$ corresponds to the Fourier transform and ω is the circular frequency. In order to simplify the writing for the introduction of the rheological models, in the following, we restrict equations to the mono-dimensional case, when the sample is subjected to a stress in tension. The constitutive law can then be written as

$$\hat{\sigma}(\omega) = E_\infty \hat{\varepsilon}(\omega) + j\omega \hat{E}^*(\omega)\hat{\varepsilon}(\omega), \tag{3}$$

where E_∞ represents the long-term elasticity modulus of the material for $t \to +\infty$ or $\omega \to 0$. This is classically written as

$$\hat{\sigma}(\omega) = E^*(\omega)\hat{\varepsilon}(\omega), \tag{4}$$

where $E^*(\omega)$ is called complex elastic modulus: in the frequency domain, linear viscoelastic problems can be solved as linear elastic problems with a complex modulus that depends on frequency. The real part of $E^*(\omega)$ is usually called storage modulus, its imaginary part being the loss modulus and the loss factor $\eta(\omega)$ being equal to the ratio between the imaginary and the real parts of the complex modulus:

$$\eta(\omega) = \frac{\mathrm{Im}(E^*(\omega))}{\mathrm{Re}(E^*(\omega))}. \tag{5}$$

4.1 Standard Rheological Models

Rheological models are classically used to define the frequency dependency of the complex modulus $E^*(\omega)$. The simplest model corresponds to constant values, which is called structural or hysteretic damping model:

$$E^* = E(1 + j\eta). \tag{6}$$

This corresponds to a very simple representation of the average viscoelastic behavior of the material. It is therefore generally used for lightly damped materials, such as metallic materials, that present a dissipated energy per cycle independent of the frequency when subjected to cyclic loading. The main drawback of this model is that it is noncausal which limits its use to the frequency domain [44]. Nevertheless, there is a way to make this model causal so that it can be used both in the frequency and time domains. The work carried out on the subject by Makris [45] leads to the formulation of a causal hysteretic model where the imaginary part is the same as that of the ideal hysteretic model:

$$E^*(\omega) = E(1 + j\eta \mathrm{sgn}(\omega)) \tag{7}$$

and where the real part is defined in order to make the model causal. Note that the ideal hysteretic model is equivalent to that expressed in Eq. (6) for positive frequencies.

In order to define a frequency dependency, rheological models have been historically built by combining simple mechanical elements like elastic springs and dampers. Figure 1 presents four standard rheological models commonly used in the literature.

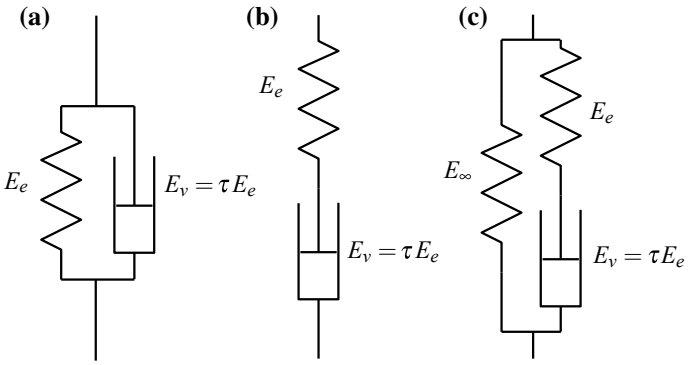

Fig. 1 Viscoelastic standard rheological models: **a** Kelvin–Voigt **b** Maxwell **c** Zener

The Kelvin–Voigt model (Fig. 1a) is a simple model composed of a spring (with a stiffness E_e) and a damper (with a viscous damping constant E_v) in parallel. Its complex modulus is written as

$$E^*(\omega) = E_e + j\omega E_v. \tag{8}$$

It can be used as the first approximation to represent a viscoelastic behavior, even if the applicability is generally restricted to a narrow frequency band. In addition, this model is only suitable for low frequencies since the damping force tends to infinity when the frequency increases.

The Maxwell model (Fig. 1b) is composed of a spring and a damper in series and the associated complex modulus can be expressed as

$$E^*(\omega) = E_e \frac{j\omega\tau}{1 + j\omega\tau}, \tag{9}$$

where $\tau = E_v/E_e$ is the relaxation time. This model can be used to describe the viscoelastic behavior but it is only applicable for a reduced frequency range as for the Kelvin–Voigt model and is not realistic at low frequency since it does not include a pure elastic component.

The Zener model, also named Standard Linear Solid model (Fig. 1c), represents a first realistic approximation of the viscoelastic behavior. Its complex modulus can be written as

$$E^*(\omega) = \frac{E_\infty + E_0 j\omega\tau}{1 + j\omega\tau}, \tag{10}$$

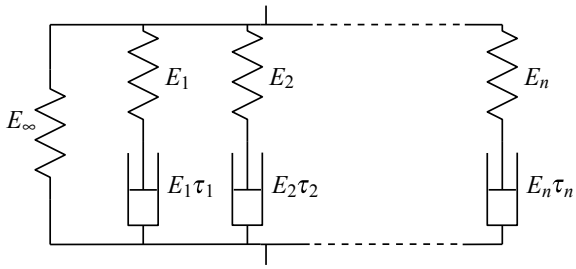

Fig. 2 Generalized Maxwell model

where E_0 corresponds to the instantaneous modulus of the material (i.e., when $t \to 0$ or $\omega \to +\infty$) and E_∞ corresponds to the long-term modulus (i.e., when $t \to +\infty$ or $\omega \to 0$).

The three parameters of the Zener model may, however, be insufficient to describe the complexity of the frequency dependency of the viscoelastic properties for some materials. In this case, higher degree model may be used. Figure 2 illustrates the Generalized Maxwell Model (GMM) which is able to generate more complex evolutions of the viscoelastic behavior of materials. By combining N Maxwell cells in parallel, it is possible to accurately represent the experimental viscoelastic behavior over a wide band of frequency in dynamics, thanks to a distribution of rational fractions shifted in frequency. The complex modulus associated with this model is written as

$$E^*(\omega) = E_\infty + \sum_{i=1}^{N} E_i \frac{j\omega\tau_i}{1 + j\omega\tau_i} = E_\infty \left(1 + \sum_{i=1}^{N} \alpha_i \frac{j\omega\tau_i}{1 + j\omega\tau_i}\right), \tag{11}$$

where E_i and τ_i represent the dynamic stiffness and the relaxation time of cell i. Up to the end of this chapter, the stiffening (or the dynamic stiffness ratio) is referred as $\alpha_i = E_i/E_\infty$. In addition, it may be noted that $E_0 = E_\infty + \sum_{i=1}^{N} E_i$.

At the price of an increase in the number of parameters that need to be identified, increasing the number of cells provides the ability of the model to describe more complex frequency dependencies (materials exhibiting several glass transitions for example).

The GMM may also be interpreted as a modeling strategy based on internal variables, where the relaxation function $C^*_{ijkl}(t)$ is approximated by a Prony series development [46]. Numerous commercial software packages propose to take into account the viscoelastic behavior of a material using Prony series: in the time domain, one has

$$\sigma(t) = \int_{-\infty}^{t} E(t-s)\dot{\varepsilon}(s)ds, \tag{12}$$

with

$$E(t) = E_\infty + \sum_{i=1}^{N} E_i e^{-t/\tau_i}, \tag{13}$$

which is sometimes written as

$$E(t) = E_0 \left(1 - \sum_{i=1}^{N} \alpha_i' (1 - e^{-t/\tau_i})\right), \tag{14}$$

where $\alpha_i' = \alpha_i/(1+\alpha_i)$, with $\alpha_i = E_i/E_\infty$ and $E_0 = E_\infty + \sum_{i=1}^{N} E_i$.

These one-dimensional rheological models are not sufficient to serve for 3D implementation, because of the couplings existing between the directions. However, the materials studied in this chapter being isotropic, the properties of the material are identical in the three directions of space. In this case, the tensor of the 3D viscoelastic constitutive law can be fully described with only two material characteristics. If we call this operator C^*_{ijkl}, such that

$$\hat{\sigma}_{ij}(\omega) = C^*_{ijkl}(\omega)\hat{\varepsilon}_{kl}(\omega) \tag{15}$$

then, C^*_{ijkl} may be written as

$$\hat{C}^*_{ijkl} = \frac{E^*(\omega)}{(1-2\nu)(1+\nu)} \begin{bmatrix} 1-\nu & \nu & \nu & 0 & 0 & 0 \\ \nu & 1-\nu & \nu & 0 & 0 & 0 \\ \nu & \nu & 1-\nu & 0 & 0 & 0 \\ 0 & 0 & 0 & \frac{1-2\nu}{2} & 0 & 0 \\ 0 & 0 & 0 & 0 & \frac{1-2\nu}{2} & 0 \\ 0 & 0 & 0 & 0 & 0 & \frac{1-2\nu}{2} \end{bmatrix}, \tag{16}$$

where ν is the Poisson's ratio, which may also be frequency-dependent, even if its variation is of second order compared to the evolution of the modulus. Nevertheless, for some materials, it may be important to access to the frequency evolution of ν. The viscoelastic behavior of the shape-memory polymers characterized in this chapter will be modeled by generalized Maxwell models.

4.2 Time–Temperature Superposition

As indicated above, the behavior of polymers is highly dependent on frequency but is also highly dependent on temperature; this is particularly true for shape-memory polymers. A lot of polymers behave, on specific temperature and frequency ranges, according to the time–temperature superposition principle [18], in particular, in the glassy and rubbery states, together with the glass transition. This comes from the observation that temperature plays a role which is the opposite of frequency: an increase in frequency has the same effect as a decrease in temperature. This principle has been shown to be valid for a wide variety of polymers but is not justified for polymer blends or composites. It can be interpreted as follows: considering a refer-

ence frequency evolution of the complex modulus $E^*(\omega, T_0)$ at a given temperature T_0, the frequency evolution of the complex modulus at another temperature T is

$$E^*(\omega, T) = E^*(a_T(T)\omega, T_0). \tag{17}$$

$E^*(\omega, T_0)$ is called the master curves. Hence, from a reduced set of measurements in frequency and temperature, the behavior of the materials can be described on larger ranges. Only the knowledge of the master curves and the shift factor $a_T(T)$ are required for this purpose. $a_T(T)\omega$ is usually called reduced frequency, and it is identified by shifting in frequency the curves measured at temperature T to the ones measured at reference temperature T_0. Manual shifting is possible but automatic procedures are preferred [47, 48]. Several parametric models are available in literature to fit the temperature evolution of the shift factor. The Williams–Landel–Ferry (WLF) law [30], based on empirical data, is one of the most popular techniques. It consists of writing the shift factor as

$$\log(a_T(T)) = \frac{-C_1^0(T - T_0)}{C_2^0 + (T - T_0)}, \tag{18}$$

where C_1^0 and C_2^0 are two constants.

Another popular way to interpolate the value of the shift factor is the Arrhenius law [49]:

$$\log(a_T(T)) = \frac{E_a}{R}\left(\frac{1}{T} - \frac{1}{T_0}\right), \tag{19}$$

where E_a is the activation energy, $R = 8.314 \times 10^3$ kJ.mol^1.K^1 is the constant of perfect gas, and T should be expressed in degree Kelvin. For a given material, the evolution of the shift factor may be fitted by one of these two equations (but may also be such that none of these models fits the experimental data).

In the following, the explicit dependency of the complex modulus to the temperature will be omitted (i.e., $E^*(\omega, T)$ will be identified to $E^*(\omega)$). The identification of the model parameters will be directly done on the master curves.

4.3 Identification of the Parameters of the Generalized Maxwell Models

In this section, a method to identify the parameters of a Generalized Maxwell Model (GMM) representing the evolution of the mechanical behavior of the shape-memory polymers is proposed. A hypothesis concerning the location of the $1/\tau_i$ poles of the GMM is formulated to facilitate its integration into computational routines in the frequency and time domains.

The identification of the parameters of a viscoelastic model requires the minimization of the difference between the measured and calculated storage and loss moduli, which is classically done using a least squares method. The real and imaginary part of the GMM can be separated by expressing, respectively, the storage module E' and the loss module E'':

$$E^*(\omega) = E'(\omega) + jE''(\omega) \tag{20}$$

$$\text{with} \quad E'(\omega) = E_\infty + \sum_{i=1}^{N} E_i \frac{\omega^2 \tau_i^2}{1 + \omega^2 \tau_i^2} \tag{21}$$

$$\text{and} \quad E''(\omega) = \sum_{i=1}^{N} E_i \frac{\omega \tau_i}{1 + \omega^2 \tau_i^2} \tag{22}$$

A total of $2N + 1$ parameters is to be identified from the master curves.

The identification of the parameters of a GMM can be conducted by an algorithm based on graphical methods such as those proposed by Dion [50]. These methods are based on a pole-zero formulation of the rheological model and make it possible to determine the number and the value of the pole-zero pairs which will be used for the construction of this model. Renaud [51] proposes to use these methods as initialization step and then to add an optimization step in order to locate more accurately these couples and thus obtain a model which has a minimal number of cells.

In this chapter, another approach, used in [52], is used. Indeed, the poles of the GMM, which are $1/\tau_i$, are fixed by the user a priori. Such a constraint tends to increase the number of Maxwell cells needed to correctly represent the viscoelastic behavior but makes the identification problem easier to implement. On this basis, only the long-term modulus E_∞ and the dynamic moduli E_i have to be found, corresponding to only $N + 1$ unknowns. There is no precise rule to define the number of poles to use, but it seems that a distribution of three poles per decade with, at least, an additional decade beyond and above the frequency range of interest leads to confident results, and helps to stabilize the procedure at the same time. This approach is preferred here since it is very easy to implement and provides good results in a very short time, at the price of a model order which is most of the time larger than the "optimal" one. Readers who are interested in finding lower order models can refer to [51].

The identification procedure consists in estimating the unknown parameters by solving in a least square sense the linear system

$$\begin{bmatrix} 1 & \frac{\tau_1^2\omega_1^2}{1+\tau_1^2\omega_1^2} & \cdots & \frac{\tau_N^2\omega_1^2}{1+\tau_N^2\omega_1^2} \\ 0 & \frac{\tau_1\omega_1}{1+\tau_1^2\omega_1^2} & \cdots & \frac{\tau_N\omega_1}{1+\tau_N^2\omega_1^2} \\ \vdots & \vdots & \cdots & \vdots \\ 1 & \frac{\tau_1^2\omega_M^2}{1+\tau_1^2\omega_M^2} & \cdots & \frac{\tau_1^2\omega_M^2}{1+\tau_N^2\omega_M^2} \\ 0 & \frac{\tau_1\omega_M}{1+\tau_1^2\omega_M^2} & \cdots & \frac{\tau_N\omega_M}{1+\tau_N^2\omega_M^2} \end{bmatrix} \begin{bmatrix} E_\infty \\ E_1 \\ \vdots \\ E_N \end{bmatrix} = \begin{bmatrix} E'_{exp}(\omega_1) \\ E''_{exp}(\omega_1) \\ \vdots \\ E'_{exp}(\omega_M) \\ E''_{exp}(\omega_M) \end{bmatrix}, \tag{23}$$

where ω_1,…, ω_M are the M measured frequency points. The pseudo-inverse of the above matrix (whose size is $[2M, (N+1)]$) is required to obtain the values of E_∞ and E_i ($i = 1$,…, N). It should be noted that in specific cases, some E_i parameters may be computed as negative values. In this kind of situation, it is necessary either to add new cells in the GMM, or to use a constrained minimization algorithm [53] to solve the following problem:

$$\begin{cases} \underset{E',\, E''}{min} \sum_{i=1}^{M} \left(|E' - E'_{exp}(\omega_i)|^2 + |E'' - E''_{exp}(\omega_i)|^2 \right) \\ \text{with} \\ E_\infty \geqslant 0 \\ E_i \geqslant 0, i = 1, \ldots, N \end{cases} \tag{24}$$

All the results presented hereafter use this strategy for the GMM identification.

5 Results

5.1 tBA/PEGDMA

Some mechanical characterizations of the tBA/PEGDMA are available in literature. In particular, the shape-memory effect has been described in [54], the recovery has been reported in [36], and nano-indentation tests have been presented in [55], while DMA tests at 1 Hz have been reported in [5]. It should be emphasized that all these tests are not performed for the same wt% components. The material used in this analysis has been deeply investigated in [4], the analysis covering large frequency and temperature ranges, but also several scales of characterization and several loading modes.

Figure 3 shows the whole set of measurements performed on the tBA/PEGDMA. The storage modulus E' varies from 0.7 MPa at low frequency in the rubbery state, to 2200 MPa at high frequency, in the glassy state. This huge change in the storage modulus at the glass transition corresponds to a very large value of the loss factor: over 1.5 in a wide frequency range with a maximal value of 2.4. These values are particularly high, and this material has been used as a composite core which provides an extremely damped structure when the environmental conditions are close to the glass temperature [20].

Figure 4 shows the master curves. Except at very high temperature, the TTS works quite well. The shift factors are very well captured by the WLF law with $C_1 = 10.87$ and $C_2 = 32.57$ K, for a reference temperature $T_0 = 40\,^\circ$C.

The results of the identification of the GMM model is shown in figure 5. The plots show the storage and loss moduli, and the loss factor. The crosses on the pictures correspond to the measured points coming from the DMA, after TTS according to WLF law. The GMM captures very well the behavior of the material on more than 12 decades, including the glassy and rubbery states, together with the glass transition.

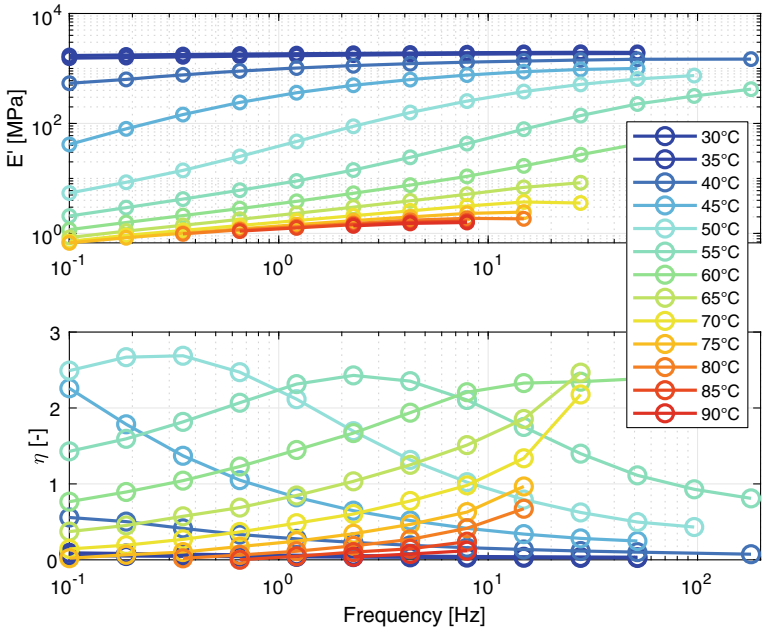

Fig. 3 DMA results on the tBA/PEGDMA

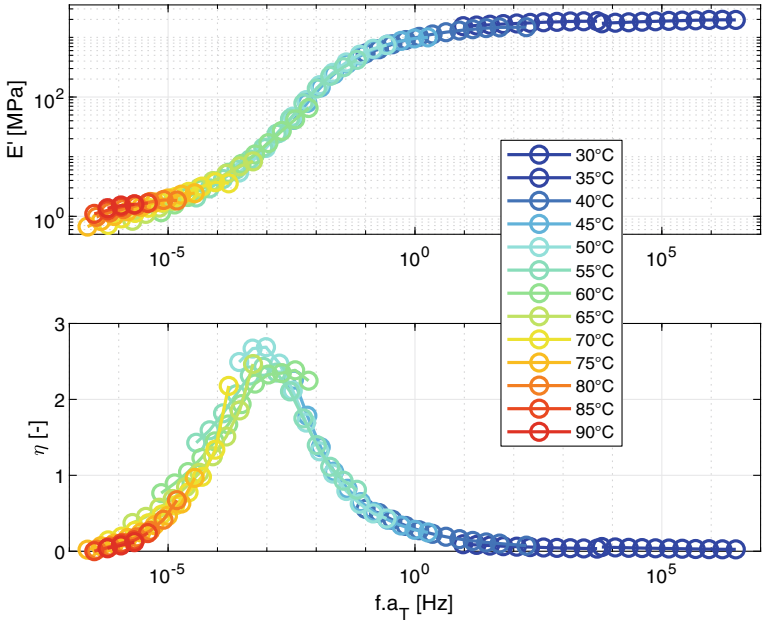

Fig. 4 Master curves of the storage modulus E' and the loss factor η according to the reduced frequency $f.a_T$ for a reference temperature $T_0 = 40\,^{\circ}\mathrm{C}$

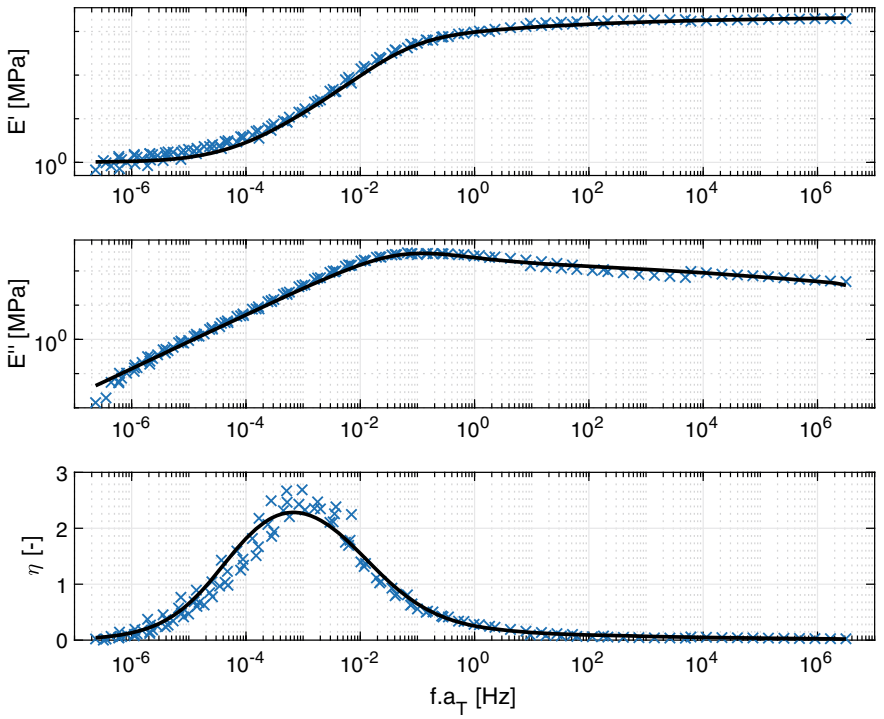

Fig. 5 Identification of the Generalized Maxwell Model for the tBA/PEGDMA for a reference temperature $T_0 = 40\,°C$ (solid lines: identified GMM; dots: measurement points)

The numerical values of the cells components are provided in Appendix. In order to cover the 12 decades, a total of 42 cells have been used in the GMM. The total number of parameters is quite high compared to models like the 2S2P1D [56] already used for this material in [4], which requires only 7 parameters. The two models have almost the same precision in the frequency domain, however the GMM can be used for time computations, which is not the case of the 2S2P1D.

5.2 SMP Filament

Figure 6 shows the whole set of measurements performed on the SMP filament. The glass transition has been measured, and the maximum value of the loss factor is about 1.5. Storage modulus has been measured around 4–5 MPa in the rubbery state, and around 1.5 GPa in the glassy state. The measurements at high temperature show a slight increase in the loss factor.

The TTS is also well verified on this material on the frequency and temperature ranges of interest. The master curves are shown in Fig. 10. Some discrepancies can

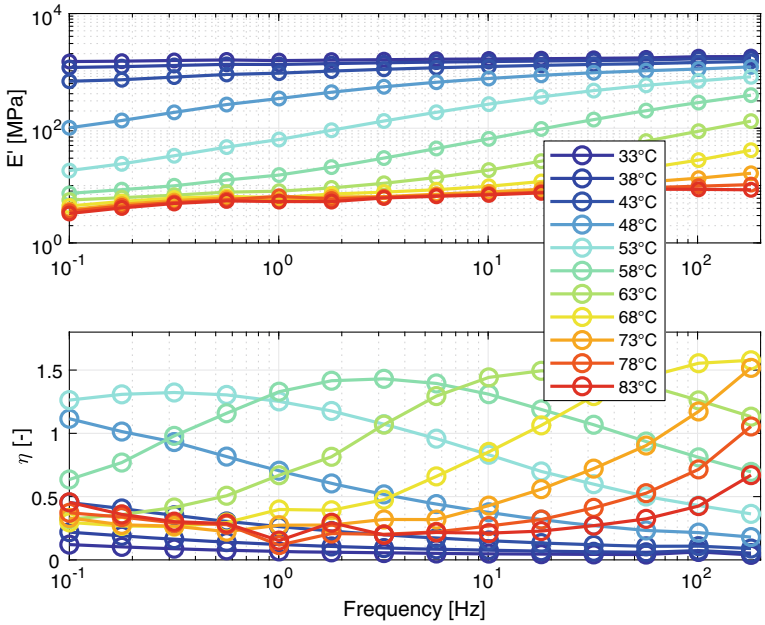

Fig. 6 DMA results on the SMP filament

be observed in the lower temperature range. The shift factors are well fitted by the WLF law with $C_1^0 = 9.66$, $C_2^0 = 55.9$ K, and $T_0 = 58\,^{\circ}$C (Fig. 7).

As shown in Fig. 8, the GMM appears to be quite representative of the behavior of the SMP filament. The model fits well on the 13 decades of reduced frequencies. Only the loss factor at the glass transition is a little bit underestimated by the model. The increase of loss factor at higher temperatures is also well captured by the GMM. Users of the model should be aware that the loss factor at very low frequency or very high temperature ($f.a_T < 2.7 \times 10^{-4}$) may be erroneous since no measurements have been done in this range where another physical phenomenon occurs. The numerical values of the model are provided in appendix.

5.3 *Vitrimer*

Figure 9 shows the whole set of measurements performed on the hard network of vitrimer. The glass transition has been measured, and the maximum value of the loss factor is about 0.72.

The TTS works quite well on this material on the frequency and temperature ranges of interest. The master curves are shown in Fig. 10. Some discrepancies can,

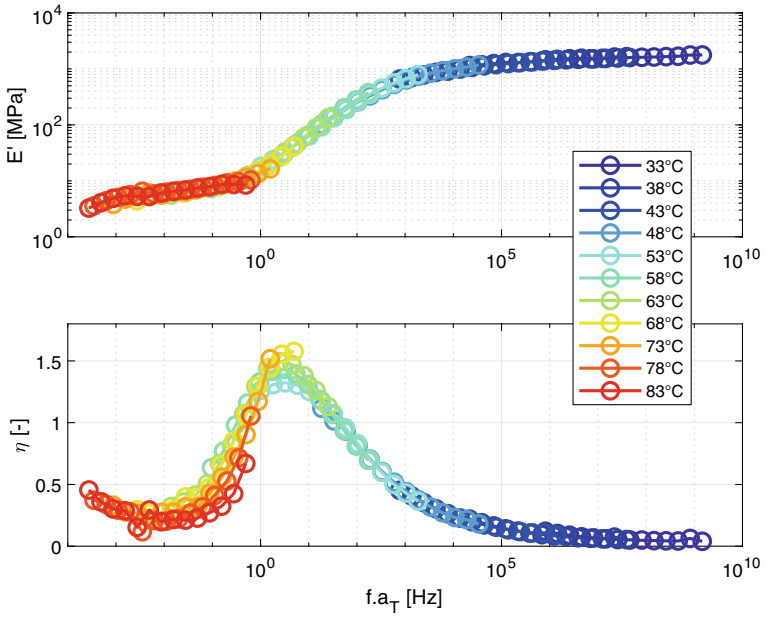

Fig. 7 Master curves of the SMP filament (reference temperature $T_0 = 58\,°C$)

however, be observed in the lower temperature range. The shift factors are well fitted by Arrhenius law with an activation energy $E_a = 1.70 \times 10^5$ J.mol^{-1}.K^{-1} and $T_0 = 46\,°C$.

The GMM appears to be quite representative of the behavior of the vitrimer. As in the master curves, some difficulties appear in the zone corresponding to the lowest temperatures analyzed during the DMA tests. The GMM has some difficulties to fit the experimental data because in the glassy state, where the storage modulus remains constant, it corresponds to a loss factor which is not converging to zero as expected by the model: it seems that the vitrimer has a constant loss factor at low temperature. The numerical values of the model are provided in appendix, and users should be aware that the data provided should not be used for values outside the reduced frequency band $10^{-11} < f.a_T < 10$ Hz (Fig. 11).

6 Conclusion

The viscoelastic properties of shape-memory polymers have been described and discussed in this chapter. An easy procedure for model identification has been presented and applied to the three materials which have been benchmarked. Starting

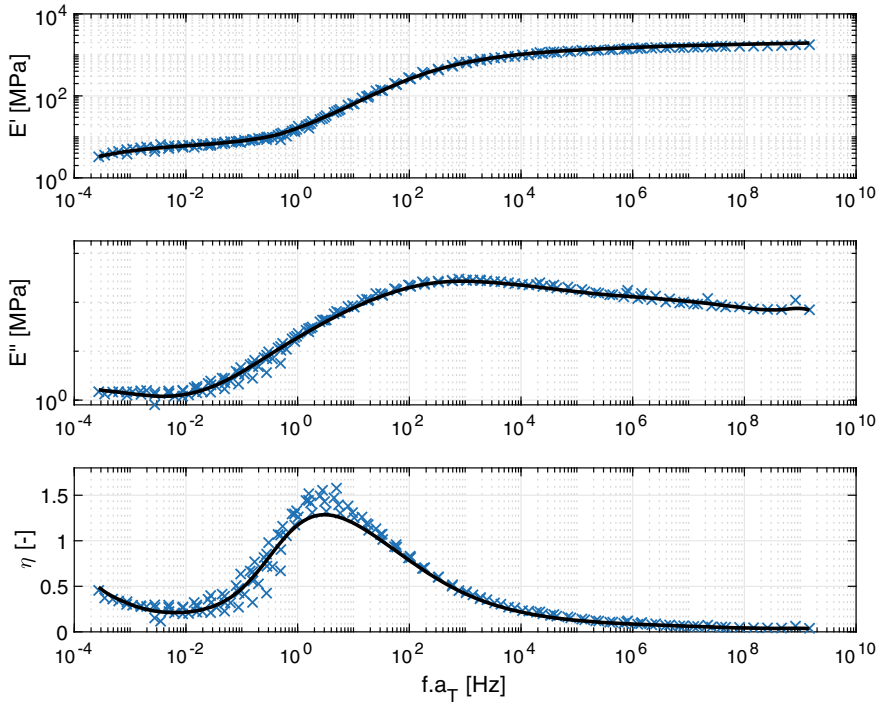

Fig. 8 Identification of the generalized Maxwell model for the SMP filament for a reference temperature $T_0 = 58\,°C$ (solid lines: identified GMM; dots: measurement points)

from dynamical mechanical thermal analysis performed on reduced sets of frequencies and temperatures, the storage modulus and loss factor are measured. Then, the time–temperature superposition has been used to identify the master curves. For the three materials, this principle is found to be representative of the measured behavior. The shift factors are then fitted using either WLF or Arrhenius laws. Finally, a generalized Maxwell model has been used to describe the master curve, using a very simple identification procedure, which provides a model with three cells by decade. The complexity of the model is higher than the optimal one, but still representative of the behavior of the material on wide frequency and temperature ranges. For the three materials, the model is found to be effective on more than 11 decades. All numerical values are provided to the readers; hence, anyone can use these models which are in accordance with the measurements performed on the three materials of interest. Among others, these models may be used to describe the shape-memory effect in the time domain [12] or to describe the mechanical properties of composite structures embedding shape-memory polymers for vibration control in the frequency domain

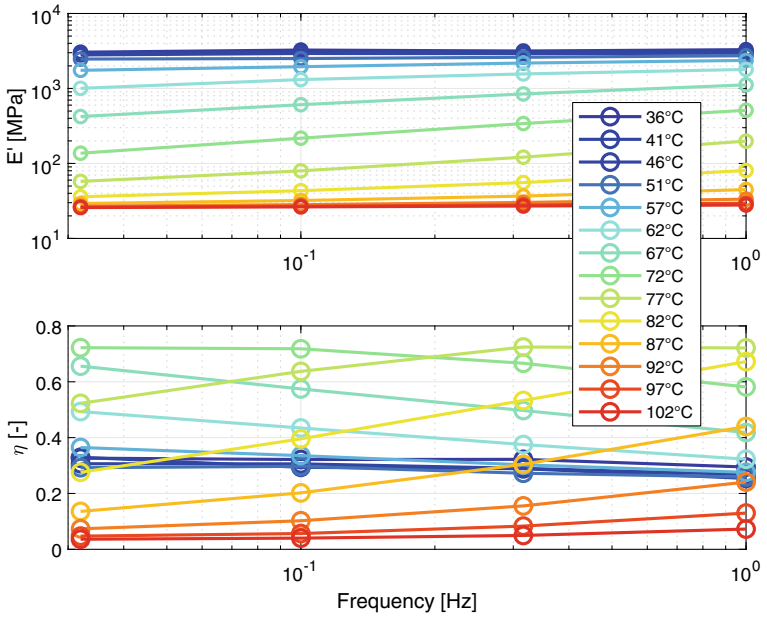

Fig. 9 DMA results on the hard network of vitrimer

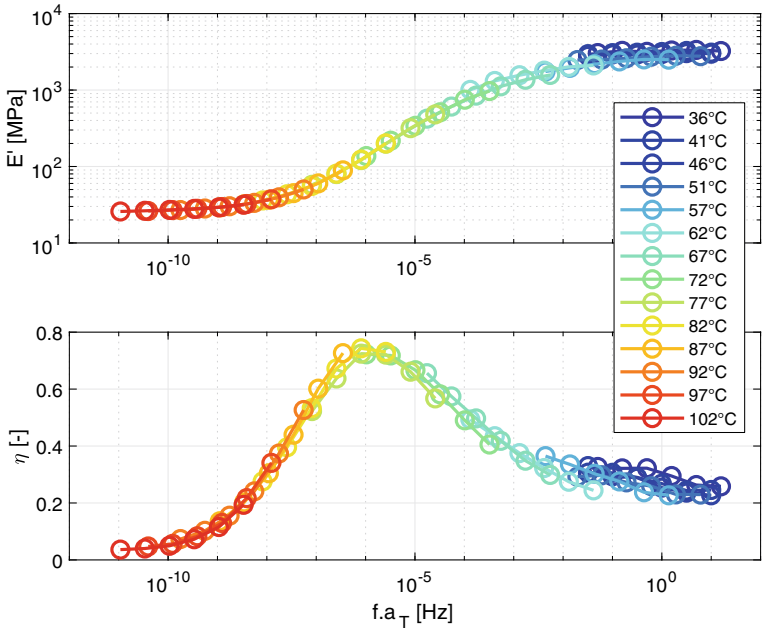

Fig. 10 Master curves of the hard network of vitrimer for a refence temperature $T_0 = 46\,°\mathrm{C}$

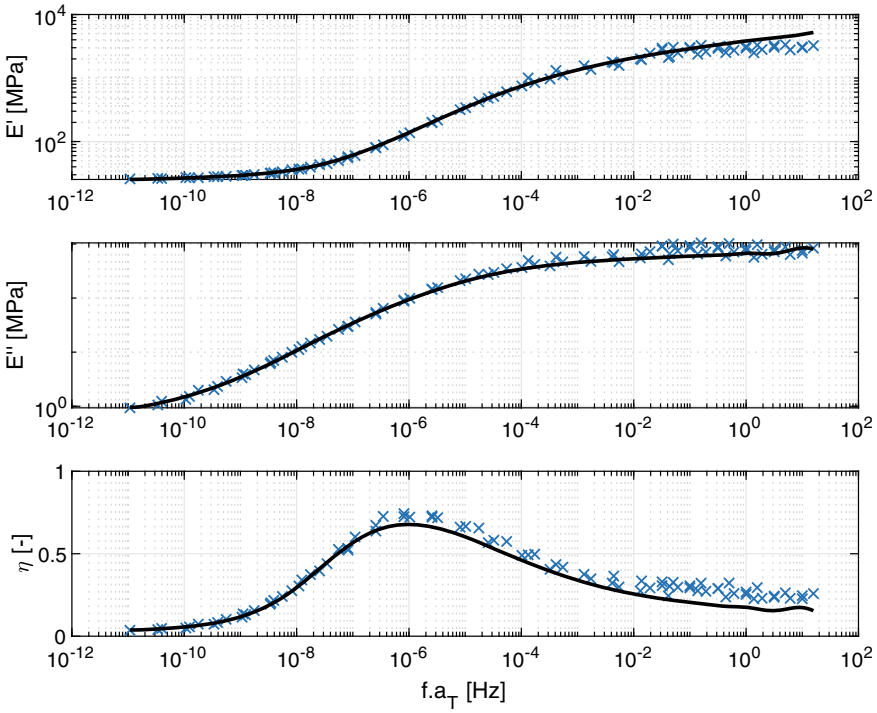

Fig. 11 Identification of the generalized Maxwell model for the hard network of vitrimer for a reference temperature $T_0 = 46\,°\mathrm{C}$ (solid lines: identified GMM; dots: measurement points)

[20]. Users should be aware that the identified models should only be used in the reduced frequency range which has been considered for the fitting: out of this range, they could no longer be representative of the physical behavior. Typical illustrations are the behavior of the vitrimer, which keeps a high loss factor at low temperature, or the SMP filament, having an increase of the loss factor at high temperatures.

Acknowledgements This work has been performed in collaboration with EUR EIPHI Graduate School (project ANR 17-EURE-0002). The authors would like to thank people who contributed to the experimental parts of this work: Renan Ferreira, Xavier Gabrion, Thomas Jeannin.

Appendix - Numerical Values of the GMM for the Master Curve of tBA/PEGDMA

Cell Id (i)	∞	1	2	3	4	5
τ_i [s^{-1}]	0	6.3559×10^{-8}	1.0593×10^{-7}	3.1780×10^{-7}	7.2089×10^{-7}	1.6353×10^{-6}
E_i [MPa]	0.97769	47.494	12.824	36.857	25.597	38.480
6	7	8	9	10	11	12
3.7094×10^{-6}	8.4144×10^{-6}	1.9087×10^{-5}	4.3297×10^{-5}	9.8215×10^{-5}	0.00022279	0.00050538
35.509	44.348	45.331	51.465	54.857	60.001	63.611
13	14	15	16	17	18	19
0.0011464	0.0026005	0.0058989	0.013381	0.030354	0.068854	0.15619
68.674	72.789	77.466	82.927	90.182	100.64	117.60
20	21	22	23	24	25	26
0.35430	0.80368	1.8231	4.1354	9.3808	21.279	48.270
147.41	195.49	236.00	181.53	88.156	38.936	17.638
27	28	29	30	31	32	33
109.50	248.38	563.42	1278.1	3149.0	7758.6	19116
8.4675	4.2157	2.0917	1.1444	0.59268	0.28032	0.13926
34	35	36	37	38	39	40
47100	1.1605×10^5	2.8593×10^5	7.0448×10^5	1.7357×10^6	4.2766×10^6	1.2830×10^7
0.067803	0.032689	0.017485	0.0050210	0.0028528	0.0049602	0.013080
41						
2.1383×10^7						
0.021141						

Appendix - Numerical Values of the GMM for the Master Curve of SMP Filament

Cell Id (i)	∞	1	2	3	4	5
τ_i [s^{-1}]	0	1.3656×10^{-10}	6.8280×10^{-10}	1.5076×10^{-9}	3.3288×10^{-9}	7.3499×10^{-9}
E_i [MPa]	0.00041175	122.25	27.421	46.242	31.513	57.238
6	7	8	9	10	11	12
1.6228×10^{-8}	3.5832×10^{-8}	7.9117×10^{-8}	1.7469×10^{-7}	3.8571×10^{-7}	8.5164×10^{-7}	1.8804×10^{-6}
46.875	62.971	58.318	66.349	68.579	73.597	81.764
13	14	15	16	17	18	19
4.1519×10^{-6}	9.1673×10^{-6}	2.0241×10^{-5}	4.4693×10^{-5}	9.8681×10^{-5}	0.00021789	0.00048109
91.310	100.64	121.28	127.62	153.02	151.15	152.60
20	21	22	23	24	25	26
0.0010622	0.0023454	0.0051786	0.011434	0.025247	0.055744	0.12308
123.22	90.911	58.486	35.484	20.420	11.493	6.0686
27	28	29	30	31	32	33
0.27176	0.60005	1.3249	2.9254	6.4592	14.262	31.490
3.2138	1.3316	0.87233	0.46338	0.63790	0.32339	0.65854
34	35	36	37	38	39	40
69.529	153.52	338.97	748.43	1652.5	3648.8	18244
0.24972	0.86167	0.87394	0.00047364	2.6729	0.66321	0.00059484

Appendix - Numerical Values of the GMM for the Master Curve of Vitrimer

Cell Id (i)	∞	1	2	3	4	5
τ_i [s^{-1}]	0	0.012689	0.063445	0.14123	0.31438	0.69983
E_i [MPa]	10.806	1517.2	9.9502	790.00	0.049548	500.70
6	7	8	9	10	11	12
1.5579	3.4678	7.7195	17.184	38.252	85.151	189.55
203.33	345.30	251.11	289.77	249.72	254.53	229.18
13	14	15	16	17	18	19
421.94	939.26	2090.8	4654.3	10361.	23063.	51339.
217.72	193.13	171.00	142.87	115.73	88.780	65.993
20	21	22	23	24	25	26
1.1428×10^5	2.5440×10^5	5.6630×10^5	1.2606×10^6	2.8062×10^6	6.2466×10^6	1.3905×10^7
47.155	33.193	22.616	15.297	9.7769	6.3134	3.8148
27	28	29	30	31	32	33
3.0954×10^7	6.8904×10^7	1.5338×10^8	3.4144×10^8	7.6005×10^8	1.6919×10^9	3.7662×10^9
2.6396	1.6391	1.3584	0.83093	0.87719	0.46957	0.69845
34	35	36	37	38		
8.3838×10^9	1.8663×10^{10}	4.1544×10^{10}	9.2478×10^{10}	4.6239×10^{11}		
0.41526	0.00059210	0.0012208	0.0050371	14.355		

References

1. Barwood MJ, Breen C, Clegg F, Hammond CL (2014) The effect of organoclay addition on the properties of an acrylate based, thermally activated shape memory polymer. Appl Clay Sci 102:41–50
2. Tsai Y, Tai CH, Tsai SJ, Tsai FJ (2008) Shape memory effects of poly (ethylene terephthalate-co-ethylene succinate) random copolymers. Eur Polym J 44(2):550–554
3. Biju R, Nair CR (2013) Synthesis and characterization of shape memory epoxy-anhydride system. J Polym Res 20(2):1–11
4. Butaud P, Ouisse M, Placet V, Renaud F, Travaillot T, Maynadier A, Chevallier G, Amiot F, Delobelle P, Foltête E, Rogueda-Berriet C (2018) Identification of the viscoelastic properties of the tBA/PEGDMA polymer from multi-loading modes conducted over a wide frequency–temperature scale range. Polym Test. https://doi.org/10.1016/j.polymertesting.2018.05.030
5. Ortega AM, Kasprzak SE, Yakacki CM, Diani J, Greenberg AR, Gall K (2008) Structure-property relationships in photopolymerizable polymer networks: Effect of composition on the crosslinked structure and resulting thermomechanical properties of a (meth) acrylate-based system. J Appl Polym Sci 110(3):1559–1572
6. Butaud P, Placet V, Ouisse M, Foltete E, Gabrion X (2015) Investigations on the frequency and temperature effects on mechanical properties of a shape memory polymer (veriflex). Mech Mater 87:50–60. https://doi.org/10.1016/j.mechmat.2015.04.002
7. Ellson G, Di Prima M, Ware T, Tang X, Voit W (2015) Tunable thiol–epoxy shape memory polymer foams. Smart Mater Struct 24(5): 055–001
8. Tandon G, Goecke K, Cable K, Baur J (2009) Durability assessment of styrene-and epoxy-based shape-memory polymer resins. J Intell Mater Syst Struct 20(17):2127–2143

9. Xie T, Rousseau IA (2009) Facile tailoring of thermal transition temperatures of epoxy shape memory polymers. Polymer 50(8):1852–1856. https://doi.org/10.1016/j.polymer.2009.02.035
10. Chen YC, Lagoudas DC (2008) A constitutive theory for shape memory polymers. part i: large deformations. J Mech Phys Solids 56(5):1752–1765
11. Diani J, Gilormini P, Frédy C, Rousseau I (2012) Predicting thermal shape memory of crosslinked polymer networks from linear viscoelasticity. Int J Solids Struct 49(5):793–799
12. Fang C, Leng J, Sun H, Gu J (2018) A multi-branch thermoviscoelastic model based on fractional derivatives for free recovery behaviors of shape memory polymers. Mech Mater 120:34–42
13. Li Y, Liu Z (2018) A novel constitutive model of shape memory polymers combining phase transition and viscoelasticity. Polymer 143:298–308
14. Lin J, Chen L (1999) Shape-memorized crosslinked ester-type polyurethane and its mechanical viscoelastic model. J Appl Polym Sci 73(7):1305–1319
15. Zeng H, Leng J, Gu J, Yin C, Sun H (2018) Modeling the strain rate-, hold time- and temperature-dependent cyclic behaviors of amorphous shape memory polymers. Smart Mater Struct
16. Zhao Q, Qi HJ, Xie T (2015) Recent progress in shape memory polymer: New behavior, enabling materials, and mechanistic understanding. Prog Polym Sci 49:79–120
17. Chun BC, Cha SH, Chung YC, Cho JW (2002) Enhanced dynamic mechanical and shape-memory properties of a poly (ethylene terephthalate)-poly (ethylene glycol) copolymer crosslinked by maleic anhydride. J Appl Polym Sci 83(1):27–37
18. Ferry JD (1980) Viscoelastic properties of polymers. Wiley, New York
19. Rao MD (2003) Recent applications of viscoelastic damping for noise control in automobiles and commercial airplanes. J Sound Vib 262(3):457–474
20. Butaud P, Foltête E, Ouisse M (2016) Sandwich structures with tunable damping properties: on the use of shape memory polymer as viscoelastic core. Compos Struct 153:401–408. https://doi.org/10.1016/j.compstruct.2016.06.040
21. Araujo A, Soares CM, Soares CM, Herskovits J (2010) Optimal design and parameter estimation of frequency dependent viscoelastic laminated sandwich composite plates. Compos Struct 92(9):2321–2327
22. Grootenhuis P (1970) The control of vibrations with viscoelastic materials. J Sound Vib 11(4):421–433
23. Berthelot JM, Assarar M, Sefrani Y, Mahi AE (2008) Damping analysis of composite materials and structures. Compos Struct 85(3):189–204
24. Ege K, Roozen N, Leclere Q, Rinaldi RG (2018) Assessment of the apparent bending stiffness and damping of multilayer plates; modelling and experiment. J Sound Vib 426:129–149
25. Li J, Narita Y (2012) The effect of aspect ratios and edge conditions on the optimal damping design of thin soft core sandwich plates and beams. J. Vib Control 1077546312463756
26. Lifshitz J, Leibowitz M (1987) Optimal sandwich beam design for maximum viscoelastic damping. Int J Solids Struct 23(7):1027–1034
27. Diani J, Gilormini P, Agbobada G (2014) Experimental study and numerical simulation of the vertical bounce of a polymer ball over a wide temperature range. J Mater Sci 49(5):2154–2163
28. Hu J, Chen W, Fan P, Gao J, Fang G, Cao Z, Peng F (2017) Epoxy shape memory polymer (smp): Material preparation, uniaxial tensile tests and dynamic mechanical analysis. Polym Test 62:335–341
29. Stark W, Jaunich M, McHugh J (2015) Dynamic mechanical analysis (dma) of epoxy carbon-fibre prepregs partially cured in a discontinued autoclave analogue process. Polym Test 41:140–148
30. Williams ML, Landel RF, Ferry JD (1955) The temperature dependence of relaxation mechanisms in amorphous polymers and other glass-forming liquids. J Am Chem Soc 77(14):3701–3707
31. Seitz J, Balazs C (1968) Application of time-temperature superposition principle to long term engineering properties of plastic materials. Polym Eng Sci 8(2):151–160
32. Hutcheson S, McKenna G (2008) In: 6th International Conference on mechanics of time dependent materials conference. Monterey, California

33. Diani J, Gilormini P (2017) On necessary precautions when measuring solid polymer linear viscoelasticity with dynamic analysis in torsion. Polym Test 63:275–280
34. Billon K, Ouisse M, Sadoulet-Reboul E, Collet M, Butaud P, Chevallier G, Khelif A (2019) Design and experimental validation of a temperature-driven adaptive phononic crystal slab. Smart Mater Struct. https://doi.org/10.1088/1361-665X/aaf670
35. Srivastava V, Chester SA, Anand L (2010) Thermally actuated shape-memory polymers: Experiments, theory, and numerical simulations. J. Mech. Phys. Solids 58(8):1100–1124
36. Yakacki CM, Shandas R, Lanning C, Rech B, Eckstein A, Gall K (2007) Unconstrained recovery characterization of shape-memory polymer networks for cardiovascular applications. Biomaterials 28(14):2255–2263
37. Leibler L, Montarnal D, Tournilhac FG, Capelot M (2016) Thermoset/supramolecular hybrid composites and resins that can be hot-formed and recycled. US Patent 9,359,467
38. Montarnal D, Capelot M, Tournilhac F, Leibler L (2011) Silica-like malleable materials from permanent organic networks. Science 334(6058):965–968
39. Caputo M, Mainardi F (1971) Linear models of dissipation in anelastic solids. La Rivista del Nuovo Cimento (1971–1977) 1(2):161–198
40. Lakes RS (1998) Viscoelastic solids, vol 9. CRC Press, New York
41. Lesieutre G, Bianchini E (1995) Time domain modeling of linear viscoelasticity using anelastic displacement fields. J Vib Acoust 117(4):424–430
42. Salençon, J (2009) Viscoélasticité pour le calcul des structures. Editions Ecole Polytechnique
43. Chevalier Y, Tuong JV (2010) Mechanics of viscoelastic materials and wave dispersion. Iste
44. Gaul L, Klein P, Kemple S (1991) Damping description involving fractional operators. Mech Syst Signal Process 5(2):81–88
45. Makris N (1997) Causal hysteretic element. J Eng Mech 123(11):1209–1214
46. Simo JC, Hughes TJ (2006) Computational inelasticity, vol 7. Springer Science and Business Media, Berlin
47. Dealy J, Plazek D (2009) Time-temperature superposition-a users guide. Rheol Bull 78(2):16–31
48. Rouleau L (2013) Modélisation vibro-acoustique de structures sandwich munies de matériaux visco-élastiques. Ph.D. thesis, Paris, CNAM
49. Seitz J, Balazs C (1968) Application of time-temperature superposition prin- ciple to long term engineering properties of plastic materials. Polym Eng Sci 8(2):151–160
50. Dion J, Vialard S (1997) Identification or rubber shock absorber mounts. Mécanique industrielle et matériaux 50(5):232–237
51. Renaud F, Dion JL, Chevallier G, Tawfiq I, Lemaire R (2011) A new identification method of viscoelastic behavior: Application to the generalized maxwell model. Mech Syst Signal Process 25(3):991–1010
52. Jaboviste K, Sadoulet-Reboul E, Peyret N, Arnould C, Collard E, Chevallier G (2019) On the compromise between performance and robustness for viscoelastic damped structures. Mech Syst Signal Process 119:65–80
53. Byrd RH, Gilbert JC, Nocedal J (2000) A trust region method based on interior point techniques for nonlinear programming. Math Program 89(1):149–185
54. Nair DP, Cramer NB, Scott TF, Bowman CN, Shandas R (2010) Photopolymerized thiol-ene systems as shape memory polymers. Polymer 51(19):4383–4389
55. Wornyo E, Gall K, Yang F, King W (2007) Nanoindentation of shape memory polymer networks. Polymer 48(11):3213–3225
56. Olard F, Di Benedetto H (2003) General 2s2p 1 d model and relation between the linear viscoelastic behaviours of bituminous binders and mixes. Road Mater Pavement Des 4(2):185–224

Differential Scanning Thermal Analysis of Shape-Memory Polymers, Polymer Blends and Composites

Giuliano Siniscalchi Martins

Abstract Calorimetry is the primary technique for measuring the thermal properties of materials. From calorimetric methods, it is possible to perform a correlation between temperature, structure, and the physicochemical properties of the materials. The differential scanning calorimeter (DSC) is one of the most common methods used to determine the thermal properties in polymeric materials. To determine the thermal properties of thermally activated polymeric materials is fundamental for the development of the programming cycle of these materials. This chapter presents a brief discussion about the application of the DSC in determining the thermal transitions of the materials and its correlation with the structure and memory effect.

1 Differential Thermal Analysis of Shape-Memory Polymers

Shape-memory polymers (SMP) are materials that can recover an original shape with a specific stimulus after programming steps. The shape-memory process is intrinsically related to a specific stimulus applied to the material (light, heat, electric field, magnetic field, pH, enzymes, ions, etc.) [1–3]. In this way, when a shape-memory polymer is developed, the behavior as a function of a specific stimulus must be studied to determine the future working conditions of this material.

Nowadays, most of the shape-memory polymers developed are based on thermal stimulus (thermally activated memory effect). The thermal transitions temperatures (melting temperature, glass transition temperature, for example) of specific segments in the polymer chain are the start parameters to the development and programming of the shape-memory cycle [4].

In this way, the polymer chain structural organization must be considered to study the shape-memory effects on polymers. The shape-memory programming process is

G. S. Martins (✉)
Federal Institute of Minas Gerais (IFMG), Av. Professor Mário Werneck, 2590, Buritis, Belo Horizonte, MG 30575-180, Brazil
e-mail: giuliano.martins@ifmg.edu.br

J. Parameswaranpillai et al. (eds.), *Shape Memory Polymers, Blends and Composites*, Advanced Structured Materials 115,
https://doi.org/10.1007/978-981-13-8574-2_7

Fig. 1 Schematic representation of the hard and soft segments in shape-memory polymers [9]

performed from structures responsible for the "permanent shape" and the "temporary shape" generally denoted as "hard domains/hard segments" and "soft domains/soft segments" with different thermal transitions (Fig. 1). These structures determine the initial thermal parameters in the development of the polymer. The hard domains are generally formed by regions with high cross-linking density, entanglement between the polymer chains and groups, or chemical functions that hinder the mobility of the chain. These domains are responsible for the permanent shape and have normally the higher thermal transition temperatures. By the other side, the soft domains are formed by chemical groups with high molecular mobility and the structures build during the mechanical deformation [5]. These domains are responsible for the temporary shape. The soft domains are rigid below the temperature of transition, when heated above this temperature they turn flexible and can be deformed when subjected to mechanical stress. The shape can be maintained during the cooling process if the deformation is maintained. The polymer restores the original shape when heated again above the transition temperature of soft domains [6–8]. The material returns to the original shape due to structural tension stored in the hard segments.

Liu et al. [7] stated that the mechanisms of memory are based on the intrinsic elasticity of the polymer networks. This model is based on the structural crystallinity of the polymer. Shape-memory polymers are constituted of covalent or physical cross-links. They are flexible when subjected to high stresses at temperatures above the glass transition temperature (T_g, amorphous case) or the melt temperature (T_m, crystalline case) [3, 7].

At temperatures higher than the thermal transition temperatures, the polymer networks exhibit superelasticity. In these conditions, the chain segments between the bonding points are able to freely deform and can be twisted randomly, via rotations over the bonds, maintaining a maximum entropy and minimum internal energy [7].

Macroscopically, the shape-memory effect on polymers can be graphically described in the form of the temperature × stress × strain measurement (Fig. 2). Initially, polymer is heated above the transition temperature of the soft segments. The material is then deformed from the application of stress (step 1). Subsequently, the applied stress is maintained and the material is cooled at temperatures below the thermal transition of the soft segments (step 2). After cooling, the stress is withdrawn. At this stage, the deformation is frozen. Finally, the material is reheated and returns the original shape (step 3).

Shape-memory polyurethanes (SMPU), by the example, are structurally formed by block copolymers with alternating segments having different properties called "segmented polyurethanes" (Fig. 3) [10, 11]. These polymers are formed by differ-

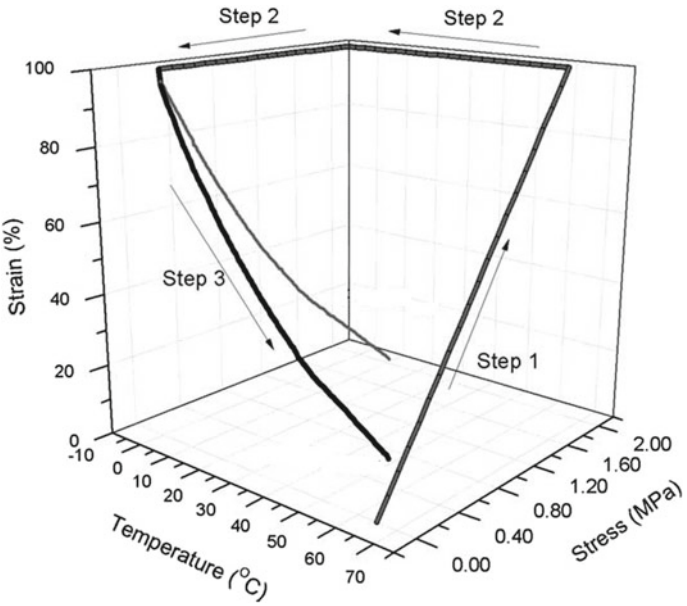

Fig. 2 Shape-memory effect in polymers: temperature × stress × strain [10]. Reproduced with permission

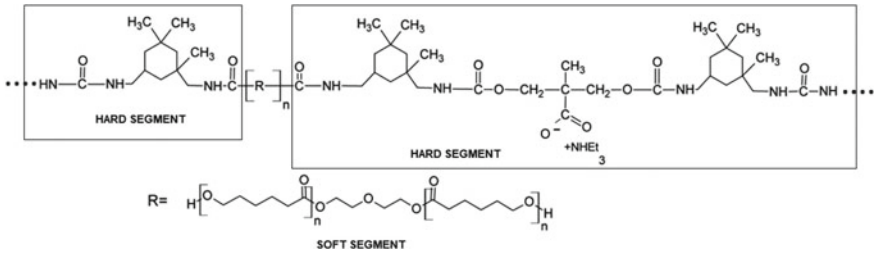

Fig. 3 Structure of an SMPU repeat unit [10]. Reproduced with permission

ent alternating polymeric monomers linked by covalent bonds and polymer chains bonded by reversible secondary bonds. Such bonds are weak and may include hydrogen bonds and ionic bonds [9]. Usually, SMPU are formed of two phases: one permanent and one reversible. The permanent shape consists of hard segments that can be formed via hydrogen bonding and crystallization below the melting temperature. The reversible phase consists of soft segments and is mainly responsible for the memory effect and to the temporary shape [12].

The segments can be manipulated to have different transition temperatures to build a shape-memory polymer thermally activated. The memory effect can be controlled via the molar mass of the soft segment that affects directly the thermal transition of this segment and the molar ratio of the rigid and soft segments [13]. In polyurethanes, the

rigid segments are formed of diisocyanates and chain extenders, and are responsible for the permanent shape. The soft segments are formed by polyols and are responsible for the temporary shape (reversible phase). Normally, this transition is associated with the glass transition temperature or other transition of the soft segment. In this type of polymer, it is possible to change the shape-memory properties by modifying the thermal transitions. This process is carried out by manipulating the composition of the polymer by the ratio of the rigid and soft segments to obtain different glass transition temperatures (−30 °C to 70 °C) [13, 14].

Typically, the shape-shifting activity of memory polymers is identified by a one-way behavior, in which the material has a permanent initial shape, can be deformed and fixed in a temporary shape, and recovers the permanent shape through a stimulus [15].

Some polymers have multiple memory effects, i.e., there is more than one temperature at which temporary shapes can be programmed, allowing these polymers to memorize many shapes that are produced during the cooling of the material and restored during the heating process [15]. The property of polymers to memorize many shapes comes from the ability to stretch the chains during heating and fix them during cooling [16, 17]. The maximum number of temporary shapes that a polymer can memorize correlates directly with the number of discrete reversible phase transitions (shape-memory transitions) [2, 18]. Xie [16], for example, developed a polymer with quadruple shape-memory (Fig. 4a, b). This effect is produced by introducing an additional reversible phase transition. However, synthesizing a polymer with more than two distinct and tightly bound reversible phases is extremely difficult [16, 18].

The determination of the thermal transitions in shape-memory materials is essential to the development of the shape programming process. The main method for measuring the thermal properties of materials is calorimetry. Calorimetrically, it is possible to establish a correlation between the physicochemical properties of the substances and the temperature. It is also the main method for direct determination of the enthalpy associated with the process of interest [19]. The most employed calorimetric technique is the differential scanning calorimeter (DSC). This technique measures the change in thermal properties as a function of temperature along with the time (heat flow). The thermal transitions and parameters detected in DSC (melting temperature, crystallization temperature, glass transition temperature, crystallization enthalpy, melting enthalpy, etc.) are associated with alteration in the microstructure of the polymeric material.

The use of DSC has many advantages, such as the low cost of the test, use of small amounts of sample, control of the time test and precision in the results. However, DSC is a destructive calorimetric method. During measurement on the DSC, the sample is degraded and cannot be recovered.

DSC analysis is performed using the sample and a reference material. The reference material is inert (does not undergo thermal transitions or structural modifications during the analysis), usually alumina (Al_2O_3) or platinum (Pt). During the test, the sample temperature (Ts) and the temperature of the reference material are maintained equal (Fig. 5). The energy difference to keep the sample and the reference at the same temperature are quantified to determine the thermal transitions in the sample.

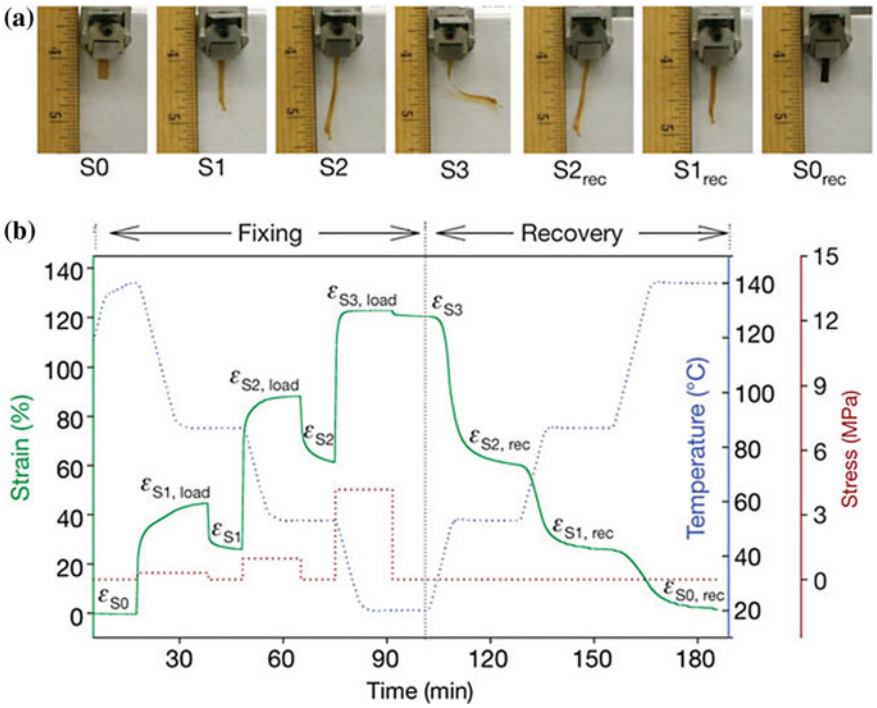

Fig. 4 Quadruple-shape-memory properties of perfluorosulphonic acid ionomer (PFSA): **a** Visual demonstration. S0: permanent shape; S1: first temporary shape (T_{d1}: 140 °C); S2: second temporary shape (T_{d2}: 107 °C); S3: third temporary shape (T_{d3}: 68 °C); $S2_{rec}$: recovered second temporary shape (T_{r1}: 68 °C); $S1_{rec}$: recovered first temporary shape (T_{r2}: 107 °C); $S0_{rec}$: recovered permanent shape (T_{r3}: 140 °C). **b** Quantitative thermal mechanical cycle ($T_{d1} = T_{r3} = 140$ °C, $T_{d2} = T_{r2} = 90$ °C, $T_{d3} = T_{r1} = 53$ °C). Shape fixity, R_f, (S0 → S1): 58.7%, R_f(S1 → S2): 57.1%, R_f(S2 → S3): 96.1%, shape recovery, R_r(S3 → S2): 100.0%, R_r(S2 → S1): 99.6%, R_r(S1 → S0): 93.0% [16]. Reproduced with permission

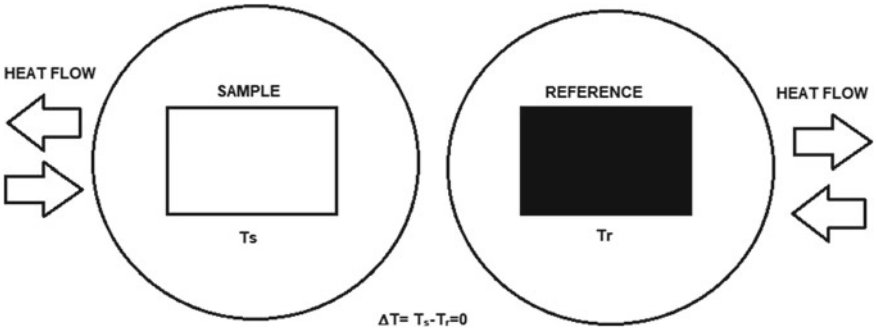

Fig. 5 Schematic representation of the DSC

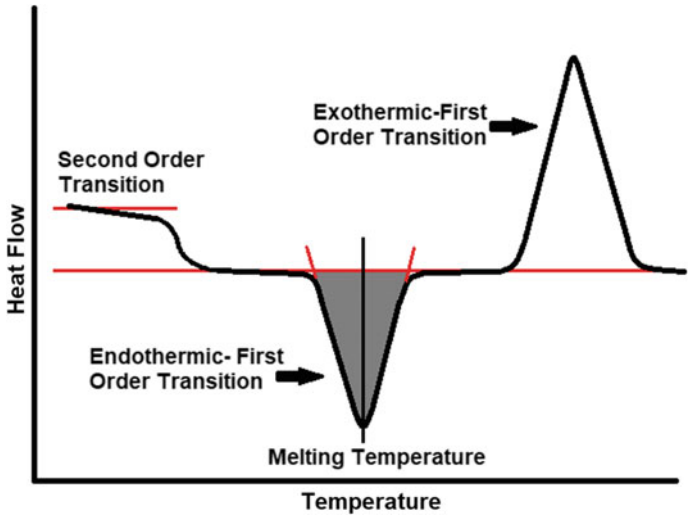

Fig. 6 DSC thermal transitions of first and second order

Many thermal events can be quantified from the energy used to maintain the same temperatures between the materials (reference and sample). These thermal events are usually transitions of second and first order (Fig. 6). First-order transitions can absorb energy (melting, loss of mass, desorption, or reactions of reduction, etc.) giving rise to endothermic peaks or releasing energy (crystallization, polymerization reactions, cure, oxidation, oxidative degradation, adsorption, etc.) giving rise to exothermic peaks. By another side, the second-order transitions do not modify the enthalpy and do not give origin to events endothermic or exothermic. The second-order transitions (glass transition and relaxations of thermal stresses of the polymer chain, for example) only provoke alterations in calorific capacity alternating the position of the baseline.

Shape-memory polymers may be amorphous or semicrystalline materials. Amorphous polymers showed a disordered structure throughout the length of the polymer chain. The absence of organization in the polymer structure results in the absence of marked thermal events in the DSC readings. By other side, semicrystalline polymers have partially ordered regions (short-range organization) accompanied by disordered structures in the chain extension. During the heating process, the crystalline segments absorb thermal energy and melt. The melting process is responsible for the origin of the endothermic peaks (Fig. 6). The melting event can occur at a given temperature resulting in high amplitude peaks when the material is highly crystalline or in a range of temperatures in the material that have a large size distribution of the crystalline regions in polymer chains. In the endothermic melting event, the region correspondent to central peak showed in the curves is associated with the melting point. Conversely, the cooling process, responsible for the formation of crystals, gives origin to exothermic peaks (opposite to the previous ones). Figure 7 shows the first heating obtained from shape-memory polyurethane samples synthesized in aqueous

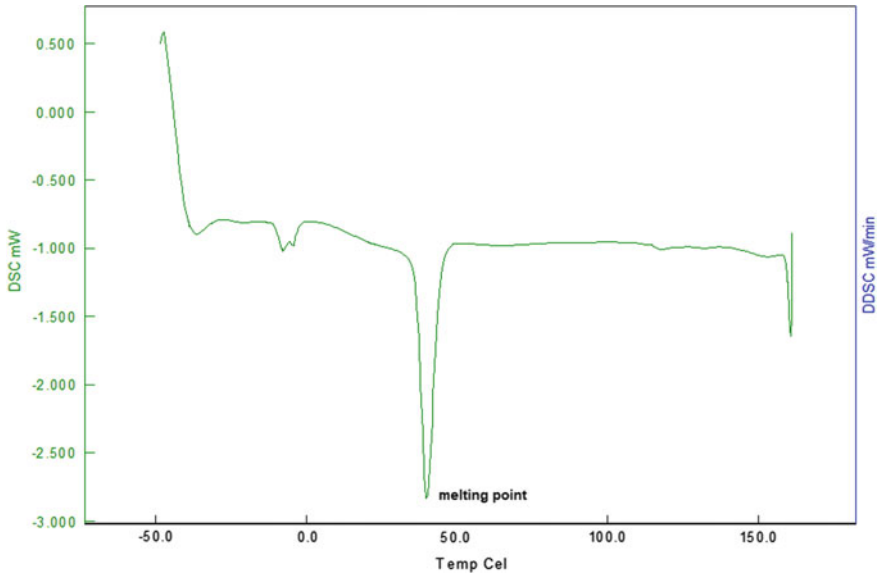

Fig. 7 DSC assay performed with shape-memory polyurethane sample

dispersion. The heating behavior is typical of semicrystalline materials. This material has in its structure polycaprolactone diol (PCL) which are crystalline at temperatures below 40 °C (melting point) showing an endothermic event near to this temperature [10].

The experimental parameters can be modified considering the result to be obtained. Some procedures can be performed to get more accurate results. Typically, the DSC assay is performed using a complete heating and cooling thermal cycle to determine the major thermal transitions related to heating and cooling. However, for the readings relating to the crystallization process to be respected, it is necessary that the cooling rate allows crystal formation and rearrangement of the polymer chains. The relationship between temperature and time variation (heat flow) is extremely important to understand the kinetics of crystallization. Figure 8 shows a DSC assay performed with shape-memory polyurethane samples from a complete cycle (heating and cooling) followed by a heating step. Note that the heating process has an endothermic peak related to the melting of the soft domains. For the cooling, we would expect the appearance of an exothermic peak related to the crystallization process; however, the same is not detected. This phenomenon occurs due to the heat flux applied. When the applied rate is high, the segments that have undergone fusion cannot organize during the cooling process to form crystals.

The endothermic peak related to the melting process of the crystalline segments, besides allowing the determination of the melting temperature of these segments, is an important tool to study the degree of crystallization of the polymer. The calculation of the area belonging to the exothermic peak is a measure of the melting enthalpy

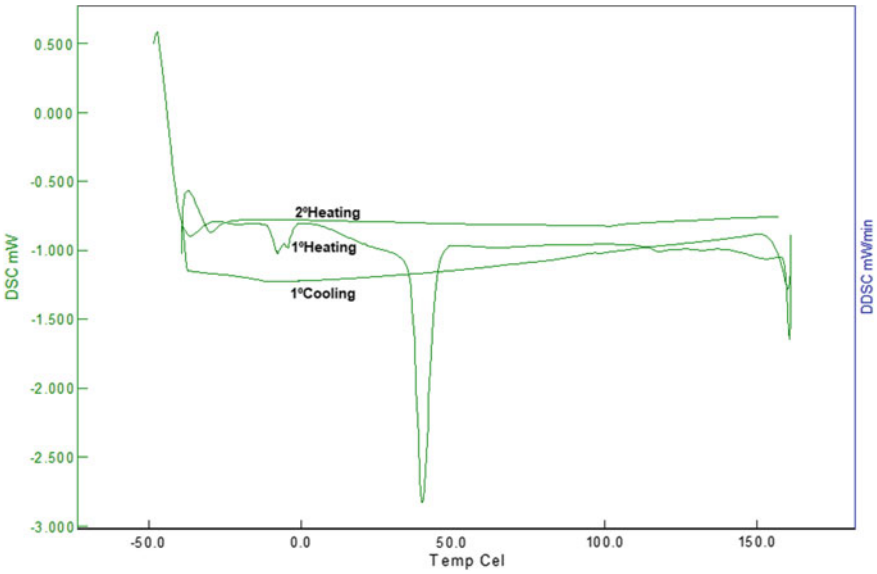

Fig. 8 DSC assay with shape-memory polyurethanes: the samples were submitted to a complete cycle of heating and cooling followed by second heating

of the material (Fig. 9). By this process, we can determine the energy used to melt the crystalline segments of the material. The higher the enthalpy value obtained, the more crystalline the polymer is; in this way, it is possible to estimate the degree of crystallinity present in the polymer structure. The same process can be applied in the exothermic peaks of the cooling, considering in this case that the calculated enthalpy and the respective degree of crystallinity determine the proportion of crystallized segments during the cooling. The difference of the areas between the endothermic peak of the melting process and the exothermic peak of the crystallization process can help to determine the ideal heat flow rate for the experiment.

2 Blends

Polymers blends are a physical mixture of two or more homopolymers or copolymers [1, 20]. The polymers are combined to produce a new material with desirable from the combination of known polymers.

Thermal analysis is an important tool to aid in the development of polymer blends. The amorphous polymeric molecule exhibits a glassy state at low temperatures where the molecular motion is frozen. The molecular motion of the polymeric start with the increase of temperature in the glass transition temperature (T_g) [20]. The glass transition temperature (T_g) is a relevant thermal criterion for the blends miscibility

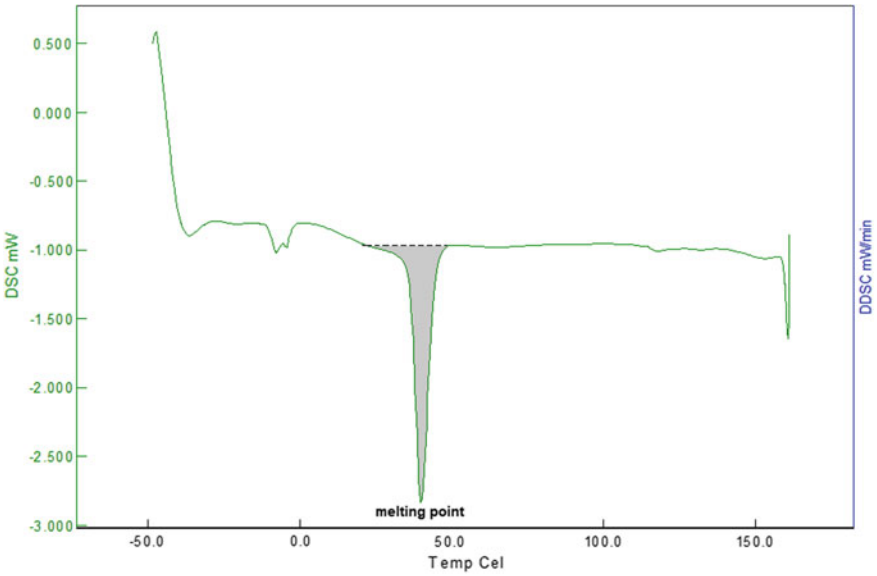

Fig. 9 DSC enthalpy: the enthalpy of melting/crystallization is determined from the area relative to the endothermic/exothermic peak

evaluation [6]. Following this criterion, the blend is considered to be "miscible" if it exhibits only a single T_g lying in a temperature range intermediate to the T_g of the original components of the blend. The condition for the application of this criterion is that there is a difference of at least 20 °C between the T_g of the components of the phases of the polymer mixture. When a blend exhibits two or more T_g corresponding to the different phases displaced relative to the T_g of the pure components is considered to be "partially miscible." In this case, each phase consists of a miscible mixture containing different compositions. Finally, "immiscible mixtures" exhibit the same glass transition temperatures of pure raw materials.

The melting temperature of the crystallization and the melting enthalpy may also be employed to study the miscibility of the components of the phases of the blend [21]. The information about the polymeric structure and its correlation to the physical and thermal properties could be provided in the melting temperature.

The following figure (Fig. 10), for example, shows the DSC (first heating) curves of polystyrene and the shape-memory polyurethane (PS/SMPU) blends produced by thermomechanical mixing [21]. Note that the curves show two thermal transitions correlated with the melt temperature of the soft segments (approximately 45 °C) of the SMPU and the glass transition temperature of the polystyrene phase (approximately 90 °C) [10]. Note that the glass transition temperature of the polystyrene was slightly reduced when the SMPU concentration was increased. At the same time, the enthalpy of fusion becomes higher. Modifications in the parameters occur because the interaction between the PS and SMPU chains in the mixing interfaces restricts

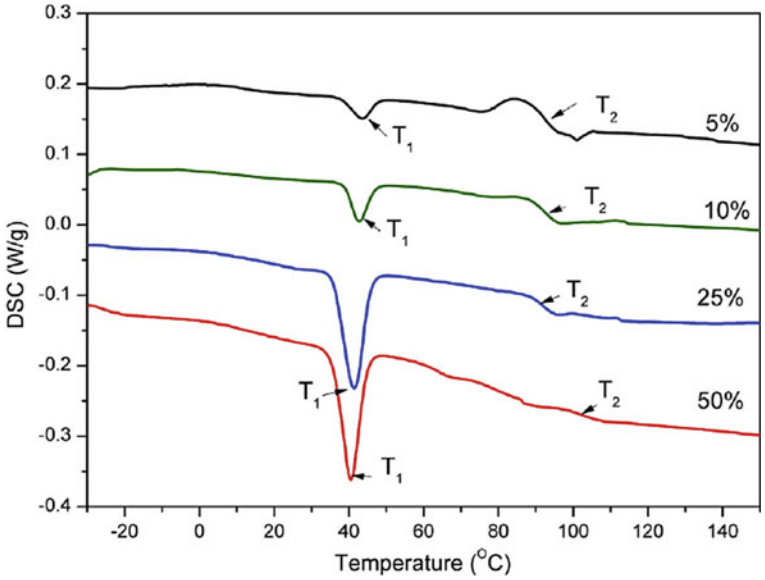

Fig. 10 DSC curves of the non-compatibilized blends (Polystyrene—PS/shape-memory polyurethane—SMPU). The curves show blends of composition of 5% wt% (5%PU/95%PS), 10% wt% (10%PU/90%PS), 25% wt% (25%PU/75%PS), and 50% wt% (50%PU/50%PS). Reproduced with permission [21]

the crystallization in the SMPU phases and contributes to the reduction of the glass transition temperature of the PS.

The addition of compatibilizer is an alternative to increase the dispersion and adhesion between the phases of a blend formed by immiscible polymers. The compatibilizers are usually blocked or graft copolymers, which act at the interface, reducing interfacial tension [22]. According to Bellin et al. [18], compatibilizers act as emulsifiers by reducing phase interfacial energy and domain size. According to Araújo et al. [23], another alternative is to generate this copolymer in situ during the preparation of the mixture through grafting reactions using functionalized polymers. In this case, the compatibilizing copolymer would migrate to the interfacial region of the dispersed phase, increasing interfacial adhesion and reducing the size of the dispersed phase [24]. When the compatibilization process is effective, it can modify the thermal transitions in the material, causing a reduction of the melting temperature of the crystallized phases.

The glass transition temperature and the melt temperature may be used as a parameter for studying the miscibility of the blends with the addition of compatibilizer. Figure 11 shows the effect of the addition of compatibilizer (maleic polystyrene anhydride) on the thermal transitions of the blends of shape-memory polyurethane and polystyrene. In Fig. 11a, the compatibilization was performed using a pre-compatibilized shape-memory polyurethane (shape-memory polyurethane exerted

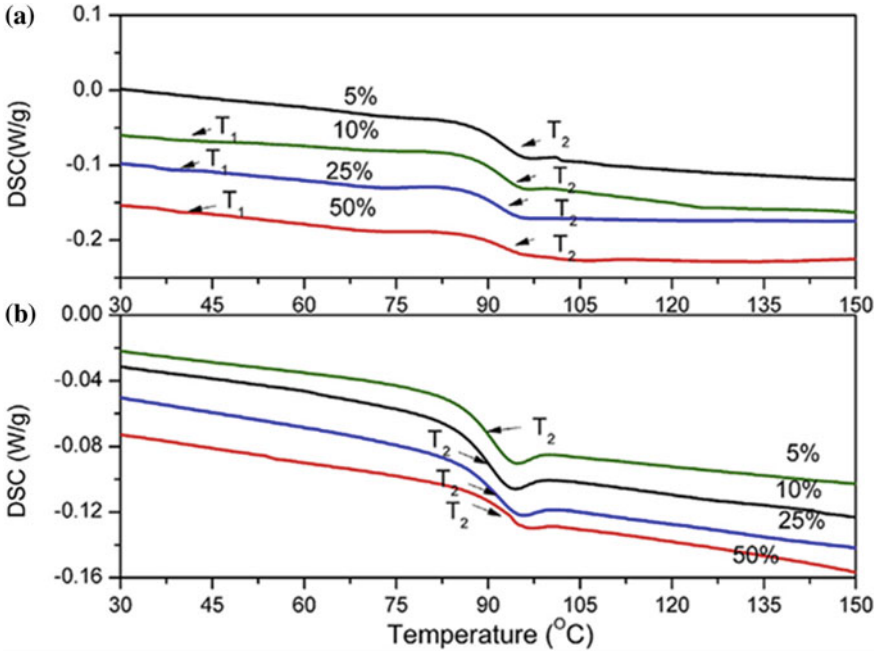

Fig. 11 DSC curves of the compatibilized blends (Polystyrene/Shape-Memory Polyurethane/Polystyrene co-anhydride maleic). The curves show blends of composition of 5% wt% (5%PU/95%PS), 10% wt% (10%PU/90%PS), 25% wt% (25%PU/75%PS), and 50% wt% (50%PU/50%PS): **a** the compatibilization was performed using a pre-compatibilized shape-memory polyurethane; **b** the compatibilizer was added during the thermomechanical cycle. Reproduced with permission [21]

with maleic polystyrene anhydride) blended with polystyrene. In Fig. 11b, the compatibilizer was added during the thermomechanical cycle (thermomechanical mixture of polystyrene/shape-memory polyurethane/maleic polystyrene anhydride). Note that the melt transition is reduced (temperature close to 40 °C). This reduction occurred because the degrees of phase mixing in these systems restrict the crystallization of soft segments. The presence of PS units in the SMPU and SMA chains hinders the crystallization of the soft segments [25].

According to Song and Liao [25], the study of heat capacity differential, dCp/dT, with temperature signal is an important resource to study the miscibility between two components of a blend. This is because the differential is sensitive to change the components of blend [26].

The analysis is performed from the study of derivative (dCp/dT) as a function of temperature. For a fully miscible blend of two-component polymers, the differential as a function of temperature is a single Gaussian curve. For a mixture of fully immiscible two-component polymers, it is a two-separate Gaussian. For partially miscible two-component polymer blends, the signal is a sum of multiple Gaussian [25, 26].

3 Composites

Composites are materials constructed of two or more components with different physical or chemical properties. These components are combined to produce a material having different properties than the individual components. There is no chemical interaction. The individual components remain separate and distinct within the final structure. The materials are combined for the purpose of obtaining better properties than the source materials for specific technological applications.

The studies of the thermal transitions of the materials' constituents of the composite are fundamental to obtain materials with satisfactory properties. Many works showed the importance of the thermal characterization for the development and the study of composites materials. The parameters are strictly related to the structure. The principal parameters are melting point, glass transition temperature, and heat capacity.

Song and Liao [25], by example, has been developed modulated differential scanning calorimetric (MDSC) method combining transmission electron microscopy (TEM) for characterizing the morphology of composite latex particles. The polymer composites' properties are strictly related to the degree of crystallization, crystalline structure, and morphology [27].

The possibilities of thermal analysis applications for composite materials depend on the composition and number of materials used to produce them. However, the basic principles used in the analysis of a constituent phase can be used to analyze the properties of the materials. Thermal transitions are used to determine composite morphology. Melting transitions, for example, are employed to study the degree of crystallization of the phases of the composite material and possible structural changes in the polymers after the production of the composite material. From this transition, the properties directly related to the crystallization of the polymers can be determined. Basically, the same thermal parameters (melting point, glass transition, melting enthalpy, melting crystallization, etc.) can be used to determine or predict the properties of a composite material. The changes existing in these parameters before and after the production of the composite material are taken as reference for study in the structural changes and in the degree of interaction between the constituent phases of the composite material.

4 Conclusion

The characterization of material properties during the design steps is essential for cost and time reduction. The characterization of a material during development allows to partially predict the behavior during its useful life.

Considering this point of view, DSC is an essential tool for the development and characterization of shape-memory polymers, polymer blends, and composites. This is because the thermal transitions from the constituent structures of the polymer

chain determine the behavior of these materials. In shape-memory polymers, thermal transitions are responsible for determining how programming processes can occur. The glass transition and the melt temperature are intrinsically associated with the mobility of the polymer, structural, and morphological characteristics. High thermal transition temperatures are generally associated with high molar mass, crystallinity, and high entanglement.

On the other hand, in composites and mixtures, the thermal transitions are an important parameter to study the affinity between the constituents of the polymer phases, interfacial adhesion, and degree of mixtures between the constituents of the polymers forming a blend or composite.

References

1. Meng Q, Hu J (2009) A review of shape memory polymer composites and blends. Compos A 40:1661–1672
2. Xie T, Xiao X, Cheng YT (2009) Revealing triple-shape memory effect by polymer bilayers. Macromol Rapid Commun 30:1823–1827
3. Behl M, Lendlein A (2007) Shape memory polymers. Mater Today 10(4):20–28
4. Xie T, Rousseau IA (2009) Facile tailoring of thermal transition temperatures of epoxy shape memory polymers. Polymer 50:1852–1856
5. Mondal S, Hu JL (2006) Segmented shape memory polyurethane and its water vapor transport properties. Des Monomers Polym 9(9):527–550
6. Otsuka K, Wayman CM (1998) Shape memory materials. Cambridge University Press, Cambridge
7. Liu C, Qin H, Mather PT (2007) Review of progress in shape-memory polymers. J Mater Chem (17):1543–1548
8. Sun L, Huang WM, Ding Z, Zhao Y, Wang CC (2012) Stimulus-responsive shape memory materials: a review. Mater Des 33:577–640
9. Pereira IM, Oréfice RL (2010) In situ evaluation of structural changes in poly(ester-urethanes) during shape-memory cycles. Polymer (Guildford) 51(8):1744–1751
10. Martins GS, Pereira IM, Hoehne NML, Oréfice RL (2017) Influence of aqueous dispersions in place of organic solvents during the synthesis of shape memory polyurethanes on their structure and properties. Polym Eng Sci 57(4):432–440
11. Pereira IM, Oréfice RL (2009) The morphology and phase mixing studies on poly(ester-urethane) during shape memory cycle. J Mater Sci 45:511–522
12. Lee BS, Chun BC, Chung YC, Sul KI, Cho JW (2001) Structure and thermomechanical properties of polyurethane block copolymers with shape memory effect. Macromolecules 34:6431–6437
13. Zhuohong Y, Jinlian H, Yeqiu L, Lapyan Y (2006) The study of crosslinked shape memory polyurethanes. Mater Chem Phys 98(2):368–372
14. Yang B, Huang WM, Li C, Lee CM, Li L (2004) On the effects of moisture in a polyurethane shape memory polymer. Smart Mater Struct 13(1):191–198
15. Pandini S, Passera S, Messori M, Paderni K, Toselli M, Gianoncelli A, Bontempi E, Riccò T (2012) Two-way reversible shape memory behaviour of crosslinked poly(ε-caprolactone). Polymer 53:1915–1924
16. Xie T (2010) Tunable polymer multi-shape memory effect. Nature 464:267–270
17. Basit A, L'Hostis G, Durand B (2012) Multi-shape memory effect in shape memory polymer composites. Mater Lett 74:220–222

18. Bellin I, Kelch S, Langer R, Lendlein A (2006) Polymeric triple-shape materials. Proc Natl Acad Sci USA 103:18043–18047
19. Sohel A, Mandal A, Mondal A, Pan S (2017) Thermal analysis of ABS/PA6 polymer blend using differential scanning calorimetry. J Therm Anal Calorim 129:1689–1695
20. Sohel MA, Mandal A, Mondal A, Pan S, SenGupta A (2018) Calorimetric analysis of uncompatibilized polypropylene/polystyrene blend using DSC. In: Macromolecular symposia, vol 379, pp 1–4
21. Martins GS, Pereira IM, Oréfice RL (2018) Toughening brittle polymers with shape memory polymers. Polymer 135:30–38
22. Grassi VG, Pizzol MV (2008) Morphological characterization of high impact polystyrene (HIPS). Polímeros 18(1):12–19
23. Araújo ME, Carvalho LH, Fook MVL, Almeida JMD (1997) Propriedades Mecânicas de blendas de PS/Resíduo de Borracha - Influência da Concentração, Granulometria e Método de Moldagem. Polímeros: Ciência e Tecnologia 45–52
24. Liu NC, Baker WE (1992) Reactive polymers for blend compatibilization. Polym Technol 11:249–262
25. Song M, Liao B (2004) A modulated DSC characterization of morphology of composite latex particles. Thermochim Acta 423:57–61
26. Song M, Hourston DJ, Schafer F-U, Pollock HM, Hammiche A (1998) Modulated differential scanning calorimetry: XVI. Degree of mixing in interpenetrating polymer networks. Thermochim Acta 315(1):25–32
27. Wang Y, Zhang L, Zhou S, Huang D, Morsi Y, Gao S, Gong M, Li Y (2011) Investigation of nonisothermal crystallization of hydroxyapatite/ethylene-vinyl acetate (HA/EVA) composite. J Appl Polym Sci

Thermal Stability of Shape Memory Polymers, Polymer Blends, and Composites

Sunan Tiptipakorn and Sarawut Rimdusit

Abstract This chapter will focus on the thermal analysis and interesting related properties of high performance shape memory polymers (SMPs), shape memory polymer blends (SMPBs), and shape memory polymer composites (SMPCs) in different length scales. In general, thermal behaviors of shape memory materials are very relevant to the potential uses in many demanding applications. In order to develop durable industrial products, it is necessary to investigate the thermal stability of these polymers. The polybenzoxazine (PBZ)-based shape memory materials are mainly mentioned in this chapter due to the outstanding properties and high thermal stability of the novel phenolic polymers. This kind of thermoset can be alloyed with other polymers such as epoxy and polyurethane suitable to be used to produce SMPCs in high temperature applications with synergistic behaviors. Therefore, the PBZ/epoxy alloy-based systems and PBZ/polyurethane alloys-based systems are mentioned as well.

Keywords Shape memory polymer · Thermal stability · Blends · Composites · Benzoxazine

1 Introduction

Shape memory materials (SMMs) have been well known for a long time as stimuli-responsive materials having recoverability of their original shape. Generally, various kinds of external stimulus such as temperature change [1–4], light induction [5],

S. Tiptipakorn
Department of Chemistry, Faculty of Liberal Arts and Science, Kasetsart University, Malaiman Road, 73140 Nakhon Pathom, Thailand
e-mail: faassntk@ku.ac.th

S. Rimdusit (✉)
Department of Chemical Engineering, Faculty of Engineering, Chulalongkorn University, 10330 Bangkok, Thailand
e-mail: sarawut.r@chula.ac.th

J. Parameswaranpillai et al. (eds.), *Shape Memory Polymers, Blends and Composites*, Advanced Structured Materials 115,
https://doi.org/10.1007/978-981-13-8574-2_8

Table 1 Comparison on characteristics between typical SMAs and SMPs [1, 14]

Characteristic	SMAs	SMPs
Density (g/cm^3)	Approximately 6.5	Approximately 0.9–1.1
Transformation strain (%)	8% at max.	Up to 800%
Thermal conductivity (W m^{-1} K^{-1})	As high as 20 for NiTi	0.15–0.30
Processing condition	Over 1000 °C/high pressure	Lower than 200 °C/low pressure
Cost	High	Low

electrical current [6], solvents [7], ions [8], magnetic field [9], pH variation [10] or even irradiation [11] are applicable. The temperature is typically the most common stimuli [12–15]. Recently, shape memory polymers (SMPs) and shape memory metallic alloys (SMAs) as two main types of SMMs that are widely used in many applications such as smart medical devices, smart actuators and sensors, deployable structure, smart fabrics etc. [16–19]. The characteristics of typical SMPs and SMAs are compared in Table 1.

It could be seen that SMPs provided comparatively greater advantages than shape memory alloys (SMAs) in aspects of lower density, higher elastic deformation, greater processability, and lower cost [19–22]. Moreover, the strain of SMP was reported to be up to 800% (for some polymers) [11]. That is higher than the maximum values of SMA, shape memory ceramics, shape memory glasses (10, 1, and 0.1%, respectively) [23, 24]. The shape memory behaviors of SMP could be demonstrated as shown in Fig. 1. It could be seen that the shape of SMP can be deformed when applying external force and heating above switching temperature or transition temperature (T_{trans}) of the polymer component, i.e., melting temperature (T_m) or glass transition temperature (T_g) [19, 25]. The deformed shape can be kept after cooling to temporary shape. At this state, the energy was stored. When further heated, the kept energy is released. The shape can automatically recover to its original shape.

Typically, SMPs are categorized into two types, i.e., thermoset-shape memory polymers (TS-SMPs) and thermoplastic-shape memory polymers (TP-SMPs). The TS-SMPs are more preferable for some severe applications such as light weight deployable spacecraft structures, and smart actuators [26, 27]. Although both TS-SMPs and TP-SMPs possess more interesting intrinsic advantages than SMA, some major shortcomings of SMP are their lower modulus [28–35] and longer response time [36, 37]. Recently, most researches relevant to SMP have been mainly focused on some areas, e.g., searching for the new applications, modification of molecular structure to meet the usage requirement, and exploration of the new shape memory effects [19]. In order to develop the thermomechanical properties of the SMPs to meet the requirement of applications, there are many approaches, i.e., blending or alloying with other polymeric components as shape-memory polymer blends (SMPBs) and

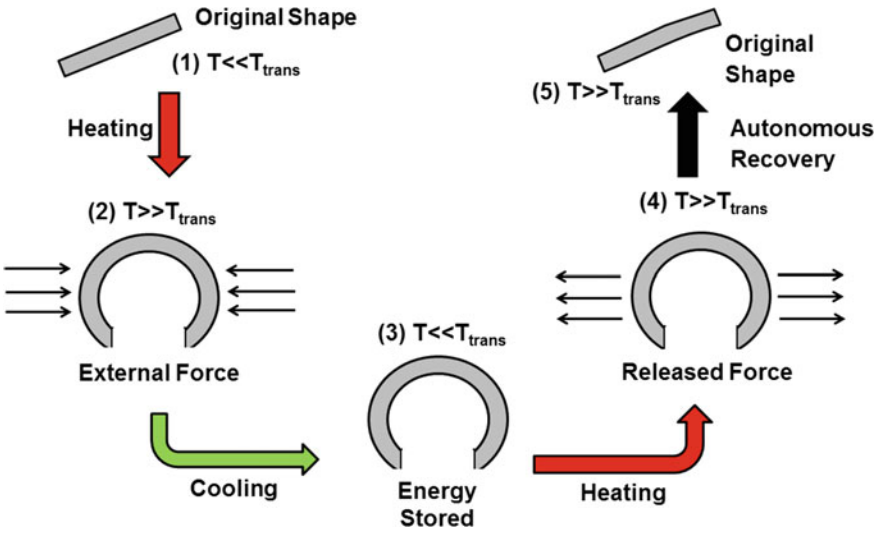

Fig. 1 SMP behaviors upon heating and applying force [25]

Table 2 Selected analytical techniques for decomposition investigation of polymers [42]

Scale of decomposition	Observed aspect	Analytical technique
Macroscopic scale	Reduction of mechanical properties	Mechanical test
Microscopic scale	Progress of Micro-cracking	Optical microscope
Supramolecular scale	Morphology change	TEM, DSC
Macromolecular scale	Molecular weight distribution change	GPC
Chemical structure scale	Generated degradation products	FTIR, Raman, NMR

the addition of functional fillers as shape memory polymer composites (SMPCs) [38–41].

The thermal stability of the SMPs, SMPBs, and SMPCs is a key parameter, indicating the limitation for the usage of the materials. In general, many methodologies for decomposition investigation of polymers in various scales have been proposed as shown in Table 2.

Although many techniques have been developed as previously mentioned, the most commonly used methodology to determine the thermal stability of shape memory materials are carried out via thermogravimetric analysis (TGA) [43], which could provide the information in terms of thermal decomposition temperature, and char yield. In the degradation process, the change in thermal decomposition of the polymers is from the chemical reaction by means of chain scission of the macromolecules. Many steps are composed in the thermal degradation pathway, i.e., (a) initiation, (b) propagation, and (c) termination steps. In the composite system, the thermal stability of the multicomponent materials not only rely on the individual thermal stability of the polymeric matrix and the functional filler, but also the degree of filler dispersion

in the matrix, and interfacial adhesion [42, 44, 45]. In aspects of char formation, the residual solid remained upon the decomposition process generally occurs from crosslink reactions. The char residues are able to act as a physical barrier for heat and oxygen diffusion, and prevent the component from further decomposition [42].

Though some reviews on SMPs, SMPBs, and SMPCs have been reported. A review focusing on the thermal stability and related thermal properties has been rarely mentioned. This chapter focuses on the shape memory polymer and associated systems derived from high temperature polymers such as polybenzoxazine-based SMPs and other polymeric materials with high stability SMP systems.

2 SMPs and SMPBs and Their Thermal Characteristics

2.1 A Brief Overview of SMPs and SMPBs

In general, SMPs and SMPBs are composed of two portions, i.e., (i) hard portion having a function to keep the structure stable, (ii) soft portion having a function to recover the shape of the materials [17]. The hard portion can be derived from the stable network segment from chemical or physical linkage; while the soft portion is acted as a reversible switching transition segment. In the soft portion, the melting/crystallization transition and glassy/rubbery transition exhibit a reversible phase transition at T_m and T_g, of the polymeric domain, respectively [46, 47]. The SMPs and SMPBs can be categorized into four classes based on types of polymeric components and type of linkage in the materials as presented below [48].

(a) Chemically linkaged thermoset polymers (Class I)
The elasticity of Class I SMPBs is attributed to the covalent bonds. The advantage of this class is its high shape recovery (as close as 100%) from strong chemical bonds. This class possesses the difficulty to recover the original shape more than one time. The examples of the materials in this class are polynorbonene (T_{trans} = 40 °C) [29], and dehydrochorinated crosslinked PVC (T_{trans} = 80 °C) [49].

(b) Chemically linkaged semi-crystalline polymers (Class II)
The deformed shape of the materials in this class can be recovered when heating beyond the melting temperature of the crystalline domain. The shape recovery is in the range of 30–95% [50]. The examples of the materials in this class are gamma radiated polycaprolactone (T_{trans} = ca. 55 °C) [51], and ethylene vinyl acetate (EVA) blended with nitrile rubber (T_{trans} = 85 °C) [52].

(c) Physically linkaged amorphous thermoplastics (Class III)
In this class, physical bonds (such as Van der Waals forces and hydrogen bonds) exist in a blend of two thermoplastic components. The T_g value of hard portion in this material is higher than that of the soft one. The modulus of the material in this class is greater than that of two former classes [53, 54]. The examples of the materials in this class are polypropylene (PP)—poly(1-hexadecene) (PHD)

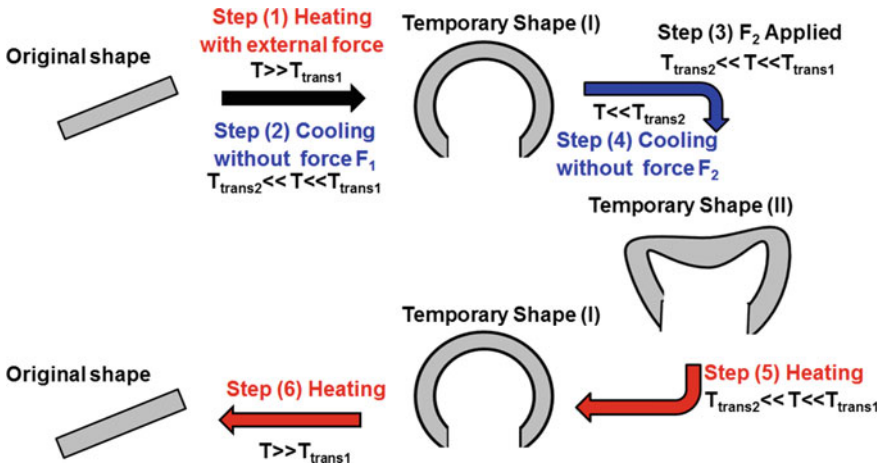

Fig. 2 Triple-shape memory polymers [23]

(T_{trans} = ca. 65 °C) [53], and polyhedral oligomeric silsesquioxane (POSS)-poly(ethylene glycol) (PEG) (T_{trans} = 55 °C) [54].

(d) Physically linkaged semi-crystalline block copolymers (Class IV)
This class is similar to Class III; but, the melting temperature (T_m) of the soft portion exhibits as T_{trans}.. The examples of the materials in this class are polyurethane (PU)- poly(tetramethylene glycol) (PTMG) with 1,4 butanediol (T_{trans} = 0–46 °C) [55], and polyurethane (PU)-PCL diol with 1,4 butanediol (T_{trans} = ca. 60 °C) [56].

Based on the number of temporary shape of the materials, shape memory polymeric materials can be categorized into two main types. In case of dual shape memory polymers as shown in Fig. 1, only one temporary shape is presented; the triple-shape and multi-shape memory polymers have more than one temporary shape as shown in Fig. 2 [57–59].

2.2 Benzoxazine-Based Shape Memory Polymers/Blends

Benzoxazine resins (BA-a) has been well known as a novel kind of thermosetting phenolic resin. The monomer of BA-a can polymerize by heating without any need of catalyst or curing agent. Polybenzoxazine (PBZ) exhibits many outstanding characteristics such as high thermal stability and high mechanical properties with good processability from low viscosity before curing; this noble polymer with high glass transition temperature (T_g) provides great potential for many usage areas [60]. Polybenzoxazine can be used as shape memory materials due to its chemical crosslink structure related to permanent shape for SMPs [61]. Recently, two siloxane-containing PBZ

types (i.e., poly(TMDSBPDP-a) and poly(TMDSBPDP-m)) were synthesized from the reaction between a siloxane-containing ortho-substituted diphenol, formaldehyde, and either aniline or methylamine [62]. Both of them show one-way dual shape memory behavior with excellent shape fixity ratios (ca. 100%) in tensile and bending modes. The T_g values of poly(TMDSBPDP-a) and poly(TMDSBPDP-m) are 53 and 39 °C, respectively. In the recent year, shape memory polybenzoxazines were developed from polyetheramine (PEA), formaldehyde and one of five different compounds, i.e., phenol, o-allylphenol, o-cresol, p-cresol, and m-cresol [61]. All five PBZ-based materials exhibit one-way dual shape memory behaviors. From the dynamic mechanical analysis, the glassy moduli of PBZ synthesized from p-cresol and o-cresol are close and lower than the other three types of PBZ. The T_g values are ranged from 40 to 97 °C. The difference in the chemical structure affects shape memory behaviors. From the three thermomechanical cycles in a tensile mode, the two PBZ based on the ortho-substituted phenols could exhibit better shape memory effect than those based on para- and meta-substituted phenol and unsubstituted phenol. The PBZ based on o-cresol provides the greatest values of shape fixity ratio.

2.2.1 Polybenzoxazine/Epoxy Alloy-Based SMP

One of the intriguing characteristics of polybenzoxazine is its wide molecular design flexibility and ability to be alloyed with other polymers such as epoxy and polyurethane. Moreover, the novel phenolic thermoset has been reported to act as a curing agent with epoxy [63]. That could be attributed to the fact that the phenolic products generated from the thermal polymerization of benzoxazine monomer could have a function as a hardener of the curing process of epoxy [64]. Also, the synergistic behaviors for some properties of copolymers between benzoxazine and epoxy were reported [65, 66]. Epoxy resins are thermosetting polymers containing more than one epoxide functional groups per molecule [67]. Typically, the epoxy resins possess preferable characteristics, such as low viscosity, low shrinkage, good chemical resistance, high adhesive strengths, great mechanical properties, and high electrically insulative properties. In a pioneering work, Rimdusit and Ishida [64] reported the synergistic behaviors of the T_g of ternary systems based on benzoxazine, epoxy, and phenolic resins. The maximum of T_g was presented at approximately 180 °C in the mass ratio of benzoxazine/epoxy/phenolic at 5/4/1. The T_g of neat polybenzoxazine was reported at ca. 160–170 °C, and that of phenolic Novolac was at ca. 170 °C. The T_g of EPON825 epoxy resin was in the range of 100–170 °C. Because synergistic behavior was observed in both the binary of benzoxazine and epoxy resins [68]. The effects of benzoxazine resin and Jeffamine D230 mol ratios on thermal stability, mechanical and shape memory properties were investigated later by Rimdusit et al. [69]. From Table 3, the notation of E, N, D, and B stands for EPON 826 (aromatic epoxy), NGDE (alphatic epoxy), Jeffamine D230 (curing agent) and BA-a, respectively. The researchers reported that the increase of BA-a content leads to the increase in storage modulus, crosslink density, and T_g. They also reported that the recovery time was shortened with increasing epoxy contents. At high temperature,

Table 3 Storage modulus, crosslink density, and glass transition temperature (T_g) of benzoxazine-modified epoxy SMP [69]

Molar ratio of E:N:D:B	Storage modulus at 35 °C (GPa)	Crosslink density (mol/cm^3)	T_g from DMA analysis (°C)
1:1:0:1	4.70	4.29×10^{-3}	120
1:1:0.2:0.8	4.62	3.81×10^{-3}	92
1:1:0.4:0.6	4.44	3.79×10^{-3}	85
1:1:0.6:0.4	4.34	3.62×10^{-3}	80
1:1:0.8:0.2	3.90	3.25×10^{-3}	72
1:1:1:0	3.18	2.90×10^{-3}	47

the movement of chain segments was accelerated with heat, leading to increase the recovery force on the samples [69].

In general, the aromatic epoxy was used in the epoxy-based SMPs. However, Tanpitaksit et al. [70] recently fabricated SMP derived from polybenzoxazine (PBZ)/NGDE epoxy alloys without the use of aromatic epoxy. Benzoxazine resin (BA-a) was used as the curing agent and a stable network segment in the system [67]. From FTIR spectra, the network formation between BA-a and NGDE aliphatic epoxy after thermal cure were observed [70]. The breakage of a C–O bond in the oxazine ring of BA-a resin was observed, and then a network structure generated. The epoxide functional group could form ether linkage with phenolic hydroxyl group. The chemical structure rings of both benzoxazine resin and aliphatic epoxy can be opened, and the curing process was conducted without other curing agents [71, 72]. These results were corresponding to the previous works of Rimdusit et al. [64] and Kimura et al. [73] using the different epoxy types. The polymerization of BA-a monomers and the chemical reaction between benzoxazine monomer (BA-a) and aliphatic epoxy (NGDE) were proposed in Fig. 3, respectively.

For the DMA thermogram [67], the storage moduli at room temperature (at glassy region) were observed ranging from approximately 2.8 to 4.5 GPa at BA-a contents ranging from 30 to 50 mol%. The values tended to increase with increasing BA-a content in the alloys because of the addition of the more rigid molecular segment of PBZ in the alloy SMPs [74]. The addition of BA-a resin from 30 to 50 mol% could also systematically increase the modulus in rubbery plateau region in the range from 40 to 172 MPa due to significant improvement of crosslink density of the alloy. The crosslink density can be predicted from the storage modulus curve at high rubbery plateau over 10^7 Pa according to the equation proposed by Nielsen [75]. From the calculation, the crossslink density of the alloys was increased with increasing BA-a content ranging from 3.8×10^{-3} to 6.0×10^{-3} mol/cm^3. The enhancement of crosslink density could lead to an increase in char formation upon thermal decomposition [44, 45]. Furthermore, the great value of crosslink density leads to the high values of storage modulus and T_g. That is attributed to higher rigidity in the molecular structure of PBZ component [76]. Moreover, the increase in T_g value directly reflected that the segmental mobility of polymer chains was decreased, and

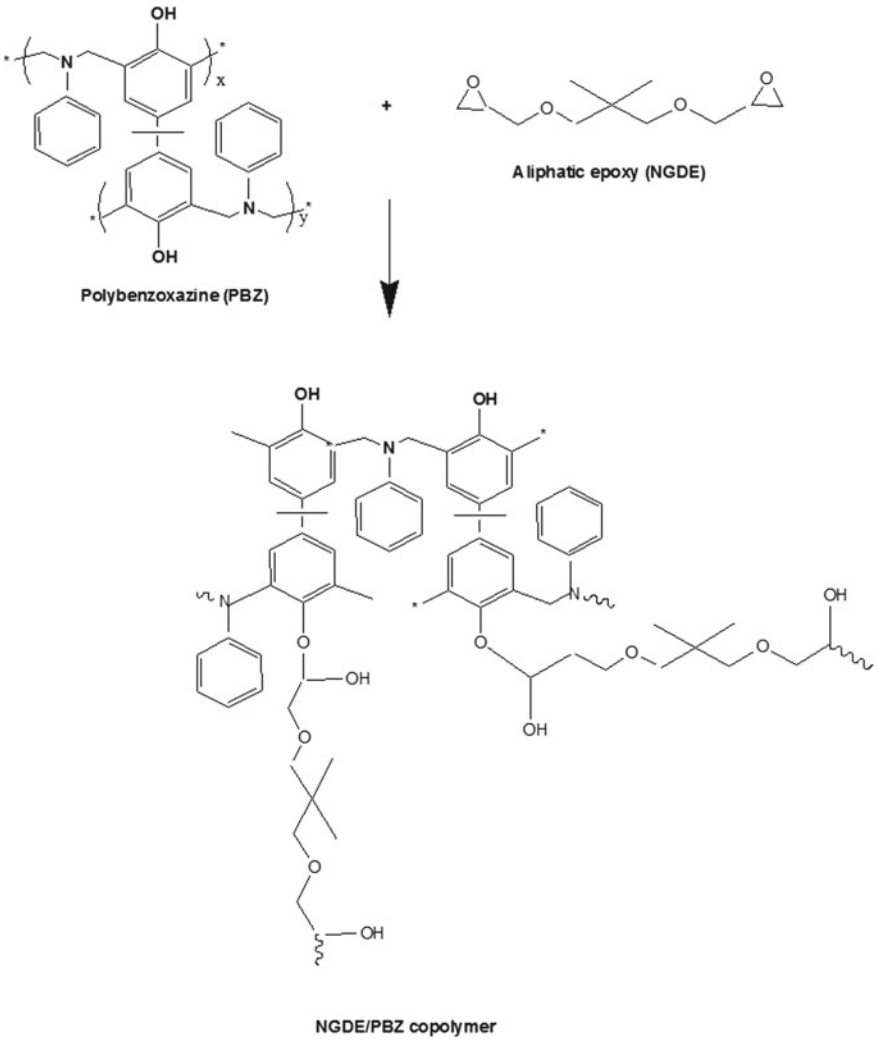

Fig. 3 Proposed synthesis reaction of BA-a/epoxy copolymer [73]

the stiffness of the alloys was increased with increasing crosslinked density upon increasing benzoxazine component in the alloy. Additionally, the peak height of the loss tangent curve was reported to decrease with increasing the benzoxazine content, indicating that the elastic behavior of the alloys was increased with the benzoxazine component. It could be noticed that the width at half height of the curves was increased, when increasing the amount of benzoxazine. That implied more network heterogeneity was observed when benzoxazine was added in the resin mixtures. The single broad switching transition region in some ratios when alloying epoxy with benzoxazine could have some benefits to provide multiple-shape memory

effects [77], which are highly beneficial for various applications, e.g., packaging and robotic uses. For the SMPBs derived from the NGDE/PBZ alloys, the shape recovery time of the SMPs was ranged from 75 s at T_g (of 51 °C for 30 mol% BA-a) to 145 s at $T_{g,}$ (of 140 °C for 50 mol% BA-a), and ranged from 64 to 120 s at $T_g + 20$ °C [70]. That means shape recovery time was shortened with increasing the active temperature. That was attributed to the fact that the activated molecular chain segments intensely moved with increasing temperature. In addition, the shape recovery time was increased with increasing BA-a content because the molecular chain segment of the alloys could be impeded with increasing crosslink density. Comparatively, the recovery times of the SMPBs derived from benzoxazine alloyed with aliphatic epoxy were less than that of the SMPs of neat epoxy resin E-51 (WSR 618) cured by aromatic amine as reported by Liu et al. [78]. In the alloy system, the addition of BA-a component into SMP was able to adjust the shape recovery time, and broaden the applications of the resulting alloy SMPs. The shape fixity of NGDE/PBZ alloys-based SMPBs was reported to be almost 100%. Moreover, their flexural strength and flexural modulus were increased with the increase of BA-a content. From the study, the NGDE/PBZ SMPs possess flexural strength ranging from 52 MPa (for 30 mol% BA-a) to 132 MPa (for 50 mol% BA-a), and flexural modulus ranging from 1.6 GPa (for 30 mol% BA-a) to 4.0 GPa (for 50 mol% BA-a). That was attributed to the fact that flexural strength and flexural modulus of pure PBZ are as high as approximately 126–139 MPa and 4.5–5.8 GPa, respectively. In addition, it was due to an enhanced crosslink density of the obtained polymer network as previously described.

2.2.2 Shape Memory Epoxy Polymers

For many years ago, Wu et al. [79] prepared shape memory epoxy polymers by mixing epoxy resin at varied hardeners contents, i.e., 27–41 wt%. The T_g values of the fabricated SMP sheet were in the range of 75–114 °C and increased with the hardener content. The decomposition temperature at 10% weight loss from TGA thermograms were reported to be over 300 °C for all SMPs. The obtained epoxy SMP possesses a high thermal stability possibly due to the component of the network structure. Later, Lu et al. [80] prepared the epoxy SMPs based on diglycidyl ether of bisphenol A (DGEBA) and tricarballylic acid. The SMP system obtained the modulus of 1.3 GPa at room temperature and was thermally stable up to 380 °C. From the thermomechanical cycle test for the epoxy SMPs, the compressive stress was 2.3 MPa when the strain was 10% at elevated temperature. Recently, Kuang et al. [81] prepared a series of tripe-shape memory epoxy materials through the reaction of a conventional epoxy oligomer, an aliphatic diamine and a diamine Dielse–Alder (DA) adduct cross-linker via a one-pot approach with varying the molar ratio of the diamine adduct cross-linker from 33 to 67. The thermal resistance of epoxy polymers was reported as the degradation temperature at 2% weight loss (T_{d2}). The values for all epoxy-based SMPs were greater than 280 °C. The char yield at 600 °C was increased with increasing the DA adduct content. One stage of weight loss was found in the

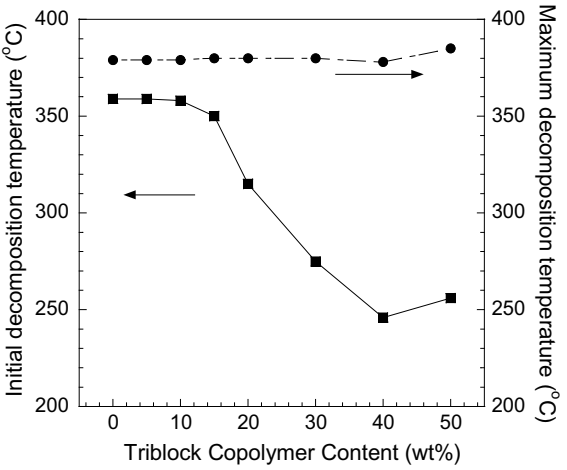

Fig. 4 Initial decomposition temperature and maximum decomposition temperature at various triblock copolymer contents [84]

range of 393–411 °C. The service temperature of this system could be less than 160 °C [81, 82]. In the recent year, Parameswaranpillai et al. [81] prepared the SMPB system of poly(propylene glycol)-block poly(ethylene glycol)-block-poly(propylene glycol) (PPO-PEO-PPO) triblock copolymer blended with DGEBA epoxy. They reported that the blends possessed UV resistance and high thermal stability. The glass transition temperature of the blends could be tunable as the composition ratio of the components. In addition, the parameters from TGA analysis were reported as shown in Fig. 4. It could be observed that the initial decomposition temperatures of the SMPBs was decreased with the addition of the triblock copolymer. However, it was reported that there was no significant difference between the temperatures at maximum decomposition rate of the blends at all triblock copolymer contents [81]. In the recent time, Wei et al. [83] reported that the hydrogenated bisphenol A epoxy resin with different curing agents provided better shape memory properties than bisphenol A epoxy resin. The hydrogenated bisphenol A possesses lower T_g, greater toughness, and much higher shape recovery rate because of its rigidity cyclohexane rings in the chemical structure.

2.2.3 SMPBs from Bio-Based Polybenzoxazine/Bio-Based Epoxy Copolymer

As previously mentioned, Tanpitaksit et al. [70] fabricated SMPs from aliphatic epoxy modified with benzoxazine resin. They reported that benzoxazine resin was acted as a curing agent and a stable network segment which has the ability to enhance the properties of SMPBs, such as outstanding shape fixity, and short recovery time. However, these kinds of rendered products are petroleum-based materials. Due to environmental concern, there has been an idea to develop renewable natural materials as an alternative choice to reduce the consumption of petroleum-based prod-

ucts. These bio-based resins have attracted increasing attention due to low cost and biodegradability of the products [82] In the recent time, bio-based polybenzoxazine was synthesized by using natural compounds such as cardanol [85, 86], vanillin [87, 88], furfurylamine [89], stearylamine [89], and eugenol [89], Recently, Sini et al. [87] prepared monofunctional benzoxazine based on vanillin and furfurylamine. The obtained bio-based benzoxazine with highly crosslinked structure showed a lower curing temperature, extremely higher T_g and higher char yield than petroleum-based benzoxazines. Thirukumaran et al. [89] synthesized and investigated the properties of bio-based benzoxazine monomer systems based on eugenol, furfurylamine and stearylamine.They successfully synthesized bio-based benzoxazine monomers (F-BZ and S-BZ) via a solventless method. Both the F-BZ based polybenzoxazine (PF-BZ) and the S-BZ based polymer (PS-BZ) exhibited excellent flame retardant properties. However, PF-BZ possessed much higher thermal stability than PS-BZ.

Not long ago, Hombunma et al. [90] prepared two bio-based alloys, i.e., the eugenol and furfurylamine-based polybenzoxazine/NGDE epoxy. The related characteristics of bio-based shape memory polymer such as shape fixity, shape recovery, thermal and mechanical were determined. Eugenol-based benzoxazine resin (E-fa) was synthesized from eugenol, furfurylamine and formaldehyde at the mole ratio of

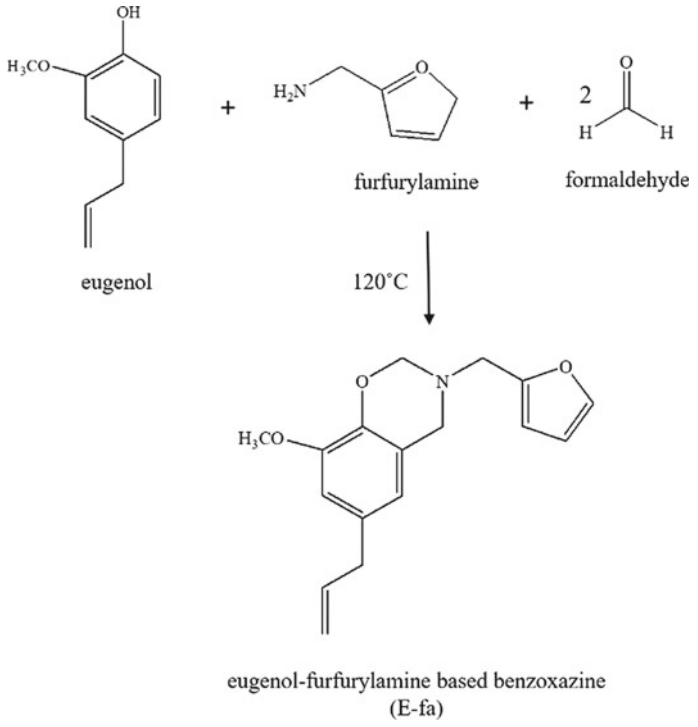

Fig. 5 Synthesis reaction of E-fa monomer [90]

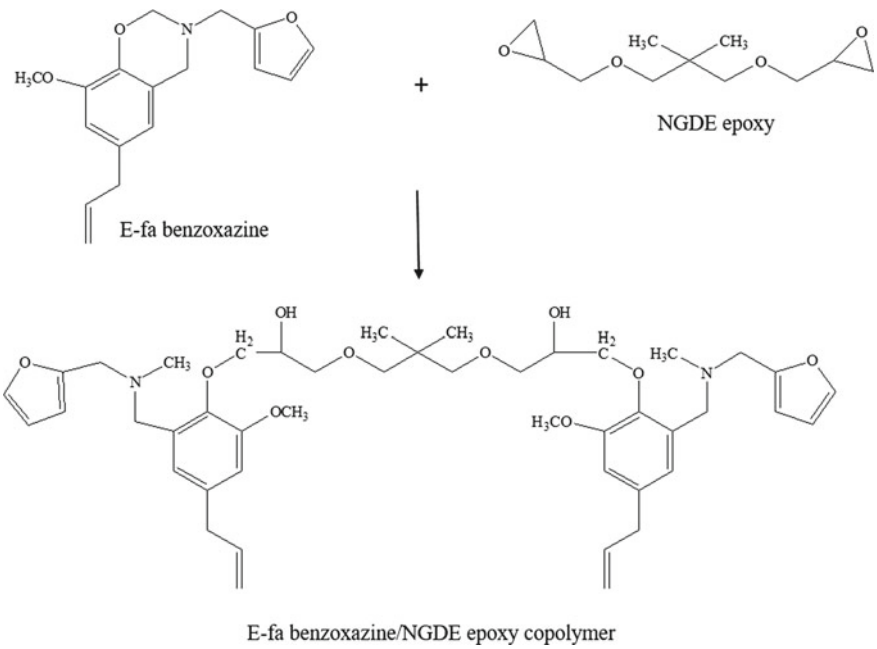

Fig. 6 Proposed chemical reaction between E-fa monomer and NGDE epoxy resin [90]

1:1:2 as shown in Fig. 5. Then, the mixture was heated and stirred until a homogeneous mixture was obtained. The chemical reaction between E-fa monomer and NGDE epoxy resin are presented in Fig. 6. The obtained E-fa monomer was pale yellow. The copolymers were prepared by mixing E-fa monomer with NGDE.The thermally cured films of the mixture were obtained. The IR spectra of E-fa based benzoxazine monomer displayed the peak at 1226 cm^{-1} from the aromatic ether C–O–C stretching mode of an oxazine ring. The peak at 919 cm^{-1} confirmed the presence of a benzene ring attached with an oxazine ring. The spectrum showed a peak at 1151 cm^{-1} from the C−N−C symmetric stretching vibrations. The peaks observed at 1001 and 738 cm^{-1} might be attributed to the vibrations of the furan ring [89].

From the analysis of the thermomechanical properties of E-fa based polybenzoxazine alloyed with NGDE, the modulus of the alloys was increased with increasing E-fa content because of the high rigidity of E-fa. The glass transition temperature (T_g) observed from the peak of loss tangent as exhibit in Fig. 7. It could be noticed that the T_g values were added from 26 to 51 °C when E-fa was increased from 30 to 50 wt%. That was because the greater rigidity segment of E-fa hindered chain mobility of the polymer [91]. The thermal degradation, char yield and shape fixity of the E-fa based polybenzoxazine (poly(E-fa)) alloyed with NGDE was summarized in Table 4. It could be noticed that the increase of E-fa content led to the increase of thermal stability, while the shape fixity of the obtained alloys was ca. 98–99%.

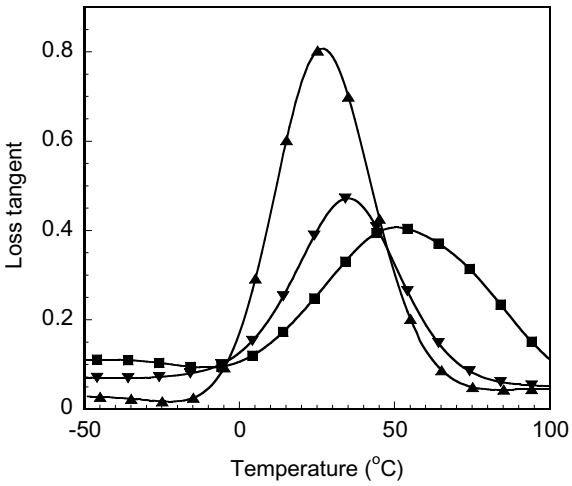

Fig. 7 Loss tangent of NGDE alloys at various E-fa contents: (▲) 30 wt%, (▼) 40 wt%, and (■) 50 wt% [91]

Table 4 thermal stability and shape fixity properties of poly(E-fa/NGDE) alloys [91]

E-fa content	$T_{d,5}$ (°C)	Residual weight (%)	Shape fixity (%)
0	196	5	–
30	269	18	98.0
40	271	22	98.7
50	279	28	98.7
100	310	43	–

In the recent year, Rimdusit et al. [92] successfully prepared the shape memory polymer from vanillin-based polybenzoxazine alloyed with castor oil-based epoxy copolymer. Vanillin-based benzoxazine resin (V-fa) was synthesized from vanillin, furfurylamine and formaldehyde at a mole ratio of 1:1:2 according to the patented solventless method as shown in Fig. 8. The copolymer was prepared by mixing V-fa monomer with epoxidized castor oil (ECO) at various contents ranging from 30 to 50 wt%. The thermal curing was conducted without other chemicals needed. The reaction between two polymeric components was proposed as shown in Fig. 9. The thermal stability of the V-fa/ECO copolymer can be exhibited as shown in Table 5. It could be noticed that the thermal degradation at 5% weight loss (T_{d5}) was decreased from 318 to 314 °C at the ECO content ranging from 30 to 50 wt%. In addition, the char yield at 800 °C was decreased with increasing ECO. In this system, the shape fixity at 25 °C decreased with increasing ECO content ranging from 93 to 86%. While the shape recovery at $T_g + 20$ °C was increased ranging from 87 to 96%.

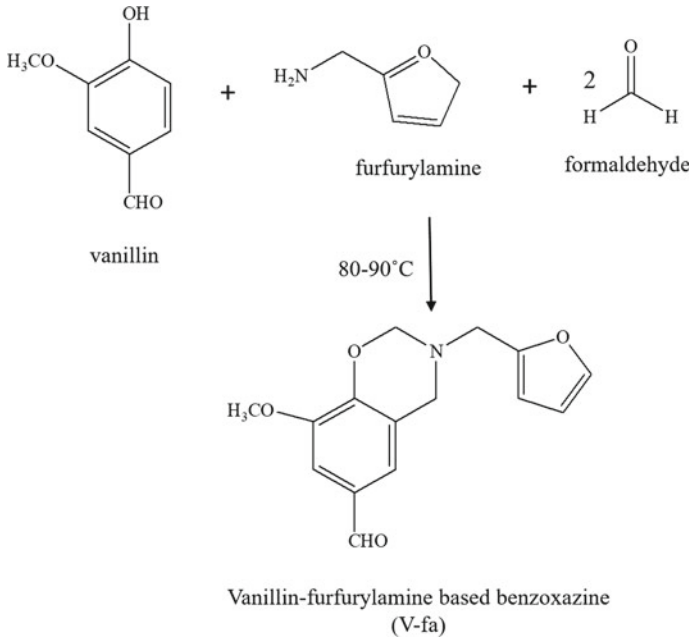

Fig. 8 Proposed synthesis reaction of E-fa monomer [92]

Table 5 Thermal properties of V-fa/ECO copolymer at various ECO contents [92]

ECO content (wt%)	$T_{d,5}$ (°C)	Char yield (%)
30	318	48
40	317	35
50	314	34

2.2.4 Polybenzoxazine/PU Alloy-Based SMP

In the recent year, Erden and Jana prepared the SMP from polybenzoxazine (BA-a) compounded with polyurethane. They reported the ability of polybenzoxazine to act as an additional hard portion of SMP because of its high glass transition temperature and much higher storage modulus than the soft portion of SMP [93]. It has been reported that the alloys between bifunctional BA-a monomer and urethane prepolymer exhibited only one glass transition temperature (T_g), indicating no phase segregation between two components. Moreover, only small amount of added benzoxazine could enhance the thermal stability of the polyurethane [76]. The hydroxyl group of benzoxazine resin generates ether linkage with the isocyanate group of urethane prepolymer as demonstrated in Fig. 10. In the alloy system, the synergistic behaviors of T_g value was observed. For instance, the alloy at PU content of 30 wt% showed the T_g at ca. 220 °C, which was greater than −70°C of neat PU and 165 °C of pure polybenzoxazine [94, 95].

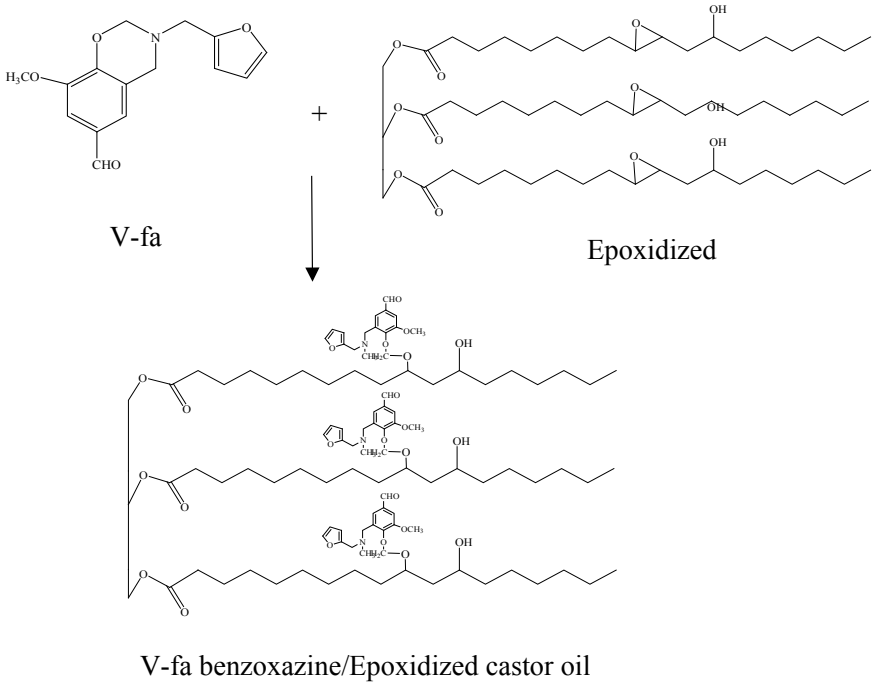

Fig. 9 Proposed chemical reactions between V-fa and epoxidized castor oil [92]

The properties of shape memory polymer from polyurethane (PU) has been investigated and reported for a long period of time. Lee et al. [55] studied the thermomechanical properties of shape memory polyurethane (PU) block copolymers composed of 4,4-methylenebis-(phenylisocyanate), and poly(tetramethylene glycol). The 1,4-butanediol was used as a chain extender. The maximum stress, tensile modulus, elongation at break, and highest loss tangent was observed at 30 wt% of hard segment content. It has been reported that the type of chain extender has an effect on the properties of SMP. In some studies, the pyridine rings in the chemicals such as 2,6-pyridinedicaroxamide was used as a chain extender to synthesize linear and crosslinked polyurethane. The thermal stability from TGA analysis was significantly enhanced [96]. Recently, Weng et al. [97] prepared 2,6-diaminoyridine and 4-hydroxybenaldehyde to provide the pyridine-containing chain extender N, N'-bis(4-hydroxybenylidene)-2,6-diaminopyridine (BHBP). The hydrogen bonding was generated between nitrogen atoms of pyridyl and imine functional groups and N-H functional group of polyurethane. This could improve the thermal stability and mechanical properties of the obtained polymers. In their system, polytetramethylene glycol (PTMG) and 4,4′-diphenylmethane diisocyanate (MDI) were used as reactants to synthesize PU prepolymer. Then, the reaction between BHBP and the prepolymer was proceeded as shown in Fig. 11. In the study, the greater content of

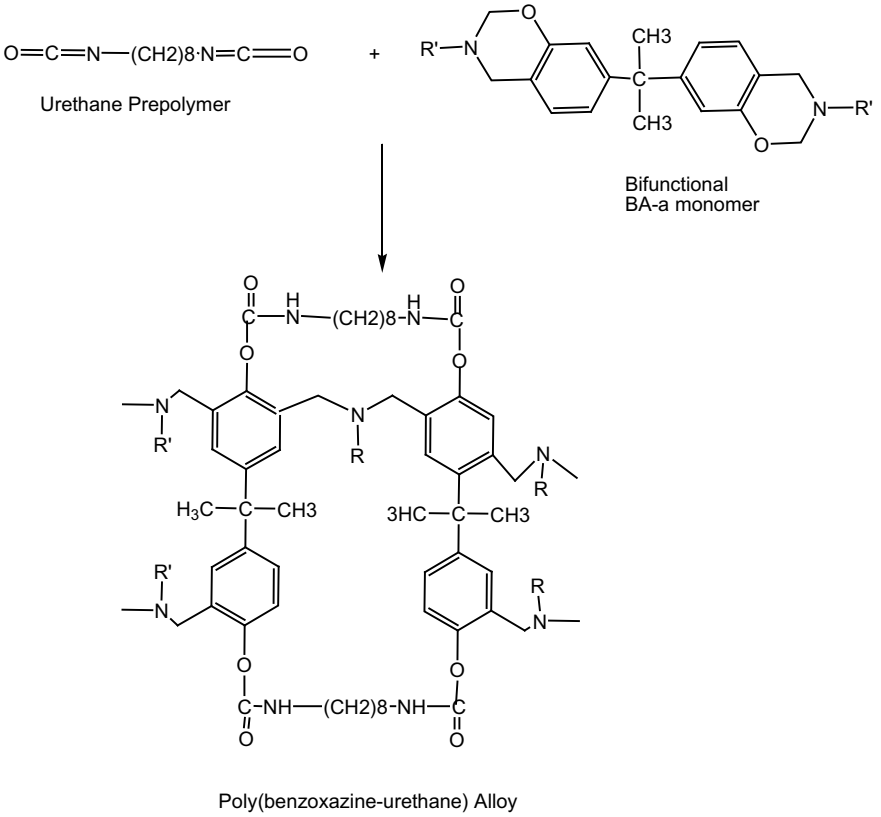

Fig. 10 Proposed chemical reaction between BA-a monomer and urethane prepolymer [76]

Table 6 Thermal decomposition onset temperature, temperature at maximum decomposition rate, and char yield at various amounts of chain extender [97]

MDI (mol)	PTMG (mol)	BHBP (mol)	T_d, onset (°C)	T_d, max (°C)	Char Yield at 700 °C (%)
4	3.50	0.50	334	403	3.5
4	3.25	0.75	338	408	8.5
4	3.00	1.00	342	413	9.2

BHBP could provide higher value of molecular weight and the greater percentage of hard segment in the obtained polymer. From TGA analysis, the thermal properties of the polyurethane at different BHBP contents were presented in Table 6.

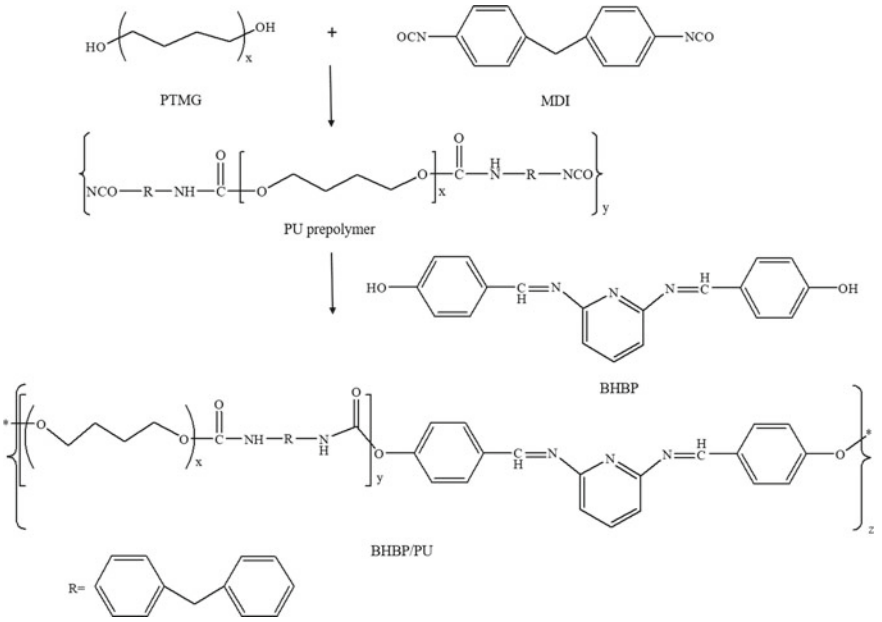

Fig. 11 Proposed chemical reaction between BHBP and PU prepolymer [97]

2.2.5 Multiple-Shape Memory Polymers

As previously mentioned, multiple-SMPs possess more than one temporary states. Two procedures are proposed for the design of multiple-SMPs, i.e., (i) a very wide range of thermal transition temperature, and (ii) multiphase design which each of them provides independent transition and correspond to shape memory effect [98]. Recently, many multiple-SMP systems have been studied. Xie [99] presented that the perfluorosulphonic acid ionomer (PFSA), possessing only one wide glass transition temperature region starting from 55 to 130 °C, revealed multi-shape memory effects without any adjustment of the material composition. Hoeher et al. [100] prepared the crosslinked polyethylene blends composed of ethylene-1-octene copolymers (EOC), low density polyethylene (LDPE), and high density polyethylene (HDPE). The mass ratio of EOC: LDPE: HDPE in the blends was 80:15:5. The results reveal that the programmed material exhibits an excellent recovery ratio of $99.7 \pm 0.3\%$. In addition, a wide transition temperature region of triple-shape memory starting from 35 to 150 °C. In the recent year, Samuel et al. [101] prepared SMPs from the miscible polymer blends between poly-L-lactic Acid (PLLA) and poly(methyl methacrylate) (PMMA). The mass blending ratio of PLLA: PMMA at 50:50 could provide the broadest region of glass transitions temperature starting from 60 to 100 °C. Lee et al. [55] synthesized shape memory polyurethane (PU) block copolymers composed of 4,4-methylenebis-(phenylisocyanate), and poly(tetramethylene glycol) via a two-step process. The 1,4-butanediol was used as a chain extender. The obtained SMPs exhibited multiple-

Table 7 Glass transition temperature of BA-a/PU copolymers at various contents [94]

BA-a:PU mass ratio	T_g (°C)	T_g range (°C)	ΔT_g (°C)
55:45	130	120–220	100
60:40	135	100–214	114
70:30	157	90–180	90
80:20	180	80–180	100
100:0	170	130–190	60

shape memory effect. When the hard segment of PU was increased from 30 to 45%, the T_g and shape fixity were reported to be increased in the range of −3.6 to 0.3 °C and 89 to 92%, respectively. Moreover, the shape recovery of 80–95% was obtained. Erden and Jana [93] examined the properties of SMPs from polyurethane-polybenzoxazine copolymer synthesized form 4,4′-methylenebis phenyl isocyanate (MDI), polytetramethylene glycol (PTMG), and benzoxazine (BA-a) monomer. The 1,4-butanediol was applied as a chain extender. When MDI and PTMG were kept at 5 and 1 mol, respectively, it was reported that the hard segment of SMPs was increased with BA-a contents. A single peak of loss tangent from the dynamic mechanical analysis (DMA) revealed an increase in T_g (51, 65, and 91 °C) with increasing BA-a content (at 0, 0.5, and 1 mol, respectively).

From the work of Rimdusit et al. [94], not only the synergism of glass transition temperature was observed in the benzoxazine-urethane copolymers, the broad region of glass transition temperature was shown in the range of 90–110 °C at PU content of 0 to 40 wt%. This characteristic was important for the determination of the number of temporary shapes for the multiple-shape memory system. Recently, Prathumrat et al. [102] determined the feasibility of benzoxazine-urethane copolymers as multiple-shape memory polymers. The thermal stability of the copolymers was shown as Fig. 12. It could be noticed that the addition of BA-a content could lead to an increase in both degradation temperature at 5% weight loss (T_{d5}) and char yield at 800 °C of the alloys. For instance, the T_{d5} value and char yield of the alloy at BA-a/PU weight ratio of 55:45 were reported to be 268 °C and 16.2%, respectively. While those of the alloy at 80:20 were presented at 333 °C and 24.6%, respectively. They reported that the suitable curing conversion of the alloy mixture could affect the shape memory behaviors. From the testing result of the flexural strength and flexural modulus at various temperature of the alloys, the mechanical properties are increased with increasing BA-a content. The glass transition temperature range observed from loss tangent of DMA for pure polybenzoxazine and BA-a/PU copolymers are presented in Table 7. The broadest range of glass transition temperature was reported at suitable composition.

Recently, Zhuo et al. [103] prepared the novel multiple-SMPs from the copolymer of 2-methoxyethyl acrylate and N-methylol acrylamide with different molar fractions of acrylate component. The physical crosslinks generated by entanglement and hydrogen boding between the polymeric chains. With increasing acrylamide con-

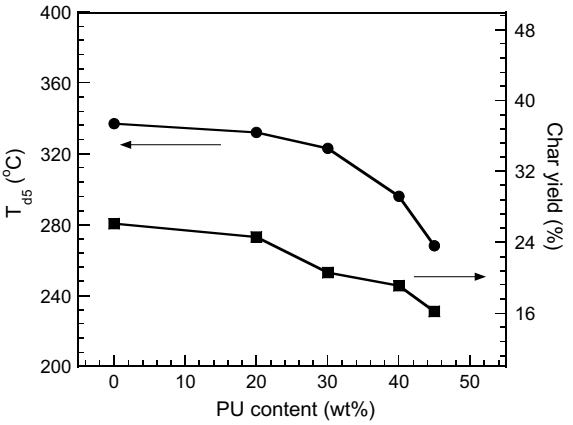

Fig. 12 Thermal degradation temperature at 5% weight loss (T_{d5}) and char yield at 800 °C of benzoxazine-urethane multiple-SMPs at various PU contents [102]

tent, the T_g values were increased in the range of 7.5–55.2 °C, and the tensile strength enhanced from 10.7 to 71.5 MPa. They also reported that the obtained multiple-SMPs presented superior multiple-shape memory effect in a broad range of temperature. The recovery ratio was reported at greater than 93%, and the fixing efficiencies was closed to 100%. The obtained multiple-SMPs could be a good candidate for the uses in potential deployable structure. At a recent time, Zheng et al. [104] prepared the multiple-SMPs by means of the multilayer between thermoplastic polyurethane (TPU) and co-continuous poly(bytylene succinate) (PBS)/polycaprolactone (PCL) blends. The shape fixity and recovery ratio of obtained dual- and triple-SMPs were increased with increasing the number of layers, and reported at 95% and 85%, respectively at the number of layers of 128. They also reported that the multilayer systems could have greater shape fixity and recovery ratio than those of the blending system at the same components.

2.2.6 Polyimide-Based SMP

Polyimide is a kind of engineering polymers possessing high thermal stability and mechanical properties. In the recent years, Xiao et al. [105] synthesized shape memory polymer based on polyimide with tunable glass transition temperature in the range of 299–322 °C. In their study, the thermoplastic polyimide-based SMPs were prepared by polycondensation reaction between 4,4′-(hexafluorisoproylidene) diphthalic anhydride (6FDA) and 4,4′-diaminodiphenyl ether (ODA). Other systems of the polyimide-based SMPS from bisphenol A dianhydride (BPADA) and 4,4′-diaminodiphenyl ether (ODA) were also prepared [106]. The ether bonds within the backbone were acted as recovery phase of shape memory effect, while the high molecular weight of polyimide could generate physical crosslinking as fixed phase. They also prepared the thermoset polyimide-based SMPs by using tris(4-aminophenyl)amine (TAP) cross-linker. From their report, the thermosetting

Table 8 Glass transition temperature and degradation temperature of SMPs based on ODA/6FDA polyimide and ODA/BPADA polyimide [105, 106]

ODA/6FDA Shape memory polyimide					
Molar ratio of ODA/6FDA		0.9250	0.9400	0.9625	0.9825
Thermoplastic ODA/6FDA	T_g (°C)	299	304	311	304
	T_{d5} (°C)	510	510	515	522
Thermoset ODA/6FDA	T_g (°C)	322	323	322	321
	T_{d5} (°C)	519	520	517	518
ODA/BPADA shape memory polyimide					
Molar ratio of ODA/BPADA		0.9100	0.9250	0.9550	0.9850
Thermoplastic ODA/BPADA	T_g (°C)	229	231	234	236
	T_{d5} (°C)	486	488	490	491
Thermoset ODA/BPADA	T_g (°C)	240	241	243	242
	T_{d5} (°C)	495	497	501	499

polyimide-based SMP rendered higher storage modulus and greater shape memory effect than the thermoplastic polyimide-based SMP because of its chemical crosslinking and high crosslink density. As shown in Table 8, the degradation temperatures at 5 wt% loss (T_{d5}) for all polyimide-based SMPs were over 500 °C. Comparatively, the glass transition temperature values of thermoset polyimide-based SMPs were over 320 °C, being higher than those of thermoplastic ones. Moreover, it was reported that the residual weights for both polyimide systems were over 50% due to the remained aromatic group. Another interesting polyimide-based SMPB system was prepared from 4,4′-(1,1'-biphenyl-4,4′-diyldioxy)-dianiline (BAPB)/bisphenol A dianhydride (BPADA) in dimehtylformide (DMF) by Kong and Xiao [107]. The researchers reported that the obtained polyimide could keep high shape fixity and shape recovery after over 1000 thermomechanical bending cycles. In an aspect of thermal stability, the degradation temperature at 5 wt% loss was reported at 505 °C, and the temperature at maximum weight loss was found at ca. 536 °C. That confirmed that the obtained polyimide-based SMPB possessed greater thermal stability.

3 Shape Memory Polymer Composites and Their Thermal Characteristics

3.1 A Brief Overview of SMPCs

As previously mentioned, shape memory polymers generally had some shortcomings on their low recovery stress and low mechanical performance. These drawbacks are able to limit the applications of smart materials. The addition of reinforcing fillers in

the polymeric matrix to form shape memory polymer composite (SMPC) is able to enhance recovery stress and mechanical characteristics [74]. Currently, SMPCs have been developed to gain potentials for a broad range of usage areas such as deployable components in aerospace, smart textiles, automobiles, actuators, and medical devices [2]. Moreover, many patents related to the uses of SMPCs (such as intravascular delivery system, hood/seat assembly, and tunable automotive brackets in vehicles) have been issued [108, 109]. Generally, two main types of SMPC can be categorized as particle-filled SMPC and fiber-filled SMPC [2].

3.1.1 Particle-Filled SMPCs

The particle-filled SMPC are developed with many types of reinforcing elements in forms of particulate matter, such as carbon black, carbon nanotubes, carbon nanofibers, silicon carbide, nickel powder, ferromagnetic (Fe_3O_4), and clay in order to meet various requirements for practical applications [30, 110–112]. The particle-filled SMPCs typically are developed for certain specific functions, e.g., great electrically conductive characteristic, magneto-responsive properties, etc. Therefore, the smart materials with multifunctional properties have been developed with particle-filled SMPCs [2]. Generally, this type of SMPCs is not applied for structural materials, but it is for some specific characteristics. The examples of the particle fillers possessing particular functions for SMPCs are electrically conductive carbon black, carbon nanotubes, and nickel powders, which are incorporated for fabricating electroactive SMPs. While Fe_3O_4 filler is added to generate magnetism induced SMPs [2]. Additionally, silicon carbide (SiC) with dielectric properties is composited with SMPs to develop microwave-induced SMPs [113].

3.1.2 Fiber-Filled SMPCs

As mentioned above, SMPCs embedded with particles or short fibers are not suitable for using as structural materials. On the other hand, significant improvement in stiffness, strength, and resistance against relaxation and creep can be obtained in the SMPCs reinforced with continuous fiber. The fiber-filled SMPCs have high potential for many advanced applications such as the use in deployable structures including antennas and solar arrays [2].

3.2 Epoxy-Based SMPCs

Epoxy resin is thermoset polymers used in many industrial fields, e.g., adhesive, coating, and sealant due to its high adhesive properties, good thermal and mechanical properties [114]. The recent researches had focused on the properties modification of SMP. Nowadays, shape memory epoxies have gained much attention from industrial

researches. This kind of SMP provides higher properties than other shape memory polymers (such as polyurethane, and styrene rubber systems) due to great thermal, thermo-physical and mechanical characteristics with its easiness for fabrication. For instance, the systems of SMP based on aromatic epoxy, aliphatic epoxy and curing agent (Jeffamine D230) have been reported to exhibit good shape fixity and, the complete shape recovery [115]. Although many types of epoxy resins have been known, diglycidyl ether of bisphenol A (DGEBA) is the most common type for fabrication of SMPs [116].The systems of thermoset epoxy filled with functional filler have been studied for a long period of time. Gall et al. [117] successfully prepared the epoxy-based SMPs nanocomposites filled with silicon carbide nano-filler. They reported that the increase in SiC content led to the improvement of elastic modulus and bending recovery force in the composites. In the later year, Athimoolam and Moorthy [116] successfully prepared the SMPCs from epoxy blended with polyurethane filled with amine treated nanoclay. They reported that the thermal stability of the composite was improved with the addition of nanoclay filler. Recently, Liu et al. [118] prepared a series of SMPC based on polymeric mixture between DGEBA and metylhexahydrophthalic anhydride (MHHPA) filled with multi-walled carbon nanotube (MWCNT). The molar ratios of DGEBA/MHHPA were varied from 0.5 to 1.2, while the MWCNT nano-filler contents were in the range of 0.25 to 0.75 wt%, respectively. The T_g values of the obtained nanocomposite SMPCs were in the broad range from approximately 65 to 140 °C. From the thermogravimetric analysis, the starting degradation temperature (at approximately 2 wt% loss) of the blends at the DGEBA/MHHPA ratio of 0.5 (ca. 243 °C), which was less than that of the blends at the ratio of 1.0 (ca. 335 °C). This could be due to the amount of uncured epoxy providing less thermal stability. The temperature at the high decomposition rate for all studied samples was found at ca. 412 °C. Furthermore, the increase of nano-filler content in the studied range could lead to a slight improvement in decomposition temperature [118]. Later, Chen et al. [119] prepared the nanocomposites of shape memory polymer based on epoxy filled with thermally reduced graphite oxide (TGO). They reported that added TGO nano-filler could provide the 41–71% enhancement of the modulus and 44–64% improvement of tensile strength with 1–3 wt% TGO. The thermal stability of the obtained SMPCs was significantly improved when applying 1–2 wt% of TGO. This could be due to barrier effects of TGO filler [120]. The nano-filler, which possesses high surface area, could act as a barrier to prevent the displacement of broken polymeric chains, and impede the diffusion of volatile products and generate the char [121]. However, the amount of 3wt% TGO could lower the thermal stability of the SMPCs. The possible reasons could be due to the partial aggregation of the nano-filler. Furthermore, the high loading of TGO filler could provide higher thermal conductivity than polymeric matrix. That could support the thermal degradation of the SMPCs [122]. In the recent year, the electroactive shape memory polymers composites from epoxy/cyanate ester nanocomposites filled with graphene were prepared by Wang et al. [123]. The graphene was dispersed in N,N- dimethylformamide and then the mixture was fed into the polymeric mixture to fabricate the SMPC. They reported that the incorporation of graphene could lead to the enhancement of the shape memory behavior. In addition, the degradation tem-

perature of the nanocomposite-based SMP was improved with the nano-filler. The reason for the improvement of thermal stability was related to the tortuous path effect of the nano-filler, which could be able to form the char and impede the diffusion of volatile degradation products [123, 124].

Not long ago, Biju and Nair [125] fabricated the SMPCs from the reaction between DGEBA epoxy and pyromellitic dianhydride (PMDA). Carboxyl telechelic poly(tetramethylene oxide) (PTAC) was used as the polymer precursor. They reported that the SMPCs for all composition was stable at least 300 °C. In the later year, the polycaprolactone (PCL)/epoxy-based SMPC microfiber has been developed by Zhang et al. [126]. In this system, the core layer of epoxy and the shell layer of PCL were fabricated via coaxial electrospinning. They reported that the entire shape memory was recovered by only approximately 6 s at 70 °C. From the TGA analysis, two decomposition steps were observed, i.e., at the range of 300–350 °C exhibiting the decomposition range of epoxy, and the range of 350–450 °C relating to the PCL degradation range.

3.2.1 Benzoxazine-Epoxy Alloy-Based SMPCs

As previously mentioned, Tanpitaksit et al. [70] developed SMPs from the alloys between BA-a and aliphatic epoxy (neopentyl glycol diglycidyl ether, NGDE). In the system, BA-a was acted as a latent curing agent for epoxy resin. The rendered SMPs provided high thermo-mechanical characteristic and great shape memory properties. Recently, Likitaporn et al. [124] studied the characteristics of slicon-carbide whisker (SiC_w)-filled in benzoxazine-epoxy SMPC. The reported that the T_g value from loss tangent was increased with SiC_w contents, i.e., 154 °C (at 0 wt%) to 170 °C (at 20 wt%). Moreover, at $T_g + 20$ °C and room temperature, the increase in SiC_w contents could lead to an increase of flexural strength and flexural modulus. In addition, the degradation temperature at 5 wt% loss (T_{d5}) and char yield of the SMPC from benzoxazine-epoxy alloys were increased with increasing SiC_w content as shown in Fig. 13. The degradation temperature at 5 wt% (T_{d5}) was systematically increased from 293 to 303 °C when SiC_w filler was increased from 0 to 20 wt%. This is attributed to the physical barrier effect of SiC_w, which could prevent the thermal transmission, and reduce the escaping rate of pyrolysis products. Moreover, it could impede the further degradation of the polymeric matrix [42]. For the amount of char residue at 800 °C, the value was found to increase with increasing SiC_w contents, i.e., ranging from 28.1 to 43.0% when the filler content varying from 0 to 20wt%. This phenomenon well corresponded to the rule of mixture. Interestingly, in this system, the increase of SiC_w contents led to shorten the recovery time, i.e., the recovery time when microwave-induction and conventional heating induction were in the range of approximately 3.5 to 5 min and ca. 8.5 to 18 min, respectively. Moreover, the addition of SiC_w could drastically enhance the recovery stress from 3.4 MPa (for neat benzoxazine/epoxy alloy) to 11.2 MPa (at 20 wt% SiC_w). That was attributed to the intrinsically great elastic modulus of the filler. In addition, the outstanding shape fixity of approximately 99% was reported in the system.

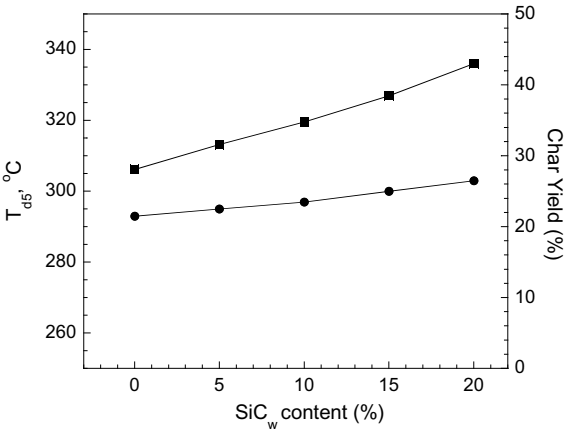

Fig. 13 TGA results of SMPCs at various filler contents: (●) Degradation temperature at 5% weight loss, and (■) Char Yield [124]

Table 9 Thermal stability of the BA-a/epoxy alloys reinforced with woven carbon fiber at various filler contents [127]

Woven carbon fiber content (vol.%)	Degradation temperature at 5 wt% loss (°C)	Char Yield at 800 °C (%)
0	306	24.6
23	289	45.6
47	314	63.5
57	323	73.7
100	850	95.4

In recent times, benzoxazine-epoxy alloys filled with carbon fiber has been prepared by Plylaharn et al. [127]. They revealed that the BA-a/epoxy systems could be reinforced with woven carbon fiber. The shape recovery was reported to be close to 100%. In their work, the recovery stress of the SMPCs has been enhanced from 3.4 MPa (without reinforcing fiber) to 28.9 MPa (at the filler content of 47 vol.%). The thermogravimetric analysis of the SMPCs was presented in Table 9. It could be noticed that the values of T_{d5} and char yield were increased with the woven carbon fiber content. This could be due to the thermal properties of carbon fiber.

3.2.2 Polyurethane-Based SMPCs

Polyurethane (PU) is one of the polymeric materials commonly used for fabrication of SMPCs because of its high strain recovery and good physical properties. Moreover, its versatility can be extended through compositing with other functional fillers. In recent time, Deka et al. [128] prepared hyperbranched polyurethane (HPU) reinforced with multi-walled carbon nanotube (MWCNT). The tensile strength of the SMPC was 300% higher than that of neat HPU. The notable improvement of thermal

Table 10 Decomposition temperature of TPU/ABS/MWCNT composites at various compositions [130]

TPU (wt%)	ABS (wt%)	MWCNT (wt%)	T_d max (°C)	T_d offset (°C)	Char Yield (%)
80	20	0	407	515	4.5
79	20	1	412	544	6.5
77	20	3	413	555	7.4
75	20	5	410	573	10.0

stability, i.e., onset T_d of 275 °C for 1 wt% of MWCNT higher than that of 215 °C for neat HPU. They reported that one degradation step was observed for all SMPC samples, exhibiting great interactions between nano-filler and HPU matrix. Later, Mahapatra et al. [129] prepared SMPCs from functionalized HPU reinforced with graphene oxide (GO) sheet. The GO sheet was functionalized by adding aliphatic hydroxyl groups on its surface. In general, the reduction of GO could lead to high thermal stability because of the elimination of the oxygen-containing functional groups. The addition of GO into the HPU matrix led to the increase of initial decomposition temperature. The given reason for the enhancement of thermal stability is the barrier effect that could prevent the permeation of oxygen and the emission of volatile decomposition products. Moreover, the surface of nano-filler could serve as a radical remover, leading to the delay of onset T_d. In the recent year, Memarian et al. [130] SMPCs derived from thermoplastic polyurethane (TPU) compositing with acrylonitrile-butadiene-styrene (ABS) and MWCNT by melt blending process. The addition of MWCNT into SMPCs could increase the tensile strength and modulus but decrease the elongation at break. The TGA analysis revealed the thermal stability as shown in Table 10. It could be noticed that the improvement of the thermal decomposition temperature was observed because of great thermal stability and high thermal conductivity of MWCNT.

4 Conclusions

The thermal stability is one of the crucial parameters that can indicate the limitation for the usage of the shape memory materials (i.e., SMPs, SMPBs, and SMPCs). In general, the thermal stability could be identified in terms of thermal degradation temperatures, and char yield. For SMP and SMPB system, the chemical structures of the materials have an effect on the thermal stability, i.e., the aromatic structures and/or the network structure could provide high thermal degradation and char yield to the materials. The degradation process is composed of many steps such as initiation, propagation, and termination steps. For SMPC systems, the thermal stability does not depend on the individual thermal stability of each component. Some of the phenomena are relevant, e.g., the barrier effect to prevent the oxygen emission, and the

char formation. This chapter provides the information related to the thermal stability of high-temperature shape memory materials, i.e., shape memory materials based on polybenzoxazine, epoxy, polyurethane, and polyimide. Polybenzoxazine is an interesting novel thermosetting resin that could be alloyed with other polymeric such as epoxy and urethane. Its alloy systems provide high degradation temperature and char yield. For example, the SMPS based on V-fa/ECO copolymer, the degradation was over ca. 300 °C with high char yield over 30%. Furthermore, the synergistic behaviors of T_g for the systems of benzoxazine/epoxy alloys and benzoxazine/urethane alloys were reported. The SMPs based on polyimide are generally fabricated in forms of films. It could provide a high decomposition temperature over 400 °C and char yield over 50%.

References

1. Wei ZG, Sandstorm R, Miyazaki S (1998) Review Shape-memory materials and hybrid composites for smart systems: Part I Shape-memory materials. J Mater Sci 33:3743–3763
2. Leng JS, Lan X, Du S (2011) Shape-memory polymers and their composites: Stimulus method and applications. Prog Polym Sci 56:10771135
3. Chatterjee T, Dey P, Nando GB, Naskar K (2015) Thermo-responsive shape memory polymer blends based on alpha olefin and ethylene propylene diene rubber. Polymer 78:180–192
4. Zheng N, Fang G, Cao Z, Zhao Q, Xie T (2015) High strain epoxy shape memory polymer. Polym Chem 6:3046–3053
5. Lendlein A, Jiang H, Junger O, Langer R (2005) Light-induced shape-memory polymers. Nature 434:879–882
6. Chen S, Yang S, Li Z, Xu S, Yuan H, Chen S, Ge Z (2015) Electroactive two-way shape memory polymer laminates. Polym Compos 36:439–444
7. Xiao R, Guo J, Safranski DL, Nguyen TD (2015) Solvent-driven temperature memory and multiple shape memory effects. Soft Matter 11:3977–3985
8. Xu B, Li Y, Gao F, Zhai X, Sun M, Lu W, Cao Z, Liu W (2015) High strength multifunctional multiwalled hydrogel tubes: Ion-triggered shape memory, antibacterial, and anti-inflammatory efficacies. ACS Appl Mater Interfaces 7:16865–16872
9. Buckley PR, McKinley GH, Wilson TS, Small W IV, Benett WJ, Bearinger J, McElfresh MW, Maitland DJ (2006) Inductively heated shape memory polymer for the magnetic actuation of medical device. IEEE Trans Biomed Eng 53:2075–2083
10. Guo W, Lu CH, Orbach R, Wang F, Qi XJ, Cecconello A, Seliktar D, Willner I (2015) pH-Stimulated DNA hydrogels exhibiting shape-memory properties. Adv Mater 27:73–78
11. Koeme H, Price G, Pearce N, Alexander M, Vaia RA (2004) Remotely actuated polymer nanocomposites—stress-recovery of carbon-nanotube-filled thermoplastic elastomers. Nat Mater 3:115–120
12. Leng JS, Lv HB, Lui YJ, Du SY (2007) Electroactivate shape-memory polymer filled with nanocarbon particles and short carbon filler. Appl Phys Lett 91: art. no. 114105
13. Lu H, Liu Y, Leng JS, Du S (2009) Qualitative separation of the effect of the solubility parameter on the recovery behavior of shape-memory polymer. Smart Mater Struct 18: art. no. 085003
14. Mohr R, Kratz K, Weigel T, Lucka-Gabor M, Moneke M, Lendlein A (2006) Initiation of shape memory effect by inductive heating of magnetic nanoparticles in thermoplastic polymers. Proc Natl Acad Sci 103:3540–3545
15. Maitlan DJ, Metzger MF, Schumann D, Lee A, Wilson TS (2003) Photothermal properties of shape memory polymer micro-actuators for treating stroke. Laser Surg Med 30:1–11

16. Ansari M, Golzar M, Baghani M, Soleimani M (2018) Shape memory characterization of poly(ε-caprolactone) (PCL)/polyurethane (PU) in combined torsion-tension loading with potential applications in cardiovascular stent. Polym Test 68:424–432
17. Hu J, Zhu Y, Huang H, Lu J (2012) Recent advances in shape memory polymers: structure, mechanism functionality, modeling and applications. Prog Polym Sci 37:1720–1763
18. Kumar B, Hu J, Pan N, Narayan H (2016) A smart orthopedic compression device based on a polymeric stress memory actuator. Mater Des 97:222–229
19. Zhao Q, Qi HJ, Xie T (2015) Recent progress in shape memory polymer: new behavior, enabling materials, and mechanistic understanding. Prog Polym Sci 49–50:79–120
20. Hu J, Chen W, Fan P, Gao J, Fang G, Cao Z, Peng F (2017) Uniaxial tensile tests and dynamic mechanical analysis of satin weave reinforced epoxy shape memory polymer composite. Polym Test 62:335–341
21. Dhulst EA, Heath WH, Torkelson JM (2016) Hybrid thiol-acrylate-epoxy polymer networks: comparison of one-pot synthesis with sequential reactions and shape memory properties. Polymer 96:198–204
22. Li Q, Zhou J, Vatankhah-Varnoosfaderani M, Nykypanchuk D, Gang O, Sheiko SS (2016) Advancing reversible shape memory by tuning the polymer network architecture. Macromolecules 49:1383–1391
23. Wei ZG, Sandstrom R, Miyazaki S (1998) Shape memory materials and hybrid composites for smart systems: part II shape-memory hybrid composites. J Mater Sci 33:3763–3783
24. Rousseau IA (2008) Challenges of shape memory polymers: a review of the progress toward overcoming SMP's limitations. Polym Eng Sci 48:2075–2089
25. Tiptipakorn S, Rimdusit S (2017) Shape memory polymers from polybenzoxazine-modified polymers. Advanced and emerging polybenzoxazine science and technology. In: Ishida H, Froimowicz P (ed), Elsevier, Cambridge, pp 1029–1049
26. Ehrenstein GW (2001) Polymeric materials-structure, properties, applications. Hanser Gardner Publications, Cincinnati, USA
27. Lake MS, Campbell D (2004) The fundamentals of designing deployable structures with elastic memory composites. IEEE aerospace conference proceeding. Compos Tech Develop, 6–13 March 2004, 2745–2756, MT, USA
28. Cao F, Jana S (2007) Nanoclay-tethered shape memory polyurethane nanocomposites. Polymer 48:3790–3800
29. Xu J, Shi W, Pang W (2006) Synthesis and shape memory effects of Si-O-Si cross-linked hybrid polyurethanes. Polymer 47:457–465
30. Ohki T, Ni QQ, Ohsako N, Iwamoto M (2004) Mechanical and shape memory behavior of composites with shape memory polymer. Compos A 35:1065–1073
31. Jeong HM, Kim BK, Choi YJ (2000) Synthesis and properties of thermotropic liquid crystalline polyurethane elastomers. Polymer 41:1849–1855
32. Liu Y, Gall K, Dunn ML, McCluskey P (2004) Thermomechanics of shape memory polymer nanocomposites. Mech Mater 36:929–940
33. Gall K, Dunn ML, Liu Y, Stefanie G, Balzar D (2004) Internal stress storage in shape memory polymer nanocomposites. Appl Phys Lett 85:290–292
34. Li F, Qi L, Yang J, Xu M, Luo X, Ma D (2000) Polyurethane/conducting carbon black composites: structure, electric conductivity, strain recovery behavior, and their relationships. J Appl Polym Sci 75:68–77
35. Zhang CS, Ni QQ (2007) Bending behavior of shape memory polymer based laminates. Compos Struct 78:153–161
36. Liu C, Mather PT (2005) A. shape memory polymer with improved shape recovery. Mater Res Soc Symp Proc 855E, W4.7.1
37. Razzaq MY, Frrormann L (2007) Thermomechanical studies of aluminum nitride filled shape memory polymer composites. Polym Compos 28:287–293
38. Guo J, Wang Z, Tong L, Lv H, Liang W (2015) Shape memory and thermos-mechanical properties of shape memory polymers/carbon fiber composites. Compos A 76:162–171

39. Meng Q, Hu J (2009) A review of shape memory polymer composites and blends. Compos Part A 1661–1672
40. Mu T, Liu L, Lan X, Liu Y, Leng J (2018) Shape memory polymers for composites. Compos Sci Tech 160:169–198
41. Wang W, Liu Y, Leng J (2016) Recent developments in shape memory polymer nanocomposites: actuation methods and mechanisms. Coord Chem Rev 320–321:38–52
42. Ray S, Cooney RP (2012) Chapter 7 thermal degradation of polymer and polymer composite. In: Kutz M Handbook of environmental degradation of materials, Waltham, USA, pp 212–242
43. Peterson JD, Vyazovkin S, Wight CA (2001) Kinetics of the thermal and thermos-oxidative degradation of polystyrene, polyethelene and poly(propylene). Macromol Chem Phys 202:775–784
44. Hamid SH, Amin MB (1992) Handbook off polymer degradation. Marcel Dekker, New York
45. Tiptipakorn S, Damrongsakkul S, Ando S, Hemvichian K, Rimdusit S (2007) Thermal degradation behaviors of polybenzoxazine and silicon-containing polyimide blends. Polym Degrad Stab 92:1265–1278
46. Shi S, Shen D, Xu T (2017) Programming effects on thermal decomposition of shape memory polymer-based composites. J Therm Anal Calorim 130:1953–1960
47. Rousseau IA, Xie T (2010) Shape memory epoxy: Composition, structure, properties and shape memory performances. J Mater Chem 20:3431–3441
48. Hu JL (2014) Shape memory polymers: fundamentals, advances and applications. Shawbury, Shrewsbury, Shropshire, SY4 4NR, United Kingdom: Smithers Rapra, pp 89–115
49. Liu G, Guan H, Xia H, Guo F, Ding X, Peng Y (2006) Novel shape-memory polymer based on hydrogen bonding. Macromol Rapid Commun 27:1100–1104
50. Chun BC, Cha SH, Park C, Chung YC, Park MC, Chao JW (2003) Dynamic mechanical properties of sandwich-structured epoxy beam composites containing poly(ethyleneterephthalate)/poly(ethyleneglycol) copolymer with shape memory effect. J Appl Polym Sci 90:3141–3149
51. Lendlein A, Schmidt AM, Langer R (2001) AB-polymer networks based on oligo(ε-caprolactone) segments showing shape-memory properties. Proc Natl Acad Sci USA 98: 842–847
52. Chowdhury SRM, Mishra JK, Das CK (2001) Study of heat shrinkability and flame retardancy of Poly(ethylene vinyl acetate)/Epichlorohydrin blends. Macromol Mater Eng 286:243–247
53. Jeong HM, Lee SH, Cho KJ, Jeong YT, Kang KK, Oh JK (2002) Thermal and mechanical properties of the polymers synthesized by the sequential polymerization of propylene and 1-hexadecene. J Appl Polym Sci 84:1709–1715
54. Mather PT, Kim BS, Ge Q, Liu C (2004) Synthesis of Nonioinic Telechelic Polymers Incorporating Polyhedral Oligo-silesquioxane and Uses Thereof. US Patent 2,004,024,098
55. Lee BS, Chun BC, Chung YC, Sul KI, Cho JW (2001) Structure and thermomechanical properties of polyurethane block copolymers with shape memory effect. Macromolecules 34:6431–6437
56. Ping P, Wang H, Chen X, Jing X (2005) Poly(α-caprolactone) polyurethane and its shape-memory property. Biomacromolecules 6:587–592
57. Hu J (2007) Characterization of shape memory properties in polymers, in shape memory polymers and textiles. Wood head Publishing Limited: England, pp 197–217
58. Li J, Rodgers WR, Xie T (2011) Semi-crystalline two-way shape memory elastomer. Polymer 52:5320–5325
59. Xie T, Xiao X, Cheng YT (2009) Revealing triple-shape memory effect by polymer bilayers. Macromo Rapid Commun 30:1823–1827
60. Kumar KS, Biju R, Nair Reghunadhan (2013) Progress in shape memory epoxy resins. React Funct Polym 73:421–430
61. Liu Y, Li Y, Zhang C, Wang R, Run M, Song H (2016) Shape memory polybenzoxazine based on a siloxane-containing diphenol. J Polym Sci, Part B Polym Phys 54:1255–1266
62. Liu Y, Huang J, Su X, Han M, Li H, Run M, Song H, Wu Y (2016) Shape memory Polybenzoxazine based on polyetheramine. React Funct Polym 102:62–69

63. Jubsilp C, Punson K, Takeichi T, Rimdusit S (2010) Curing kinetics of benzoxazine-epoxy copolymer investigated by non-isothermal differential scanning calorimetry. Polym Degrad Stab 95:918–924
64. Ning X, Ishida H (1994) Phenolic materials via ring-opening polymerization: Synthesis and characterization of bisphenol-A based benzoxazines and their polymers. J Polym Sci Part A 32:1121–1129
65. Rimdusit S, Kunopast P, Dueramae I (2011) Thermomechanical properties of arylamine-based benzoxazine resins alloyed with epoxy resin. Polym Eng Sci 51:1797–1807
66. Lee SM (1991) International encyclopedia of composites. VCH Publishers, New York
67. Rimdusit S, Ishida H (2000) Synergism and multiple mechanical relaxations observed in ternary systems based on benzoxazine, epoxy, and phenolic resins. J Polym Sci Part B 38:1687–1698
68. Ishida H, Allen DJ (1996) Mechanical characterization of copolymers based on benzoxazine and epoxy. Polymer 37:4487–4495
69. Rimdusit S, Lohwerathama M, Hemvichian K, Kasemsiri P, Dueramae I (2013) Shape memory polymers from benzoxazine-modified epoxy. Smart Mater Struct 22: art no. 075033
70. Tanpitaksit T, Jubsilp C, Rimdusit (2015) Effects of benzoxazine resin on property enhancement of shape memory epoxy: a dual function of benzoxazine resin as a curing agent and a stable network segment. eXPRESS Polym Lett 9:824–837
71. Dunkers J, Ishida H (1999) Reaction of benzoxazine-based phenolic resins with strong and weak carboxylic acids and phenols as catalysts. J Polym Sci Part A 37:1913–1921
72. Jubsilp C, Punson K, Takeichi T, Rimdusit S (2010) Curing kinetics of Benzoxazine–epoxy copolymer investigated by non-isothermal differential scanning calorimetry. Polym Degrad Stabil 95:918–924
73. Kimura H, Matsumoto A, Hasegawa K, Ohtsuka K, Fukuda A (1998) Epoxy resin cured by bisphenol A based benzoxazine. J Appl Polym Sci 68:1903–1910
74. Jubsilp C, Takeichi T, Hiziroglu S, Rimdusit S (2008) High performance wood composites based on benzoxazine-epoxy alloys. Bioresour Technol 99:8880–8886
75. Nielsen LE, Landel RF (1994) Mechanical properties of polymers and composites, 2nd edn. Marcel Dekker Inc., New York
76. Rimdusit S, Pirstpindvong S, Tanthapanichakoon W, Damrongsakkul S (2005) Toughening of polybenzoxazine by alloying with urethane prepolymer and flexible epoxy: A comparative study. Polym Eng Sci 45:288–296
77. Meng H, Li G (2013) A review of stimuli-responsive shape memory polymer composites. Polymer 54:2199–2221
78. Liu Y, Han C, Tan H, Du X (2010) Thermal, mechanical and shape memory properties of shape memory epoxy resin. Mater Sci Eng A 527:2510–2514
79. Wu X, Zheng H, Liu Y (2010) Thermomechanical property of epoxy shape memory polymers. Int J Mod Phys B 24:2386–2391
80. Lu L, Fan J, Li G (2016) Intrinsic healable and recyclable thermoset epoxy based on shape memory effect and transesterification reaction. Polymer 105:10–18
81. Kuang X, Liu G, Dong X, Wang D (2016) Triple-shape memory epoxy based on Diels-Alder adduct molecular switch. Polymer 84:1–9
82. Jin FL, Li X, Park SJ (2015) Synthesis and application of epoxy resins: a review. J Ind Eng Chem 29:1–11
83. Wei J, Ma S, Yue H, Wang S, Zhu J (2018) Comparison of hydrogenated bisphenol A and bisphenol A epoxies: curing behavior, thermal and mechanical properties, shape memory properties. Macromol Res. https://doi.org/10.1007/s13233-018-6075-3
84. Parameswaranpillai J, Ramanan SP, Seno J, Siengchin S, Magueresse A, Janke A, Pionteck J (2017) Shape memory properties of Epoxy/PPO–PEO–PPO Triblock copolymer blends with tunable thermal transitions and mechanical characteristics, industrial and engineering chemistry research. Am Chem Soc 56:14069–14077
85. Li S, an S (2015) Synthesis and characterization of novel biobased benzoxazines from cardbisphenol and the properties of their polymers. RSC Adv 5:61808–61814

86. Lochab B, Varma IK, Bijwe J (2010) Thermal behaviour of cardanol-based benzoxazines. J Therm Anal Calorim 102:769–774
87. Sini NK, Bijwe J, Varma IK (2014) Renewable benzoxazine monomer from Vanillin: Synthesis, characterization, and studies on curing behavior. J Polym Sci Part A 52:7–11
88. Van A, Chiou K, Ishida H (2014) Use of renewable resource vanillin for the preparation of benzoxazine resin and reactive monomeric surfactant containing oxazine ring. Polymer 55:1443–1451
89. Thirukumaran P, Shakila Parveen A, Sarojadevi M (2014) Synthesis and copolymerization of fully biobased benzoxazines from renewable resources. ACS Sust Chem Eng 2:2790–2801
90. Hombunma P, Okhawilai M, Rimdusit S (2018) Characterization of novel shape memory polymer from Green-Polybenzoxazine/Epoxy alloy. In: Proceedings in the 2018 pure and applied chemistry international conference (PACCON2018), Songklanakarin, Thailand
91. Tobushi H, Hayashi S, Hoshio K, Makino Y, Miwa N (2006) Bending actuation characteristics of shape memory composite with SMA and SMP. J Intell Mater Syst Struct 17:1075–1081
92. Rimdusit S, Hombunma P (2018) Shape memory polymer from Vaniline based Polybenzoxazine/castor oil-based epoxy copolymer. In: Proceeding in ICCE, 26 July 15–21 2018, France
93. Erden N, Jana SC (2013) Synthesis and characterization of shape-memory polyurethane-polybenzoxazine compounds. Macro Chem Phys 214:1225–1237
94. Rimdusit S, Bangsen W, Kasemsiri P (2011) Chemorheology and thermomechanical characteristics of benzoxazine-urethane copolymers. J Appl Polym Sci 1321:3669–3678
95. Rimdusit S, Mongkhonsi T, Kamonchaivanich P, Sujirot K, Tiptipakorn S (2008) Effects of polyol molecular weight on properties of benzoxazine-urethane polymer alloys. Polym Eng Sci 48:2238–2246
96. Oprea S, Potolinca VO, Varganici CD (2016) Synthesis and properties of polyurethane urea with pyridine-2,6-dicarboxamide moieties in their structure. RSC Adv 6:106904–106913
97. Weng NC, Wu CF, Tsen WC, Wu CL, Suen MC (2018) Synthesis and properties of shape memory polyurethanes generated from schiff-base chain extender containing benzoyl and pyridyl rings. Design Monom Polym 21:55–63
98. Hager MD, Bode S, Weber C, Schubert US (2015) Shape memory polymers: past, present and future developments. Prog Polym Sci 49–50:3–33
99. Xie T (2010) Tunable polymer multi-shape memory effect. Nature 464:267–270
100. Hoeher R, Raidt T, Krumm C, Meuris M, Katzenberg F, Tiller JC (2013) Tunable multiple-shape memory polyethylene blends. Macro Chem Physics 214:2725–2732
101. Samuel C, Barrau S, Lefebvre JM, Raquez JM, Dubois P (2014) Designing multiple-shape memory polymers with miscible polymer blends: Evidence and origins of a triple-shape memory effect for miscible PLLA/PMMA blends. Macromolecules 47:6791–6803
102. Prathumrat P, Tiptipakorn S, Rimdusit S (2017) Multiple-shape memory polymers from benzoxazine-urethane copolymer. Smart Mater Struct 26: art no. 065025
103. Zhuo S, Zhang G, Feng X, Jiang H, Shi J, Liu H, Li H (2016) Multiple shape memory polymers for self-deployable device. RSC Adv 6:50581–50586
104. Zheng Y, Ji X, Yin M, Shen J, Guo S (2017) Strategy for fabricating multiple-shape memory polymeric materials via the multilayer assembly of co-continuous blends. ACS Appl Mater Interfaces 9:32270–32279
105. Xiao X, Kong D, Qiu X, Zhang W, Zhang F, Liu L, Liu Y, Zhang S, Hu Y, Leng J (2015) Shape-memory polymers with adjustable high glass transition temperature. Macromolecules 48:3582–3589
106. Xiao X, Kong D, Qiu X, Zhang W, Liu Y, Zhang S, Zhang F, Hu Y, Leng J (2015) Shape memory polymers with high and low temperature resistant properties. Sci Rep, 5: art no. 14137
107. Kong D, Xiao X (2016) High Cycle-file Shape Memory Polymer at High Temperature, Sci Rep 6: art no. 33610
108. Browne AL, Johnson NL (2007) Shape memory polymer seat assemblies. GM Global Technology Operations: US

109. Browne AL, Johnson NL (2005) Airflow control devices based on active materials. Genaral Motors Corporation: US
110. Fejos M, Romhány G, Karger-Kocsis J (2013) Shape memory characteristics of woven glass fibre fabric reinforced epoxy composite in flexure. J Reinf Plas Compos 31:1532–1537
111. Ni QQ, Zhang CS, Fu Y, Dai G, Kimura T (2007) Shape memory effect and mechanical properties of carbon nanotube/shape memory polymer nanocomposites. Compos Struct 81:176–184
112. Lu HB, Yu K, Sun SH, Liu YJ, Leng JS (2010) Mechanical and shape-memory behavior of shape-memory polymer composites with hybrid fillers. Polym Int 59:766–771
113. Du H, Song Z, Wang J, Liang Z, Shen Y, You F (2015) Microwave-induced shape-memory effect of silicon carbide/poly(vinyl alcohol) composite. Sens Actuat A 228:1–8
114. Lan X, Liu Y, Lv H, Wang X, Leng J, Du S (2009) Fiber reinforced shape-memory polymer composite and its application in a deployable hinge. Smart Mat Struct 18: art no. 024002
115. Kumar KSS, Biju R, Nair CPR (2013) Progress in shape memory epoxy resin. React Funct Polym 73:421–430
116. Athimoolam M, Moorthy TV (2015) Tensile behaviour and characterization of amine treated nanoclay reinforced epoxy/ polyurethane blends and composites for shape memory applications. Ind J Eng Mater Sci 22:435–442
117. Gall K, Dunn ML, Liu Y, Finch D, Lake M, Munshi NA (2002) Shape memory polymer nanocomposites. Acta Mater 50:5115–5126
118. Liu Y, Zhao J, Zhao L, Li W, Zhang H, Yu X, Zhang Z (2016) High performance shape memory epoxy/carbon nanotube nanocomposites. ACS Appl Mater Interfaces 8:311–320
119. Chen L, Li W, Liu Y, Leng J (2016) Nanocomposites of epoxy-based shape memory polymer and thermally reduced graphite oxide: mechanical, thermal and shape memory characterizatuions. Compos B 91:75–82
120. Jeon CW, An JE, Jeong YG (2012) High Performance cellulose acetate propionate composites reinfoced with exfolliated graphene. Compos B 43:3412–3418
121. Zhoa YH, Zhang YF, Wu ZK, Bai SL (2016) Synergic enhancement of thermal properties of polymer composites by graphene foam and carbon black. Compos B 84:52–58
122. Lee YR, Raghu AV, Jeong HM, Kim BK (2009) Properties of waterborne polyurthan/functionalized graphene sheet/nanocomposites prepared by an in situ method. Macromol Chem Phys 210:1247–1254
123. Wang Y, Ma T, Tian W, Ye J, Wang X, Jiang X (2018) Electroactive shape memory properites of graphene/epoxy-cyanate ester nanocomposites. Pig Resin Techno 47:72–78
124. Likitaporn C, Mora P, Tiptiptkorn S, Rimdusit S (2018) Recovery stress enhancement in shape memory composites from silicon carbide whisker-filled benzoxazine epoxy polymer alloy. J Intell Mater Sys Struct 29:388–396
125. Biju R, Reghunadhan Nair CP (2013) Synthesis and characterization of shape memory epoxy-anhydride system. J Polym Res 20:82
126. Zhang F, Zhang Z, Liu Y, Cheng W, Huang Y, Leng J (2015) Thermosetting epoxy reinforced shape memory composites microfiber membranes: fabrication, structure and properties. Compos A 76:54–61
127. Plylaharn J, Okhawilai M, Rimdusit S (2018) High recovery stress obtained in benzoxazine-epoxy shape memory polymers reinforced with carbon fiber. In: Proceeding in the 2018 pure and applied chemistry international conference (PACCON 2018), Songklanakarin, Thailand
128. Deka H, Ranjan N (2010) Biocompatible hyperbranched polyurethane/multi-walled carbon nanotube composites as shape memory materials. Carbon 48:2013–2022
129. Mahapatra SS, Ramasamy MS, Yoo HJ, Cho JW (2014) A reactive graphene sheet in situ functionalized hyperbranched polyurethane for high performance shape memory material. RSC Adv 4:15146–15153
130. Memarian F, Fereidoon A, Ahangari MG (2016) Shape memory, mechanical and thermal properties of TPU/ABS/CNT: a ternary polymer composite. RSC Advances 6:101038–101047

Mechanical Properties of Shape-Memory Polymers, Polymer Blends, and Composites

P. Poornima Vijayan

Abstract Shape-memory polymers (SMPs) are widely employed in aerospace, biomedical, portable electronic devices, etc., where their multiple-shape capabilities are considered. In order to avoid the failure of the SMPs before shape change, it is critical to possess excellent mechanical properties along with their inherent shape-memory ability. Recent research reports highlight the importance of SMPs with high strength and toughness. Conventional mechanical testing procedures such as tensile, bending, and fracture toughness are used to outline the static mechanical performance of SMPs. The cyclic mechanical testing facilitates the evaluation of shape-memory parameters such as shape fixity (R_f) and shape recovery (R_r) ratio. In a recent development, nanoindentation technique is used to probe the shape-memory process at nanolevel. SMPs based on epoxy, polyurethane, PCL, etc., were investigated for their both static and cyclic mechanical performance. Well-balanced mechanical and shape-memory performance can be tailored in SMPs by careful tuning of crystallinity, cross-link density, and fiber/filler reinforcement.

1 Introduction

Shape-memory polymers (SMPs) are mechanically active materials which memorize a permanent shape that is substantially differ from their initial temporary shape. SMPs are important category of stimuli responsive polymers, which can recover their original or permanent shape upon exposure to external stimuli such as heat [1–3], light [4], moisture [5], pH [6], etc. Among them, thermo-initiated shape-memory polymers are more common and widely studied. SMPs consists of two segments, of which the hard segment to determine the permanent shape and the switching (soft) segments to fix the temporary shape. The polymer chains in switching segment are able to fix a given deformation by cooling below a transition temperature (T_{trans}). T_{trans} can be the glass transition (T_g) or the melting point (T_m) of the polymer. When

P. Poornima Vijayan (✉)
Department of Chemistry, Sree Narayana College for Women, Kollam 691001, Kerala, India
e-mail: poornimavijayan2007@gmail.com

J. Parameswaranpillai et al. (eds.), *Shape Memory Polymers, Blends and Composites*, Advanced Structured Materials 115,
https://doi.org/10.1007/978-981-13-8574-2_9

reheating above T_{trans}, the oriented or crystalline chains in the polymer network, restore their random coil conformation to recover its original shape.

Shape-memory polymers are getting popular than their alloys and ceramic counterparts, as they are cheap, lightweight, and easily processable. Above all, the shape-memory polymers have the mechanical advantage of higher percentage of strain recovery than shape-memory alloys (SMA) [7, 8]. While SMA can store strains on the order of 10%, the shape-memory polymers can recover strains on the order of several 100%. However, shape-memory polymers have low stiffness and strength which limits their wider application. Both strength and stiffness of SMPs could be dramatically improved by reinforcement with fillers [9].

For SMPs, both static and cyclic mechanical tests are used to determine the mechanical and shape-memory properties, respectively. The strain fixity rate R_f and strain recovery rate R_r are important characteristics of SMPs for describing their shape-memory properties. The strain recovery rate quantifies the ability of the material to memorize its permanent shape, whereas strain fixity rate describes the ability of the switching segment to fix the mechanical deformation and are expressed as below

$$R_r(N) = \frac{\varepsilon_u - \varepsilon_p(N)}{\varepsilon_m - \varepsilon_p(N-1)} \times 100\% \tag{1}$$

$$R_f = \frac{\varepsilon_u}{\varepsilon_m} \times 100\% \tag{2}$$

Strain recovery rate is a measure of the strain that was applied in the course of the programming $\varepsilon_m - \varepsilon_p(N-1)$ is recovered in the following shape-memory transition. By definition, the strain fixity ratio (R_f) is the ratio of the strain in the stress-free state after the retraction of the stress in the N-th cycle ε_u and the maximum strain ε_m.

Usually, the shape-memory properties were quantified using cyclic thermomechanical tests, which allows simultaneous control over stress or strain and temperature during programming and recovery [10]. Apart from dynamic mechanical analyzer, mechanical testing devices equipped with a thermochamber are used to estimate the shape recovery of thermally initiated SMPs. The cyclic mechanical test can be done in tensile, bending, and compression modes. The current chapter gives an overview of these test methods, which is used to predict the shape recovery in SMPs. In addition to cyclic mechanical tests, the current chapter also discusses the static tensile and three-point bending, nanoindentation, toughness, fracture toughness of SMPs, their composites, and blends.

2 Static Tensile Tests

For a shape-memory polymer, it is essential to possess enhanced static mechanical strength before shape changing. Static tensile tests are performed at a fixed temperature and allow the variation of the applied strain or stress as well as the strain rate.

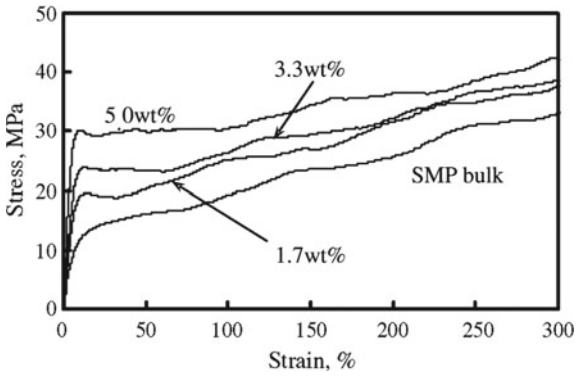

Fig. 1 Stress–strain curves in static tensile tests for four materials—SMP bulk, 1.7, 3.3 and 5.0 wt% at testing temperatures of 25 °C [12]

The resulted stress–strain curve is used to evaluate tensile properties such as Young's modulus, the yield point as well as elongation at break, and stress at break.

Similar to reinforcing of polymers, the researcher made attempts to reinforce the shape-memory polymers. Static tensile tests were used to evaluate the reinforcing ability of fillers on SMP-based composite [11, 12]. Ni et al. [12] used vapor growth carbon fibers (VGCFs) to enhance the mechanical properties of the SMP based on polyurethane with excellent ductility similar to unmodified SMP (Fig. 1). The yield region became long as the VGCFs weight fraction increased.

Static tensile tests were also used to evaluate the mechanical performance of SMPs at above and below glass transition temperature. In polyurethane reinforced with VGCNF, a significant difference in tensile properties (Young's modulus and tensile strength) above and below glass transition temperature were noticed [12]. Below T_g, the deformation resistance is large due to frozen micro-Brownian motion of the soft segment at low temperature. However, above T_g, the soft segment becomes free to move to facilitate easy deformation.

Cho et al. [13] studied the role of arrangement of soft segment in SMPs by using tensile testing. Different types of soft-segment arrangement in shape-memory polyurethane (PU) was achieved where two poly(tetramethylene glycol) (PTMGs) is randomly arranged to get random co-polymer and block distribution of PTMGs to give a block copolymer. Polyurethane copolymers with a random or block soft-segment arrangement were found to have higher stresses at break and elongations at break than those with only one kind of soft segment. Physical interactions include hydrogen bonding, dipole–dipole, and induced dipole–dipole interactions can occur among copolymer. The presence of two PTMGs together in the soft segment reduced the interactions among the hard segments, and this made the copolymers easily elongated. Random copolymers showed higher elongation than block copolymers as disturbance in uniform distribution of soft segments resulted in reduction in this effective interaction.

Poly(ε-caprolactone) (PCL) and poly(ω-pentadecalactone) (PPDL) are suitable shape transition component for SMPs, while the earlier is used in low transition temperature SPMs and later is used in high transition temperature SPMs. PCL and

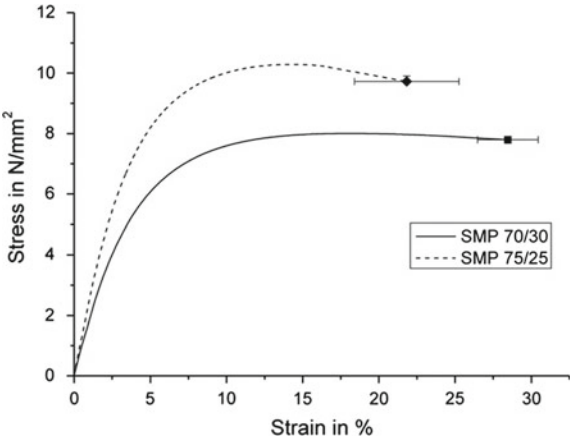

Fig. 2 Mean value of stress–strain curves of the partially crystalline and shape fixed SMP 70/30 and SMP 75/25 measured after polymerization and one weak at 20 °C [14]

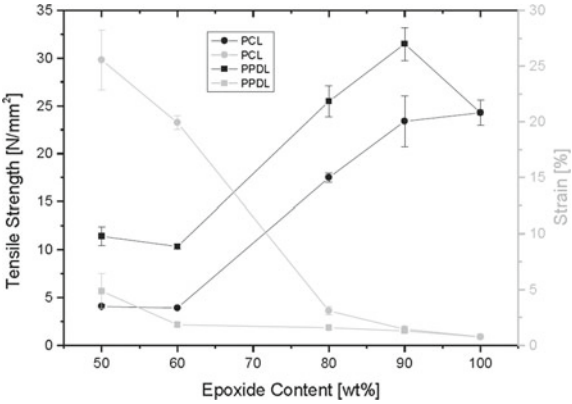

Fig. 3 Tensile strength (black) and strain at break (gray) for both epoxy-based polymers containing PPDL and PCL [15]

PPDL are used to develop interesting cationically polymerized epoxy-based SMPs. The blend ratio in PCL/epoxy SMPs are critically important as the physical cross-linking due to the crystalline interactions leads to less flexible but stiff PCL segments [14]. This leads to brittleness in PCL/epoxy-based SMPs with low epoxy content. Figure 2 shows the tensile behavior of PCL/epoxy SMPs with varying blend ratio. SMP containing 75 wt% PCL and 25 wt% epoxy showed an adequate crystallinity and shape fixity time with good material cohesion under mechanical load.

Arnebold et al. [15] studied the tensile behavior of epoxy-based SMP with poly(ω-pentadecalactone) (PPDL) as soft segment. Under certain polymerization conditions, PPDL/epoxy SMPs generated a high degree of crystallinity compared to the respective poly(ε-caprolactone) (PCL) counterpart. SMPs containing PPDL instead of PCL exhibit distinctly higher tensile strength due to increased crystalline macrophase formation (Fig. 3).

POSS–PCL network, another excellent PCL-based SMP, were investigated for their mechanical performance [16]. Star-shaped POSS–PCL SMPs with different

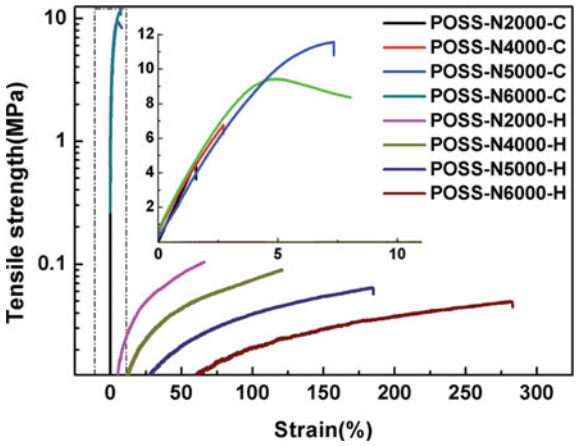

Fig. 4 Tensile stress–strain curves of POSS–PCL networks with different PCL arm lengths at room temperature and at elevated temperature; where 2000, 4000, 5000, and 6000 stands for molecular weight of PCL diol used to fabricate network; C stands for room temperature, and H stands for elevated temperature [16]

PCL arm lengths were synthesized via. ring opening polymerization of epoxy group by PCL diol. Tensile behavior of POSS–PCL networks with different PCL arm lengths is shown in Fig. 4. It was found that with shorter PCL arm lengths, lower crystallinity reduced the tensile strength and higher cross-links density resulted in brittle fracture of POSS-N2000 and POSS-N4000 samples. At the same time, more dangling ends with longer PCL chain generated high level of crystallinity in POSS-N5000 and POSS-N6000. The energy generated by stretching during tensile test stored in the crystalline domain. Above Tm, all POSS–PCL samples behave like elastomers, with sharply declining tensile strength.

3 Physical Bending Test

Physical bending test is used to characterize cycle-life of the shape-memory polymers. Various approach was adopted by researchers and some of them are illustrated in this chapter. Kong et al. [17] studied the cycle life of a shape-memory polyimide, which is synthesized by two-step polycondensation of 4,4′-(1,1′-biphenyl-4,4′-diyldioxy)-dianiline and bis phenol A dianhydride, by physical bending test. The schematic illustration of shape-memory bending cycle adopted in their study is shown in Fig. 5a. The corresponding performance of polyimide is shown in Fig. 5b.

R_f and R_r of bending deformation are calculated with Eqs. 3 and 4, respectively.

$$Rf = \frac{180^\circ - \theta_f}{180^\circ} \times 100\% \tag{3}$$

$$R_r = \frac{180^\circ - \theta_r}{180^\circ} \times 100\% \tag{4}$$

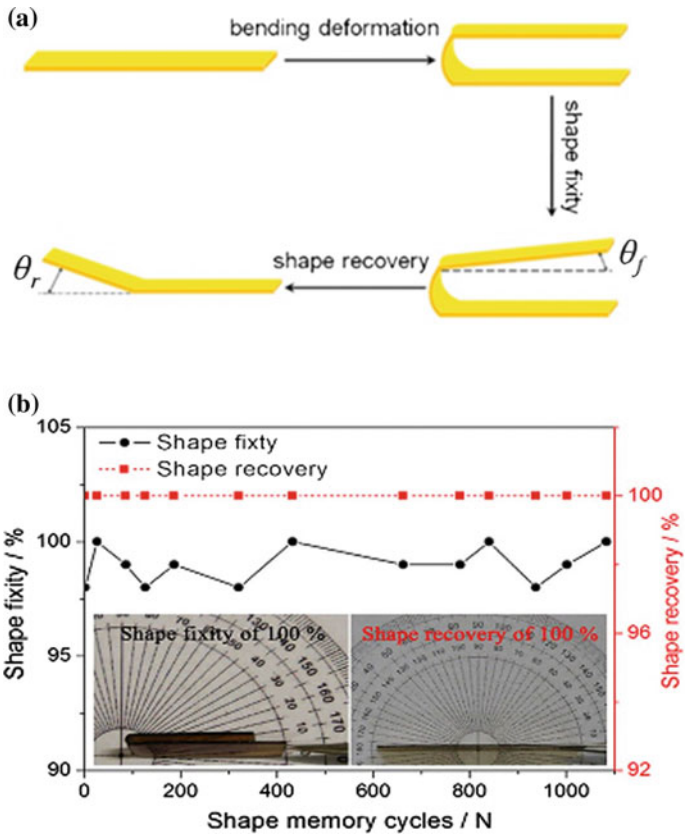

Fig. 5 **a** Schematic illustration of the shape fixity and shape recovery test in bending deformation **b** overview of shape-memory performances of the polyimide during the bending cycles [17]

where θ_f and θ_r represent the released angle after cooling and the recovered angle, respectively. This procedure was used to determine R_f and R_r of polyimide possessing large content of aromatic groups and highly twisted molecular chains. This polyimide maintained both high R_f and R_r of about 100% during the more than 1000 shape-memory cycles tested.

In another study, Lin et al. [18] performed the physical bending using cylinder-shaped polyvinyl alcohol (PVA) hydrogel specimens, which were bent to a "L" shape at a temperature equivalent to T_g of the SMP. The deformed shapes were fixed by quickly cooling them at room temperature and maintaining them at a deformation load. The shape recovery was recorded by a digital camera after putting the specimens back to 85 °C. The angle of the specimen after cooling was recorded as θ_f and the final angle of the specimen after recovery was recorded as θ_r. The shape fixity ratio, R_f, and shape recovery ratio, R_r, were determined using Eqs. (5) and (6) below

$$R_f = \frac{\theta_f}{90} \times 100\% \tag{5}$$

$$R_r = \frac{\theta_f - \theta_r}{\theta_f} \times 100\% \tag{6}$$

Physical bending studies on polyvinyl alcohol (PVA) hydrogel chemically cross-linked with glutaraldehyde (GA) revealed that an increase in the content of GA in PVA hydrogel reduces the recovery force and increase the recovery time. PVA hydrogel with 5 wt% GA showed best shape recoverability and one with above 7 wt% GA content limited the movement of the PVA soft chain resulting in a relatively lower recovery rate and longer recovery time.

4 Cyclic Tensile Test

Conventional tensile testing machine equipped with a thermochamber is used to carry out cyclic thermomechanical tests for shape-memory polymers [10]. The thermochamber enables an accurate temperature control during mechanical deformation and recovery process. The temperature (T_s) selected to carry out the cyclic tensile test is generally an intermediate temperature between the melting temperature of the soft segments ($T_{m,s}$) and the melting temperature of the hard segments ($T_{m,h}$). Once the shape-memory polymer is deformed at T_s and subsequently cooled below $T_{m,s}$, the deformed shape is fixed to a large extent because of the frozen micro-Brownian movement of polymer chains. When the sample is reheated at T_s, the original shape is recovered due to the elastic energy stored during the deformation process. The result obtained from such measurement is usually presented in a stress–strain curve. The shape recovery and shape fixity ratios are calculated from the obtained stress–strain curve using Eqs. (1) and (2).

Cyclic tensile testing is also used to study the cyclic photomechanical behavior of light-induced shape-memory polymers [4]. The cyclic photomechanical experiment is similar to cyclic thermomechanical experiments. Lendlein et al. [4] studied the cyclic photomechanical behavior of polymer containing cinnamic groups, which can deformed and fixed into predetermined shapes by ultraviolet light illumination. Figure 6a gives elongation–time diagram of the grafted polymer in which cinnamic acid (CA) molecules are grafted onto the permanent polymer network, which was obtained during a cyclic photomechanical test under stress controlled conditions using tensile tester equipped with a thermochamber. Initially, the elongated sample is kept at constant stress and during the first cycle, the elongation stayed constant in the stretched state, indicating no relaxation of the polymer. Upon removing the stress and switching off the UV light ($\lambda > 260$ nm), a temporarily fixed elongation (ε_u) was observed. The fixed temporary shape is maintained till the sample is exposed to UV light of $\lambda < 260$ nm, activating the shape recovery of the temporarily fixed shape to nearly its original length characterized by a remaining elongation ε_p. This

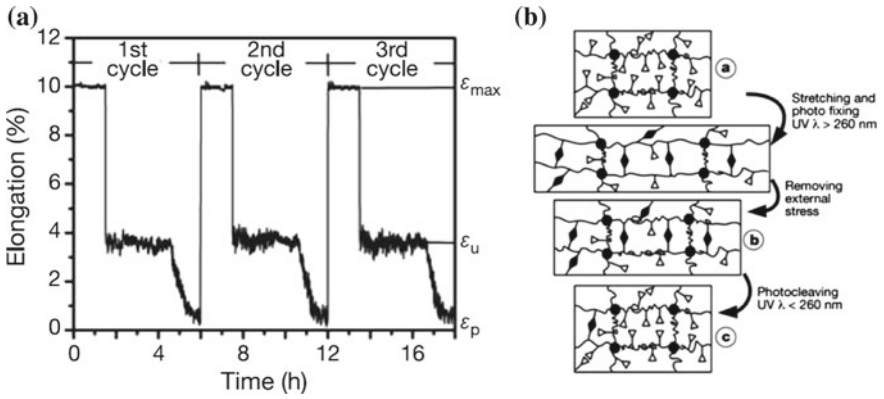

Fig. 6 **a** Cyclic photomechanical experiment on a grafted polymer under stress-controlled conditions and **b** molecular mechanism of shape-memory effect of the grafted polymer network: the chromophores (open triangles) are covalently grafted onto the permanent polymer network (filled circles, permanent cross-links), forming photoreversible cross-links (filled diamonds); fixation and recovery of the temporary shape are realized by UV light irradiation of suitable wavelengths [4]

cycle of experiment is repeated twice to find out R_f and R_r. When compared with thermoresponsive shape-memory polymers, similar strain recovery rate and much lower strain fixity rate is observed for photoresponsive shape-memory polymers due to the change in shape recovery mechanism. While, segments having a thermal transition at T_{trans} act as molecular switches in thermoresponsive SMPs, reversible photoreactive entities serve as molecular switches in photoresponsive shape-memory polymers. The molecular mechanism in photoresponsive shape memory is depicted in Fig. 6b.

Cyclic tensile properties both at constant strain and constant stress loading are evaluated for fiber-reinforced SMPs [19]. The stress–strain curves at constant stress for non-reinforced and reinforced SMPs were studied. The yield phenomenon occurred in the non-reinforced specimen before reaching the prescribed cycle number. In SMP with 10 wt% fiber, the residual strain increased with cycle number, whereas in SMP with 20 and 30 wt% fiber, there was no obvious increment in residual strain with the cycle number. Similarly, the stress–strain curves at constant strain cycle were also studied. At the first cycle, a large hysteresis loop was observed for fiber-reinforced SMPs with different fiber loadings and is mainly contributed by matrix deformation and failures around fibers. There was no hysteresis following the first cycle. This is called training effect, where stable strain recovery ability can be achieved after several cycles of training. This makes this SMPs for several cycle use in daily life.

Auad et al. [20] studied the shape-memory behavior of nanocellulose reinforced PU using cyclic tensile test. It was found that the presence of nanocellulose doesn't have any significant effect on shape fixity or recovery of the material. The shape-

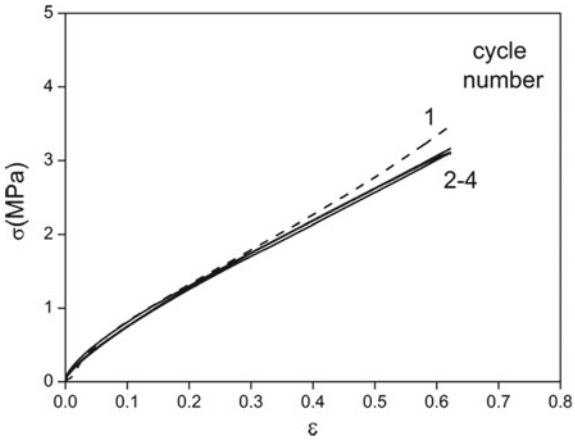

Fig. 7 Uniaxial stress–strain curves at 55 °C for SMP based on epoxy with both chemical and physical cross-links during the four cycles are used to determine shape-memory properties [22]

memory behavior of nanocellulose reinforced PU is controlled by the polymer properties rather than polymer–filler interaction.

The influence of loading rate, loading levels, preconditioning loading–unloading treatment, and temperature on the shape recovery behavior of styrene SMP are studied using cyclic tensile testing [21]. It was observed that loading level and loading rate have little effect on the shape recovery behavior of styrene SMP. A prior cyclic loading–unloading treatment will make styrene SMP to obtain a better shape recovery property due to the formation of super-molecular structure. A cyclic loading–unloading test will make styrene SMP enter into rubbery state at low temperature and show a better shape recovery behavior.

An epoxy polymer designed with both chemical and physical cross-links were analyzed with cyclic tensile testing to estimate their shape fixity and shape recovery [22]. These polymers showed excellent shape-memory behavior with a combination of relatively high tensile strains (75%) and recovery stresses (3 MPa) without shape hysteresis between the first and subsequent cycles (Fig. 7). Very good values of shape fixity (98%) and shape recovery (96%) were obtained and no shape hysteresis was observed between the first and subsequent cycles. This was assigned to the presence of physical associations among pendant alkyl chains.

Cyclic tensile test was used to compare the shape recovery and shape fixity ratio of POSS–PCL network as a function of PCL arm length (Table 1) [16]. Shape fixity ratio has a slightly higher value for POSS–PCL network with shorter PCL arm length. As the cross-link density reduces with increase in PCL arm length, the shape fixity ratio decreased from POSS-N2000 to POSS-N6000. Shape recovery (R_r) ratio also decreased with increase in PCL arm length as the shorter PCL chain tended to return to its initial shape more easily. These phenomena may be attributed to the plastic deformation of PCL chain and the cumulative breakage of covalent bonds.

Table 1 Shape-memory properties of POSS–PCL networks at 60 °C [16]

Sample	R_f (N = 1) (%)	R_f (N = 2, 3) (%)	R_r (N = 1) (%)	R_r (N = 2, 3) (%)
POSS-N2000	97.3 ± 0.2	97.3 ± 0.2	99.8 ± 0.2	99.6 ± 0.2
POSS-N4000	95.5 ± 0.2	95.2 ± 0.2	99.1 ± 0.2	98.7 ± 0.3
POSS-N5000	94.2 ± 0.2	94.0 ± 0.2	98.6 ± 0.2	98.1 ± 0.2
POSS-N6000	93.6 ± 0.2	93.3 ± 0.2	97.5 ± 0.2	97.0 ± 0.3

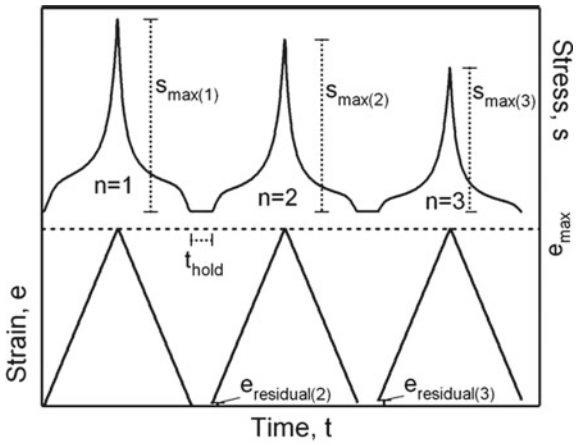

Fig. 8 Schematic of the cyclic compression test [23]

5 Cyclic Compression Test

In addition to tensile mode, compression mode has also been used to study the cyclic thermomechanical behavior of shape-memory polymer especially for foams and gels. For instance, one such experimental procedure for cyclic compression test is schematically shown in Fig. 8. Compressive strain is applied to a maximum level, e_{max}, then the sample is unloaded by moving the cross-head, until the preload force is reached; for nonzero hold times, the cross-head is further raised to completely unload the sample. The sample is held in this unloaded state for a hold time, t_{hold}, and then reloaded to the same e_{max} level, taking note of the residual strain, $e_{residual}$, on the sample after the cycle, including the hold time.

Cyclic compressive behavior of epoxy shape-memory polymer foam were studied by Di Prima et al. [23, 24]. Their studies revealed the correlation between the strain to failure as a function of temperature and the cyclic damage accumulation in epoxy shape-memory foams (Fig. 9). As the deformation temperature approached corresponding to the peak of the strain-to-failure behavior in such materials, there was significantly less cyclic damage. Hence, the damage under compression in epoxy shape-memory foams can be greatly minimized by lowering the maximum strain or changing the deformation temperature to a temperature where tensile ductility is maximized.

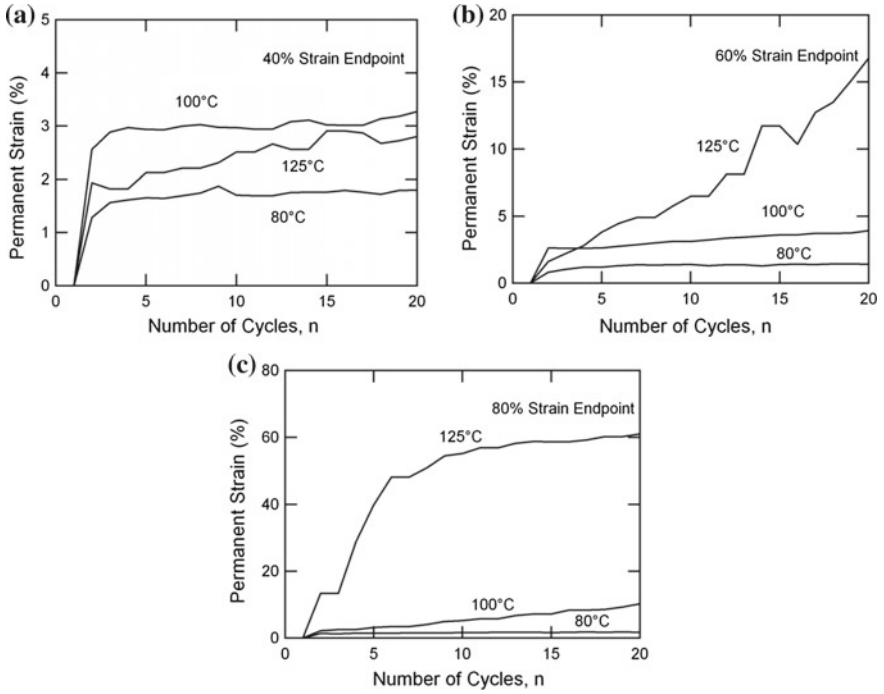

Fig. 9 Temperature dependence on permanent strain during cyclic loading with varying strain endpoints: **a** 40% compressed, **b** 60% compressed, and **c** 80% compressed [24]

The effects of pre-strain and hold period between compressive cycles on cyclic behavior on epoxy shape-memory polymer foam with varying relative density were also investigated [24]. Cyclic compression behavior of epoxy SMP foams with 20% and 30% relative density (RD) is shown in Figs. 10 and 11. The maximum strain is a driving factor in the cyclic behavior of epoxy SMP foam across relative densities and there is a strain threshold for damage. Upon increasing the relative density of the foam, the strain threshold for damage gets decreased. Moreover, the addition of a hold time between compression cycles was found to extend the strain damage threshold.

6 Toughness of SPMs

The understanding of strain-to-failure behavior and corresponding toughness of SMPs is crucial as it governs the available work capacity in the materials. Especially, SMPs used in medical implant and space structure materials need to meet specific load-bearing capability. Toughness is defined as the amount of energy required to

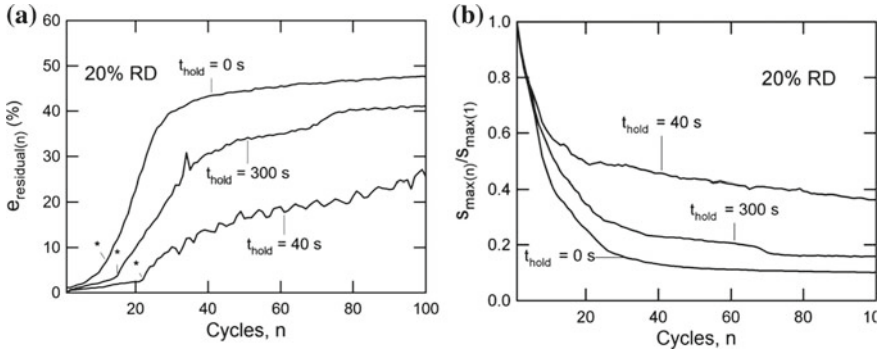

Fig. 10 Cyclic behavior of 20% RD foam for 100 cycles with a maximum strain of 80% with hold times of 0, 40, and 300 s. Both the residual strain (**a**) and the maximum stress normalized to the first cycle (**b**) were tracked. For residual strain (**a**), the * marks the onset of macroscopic failure [23]

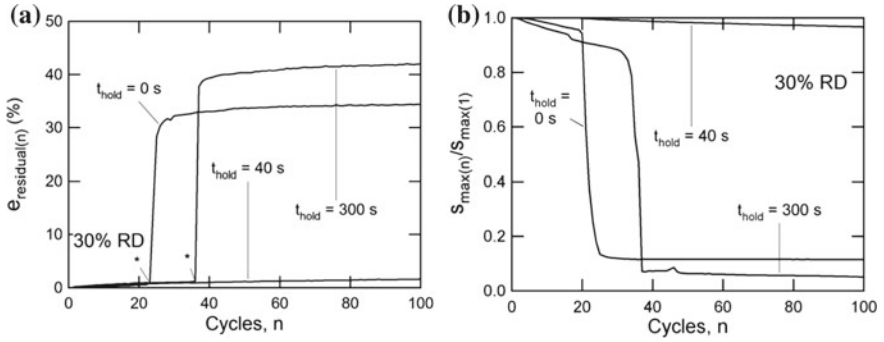

Fig. 11 Cyclic behavior of 30% RD foam for 100 cycles with a maximum strain of 50% with hold times of 0, 40, and 300 s. Both the residual strain (**a**) and the maximum stress normalized to the first cycle (**b**) were tracked. For residual strain (**a**), the * marks the onset of macroscopic failure [23]

break a material. Toughness also relates to the ability of a material to resist fracture under acute loading due to geometric flaws and is known as fracture toughness. Fracture toughness reveals resistance of a material to crack propagation. In order to estimate the inherent toughness, a strain-to-failure test performed in either tension or compression mode is usually used. On the other hand, fracture toughness, can be measured by determining the failure of a specimen containing a crack, like a compact tension specimen or center cracked plate. The parameter called "critical stress intensity factor" (K_{IC}), a measure of fracture toughness is determined from ultimate failure stress using the following equation:

$$K_{IC} = \left(\frac{F_{max}}{BW}\right) a^{\frac{1}{2}} f\left(\frac{a}{w}\right) \tag{7}$$

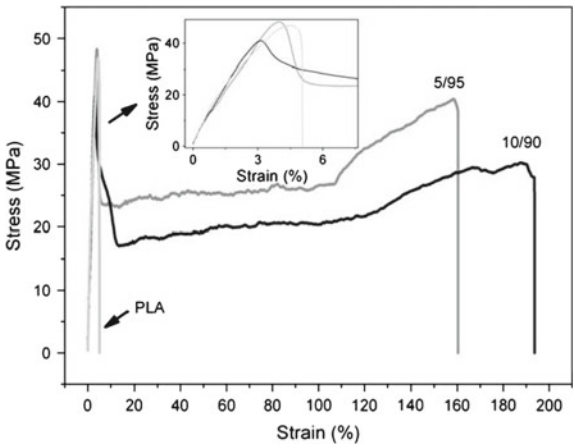

Fig. 12 Tensile stress–strain curves of the PAE/PLA blends with varying compositions [27]

where F_{max} is a maximum force from the load–elongation curve, B is the thickness of the specimen, W is the width of the specimen, and a is the total notch length.

$f\left(\frac{a}{w}\right)$ is the geometry correction factor, expressed as

$$f\frac{a}{w} = 1.99 - 0.41\left(\frac{a}{w}\right) + 18.7\left(\frac{a}{w}\right)^2 - 38.48\left(\frac{a}{w}\right)^3 + 53.85\left(\frac{a}{w}\right)^4 \quad (8)$$

The toughness of brittle polymers could be drastically increased by blending with another polymer [25, 26]. Similarly, in SMPs, the combination of two polymers mostly resulted in a toughness enhancement along with shape-memory effect. The intrinsic brittleness of PLA (polylactic acid) limited the shape-memory effect as it breaks up above 5% of deformation ratio. Melt blending of PLA and biodegradable polyamide elastomer (PAE) has generated an efficient SMP for biomedical application with high toughness performance [27]. An elongation of 194.6% was recorded for PAE/PLA blend with 10% of PAE content (Fig. 12). The shape recovery process in PAE/PLA blends is different from the traditional shape-memory polymers. In PAE/PLA blend, the temporary shape is formed at room temperature. While the amorphous PAE region deforms upon elongation, the crystalline PLA region act as the cross-link points to keep the original structure. The entire recovery process is shown in Fig. 13.

Polyurethane (PU)-based SMP with tunable toughness suitable for biomedical applications was developed by a post-polymerization cross-linking method [28]. Post-polymerization cross-linking was achieved by solution blending of PU with polythiol cross-linking agents and photoinitiator and subsequent UV irradiation. Stress to failure behavior of PU based SMP with different cross-link density was studied. They exhibit high toughness, especially the low cross-link density PU, for which toughness exceeds 90 MJ/m^3 at select straining temperatures. Similarly, polymer networks based on (meth) acrylate monomers are strong candidate for shape-memory polymers. Stress–strain response of (meth) acrylate-based SMPs systematically var-

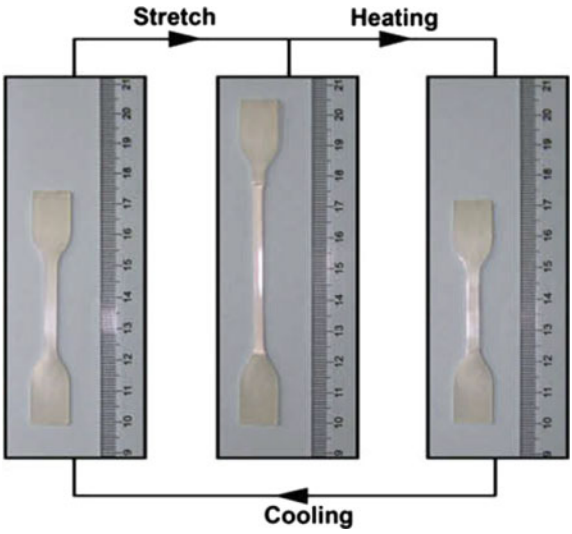

Fig. 13 Illustration of cyclic stretch-recovery process in PLA/PAE blend with 10% PAE contents [27]

ied with monomer functionalities, concentrations, and chemistries [29]. By varying chemistry and cross-linking density, a divergence point in network toughness was revealed.

The inherent brittleness of epoxy-based SMP due to their high cross-link density limit their applications as smart engineering and structural materials. Different strategies were adopted by researchers to improve the toughness of epoxy-based SMPs. Introduction of partial crystallinity into the epoxy network, by cationic polymerization with PCL and PPDL effectively increased the toughness of SMP [15]. Figure 14 represents the variation of fracture energies with epoxy content. As the concentration of PCL or PPDL increased, the toughness of SMP increased but the effect of PCL is more significant. This difference in toughness is due to the higher degree of crystalline macrophase formation due to strong segregation of PPDL in PPDL/epoxy-based SMPs when compared to PCL-based system.

7 High-Temperature Nanoindentation Technique

The shape-memory effect in homogenous bulk materials are well studied using dynamic mechanical analysis (DMA), while nanoindentation provides information on shape-memory process at the nanoscale. Understanding of shape recovery at nanoscale will be applicable in the design of small-scale actuators for various biomedical and microsystems [30]. Nanoindentation is a depth-sensing technique, conventionally used to study the mechanical properties of nanometer-scaled volumes of materials. In an advanced attempt, high-temperature nanoindentation test is used for the characterization of thermally induced shape-memory property. For this purpose,

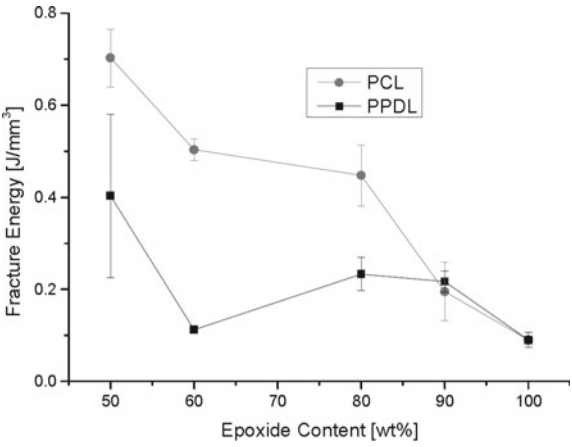

Fig. 14 Fracture energy of epoxy/PPDL-based SMPs (black) and epoxy/PCL-based SMPs (gray) [15]

the nanoindenter is integrated with a microheater and a temperature control and monitoring system. So that, the SMP specimen to be activated at elevated temperatures enable proper implementation of the thermomechanical cycle. The load–depth curves of the SMP are obtained at various temperatures, from which the instantaneous moduli are calculated using the following equation:

$$E = \frac{1-\nu^2}{\frac{1}{E_r} - \frac{1-\nu_i^2}{E_i}} \tag{9}$$

where $E_r = \left(\frac{\sqrt{\pi}}{2} \cdot (1.034)\right)(S/\sqrt{\pi a^2})$, S is the elastic contact stiffness and a is the indenter-sample contact radius. E_i and ν_i are the elastic modulus and Poisson's ratio of the indenter.

The temperature dependent modulus of the SMP has a similar trend as that from dynamic mechanical analysis, which makes nanoindentation as a promising technique for characterizing the shape-memory cycle.

Fulcher et al. [31] used nanoindentation technique to study the shape-memory properties of epoxy-based SMPs. Nanoindentation test enables to follow up the shape-memory process by analyzing the load–depth curve and surface profile below and above T_g of the SMPs. The load–depth curve becomes less stiff with an increase in temperature, since the material changes its state from a rigid plastic to a soft rubber as shown in Fig. 15a. When SMPs is activated at high temperatures, they can undergo larger deformation as shown in Fig. 15a, which is favorable for applications involving morphing deployable structures. When activated at elevated temperatures, the SMP surface has a large amount of "sink-in" which indicates large-strain elastic deformation (Fig. 15b).

Wornyo et al. [32] studied the effect of cross-link density on thermally induced shape-memory properties of copolymer based on diethylene glycol dimethacrylate and polyethylene glycol dimethacrylate using nanoindentation technique. They

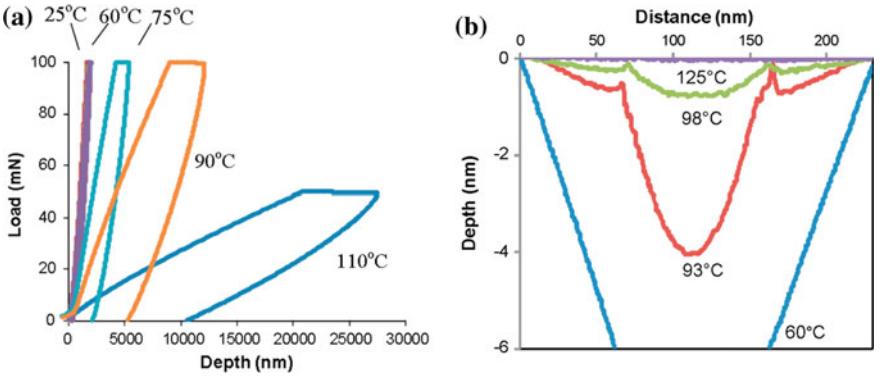

Fig. 15 **a** Indentation load–depth responses at various temperatures, **b** surface profiles of obtained at various recovery temperatures for epoxy-based SMP [31]

observed the temperature-induced shape recovery of the nanoindentations using atomic force microscopy (AFM). AFM images, which monitor the recovery process in acrylate monomer and acrylate monomer/cross-linker combinations is given in Fig. 16. The indents was found to shrink as increasing temperature. The indents eventually diminished in the vicinity of T_g. For impressions placed at ambient temperature, the indent shape recovery profile shifts to higher temperatures as cross-link density and glass transition temperature increase.

8 Conclusions

As emerging smart materials, shape-memory polymers are capable to make key changes in biomedical, automobile, electronic, textile, and aerospace industries. Evaluation of both static and cyclic mechanical properties of these shape-memory polymers are critical to assess their suitability for the abovementioned applications. The current chapter outlined the fundamentals of both static and cyclic mechanical properties used to characterize the shape-memory polymers. The factors influencing the static mechanical strength, toughness, and shape-memory parameters are discussed by citing the examples of epoxy, polyurethane, and PCL-based SMPs, their blends, and composites.

Various factors affecting the strength and toughness were discussed. In fiber-reinforced SMP composites, the fiber content has a significant role in enhancing the mechanical properties including the strength, modulus, and toughness. At the same time, reinforcing fillers have little effect on shape-memory properties as it mainly depends on polymer chain interactions rather than polymer–filler interaction. While cyclic compression tests were effectively used to study the shape-memory behavior of SMP foams and gels, physical bending tests are found suitable for high cycle

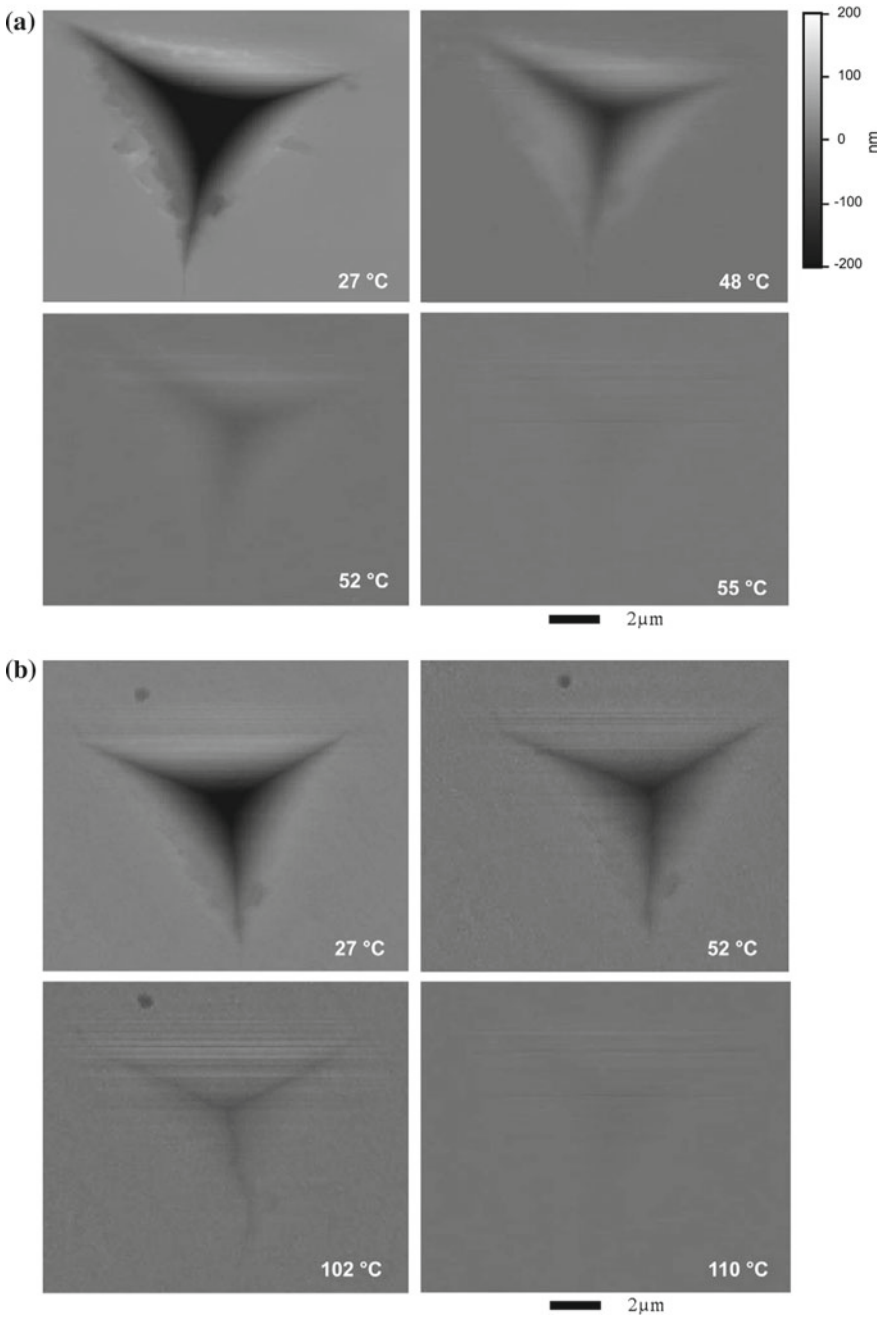

Fig. 16 Tapping mode AFM images show the evolution of shape recovery from room temperature to the recovery temperature for **a** tert-butyl acrylate monomer (l00tBA) and **b** diethylene glycol dimethacrylate (DEGDMA) cross-linker/tert-butyl acrylate monomer (50DEG50tBA) [32]

life determination in SMPs. The role of crystallinity, cross-link density, and reinforcement on mechanical and shape-memory performance are well studied using the mechanical testing procedures. The cyclic mechanical tests have been proved as efficient shape-memory probing tools, which contributes in developing potential SMPs for various future applications ranging from portable electronic devices to aerospace. The efficiency of nanoindentation to follow up the shape-memory properties in nanoscale dimension has been well discussed in this chapter. It has been proved as a promising technique in designing small-scale actuators for biomedical and microsystems.

References

1. Kagami Y, Gong JP, Osada Y (1996) Shape memory behaviors of crosslinked copolymers containing stearyl acrylate. Macromol Rapid Commun 17:539–543
2. Kim BK, Lee SY, Xu M (1996) Polyurethanes having shape memory effects. Polymer 37:5781–5793
3. Lendlein A, Langer R (2002) Biodegradable, elastic shape-memory polymers for potential biomedical applications. Science 296:1673–1676
4. Lendlein A, Jiang H, Jünger O, Langer R (2005) Light-induced shape-memory polymers. Nature 434:879–882
5. Chen S, Hu J, Chen S (2012) Studies of the moisture-sensitive shape memory effect of pyridine-containing polyurethanes. Polym Int 61:314–320
6. Han X-J, Dong Z-Q, Fan M-M, Liu Y, li J-H, Wang Y-F, Yuan Q-J, Li B-J, Zhang S (2012) pH-induced shape-memory polymers. Macromol Rapid Commun 33:1055–1060
7. Ratna D, Karger-Kocsis J (2008) Recent advances in shape memory polymers and composites: a review. J Mater Sci 43:254–269
8. Xu B, Fu YQ, Ahmad M, Luo JK, Huang WM, Kraft A, Reuben R, Pei YT, Chen ZG, De Hosson JThM (2010) Thermo-mechanical properties of polystyrene-based shape memory nanocomposites. J Mater Chem 20:3442–3448
9. Abrahamson ER, Lake MS, Munshi NA, Gall K (2003) Shape memory mechanics of an elastic memory composite resin. J Intell Mater Syst Struct 14:623–632
10. Sauter T, Heuchel M, Kratz K, Lendlein A (2013) Quantifying the shape-memory effect of polymers by cyclic thermomechanical tests. Polym Rev 53:6–40
11. Cho J-W, Kim J-W, Jung Y-C, Goo N-S (2005) Electroactive shape-memory polyurethane composites incorporating carbon nanotubes. Macromol Rapid Commun 26:412–416
12. Ni Q-Q, Zhang C-S, Fu Y, Dai GS, Kimura T (2007) Shape memory effect and mechanical properties of carbon nanotube/shape memory polymer nanocomposites. Compos Struct 81:176–184
13. Cho J-W, Jung Y-C, Chung Y-C, Chun B-C (2004) Improved mechanical properties of shape-memory polyurethane block copolymers through the control of the soft-segment arrangement. J Appl Polym Sci 93:2410–2415
14. Lützen H, Gesing TM, Kim B-K, Hartwig A (2012) Novel cationically polymerized epoxy/poly(ε-caprolactone) polymers showing a shape memory effect. Polymer 53:6089–6095
15. Arnebold A, Hartwig A (2016) Fast switchable, epoxy based shape-memory polymers with high strength and toughness. Polymer 83:40–49
16. Yang P, Zhu G, Shen X, Yan X, Nie J (2016) Poly(3-caprolactone)-based shape memory polymers crosslinked by polyhedral oligomeric silsesquioxane. RSC Adv 6:90212
17. Kong D, Xiao X (2016) High cycle-life shape memory polymer at high temperature. Sci Rep 6:33610

18. Lin L, Zhang L, Guo Y (2018) Mechanical properties and shape memory effect of thermal-responsive polymer based on PVA. Mater Res Express 5:015702
19. Ohki T, Ni Q-Q, Iwamoto M (2004) Creep and cyclic mechanical properties of composites based on shape memory polymer. Sci Eng Compos Mater 11:137–148
20. Auad ML, Contos VS, Nutt S, Aranguren MI, Marcovich NE (2008) Characterization of nanocellulose reinforced shape memory polyurethanes. Polym Int 57:651–659
21. Liu R, Li Y, Liu Z (2018) Experimental study of thermo-mechanical behavior of a thermosetting shape-memory polymer. Mech Time Depend Mater. https://doi.org/10.1007/s11043-018-9377-0
22. Leonardi AB, Fasce LA, Zucchi IA, Hoppe CE, Soule ER, Perez CJ, Williams RJJ (2011) Shape memory epoxies based on networks with chemical and physical crosslinks. Euro Polym J 47:362–369
23. Di Prima MA, Gall K, McDowell DL, Guldberg R, Lin A, Sanderson T, Campbell D, Arzberger SC (2010) Cyclic compression behavior of epoxy shape memory polymer foam. Mech Mater 42:405–416
24. Di Prima MA, Lesniewski M, Gall K, McDowell DL, Sanderson T, Campbell D (2007) Thermo-mechanical behavior of epoxy shape memory polymer foams. Smart Mater Struct 16:2330–2340
25. Anderson KS, Hillmyer MA (2004) The influence of block copolymer microstructure on the toughness of compatibilized polylactide/polyethylene blends. Polymer 45:8809–8823
26. Jaratrotkamjorn R, Khaokong C, Tanrattanakul V (2012) Toughness enhancement of poly(lactic acid) by melt blending with natural rubber. J Appl Polym Sci 124:5027–5036
27. Zhang W, Chen L, Zhang Y (2009) Surprising shape-memory effect of polylactide resulted from toughening by polyamide elastomer. Polymer 50:1311–1315
28. Hearon K, Wierzbicki MA, Nash LD, Landsman TL, Laramy C, Lonnecker AT, Gibbons MC, Ur S, Cardinal KO, Wilson TS, Wooley KL, Maitland DJ (2015) A processable shape memory polymer system for biomedical applications. Adv Healthc Mater 4:1386–1398
29. Safranski DL, Gall K (2008) Effect of chemical structure and crosslinking density on the thermo-mechanical properties and toughness of (meth)acrylate shape memory polymer networks. Polymer 49:4446–4455
30. Yang F, Wornyo E, Gall K, King WP (2008) Thermomechanical formation and recovery of nanoindents in a shape memory polymer studied using a heated tip. Scanning 30:197–202
31. Fulcher JT, Lu YC, Tandon GP, Foster DC (2010) Thermomechanical characterization of shape memory polymers using high temperature nanoindentation. Polym Test 29:544–552
32. Wornyo E, Gall K, Yang F, King W (2007) Nanoindentation of shape memory polymer networks. Polymer 48:3213–3225

Biodegradable Shape-Memory Polymers

Leire Ruiz-Rubio, Leyre Pérez-Álvarez and José Luis Vilas-Vilela

Abstract Biodegradable shape-memory polymers (BSMP) have arisen as highly promising materials for biomedical applications due to their valuable properties. Their chemical and structural diversities, low toxicity, biodegradation, and resorption added to their capability to adapt their shape due to their shape-memory property make them excellent materials for many implantable devices. In this chapter, the main characteristics of these materials and their applications in biomedicine are described.

1 Introduction

Biomaterials need to fulfill complex requirements, which are determined by a specific application. As such requirements can differ significantly from case to case, materials should be adjusted for any specific application [1, 2]. The choice of a suitable material in order to get the desired functions is crucial and will be only possible when the characteristics on the molecular level can be tailored to obtain the desired properties in the final material. Multifunctional biopolymers that combine two functions such as shape-memory effect and biodegradability [3, 4] are of special interest, specifically in uses into the human body.

On the other hand, growing environmental concerns of the necessity of sustainable growth promote the production and use of biodegradable polymers, especially those which are obtained from renewable resources. The major part of biodegradable polymers are polyesters, and in particular, aliphatic polyesters. Even more, to obtain aliphatic polyesters practically all monomers can be synthesized from renewable resources [5], although biodegradable polymers can be produced from petrochemical sources as well.

L. Ruiz-Rubio · L. Pérez-Álvarez · J. L. Vilas-Vilela (✉)
Grupo de Química Macromolecular (LABQUIMAC), Departamento de Química Física, Facultad de Ciencia y Tecnología, Universidad del País Vasco UPV/EHU, 48940 Leioa, Spain
e-mail: joseluis.vilas@ehu.eus

BCMaterials, Basque Center for Materials, Applications and Nanostructures, UPV/EHU Science Park, 48940 Leioa, Spain

J. Parameswaranpillai et al. (eds.), *Shape Memory Polymers, Blends and Composites*, Advanced Structured Materials 115,
https://doi.org/10.1007/978-981-13-8574-2_10

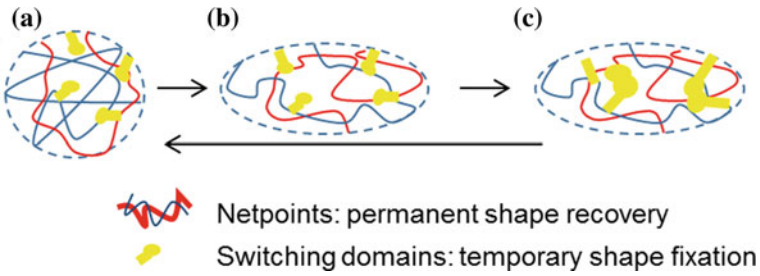

Fig. 1 Schematic representation of an SMP. **a**, **b** temporary shape by deformation of the network, **b**, **c** fixation of temporary shape, and **c**, **b** recovery of permanent shape

Shape-memory polymers (SMPs) are emerging as advanced materials for many demanding applications, such as biomedical or engineering. This kind of materials can be described as dual, triple, or even multi-shape memory depending on the number of temporal/permanent shape transitions that the material could have undergone as a response to an external stimulus. The main stimuli capable of triggering the response of the material are temperature, pH, light irradiation [6–8], and redox condition, among others [9]. However, the most reported shape-memory polymers respond to a thermal variation, being the temperature in which the shape change induced defined as "switching" or transformation temperature (T_{trans}). At this temperature, the shape of the materials changes from temporary to permanent shape. The transition temperature of the shape memory is related to the main transitions of the polymers, that is, to the glass transition (T_g) or the melting temperature (T_m), being often the SMPs subcategorized as T_g- or T_m-based SMPs [10].

The permanent shape could be fixed by physical interactions (physical bonds, forming interpenetrating networks or/and similar structures) or chemical interactions (covalent bonds). These interactions form the network capable to establish the shape memory and the bonded sites are commonly termed as netpoints. Although both interactions could successfully form SMP, chemical cross-linked SMP establish more stable permanent shape. A general shape-memory transition scheme is depictured in Fig. 1. It is important to notice that every SMP presents two key components that could define the permanent shape and the triggering zones, these are the netpoints and switching domains [11, 12]. The switching domains could be fixed by crystallization and vitrification of the SM polymer depending on the main thermal transition, T_g or T_m [9].

Among all the polymeric materials used to fabricate SMPs, biodegradable polymers have emerged as interesting materials. Their biodegradability made them highly suitable materials to develop temporal biomedical devices (i.e., sutures, catheters, and stents) that could be absorbed in the human body avoiding the necessity of being removed then after their implantation. The other, not less important, aspect is that an adequate synthesis of these BSMP could allow obtaining a transition temperature close to body temperature.

2 Biodegradable Shape-Memory Polymers (BSMP)

The use of biodegradable polymers has arisen due to the growing environmental concerns. The environmental issues are derived from the disposable polymers. Biodegradable polymers are promising materials capable of replacing the most commonly used petroleum-based polymers. The bio-based materials have been synthesized from microorganisms (polyhydroxyalkanoates, (PHAs)), by diverse polymerizations (polylactic acid (PLA)) or from biomass (starch). In addition, some widely used biodegradable polymers have petroleum-based origin, such as poly(ε-caprolactone) (PCL) and several aliphatic polyesters, among others [13–15]. In general, these polymers present in their structure hydrolytically or enzymatically breakable groups, including esters, amides, carbamates, or similar groups.

The degradability of biodegradable polymers is considered essential in some biomedical applications. The biodegradability added to the shape-memory properties has given rise to the interest on biodegradable shape-memory polymers (BSMP). The main advantages of BSMP are the capacity of adapting their shape, due to the shape memory, and the possibility to avoid a second surgery to remove the device since they are biodegraded in the body. The exposition to biological fluid and/or tissues allows the biodegradation of these polymers.

2.1 Poly(Lactide) and Its Derivatives

Poly(lactide) (PLA) and their derivatives are one of the most widely used class of BSMP. Poly(L-lactide) (PLLA) presents good mechanical strength, biocompatibility, and biodegradability, making it highly desirable for biomedical applications. However, PLLA presents some limitations such as reduced hydrophilicity and processability, and high crystallinity and rigidity [16]. In addition, significant variations on its properties have been described depending on its microstructure. That is, poly(L-lactide) (PLLA) is semicrystalline whereas poly(D, L-lactide) (PDLLA) is amorphous. PLLA presents a T_g between 60 and 65 °C and a T_m of 175 °C, besides PDLLA a T_g of 55–60 °C [14, 17].

The crystalline region of PLLA has been used as a permanent physical network, being the shape-memory drive its T_g [18–20]. In addition, some authors have described shape-memory effect based on physical cross-links in its copolymers [21, 22]. Among the PLA-based copolymers, poly(lactide-co-glycolide) has emerged as very important materials in biomedicine and several studies have reported the shape-memory effect on materials based on this polymer [23–25].

2.2 *Poly(caprolactone)*

Poly(ε-caprolactone) is a semicrystalline polymer prepared by ring-opening polymerization from ε-caprolactone, a seven-membered cyclic monomer. It has a T_g around −60 °C and T_m between 59 and 64 °C. But it degrades more slowly than PLLA [26, 27]. Salvekar et al. [28] have reported the shape-memory effect (SME) of unmodified PCL at low temperatures. Both copolymerization process and/or cross-linking make PCL with tailored mechanical and shape-memory properties. Since the T_g is below zero, the shape memory is triggered by T_m. So the modification of the $T_{m,}$ by blending, by copolymerization of PCL, or by adding a covalent network modulates the shape-memory effect of PCL [29–33]. As an example, some authors [33–35] have described PCL-based semicrystalline polymers with SME prepared by Diels–Alder reaction.

2.3 *Other Polymers*

There are limited examples of BSMP non-related with PLA and PCL, being polyurethane-based materials the most used after these main groups [36, 37]. Wang and co-workers [38] have reported the polyurethane-based poly(lactide-co-p-dioxane) BSMP synthesized by diosiisocyanate and butanediamine.

Less used but also present are natural polysaccharide-based BSMPs. Starch-based shape-memory polymers have good SME compared with some synthetic SMP as was reported by Véchambre et al. [39, 40]. In addition, chitosan has been used in several BSMP formulations with epoxy compounds to develop biodegradable materials [41].

3 Applications of Shape-Memory Polymers

There are numerous applications in which shape-memory polymers could be used such as intelligent packaging, sensors, self-repairing bodies of cars, or electrodomestics [42]. However, shape-memory polymers have emerged in the last decades as an important class of materials mainly for biomedical applications. One of the first attempts to apply this kind of materials was described by Echigo and co-workers in 1990 [43]. In their study, an occlusion device for a percutaneous ductus arteriosus occlusion technique was described based on the shape-memory effect of polynorbornene. In addition, the use of biodegradable polymers for biomedical applications has significantly improved their applicability. Lendlein and Langer were pioneers in the use of biodegradable shape-memory polymers in biomedical applications, describing temperature-responsive shape-memory self-tightening sutures fabricated with caprolactone oligomers [3].

Biodegradable shape-memory polymers usually present low toxicity, excellent biocompatibility, and tunable properties which, added to their shape-memory capability, make them a highly interesting type of multifunctional materials. This multifunctionality could be essential to develop advanced medical devices used for minimally invasive surgery. The main applications of these materials in biomedicine are in implantable devices, drug delivery, tissue engineering, stents, and wound closure.

3.1 Tissue Engineering

Injuries, traumas, and several diseases could produce tissue degeneration in the human body. Since conventional tissue transplantation from the same or another patient is not always available, the need to regenerate these damaged tissues has given rise to the so-called tissue engineering. The shape-memory capacity of the BSMP added to the biodegradability allows the facile implantation of the device and the biodegradation of the scaffold once the tissue has been regenerated [44, 45]. BSMP-based scaffolds have been developed for different tissue regenerations such as skeletal muscle [46–48], nerve [25, 49, 50], or vascular tissue [51]; however, the main application of these materials is bone tissue regeneration [52–56].

The pioneering studies in this area had focused on the development of 2D scaffolds. Neuss et al. [57] studied the influence of the shape-memory effect on the cell adhesion onto poly(ε-caprolactone)dimethacrylate (PCLDMA) scaffolds and the biocompatibility of this material. Oligo(ε-caprolactone)dimethacrylate (PCLDMA) networks were obtained by photocuring of the DMA into a mold above the T_m of the material (52 °C). Cylindrical samples 12 mm in diameter and sample weight approx. 100 mg were used as scaffolds for biological tests. They reported the cytocompatibility of PCLDMA with three primary cell types (*Human mesenchymal stem cells* (hMSC), *Human omentum majus cells* (HOMC), and *Rat omentum majus cells* (ROMC)). The direct influence of thermally activated shape memory on the adhered cells was evaluated for the first time. After activation of the shape-memory effect, the cell monolayer was disconnected, the shears forces induced by the shape variation reduced the cells present in the surface (some cells underwent apoptosis), although no necrotic cells were observed by the authors. In addition, this study revealed that temperature elevation that triggers the shape memory did not affect the cell survival, being the mechanical stimulation responsible for the cell monolayer disruption. It is worthy to notice that 3D cell culture by using 3D scaffolds has arisen as a highly interesting method. Several advantages have been described for this method. Among others, it could promote levels of cell differentiation and tissue organization that the 2D culture systems are not capable to reach [58].

BSMP-based 3D scaffolds have also been developed for tissue regeneration. Several strategies have been used to fabricate this kind of structures, such as casting, [59, 60] electrospinning [56], or 3D printing [61, 62]. As an example, Bao and co-workers [56] studied the osteoblast adhesion and growth on poly(D,L-lactide-co-trimethylene carbonate) (PDLLA-co-TMC) scaffolds fabricated by electrospinning technique.

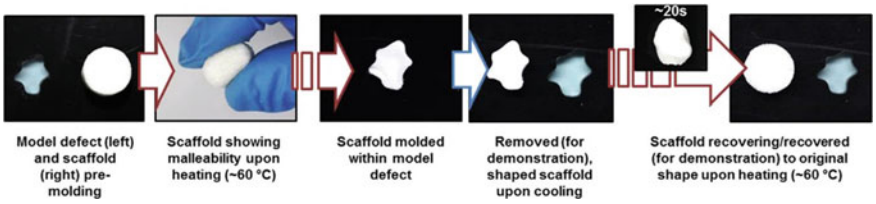

Fig. 2 Simulation of the implantation of biodegradable shape-memory scaffold adapted to an irregular bone defect. Reproduced from Woodard et al. [63] with permission. Copyright 2017. ACS

They reported the excellent biocompatibility of these materials and the good adhesion and proliferation of the osteoblast. The results of biomineralization, including alkaline phosphatase (ALP) expression and mineral deposition, were reported. These results give information about the effectiveness of the bone formation in PDLLA-co-TMC scaffolds. The studies revealed that the biomineralization-relevant alkaline phosphatase expression and mineral deposition in vitro were promoted, that is, the material presents good bone-forming ability.

Another possible application of biodegradable shape-memory polymer scaffolds is to repair bone defects. The capability of BSMP to adapt their shape makes them highly interesting materials to repair irregular bone defects. In this context, Woodard et al. [60] reported the use of shape-memory scaffolds fabricated by solvent casting. They used poly(ε-caprolactane)-poly(L-lactic acid) semi-interpenetrating networks to repair irregular cranial bone defects. These biodegradable structures were capable to successfully fit in irregular cranial defects and to improve the osteointegration. In Fig. 2, a simulation of the designed device is shown.

Shape-memory capability of these materials could modify the surface topography allowing the control over cell orientation, growth, and differentiation. Several authors have reported that the microgrooves present on BSMP surfaces could induce aligned cell culture. When the shape recovery is triggered, anisotropic topographies change to flat featureless surface, this loss of the topography decreases the cell alignment without losing their viability. The control over the cell orientation allows the control of cellular function/differentiation [64–68]. An excellent example of this behavior was described by Mengsteab and co-workers [65]. The fabricated PCL-based surfaces patterned with nanogrooves are capable to switch their orientation at 32–37 °C; this reorganization allows the regulation of cellular differentiation, maturation, and function. In this case, the shape transition is thermally triggered, and induces a variation of 90º on the nanogroove pattern. This variation produces a modification on the contractile direction and structural organization of cardiomyocyte sheets (Fig. 3).

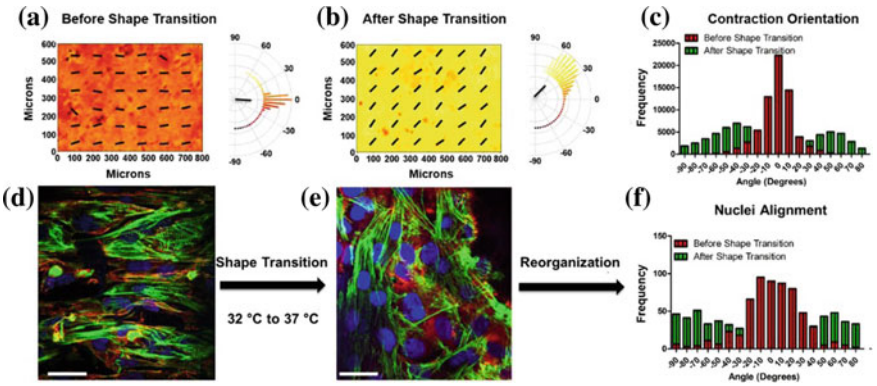

Fig. 3 Contraction analysis of cardiac cell monolayer reorganization culture on PCL-based SMP before and after its shape transition. **a** and **b** indicate the direction of contraction at each location in the heat map and the semicircular histograms indicate the directionality of contracting cardiac cells before and after shape transition, respectively. Pictures **d** and **e** are examples of images of NRVM alignment on surfaces before and after the transition, respectively. Reproduced from Mengsteab and co-workers [65] with permission. Copyright 2016 Elsevier

3.2 Wound Closure Devices

In endoscopic surgeries, one real challenge is tying a knot which is able to press wound lips together with the adequate stress to close the wound. When the force is too strong, necrosis of the surrounding tissue can occur, whereas for a force too weak, scar tissue has poorer mechanical properties, and hernias formation could be induced [3]. As a response to this, biodegradable shape-memory polymers have a special importance to solve this problem since these materials are capable to tying themselves and their removal is not necessary, because they degrade within a controlled time interval. These sutures could be loosely applied in their temporary shape and then heated above the critical temperature (T_{trans}) to trigger the shape recovery and tighten the knot, applying the optimum force [3, 69–71]. An opposite behavior was described by Huang et al. in their study and they have reported self-untying properties [72].

First, BSMP-based sutures were prepared by Lendlein and Langer. BSMP fibers used as sutures were fabricated from multi-block copolymers by ring-opening polymerization of oligo(ε-caprolactone)diol and oligo(p-dioxane)diol and linked by 2,2(4)-trimethylhexanediisocyanate [3]. These materials were successfully used in a rat belly, the BSMP-based suture is first stretched to an elongation ratio of 200% and then the temporary shape is fixed. The wound was closed loosely with the shape-memory fiber at 20 °C. Then, by increasing the temperature, the shape-memory effect is activated and as the result, the wound is perfectly closed [3, 9, 22, 27, 73].

3.3 Stents

The treatment of coronary arterial stenosis (vascular obstruction diseases) can be performed by the implantation of stents during percutaneous transluminal coronary angioplasty. The use of balloon-expandable coronary stents was approved in 1994 by the Food and Drug Administration (FDA). However, the first clinical application of a metallic stent was carried out in 1986. Since then, many advances have been made in the field of stent engineering, improving both the design and the materials used in their development. Metal stents can produce a re-narrowing of the artery after 6 months, increasing the possibility of being blocked again. These first-generation stents, also, needed to overcome some limitations such as low flexibility, stiffness and compliance mismatches, or thrombogenicity, among others. Many materials have been used in the improvement of these devices, being biodegradable shape-memory polymers are the most attractive candidates [74–77].

One of the first stents developed with BSMP was the so-called Igaki-Tamai stent. This self-expansible stent is fabricated with PLLA and is capable to recover its shape at 37 °C in 20 min [78]. Another example of PLLA-based biodegradable stent is a bi-layered poly-l-lactic acid (PLLA) and polyglycolic acid (PLGA) device, which is fully degradable at biological conditions [79].

Several other BSMPs have been used for stent fabrication such as PCL, PLGA, PHBV, and chitosan, among others. PCL-based stents have been extensively studied. Nagata et al. have developed photocurable and biodegradable PCL/PEG copolymers with T_{trans} that could be tailored in the 37–60 °C temperature range [80]. Block copolymers of PCL and PHBV were studied by Xue and co-workers reporting a complete self-expansion at body temperature within 25 s, much faster shape transition than most of these devices [81].

Some studies have reported the successful use of chitosan as a main material for biodegradable shape-memory stents [82]. Nonthermal stimuli-responsive biodegradable stent was developed by Chen et al. Chitosan was cross-linked with an epoxy compound to obtain the biodegradable material used for the stent. The shape-memory effect was trigged by a hydration of chitosan segments, obtaining a rapid transition (∼150 s), which is advantageous because it avoids the migration of the device during its in vivo use [41].

Recently, Zheng and co-workers [13] have reported a biocompatible shape-memory stents of poly(propylene carbonate) (PPC)/polycaprolactone (PCL) blends, which showed a fast response and self-expansion at 37 °C (Fig. 4). These devices present adequate blood biocompatibility, biodegradation, and drug release capability.

Moreover, triple-shape-memory stents have been described by Bellin et al. [83]. They developed two triple-shape-memory systems, one based on PCL and poly(cyclohexyl methacylate) (PCHMA) and other based on PCL and PEG. These materials could allow the fabrication of removable stents that could be inserted in a compressed shape (A). Once they are adequately placed, they can be expanded, shape (B), and contracted to shape (C) when they are going to be removed.

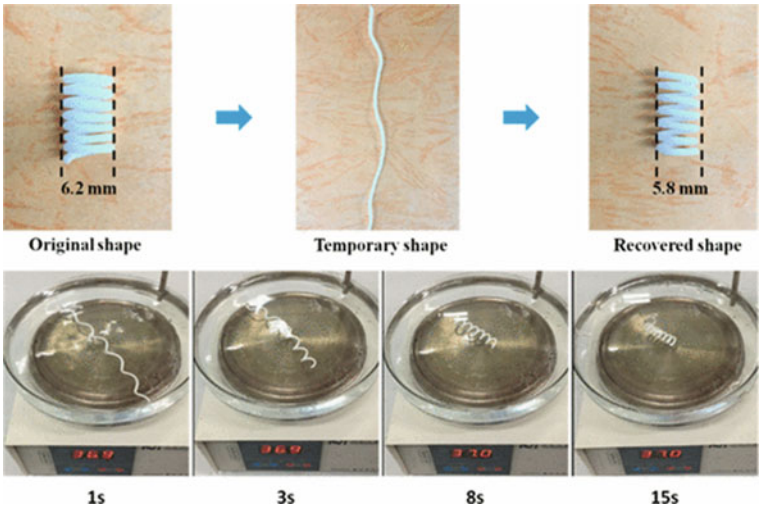

Fig. 4 Images of shape-memory stents based on poly(propylene carbonate)/polycaprolactone blends designed by Zheng et al. [13]. Reproduced from Zheng et al. with permission. Copyright 2017. ACS

Finally, drug-eluting stents (DESs) are one of the most recent developed approaches to prevent in-stent restenosis (ISR). It has been demonstrated that the local drug delivery reduces restenosis rate. Mainly, the drugs used in this kind of stent have antibacterial properties, and some devices have also incorporated antiplatelet drugs [84–90]. An example of BSMP-based drug-eluting stents has been reported by Yang and co-workers [91]. They fabricated a stent by cross-linking PEG-PCL copolymer loaded with a mitomycin C and curcumin. The stent is capable to recover a spiral shape (permanent) from a linear shape (temporal) with a transition temperature around body temperature (Fig. 5). The biological results reveal that the release of mitomycin C and curcumin reduces platelet adhesion in the early stages and inhibits smooth muscle cell hyperproliferation.

3.4 Embolization

Sub-arachnoid hemorrhage from aneurysm rupture could severely debilitate a patient or even cause death [92, 93]. Most common treatment method of this disease since is minimally invasive for the patients which is based on occlusion Guglielmi detachable coils (GDCs) and derivative devices. However, even if these platinum devices require a small incision for their collocation, there are several complications associated to this procedure, such as a low endothelial cell attachment, low fill volume (of coils in the aneurysm) and coil compaction, shifting, or migration. The use of BSMP in this kind of devices has been focused in two strategies: (a) coating platinum devices

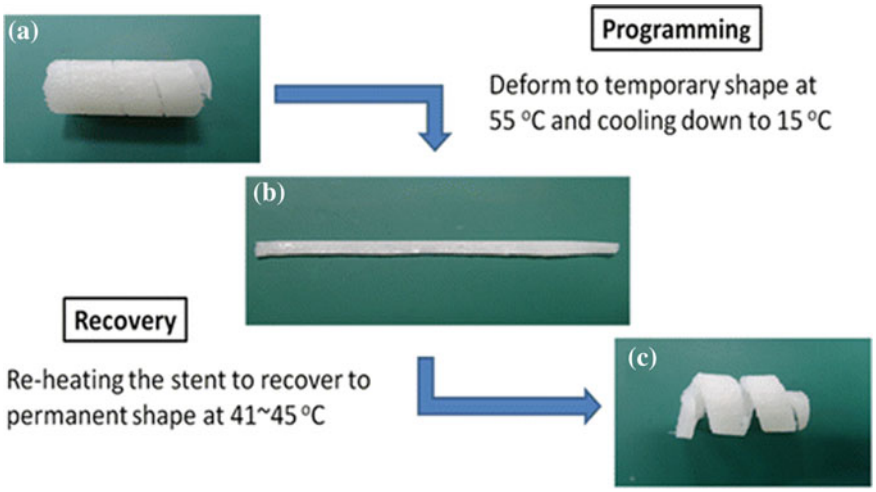

Fig. 5 Shape-memory effect of a cross-linked PEG-PCL reported by Yang et al. **a** permanent shape of the stent, **b** temporary shape, and **c** permanent shape recovery after the thermal stimulus. Reproduced from Yang et al. [91], with permission. Copyright 2013. ACS

(coils) with a polyurethane-based foam [94–96] and (b) design devices constructed entirely by shape-memory polymers [97–99].

BSMPs-based polyurethanes present low thrombogenicity and biocompatibility being widely used in the construction of hematology-related devices. The shape-memory effect of these materials combined with the elastic recovery of foams could present useful properties for an occlusive material for embolization [100]. In addition, the possible risk associated with using a coil design has increased the interest on this type of BSMP foams for aneurysm occlusion. In these devices, a compacted foam is delivered to the aneurysm, and a change in the temperature activates the shape-memory effect leading to the expansion of the foam and filling of the cavity (Fig. 6).

A great effort has been made in the last years in the development of embolization devices based on biodegradable SMP. In this context, it is interesting to notice the preliminary in vivo studies of BSMP foams reported by Rodriguez et al. showing promising results. This work reported a complete vessel wall formation in a porcine aneurysm [94]. Similarly, recent studies have also reported the use of biodegradable SMP based on polyurethane foams as peripheral occlusion devices in order to control abnormal blood flow through vessels. Peripheral occlusion devices could successfully block or reduce the direct blood flow reducing pain, dysfunction, and potential hemorrhage associated with venous insufficiency [101, 102].

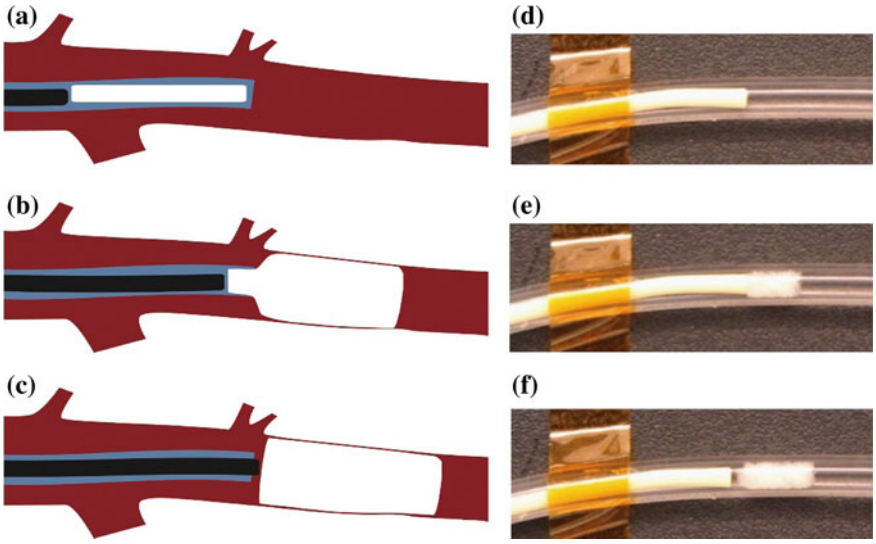

Fig. 6 Schematic diagram of endovascular occlusion device based on BSMP foam: **a** the device is pushed near catheter tip by the guidewire, **b** the guidewire pushes the device out of the catheter, and **c** then fills the vessel lumen. **d–f** In vitro demonstration of developed occlusion device in 37 °C. Reproduced from Rodriguez et al. [98], with permission. Copyright 2014. Elsevier

3.5 Drug release

Biodegradable shape-memory polymers, in contrast with classic SMP, are multifunctional materials capable of having at least two functions; however, there are few examples of materials that present not only shape-memory effect and biodegradation but also a drug releasing capability [4, 103]. The biodegradability of these kinds of drug delivery systems (DDS) is crucial, since it could avoid the surgical removal of the implant or device. In contrast with hydrogels, in which their drug release is based on the swelling capability, SMPs present low swell, so their diffusion coefficients are low. This low diffusion, added to their toughness, makes fabricating devices capable of releasing the embedded drugs over long periods of time.

In this context, the drug delivery based on shape-memory polymers could be divided into two types: (a) drug release induced or enhanced by shape-memory effect or (b) drug release independent from shape memory [103, 104]. In addition to the shape-memory effect, the biodegradability of BSMP could have influence on drug releasing process, since drug diffusion could be increased due to the degradation of the polymer matrix, increasing the release rate as the degradation advances. It is important to notice that this delivery based on a degradation process is slower than processes of the common DDS, such as hydrogels and nanoparticles, being the release prolonged along the lifetime of the BSMP.

Only a few examples in which shape memory and drug release are related have been reported until now. These drug delivery systems described a polymer matrix with cavities filled with drug and covered with polymer without shape memory that after a deformation breaks the non-shape-memory cover releasing the drug. Bao et al. [23] fabricated a drug delivery system based on PLGA microspheres with a shape-memory effect triggered by ultrasound that is capable to successfully release lysozyme when the shape memory is activated.

However, the most developed drug carriers are based on systems in which release and shape memory are independent [22, 103, 105–107]. The key requirements for designing a device in this kind of delivery systems are (1) shape-memory effect and degradation behavior should not be modified by drugs, (2) diffusion controlled release should be enabled, which is independent of the SMP biodegradation, and (3) the shape programming and recovery processes, which a device should undergo during its implantation should not change the drug release kinetics [4]. The presence of the drug could vary the T_g and T_m of the polymer matrix. This could change the shape-memory behavior of the materials. This variation has been reported in many developed systems in which the presence of drugs loaded in the polymer matrix reduces shape-memory behavior [105–107], being in some cases responsible for a complete loss of the shape-memory effect [108].

4 Conclusion and Future Perspectives

The versatility of biodegradable shape-memory polymers allows their adaptation to the different requirements demanded by biomedical applications. In addition, the capability to tailor some of the properties such as chemical stability, biocompatibility, flexibility, and biodegradability, along with their ability as drug carrier, will potentiate the research based in the development of SMPs.

Such a combination of functions, biodegradability, shape memory, and drug delivery capability is demanded by biomaterial-assisted therapies, scaffold materials for reconstructive or aesthetic surgery, and in tissue engineering applications. Multimaterial systems presently applied in these areas cannot fulfill the demands, so materials that combine the three functions will receive a high interest.

Even more, the use of biodegradable materials not only allows the use as a drug carrier and avoids the necessity of being removed after their use in the body, but also is highly used to reduce environmental problems derived from plastic waste.

Acknowledgements This work has been funded by UPV/EHU (IT718-13), MINECO (MAT2017-89553-P).

References

1. Kim J, Lee JE, Lee SH et al (2008) Designed fabrication of a multifunctional polymer nanomedical platform for simultaneous cancer-targeted imaging and magnetically guided drug delivery. Adv Mater 20:478–483. https://doi.org/10.1002/adma.200701726
2. Alexander C, Shakesheff KM (2006) Responsive polymers at the biology/materials science interface. Adv Mater 18:3321–3328. https://doi.org/10.1002/adma.200502640
3. Lendlein A, Langer R (2002) Biodegradable, elastic shape-memory polymers for potential biomedical applications. Science 80, 296:1673–1676. https://doi.org/10.1126/science.1066102
4. Neffe AT, Hanh BD, Steuer S, Lendlein A (2009) Polymer networks combining controlled drug release, biodegradation, and shape memory capability. Adv Mater 21:3394–3398. https://doi.org/10.1002/adma.200802333
5. Bikiaris DN (2013) Nanocomposites of aliphatic polyesters: an overview of the effect of different nanofillers on enzymatic hydrolysis and biodegradation of polyesters. Polym Degrad Stab 98:1908–1928. https://doi.org/10.1016/j.polymdegradstab.2013.05.016
6. Stocum DL (1998) Regenerative biology and engineering: strategies for tissue restoration. Wound Repair Regen 6:276–290. https://doi.org/10.1046/j.1524-475X.1998.60404.x
7. Lendlein A, Jiang H, Jünger O, Langer R (2005) Light-induced shape-memory polymers. Nature 434:879–882. https://doi.org/10.1038/nature03496
8. Yu Y, Ikeda T (2005) Photodeformable polymers: A new kind of promising smart material for micro- and nano-applications. Macromol Chem Phys 206:1705–1708. https://doi.org/10.1002/macp.200500318
9. Behl M, Lendlein A (2007) Shape-memory polymers. Mater Today 10:20–28. https://doi.org/10.1016/S1369-7021(07)70047-0
10. Hu J, Zhu Y, Huang H, Lu J (2012) Recent advances in shape-memory polymers: Structure, mechanism, functionality, modeling and applications. Prog Polym Sci 37:1720–1763. https://doi.org/10.1016/j.progpolymsci.2012.06.001
11. Parameswaranpillai J, Ramanan SP, George JJ et al (2018) PEG- ran -PPG modified epoxy thermosets: a simple approach to develop tough shape memory polymers. Ind Eng Chem Res 57:3583–3590. https://doi.org/10.1021/acs.iecr.7b04872
12. Parameswaranpillai J, Ramanan SP, Jose S et al (2017) Shape memory properties of Epoxy/PPO-PEO-PPO triblock copolymer blends with tunable thermal transitions and mechanical characteristics. Ind Eng Chem Res 56:14069–14077. https://doi.org/10.1021/acs.iecr.7b03676
13. Zheng Y, Li Y, Hu X et al (2017) Biocompatible shape memory blend for self-expandable stents with potential biomedical applications. ACS Appl Mater Interfaces 9:13988–13998. https://doi.org/10.1021/acsami.7b04808
14. Nair LS, Laurencin CT (2007) Biodegradable polymers as biomaterials. Prog Polym Sci 32:762–798. https://doi.org/10.1016/j.progpolymsci.2007.05.017
15. Tian H, Tang Z, Zhuang X et al (2012) Biodegradable synthetic polymers: Preparation, functionalization and biomedical application. Prog Polym Sci 37:237–280. https://doi.org/10.1016/j.progpolymsci.2011.06.004
16. Södergård A, Stolt M (2002) Properties of lactic acid based polymers and their correlation with composition. Prog Polym Sci 27:1123–1163. https://doi.org/10.1016/S0079-6700(02)00012-6
17. Xu J, Song J (2015) Polylactic acid (PLA)-based shape-memory materials for biomedical applications. Shape Mem Polym Biomed Appl 197–217. https://doi.org/10.1016/b978-0-85709-698-2.00010-6
18. Wong YS, Xiong Y, Venkatraman SS, Boey FYC (2008) Shape memory in un-cross-linked biodegradable polymers. J Biomater Sci Polym Ed 19:175–191. https://doi.org/10.1163/156856208783432516

19. Meng B, Wang J, Zhu N et al (2006) Study of biodegradable and self-expandable PLLA helical biliary stent in vivo and in vitro. J Mater Sci Mater Med 17:611–617. https://doi.org/10.1007/s10856-006-9223-9
20. Wong YS, Venkatraman SS (2010) Recovery as a measure of oriented crystalline structure in poly(l-lactide) used as shape memory polymer. Acta Mater 58:49–58. https://doi.org/10.1016/j.actamat.2009.08.075
21. Lu XL, Cai W, Gao ZY (2008) Shape-memory behaviors of biodegradable poly(L-lactide-co-ε-caprolactone) copolymers. J Appl Polym Sci 108:1109–1115. https://doi.org/10.1002/app.27703
22. Lendlein A, Kelch S (2002) Shape-Memory Effect From permanent shape. Angew Chemie 41:2034–2057. https://doi.org/10.1016/1433-7851/02/4112-2035
23. Bao M, Zhou Q, Dong W et al (2013) Ultrasound-modulated shape memory and payload release effects in a biodegradable cylindrical rod made of chitosan-functionalized PLGA microspheres. Biomacromolecules 14:1971–1979. https://doi.org/10.1021/bm4003464
24. Matsumura S, Hlil AR, Lepiller C et al (2008) Ionomers for proton exchange membrane fuel cells with sulfonic acid groups on the end-groups: novel branched poly(ether-ketone)s. Am Chem Soc Polym Prepr Div Polym Chem 49:511–512. https://doi.org/10.1002/pola
25. Chen C, Hu J, Huang H et al (2016) Design of a smart nerve conduit based on a shape-memory polymer. Adv Mater Technol 1:1–10. https://doi.org/10.1002/admt.201600015
26. Woodruff MA, Hutmacher DW (2010) The return of a forgotten polymer—polycaprolactone in the 21st century. Prog Polym Sci 35:1217–1256. https://doi.org/10.1016/j.progpolymsci.2010.04.002
27. Lendlein A, Kelch S (2005) Degradable, multifunctional polymeric biomaterials with shape-memory. Mater Sci Forum 492–493:219–224. https://doi.org/10.4028/www.scientific.net/MSF.492-493.219
28. Salvekar AV, Zhou Y, Huang WM et al (2015) Shape/temperature memory phenomena in uncrosslinked poly-ε-caprolactone (PCL). Eur Polym J 72:282–295. https://doi.org/10.1016/j.eurpolymj.2015.09.027
29. Zarek M, Mansour N, Shapira S, Cohn D (2017) 4D printing of shape memory-based personalized endoluminal medical devices. Macromol Rapid Commun 38:1–6. https://doi.org/10.1002/marc.201600628
30. Yang P, Zhu G, Shen X et al (2016) Poly(ϵ-caprolactone)-based shape memory polymers crosslinked by polyhedral oligomeric silsesquioxane. RSC Adv 6:90212–90219. https://doi.org/10.1039/c6ra20431g
31. Defize T, Riva R, Raquez JM et al (2011) Thermoreversibly crosslinked poly(ε-caprolactone) as recyclable shape-memory polymer network. Macromol Rapid Commun 32:1264–1269. https://doi.org/10.1002/marc.201100250
32. Erndt-Marino JD, Munoz-Pinto DJ, Samavedi S et al (2015) Evaluation of the osteoinductive capacity of polydopamine-coated poly(-caprolactone) diacrylate shape memory foams. ACS Biomater Sci Eng 1:1220–1230. https://doi.org/10.1021/acsbiomaterials.5b00445
33. Dolynchuk O, Kolesov I, Jehnichen D et al (2017) Reversible shape-memory effect in cross-linked linear poly(ϵ-caprolactone) under stress and stress-free conditions. Macromolecules 50:3841–3854. https://doi.org/10.1021/acs.macromol.7b00481
34. Zou W, Dong J, Luo Y, et al (2017) Dynamic covalent polymer networks: from old chemistry to modern day innovations. Adv Mater. https://doi.org/10.1002/adma.201606100
35. Defize T, Riva R, Jérôme C, Alexandre M (2012) Multifunctional Poly (ε -caprolactone) -forming networks by Diels–Alder cycloaddition: effect of the adduct on the shape-memory properties. Macromol Chem Phys 213:187–197. https://doi.org/10.1002/macp.201100408
36. Weems AC, Wacker KT, Carrow JK et al (2017) Shape memory polyurethanes with oxidation-induced degradation: in vivo and in vitro correlations for endovascular material applications. Acta Biomater 59:33–44. https://doi.org/10.1016/j.actbio.2017.06.030
37. Weems AC, Szafron JM, Easley AD et al (2017) Shape memory polymers with enhanced visibility for magnetic resonance- and X-ray imaging modalities. Acta Biomater 54:45–57. https://doi.org/10.1016/j.actbio.2017.02.045

38. Wang Y, Huang M, Luo Y, Li Y (2010) In vitro degradation of poly(lactide-co-p-dioxanone)-based shape memory poly(urethane-urea). Polym Degrad Stab 95:549–556. https://doi.org/10.1016/j.polymdegradstab.2009.12.016
39. Véchambre C, Buléon A, Chaunier L et al (2011) Understanding the mechanisms involved in shape memory starch: macromolecular orientation, stress recovery and molecular mobility. Macromolecules 44:9384–9389. https://doi.org/10.1021/ma202019v
40. Véchambre C, Buléon A, Chaunier L et al (2010) Macromolecular orientation in glassy starch materials that exhibit shape memory behavior. Macromolecules 43:9854–9858. https://doi.org/10.1021/ma101704k
41. Chen MC, Tsai HW, Chang Y et al (2007) Rapidly self-expandable polymeric stents with a shape-memory property. Macromolecules 8:2774–2780. https://doi.org/10.1021/bm7004615
42. Ratna D, Karger-Kocsis J (2008) Recent advances in shape memory polymers and composites: a review. J Mater Sci 43:254–269. https://doi.org/10.1007/s10853-007-2176-7
43. Echigo S, Matsuda T, Kamiya T, et al (1990) Development of a new transvenous patent ductus arteriosus occlusion technique using a shape memory polymer. ASAIO J. 36
44. Hardy JG, Palma M, Wind SJ, Biggs MJ (2016) Responsive biomaterials: advances in materials based on shape-memory polymers. Adv Mater 28:5717–5724. https://doi.org/10.1002/adma.201505417
45. Wu Y, Wang L, Zhao X et al (2016) Self-healing supramolecular bioelastomers with shape memory property as a multifunctional platform for biomedical applications via modular assembly. Biomaterials 104:18–31. https://doi.org/10.1016/j.biomaterials.2016.07.011
46. Deng Z, Guo Y, Zhao X et al (2016) Stretchable degradable and electroactive shape memory copolymers with tunable recovery temperature enhance myogenic differentiation. Acta Biomater 46:234–244. https://doi.org/10.1016/j.actbio.2016.09.019
47. Zhao X, Dong R, Guo B, Ma PX (2017) Dopamine-Incorporated dual bioactive electroactive shape memory polyurethane elastomers with physiological shape recovery temperature, high stretchability, and enhanced C2C12 myogenic differentiation. ACS Appl Mater Interfaces 9:29595–29611. https://doi.org/10.1021/acsami.7b10583
48. Xie M, Wang L, Guo B et al (2015) Ductile electroactive biodegradable hyperbranched polylactide copolymers enhancing myoblast differentiation. Biomaterials 71:158–167. https://doi.org/10.1016/j.biomaterials.2015.08.042
49. Tao J, Hu Y, Wang S et al (2017) A 3D-engineered porous conduit for peripheral nerve repair. Sci Rep 7:1–13. https://doi.org/10.1038/srep46038
50. Kai D, Tan MJ, Prabhakaran MP et al (2016) Biocompatible electrically conductive nanofibers from inorganic-organic shape memory polymers. Colloids Surfaces B Biointerfaces 148:557–565. https://doi.org/10.1016/j.colsurfb.2016.09.035
51. Cha KJ, Lih E, Choi J et al (2014) Shape-memory effect by specific biodegradable polymer blending for biomedical applications. Macromol Biosci 14:667–678. https://doi.org/10.1002/mabi.201300481
52. Xie R, Hu J, Hoffmann O et al (2018) Self-fitting shape memory polymer foam inducing bone regeneration: a rabbit femoral defect study. Biochim Biophys Acta Gen Subj 1862:936–945. https://doi.org/10.1016/j.bbagen.2018.01.013
53. Turnbull G, Clarke J, Picard F et al (2018) 3D bioactive composite scaffolds for bone tissue engineering. Bioact Mater 3:278–314. https://doi.org/10.1016/j.bioactmat.2017.10.001
54. Xie R, Hu J, Ng F et al (2017) High performance shape memory foams with isocyanate-modified hydroxyapatite nanoparticles for minimally invasive bone regeneration. Ceram Int 43:4794–4802. https://doi.org/10.1016/j.ceramint.2016.11.216
55. Baker RM, Tseng LF, Iannolo MT et al (2016) Self-deploying shape memory polymer scaffolds for grafting and stabilizing complex bone defects: a mouse femoral segmental defect study. Biomaterials 76:388–398. https://doi.org/10.1016/j.biomaterials.2015.10.064
56. Bao M, Lou X, Zhou Q et al (2014) Electrospun biomimetic fibrous scaffold from shape memory polymer of PDLLA- co -TMC for bone tissue engineering. ACS Appl Mater Interfaces 6:2611–2621. https://doi.org/10.1021/am405101k

57. Neuss S, Blomenkamp I, Stainforth R et al (2009) The use of a shape-memory poly(ε-caprolactone)dimethacrylate network as a tissue engineering scaffold. Biomaterials 30:1697–1705. https://doi.org/10.1016/j.biomaterials.2008.12.027
58. Huh D, Hamilton GA, Ingber DE (2011) From 3D cell culture to organs-on-chips. Trends Cell Biol 21:745–754. https://doi.org/10.1016/j.tcb.2011.09.005
59. Zheng X, Zhou S, Li X, Weng J (2006) Shape memory properties of poly(d, l-lactide)/hydroxyapatite composites. Biomaterials 27:4288–4295. https://doi.org/10.1016/j.biomaterials.2006.03.043
60. Zhang D, George OJ, Petersen KM et al (2014) A bioactive "self-fitting" shape memory polymer scaffold with potential to treat cranio-maxillo facial bone defects. Acta Biomater 10:4597–4605. https://doi.org/10.1016/j.actbio.2014.07.020
61. Senatov FS, Niaza KV, Zadorozhnyy MY et al (2016) Mechanical properties and shape memory effect of 3D-printed PLA-based porous scaffolds. J Mech Behav Biomed Mater 57:139–148. https://doi.org/10.1016/j.jmbbm.2015.11.036
62. Senatov FS, Zadorozhnyy MY, Niaza KV et al (2017) Shape memory effect in 3D-printed scaffolds for self-fitting implants. Eur Polym J 93:222–231. https://doi.org/10.1016/j.eurpolymj.2017.06.011
63. Woodard LN, Kmetz KT, Roth AA et al (2017) Porous poly(ϵ-caprolactone)-Poly(l-lactic acid) semi-interpenetrating networks as superior, defect-specific scaffolds with potential for cranial bone defect repair. Biomacromolecules 18:4075–4083. https://doi.org/10.1021/acs.biomac.7b01155
64. Ebara M, Uto K, Idota N et al (2014) The taming of the cell: shape-memory nanopatterns direct cell orientation. Int J Nanomed 9:117–126. https://doi.org/10.2147/IJN.S50677
65. Mengsteab PY, Uto K, Smith AST et al (2016) Spatiotemporal control of cardiac anisotropy using dynamic nanotopographic cues. Biomaterials 86:1–10. https://doi.org/10.1016/j.biomaterials.2016.01.062
66. Ebara M, Uto K, Idota N et al (2012) Shape-memory surface with dynamically tunable nano-geometry activated by body heat. Adv Mater 24:273–278. https://doi.org/10.1002/adma.201102181
67. Davis KA, Burke KA, Mather PT, Henderson JH (2011) Dynamic cell behavior on shape memory polymer substrates. Biomaterials 32:2285–2293. https://doi.org/10.1016/j.biomaterials.2010.12.006
68. Shou Q, Uto K, Lin WC et al (2014) Near-infrared-irradiation-induced remote activation of surface shape-memory to direct cell orientations. Macromol Chem Phys 215:2473–2481. https://doi.org/10.1002/macp.201400353
69. Jing X, Mi HY, Huang HX, Turng LS (2016) Shape memory thermoplastic polyurethane (TPU)/poly(ε-caprolactone) (PCL) blends as self-knotting sutures. J Mech Behav Biomed Mater 64:94–103. https://doi.org/10.1016/j.jmbbm.2016.07.023
70. Zhang H, Wang H, Zhong W, Du Q (2009) A novel type of shape memory polymer blend and the shape memory mechanism. Polymer (Guildf) 50:1596–1601. https://doi.org/10.1016/j.polymer.2009.01.011
71. Bai Y, Jiang C, Wang Q, Wang T (2013) A novel high mechanical strength shape memory polymer based on ethyl cellulose and polycaprolactone. Carbohydr Polym 96:522–527. https://doi.org/10.1016/j.carbpol.2013.04.026
72. Huang WM, Song CL, Fu YQ et al (2013) Shaping tissue with shape memory materials. Adv Drug Deliv Rev 65:515–535. https://doi.org/10.1016/j.addr.2012.06.004
73. Lendlein A, Kelch S (2005) Shape-memory polymers as stimuli-sensitive implant materials. Clin Hemorheol Microcirc 32:105–116
74. Serruys PW, Kutryk MJB, Ong ATL (2006) Coronary-artery stents. N Engl J Med 354:483–495. https://doi.org/10.1056/NEJMra051091
75. Palmaz JC (2004) Intravascular stents in the last and the next 10 years. J Endovasc Ther 11:II-200-II-206. https://doi.org/10.1583/04-1363.1
76. Hu T, Yang C, Lin S et al (2018) Biodegradable stents for coronary artery disease treatment: Recent advances and future perspectives. Mater Sci Eng, C 91:163–178. https://doi.org/10.1016/j.msec.2018.04.100

77. Wang R, Zhang F, Lin W et al (2018) Shape Memory properties and enzymatic degradability of poly(ε-caprolactone)-based polyurethane urea containing phenylalanine-derived chain extender. Macromol Biosci 18:1800054. https://doi.org/10.1002/mabi.201800054
78. Tamai H, Igaki K, Kyo E et al (2000) Initial and 6-month results of biodegradable poly-l-lactic acid coronary stents in humans. Circulation 102:399–404. https://doi.org/10.1161/01.CIR.102.4.399
79. Venkatraman SS, Tan LP, Joso JFD et al (2006) Biodegradable stents with elastic memory. Biomaterials 27:1573–1578. https://doi.org/10.1016/j.biomaterials.2005.09.002
80. Nagata M, Inaki K (2011) Biodegradable and photocurable multiblock copolymers with shape-memory properties from poly(ε-caprolactone) diol, poly(ethylene glycol), and 5-cinnamoyloxyisophthalic acid. J Appl Polym Sci 120:3556–3564. https://doi.org/10.1002/app.33531
81. Xue L, Dai S, Li Z (2010) Biomaterials Biodegradable shape-memory block copolymers for fast self-expandable stents. Biomaterials 31:8132–8140. https://doi.org/10.1016/j.biomaterials.2010.07.043
82. Lauto A, Ohebshalom M, Esposito M et al (2001) Self-expandable chitosan stent: Design and preparation. Biomaterials 22:1869–1874. https://doi.org/10.1016/S0142-9612(00)00371-9
83. Bellin I, Kelch S, Langer R, Lendlein A (2006) Polymeric triple-shape materials. Proc Natl Acad Sci 103:18043–18047. https://doi.org/10.1073/pnas.0608586103
84. Kraitzer A, Kloog Y, Zilberman M (2008) Approaches for prevention of restenosis. J Biomed Mater Res Part B Appl Biomater 85:583–603. https://doi.org/10.1002/jbm.b.30974
85. Jang HS, Nam HY, Kim JM et al (2009) Effects of curcumin for preventing restenosis in a hypercholesterolemic rabbit iliac artery stent model. Catheter Cardiovasc Interv 74:881–888. https://doi.org/10.1002/ccd.22047
86. Nakazawa G, Finn AV, Kolodgie FD, Virmani R (2009) A review of current devices and a look at new technology: drug-eluting stents. Expert Rev Med Devices 6:33–42. https://doi.org/10.1586/17434440.6.1.33
87. Huang S, Wang YY-J, Ge S et al (2010) Quantification of Staphylococcus epidermidis using a wireless, mass-responsive sensor. Sensors Actuat B Chem 150:412–416. https://doi.org/10.1016/j.snb.2010.06.037
88. Puranik AS, Dawson ER, Peppas NA (2013) Recent advances in drug eluting stents. Int J Pharm 441:665–679. https://doi.org/10.1016/j.ijpharm.2012.10.029
89. McFadden EP, Stabile E, Regar E et al (2004) Late thrombosis in drug-eluting coronary stents after discontinuation of antiplatelet therapy. Lancet 364:1519–1521. https://doi.org/10.1016/S0140-6736(04)17275-9
90. Parker T, Dave V, Falotico R (2010) Polymers for drug eluting stents. Curr Pharm Des 16:3978–3988. https://doi.org/10.2174/138161210794454897
91. Yang CS, Wu HC, Sun JS et al (2013) Thermo-induced shape-memory PEG-PCL copolymer as a dual-drug-eluting biodegradable stent. ACS Appl Mater Interfaces 5:10985–10994. https://doi.org/10.1021/am4032295
92. Connolly ES, Rabinstein AA, Carhuapoma JR et al (2012) Guidelines for the management of aneurysmal subarachnoid hemorrhage: a guideline for healthcare professionals from the American heart association/American stroke association. Stroke 43:1711–1737. https://doi.org/10.1161/STR.0b013e3182587839
93. Murayama Y, Viñuela F, Duckwiler GR et al (1999) Embolization of incidental cerebral aneurysms by using the Guglielmi detachable coil system. J Neurosurg 90:207–214. https://doi.org/10.3171/jns.1999.90.2.0207
94. Rodriguez JN, Clubb FJ, Wilson TS et al (2014) In vivo response to an implanted shape memory polyurethane foam in a porcine aneurysm model. J Biomed Mater Res Part A 102:1231–1242. https://doi.org/10.1002/jbm.a.34782
95. Hampikian JM, Heaton BC, Tong FC et al (2006) Mechanical and radiographic properties of a shape memory polymer composite for intracranial aneurysm coils. Mater Sci Eng C 26:1373–1379. https://doi.org/10.1016/j.msec.2005.08.026

96. Landsman TL, Touchet T, Hasan SM et al (2017) A shape memory foam composite with enhanced fluid uptake and bactericidal properties as a hemostatic agent. Acta Biomater 47:91–99. https://doi.org/10.1016/j.actbio.2016.10.008
97. Rodriguez JN, Clubb FJ, Wilson TS et al (2013) In vivo response to an implanted shape memory polyurethane foam in a porcine aneurysm model. J Biomed Mater Res Part A 102:1231–1242. https://doi.org/10.1002/jbm.a.34782
98. Rodriguez JN, Miller MW, Boyle A et al (2014) Reticulation of low density shape memory polymer foam with an in vivo demonstration of vascular occlusion. J Mech Behav Biomed Mater 40:102–114. https://doi.org/10.1016/j.jmbbm.2014.07.037
99. Small W IV, Gjersing E, Herberg JL et al (2009) Magnetic resonance flow velocity and temperature mapping of a shape memory polymer foam device. Biomed Eng Online 8:1–7. https://doi.org/10.1186/1475-925X-8-42
100. Metcalfe A, Desfaits AC, Salazkin I et al (2003) Cold hibernated elastic memory foams for endovascular interventions. Biomaterials 24:491–497. https://doi.org/10.1016/S0142-9612(02)00362-9
101. Nathan AL, Fletcher GK, Monroe MBB et al (2017) Particulate release from nanoparticle-loaded shape memory polymer foams. J Med Device 11:011009. https://doi.org/10.1115/1.4035547
102. Landsman TL, Bush RL, Glowczwski A et al (2016) Design and veri fi cation of a shape memory polymer peripheral occlusion device. J Mech Behav Biomed Mater 63:195–206. https://doi.org/10.1016/j.jmbbm.2016.06.019
103. Wischke C, Neffe AT, Lendlein A (2010) Controlled drug release from biodegradable shape-memory polymers. In: Lendlein A (ed) Shape-memory polym. Springer, Berlin Heidelberg, Berlin, Heidelberg, pp 177–205
104. Peterson GI, Dobrynin AV, Becker ML (2017) Biodegradable Shape Memory Polymers in Medicine. Adv Healthc Mater 6:1700694. https://doi.org/10.1002/adhm.201700694
105. Wischke C, Neffe AT, Steuer S et al (2010) AB-polymer networks with cooligoester and poly(n-butyl acrylate) segments as a multifunctional matrix for controlled drug release. Macromol Biosci 10:1063–1072. https://doi.org/10.1002/mabi.201000089
106. Wischke C, Neffe AT, Steuer S, Lendlein A (2010) Comparing techniques for drug loading of shape-memory polymer networks—effect on their functionalities. Eur J Pharm Sci 41:136–147. https://doi.org/10.1016/j.ejps.2010.06.003
107. Kashif M, Yun BM, Lee KS, Chang YW (2016) Biodegradable shape-memory poly(ε-caprolactone)/polyhedral oligomeric silsequioxane nanocomposites: Sustained drug release and hydrolytic degradation. Mater Lett 166:125–128. https://doi.org/10.1016/j.matlet.2015.12.051
108. Nagahama K, Ueda Y, Ouchi T, Ohya Y (2009) Biodegradable shape-memory polymers exhibiting sharp thermal transitions and controlled drug release. Biomacromolecules 10:1789–1794. https://doi.org/10.1021/bm9002078

Optical, Electrical, and Magnetic Properties of Shape-Memory Polymers, Polymer Blends, and Composites

Yu Zheng, Jiabin Shen and Shaoyun Guo

Abstract The polymeric shape-memory materials, which generally trigger the shape-memory effect (SME) via direct heating, have been the rising star in the field of smart materials. Recently, numerous efforts have been paid to explore the alternative methods for realizing SME by indirect actuation, for further extending the practical application. Incorporation of functional groups or/and fillers is the most convenient route to endow the shape-memory matrix with enhanced properties of inductive heating, which has been rapidly developed to achieve new stimulus-responsive behavior. Herein, the novel functions of the shape-memory polymers, polymer blends, and composites including optical, electrical, and magnetic properties will be introduced. Moreover, the operative mechanism and optimization method of the different properties will be substantially discussed considering the composition change, morphology control, and structure design as well as the filler type, concentration, and dispersion. Finally, an outlook is presented describing the future challenges of this promising field.

1 Introduction

Shape-memory polymers (SMPs), as a kind of intelligent materials, can afford capacity to recover from the temporary shape to the initial state upon an external stimulus [1–3]. Commonly, the shape-memory effect (SME) is realized based on a reversible thermal reaction. As the SMPs are heated above the switching temperature (T_s), the molecular chain would be activated to trigger the shape recovery progress. However, the thermo-responsive SMPs can only work by direct heating, which extremely limits their applications in some specific environments, such as in body and aerospace.

For further extending the capacity of SMPs, a great deal of work has been conducted to explore the alternative methods for triggering SME by indirect actuation

Y. Zheng · J. Shen (✉) · S. Guo
State Key Laboratory of Polymer Materials Engineering, Polymer Research Institute of Sichuan University, Chengdu 610065, Sichuan, People's Republic of China
e-mail: shenjb@scu.edu.cn

J. Parameswaranpillai et al. (eds.), *Shape Memory Polymers, Blends and Composites*, Advanced Structured Materials 115,
https://doi.org/10.1007/978-981-13-8574-2_11

[4–8]. With respect to the SMPs relying on thermal effect, the key point is to heat the materials to a temperature above T_s. Hence, the stimuli which can induce temperature rise are all theoretically feasible to be applied. Inspired by that, different kinds of functional groups or/and fillers are introduced into SMPs to achieve the enhanced properties of inductive heating. By so far, various original triggering means have been demonstrated in literatures, in which the photoirradiation, application of electrical or magnetic field are the most frequently investigated [7, 8].

With incorporation of light-sensitive fillers or/and groups, such as the carbon nanoparticles, cinnamic acid, and azobenzene groups, SMPs can obtain optical properties of photothermal effect (PTE) and reversible photochemical reaction under light irradiation [9]. The former one can convert the light energy into heat and induce temperature rise to trigger SME, which is similar to the thermal effect. In contrast, the latter one acting as the shape-memory switch can achieve SME by using light of alternative wavelength (λ) instead of increasing the sample's temperature. Since light can travel a long distance, it is easy to realize remote activation of molecular motion inside materials. Moreover, the spatially controlled recovery is achievable via micro-localized light stimulation. Particularly, the light-responsive processes can be halted and resumed "on-demand" by turning the light off and on. With these advantages, the light-responsive SMPs (LSMPs) provide a great potential to be applied as biomedical instruments, photonics, and photo-driven actuators [10–12].

As another typical heating source, Joule heating created by passing the electricity through the conductive network is the most convenient one of all kinds of indirect stimulation. On the basis of the Joule's law, the heat generated in unit time at a certain voltage is governed by the electrical property of the SMP composites (SMPCs). Hence, the challenge for realizing fast electrical response is optimizing the conductivity. With this regard, many chemical and physical methods, including ultrasonic treatment, surface modification, hybrid fillers, and assembly of conductive channels and layers, have been carried out to improve the distribution of conductive fillers (e.g., carbon nanotubes (CNTs), carbon black (CB), and graphene), for ensuring the efficient transfer of their electrical property to the SMP matrix [4]. On the other hand, fillers can usually promote the mechanical properties of SMPs, resulting in a stronger recovery stress to execute some mechanical works. These superior performances develop the electro-responsive SMPCs (ESMPCs) to be used as smart actuators, which are important in extensive applications such as self-deployable instruments for aerospace environment valuation and related testing [13].

Besides, the inductive heating can be also achieved by the creation of magnetic-responsive SMPCs (MSMPCs). In an alternating magnetic field (AMF), the magnetic nanoparticles can generate heat through eddy current loss, hysteresis loss, or/and additional mechanisms dominated by the sizes of the particles [14, 15]. When a deformed MSMPC is heated by the fillers to a temperature exceeded T_s, shape recovery would be observed. Numerous types of magnetic nanoparticles, such as

Ni, Fe, Fe_2O_3, and Fe_3O_4, have been used to fabricate MSMPCs. In addition, different methods have been employed to enhance the dispersion of fillers, including solution mixing, in situ polymerization, and surface modification, for better spreading of the magnetic-induced heat into the SMP matrix [16]. With the advantages of remote and spatial control provided by magnetic stimulus, MSMPCs can be designed and tailored to meet potential applications such as biomedical devices, drug release, sensors, etc. [17, 18].

In this chapter, the above three different functions resulting from adding groups or/and fillers to shape-memory matrix will be sufficiently discussed: optical property (Sect. 2), electrical property (Sect. 3), and magnetic property (Sect. 4). The new stimulation ways developed by these properties will be highlighted. Moreover, different methods to tailor and optimize the corresponding property are comprehensively introduced. Finally, an outlook on the future research trends of this promising field will be presented.

2 Optical Properties

2.1 Optical Response

After incorporating with light-sensitive groups or/and fillers, SMPs would be endowed with light-responsive property to realize SME through light irradiation. As schematically shown in Fig. 1, two common routes are known in the literature. The first method is based on the reversible photochemical reaction, such as the reversible photocross-linking. In this case, light plays a role in both processes of the temporary shape fixation and permanent shape recovery, thus the stimulation has no relation with the temperature effect. In contrast, the second strategy is to heat the SMPs to $T > T_s$ by PTE, and light is used only for triggering the shape recovery progress but is not involved in the formation of temporary shape.

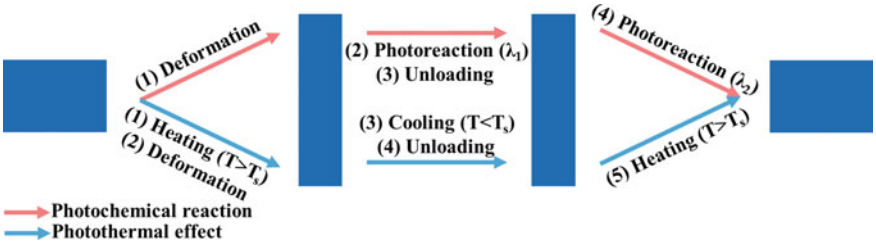

Fig. 1 Schematic illustration of the light-responsive shape-memory progress based on either the reversible photochemical reactions or PTE

2.1.1 Photochemical Reaction

The LSMPs containing photosensitive groups can undergo the desired photochemical reaction via absorption of photons. Instead of directly heating the materials, light is applied to trigger the shape fixation and shape recovery stages. This kind of LSMP was first reported by Lendlein et al. at [19]. In their work, cinnamic acid (CA) and cinnamylidene acetic acid (CAA), which enable efficient reversible [2 + 2] cycloaddition reactions when irradiated with alternating λ, were used as the molecular switches to prepare the amorphous LSMPs. Figure 2 exhibited the light-triggered shape-memory cycle, together with schematic diagram showing the operative mechanism. When the polymer film was deformed by external stretching stress and then was exposed to UV light of λ > 260 nm while maintaining the stress, the new cross-links would be formed through dimerization of CA (Fig. 2A) or CAA (Fig. 2B) groups so that the elongated chain segments could be partially fixed in their uncoiled conformation. After removing the external force, a temporary shape could be fixed without cooling. Upon exposure to UV light of λ < 260 nm, the cross-links were reversibly cleaved and the permanent shape was recovered. By comparison, the sample with CA groups exhibited a better shape recovery performance. However, the efficiency of the temporary shape fixation was rather limited because that the light-induced cross-linking network failed to completely restrain the recovering tendency

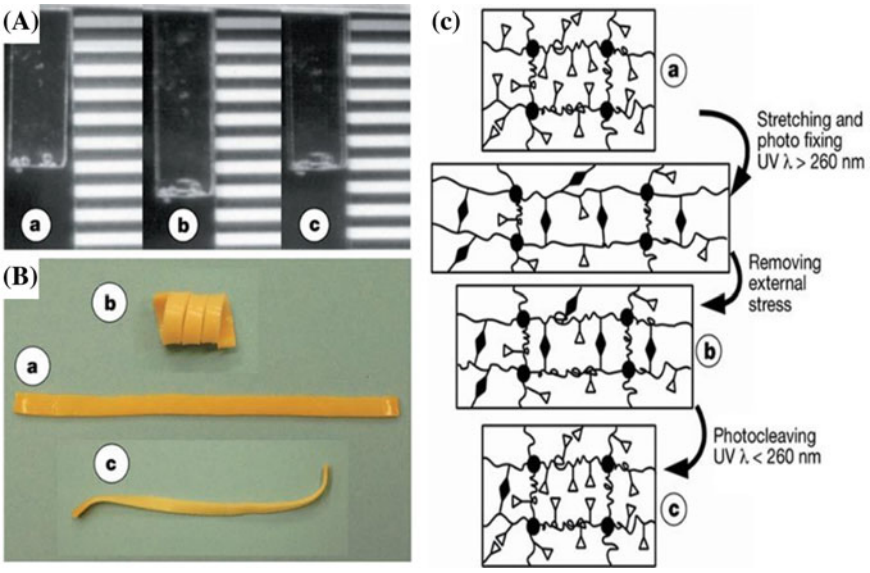

Fig. 2 Light-responsive shape-memory performances: the shape-memory progress of **A** the polymer containing CA side groups upon irradiation of UV light, and **B** the interpenetrating polymer network containing CCA groups exposed to UV light, and **C** the feasible molecular mechanism (photos a, b, and c in each figure are the permanent, temporary, and recovered shapes, respectively). Adapted and reproduced from [19] with permission from Nature Publishing Group

of the deformed sample. Moreover, it was hard to realize a full recovery due to the incomplete photocleavage of the new cross-links [19].

On the basis of the same mechanism, a light-responsive polyesterurethane comprising poly(L-lactide) (PLA) and poly(ε-caprolactone) (PCL) bearing photosensitive cinnamamide pendant groups (CPG) were synthesized. When the deformed sample was exposed to UV light of $\lambda > 260$ nm, the PCL chains would be photocross-linked through the dimerization of CPG, affording ability to fix the temporary shape to some extent after removing the external force. However, the fixity ratio (R_f) of the sample with 20 wt% content of CPG was only 50%. Under the stimulation of UV light of $\lambda < 260$ nm, shape recovery was triggered by photoinduced breakup of cyclobutane bridges between the PCL chains. Moreover, the recovery ratio (R_r) could be optimized to 95% via tailoring the composition of PLA and PCL [20]. In a more recent study, the light-responsive monomer N,N-bis(2-hydroxyethyl)-9-anthracene-methanamine was embedded into poly(ethylene glycol) (PEG), and then this anthracene-functionalized PEG precursor was coupled with PLA to produce a novel LSMP. By applying UV light of alternating λ (365 and 254 nm), this material exhibited SME because of the reversibility of [4 + 4] cycloaddition reaction between pendant anthracene groups [21].

Another typical class of light-responsive material is the azobenzene-containing liquid crystalline network (azo-LCN) possessing ability to realize reversible trans–cis photoisomerization. A light-driven film containing azo-LCN was prepared by thermal cross-linking the liquid-crystal monomer (4′-ethoxy-azobenzyl-4-(6-oxyhexyl-1-alcohol) acrylate, molecular 1) with a diacrylate cross-linker (4,4′-Azo-bis[6′-(phenoxy)hexyl acrylate], molecular 2), both of which have azobenzene moieties (see Fig. 3). The film could be bent upon exposure to 366 nm light at $T > T_g$ and the deformation direction kept parallel to the direction of light polarization. When visible light of $\lambda > 540$ nm was applied to the curly film, it reverted to the initial flat form. As irradiated with the linearly polarized light, the conversion of trans isomer into cis isomer of the azobenzene moieties would induce reduction in microscopic size and ordering of the liquid-crystal components, leading to surface contraction along the direction of light. Subsequently, the bending deformation of the film was recovered through visible light irradiation which triggered the configurational change from cis form to trans form [22]. Besides, the bending direction could also be changed to be away from light through aligning the azobenzene mesogens perpendicular to the film surface. This fantastic performance developed the potential application of novel photomechanical devices, such as the light-driven plastic motor [23].

Instead of using light of alternating λ to control the isomerization of azobenzene mesogens, the 442 nm visible light which can simultaneously trigger trans–cis and reverse cis–trans transition was applied to realize SME of azo-LCN at room temperature. As shown in Fig. 4, a bended shape was obtained by irradiation with the linear polarization light (E) whose direction is parallel to the long axis (x) of the sample. Subsequently, the temporary shape was maintained by removing E, and then recovered to the straight form by using circularly polarized light (CPL). Particularly, the fixed shape after exposure with 442 nm light could be maintained for a long time. It was speculated that the stimulation directly changed the entanglement and configu-

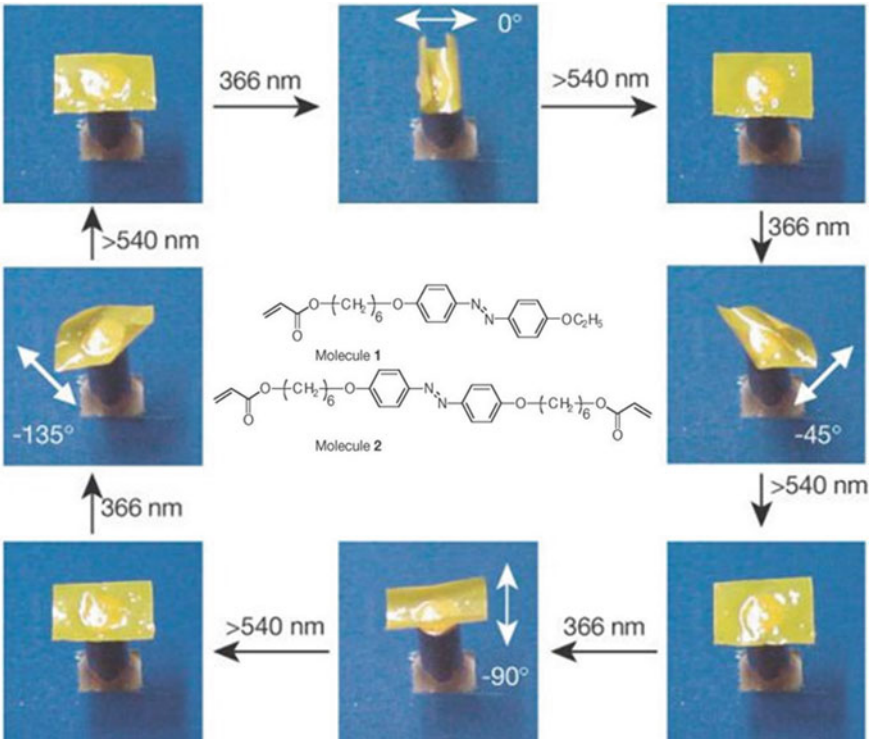

Fig. 3 Chemical structures of the liquid-crystal monomer (molecule 1) and cross-linker (molecule 2), and the photographs of the film bending in different directions as irradiated by linearly polarized light of different polarized angels at 366 nm, and then being recovered to the flat form again by visible light longer than 540 nm. Adapted and reproduced from [22] with permission from Nature Publishing Group

ration of the polymer chains, resulting in the similar effect of thermal fixing of glassy SMP. As exposed with CPL, the reconfigured polymer network was randomized and recovered to its original state [24]. Furthermore, Fig. 5 exhibited that the visible light with tunable oscillation angle could make azobenzene mesogens undergo repeated isomerization back and forth, inducing polarization-controlled bidirectional bending of azo-LCN. Inspired by that, the light-driven cantilevers composed of azo-LCN were produced, and the frequency and amplitude of the oscillations could be tuned by adjusting the sample length, laser beam power density, and air pressure [25–27].

2.1.2 Photothermal Effect

Considering that the shape-memory switch is usually controlled by T_s, the additives or fillers which can induce PTE by strong absorption of light and efficient conversion

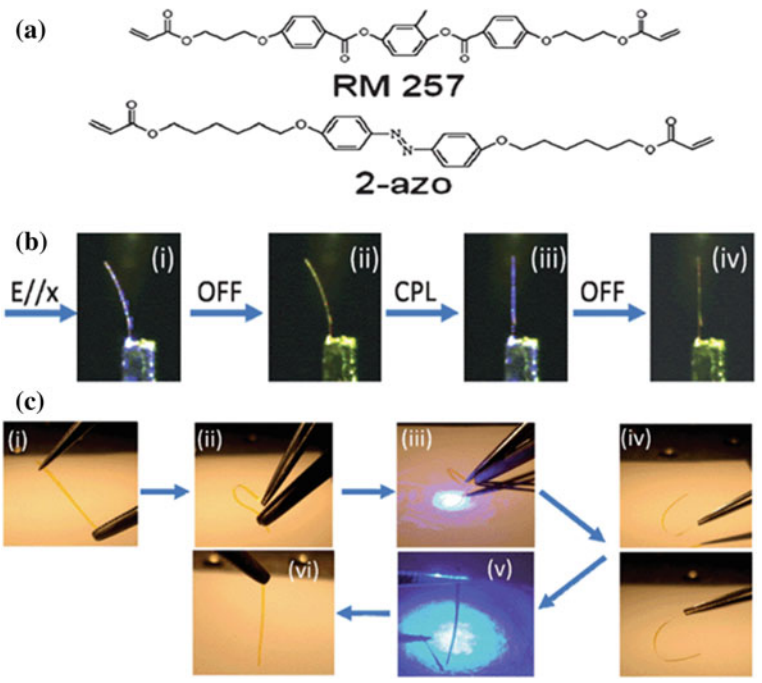

Fig. 4 **a** Chemical structures of the cross-linking monomers and azo-LCN. **b** The bend state of a cantilever formed by exposure to the paralleled E (i), fixation of the bent form after turning off E (ii), recovery to the flat shape upon CPL irradiation (iii), and after turning off the excitation light (iv). **c** Light-responsive shape-memory progress of a freestanding film: the initial shape (i), mechanical bending (ii), fixation by light irradiation (iii), the temporary shape retention after removing the light (iv), shape recovery by exposure to CPL (v), and the recovered shape (vi). Adapted and reproduced from [24] with permission from Royal Society of Chemistry

of light into heat have been used to realize light actuation, such as ligands, CNTs, CB, graphene, and gold particles, among others. Unlike the SME achieved by reversible photochemical reaction, the temporary shape of the photothermal-triggered materials is formed through thermal–mechanical programming and then recovered to the initial form via photoheating.

The organic ligands can be incorporated into the molecular structure to ensure a homogeneous material. Kumpfer and coworkers prepared a light-responsive metallo-supramolecular polymer by adding the metal salts into the covalently cross-linked polybutadiene (PB) end-capped with a metal chelating ligand, 4-oxr-2,6-bis(N-methylbenzimidazolyl). The dynamic metal–ligand complexes separated by the cross-linkable PB core played the key role in determining the fixation and release of the temporary shape. As shown in Fig. 6, the absorbance of 320–390 nm UV light by the ligands would induce PTE and dissociate the metal–ligand complex, allowing the material to be deformed. After removing the light at the temporary shape stage, the new metal–ligand complexes were formed and acted as the cross-links to

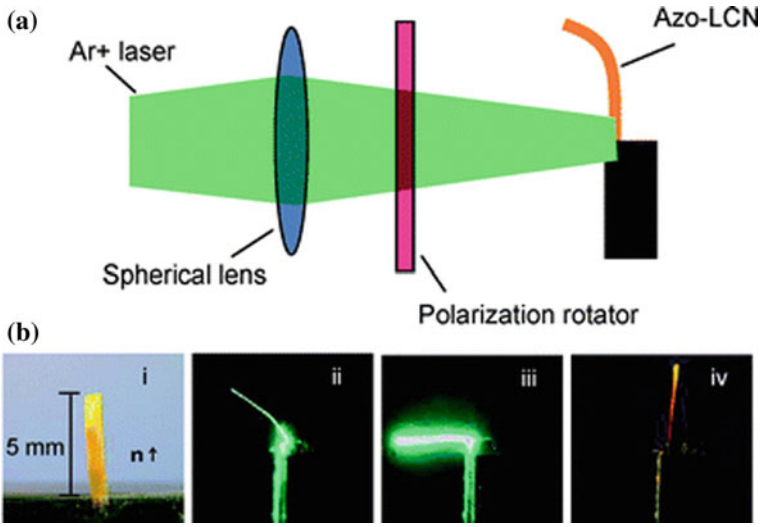

Fig. 5 **a** The optical setup for azo-LCN cantilever: argon-ion (Ar^+) laser, spherical lens, and polarization rotator. **b** The azo-LCN cantilever placed with the nematic director (n) parallel to the x (i), bending 42° as exposed to E polarized orthogonal to n (E⊥n) (ii), bending to almost 90° as exposed to E polarized parallel to n (E//n) (iii), and recovering to its original position upon blocking the laser at any point (iv). Reprinted from [25] with permission from Royal Society of Chemistry

fix the deformation. Upon irradiation with the UV light again, the PTE dissociated the physical cross-links and actuated the shape recovery [28]. In another example, a light-responsive liquid crystalline elastomer was further fabricated via incorporating a mesogenic derivative of the 2,6-bisbenzimidazolylpyridine ligand. As the ligand absorbed UV light, the sample was heated above the liquid crystal transition through PTE, which in turn triggered the shape recovery back to the permanent shape [29].

Unlike the ligands that can be designed as a part of the polymer, the other fillers need to be homogeneously dispersed in the SMP matrix so as to fabricate efficient light-responsive SMPCs (LSMPCs). As early as in 2004, the light-driven recovery has been achieved based on thermoplastic polyurethane (TPU) elastomer incorporating with well-dispersed multiwalled CNTs (MWCNTs). Stretching the material at room temperature induced crystallization of TPU and the newly formed crystals could act as physical cross-links to fix the temporary shape. On exposure to near-infrared (NIR) irradiation, the nanocomposite with only 1 wt% MWCNTs could be heated to the temperature above T_m of the TPU crystals (~48 °C), indirectly triggering the shape recovery progress [30]. In another work, the sulfonated graphene sheets were introduced into TPU to fabricate light-driven actuator with excellent mechanical properties by distribution control. The sample with 1 wt% graphene showed striking contraction from the stretched shape to the permanent state on exposure to NIR light, accompanied by the release of strain energy with energy density of 0.33 J g^{-1} [31]. Additionally, CB with PTE can act as the heating agent to activate shape recovery.

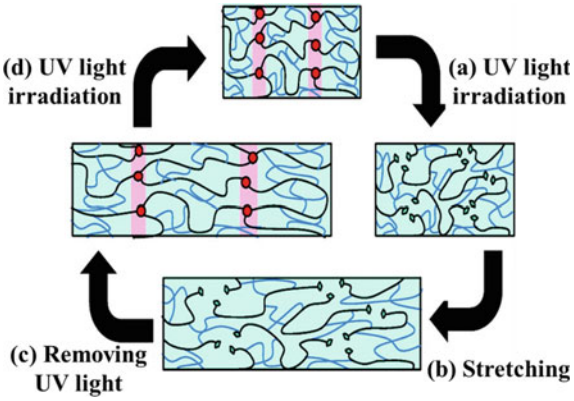

Fig. 6 The shape-memory cycle combining UV light irradiation: **a** dissociation of the metal–ligand complex via UV light irradiation, **b** deforming the sample by manual stretching while irradiated with UV light, **c** removing force and UV light to achieve temporary shape fixation, and **d** shape recovery via UV light irradiation again. Adapted and reproduced from [28] with permission from American Chemical Society

However, the CB filled LSMPCs usually require a higher addition attribute to its relatively lower efficiency in converting the light into heat [32].

Besides, using the hybrid fillers is another ideal strategy for producing LSMPCs. Feng et al. observed the infrared (IR)-responsive SME of TPU incorporated by 1 wt% sulfonated reduced graphene oxide (SRGO)/sulfonated CNT (SCNT) hybrid fillers. When the weight ratio of SRGO to SCNT was 3:1, the TPU nanocomposite showed an outstanding IR-actuated recovery with a high energy density of 0.63 J g^{-1} and recovery stress up to 1.2 MPa, which could lift a 107.6 g weight up to 4.7 cm in only 18 s [33]. Additionally, the hybrid filler network composed of CNTs and boron nitride (BN) was constructed in the epoxy-based SMP to realize IR-induced SME. In the nanocomposite, CNTs were employed to absorb light and convert it into heat and BNs enhanced the heat transfer from CNTs to the polymer matrix, thus synergistically optimizing the shape recovery performance. The sample with 4 wt% BNs and 4 wt% CNTs could finish 100% recovery under IR irradiation within 60 s [34]. In a more recent work, a hyperbranched polyurethane (HPU)-based SMPC incorporating hybrid filler of TiO_2 and RGO was presented. The nanocomposite system could self-deploy under sunlight stimulation and demonstrate excellent R_r of 91–95% [35]. Moreover, Yu et al. designed a multicomponent LSMPC consisting of three typical segments, neat epoxy, and the p-aminodiphenylimide (p-Ap)/epoxy and MWCNTs/epoxy composites. The p-AP and MWCNTs featuring wavelength-selective and micro-localized light-responsive behavior not only acted as photoabsorbers to induce SME but also as functional components to accurately control the quantity of temporary shapes and the shape recovery process. With the segmental structure and multifunctional property, the LSMPC could exhibit multi-

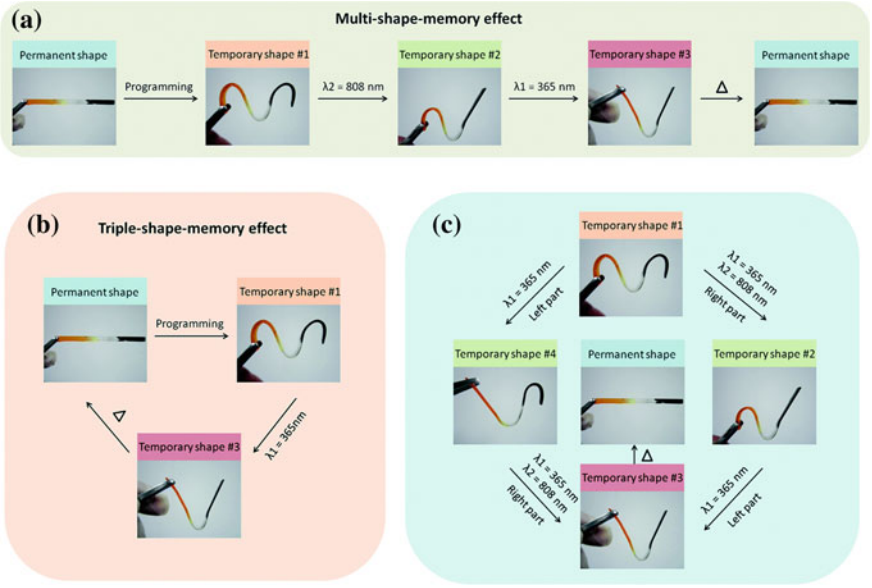

Fig. 7 Pictures exhibiting the micro-localized and photo-manipulatable shape recovery processes of a wavelength-selective multicomposite: **a** multi-shape-memory effect achieved by irradiation with light of $\lambda 2 = 808$ nm and $\lambda 1 = 365$ nm, **b** triple-shape-memory effect achieved by only irradiation with light of $\lambda 1 = 365$ nm, and **c** photo-manipulation of shape recovery processes by micro-localized light irradiation. Reprinted from [36] with permission from Royal Society of Chemistry

shape-memory behavior through the designed shape programming process combined with photo-manipulation procedure, as exhibited in Fig. 7 [36].

Except the carbon fillers, gold nanorods (AuNRs) and gold nanoparticles (AuNPs) can also convert light into heat through the surface plasmon resonance. Hribar et al. investigated the PTE of an SMPC produced by cross-linking the amorphous poly(tertbutyl acrylate) with poly(β-amino ester) and AuNRs. With an extremely low content of AuNRs (<1 vol%), the composite could be heated to above its T_g by applying the NIR light with intensity of 0.3 w and then finish a full shape recovery [37]. More recently, some further developments in using AuNRs or AuNPs for LSMPCs have been reported [38–40]. As a representative work, the chemically cross-linked poly(ethylene oxide) (PEO) loaded with only 0.5 wt% AuNPs could exhibit photoinduced temperature gradient effect to control polymer chain relaxation and strain energy release. Based on that, the material realized sophisticated and controllable motions upon exposure to 532 nm light, which could be applied to execute mechanical work [40] (Fig. 8).

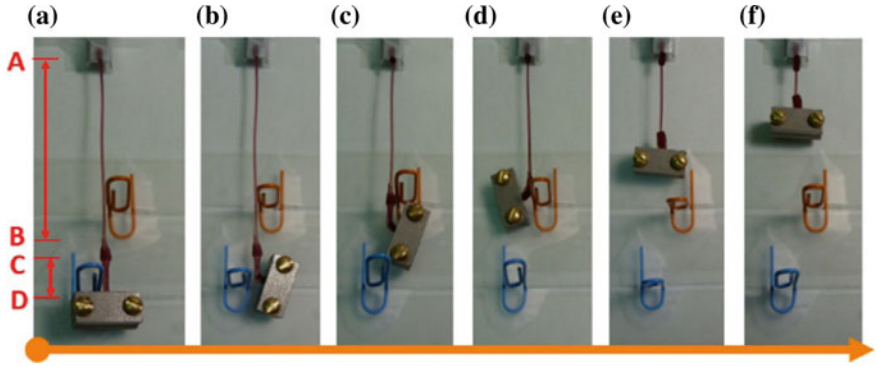

Fig. 8 The light-driven lifting progress of a piece of metal attached to the AuNP-loaded cross-linked PEO. Reprinted from [40] with permission from American Chemical Society

2.2 Optical Reversibility

Generally, the optical properties are significantly influenced by the surficial and internal macrostructures of the materials [41–43]. Since the molecular chains could be deformed and recovered in the shape-memory progress, SMPs are potential to gain reversible optical property. Zheng et al. prepared LSMPs by introducing 0.1–0.2 mol% AuNRs into the SMP composed of bisphenol A diglycidyl ether, and then shaped them into micropillar arrays by pouring the AuNRs-filled LSMP solution into the poly(dimethylsiloxane) (PDMS) mold (10 μm in diameter, 40 μm in height and 20 μm pillar-to-pillar distance), followed by curing at 100 °C for 1.5 h and at 130 °C for 1 h, respectively. A bent form of pillars was obtained through thermal deforming and fixing, and then recovered to the straight form as exposed to visible light. By locally inducing shape recovery with light, switchable optical properties of the film from opaque (bent pillar) to transparent (straight pillar) were realized in the confined region, as shown in Fig. 9 [44]. Similarly, the lightly cross-linked azo-LCN has been used to fabricate light-responsive microstructured surfaces which were covered with micropillar arrays. The SME of azo-LCN actuated by UV light irradiation would induce contraction and recovery of the surfaces, resulting in tunable light transmittance [45].

In addition to LSMPs, the directly thermal-induced SME has also been employed to explore reversible optical properties. Xu et al. prepared some micro-optic components using the cross-linked poly(ethylene-co-vinyl acetate) with thermal SME. The surface features of the micro-optics could be easily tailored in a single step via compression molding. After that, a hot stretching or pressing deformation would reform their surface features to manipulate the corresponding optical property. The opaque thin film could become transparent by compressing the uneven surface into flat form, and regained opacity through heat-induced shape recovery [46]. With the same method of surface structure control, the multilayer shape-memory mate-

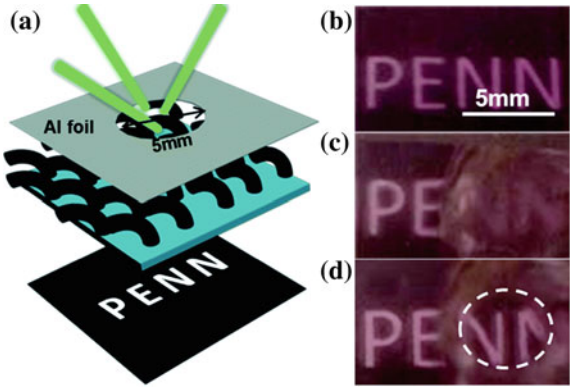

Fig. 9 **a** Schematic illustration of the setup for light exposure. **b–d** Images of the SMP/AuNR micropillars at different stages: **b** pristine pillars, **c** the right half of the sample became opaque by deformation, and **d** the selected domain of the sample regained transparency after laser exposure. Reprinted from [44] with permission from Royal Society of Chemistry

rials containing alternating layers of polyvinyl acetate (PVAc) and PU also realized switchable optical property in the thermal–mechanical cycling progress [47]. In another work, tunable diffractive optical elements (DOEs) were produced based on a transparent TPU SMP. The material could be easily structured with diverse diffractive microstructures by hot embossing, and its diffractive capacity could be further adjusted via thermal–mechanical deformation. Upon exposure to the stimulus heat, the deformed DOE was gradually recovered back to the original state in a predefined way, displaying the morphing diffractive pattern of a height-tunable or a period-tunable structure [48] (Fig. 10).

3 Electrical Properties

Joule heating, which is induced by passing the current through the conductive network, is an ideal heating source for actuating SME. With incorporation of conductive fillers, such as metal particles, CB, CNTs, carbon nanofibers (CNFs), and graphene, SMPs are endowed with electrical property and able to generate heat at an electrical field [4–6]. When the ESMPCs are heated to temperature above T_s, the shape recovery would be triggered, as schematically shown in Fig. 11. According to the Joule's law, the heat generated in unit time at a certain voltage is governed by the conductivity of the composite. Thus, optimizing the electrical property governed by the dispersion of particles is critical for achieving excellent shape-memory performance.

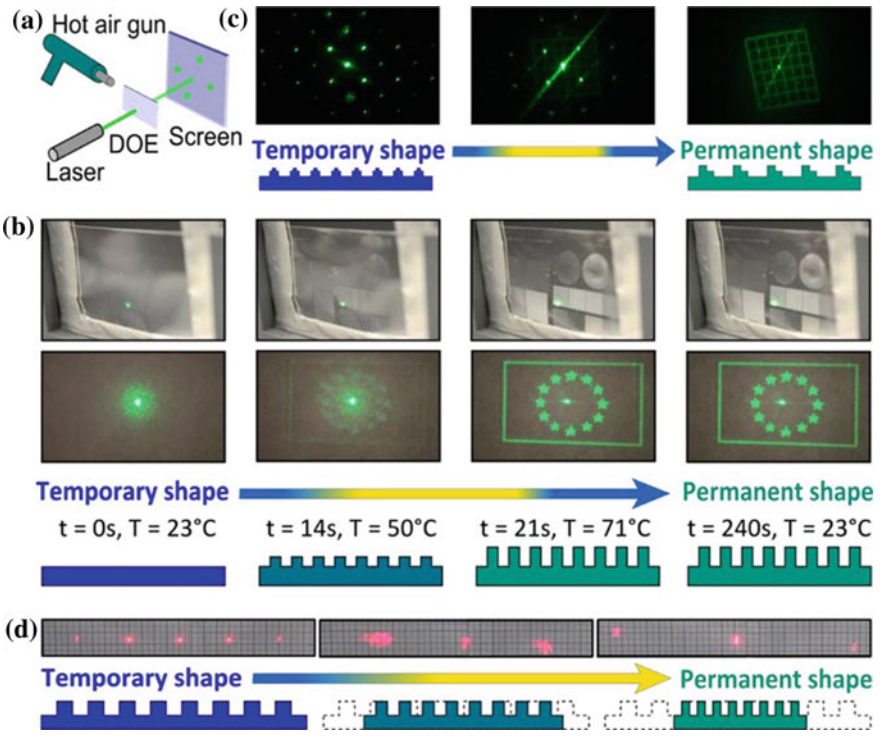

Fig. 10 **a** Schematic of the setup applied to visualize the recovery of the SMP-based DOE. **b–d** The change of diffraction pattern on the screen following the recovery progress of the different temporarily diffractive microstructure: **b** recovery from the temporarily flattened macrostructure to the structure with full height resulted in the change from a blurry spot to the European Union flag; **c** recovery from the temporary 2D phase grating to the complex microstructure resulted in the change from a grid of dots into a grid of lines; and **d** recovery from the stretched sample to the original shape with the smaller grating period resulted in the increasing distance between the maxima of the diffraction pattern. Reprinted from [48] with permission from American Chemical Society

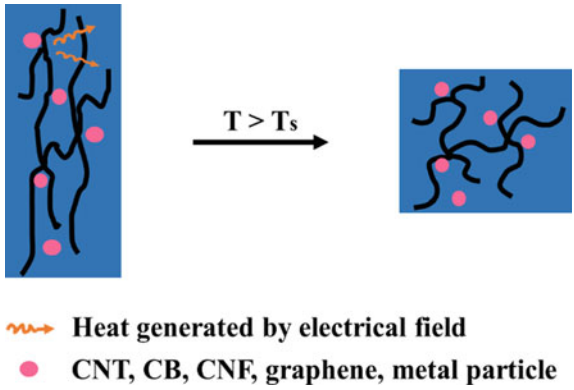

Fig. 11 Schematic illustration of ESMPCs containing diverse fillers as a nanoscale heater upon stimulation of electrical field

3.1 Electrical Property via Improved Dispersion of Conductive Fillers

With the advantages of superior mechanical and electrical properties, CNTs are the efficient agents for improving the conductivity of SMPs. However, CNTs often aggregate into bundles because of their high aspect ratio and van der Waals interactions, limiting the efficient transfer of their conductive property to the SMP matrix [49]. For addressing that issue, both physical and chemical methods have been conducted to improve the dispersion of CNTs. As an example, the ultrasound-assisted in situ polymerization, which can promote the dispersion of CNTs and the formation of conductive networks has been applied to fabricate ESMPCs with enhanced electrical conductivity and responsive speed. By selecting the place where the electrical voltage is applied, the produced composites could even present localized electro-responsive SME (ESME) [50]. Besides, using polymer or surfactant to functionalize the surface of fillers prior to mixing with SMPs is another feasible route to mitigate the aggregation. With incorporation of 5 wt% acid surface-modified MWCNTs, the PU-based ESMPCs could obtain improved mechanical properties and quick electro-induced recovery attributed to the strong interfacial-bonding strength between the polymers and fillers [51]. Appling the same strategy, the efficient ESME was realized via bonding the modified MWCNTs with PU/PLA shape-memory blend (SMPB) as well as PU/poly (vinylidene difluoride) (PVDF) SMPB [52, 53]. In addition, homogeneous dispersion of fillers could also be achieved through polymer-assisted effect without any surface modification. Mahapatra et al. developed an ESMPC by introducing MWCNTs into the synthesized PCL-based hyperbranched PU through solvent casting. It was demonstrated that the branched structure with numerous cavities and surface groups could significantly improve the dispersion of MWCNTs, resulting in improved mechanical properties. As shown in Fig. 12, the hyperbranched PU with 5 wt% MWCNTs finished 98% recovery within only 9 s at 40 V [54].

3.2 Electrical Property via Formation of Double-Percolation Conductive Network

Double-percolation conductive network, which is formed by confined dispersion of conductive fillers in a co-continuous SMPB, can dramatically reduce the percolation threshold, thus giving a promising strategy for fabricating ESMPCs [55]. Wang et al. prepared an ESMPC by chemically cross-linking polycyclooctene (PCO)-MWCNTs/polyethylene (PE) with co-continuous structure and selective distribution of fillers in the PCO phase. The content of MWCNTs in PCO is 15 vol% and the composition ratio of MWCNTs-filled PCO and PE is 70/30 vol%. With the well-separated T_m's, respectively, afforded by PCO and PE, the prepared composites exhibited pronounced triple-shape-memory effect (TSME) on the visual observation by electrical heating at a voltage of 150 V for 2 min, see Fig. 13 [56]. In recent years,

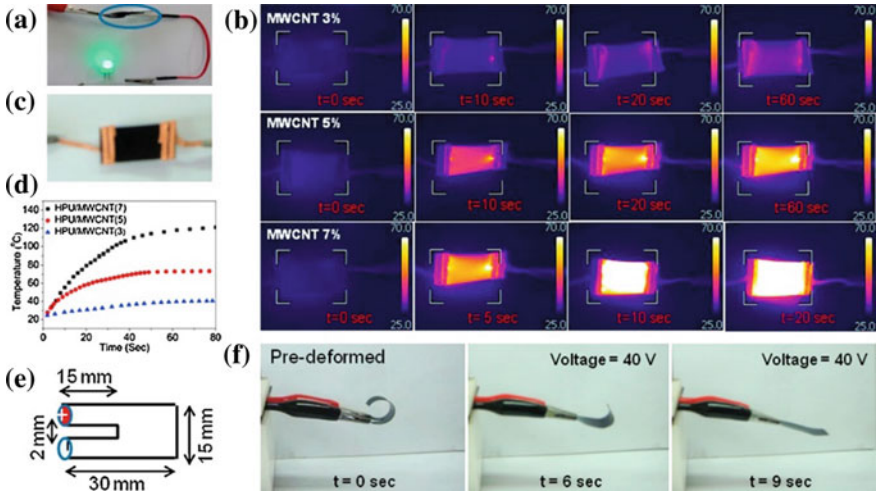

Fig. 12 **a** The hyperbranched PU/MWCNT film showing DC conductivity at 9 V. **b** Forward-looking infrared radar (FLIR) images of nanocomposites. **c** The photograph of FLIR testing sample. **d** Evolution of the surface temperature with conducting time. **e** Dimensions of ESME testing sample. **f** Pictures exhibiting the electro-responsive recovery progress. Reprinted from [54] with permission from Elsevier

Qi and coworkers reported some developments of realizing ESME based on double-percolation effect. They blended PLA with poly(propylene carbonate) (PPC) and tailored the phase structure to be co-continuous via composition control. After that, the MWCNTs were selectively introduced into the PPC phase, and the composite with only three phr MWCNTs could reach R_r of 97% within 30 s at 30 V [57]. The same route was also applied to produce TPU-MWCNTs/PLA and poly(ethylene vinyl acetate) (EVA)-MWCNTs/PCL ESMPCs [58, 59]. Moreover, they transformed the phase morphology of TPU/PLA (70/30 by weight) blend from sea–island structure to co-continuous structure by the self-networking capability of CB nanoparticles. The composites could recover back to their original shape within 80 s at 30 V because of the stronger recovery driving force provided by the high phase continuity and excellent electrical conductivity induced by the double-percolation effect [60].

3.3 Electrical Property via Assembly of Conductive Channels

At an external electric or magnetic field, the electronic polarized CNTs would tend to assemble into conductive chains with electrode distance in micrometer or even nanometer ranges, which can significantly reduce the electrical resistivity of the composites [61, 62]. Inspired by this, Leng et al. conducted many researches on preparing ESMPCs via assembling of conductive channels. A simple way was employed to sig-

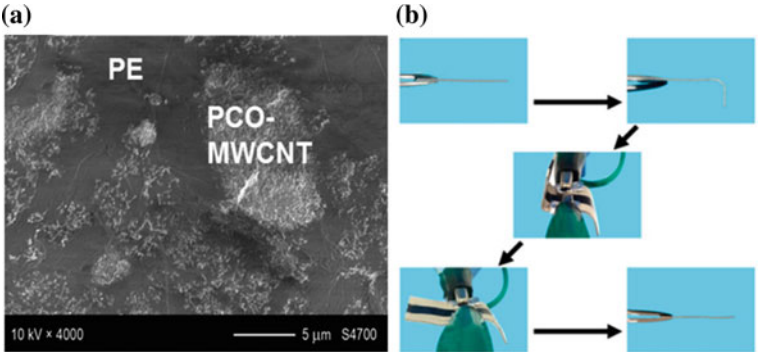

Fig. 13 **a** SEM image of the cryo-fractured surface of the PCO-MWCNT (15 vol%)/PE 70/30 vol% nanocomposite. **b** The visual TSME of the PCO-MWCNT (15 vol%)/PE 70/30 vol% nanocomposite induced by electrical heating. Reprinted from [56] with permission from American Chemical Society

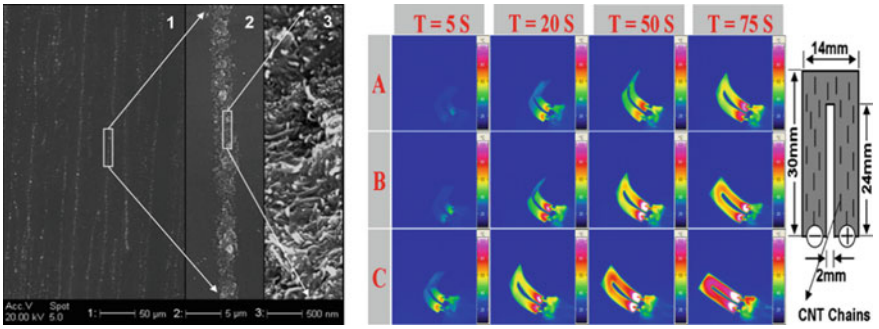

Fig. 14 SEM image of the SMP/CB composite with chained CNTs (insets: zoom-in views of one CNTs chain) and pictures exhibiting the shape recovery progress and the temperature distributions (sample A: SMP/CB, sample B: SMP/CB/random CNTs, and sample C: SMP/CB/chained CNTs). Adapted and reproduced from [65] with permission from American Institute of Physics

nificantly improve the electrical conductivity of SMPCs by constructing conductive Ni chains under a weak magnetic field (0.03 T), which made it more efficient for ESME [63]. Then, they aligned the Ni macroparticles into chains in an SMPC filled with CB with the same strategy, resulting in reduction of the electrical resistivity by over ten times as compared to the same sample with randomly distributed fillers. The composite with 10 vol% CB and 0.5 vol% chained Ni could realize shape recovery at 30 V [64]. In addition, the SMP/CB composites with embedded CNTs chains were fabricated by applying an alternating current electric field. Compared with the conventional SMP/CB/CNTs composite, the electrical resistivity of those containing chained CNTs was reduced by over 100 times. Figure 14 exhibited that the sample with 1 wt% chained CNTs and 15 wt% CB could complete a full recovery within 75 s at 25 V [65].

3.4 *Electrical Property via Incorporation of Conductive Layers*

3.4.1 Coating of Conductive Nanopaper

By assembling the conductive fillers into nanopapers and then coating them as heating source on the surface of the shape-memory matrix, it would be much easier to pass current and generate Joule heating. Lu et al. coated a self-supporting network-CNT nanopaper on the surface of the epoxy-based SMP/CNFs composite to achieve ESME. The CNFs embedded in the SMP resin could improve the thermal conductivity to efficiently transfer the heat created by the nanopaper to the underlying composite, thus could accelerate the electro-stimulus response. At a relatively low voltage of 16.2 V, the prepared composite realized 98% recovery within 330 s [66]. Then, the same group presented a work of synthesizing three-dimensional self-assembled MWCNT nanopaper on the PCL-based shape-memory membrane. With the synergetic effect of the electrical property of nanopaper and the shape recovery behavior of SMP, the developed composites were integrated with sensing and actuating performances. Moreover, the electro-driven shape recovery was used to drive up a 5 g mass from 0 to 30 mm in height [67]. In their another work, the ESMPCs were fabricated by coating the RGO paper onto the surface of the epoxy-based shape-memory sheets through resin transfer molding. The RGO paper acted as conductive layer to generate Joule heating and trigger the shape recovery progress. As shown in Fig. 15, the composite demonstrated adequate electric heating performance and possessed uniform surface temperature distribution. Besides, the R_r approximated 100% within only 5 s at a much lower voltage of 6 V [68].

3.4.2 Fabrication of Bilayer Structures

The digitally controlled spin-coating and spraying-evaporation deposition technologies, which can produce functional membranes with arbitrary thickness and patterns, are very convenient to fabricate conductive layers. Luo et al. first prepared the silver nanowire (AgNW) percolating network on a glass substrate by spin coating, and then added the shape-memory PU solution onto AgNWs, forming a bilayer composite comprising an AgNWs layer inlaid in the surface SMP layer. As a result, the composite showed superior conductivity and good ESME with R_r more than 80% within 5 s at 5 V. Particularly, the composite also possessed good flexibility and could maintain most of the conductivity as the elongation of 12%, demonstrating a great potential to be applied as sensors [69]. Furthermore, the bilayer ESMPCs were also prepared by depositing the printed CNT layers on defined locations of the SMP films. As shown in Fig. 16A, the thicknesses and patterns of the CNT layers could be easily tuned and designed through spraying-evaporation deposition molding. Thus, it was simple to adjust the maximum surface temperature and the even temperature distribution or gradient. The results revealed that the composite with 50 CNT layers

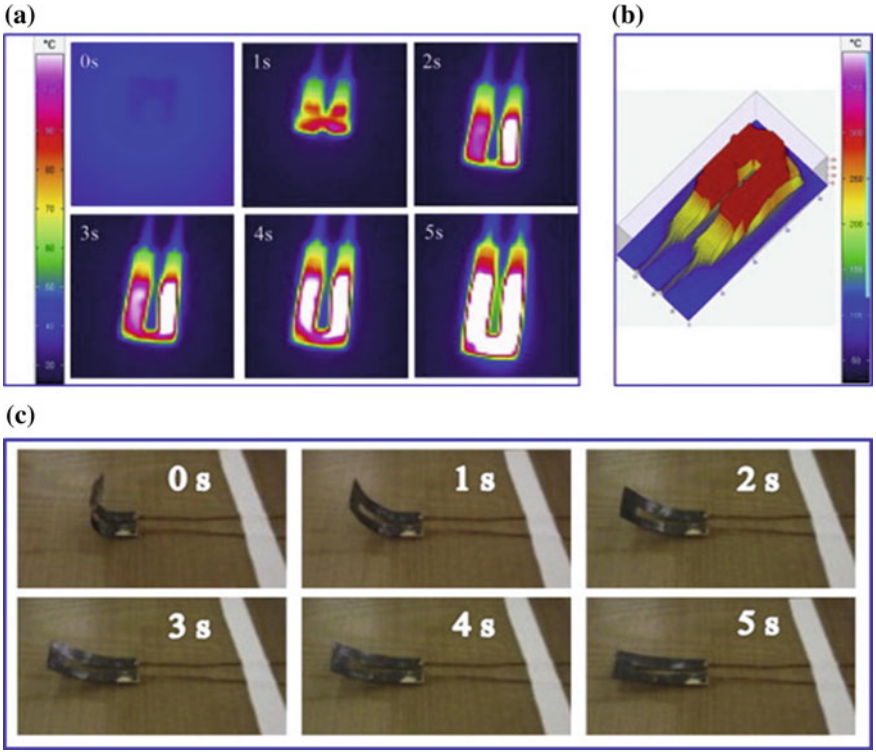

Fig. 15 **a** Infrared thermal images of the shape recovery process of the epoxy-based shape-memory sheet coated with the RGO paper at the voltage of 6 V. **b** 3D surface temperature distribution photo after conducting for 5 s. **c** Visual shape recovery process of the epoxy-based shape-memory sheet coated with the RGO paper at the voltage of 6 V. Adapted and reproduced from [68] with permission from Elsevier

exhibited the best electrical property and approximately 100% shape recovery within 30 s at 40 V, Fig. 16B [70].

3.4.3 Construction of Multilayer Structures

The multilayer structure, as a special co-continuous morphology, has extensively existed in the nature world [71, 72]. Particularly, the property of individual layer in that architecture can be tailored independently, thus providing an easy method for preparing functional composites by integrating the capacity of each layer. Lu et al. formed self-assembled CNF and BN nanopapers through the means of deposition on carbon fibers at a high pressure. The nanopapers were then coated on the surface of SMP to fabricate a three-layer composite for enabling electrical actuation via passing an electrical current through CNFs and carbon fiber. Moreover, the BN nanopaper

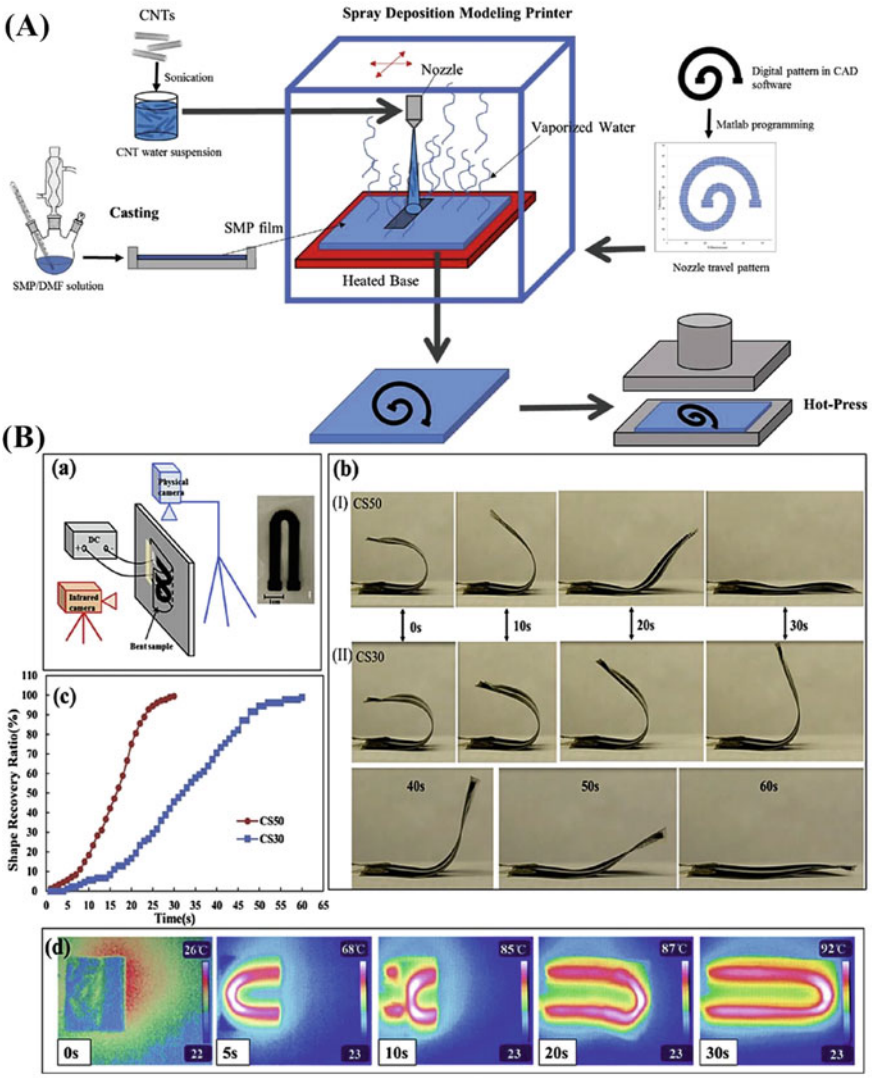

Fig. 16 **A** Schematical illustration of the fabrication process of CNT/SMP bilayer nanocomposites. **B** ESME of the CNT/SMP bilayer nanocomposites: (a) the schematics of the specimen and the testing setup, (b) shape recovery process of the composites with (I) 50 and (II) 30 CNT layers at 40 V, (c) R_r over the conducting time, and (d) photos of temperature distribution of the composite with 50 CNT layers during the shape recovery process. Adapted and reproduced from [70] with permission from Elsevier

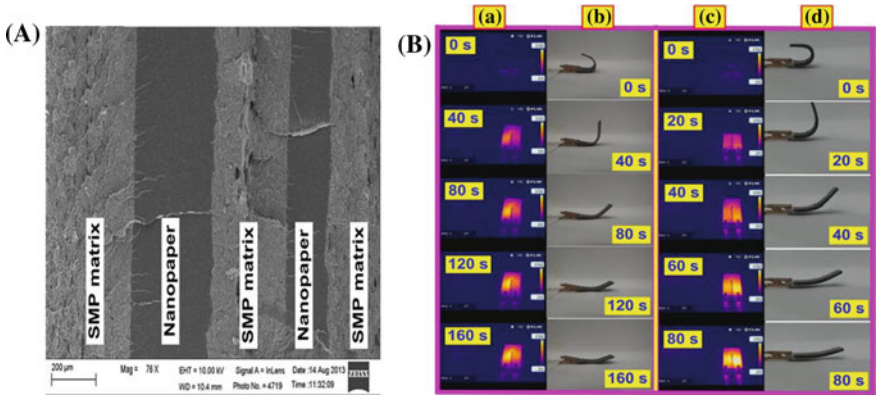

Fig. 17 **A** Structural morphology of the multilayered nanopaper/SMP nanocomposite. **B** The temperature distribution and shape recovery progress of the multilayered nanocomposites: (a, b) the sample incorporated with two-layered CNF nanopaper and (c, d) the sample incorporated with four-layered CNF nanopaper. Adapted and reproduced from [74] with permission from American Institute of Physics

could enhance the thermal conductivity of the composite so that the Joule heating could be more efficiently transferred from the nanopapers into SMP, resulting in full shape recovery within 80 s at a low voltage of 4.8 V [73]. They also reported an interesting work in using multilayer structure to realize ESME. As shown in Fig. 17, a multilayered composite comprising alternating layers of self-assembled CNF nanopaper and SMP was fabricated. By varying the layer number, the synergistic effect of the conductive nanopaper and the multilayered interface on the electrical property and recovery performance was researched. The results demonstrated that the CNF nanopaper could not only significantly enhance the bonding strength between the nanopaper and SMP via van der Waals force but also promote the electrical conductivity and temperature distribution in the composites. By comparison, the sample with four-layered nanopaper achieved the best EMSE of full shape recovery within 80 s at 30 V [74].

4 Magnetic Properties

Commonly, the straight way for SMPs to obtain magnetic properties is incorporating magnetic nanoparticles, such as iron, iron oxide, nickel, and cobalt, which can generate heat in an AMF through eddy current loss, hysteresis loss, and/or rotational loss [14, 15]. When the MSMPC with a temporary shape is heated to the temperature above T_s, the recovery progress would be induced. Moreover, the heating efficiency produced in an AMF was significantly influenced by the particle size. For the particles in the nanoscale, enough amount of heat required for triggering SME could be

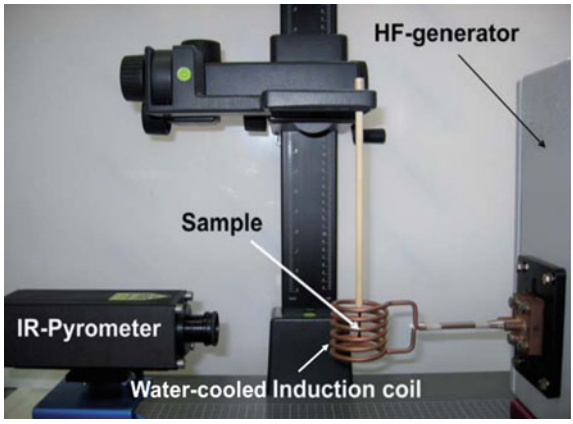

Fig. 18 Schematic of the setup for testing the magnetic-responsive SME in an AMF. Reprinted from [75] with permission from Springer

induced only at high frequency. On the contrary, the micro-sized particles generated heat via hysteresis and eddy current losses under relatively low f. Figure 18 showed the typical equipment for exploring the magnetic-induced SME consisting of a high-frequency (HF) generator, a water-cooled coil, and an IR pyrometer for temperature measurement [75].

4.1 Magnetic Properties for Shape-Memory Effect

4.1.1 Dual-Shape-Memory Effect

Considering that the magnetic medium has distinct boundaries with the polymer matrix, surface modification of the particle or cross-linking it to form network are usually employed to induce dual-shape-memory effect (DSME), which can memorize only one temporary shape in a shape-memory cycle. Back to 2006, MSMPCs have been fabricated by introducing the nanoparticles composed of Fe_2O_3 core in silica matrix into a shape-memory multi-block copolymer with poly (p-dioxanone) as hard segment and PCL as soft segment. The silica could dramatically improve the compatibility between the fillers and the SMP matrix, leading to a homogeneous distribution of nanoparticles. Since the mean domain size of the nanoparticle was slightly higher than 20 nm, hysteresis and/or relaxational losses were regarded to be responsible for heating. As an AMF (f = 258 kHz, strength (H) = 30 kA m^{-1}) was switched on, the nanocomposite with 10 wt% surface-modified Fe_2O_3 recovered back to the initial shape by inductive heating, see Fig. 19. Moreover, the final R_r's were close to those obtained by directly heating, further demonstrating that MSMPC was comparable to thermal-responsive SMP [76]. In other work, PEG-10000 was used as the dispersing surfactant to synthesize Fe_3O_4 nanoparticles with a diameter of 20 nm by co-precipitation of divalent and trivalent iron salts. After that, PLA/Fe_3O_4

composites were produced through hot compression molding, which possessed a uniform structure because of the weak hydrogen bonding between the Fe–OH group of nano-Fe_3O_4 and the C=O of the PLA matrix. The enhanced interfacial interaction endowed the optimization of tensile properties and DSME of the nanocomposites [77]. Besides, polymerization of reactive monomer was employed to give rise to MSMPCs. With the incorporation of Fe_3O_4 through in situ polymerization, the mechanical properties and DSME of the cross-linking PCL-based nanocomposites were synergistically enhanced [78].

4.1.2 Triple-Shape-Memory Effect

By incorporation of magnetic-sensitive particles in a multiphase shape-memory network (MSMN), the magnetically switchable TSME could be achieved for memorizing two temporary shapes. An example of the triple MSMPC was reported by a series of nanocomposites which were synthesized through dispersing the silica-coated Fe_2O_3 nanoparticles into an MSMN containing PCL and poly(cyclohexyl methacrylate) (PCHMA) segments. Different bending procedures were applied to create temporary shapes, as shown in Fig. 20A. By increasing the H of AMF at the f of 258 kHz, the material could be heated to unfreeze PCL and PCHMA step by step, thus enabling two-step recovery. Figure 20B exhibited that the sample with 40 wt% PCL could present an excellent TSME of different temporary shapes through step-wise enhancing of the magnetic field strength [79]. In addition to that, another MSMPC with two crystallizable switches was fabricated by the incorporation of silica-coated magnetite nanoparticles into an MSMN comprising PEG side chains and PCL cross-links. It was demonstrated that the nanocomposites with high PEG weight fraction could achieve efficient TSME by applying two-step programming procedures [80]. Instead of MSMN, the polymer with a broad transition temperature range could also act as the matrix to realize magnetic-responsive TSME. The electrospun Nafion membranes, which possess a broad T_g transition from 60 to 170 °C,

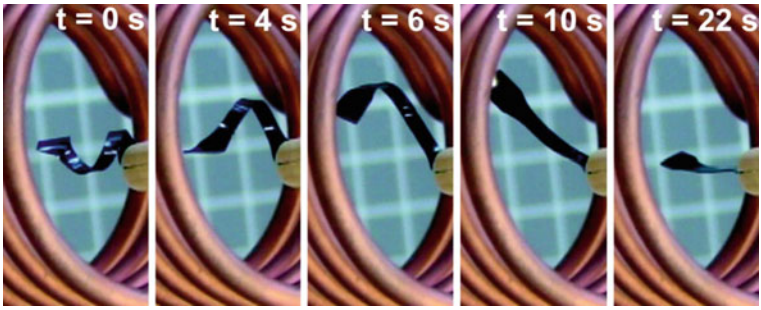

Fig. 19 Photographs showing the magnetic-induced SME of the sample with 10 wt% surface-modified Fe_3O_4 in an AMF of f = 258 kHz and H = 30 kA m^{-1}. Reprinted from [76] with permission from National Academy of Sciences

have been proved to exhibit thermal-induced multiple SME [81]. Based on that, Nafion nonwoven nanofiber fabrics embedded with Fe_3O_4 were produced through electrospinning, which could realize magnetic-responsive triple- and quadruple-SME remotely by controlling the intensities of AMF [82].

4.1.3 Two-Way Shape-Memory Effect

Recently, the SMPs with two-way SME were used as the matrix to create unique magnetic-responsive behaviors. Du et al. investigated the SME of the hybrid networks formed by metal coordination interaction between Fe_3O_4 and catechol-telechelic PCL. The strong netpoints acted by Fe_3O_4 allowed the materials with two-way shape fixation and recovery because of the crystallization-induced elongation and melting-induced contraction of the PCL segments by turning off/on AMF. This fantastic performance of the material could be applied to fabricate magnetic-triggered actuator, as schematically shown in Fig. 21 [83].

4.2 Magnetic Properties for Temperature Control

As another outstanding advantage, some ferromagnetic particles with an appropriate scale enabled the innate thermoregulation because of Curie temperature (TC) effect [84, 85]. When the temperature is increased to TC, the magnetic particles which cause heating via only hysteresis loss mechanism instead of eddy current mechanism would

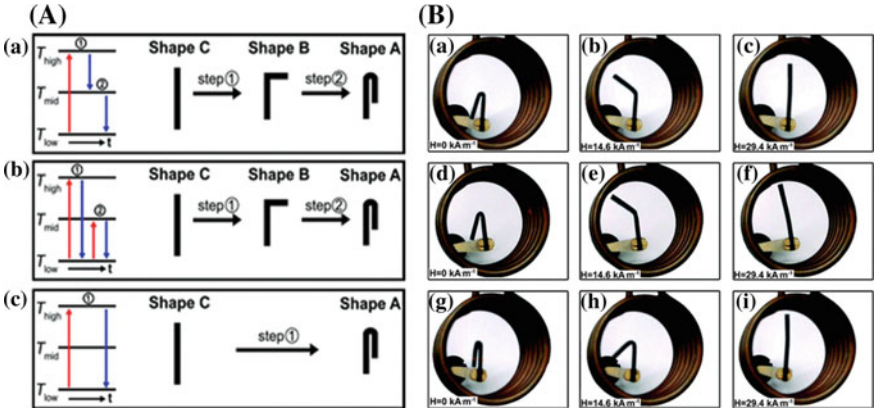

Fig. 20 **A** Schematic of the different triple-shape creation procedures: (a), (b) type-I and type-II two-step triple-shape creation procedure (TCP-2s-I and TCP-2s-II), (c) one-step triple-shape creation procedure (TCP-1s). **B** Images showing the shape recovery progress of the sample with 40 wt% PCL in an AMF of H = 0, 14.6 and 29.4 kA m^{-1}. (a)–(c): TCP-2s-I; (d)–(f): TCP-2s-II; (g)–(i): TCP-1s. Adapted and reproduced from [79] with permission from Royal Society of Chemistry

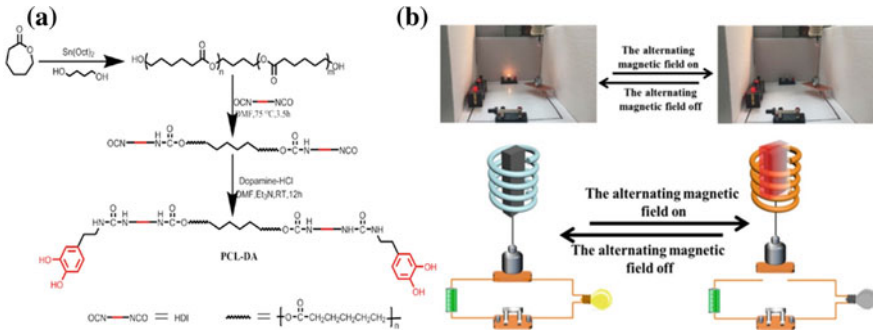

Fig. 21 **a** The preparation route of catechol-telechelic PCL and **b** the model of magnetic-triggered two-way shape-memory actuator used to realize on/off control in a circuit. Reprinted from [83] with permission from American Chemical Society

become paramagnetic, losing the capacity to further heat. This effect can be applied to limit the maximum achievable temperature and avoid overheating in biomedical applications. Buckley et al. fabricated MSMPCs by dispersing nickel zinc ferrite ferromagnetic particles in an amorphous shape-memory PU with T_g of 55 °C for the switching domains. Because of the negligible contribution of eddy current heat, the particles with an average size of approximately 50 μm mainly were heated by hysteresis loss mechanism. As a result, the composites exhibited a TC which could be further adjusted to be clinically acceptable via tailoring the composition of filler material. Moreover, the MSMPC with 10 vol% fillers could be inductively heated to realize self-deployment in an AMF (f = 12.2 MHz, H = 545 kA m^{-1}), providing a great potential to be applied as the endovascular thrombectomy device [86].

Besides limiting the maximum achievable temperature, another strategy for adjusting the application relevant temperature is controlling the apparent switching temperature ($T_{s,a}$). Generally, $T_{s,a}$ is determined as the environmental temperature (T_e) at which the shape recovery occurs. For an MSMPC without stimulation of magnetic field, T_e should be suitably higher than its T_m or T_g. However, as located in an AMF, the internal heating generated by the interaction with the magnetic field, in certain degree, would induce temperature rise of MSMPC. Thus, the heat flow from the environment required for triggering SME can be decreased, affording a feasible route to reversibly adjust $T_{s,a}$. The synergetic influence of the environmental and magnetic heating has been explored based on the different SMP matrixes with DSME and TSME. The dual-MSMPC named as CLC05 was prepared by cross-linking PCL diisocyanatoethyl methacrylate (PCLDIMA) in the presence of 5 wt% silica-coated magnetite nanoparticles. The triple-MSMPCs named CLEGC05 and CLEGC10 were fabricated by copolymerization of PCLDIMA with 60 wt% of PEG monomethyl ether monomethacrylate (PEGMA) in the presence of 5 and 10 wt% silica-coated magnetite nanoparticles, respectively. It was found that the bulk temperature (T_b) of each sample demonstrated a correlation to H by the power of two at a constant T_e. On the other hand, the environmental heating tests were conducted

at various fixed H of AMF and a linear correlation between T_b and T_e was observed for all samples. T_b was initially identical with T_e, whereas application of a constant H led to an increase in T_b attributed to the contribution of magnetic-induced inductive heating. As a result, $T_{s,a}$ of CLC05 could be decreased up to 13 °C and $T_{s,a}$ of CLEGC05 and CLEGC10 at the different shape-memory stages could be lowered by up to 9 °C and 19 °C, respectively [87].

5 Outlook

The optical property of reversible photochemical reaction provides an innovative mechanism for achieving SME without temperature effect, which can be used to fabricate remote shape-memory materials due to the long travel distance of light. On the other hand, the optical, electrical, and magnetic properties which may induce the rise of temperature upon the external stimuli (light, electrical field, or AMF) can also be the choice for designing smart materials triggering SME via indirect actuation. Although the underlying mechanism is also thermal effect that heats the sample to $T > T_s$, the none-contact stimulation ways enable remote activation of the shape recovery process and spatial control of the shape recovery behavior. Moreover, the SME induced by inductive heating resides in the fact that the recovery temperature, speed, and level can be tailored by choosing an appropriate filler combined with varying the intensity of stimulation, e.g., the λ of light, voltage of electrical field, and f as well as H of AMF. This feature is crucial for some applications, such as that the light-responsive biomedical devices limited by the physiological environment generally prefer the lower energy NIR light rather than UV or visible light, while the higher energy electrical or magnetic fields are favorable for ESMPCs and MSMPCs to realize quick recovery.

Although the remote and spatial activation as well as tunable performance of SME have been achieved, there are still some issues to be solved.

(1) The tailored distribution of functional nanoparticles can induce uniform induction heating and optimize the shape recovery performance (see Sect. 3.4.1 "Coating of Conductive Nanopaper"). However, for the conventional composites, the micro-localized aggregation of nanoparticles seems inevitable, which usually results in local overheating and unstable SME. Thus, the advanced methods should be further developed to realize completely homogenous dispersion of nanoparticles. On the other hand, the SME is not promoted constantly with increasing the efficiency of inductive heating. For example, the ESMPCs with high electrical conductivity would generate dramatic temperature rise at a relatively high voltage, which may cause the melting of the memorize component acted by a thermoplastic polymer (such as rubber or elastomer) and finally lead to the failure of SME. Nevertheless, that issue is conventionally ignored in literatures. Accordingly, an effective range of the stimulus intensity should be given in future researches, for better controlling the shape recovery performance.

(2) The enhanced property of inductive heating is generally achieved by forming a filler network in the shape-memory matrix. As a result, the SMPCs fail to complete the stretching or other complex deformations which may destroy the functional network. Similarly, it is difficult for SMPCs to undergo repeat application through running consecutive shape-memory cycles. Moreover, most of the SMPCs are limited by the great shortcoming of one-way deformation. These imperfections lead to that the SMPCs are commonly trapped in a small application area, such as the self-deployable instruments. Hence, stretchable SMPCs with stable property should be explored and SME needs to be extended to two-way (see Sect. 4.1.3 "Two-Way Shape-Memory Effect") or other deformation principles (see Sect. 4.1.2 "Triple-Shape-Memory Effect") in future studies, which can provide the more greater freedom in practical applications.
(3) Despite the indirect actuation methods have been abundantly researched, most of the shape recovery progress can only be triggered by one kind of specific stimulation. In order to further broaden the application field, the multi-responsive materials which can trigger SME via two or more stimulation ways should be developed to meet the requirement of different application environments. However, it is still challenging for a material to obtain multi-responsive properties because of the difficulties in simultaneously achieving well dispersion of hybrid fillers and efficiently integrating their functions. By so far, some related works have been successfully accomplished [88], but the fabrication technologies still need improvement and development.

Apart from these arduous challenges, the research opportunities and promising strategies which may promote the development of shape-memory field are also worth noticing. For instance, the multilayer structure as a special co-continuous morphology which holds a great promise in optimizing DSME and TSME [89, 90] has been applied to produce ESMPCs through incorporating conductive layers (see Sect. 3.4.3 "Construction of Multilayer Structures"). On the basis of the same mechanism, it is believed to be feasible to fabricate light- and magnetic-responsive materials by incorporating the corresponding function layers. Moreover, the multilayer composites can easily obtain multifunctional properties by selectively or alternatively layered distribution of different particles [91, 92], providing a conceivable route to produce multi-responsive materials. However, to the best of our knowledge, there are few reports on using that architecture to prepare multi-responsive shape-memory materials. Accordingly, this promising method is worthy to be explored and applied for creation of multi-responsive materials in future studies.

6 Summary

In this chapter, a comprehensive overview has been presented introducing the recent developments and progress in the optical, electrical, and magnetic properties of SMPs, SMPBs, and SMPCs. Functional groups or/and fillers are introduced into

the shape-memory materials to serve as switches or heaters as well as functional components, which finally induce SME via indirect actuation and simultaneously improve the overall material properties. The triggering methods of light, electrical field, and AMF developed by these properties can achieve remote and spatial control to meet the requirement of the specific applications.

The optical property of photochemical reaction created by incorporation of photosensitive groups (e.g., cinnamic acid, anthracene, and azobenzene), such as reversible photocross-linking and reverse cis–trans transition which can act as the shape-memory switch, enables the materials to present light-responsive SME without any relation with the temperature effects. On the other hand, the PTE induced by the groups or fillers (such as ligands, CNTs, CB, graphene, and gold particles) possessing the ability to absorb light and convert it into heat can increase the temperature of the matrix to trigger SME in thermal form. Because of the none-contact and micro-localized advantages of light irradiation, the materials with optical response are able to achieve remote and spatial control in the shape recovery progress, demonstrating the great potential to be applied as light-driven actuator, biomedical devices, etc. Besides, the shape-memory materials can achieve reversible optical property because they could be shaped into a tailored optical structure and then recovered back to the original state in the shape-memory cycling progress.

For the electrical property which is generally obtained by incorporating the conductive particles, including metal particles, CB, CNTs, CNFs, and graphene, the optimization of the particle dispersion is of importance to enhance the performance. Numerous methods including the use of ultrasonic treatment, surface modification, hybrid fillers, and assembly of conductive channels and layers combined with morphological control and structural design have been used to tailor the conductive network in the shape-memory matrix, for achieving superior mechanical properties and shape recovery performance. The higher conductivity can generate more efficient Joule heating by passing the current through the conductive particles, resulting in fast temperature rise and recovery speed at the given voltage. Moreover, the dramatically increased recovery stress of the ESMPCs can be applied to complete mechanical works of mini lifts, self-deployable instruments, and actuators.

Similarly, the magnetic particles embedded in the polymer matrix can produce magnetic property and act as heaters to actuate SME by inductive heating in an AMF. The methods of improving the particle dispersion proposed in ESMPCs are also applied to optimize magnetic property. Particularly, the heating efficiency is significantly influenced by the type and size of the magnetic particles. The maximum achievable temperature can be adjusted by choosing the particles with a proper size based on the fantastic phenomenon of TC, which was favorable in biomedical applications. In addition, the application relevant temperature can also be tailored by combining the contributions from magnetic-induced heating and the environmental heating.

Apart from the reversible photochemical reaction, the optical, electrical, and magnetic properties of inducing SME upon inductive heating rely on the same mechanism of thermal effect that heats the sample to $T > T_s$. These none-contact stimulation ways can remotely tailor the recovery temperature, speed, and level by choosing an appro-

priate filler and varying the intensity of stimulation, e.g., the λ of light, voltage of electrical field, and f as well as H of AMF. In addition, versatile shape-memory behaviors of DSME, TSME, and two-way SME can be realized by using the corresponding shape-memory matrix. Based on the developed studies, it is prospected that SME triggered by indirect actuations instead of environmental heating would significantly expand the applications of shape-memory materials ranging from biomedical devices to aerospace equipment.

References

1. Hu JL, Zhu Y, Huang HH, Lu J (2012) Recent advances in shape–memory polymers: structure, mechanism, functionality, modeling and application. Prog Polym Sci 37:1720–1763
2. Zhao Q, Qi HJ, Xie T (2015) Recent progress in shape memory polymer: new behavior, enabling materials, and mechanistic understanding. Prog Polym Sci 49–50:79–120
3. Martin Hager MD, Bode S, Weber C, Schubert US (2015) Shape memory polymers: past, present and future developments. Prog Polym Sci 49–50:3–33
4. Liu YJ, Lv HB, Lan X, Leng JS, Du SY (2009) Review of electro-active shape-memory polymer composite. Compos Sci Technol 69:2064–2068
5. Leng JS, Lan X, Liu YJ, Du SY (2011) Shape-memory polymers and their composites: stimulus methods and applications. Prog Mater Sci 56:1077–1135
6. Meng H, Li GQ (2013) A review of stimuli-responsive shape memory polymer composites. Polymer 54:2199–2221
7. Mu T, Liu LW, Lan X, Liu YJ, Leng JS (2018) Shape memory polymers for composites. Compos Sci Technol 160:169–198
8. Liu TZ, Zhou TY, Yao YT, Zhang FH, Liu LW, Liu YJ, Leng JS (2018) Stimulus methods of multi-functional shape memory polymer nanocomposites: a review. Compos A 100:20–30
9. Habault D, Zhang HJ, Zhao Y (2013) Light-triggered self-healing and shape-memory polymers. Chem Soc Rev 42:7244–7256
10. Li HM, Keller P, Li B, Wang XG, Brunet M (2003) Light-driven side-on nematic elastomer actuators. Adv Mater 15:7–8
11. Ikeda T, Mamiya JI, Yu YL (2007) Photomechanics of liquid-crystalline elastomers and other polymers. Angew Chem Int Ed 46:506–528
12. Pei ZQ, Yang Y, Chen QM, Terentjev EM, Wei Y, Ji Y (2014) Mouldable liquid-crystalline elastomer actuators with exchangeable covalent bonds. Nat Mater 13:36–41
13. Liu YJ, Du HY, Liu LW, Leng JS (2014) Shape memory polymers and their composites in aerospace applications: a review. Smart Mater Struct 23:023001
14. Li CH, Hodgins P, Peterson GP (2010) Experimental study of fundamental mechanisms in inductive heating of ferromagnetic nanoparticles suspension (Fe_3O_4 iron oxide ferrofluid). J Appl Phys 110:054303
15. Heuchel M, Razzaq MY, Kratz K, Behl M, Lendlein A (2015) Modeling the heat transfer in magneto-sensitive shape-memory polymer nanocomposites with dynamically changing surface area to volume ratios. Polymer 65:215–222
16. Razzaq MY, Behl M, Lendlein A (2012) Memory-effects of magnetic nanocomposites. Nanoscale 4:6181–6195
17. Gass J, Poddar P, Almand J, Srinath S, Srikanth H (2006) Superparamagnetic polymer nanocomposites with uniform Fe_3O_4 nanoparticle dispersions. Adv Funct Mater 16:71–75
18. Kalia S, Kango S, Kumar A, Haldorai Y, Kumari B, Kumar R (2014) Magnetic polymer nanocomposites for environmental and biomedical applications. Colloid Polym Sci 292:2025–2052

19. Lendlein A, Jiang HY, Jünger O, Langer R (2005) Light-induced shape-memory polymers. Nature 434:879–882
20. Wu LB, Jin CL, Sun XY (2011) Synthesis, properties, and light-induced shape memory effect of multiblock polyesterurethanes containing biodegradable segments and pendant cinnamamide groups. Biomacromolecules 12:235–241
21. Xie H, He MJ, Deng XY, Du L, Fan CJ, Yang KK, Wang YZ (2016) Design of poly(l-lactide)-poly(ethylene glycol) copolymer with light-induced shape-memory effect triggered by pendant anthracene groups. ACS Appl Mater Interfaces 8:9431–9439
22. Yu YL, Nakano M, Ikeda T (2003) Directed bending of a polymer film by light. Nature 425:145
23. Yamada M, Kondo M, Mamiya JI, Yu YL, Kinoshita M, Barrett CJ, Ikeda T (2008) Photomobile polymer materials: towards light-driven plastic motors. Angew Chem Int Ed 47:4986–4988
24. Lee KM, Koerner H, Vaia RA, Bunning TJ, White TJ (2011) Light-activated shape memory of glassy, azobenzene liquid crystalline polymer networks. Soft Matter 7:4318–4324
25. White TJ, Tabiryan NV, Serak SV, Hrozhyk UA, Tondiglia VP, Koerner H, Vaia RA, Bunning TJ (2008) A high frequency photodriven polymer oscillator. Soft Matter 4:1796–1798
26. White TJ, Serak SV, Tabiryan NV, Vaiaa RA, Bunning TJ (2009) Polarization-controlled, photodriven bending in monodomain liquid crystal elastomer cantilevers. J Mater Chem 19:1080–1085
27. Serak S, Tabiryan N, Vergara R, White TJ, Vaia RA, Bunning TJ (2010) Liquid crystalline polymer cantilever oscillators fueled by light. Soft Matter 6:779–783
28. Kumpfer JR, Rowan SJ (2011) Thermo-, photo-, and chemo-responsive shape-memory properties from photo-cross-linked metallo-supramolecular polymers. J Am Chem Soc 133:12866–12874
29. Michal BT, McKenzie BM, Felder SE, Rowan SJ (2015) Metallo-, thermo-, and photoresponsive shape memory and actuating liquid crystalline elastomers. Macromolecules 48:3239–3246
30. Koerner H, Price G, Pearce NA, Alexander M, Vaia RA (2004) Remotely actuated polymer nanocomposites-stress-recovery of carbon-nanotube-filled thermoplastic elastomers. Nat Mater 3:115
31. Liang JJ, Xu YF, Huang Y, Zhang L, Wang Y, Ma FF, Li FF, Guo TY, Chen YS (2009) Infrared-triggered actuators from graphene-based nanocomposites. J Phys Chem C 113:9921–9927
32. Leng JS, Wu XL, Liu YJ (2009) Infrared light-active shape memory polymer filled with nanocarbon particles. J Appl Polym Sci 114:2455–2460
33. Feng YY, Qin MM, Guo HQ, Yoshino K, Feng W (2013) Infrared-actuated recovery of polyurethane filled by reduced graphene oxide/carbon nanotube hybrids with high energy density. ACS Appl Mater Interfaces 5:10882–10888
34. Lu HB, Yao YT, Huang WM, Leng JS, Hui D (2014) Significantly improving infrared light-induced shape recovery behavior of shape memory polymeric nanocomposite via a synergistic effect of carbon nanotube and boron nitride. Compos B 62:256–261
35. Thakur S, Karak NJ (2015) Tuning of sunlight-induced self-cleaning and selfhealing attributes of an elastomeric nanocomposite by judicious compositional variation of the TiO_2-reduced graphene oxide nanohybrid. J Mater Chem A 3:12334–12342
36. Yu L, Wang Q, Sun J, Li CY, Zou C, He ZM, Wang ZD, Zhou L, Zhang LY, Yang H (2015) Multi-shape-memory effects in a wavelength-selective multicomposite. J Mater Chem A 3:13953–13961
37. Hribar KC, Metter RB, Ifkovits JL, Troxler T, Burdick JA (2009) Light-induced temperature transitions in biodegradable polymer and nanorod composites. Small 5:1830–1834
38. Zhang HJ, Zhang JM, Tong X, Ma DL, Zhao Y (2013) Light polarization-controlled shape-memory polymer/gold nanorod composite. Macromol Rapid Commun 34:1575–1579
39. Zhang HJ, Zhao Y (2013) Polymers with dual light-triggered functions of shape memory and healing using gold nanoparticles. ACS Appl Mater Interfaces 5:13069–13075
40. Zhang HJ, Xia HS, Zhao Y (2014) Light-controlled complex deformation and motion of shape memory polymers using a temperature gradient. ACS Macro Lett 3:940–943
41. Shibaev V, Bobrovsky A, Boiko N (2003) Photoactive liquid crystalline polymer systems with light-controllable structure and optical properties. Prog Polym Sci 28:729–835

42. Pucci A, Bizzarri R, Ruggeri G (2011) Polymer composites with smart optical properties. Soft Matter 7:3689–3700
43. Wu WB, Tang RL, Li QQ, Li Z (2015) Functional hyperbranched polymers with advanced optical, electrical and magnetic properties. Chem Soc Rev 44:3997–4022
44. Zheng YW, Li J, Lee E, Yang S (2015) Light-induced shape recovery of deformed shape memory polymer micropillar arrays with gold nanorods. RSC Adv 5:30495–30499
45. Wu ZL, Wang ZJ, Keller P, Zheng Q (2016) Light responsive microstructured surfaces of liquid crystalline network with shape memory and tunable wetting behaviors. Macromol Rapid Commun 37:311–317
46. Xu HX, Yu CJ, Wang SD, Malyarchuk V, Xie T, Rogers JA (2013) Deformable, programmable, and shape-memorizing micro-optics. Adv Funct Mater 23:3299–3306
47. Li ZP, Black T, Rahman MA, Feng JX, Olah A, Baer E (2018) Opto-mechanical programming of micro-scale information on transparent multilayer shape memory film. Polymer 137:156–168
48. Schauer S, Meier T, Reinhard M, Röhrig M, Schneider M, Heilig M, Kolew A, Worgull M, Hölscher H (2016) Tunable diffractive optical elements based on shape-memory polymers fabricated via hot embossing. ACS Appl Mater Interfaces 8:9423–9430
49. Girifalco LA, Hodak M, Lee RS (2000) Carbon nanotubes, buckyballs, ropes, and a universal graphitic potential. Phys Rev B 62:13104
50. Fei GX, Li G, Wu LS, Xia HS (2012) A spatially and temporally controlled shape memory process for electrically conductive polymer-carbon nanotube composites. Soft Matter 8:5123–5126
51. Cho JW, Kim JW, Jung YC, Goo NS (2005) Electroactive shape-memory polyurethane composites incorporating carbon nanotubes. Macromol Rapid Commun 26:412–416
52. Raja M, Ryu SH, Shanmugharaj AM (2013) Thermal, mechanical and electroactive shape memory properties of polyurethane (PU)/poly (lactic acid) (PLA)/CNT nanocomposites. Eur Polym J 49:3492–3500
53. Raja M, Ryu SH, Shanmugharaj AM (2014) Influence of surface modified multiwalled carbon nanotubes on the mechanical and electroactive shape memory properties of polyurethane (PU)/poly(vinylidene diflouride) (PVDF) composites. Colloids Surf A 450:59–66
54. Mahapatra SS, Yadav SK, Yoo HJ, Ramasamy MS, Cho JW (2014) Tailored and strong electro-responsive shape memory actuation in carbon nanotube-reinforced hyperbranched polyurethane composites. Sens Actuators B 193:384–390
55. Deng H, Lin L, Ji MZ, Zhang SM, Yang MB, Fu Q (2014) Progress on the morphological control of conductive network in conductive polymer composites and the use as electroactive multifunctional materials. Prog Polym Sci 39:627–655
56. Wang ZW, Zhao J, Chen M, Yang M, Tang LY, Dang ZW, Chen FH, Huang MM, Dong X (2014) Dually actuated triple shape memory polymers of cross-linked polycyclooctene-carbon nanotube/polyethylene nanocomposite. ACS Appl Mater Interfaces 6:20051–20059
57. Qi XD, Dong P, Liu ZW, Liu TY, Fu Q (2016) Selective localization of multi-walled carbon nanotubes in bi-component biodegradable polyester blend for rapid electroactive shape memory performance. Compos Sci Technol 125:38–46
58. Liu TY, Huang R, Qi XD, Dong P, Fu Q (2017) Facile preparation of rapidly electro-active shape memory thermoplastic polyurethane/polylactide blends via phase morphology control and incorporation of conductive fillers. Polymer 114:28–35
59. Zhang ZX, Wang WY, Yang JH, Zhang N, Huang T, Wang Y (2016) Excellent electroactive shape memory performance of EVA/PCL/CNT blend composites with selectively localized CNTs. J Phys Chem C 120:22793–22802
60. Qi XD, Xiu H, Wei Y, Zhou Y, Guo YL, Huang R, Bai HW, Fu Q (2017) Enhanced shape memory property of polylactide/thermoplastic poly(ether)urethane composites via carbon black self-networking induced co-continuous structure. Compos Sci Technol 139:8–16
61. Chen XQ, Saito T, Yamada TH, Matsushige K (2001) Aligning single-wall carbon nanotubes with an alternating-current electric field. Appl Phys Lett 78:3714
62. Martina CA, Sandlera JKW, Windlea AH, Schwarzb MK, Bauhoferb W, Schultec K, Shafferd MSP (2005) Electric field-induced aligned multi-wall carbon nanotube networks in epoxy composites. Polymer 46:877–886

63. Leng JS, Lan X, Liu YJ, Du SY, Huang WM, Liu N, Phee SJ, Yuan Q (2008) Electrical conductivity of thermoresponsive shape-memory polymer with embedded micron sized Ni powder chains. Appl Phys Lett 92:014104
64. Leng JS, Huang WM, Lan X, Liu YJ, Du SY (2008) Significantly reducing electrical resistivity by forming conductive Ni chains in a polyurethane shape-memory polymer/carbon-black composite. Appl Phys Lett 92:204101
65. Yu K, Zhang ZC, Liu YJ, Leng JS (2011) Carbon nanotube chains in a shape memory polymer/carbon black composite: to significantly reduce the electrical resistivity. Appl Phys Lett 98:074102
66. Lu HB, Liu YJ, Gou JH, Leng JS, Du SY (2010) Synergistic effect of carbon nanofiber and carbon nanopaper on shape memory polymer composite. Appl Phys Lett 96:084102
67. Lu HB, Liu YJ, Gou JH, Leng JS, Du SY (2011) Surface coating of multi-walled carbon nanotube nanopaper on shape-memory polymer for multifunctionalization. Compos Sci Technol 71:1427–1434
68. Wang WX, Liu DY, Liu YJ, Leng JS, Bhattacharyya D (2015) Electrical actuation properties of reduced graphene oxide paper/epoxy-based shape memory composites. Compos Sci Technol 106:20–24
69. Luo HS, Li ZW, Yi GB, Zu XH, Wang H, Wang YJ, Huang HL, Hu JW, Liang ZF, Zhong BB (2014) Electro-responsive silver nanowire-shape memory polymer composites. Mater Lett 134:172–175
70. Wang X, Sparkman J, Gou JH (2017) Electrical actuation and shape memory behavior of polyurethane composites incorporated with printed carbon nanotube layers. Compos Sci Technol 141:8–15
71. Mayer G (2005) Rigid biological systems as models for synthetic composites. Science 310:1144–1147
72. Chen PY, Lin AYM, Stokes AG, Seki Y, Bodde SG, McKittrick J, Meyers MA (2008) Structural biological materials: overview of current research. JOM-US 60:23–32
73. Lu HB, Huang WM, Leng JS (2014) Functionally graded and self-assembled carbon nanofiber and boron nitride in nanopaper for electrical actuation of shape memory nanocomposites. Compos B 62:1–4
74. Lu HB, Liang F, Gou JH, Huang WM, Jinsong Leng JS (2014) Synergistic effect of self-assembled carbon nanopaper and multi-layered interface on shape memory nanocomposite for high speed electrical actuation. J Appl Phys 115:064907
75. Madbouly SA, Lendlein A (2010) Shape-memory polymers. Springer, Berlin Heidelberg
76. Mohr R, Kratz K, Weigel T, Lucka-Gabor M, Moneke M, Lendlein A (2006) Initiation of shape-memory effect by inductive heating of magnetic nanoparticles in thermoplastic polymers. Proc Natl Acad Sci USA 103:3540–3545
77. Zheng XT, Zhou SB, Xiao Y, Yu XJ, Li XJ, Wu PZ (2009) Shape memory effect of poly(d, l-lactide)/Fe_3O_4 nanocomposites by inductive heating of magnetite particles. Colloids Surf B 71:67–72
78. Gao YL, Zhu GM, Xu SG, Ma TT, Nie J (2018) Biodegradable magnetic-sensitive shape memory poly(ε-caprolactone)/Fe_3O_4 nanocomposites. J Appl Polym Sci 135:45652
79. Kumar UN, Kratz K, Wagermaier W, Behl M, Lendlein A (2010) Non-contact actuation of triple-shape effect in multiphase polymer network nanocomposites in alternating magnetic field. J Mater Chem 20:3404–3415
80. Kumar UN, Kratz K, Behl M, Lendlein A (2011a) Shape-memory properties of magnetically active triple-shape nanocomposites based on a grafted polymer network with two crystallizable switching segments. eXPRESS Polym Lett 6:26–40
81. Zhang FH, Zhang ZC, Liu YJ, Lu HB, Leng JS (2013) The quintuple-shape memory effect in electrospun nanofiber membranes. Smart Mater Struct 22:085020
82. Zhang FH, Zhang ZC, Luo CJ, Lin IT, Liu YJ, Leng JS, Smoukov SK (2015) Remote, fast actuation of programmable multiple shape memory composites by magnetic fields. J Mater Chem C 3:11290–11293

83. Du L, Xu ZY, Fan CJ, Xiang G, Yang KK, Wang YZ (2018) A fascinating metallo-supramolecular polymer network with thermal/magnetic/light-responsive shape-memory effects anchored by Fe_3O_4 nanoparticles. Macromolecules 51:705–715
84. Stauffer PR, Cetas TC, Fletcher AM, Young DW, Dewhirst MW, Oleson JR, Roemer RB (1984) Observations on the use of ferromagnetic implants for inducing hyperthermia. IEEE Trans Biomed Eng 31:76–90
85. Goldman A (1990) Modern ferrite technology. Van Nostrand Reinhold, New York
86. Buckley PR, McKinley GH, Wilson TS, Small W, Benett WJ, Bearinger JP, McElfresh MW, Maitland DJ (2006) Inductively heated shape memory polymer for the magnetic actuation of medical devices. IEEE Trans Biomed Eng 53:2075–2083
87. Kumar UN, Kratz K, Heuchel M, Behl M, Lendlein A (2011) Shape-memory nanocomposites with magnetically adjustable apparent switching temperatures. Adv Mater 23:4157–4162
88. Herbert KM, Schrettl S, Rowan SJ, Weder C (2017) 50th anniversary perspective: solid-state multistimuli, multiresponsive polymeric materials. Macromolecules 50:8845–8870
89. Zheng Y, Dong RQ, Shen JB, Guo SY (2016) Tunable shape memory performances via multilayer assembly of thermoplastic polyurethane and polycaprolactone. ACS Appl Mater Interfaces 8:1371–1380
90. Zheng Y, Ji XY, Yin M, Shen JB, Guo SY (2017) Strategy for fabricating multiple-shape-memory polymeric materials via the multilayer assembly of co-continuous blends. ACS Appl Mater Interfaces 9:32270–32279
91. Gao WL, Zheng Y, Shen JB, Guo SY (2015) Electrical properties of polypropylene-based composites controlled by multilayered distribution of conductive particles. ACS Appl Mater Interfaces 7:1541–1549
92. Zhu JM, Shen JB, Guo SY, Sue HJ (2015) Confined distribution of conductive particles in polyvinylidene fluoride-based multilayered dielectrics: toward high permittivity and breakdown strength. Carbon 84:355–364

Scattering and Other Miscellanies Techniques for the Characterization of Shape Memory Polymers

Angel Romo-Uribe

Abstract Shape memory polymers experience stress-induced macromolecular reorganization like alignment, crystallization, isotropic-to-smectic order, and temperature-induced melting (disorder), crystallization (ordering). The molecular processes involve short and/or long-range order. Hence, there is a need to apply suitable multi-scale characterization techniques to assess the molecular changes occurring during shape memory events. Ideally, the spatial resolution ranges from Å to nm- to μm-scale. This chapter focuses on the application of wide-angle and small-angle X-ray scattering (WAXS and SAXS, respectively), small-angle light scattering (SALS) and optical microscopy techniques which are ideal to get insights into the molecular mechanisms associated to shape memory in polymers. These techniques are ideally suited to enable in situ and *time-resolved* studies. It is the author's view that understanding the molecular mechanisms is at the heart of shape memory effects and novel in situ techniques and *simultaneous* monitoring of microstructure and bulk extensional properties during shape memory cycles need to be implemented. The main body of the chapter focused on fundamentals of X-ray scattering, recording techniques, and applications to the study of shape memory polymers using conventional X-ray sources and synchrotron radiation. WAXS and SAXS enable Å- and nm-scale structure analysis and synchrotron sources enable time-resolved resolution. On the other hand, in situ and *time-resolved* studies of microstructure at μm-scale are enabled by optical microscopy and SALS. These techniques combined with temperature or uniaxial testing are also a powerful tool to understand molecular mechanisms associated to shape memory behavior.

Keywords Shape memory polymer · Structure · X-ray scattering · Optical microscopy · SALS

A. Romo-Uribe (✉)
Research & Development, Advanced Science & Technology Division, Johnson & Johnson Vision Care Inc., Jacksonville, FL 32256, USA
e-mail: aromouri@its.jnj.com

J. Parameswaranpillai et al. (eds.), *Shape Memory Polymers, Blends and Composites*, Advanced Structured Materials 115,
https://doi.org/10.1007/978-981-13-8574-2_12

Glossary of Terms

d	Bragg spacing
f	Orientational distribution function (ODF)
D	Detector-specimen distance
I	Intensity of scattered radiation
$\hat{\boldsymbol{n}}$	Molecular director
$\hat{P}_n$	Weighted Legendre polynomials
$\langle P_n \rangle$	Orientational order parameters
r	Radial spatial coordinate in cylindrical coordinates or radial coordinate in flat-plate camera
R_g	Radius of gyration
$\|q\|$	Magnitude of scattering vector $\left(=\frac{4\pi}{\lambda} Sin\,\theta\right)$
Q	Invariant
λ	Radiation wavelength
2θ	Scattering angle
ϕ	Azimuthal angle

1 Shape Memory Polymers

Shape memory polymers (SMPs) are a new generation of polymeric materials with the ability to keep memory of a permanent shape. Therefore, they fall into the classification of "smart" polymers. SMPs can be programmed into a nonequilibrium temporary shape and return to their permanent shape at will by only applying an appropriate external stimulus. The external stimulus may be temperature, pH, or electric field among various possibilities [26, 30]. Many SMPs are copolymers containing a "switchable" soft phase, many based on poly-ε-caprolactone (PCL), as PCL is biodegradable and biocompatible. PCL-based copolymers may be endowed with shape memory activated by heat and designed into molecular networks with tunable transition/activation temperature, quite close to body temperature. Hence, these materials have focused on biomedical applications [26]. Triple shape memory behavior features one shape change (from temporary shape A to second temporary shape B) followed by a second shape change from shape B to the permanent shape, shape C. A combination of physical and chemical cross-linking is involved into producing triple SMPs [6, 23]. Amorphous biodegradable shape memory polymer networks were observed to be transparent and to undergo bulk degradation and could be good candidate for minimally invasive surgery in areas like ophthalmology [26]. A novel biodegradable multifunctional shape memory copolymer combines in one material shape memory, biodegradability and controlled release of drugs [9, 30]. Other applications envisioned are self-healable coatings [24, 25], and smart fabrics where smart textiles can enable reversible heat and mass transport properties required to achieve next-generation sports and leisure apparel, and Braille. A soft 2W-SMP membrane

will be coated onto a substrate with embedded heaters and constant pressure backing at discrete locations. For a Braille dimple to form, the local area is cooled so that the backing pressure easily deforms the coating. Upon heating, the dimple is erased.

An example of a SMP programmed to hold a capsule at room temperature and then release the cargo at a given temperature above the activation temperature T_a for shape memory effect is shown here [2]. In this case, $T_a = 30$ °C corresponds to the melting transition of the hybrid phase, POSS, covalently attached to PCL. The PCL-POSS SMP network is amorphous, optically transparent, and it has flat permanent shape, as shown in Fig. 1.

Then, the POSS-PCL is heated up at $T > T_a$, wrapped around a capsule and cooled down to $T < T_a$ to fix the shape. The capsule will remain wrapped by the SMP as long as the temperature is below T_a. The release of the capsule is achieved by heating up to $T = 38$ °C $> T_a$. Figure 2 shows the shape memory effect, where the SMP unwraps and releases the capsule within 10 s.

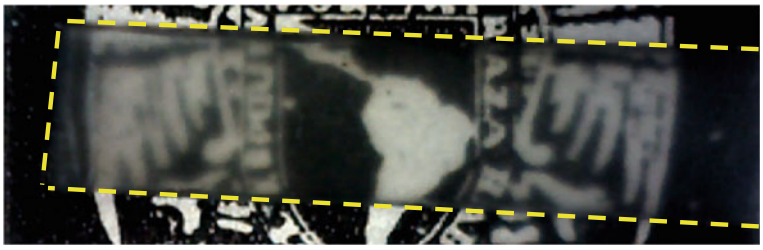

Fig. 1 POSS-PCL shape memory UV crosslinked network with activation temperature $T_a = T_{m,POSS} = 30$ °C and flat permanent shape (see [2] for more details on sample preparation)

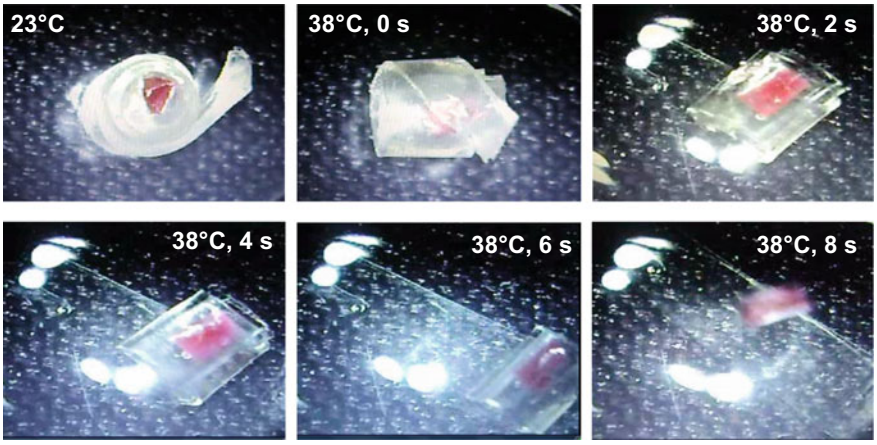

Fig. 2 One-way shape memory behavior of POSS-PCL crosslinked network with activation temperature $T_a = 30$ °C. In order to return to its permanent (flat) shape the SMP unwrapped and released the capsule (Romo-Uribe and Mather, to be published)

1.1 Shape Memory Cycles

The typical thermo-mechanical processes associated to shape memory phenomena are shown in Fig. 3. These are graphical depictions of the distinct types of thermoelasticity observed for (a) one-way (1W-SMPs) and (b) two-way shape memory polymers (2W-SMPs). 1W-SMPs are those polymers with the ability to "memorize" a macroscopic (permanent) shape, be manipulated and "fixed" to a temporary or dormant shape under specific conditions of temperature and stress, and then later relax to the original, stress-free, condition under thermal, electrical, or environmental command. This relaxation is associated with elastic deformation stored during prior manipulation. Moreover, the return of the SMP toward its equilibrium shape can be accompanied by a large force, useful for the deployment of structures, and/or macroscopic shape change. Figures-of-merit for shape memory includes the fixing percentage, R_f, the shape recovery percentage, R_s, and the fully-constrained stress (σ_c)—the stress generated when no shape change is permitted. Because external stress application is required for the elongation step, applications of 1W-SMPs are restricted to one-time actuation or deployment events, such as coronary stent deployments, and the example shown in Fig. 2.

In contrast, 2W-SMPs reversibly contract (heating) and expand (cooling) under the application of a small applied load. So far, several groups have demonstrated such reversible actuation [12, 32, 44, 59].

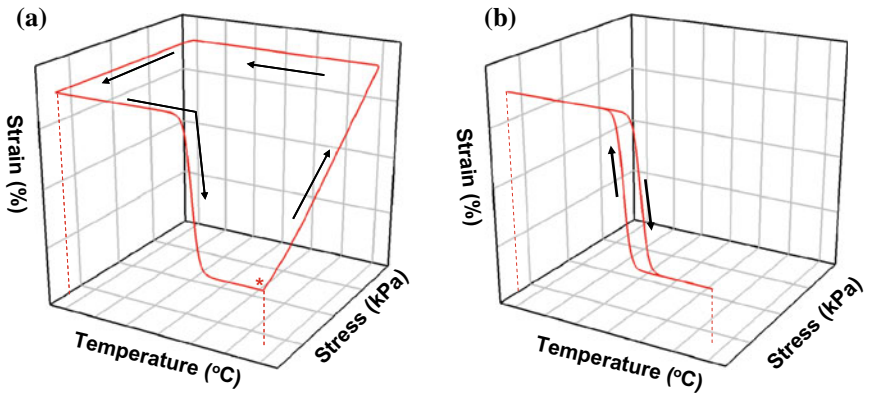

Fig. 3 **a** Shape memory cycle behavior of a high-quality 1W-SMP. Beginning the cycle at the asterix, the material is elongated by increasing stress in the compliant state. Cooling and removing load yields a temporary "fixed" strain that is recovered (more or less) upon heating. **b** 2W-SMP behavior. Heating induces contraction, while cooling induces expansion. This behavior requires small applied stress (3D plots courtesy of Prof. P. T. Mather, Bucknell University)

1.2 Shape Memory and Macromolecular Reorganization

There are undoubtedly molecular mechanisms associated to the production of shape memory phenomena. Figure 4 summarizes the type of polymer architectures utilized and the differentiation between SMPs produced by physical crosslinks or chemical (covalent) crosslinks. There is now much research on designing polymeric materials with shape memory properties including molecular networks [6, 59, 62], nanostructured molecular networks [2–3], epoxy systems [61], polyurethanes [9, 17], hyperbranched polymers/epoxy blends [51], liquid crystalline elastomers [44], smart hydrogels [38, 53], and thermoplastic/epoxy blends [23, 57].

Inducing a given, recoverable, shape comprises: (a) stress-induced macromolecular changes like alignment, crystallization, isotropic-to-smectic order and so on, and (b) temperature-induced melting, crystallization, alignment. These processes involve short and/or long-range order [1, 10, 54]. Hence, there is a need to apply suitable multi-scale characterization techniques to assess the degree of order attained under shape memory events, the spatial resolution ranging from Å to nm- to μm-scale. This chapter will focus on a set of techniques ideal to get insights into the molecular mechanisms associated to the shape memory in polymers, including in situ and *time-resolved* techniques. These are X-ray scattering, and optical microscopy.

In particular, X-ray scattering, wide-angle (WAXS) and small-angle (SAXS), are well-suited techniques for this purpose as the material preparation is relatively simple, most materials are transparent to X-ray radiation, 1D and 2D patterns can be recorded, and in situ, time-resolved studies can be enabled due to developments in instrumentation and high flux facilities [10, 18, 39, 40, 48, 60].

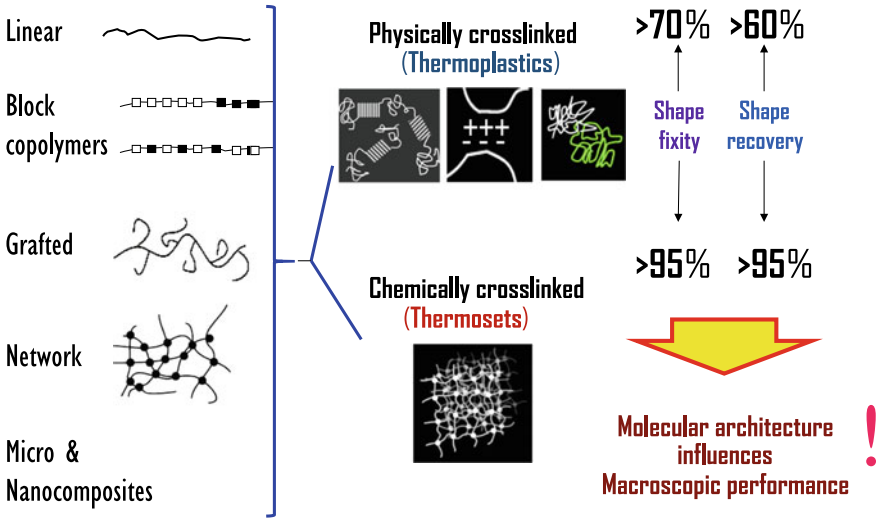

Fig. 4 Molecular architectures involved in shape memory behavior

Conventional physical characterization techniques are not only adequate but a minimum requirement to characterize SMPs. However, it is the author's view that to understand the molecular mechanisms at the heart of shape memory effects novel in situ techniques for *simultaneous* monitoring of microstructure and bulk extensional properties during shape memory cycles need to be implemented.

2 Å and nm-Scale Structure by X-ray Scattering

The special usefulness of X-ray scattering in the study of materials lies in its ability to distinguish ordered from disordered states [1, 58]. Liquids or glasses (so-called amorphous materials) produce X-ray patterns of a diffuse nature consisting of one or more halos, whereas well-crystallized substances yield patterns of numerous sharp circles or spots, Fig. 5 [1]. It may be difficult to select the optimum X-ray diffraction procedure for polymer analysis in advance since the choice rests on so many factors. For example, the stereochemistry of the polymer molecule, the thermal and mechanical pretreatment, the amount of material available, the method of preparing the material for X-ray analysis, and the presence or absence of preferred orientation [1, 58].

2.1 Properties of X-rays

The X-rays of importance in diffraction studies are generated when high-energy electrons impinge on a metal target, the more useful being iron (Fe), copper (Cu) and molybdenum (Mo). At a sufficiently high X-ray-tube voltage, the X-ray beam is found to possess a continuous spectrum of wavelengths (the continuous, or white,

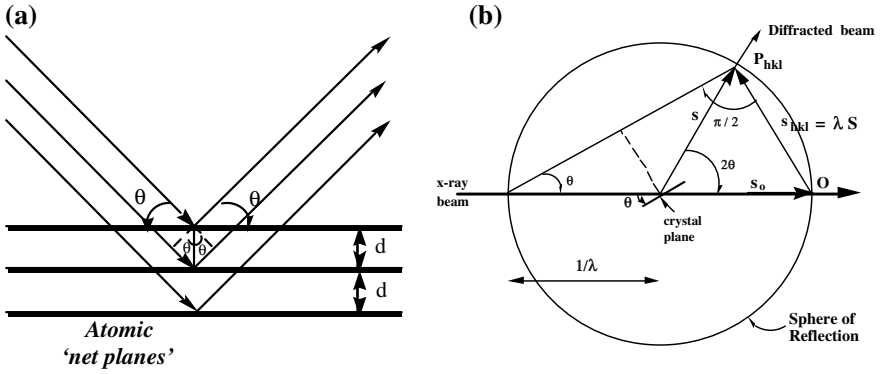

Fig. 5 **a** Bragg's condition, and **b** Ewald's sphere of reflection (for details see [1])

Table 1 Most popular X-ray targets, and wavelengths and filters

Target[a]	$\lambda_{K\alpha}$ (Å)	*Filter*	K-absorption edge (Å)
Fe	1.94	Mn	1.896
Cu	1.54	Ni	1.488
Mo	0.71	Zr	0.689

[a]Alexander [1]

radiation) with a broad maximum in the neighborhood of 0.5 Å and a characteristic spectrum superposed on it consisting of two lines, Kα and Kβ, the Kα line being the more intense (the Kα line is itself a doublet, but in studies of polymers, the separation of the Kα doublet is seldom seen) [1].

It is not possible to get a monochromatic X-ray beam, but it can pass through an appropriate absorbing material to reduce the Kβ line to a negligible level at the cost of depressing the Kα line only moderately, this kind of materials are called "filters". For a given X-ray target the proper β-filter will be evidently the element whose K-absorption edge falls between the wavelengths of the Kα and the Kβ lines of the target. Some of the most common targets and respective filters are listed in Table 1.

When a β-filter is employed, only the Kα X-rays produce sharp diffraction effects, while the residual continuous spectrum has the effect of generating diffuse background. The thickness of the filter is a compromise between reduction of the Kβ component at the cost of attenuation of the Kα intensity. For Cu target the Ni filter is usually chosen about 15–20 μm thick, hence producing the ratio Kα/Kβ of 25–50 [1, 58].

Radiation that is nearly monochromatic can be obtained by inserting a crystal monochromator in the direct X-ray beam and reflecting the Kα line from a set of planes of the monochromator on the specimen to be studied; graphite is utilized as a monochromator for a Cu target [1].

2.2 Bragg's Condition

Fine-scale structure scatters short wavelength radiation into a pattern which when analyzed gives a substantial amount of information about the structure. X-ray, electron and neutron radiation is scattered by the atoms in a crystal to give a well-defined diffraction pattern. The interaction of the incident waves with the standing waves we call crystal planes (Fig. 5a, with spacing d) can be handled in terms of the addition of wave vectors which are normal to the wavefronts (direction of incident radiation and normal to the crystal planes) and have magnitudes of $(\text{wavelength})^{-1}$. The sum of these two vectors, which closes the triangle in Fig. 5b, would represent the scattered radiation except that it is unequal in length to the incident vector and cannot, therefore, represent elastic scattering. We can see that the vector sum can only give elastically scattered radiation when, for given values of $1/\lambda$ and $1/d$, there is a partic-

ular angle θ between the incident beam and the normal to the planes. This is shown in Fig. 5b; note that both ends of the $1/\lambda$ vector lie on a sphere, the sphere of reflection, which has both incident and diffracted vectors as radii, the $1/d$ vector being of course a chord. Simple geometry gives Bragg's Law, with θ being the Bragg angle. Hence, a given set of "planes" will only diffract when Bragg's condition is fulfilled [1, 58].

$$Sin\,\theta_{hkl} = \frac{1/d_{hkl}}{2/\lambda} \tag{1}$$

2.3 Scattering by Polymers

Some of the features encountered in polymer diffraction are as follows:

a. the polymer samples are usually uniaxially oriented and give fiber diagrams that correspond to the rotation photographs of single crystals. Accordingly, it is difficult to get three-dimensional reflection data uniquely. Three-dimensional data can be obtained only for doubly oriented samples (Tadokoro 1979) and for solid-state polymerization products;
b. the diffraction spots are broad and diminish rapidly with increasing diffraction angle since the crystalline regions coexist with the amorphous ones and, furthermore, the former regions contain a considerable number of irregularities; the size of the crystallites is of the order of several hundred Angstroms;
c. Incomplete orientation of the crystallites results in broadening of the spots along the arcs at a constant diffraction angle;
d. The number of independent observable reflections is small (at most 200, usually 40–100) compared to that of single crystals (usually more than 1000) [1].

2.4 Random Microcrystalline Versus Oriented Specimens

In bulk and molded polymer specimens the orientations of the crystalline regions, which may be designated crystallites, tend to be statistically random. This is a natural consequence of the mechanisms of nucleation and crystal growth in the melt or concentrated solutions. Because of the minuteness of the crystallites, with dimensions typically about 50 nm, even a sample amounting to a few milligrams contains a vast number of crystallites, which results in all orientations being represented in equal proportions. Hence, a monochromatic X-ray beam will generate a typical powder-diffraction pattern, which consists of a number of relatively sharp concentric circles superposed on a background of diffuse X-ray scatter, Fig. 6a, b. These are called Debye-Scherrer patterns after their discoverers.

Natural and synthetic fibers exhibit various degrees of axial orientation. Small- and wide-angle photographs are most commonly prepared with the fiber axis normal

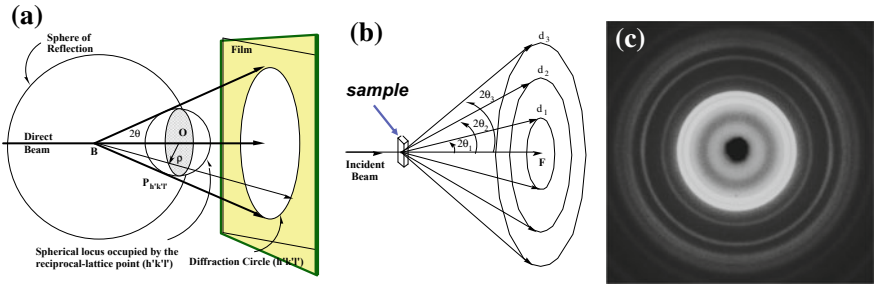

Fig. 6 **a** A set of crystallographic planes (h, k, l) assumes all orientations with equal probability P is dispersed over all positions on the surface of a sphere of radius $1/d_{hkl}$. The sphere intersects the sphere of reflection in a circular zone. **b** In the same way, another reciprocal lattice node with different indices (h', k', l') will generate a diffraction cone at a different angle, and so on thus producing a so-called Debye-Scherrer pattern (for more details see [1]). **c** Debye-Scherrer pattern of polypropylene (PP), Ni-filtered CuKα radiation

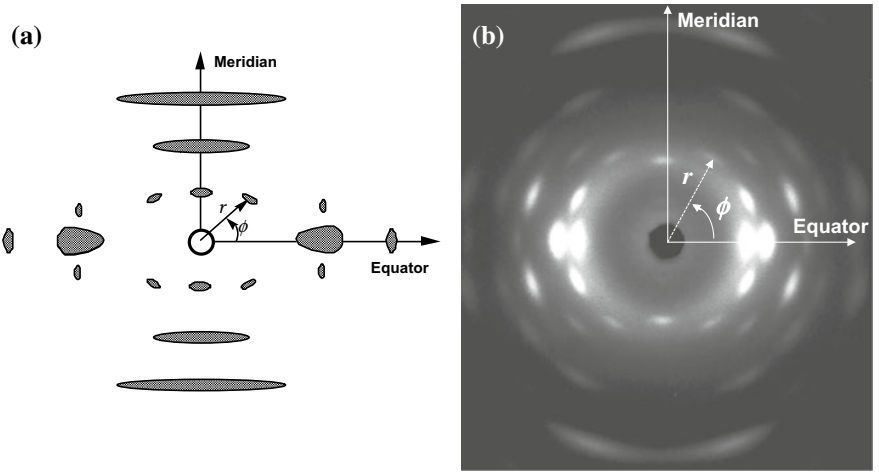

Fig. 7 **a** The figure illustrates a fiber diffraction pattern, where the *fiber axis* ***c*** is vertical. The position of any reflection on the pattern is defined by a radial coordinate r and the azimuthal angle, ϕ. **b** Fiber pattern of polyether-ether ketone (PEEK). Flat-plate camera, CuKα and graphite monochromator

to the incident X-ray beam, the direction of the film parallel to the fiber axis being designated the ***meridian***, and the direction at right angles the ***equator***. A location on the film can be designated by a radial distance r from the undeviated beam and an azimuth ϕ with respect to the equator. These conventions are illustrated in Fig. 7.

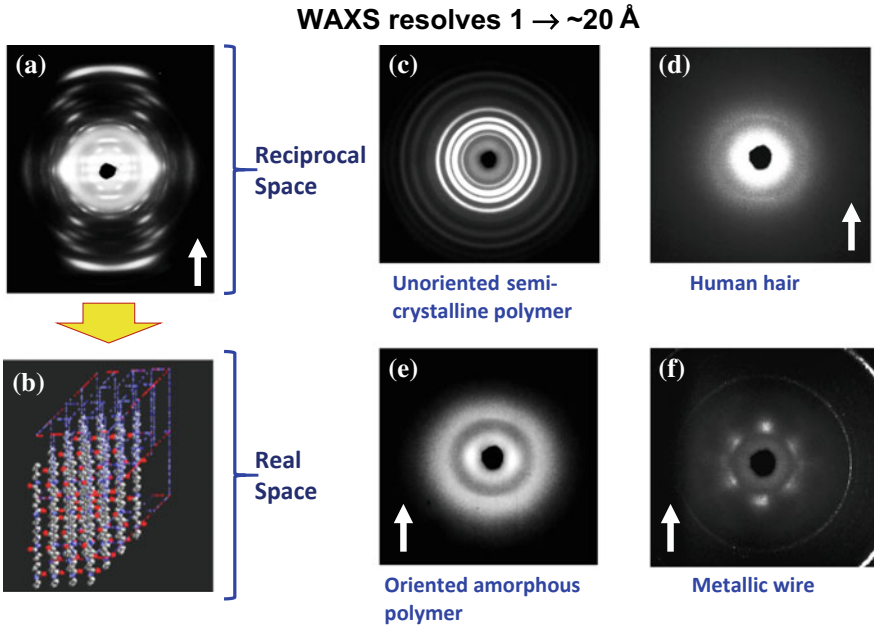

Fig. 8 WAXS resolves intra- and interchain distances; it discerns oriented versus unoriented structures, amorphous and semicrystalline phases, and structure of organic, inorganic, and hybrid compounds

2.5 Methods in X-ray Scattering

In appropriate circumstances, practically all X-ray diffraction equipment useful in the study of solid materials is also applicable to polymers. The apparatus that is best suited to obtain a specific kind of information (e.g., presence or absence of crystallinity, size of crystalline regions, degree of crystallinity, mode of preferred orientation, crystal structure, etc.) may be quite different from that suited to another goal.

Figures 8 and 9 summarize the spatial resolution achieved with WAXS and SAXS, with emphasis on 2D recording. The 2D patterns were obtained using photographic film, CCD cameras, and area detectors, and exemplifies the usefulness of X-ray scattering when analyzing a variety of materials, i.e., natural, synthetic, metallic, and in solid and liquid phases, over a broad range of spatial resolution.

2.5.1 Recording Instrumentation and Diffraction Geometries

X-ray diffraction patterns are nowadays recorded only with electronic detectors, namely counter diffractometers, position sensitive detectors (PSDs), image plates,

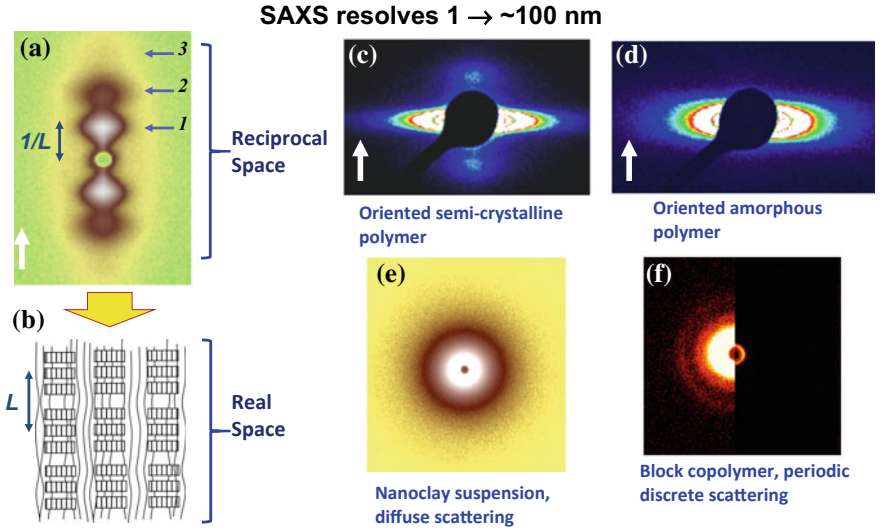

Fig. 9 SAXS resolves nanostructures; it discerns oriented versus unoriented state, spatial periodicity, fractal dimension, and particle/void size in gas, solid, and liquid state

area detectors or CCD cameras. The original and rather powerful photographic recording first applied by von Laue in 1912 has been abandoned (Ewald 1962). 1D intensity traces are recorded with counter diffractometers and PSDs, whereas 2D patterns are obtained with image plates, area detectors, and CCD cameras. 1D traces obtained with counter diffractometers can take minutes to hours and requires stable X-ray sources. Relatively fast, nearly time-resolved 1D traces can be obtained with PSDs and conventional sealed tube and rotating anode X-ray generators (an entire trace can be obtained within few seconds, as shown in examples in the next section).

There are several well-standardized diffraction techniques, which serve very satisfactorily for the great majority of polymer analysis, and the choice is mainly based on the instrumentation available. Some of the most common techniques are as follows:

(a) symmetrical transmission with flat-plate camera, Fig. 10a;
(b) symmetrical fiber diffraction with a cylindrical camera, Fig. 11a;
(c) small-angle scattering technique with (i) pin-hole (Fig. 10a), or (ii) slit collimators.

In the case of flat-plate camera the relationship between film-specimen distance D, radial distance of a given reflection r, and the Bragg angle θ is given by

$$r = D \tan 2\theta \tag{2}$$

In cylindrical or Debye-Scherrer cameras the scattering angle θ is proportional to the arc length L and the radius of the camera R,

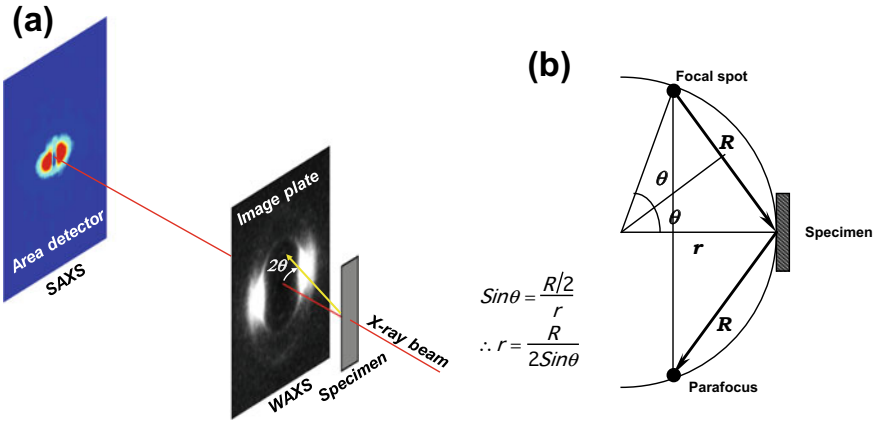

Fig. 10 **a** Symmetrical transmission mode with pin-hole collimation. **b** The parafocusing effect in the symmetrical reflection diffractometer. R = source–specimen distance = specimen–parafocus distance; r = radius of focusing circle

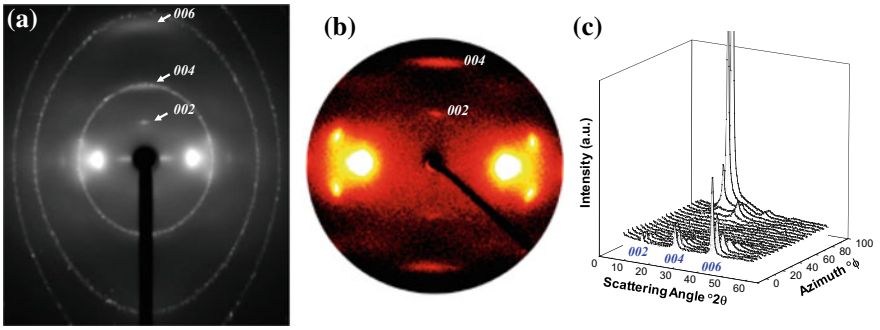

Fig. 11 WAXS patterns of same copolyester fiber, recorded with: **a** cylindrical camera and photographic film, 30 min exposure; **b** area detector, 5 min exposure; and **c** scintillation counter, symmetrical reflection mode, step scans varying radial and azimuthal angles, 360 min recording time ($\phi = 0°$ meridional, and $\phi = 90°$ equatorial axes). CuKα radiation

$$\theta = \frac{L}{4R} \tag{3}$$

In the case of counter diffractometry, the symmetrical reflection geometry is the most popular arrangement. A great advantage is the high X-ray intensity which can be achieved, due to the "parafocusing" effect which is shown in detail in Fig. 10b. The problem of low scattered X-ray intensity arises from the non-infinitesimal dimensions of a typical sample; each volume element within a real sample produces a cone of diffracted rays at the appropriate Bragg angle, which leads to an overall diffuse pattern. However, if a circle (radius R) is drawn through the focal spot and at a tangent to the specimen surface, all "reflected" rays originating from this circle would unite

at the parafocus, as shown in Fig. 10b. In practice, the specimen surface does not deviate greatly from the focusing circle, and thus a good degree of focusing of the X-rays is achieved, with the consequent improvement in the scattered intensity.

2.5.2 Wide-Angle X-ray Scattering, WAXS

WAXS is the most utilized technique in polymer structure investigation due to its apparent simplicity. Information like degree of crystallinity, quantification of macromolecular alignment, interchain spacing, and crystal structure can be readily obtained. As stated above, the X-ray generator power coupled to the recording method and geometry defines the exposure time, and the choice will depend on specific conditions and information sought. For instance, Fig. 11 shows WAXS fiber patterns of the same polymeric fiber recorded with three different devices and geometries, namely (a) photographic recording and cylindrical camera, (b) area detector, and (c) scintillation counter. The collection time varied from 5 min to 360 min (an increase >70-fold!). Note that the cylindrical camera provides a broad angular range along the meridian (°2θ) and the complete azimuthal range (°ϕ) than an area detector. On the other hand, the scintillation counter provides accurate intensity measurements in one quadrant only ($2\theta = 5 \rightarrow 50°$ and $\phi = 0 \rightarrow 90°$) as it is quite time-consuming.

Hot-Stage WAXS

Fast recording using a PSD enables time-resolved studies of, for instance, temperature-induced phase transitions in polymers. The temperature of the transition and the phase obtained can be determined by WAXS. Therefore, hot-stage WAXS results complement those obtained with a thermal analyzer, e.g., differential scanning calorimetry (DSC). Figure 12a shows a series of WAXS traces of a polymer during heating at constant rate of 10 °C/min, and each trace recorded every 20 s. The traces clearly show the sharpening of the intermolecular reflection at 150 °C ($>T_g = 110$ °C) denoting an increase of degree of crystallinity. Eventually, at 290 °C, the polymer melted and the WAXS trace shows a broad amorphous halo.

Utilization of scintillation counters can also provide information on phase transitions in polymers. The experiments, however, cannot be carried out in continuous mode, but the temperature is increased in steps, and holding isothermally during the X-ray measurements. Figure 12b shows a series of WAXS traces as a function of temperature, scanning at 2°2θ/min. Hence, each trace required 750 s collection time.

The results are shown in Fig. 12 also enable to determine the thermal expansion of the unit cell in the polymer. Figure 13 shows the results obtained from a temperature scan, where the main interchain distance (extracted from the *110* equatorial reflection) and the chain dimension (extracted from the *002* meridional reflection) are plotted as a function of temperature. The results show that temperature induced an increase of interchain distance and, most intriguingly, an increase of the length along the chain axis, i.e., chain straightening. This last result is not obvious, espe-

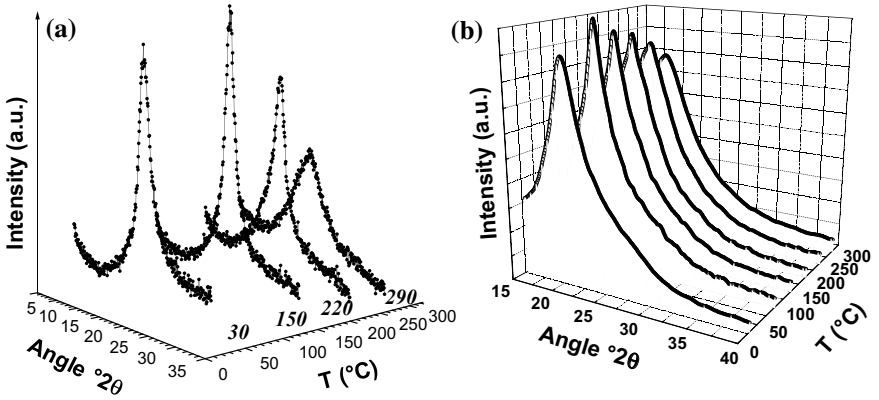

Fig. 12 WAXS traces as a function of temperature of copolyesters: **a** time-resolved WAXS traces of HBA-HNA 73:27 recorded with PSD, 20 s/trace (more details in [36]); **b** WAXS traces of B-ET 40:60 recorded with scintillation counter in continuous mode at 2°2θ/min = 750 s/trace (more details in [41]). Ni-filtered CuKα radiation

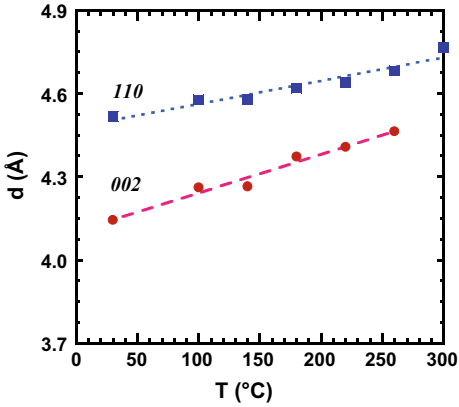

Fig. 13 Interchain distance (extracted from the *110* equatorial reflection) and the chain dimension (extracted from the *002* meridional reflection) of a thermotropic polymer as a function of temperature

cially for flexible chain polymers where random coil conformation is favored. The polymer, however, is a stiff chain aromatic thermotropic polymer. The lines in Fig. 13 are linear fits, hence, the hot-stage WAXS results also enable to determine the linear thermal expansion of the unit cell from the slope of the linear fits.

Degree of Crystallinity

The degree of crystallinity, χ, can be quantified utilizing Ruland's method [1, 47], where

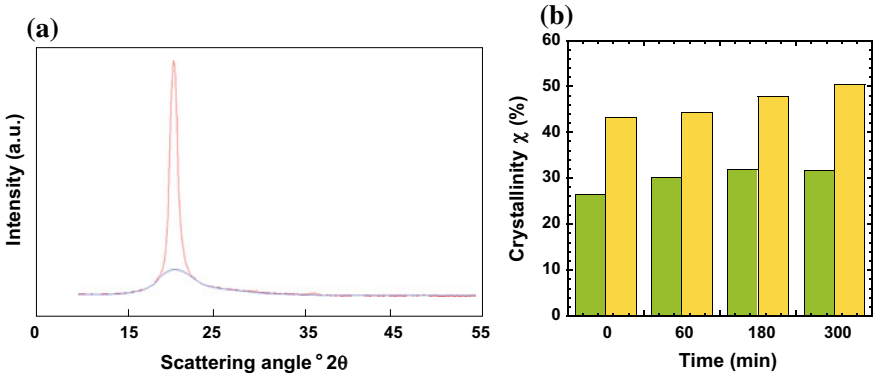

Fig. 14 **a** WAXS trace obtained with a θ/2θ diffractometer and Ni-filtered CuKα radiation. The blue line denotes the amorphous background contribution, which is subtracted from the total intensity to determine the crystalline contribution and the degree of crystallinity χ. **b** Degree of crystallinity as a function of heat treatment time of thermotropic copolyesters B-N (■) and COTBP (■)

$$\chi = \frac{\int_0^\infty I_c(q) \cdot q^2 \cdot dq}{\int_0^\infty I(q) \cdot q^2 \cdot dq} \tag{4}$$

where I_c is the intensity contribution from the crystalline phase, I is the total diffracted intensity, and q is the magnitude of the scattering vector defined as

$$|\vec{q}| = q = \frac{4 \cdot \pi \cdot \sin\theta}{\lambda} \tag{5}$$

Figure 14a shows a typical intensity trace used for the calculation of χ, and the separation of amorphous and crystalline components in the intensity traces can be carried out using commercially available software (e.g., PowderX or Polar v2.6). After numerical integration, the plot of degree of crystallinity as a function of time for two different polymers is shown in Fig. 14b. These results enable to compare the response of each polymer to thermal annealing.

Macromolecular Orientation and Order Parameter

Polymers subjected to shear and/or extensional flow, or tensile deformation exhibit some degree of macromolecular alignment along the applied field. The degree of macromolecular alignment is quantified from the integrated intensities, I(ϕ), of the main equatorial maximum as a function of the azimuthal angle ϕ, shown in Fig. 7a. Note that the azimuth $\phi = 0°$ corresponds to the equatorial axis and $\phi = 90°$ corresponds to the meridional (molecular) axis. The order parameter can be quantified by the orientational distribution function, $f(\beta)$, of the molecular axis relative to the molecular director, $\hat{n}$, as shown in Fig. 15a. The order parameters $\bar{P}_n$ are defined as

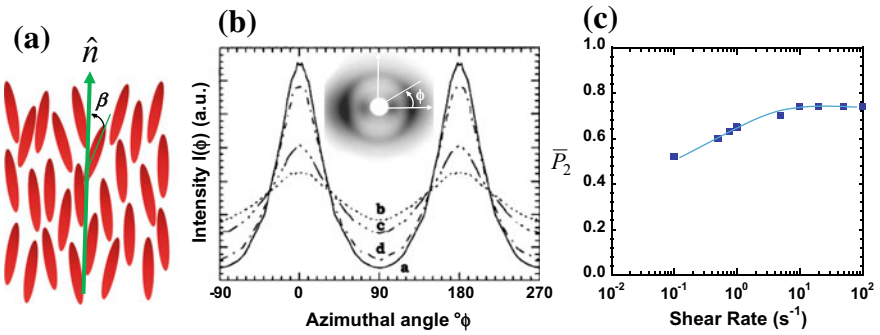

Fig. 15 **a** Nematic order, with molecular orientational order along the molecular director $\hat{n}$, and positional disorder. **b** Azimuthal intensity traces around main interchain reflection. Inset shows typical WAXS pattern of oriented polymer, and definition of azimuthal angle ϕ. **c** Order parameter $\bar{P}_2$ as a function of shear rate of nematic polymer in the molten state (T = 310 °C) (for more details see [43] and [35])

$$\bar{P}_n = \int_0^{\pi/2} P_n(Cos\,\beta) f(\beta) d(Cos\,\beta) \tag{6}$$

where $f(\beta)$ denotes the finite probability for a given molecule to have its axis at an angle β to the director $\hat{n}$, and $P_n(x)$ is the Legendre polynomial [28]. Leadbetter and Norris [22] showed that the intensity I(ϕ) around the equatorial reflection is utilized to determine the orientational distribution function using

$$I(\phi) = \int_{\phi}^{\pi/2} f(\beta) Sec^2\,\phi (Tan^2\,\beta - Tan^2\,\phi) Sin\,\beta d\beta \tag{7}$$

where ϕ is the azimuthal angle. From the analytical solution of Eq. (7), as derived by Deutsch [13], the order parameter $\bar{P}_2$ is determined. The results are

$$f_1(\beta) = -\frac{1}{NCos^3\,\beta} \int_{\beta}^{\pi/2} \left\{ \frac{d[I(\phi)Cos^2\,\phi]}{d\phi} \right\} \frac{d\phi}{(Tan^2\,\phi - Tan^2\,\beta)^{1/2}} \tag{8}$$

$$f_2(\beta) = -\frac{1}{NSin\,\beta} \frac{d}{d\beta} \left\{ \int_{\beta}^{\pi/2} \frac{I(\phi) Tan\,\phi d\phi}{(Tan^2\,\phi - Tan^2\,\beta)^{1/2}} \right\} \tag{9}$$

where N is a normalizing constant given by

$$N = \int_0^{\pi/2} f(\beta) Sin\,\beta d\beta = \int_0^{\pi/2} I(\phi) d\phi \tag{10}$$

where a factor of $(2/\pi)$ common to Eqs. (8) and (9) was eliminated. The Eqs. 8 and 9 are the requested analytic solutions of the integral equation, Eq. (7). Deutsch [13] also showed that it is possible to calculate orientational distribution functions-averaged quantities directly from the measured intensity $I(\phi)$ without having to calculate $f(\beta)$ first. This is particularly advantageous in cases when error amplification proves to be a serious problem in calculating $f(\beta)$, due to large experimental errors in, or scarcity of, the intensity data. The two lowest and most important order parameters are

$$\langle P_2 \rangle = 1 - \frac{3}{2N} \int_0^{\pi/2} I(\phi) \left\{ Sin^2\phi + Sin\phi Cos^2\phi \ln\left[\frac{1 + Sin\phi}{Cos\phi} \right] \right\} d\phi \tag{11}$$

$$\langle P_4 \rangle = 1 - \frac{1}{N} \int_0^{\pi/2} I(\phi) \left\{ Sin^2\phi \left(\frac{105}{16} Cos^2\phi + \frac{15}{24} \right) \right\} d\phi + \frac{1}{N} \int_0^{\pi/2} I(\phi) \left\{ Sin\phi \ln\left[\frac{1 + Sin\phi}{Cos\phi} \right] \left(\frac{105}{16} Cos^4\phi - \frac{15}{4} Cos^2\phi \right) \right\} d\phi \tag{12}$$

In these expressions, the order parameters are obtained from an integral over the measured intensity $I(\phi)$. The accuracy achievable in calculating the various quantities discussed above is limited only by the quality and density of the measured data, assuming, of course, that sufficiently accurate numerical methods of integration and interpolation are employed. Figure 15b shows a series of azimuthal intensity traces obtained from uniaxially oriented polymer with varying degree of orientation. The azimuthal broadness and amount of amorphous background determine the degree of macromolecular alignment $\bar{P}_2$. An application of this formalism is shown in Fig. 15c, where the order parameter $\bar{P}_2$ is plotted as a function of shear rate for a nematic molten polymer.

2.5.3 Small-Angle X-ray Scattering, SAXS

SAXS allows the characterization of any long-range order, in the order of 1–100 nm. SAXS from an inhomogeneous system may consist of either diffuse or discrete scattering [4]. The properties that can be extracted from SAXS measurements in polymers consist of (a) long-range molecular order; (b) size of crystallites (e.g., semicrystalline polymers); (c) size and type of nanophases (e.g., block copolymers); (d) morphology; (e) particle size in dilute solutions and colloidal dispersions, i.e., radius of gyration; (f) microvoid/micropore size; and (g) fractal dimension.

Diffuse SAXS Scattering

Such scattering is essentially particulate in origin but modulated to some extent by interparticle interferences. This is the basis for the concept of a dilute system, which produces pure particulate scattering [4]. The angular limit within which the scattering occurs is inversely proportional to the size of the inhomogeneities in the electron density distribution within the specimen. Hence, the diffuse scattering from a loose aggregate of oriented particles will have its largest extension in the direction of the smaller particle dimension and its smaller extension in the direction of the larger dimension. Therefore, the shape of the diffuse scattering depicts the particle shape in reverse (i.e., reciprocal space).

It is important to realize that a diffuse scattering pattern is never subject to an unequivocal structural interpretation on the basis of the X-ray data alone. Moreover, specimens that yield identical scattering patterns may be designated as *scattering-equivalent systems*. The interpretation of diffuse small-angle scattering always carries the following types of ambiguities [1]:

(a) It is not possible to distinguish the scattering by a system of particles in space from the scattering by a complementary system of micropores in a solid continuum. The choice between these alternatives is usually made on evidence bearing on the nature of the system concerned.
(b) It is not possible to differentiate, without some degree of uncertainty, the effects due to particle shape from those due to polydispersity. Hence, scattering equivalence may result from a special particulate shape and a certain distribution of particle sizes.
(c) In dense systems interparticle scattering cannot be neglected. Thus, it is difficult to discern to what extent the scattering data is determined by the isolated particles and to what extent by interparticle interferences.

Examples of nanostructured materials that exhibit small-angle diffuse scattering are colloidal and polymer solutions, equatorial scattering from polymer fibers, layered polymer nanocomposites, and catalysts. Figure 9d and e shows polymers exhibiting diffuse scattering, anisotropic and isotropic, respectively.

When the concentration of the particles is sufficiently dilute, the positions of individual particles, far apart from each other, are uncorrelated. Under these conditions, the waves scattered from different particles are incoherent among them, and the observed intensity simply becomes the sum of the individual scattering. If the particles are of irregular or unknown shape, the data may be analyzed according to the *Guinier Law* to determine the radius of gyration characterizing the size of the particles [19]. Thus, in the limit of small scattering vector q,

$$I(q) = \rho_o^2 v^2 \cdot \exp\left(-\frac{1}{3} q^2 R_g^2\right) \tag{13}$$

where $I(q)$ is the intensity of independent scattering by a particle, $q = (4\pi/\lambda)sin\theta$, and 2θ is the scattering angle. Equation (13) is called the Guinier Law, and allows for

the determination of the radius of gyration R_g of a particle or void from small-angle scattering by plotting ln I versus q^2. The Guinier Law is valid provided that:

(1) $q \ll 1/R_g$,
(2) the system is dilute so that the particles in the system scatter independently of each other,
(3) the system is isotropic, i.e., the particles assume random orientations
(4) the matrix (or the solvent) in which the particles are dispersed is of constant density and devoid of any internal structure that can by itself give scattering in the q-range of interest.

Diffuse Scattering from Nanopores

As far as SAXS is concerned a catalyst can be considered a dilute particle system where the particles are dispersed in a uniform matrix of a second material. In a catalyst, the "particles" consist of *nanovoids* and these are continuously dispersed throughout the material, the "matrix".

The SAXS measurements of Fig. 16 were carried out using the Dmax2500® rotating anode X-ray generator (Rigaku Inc.), in the scattering range 0.08°2θ to 2.5°2θ (using step scan mode, in steps of 0.005°2θ). Ni-filtered CuKα radiation was used, $\lambda = 1.54$ Å. Scattered intensities were corrected for background contribution by carrying out a scan without a sample. 1D scan took approximately 60 min to complete. The Guinier plot produced a straight line and the radius of gyration of the porous structure was determined from the slope, $R_g = 100$ Å $= 10$ nm.

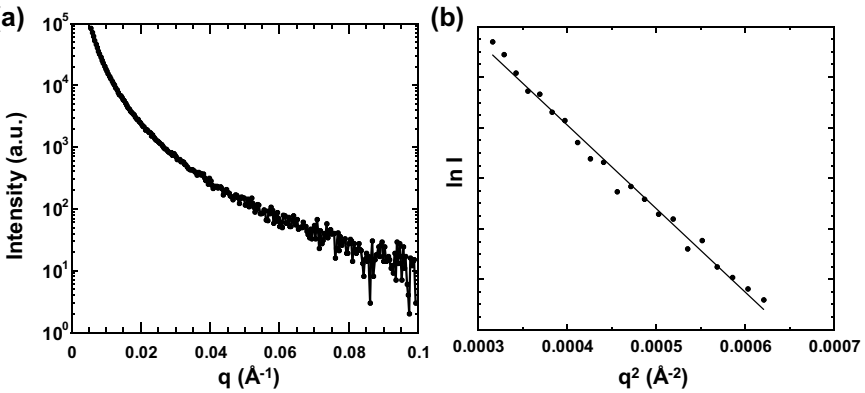

Fig. 16 **a** Typical SAXS intensity trace of a catalyst. **b** Corresponding Guinier plot in the limit of small q. Radius of gyration was determined from the slope and using Eq. 13, $R_g = 100$ Å $= 10$ nm. CuKα radiation

Diffuse Scattering from Fibrous Structure

The SAXS pattern of extruded and heat treated polymeric film is shown in Fig. 17a; it exhibits diamond-shaped intensity streaks along the equatorials axis, typically observed in highly oriented polymers, e.g., fibers. The equatorial diamond-shaped scattering corresponds to scattering objects extended along the extrusion (macromolecular) axis. Note that scattering and real space are reciprocal Hsiao and Chu [10].

Structural information can be extracted from the equatorial SAXS intensity trace shown in Fig. 17a. The trace corresponds to diffuse scattering, i.e., intensity decaying monotonically as a function of scattering vector q. The equatorial streaks can be associated with nanovoid morphology or microfibrillar structure in highly aligned semicrystalline and liquid crystalline polymers [1, 16, 40]. X-ray scattering arises from electron density differences, and therefore microfibrils and nanovoids are scat-

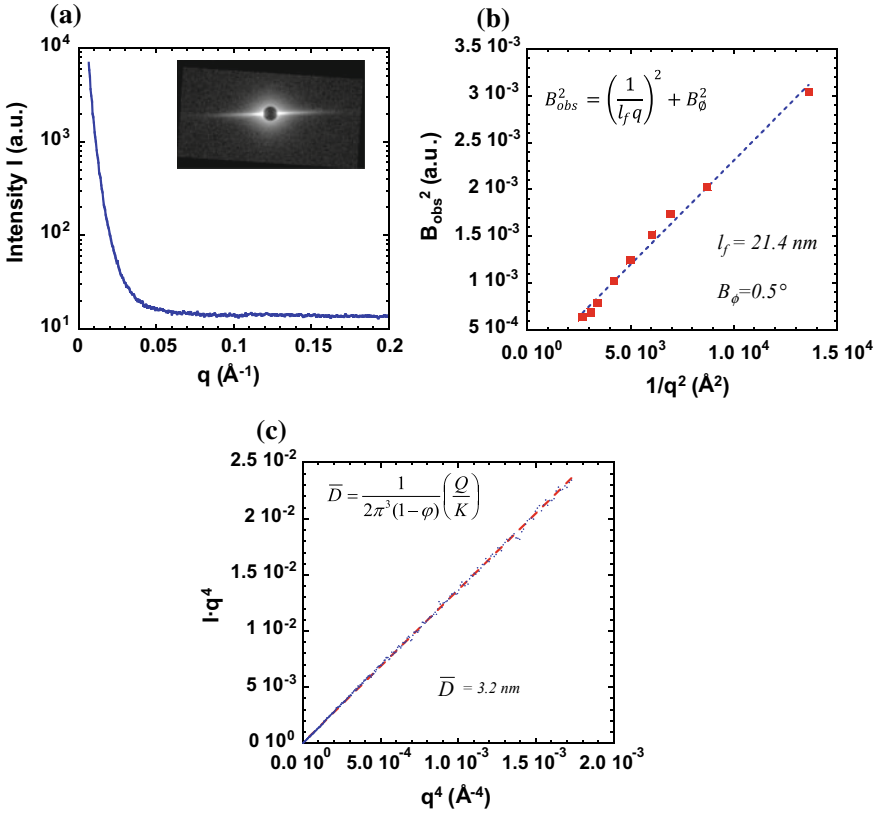

Fig. 17 **a** SAXS pattern and equatorial intensity trace. **b** Nanovoid length and misorientation angle extracted from azimuthal spread of equatorial streak as a function of $1/q^2$. **c** Porod-Debye plot from equatorial intensity (for more details see [40])

tering equivalents. Hence, a complementary technique is needed to assess the exact identity of the structure giving rise to SAXS scattering.

Nevertheless, the diamond-like scattering indicates that the scattering objects are of elongated ellipsoidal shape. Analysis of the equatorial intensity distribution is carried out according to a method proposed by Ruland and described in detail by Ran et al. [33] to determine the average length, l_f, and misorientation angle B_ϕ, from the extrusion axis of the scattering object. This is because the size distribution and the misorientation of the scattering objects contribute to the equatorial streak profile. For this, the angular spread B_{obs} of each azimuthal trace as a function of q must be determined. From the angular spread, the length (l_f) and the misorientation width B_ϕ of the scattering object can be determined using the following Gaussian fit,

$$B_{obs}^2 = \left(\frac{1}{l_f q}\right)^2 + B_{\emptyset}^2 \tag{14}$$

A Gaussian or Lorentzian function should be tested and choose the model that better fits the experimental data. The average length l_f is determined from the slope of the plot B_{obs}^2 versus $1/q^2$, and the square root of the intercept gives the angular misorientation width B_ϕ. The angular spread is the full width at half maximum (FWHM) of the azimuthal intensity trace, and the plot is shown in Fig. 17b.

Additional information can be extracted from the equatorial intensity. The lateral size and distribution of the oriented scattering objects control the distribution of intensity in the equatorial plane [10]. Porod-Debye plots, $q^4 \cdot I(q)$ versus q^4, are utilized to estimate the density of interfaces whose normal lie in the equatorial plane. If the scattering objects are approximately cylindrical, with volume fraction φ, then the mean diameter of the scattering object can be determined using the equation proposed by Grubb et al. [15], and Kumar et al. [20]:

$$\bar{D} = \frac{1}{2\pi^3(1-\varphi)}\left(\frac{Q}{K}\right) \tag{15}$$

where

$$K = \lim_{q\to\infty}\left[q^4 I(q)dq\right] \tag{16}$$

and the invariant Q is defined as

$$Q = \int_0^\infty q^2 I(q)dq \tag{17}$$

The Porod-Debye plots are shown in Fig. 17c, the data show excellent linear behavior. If φ is taken as the degree of crystallinity (determined by WAXS), then the scattering

objects correspond to crystalline fibrils and the average width of the scattering objects is 6.6 nm. If the scattering objects are nanovoids, then the average width is 3.2 nm.

Discrete SAXS Scattering

Among polymeric and biological materials there are many examples of ordered structures having a period of the order of 1–100 nm, and such structures are suitable to study by small-angle scattering. However, the degree of periodic order in these systems is usually much poorer than in crystals and dealing with the effects of such "imperfections" constitutes a significant part of the effort in the analysis [1].

The periodic systems that are subjected to small-angle scattering studies are mostly of lamellar morphology, as in folded-chain lamellar crystals, membrane structures, core-shell structures (e.g., latex particles), and block copolymers with lamellar ordering, as shown in Fig. 9a, c [10]. Figure 18a, b shows the SAXS patterns and radial intensity trace due to an ordered lamellar nanostructure in a block copolymer. The pattern exemplifies discrete small-angle scattering. The average separation between nanodomains is determined from the position of the intensity maximum, q_m, using Bragg's law [1]:

$$\bar{L} = \frac{2\pi}{q_m} \tag{18}$$

In oriented semicrystalline polymers (i.e., films and fibers) and natural fibers, the discrete scattering interferences appear in only one direction, most commonly along

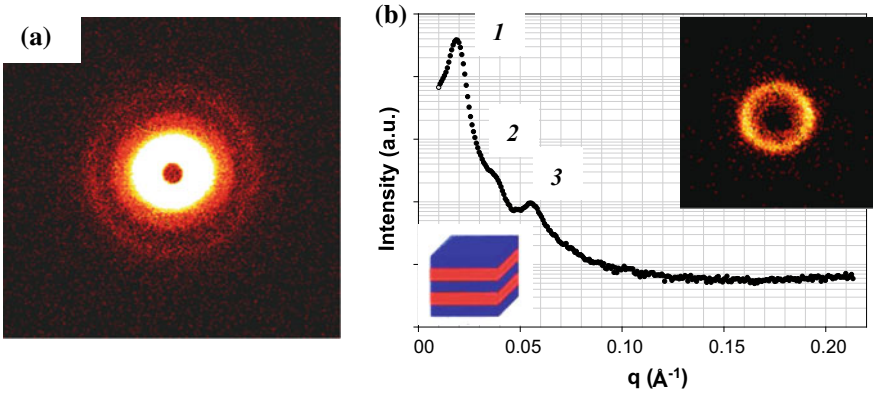

Fig. 18 Examples of discrete and diffuse small-angle scattering. **a** SAXS pattern of a block copolymer. **b** Radial intensity trace of pattern in (**a**). The inset corresponds to inner region of pattern in (**a**) obtained by reducing exposure time by 50% to enhance the first order maximum. The intensity trace shows that the maxima positions are integer multiples of the 1st order reflection and therefore the nanostructure is lamellar (for more details see [37])

the orientation axis, denoted the Meridian [39]. Meridional reflections denote some degree of large-scale periodic character in the structure parallel to the fiber axis. Analysis of these diffraction patterns enable, for instance, the determination of the lamellar or domain size in semicrystalline polymers and block copolymers, and the type of nanophase exhibited by narrow molecular weight distribution block copolymers [10, 37].

3 Structure Evolution and Shape Memory by X-ray Scattering

3.1 PCL-POSS Chemical–Physical Networks

WAXS and SAXS have been applied to study in detail the micro and nanostructure in POSS-PCL hybrid nanocomposites and their macromeric precursors. These networks feature two PCL chains tethered to a *single* POSS moiety, thus resembling an asymmetric block copolymer with crystallizable blocks, as shown in Fig. 19a [2]. These nanocomposites exhibited shape memory behavior as shown in Fig. 19b, with the molecular architecture enabling dynamic coupling between crystallization and microphase separation. Strikingly, such a system showed a highly ordered nanoscale superstructure not only in the precursors but also in the covalently crosslinked networks [2].

Analysis of the influence of stress applied during shape memory cycles by *simultaneous* WAXS/SAXS experiments showed that not only stress-induced crystallization of POSS and PCL, but a strikingly highly ordered nanostructure featuring POSS clusters coexisting with lamellar PCL nanodomains.

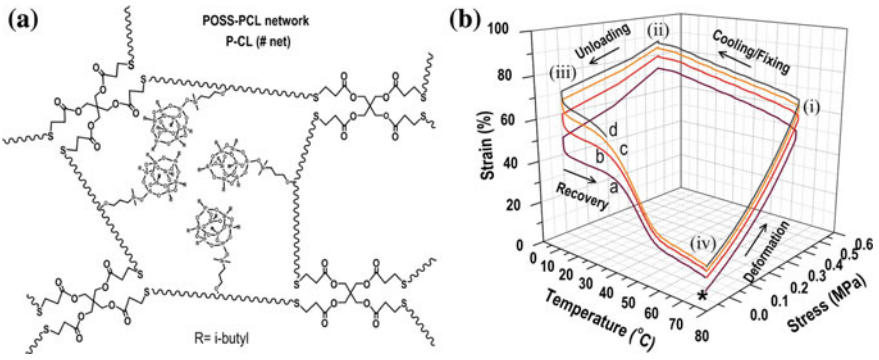

Fig. 19 **a** Idealized structure of POSS-PCL chemical/physical double molecular networks with a single POSS tethered to PCL, **b** three one-way shape memory cycles (for more details see [3])

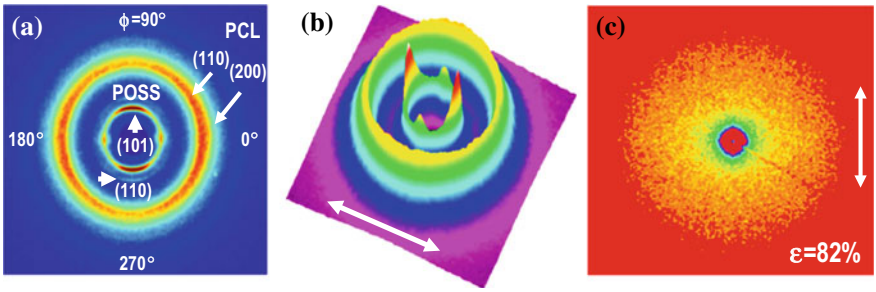

Fig. 20 Uniaxial stretched POSS-PCL 2.6 networks with diacrylate:tetrathiol molar ratio of 1:1. **a** 2D pattern, **b** 3D pattern, **c** 2D SAXS pattern. Arrow indicates the stretching direction. Room temperature and Ni-filtered CuKα radiation (more details in [3])

Simultaneous WAXS/SAXS patterns were acquired at room temperature after stretching at 80 °C to 82% strain, and the 2D and 3D WAXS patterns are shown in Fig. 20a, b. The WAXS pattern was recorded using an image plate, and the SAXS pattern was recorded using an area detector; pin-hole collimation and a rotating anode X-ray generator were utilized [3]. The patterns are anisotropic, indicating stress-induced molecular orientation. Moreover, the WAXS pattern exhibits *110* and *200* reflections for PCL crystalline phase, and *101* and *110* crystalline reflections corresponding to POSS phase. These results show that: (a) in the molecular network the POSS crystals are *biaxially* oriented (see the four internal reflections in the 3D pattern), and (b) under the restricted mobility afforded by the high degree of cross-linking of POSS-PCL2.6-net-2:1, the PCL chains are still able to orient and crystallize.

The nanoscale structure of the stretched macromolecular networks was also investigated by collecting the SAXS pattern, as shown in Fig. 20c. The pattern is anisotropic, and the stretched network exhibits strikingly ordered nanostructure. Analysis of the intensity traces along equatorial and meridional axes revealed spatial periodicity associated to PCL lamellar morphology with long-distance of 63.6 nm. This morphology coexisting with POSS oriented nanostructure [3].

The WAXS and SAXS analysis enable a schematic representation suggested for the crystalline arrangement of POSS and PCL after straining the molecular networks, this is shown in Fig. 21. The scheme depicts the crystallization of initially amorphous PCL chains upon the applied stress field and the biaxial reorientation of POSS rhombohedral crystals.

3.2 PCL-POSS Chemical Networks

Here simultaneous WAXS and SAXS experiments were carried out to study in detail the micro and nanostructure in randomly crosslinked POSS-PCL molecular net-

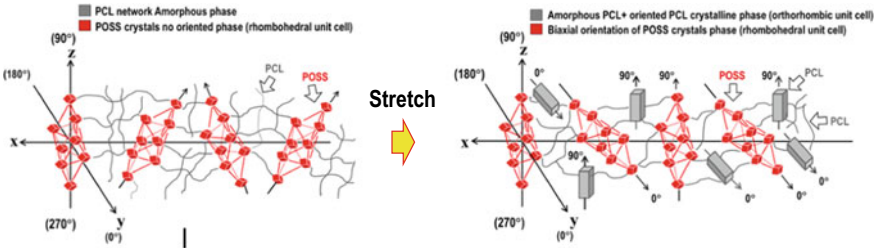

Fig. 21 Stylized sketch of phase behavior of POSS crystals and amorphous PCL network in a POSS-PCL crosslinked network (adapted from [3])

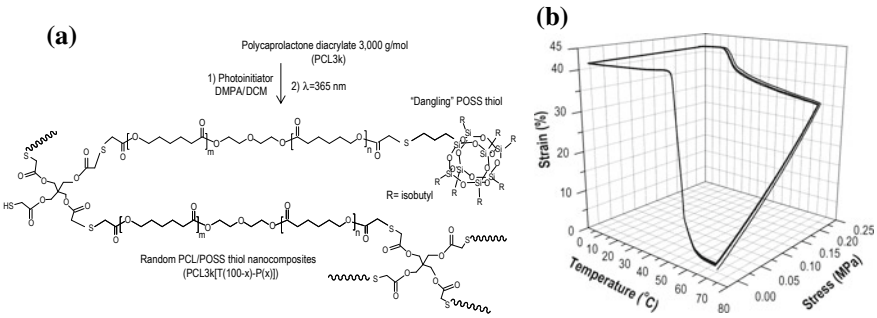

Fig. 22 **a** Idealized structure of POSS-PCL chemical molecular networks, **b** three thermally activated one-way shape memory cycles of PCL3kT70-POSS30 crosslinked network (Romo-Uribe and Mather, to be published)

works, with POSS end capping the network, as shown schematically in Fig. 22a. The topology of the molecular network thus obtained is distinctly different from the physical–chemical networks discussed in Sect. 3.1. These networks also exhibit one-way shape memory behavior, with shape recovery as high as 99% and high reproducibility after three cycles, as shown in Fig. 22b.

Figure 23 shows (a) WAXS and (c) SAXS patterns of POSS-PCL network exhibiting crystalline order (WAXS), and long-range spatial periodicity (SAXS). The patterns were acquired simultaneously. The WAXS intensity trace of Fig. 23b enables the identification of PCL crystalline structure and a weak crystalline reflection of POSS. These results show that PCL crystallizes by chain folding (*110* and *200* reflections) whereas POSS crystalline aggregates are small giving rise to a weak *101* reflection. The limited crystallization of POSS undoubtedly arises from being covalently attached to PCL chains. On the other hand, the SAXS intensity maximum of Fig. 23d shows a lamellar superstructure with periodicity of 17.9 nm. These results enable to postulate a microstructure depicted in the scheme of Fig. 23 and demonstrates the value of acquiring WAXS and SAXS patterns of a specimen.

The SAXS data was further analyzed by determining the pair-distance distribution function, and the results are shown in Fig. 24a. These results enable to postulate a

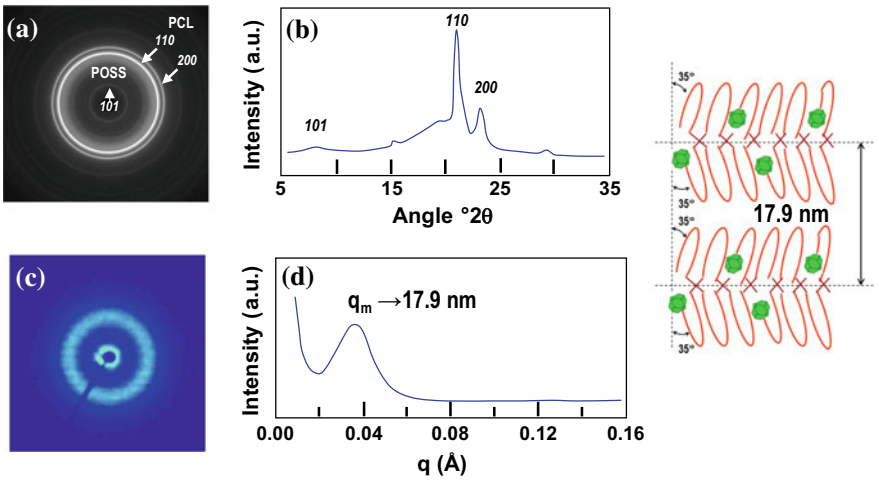

Fig. 23 PCL3k(T70-POSS30) crosslinked network. **a** WAXS pattern and **b** azimuthally averaged intensity trace. **c** SAXS pattern and **d** azimuthally averaged intensity trace. Patterns were obtained simultaneously using a Rigaku S3000 system; CuKα radiation (Romo-Uribe and Mather, to be published)

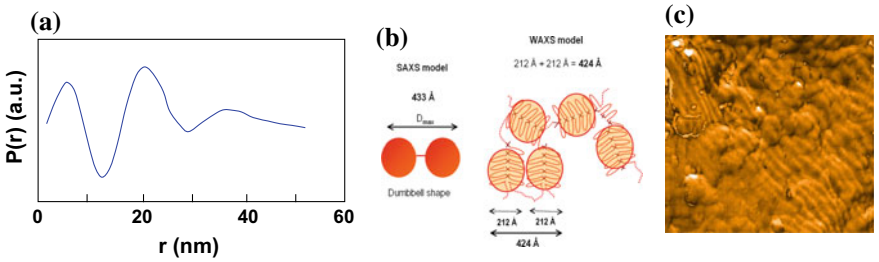

Fig. 24 **a** Pair-distance distribution function of PCL3k(T70-POSS30) network calculated from SAXS data. **b** SAXS and WAXS models for particle shape nanostructure, **c** atomic force microscopy (AFM) image exhibiting lamellar morphology consistent with X-ray scattering results (Romo-Uribe and Mather, to be published)

dumbbell shape superstructure, as shown in Fig. 24b. The lamellar superstructure of POSS-PCL networks was confirmed by atomic force microscopy, Fig. 24c.

3.3 PCO Two-Way SMP Networks

A series of poly (cyclooctene) (PCO) films with different cross-linking density were prepared through controlling the amount of thermal initiator, dicumyl peroxide (DCP), giving rise to a novel two-way shape memory effect. The cross-linking density

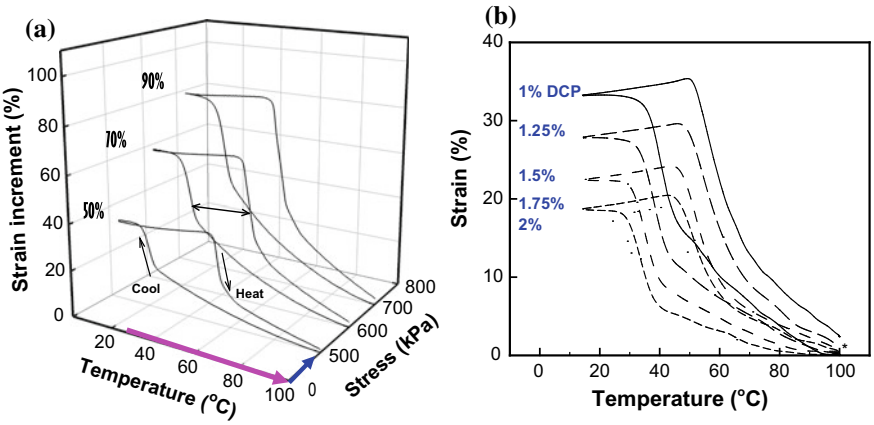

Fig. 25 Two-way shape memory behavior of PCOs cured with different DCP contents. **a** Two-way shape memory behavior for PCO-D20 at different stresses. The length of the elongated sample indicates the initial length (Li), meaning 0% in strain. The deformation step is followed by cooling and heating process (2 °C/min) under the constant stress, respectively; **b** the samples were elongated at high temperature (100 °C) under a constant stress of 600 kPa. The deformation step is followed by a cooling process (2 °C/min), inducing an increase in strain. Then, the increased strain decreases by a heating process (2 °C/min) to high temperature (adapted from [12])

influenced the thermal and mechanical properties, and these were closely associated with the shape memory effect of the PCO network [12]. Dynamic mechanical analysis (DMA) showed that the crosslinked PCOs exhibited a thermally reversible deformation behavior, that is, there is a crystallization-induced expansion on cooling and melting-induced shrinkage on heating under a constant load, as shown in Fig. 25a. Note that the degree of stretching was a function of crosslinker concentration, as shown in Fig. 25b, i.e., higher crosslink density less extensibility.

Two-dimensional WAXS patterns of the PCO-D15 specimen were obtained to investigate the microstructure and the molecular mechanisms responsible for the two-way shape memory behavior. The WAXS patterns under different degrees of stretching are shown in Fig. 26; the stretching direction is vertical. PCO crystallizes in a triclinic or monoclinic unit cell, or the mixture, depending on the conditions of crystallization. The unstretched PCO sample (Fig. 26a) shows two sharp Debye-Scherrer (crystalline) reflections. The uniform intensity around the azimuth denotes isotropic chain orientation. The reflections are located at $2\theta = 20.0°$ (4.43 Å), and $2\theta = 23.0°$ (3.85 Å), indexed as 010, and $\bar{1}00/100$ according to a triclinic unit cell. The amorphous ring close to the beam stop is an artifact produced by the tail of white radiation that cannot be eliminated by the Nickel filter [12].

Applying deformation at 400 kPa (Fig. 26b), the diffraction pattern becomes anisotropic, the *010* reflection splits into four off-equatorial reflections whereas the reflections are azimuthally spread. The equatorial axis is horizontal and the meridional axis is vertical. The anisotropy in the diffraction pattern Fig. 26b denotes molecular alignment. However, the four off-equatorial *010* reflections show that the

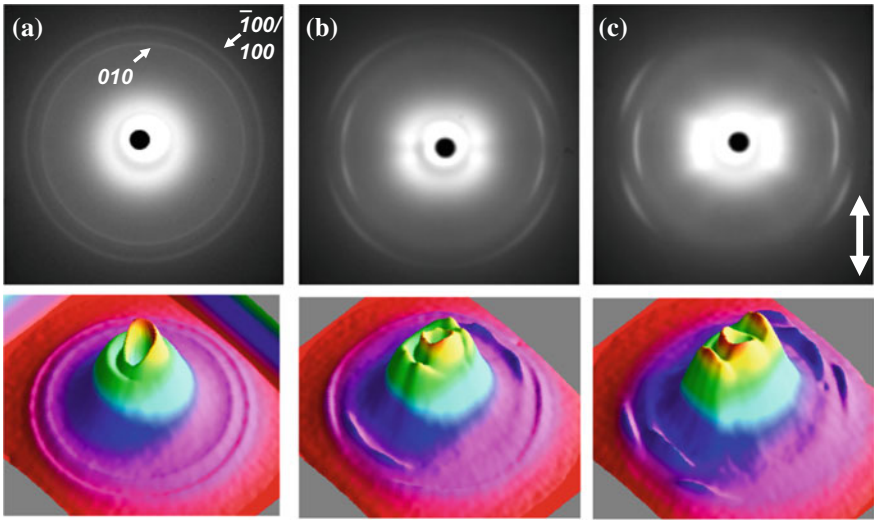

Fig. 26 Flat plate 2D WAXS patterns and corresponding 3D plots of PCO-D1.5 after stretching and cooling to room temperature. The applied stress was: **a** 0, **b** 400, and **c** 700 kPa. Stretching direction is vertical. Ni-filtered CuKα radiation (adapted from [12])

molecular orientation is neither along the stretching (vertical) axis nor uniaxial, but rather bimodal. That is, under these stretched conditions there coexist two populations of oriented crystallites. There is a distribution of orientations of the crystallites as deduced from the azimuthal spread of the *010* reflections. Furthermore, the increase of intensity on the *010* reflections indicate a stress-induced increase in crystallinity and corroborated independently by differential scanning calorimetry (DSC) [12].

Increasing the strain by increasing the applied stress showed that the *010* reflection gradually rotated towards the equatorial axis, hence forcing the macromolecules to gradually orient along the stretching axis. Eventually, at the highest load applied (700 kPa) the WAXS pattern in Fig. 26c shows fiber-like morphology. There are only a pair of *010* reflections located on the equatorial axis indicative of crystalline uniaxial orientation along the stretching axis. The *010* reflection appears more concentrated in °2θ but azimuthally spread. The azimuthal spread of intensity shows that there is still a distribution of orientations along the stretching axis. Furthermore, the intensity of the reflections further increased, became azimuthally concentrated, and formed the 1st layer along the meridional axis.

Higher stretching loads promoted an increase in strain upon cooling (see Fig. 25a, b). The WAXS results of Fig. 26 showed that the increase in strain is due to the reorientation of crystalline structure towards the stretching direction. As the crystalline structure evolves from bimodal (low stress) to uniaxial (high stress) the recrystallization occurs along a single preferred orientation thus inducing greater expansion along the stretching direction [12].

3.4 Time-Resolved Synchrotron Scattering

3.4.1 Smectic C Elastomer, Two-Way SMP Networks

Elastomers, i.e., crosslinked molecular networks endowed with smart, compliant, and biocompatible properties can respond to applied stimuli allowing for fast, possibly reversible, and high strain–amplitude response. Controlling the crosslink density can tune the mechanical properties, closely matching those of biological tissues [46, 45, 56]. Rousseau and Mather [44] designed, synthesized, and investigated the actuation behavior of liquid crystalline elastomers (LCEs) capable of forming a smectic C phase upon melting. The LCE can combine composition-dependent phase behavior with low modulus [14]. Note that careful design of LCE chemistry can produce shape memory properties arising from (a) the glass transition temperature and (b) spontaneous reversible actuation at the smectic–isotropic transition temperature. By adequately choosing the chemical composition, the latter could be switched "on" or "off", leading to pure shape memory response. Figure 27 shows a schematic of the chemical structure of side-chain liquid crystal (SCLC). Once crosslinked, the SCLC can produce a LCE, the X-ray scattering pattern of the LCE is also shown in Fig. 27.

The structural changes occurring during the stretching process was monitored by time-resolved synchrotron scattering, and typical patterns as a function of per cent of stretching are shown in Fig. 28. The patterns were recorded using a MAR area detector at the Advanced Photon Source, Argonne National Laboratory (APS, ANL).

The unstretched specimen exhibits three concentric amorphous halos typical of unoriented glassy material. Note that the inner crystalline ring corresponds to the Kapton window of the MAR detector. Interestingly, gradual stretching of the specimen (along the vertical axis as indicated by the double headed arrow) produced two structural changes: (a) a split of four sharp reflections typical of smectic C phase, and (b) equatorial intensity concentration associated to molecular chains being oriented along the stretching axis. These structural changes are clearly visualized in the corresponding 3D plots shown in Fig. 28. The elastic energy stored during the structural

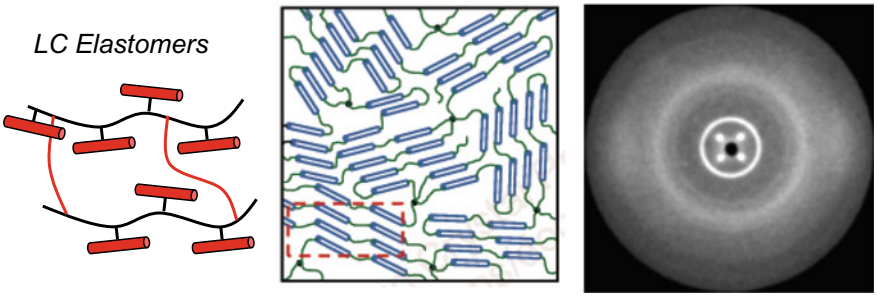

Fig. 27 Side-chain liquid crystals (LC) are crosslinked to give a LC elastomer (LCE). Scheme of μm-scale of local alignment of mesogens in the LC phase. X-ray scattering pattern of an LCE

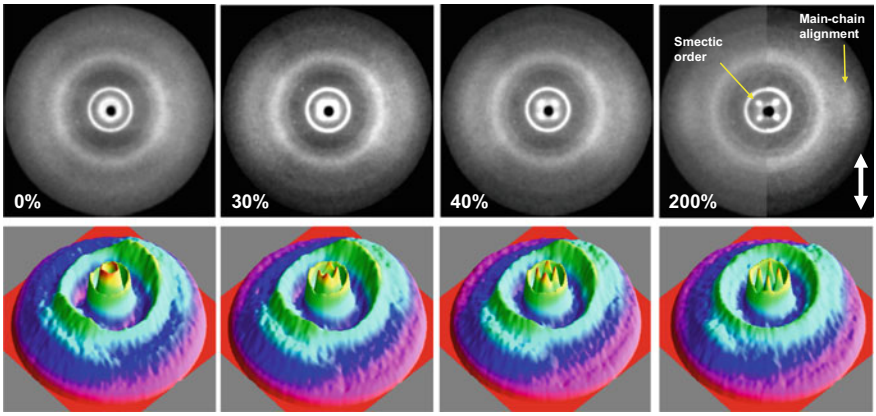

Fig. 28 Middle-angle X-ray scattering of LCE under uniaxial deformation. Structure evolution as a function of strain, indicated in each pattern. Double exposure was utilized for the pattern at 200% stretching. Synchrotron radiation, using 10 s exposure time per pattern; stretching direction is vertical. Note that the inner crystalline ring corresponds to the Kapton window of the MAR detector (Romo-Uribe and Mather, to be published)

rearrangement (i.e., smectic C order and macromolecular alignment) is thought to be responsible for the double shape memory effect exhibited by the LCEs.

Information regarding the smectic C layer spacing d_{SmC}, molecular alignment relative to the normal to the layer β, and interchain distance d_m, can be extracted from the diffraction patterns analyzing the equatorial intensity trace, the intensity trace through the smectic C reflections, and the azimuthal intensity trace around the smectic C reflections [21]. These intensity traces are shown in Fig. 29. The intensity traces show that the smectic C layer spacing is $d_{SmC} = 32.4$ Å, the interchain distance is $d_m = 6.81$ Å, and the tilting angle is $\beta = 90 - 44 = 46°$.

4 Optical Microscopy and μm-Scale Structure

As described in the previous sections, the innovation and technology development of new generation of shape memory materials requires analytical techniques which may involve the combination of two or more techniques. In situ and *time-resolved* monitoring of mechanical behavior and the microstructural changes associated to deformation, and fracture is ideal to better characterize and innovate these complex materials. Furthermore, these techniques are applicable to a broader range of polymeric materials in other fields and technologies.

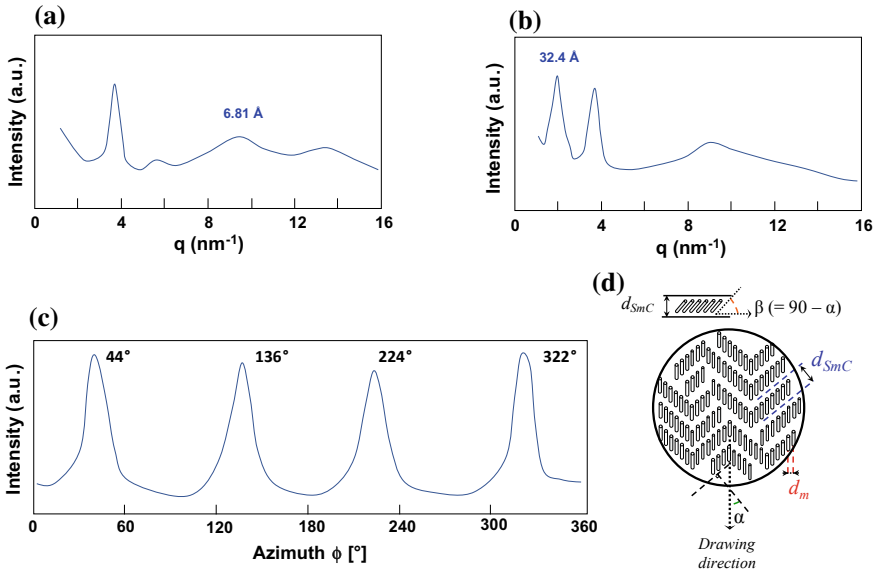

Fig. 29 Intensity traces extracted from MAXS pattern of LCE uniaxially deformed 200%. **a** Equatorial trace, **b** intensity through smectic reflection, **c** azimuthal intensity trace around the four smectic C reflections (at constant $q = 1.94$ nm^{-1}), and **d** scheme of molecular arrangement in a smectic C mesophase and parameters extracted by X-ray scattering (Romo-Uribe and Mather, to be published)

4.1 Hot-Stage Optical Microscopy

The excellent temperature control of current commercial hot-stage systems in combination with a (polarized) optical microscope enables, for instance, the accurate determination of thermal melting transitions of multilayer films typically used in packaging applications. The melting transitions of semicrystalline polymers under polarized light are characterized by changes in birefringence followed by total extinction (darkness) when melting is completed. The molten polymers are amorphous and therefore there is no birefringence to be detected under crossed polarizers [52].

Figure 30 shows a DSC trace (first heating) and a series of polarized optical microscopy (POM) micrographs of a multilayer polymeric film 106 μm thick used in packaging. The results correlate thermal endothermic transitions corresponding to the melting of polymers with POM micrographs. Furthermore, POM microscopy not only confirmed the temperature of the melting transitions but also enabled to establish the *location* of each polymer layer within the multilayer composite.

Hot-stage optical microscopy also enables recrystallization studies under either isothermal or non-isothermal conditions of semicrystalline polymers mimicking, for instance, processing conditions of polymers.

An application of hot-stage microscopy pertaining to thermally responsive shape memory polymers is shown in Fig. 31 [38]. Figure 31a shows a series of optical

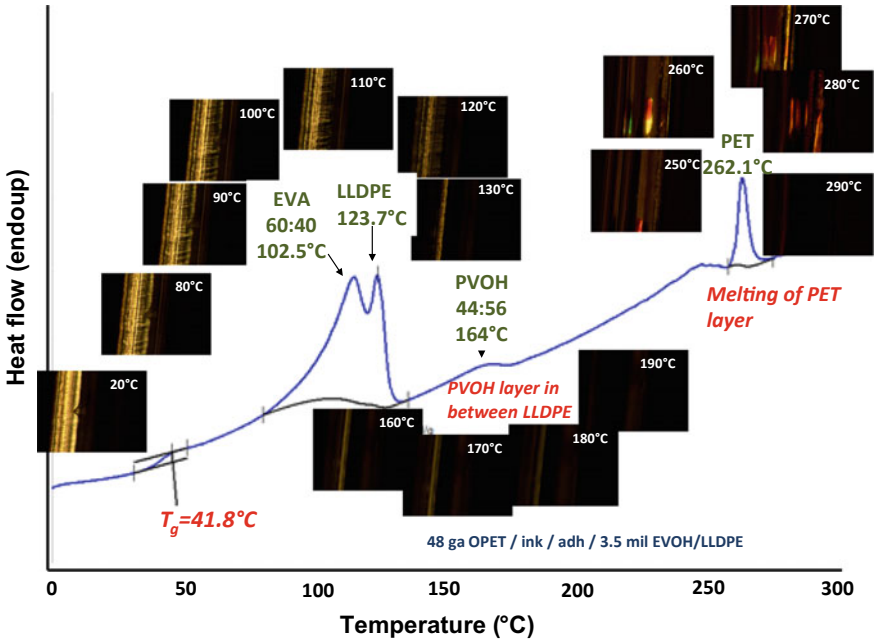

Fig. 30 DSC heating trace and in situ POM micrographs of a multilayer polymer film composed of EVA, LLDPE, PVOH and PET. Film total thickness = 106 μm

micrographs of a thermally responsive physically crosslinked hydrogel PNIPAm-POSS3.4 during a heating scan a 2 °C/min. The micrographs show the collapsing of the hydrogel as heating through the lower critical solution temperature (LCST). Then, the cooling cycle of Fig. 31b shows that the shape (and size) is largely recovered, demonstrating the shape memory behavior. However, the images also revealed a hysteresis effect, probably associated to solvent diffusion. The 2D change ΔL, relative to the equilibrated hydrogel, is plotted as a function of temperature in Fig. 31c ($\Delta L = 0$ means the size of the de-swelled copolymer, at 45 °C). The LCST of the shape memory hydrogel can be determined from onset of shape change as a function of temperature. These results showed a LCST = 26 °C. The results obtained from hot-stage optical microscopy are complemented with shear moduli measurements, as shown in Fig. 31c. The results from both techniques during the heating scan, ΔL and shear moduli, are in agreement. As water was expelled from the hydrogel the elastic modulus decreased (the gap in the rheometer was kept constant). Note that the onset of the elastic shear modulus G' corresponds to the onset in ΔL and determines the LCST.

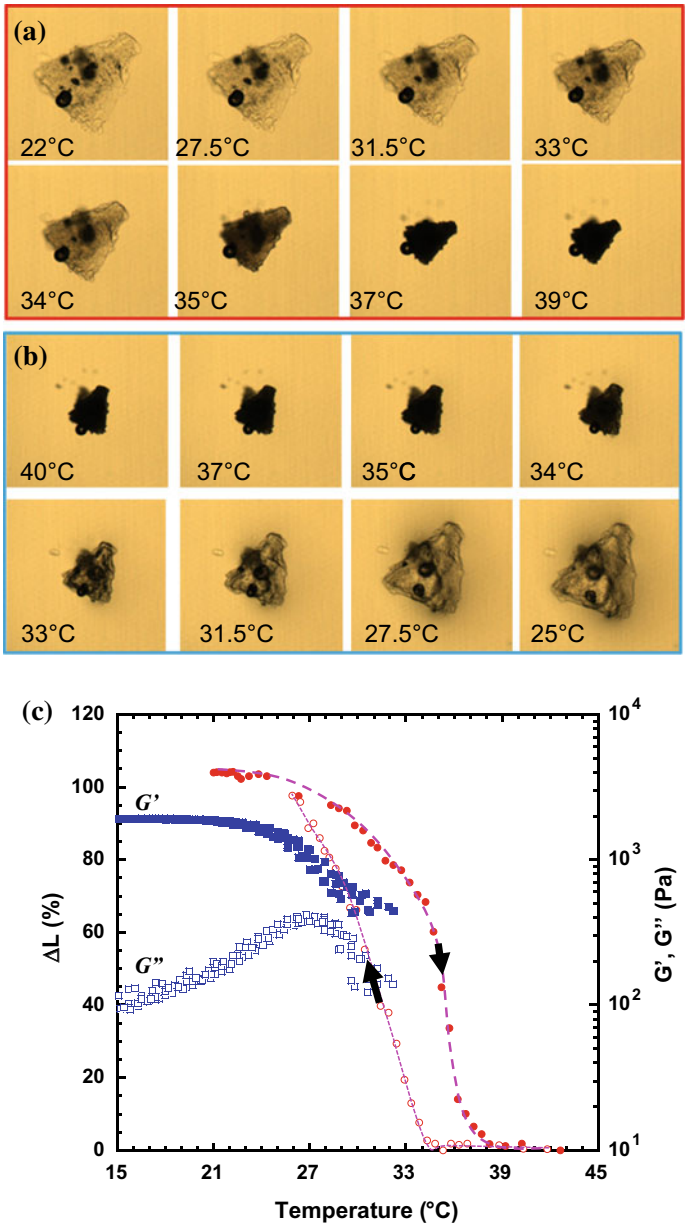

Fig. 31 Thermally-activated shape memory behavior of PNIPAm-POSS3.4 physically crosslinked hydrogel. Micrographs acquired **a** heating, and **b** cooling at 2 °C/min. **c** Size change ΔL and dynamic shear moduli (G', G'') as a function of temperature. Shear rheometry data also measured at 2 °C/min (adapted from [38])

4.2 Time-Resolved Optical Microscopy/Uniaxial Deformation

The mechanical behavior during uniaxial deformation of polymeric materials determines performance, applications, and limits of use and failure among other important properties. Polymeric materials are able to experience elastic (recoverable) deformation, yield stress, plastic (permanent) deformation, cold drawing, and strain hardening prior to fracture. The type of deformation will depend on the morphology and physical state of the polymeric material. Shape memory elastomers, crosslinked polymers, and hydrogels will exhibit elastic deformation and some, limited, plastic deformation followed by strain hardening prior to fracture. The mechanical properties like tensile strength and Young's modulus are relevant to the product's performance in handling and resistance to tear, and long-term durability. The mechanical modulus also impacts performance and it, therefore, can also be associated to comfort in many applications envisioned for shape memory polymers (e.g., biomedical applications). Mechanical properties and microstructure can be probed simultaneously by implementation of simultaneous stress–strain–microstructure studies by combining a mini tensile tester and an optical microscope with long working objectives (for high-temperature studies), as shown in Fig. 32.

The stress–strain traces of a linear low-density polyethylene (LLDPE) film of three tests are shown in Fig. 32c; a fresh specimen was used each time. The results show excellent reproducibility. The Young's modulus is determined from the elastic region of the stress–strain traces; the traces also provide the yield stress.

Figure 33 shows a series of optical micrographs acquired during the tensile test at the strains indicated in each micrograph. The micrographs were obtained at 50× magnification, but magnifications up to 500× are possible with current instrumentation. The instrumentation enables symmetrical displacement of the clamps during the specimen's stretching, hence the point of microscopic observation (rectangular, illuminated region in Fig. 32b) is always the same.

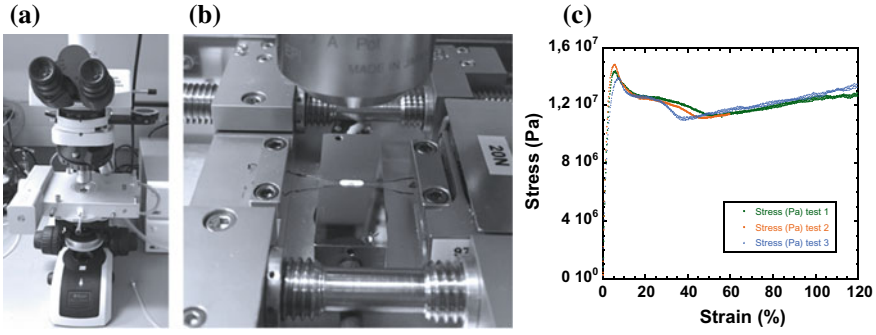

Fig. 32 **a** Tensile stress testing system TST350 mounted on optical microscope. Video recording is performed with a digital camera Quicam coupled to tensile tester controller. **b** Polymeric film clamped in tensile tester. **c** Stress–strain curves polymeric film at room temperature, straining at 5 mm/min

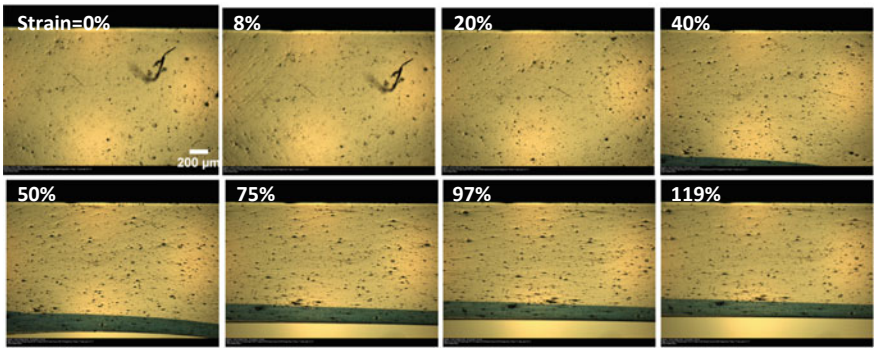

Fig. 33 In situ bright field optical micrographs of LLDPE film obtained *simultaneously* to stress–strain trace (test 1) shown in Fig. 32, while straining at 5 mm/min, room temperature. The corresponding strains are indicated in each micrograph. Tensile axis is horizontal

5 Small-Angle Light Scattering, SALS

Small-angle light scattering (SALS) is another ideal technique for in situ and time-resolved studies of polymers under deformation/temperature cycles. SALS was initially developed to characterize polymeric solutions and colloidal suspensions [34]. The usefulness of SALS is well established and the technique is routinely utilized to investigate soft condensed matter as well as complex fluids. Commercial instrumentation is scarce, however, building in-house SALS instrumentation is relatively easy and inexpensive [8, 31]. SALS is being applied to study the spherulitic microstructure of partially crystalline polymers, the microstructure in deformed polyethylene samples, and the influence of thermal annealing on polymer's crystalline microstructure [50, 55], phase separation kinetics in polymeric blends [49], and thermotropic polymers under shear [27, 42]. There are also applications to biological systems [7, 29]. In this section, we show applications of this technique to investigate the correlation of microstructure with deformation in polymer films subjected to controlled uniaxial tensile deformation.

Figure 34a shows the polarized optical micrograph (POM) and H_V SALS pattern of a polyamide 66 film (PA66). The POM micrograph exhibits a spherulitic structure whereas the SALS pattern shows a "four-leaf clover" with intensity maxima at azimuthal angle of $\phi = 45°$ with respect to the extrusion direction (vertical). The SALS pattern is typical of spherulitic microstructure in semicrystalline polymers [34].

Stein [55] developed a theory for small-angle scattering from spherulitic polymers by assuming that scattering arises from a homogeneous anisotropic sphere embedded in an isotropic medium. The equation derived by Stein et al. for H_V scattering is

$$I_{HV} = AV_o^2\left(\frac{3}{U^3}\right)\cdot\left[(\alpha_t-\alpha_r)\cdot\cos^2\theta\cdot\sin\phi\cos\phi(4\cdot\sin U - U\cos U - 3\cdot SiU)\right]^2 \quad (19)$$

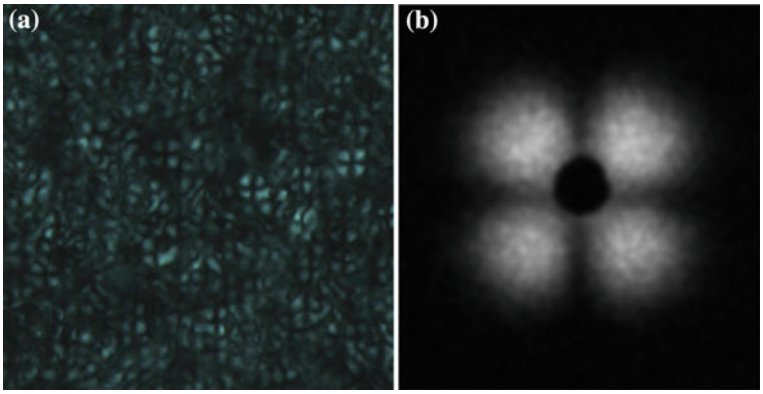

Fig. 34 **a** Polarized optical microscopy (POM) micrograph and **b** SALS pattern of extruded PA66 film. The extrusion direction is vertical. Room temperature and H_V polarization condition

where V_o is the volume of the sphere, $U = (4\pi R/\lambda)sin\theta$, where R is the radius of the sphere, λ the wavelength of the light (in the medium), and 2θ is the scattering angle. α_t and α_r are the tangential and radial polarizabilities of the sphere, and ϕ is the azimuthal scattering angle. The maxima of the "four-leaf clover" H_V patterns occur, according to Eq. (19), when

$$\frac{4\pi R}{\lambda} \sin\theta_{\max} = 3.9 \tag{20}$$

thus

$$R = \frac{3.9\lambda}{4\pi \cdot \sin\theta_{\max}} \tag{21}$$

enabling the calculation of the spherulite size from the position of the intensity maximum. Equation (21) is easily rewritten in terms of the scattering vector

$$R = \frac{3.9}{q_{\max}} \tag{22}$$

Applying Eq. (22) we obtained a spherulite radius for the PA66 film of $R = 10.1\ \mu$m, in agreement with the size determined by POM.

After uniaxially stretching the film by 60%, the POM micrograph, SALS and WAXS patterns were acquired, these are shown in Fig. 35. The POM micrograph of Fig. 35a shows nearly total extinction and a weak crisscross morphology with elongated stripes. The inset in Fig. 35a was obtained by rotating the specimen to reveal the oriented morphology.

Figure 35b shows the SALS pattern of PA66 after 60% uniaxial stretching. The SALS pattern shows a rotation of the intensity maxima towards the equatorial (hor-

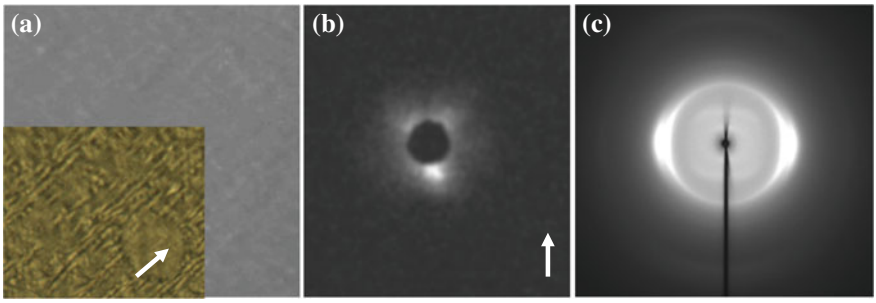

Fig. 35 **a** POM micrograph, **b** SALS and **c** WAXS patterns of PA66 film under uniaxial deformation along the extrusion (vertical) direction. Film stretched 60% as indicated by the arrow. Inset in (**a**) shows the specimen rotated 45° to reveal the oriented morphology. WAXS: CuKα radiation; SALS: H_V polarization condition

izontal) axis as well as a shifting towards the beam stop. This pattern indicates that the spherulites have been deformed and stretched along the tensile axis. There is additionally a weak streak along the equatorial axis. This streak arises from an elongated microstructure along the tensile axis (shown in the inset of Fig. 35a). Note the presence of the four-lobe morphology indicating that the spherulitic morphology is preserved under the uniaxial elongation. However, the lobes have significantly shifted towards the beam stop, a consequence of a size increase of the spherulites. Finally, Fig. 35c shows the corresponding WAXS pattern exhibiting sharp reflections, concentrated intensity on the equatorial axis and off meridional reflections. The sharp reflections are associated to crystallinity in the specimen, whereas the azimuthal spread of the equatorial reflections denote the degree of macromolecular alignment along the stretching axis.

Another example of the utilization of SALS to probe microstructure under deformation conditions is shown in Fig. 36, it shows a series of SALS patterns obtained in situ, shearing a thermotropic polymer at 180 °C, above the nematic-to-isotropic temperature. The SALS patterns revealed shear-induced isotropic-to-nematic transition, where the nematic phase was highly oriented along the shearing axis and spatially correlated (up to seven intensity maxima were detected along the meridional axis) [27].

6 Conclusions

The development and innovation of smart, shape memory polymers require fundamental understanding of the molecular mechanisms associated to the memory effect. This chapter focused largely on the author's experience, own research results, and research interests. The chapter provided an overview of the utilization of scattering and optical probes, with spatial resolution from Å-scale to μm-scale. Since

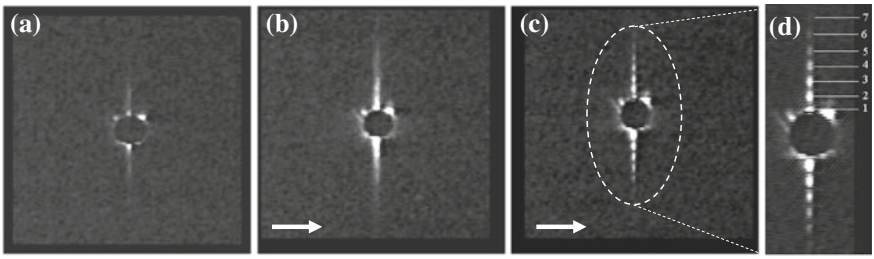

Fig. 36 SALS patterns of thermotropic polymer under shear flow, as indicated by the arrow. **a** Quiescent state. **b** and **c** Increasing shear rate. **d** Enlargement of c exhibiting a spatially correlated structure. H_V polarization condition (for more details see [27])

its discovery in 1912, X-ray scattering, WAXS first and SAXS few years later, has proved to be a particularly powerful technique to probe structure. Furthermore, X-ray scattering does not require special sample preparation and optically opaque materials are transparent to X radiation. Moreover, modern instrumentation and synchrotron sources enable in situ and *time-resolved* studies. On the other hand, SALS and optical microscopy are suitable techniques to resolve microstructure at sub-μm and μm-scale, respectively. These techniques can also be adapted with stretching/shearing devices for simultaneous, time-resolved microstructure analysis. Each technique relies on contrast, either electron density or index of refraction, and suitable dimensions, and the choice of a particular technique or the combination of several techniques relies on specific materials under study.

References

1. Alexander LE (1969) X-ray diffraction methods in polymer science. Wiley, London
2. Alvarado-Tenorio B, Romo-Uribe A, Mather PT (2011) Microstructure and phase behavior of POSS/PCL shape memory nanocomposites. Macromolecules 44:5682–5692
3. Alvarado-Tenorio B, Romo-Uribe A, Mather PT (2015) Nanoscale order and crystallization in POSS-PCL shape memory molecular networks. Macromolecules 48:5770–5779
4. Alvarado-Tenorio B, Romo-Uribe A, Mather PT (2012) Stress-induced bimodal ordering in POSS/PCL biodegradable shape memory nanocomposites. In: MRS symposium proceedings, vol 1450. https://doi.org/10.1557/opl.2012.1327
5. Alvarado-Tenorio B, Romo-Uribe A, Mather PT (2013) Nanoscale anisotropic orientation in shape memory random POSS/Polycaprolactone nanocomposites. In: MRS symposium proceedings, vol 1453. https://doi.org/10.1557/opl.2013.1117
6. Bellin I, Kelch S, Robert L, Lendlein A (2006) Polymeric triple-shape materials. Proc Natl Acad Sci USA 103:18043–18047
7. Bettelheim FA, Kumar M (1977) Small-angle light-scattering patterns of corneas of different species. Invest Ophthalmol Vis Sci 16:236–240
8. Castelleto V, Hamley IW (2006) Capillary flow behavior of worm-like micelles studied by small-angle X-ray scattering and small angle light scattering. Polym Adv Technol 17:137–144

9. Chien Y-C, Chuang W-T, Jeng U-S, Hsu S-H (2017) Preparation, characterization, and mechanism for biodegradable and biocompatible polyurethane shape memory elastomers. ACS Appl Mater Interfaces 9(6):5419–5429
10. Chu B, Hsiao BS (2001) Small-angle X-ray scattering of polymers. Chem Rev 101:1727–1761
11. Chu B, Hsiao BS (2001) Small-angle X-ray scattering of polymers. Chem Rev 101:1727–1761
12. Chung T, Romo-Uribe A, Mather PT (2008) Two-way reversible shape memory in a semicrystalline network. Macromolecules 41(1):184–192
13. Deutsch M (1991) Orientational order determination in liquid crystals by X-ray diffraction. Phys Rev A 44:8264–8270
14. Finkelmann H, Kock HJ, Rehage G (1981) Investigations on liquid crystalline polysiloxanes 3. Liquid crystalline elastomers—a new type of liquid crystalline material. Makromoleculare Chem Rapid Comm 2:317–322
15. Grubb DT, Prasad K, Adams W (1991) Small-angle X-ray diffraction of Kevlar using synchrotron radiation. Polymer 32:1167–1172
16. Hsiao BS, Verma RK (1998) A novel approach to extract morphological variables in crystalline polymers from time-resolved synchrotron SAXS data. J Synchrotron Radiat 5:23–29
17. Huitron-Rattinger E, Ishida K, Romo-Uribe A, Mather PT (2013) Thermally modulated nanostructure of poly(ε-caprolactone)–POSS multiblock thermoplastic polyurethanes. Polymer 54:3350–3362
18. Janicki J (2003) Time-resolved small-angle X-ray scattering and wide-angle X-ray diffraction studies on the nanostructure of melt-processable molecular composites. J Appl Crystal 36:986–990
19. Kasai N, Kakudo M (2005) X-ray diffraction by macromolecules, Kodansha-Springer, Japan
20. Kumar S, Werner S, Grubb DT, Adams W (1994) On the small-angle X-ray scattering of rigid-rod polymer fibres. Polymer 35:5408–5412
21. Leadbetter AJ (1979) Structural studies in nematic, smectic A, and smectic C phases. In: Luckhurst GA, Gray GW (eds) The molecular physics of liquid crystals. Academic Press, London
22. Leadbetter AJ, Norris EK (1979) Distribution functions in three liquid crystals from X-ray diffraction measurements. Mol Phys 38:669–686
23. Luo X, Mather PT (2010) Triple-shape polymeric composites (TSPCs). Adv Funct Mater 20:2649–2656
24. Luo X, Mather PT (2013) Shape memory assisted self-healing coating. ACS Macro Lett 2:152–156
25. Luo X, Ou R, Eberly DE, Singhal A, Vyratyaporn W, Mather PT (2009) A thermoplastic/thermoset blend exhibiting thermal mending and reversible adhesion. ACS Appl Mater Interfaces 1:612–620
26. Mather PT, Luo X, Rousseau IA (2009) Shape memory polymer research. Annu Rev Mater Sci 39:445–471
27. Mather PT, Romo-Uribe A, Han CD, Kim SS (1997) Rheo-optical evidence of the flow-induced isotropic-nematic transition in a thermotropic liquid crystalline polymer. Macromolecules 30:7977–7989
28. Mitchell GR, Windle AH (1982) Structural analysis of an oriented liquid crystalline copolyester. Polymer 23:1269–1272
29. Mullaney PF, Dean PN (1970) The small-angle light scattering of biological cells. Biophys J 10:764–772
30. Neffe AT, Hanh BD, Steuer S, Lendlein A (2009) Polymer networks combining controlled drug release, biodegradation, and shape memory capability. Adv Mater 21:3394–3398
31. Nishida K, Ogawa H, Matsuba G, Konishi T, Kanaya T (2008) A high-resolution small-angle light scattering instrument for soft matter studies. J Appl Cryst 41:723–728
32. Nochel U, Kratz K, Behl M, Lendlein A (2015) Relation between nanostructural changes and macroscopic effects during reversible temperature-memory effect under stress-free conditions in semicrystalline polymer networks. In: MRS symposium proceedings, vol 1718. https://doi.org/10.1557/opl.2015.427

33. Ran S, Fang D, Zong X, Hsiao BS, Chu B, Cunniff PM (2001) Structural changes during deformation of Kevlar fibers via on-line synchrotron SAXS/WAXS techniques. Polymer 42:1601–1612
34. Rhodes MB, Stein RS (1961) Light scattering study of the annealing of drawn polyethylene. J Appl Phys 32:2344–2352
35. Romo-Uribe A (2001) On the molecular orientation and viscoelastic behaviour of liquid crystalline polymers. The influence of macromolecular architecture. Proc R Soc Lond A 457:207–229
36. Romo-Uribe A (2001) Smectic-like order in the log-rolling flow of thermotropic random copolymers. A time-resolved wide-angle X-ray scattering study. Proc R Soc Lond A 457:1327–1342
37. Romo-Uribe A (2007) Hybrid-block copolymer nanocomposites. characterization of nanostructure by small-angle X-ray scattering (SAXS). Rev Mex Fis 53:171–178
38. Romo-Uribe A, Albanil L (2018) Dynamics retardation in hybrid POSS-NIPAm nanocomposites. Thermoplastic and thermally-responsive hydrogel behavior. Eur Polym J 99:350–360
39. Romo-Uribe A, Manzur A, Olayo R (2012) Synchrotron small-angle X-ray scattering study of linear low density polyethylene under uniaxial deformation. J Mater Res 27:1351–1359
40. Romo-Uribe A, Reyes-Mayer A, Calixto-Rodriguez M, Benavente R, Jaffe M (2018) Synchrotron scattering and thermo-mechanical properties of high performance thermotropic polymer. A multi-scale analysis and structure-property correlation. Polymer 153:408–421
41. Romo-Uribe A (2007) Long-range orientation correlations and molecular alignment in sheared thermotropic copolyester. In-situ light and X-ray scattering. Polym Adv Techn 18(7):503–512
42. Romo-Uribe A, Mather PT, Chaffee K, Han CD (1997) Molecular and textural ordering of thermotropic polymers in shear flow. In: MRS symposium proceedings, vol 461, pp 63–68
43. Romo-Uribe A, Windle AH (1996) Log-rolling alignment in main-chain thermotropic liquid crystalline polymers: An in-situ WAXS study, Macromolecules 29 :6246–6255
44. Rousseau IA, Mather PT (2003) Shape memory effect exhibited by smectic-C liquid crystalline elastomers. J Am Chem Soc 125(50):15300–15301
45. Rousseau IA, Qin H, Mather PT (2005) Tailored phase transitions via mixed-mesogen liquid crystalline polymers with silicon-based spacers. Macromolecules 38:4103–4113
46. Rousseau IA (2004) University of Connecticut PhD thesis, Development of soft polymeric networks showing actuation behavior: from hydrogels to liquid crystalline elastomers
47. Ruland W (1961) X-ray determination of crystallinity and diffuse disorder scattering. Acta Cryst 14:1180–1185
48. Ryan AJ (1993) Simultaneous small-angle X-ray scattering and wide-angle X-ray diffraction. A powerful new technique for thermal analysis. J Therm Anal 40:887–899
49. Sakurai S, Izumitani T, Hasegawa H, Hashimoto T, Han CC (1991) Small-angle neutron scattering and light scattering study on the miscibility of poly(styrene-ran-butadiene)/polybutadiene blends. Macromolecules 24:4844–4851
50. Samuels RJ (1966) Structured polymers. Wiley, New York
51. Santiago D, Fernandez-Franco X, Ferrando F, de la Flor S (2015) Shape memory effect in hyperbranched poly(ethyleneimine)-modified epoxy thermosets. J Polym Sci Polym Phys. https://doi.org/10.1002/polb.23717
52. Sawyer LC, Grubb DT (1987) Polymer microscopy. Chapman and Hall, New York
53. Soto-Quintero A, Meneses-Acosta A, Romo-Uribe A (2015) Tailoring the viscoelastic, swelling kinetics and antibacterial behavior of poly(ethylene-glycol)-based hydrogels with polycaprolactone. Eur Polym J 70:1–17
54. Statton WO (1959) Directional 'crystallization' of polymers. Ann N Y Acad Sci 83:27–36
55. Stein RS (1964) In: Ke B (ed) Newer methods of polymer characterization. Interscience Publishers, New York, p 155
56. Thomsen DL III, Keller P, Daciri J, Pink R, Jeon H, Shenoy D, Ratna BR (2001) Liquid crystal elastomers with mechanical properties of a muscle. Macromolecules 34:5868–5875
57. Torbati AH, Birjandi Nejad H, Ponce M, Sutton JP, Mather PT (2014) Properties of triple shape memory composites prepared via polymerization-induced phase separation. Soft Matter 10:3112–3121

58. Vainshtein BK (1966) Diffraction of X-rays by chain molecules. Elsevier, Amsterdam
59. Wang K, Jia Y-G, Zhu XX (2017) Two-way reversible shape memory polymers made of cross-linked cocrystallizable random copolymers with tunable actuation temperatures. Macromolecules 50(21):8570–8579
60. Wilke W, Bratrich M, Heise B, Peichel G (1992) The change of the superstructure of semicrystalline polymers during deformation: results from small-angle scattering with synchrotron radiation. Polym Adv Technol 3:179–190
61. Xie T, Rousseau IA (2009) Facile tailoring of thermal transition temperatures of epoxy shape memory polymers. Polymer 50:1852–1856
62. Yang Z, Song F, Wang Q, Wang T (2016) Shape memory induced structural evolution of high performance copolyamides. J Polym Sci A Polym Chem 54:3858–3867

Applications of Shape-Memory Polymers, and Their Blends and Composites

L. Santo, F. Quadrini, D. Bellisario and L. Iorio

Abstract In this chapter, applications of Shape-Memory Polymers (SMPs), and their blends and composites (SMPCs) are discussed. SMPs and SMPCs are a new class of stimuli-responsive smart materials that change their configuration reacting to specific external stimulus and remember the original shape. They are expected to have interesting applications in many engineering fields such as aerospace (e.g., in deployable structures and morphing wings), microelectronics (e.g., in flexible bio-electronics and active disassembly systems), automotive (e.g., automobile actuators and self-healing composite systems), and biomedical one (e.g., in stents and filters). This is mainly due to their lightweight, high shape reconfiguration, recovery force, good manufacturability, easily tailorable glass transition temperature, and low cost. After a brief description of SMPs, blends and their composites behavior, this chapter highlights the most attractive current and future applications.

Keywords Smart materials · Shape-memory polymer (SMP) · Shape-memory polymer composites (SMPC) · Shape-memory blends · Biomedical applications · Aerospace applications

1 Introduction

1.1 What Are SMP/SMPC Materials?

The SMPs\SMPCs are stimuli-responsive smart materials that can undergo a large recoverable deformation by application of an external stimulus (e.g., heat, electricity, light, magnetic field, water, and solvent) [1–6]. The heat-induced and electricity-induced SMPs and SMPCs are most typical. In the case of heat-induced, the shape-memory effect can be observed by performing a typical thermomechanical cycle,

L. Santo (✉) · F. Quadrini · D. Bellisario · L. Iorio
Department of Industrial Engineering, University of Rome "Tor Vergata", Via del Politecnico 1, 00133 Rome, Italy
e-mail: loredana.santo@uniroma2.it

J. Parameswaranpillai et al. (eds.), *Shape Memory Polymers, Blends and Composites*, Advanced Structured Materials 115,
https://doi.org/10.1007/978-981-13-8574-2_13

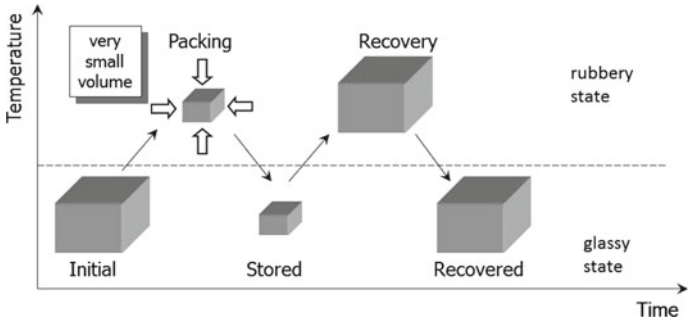

Fig. 1 Schematic representation of the typical thermomechanical cycle of an SMP/SMPC under compression testing [2]. Copyright 2016. Reproduced with permission from Elsevier

as shown in Fig. 1, in compression test. The possibility to change the configuration mainly depends on the material state that becomes from glassy to rubbery state. This occurs when the temperature reaches a characteristic value labeled transition temperature (T_{trans}) (i.e., the glass transition temperature (T_g) or melting transition temperature (T_m) depending on the nature of the polymer) [1, 2]. The chemical nature of the material, the morphology and the applied processing and programming influence the shape-memory properties and the related behavior [3]. The initial geometry can be varied. Figure 2 shows a schematic representation of some conceptual geometries for reliable actuators. In some cases, the memorizing cycle allows deformation of up to 400%.

Among the polymers developed with remarkable shape-memory properties, the most important are epoxy resin, polyurethane resin, cross-linked polyethylene, diverse styrene-butadiene copolymers, and other formulation.

The preparation of SMP composites and blends is mainly performed to improve some material properties and to make easier the process of memorizing and shape recovery. In particular, they are fabricated to improve shape recovery stress and mechanical properties, and to decrease shape recovery time by increasing thermal conductivity. Moreover, it is possible to create new polymer/polymer blends with shape-memory effect (SME), to set properly switch temperature, mechanical properties and biomedical properties of SMPs, and to manufacture shape-memory materials sensitive to various stimuli [7, 8].

Many studies deal with the fabrication methods and characterization of this class of emerging smart materials [1–17].

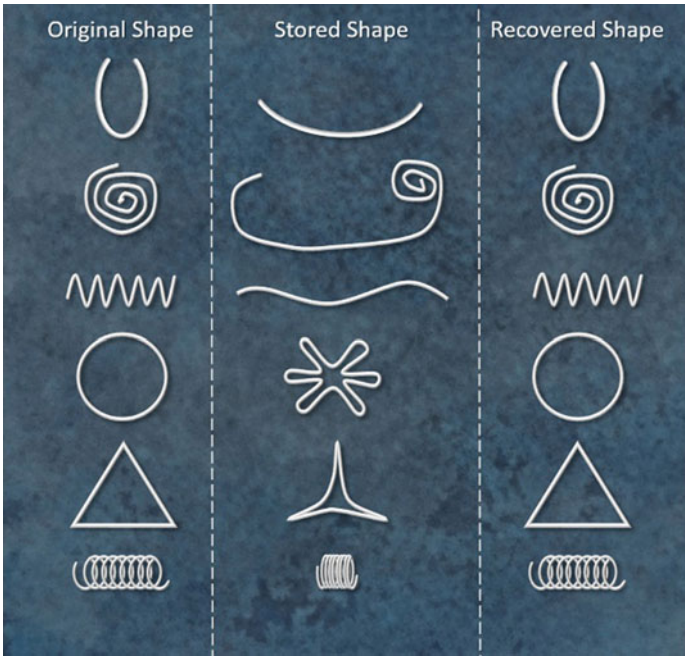

Fig. 2 Schematic representation of some conceptual geometries for reliable actuators based on shape-memory polymers

2 Applications

SMPs, blends, and their composites can be used in many areas ranging from outer space to automobiles.

Recently, the most attractive applications are in aerospace for deployable components and structures, including hinges, trusses, booms, antennas, optical reflectors, solar sails, and morphing skins [1, 2, 11, 18–23]. In addition, there are further interesting applications in areas of biomedicine (scaffolds for tissue engineering, implants for minimally invasive surgery procedures, self-tightening sutures, self-retractable and removable stents, drug delivery systems) [24–27], microelectronics (flexible bioelectronics and active disassembly systems), automotive (automobile actuators and self-healing composite systems, seat and adaptive lens assemblies, reconfigurable storage bins, airflow control devices), food packaging for thermal and light-sensitive products, deployable structures (reflectors, ground-based deployable mirrors), smart textile (life jacket, floating wheels), and others [11].

At present, some applications are already utilized and others are an object of research for future development. Some remarkable applications are described in the following sections.

3 Applications for Aerospace

Nowadays, many researches are devoted to the SMP/SMPC applications in aerospace. In particular, SMPs/SMPCs are of great interest for building low-cost self-deployable structures, e.g., solar sails, solar arrays, sunshields, radar antennas, systems for space debris capture, morphing wings [1, 11, 18–23, 28].

Figure 3 shows some prototypes made of shape-memory materials from epoxy matrix composites for space applications; in particular, prototypes of solar sail, de-orbiting sail, solar panel, and a self-deploying cross [19].

Commercial materials are generally used for the fabrication of such prototypes of SMC with a bulk SMP interlayer. The composite layers are carbon/epoxy prepreg (HexPly® M49/42%/200T2X2/CHS-3K, nominal epoxy resin content of 42 wt%, nominal area weight of 200 g/m^2, thickness of 0.35 mm), while the SMP interlayer is an epoxy resin 3M Scotchkote 206 N [18–20].

Figure 4 shows the configuration of the prototypes of Fig. 3 after the memorizing step, in stored configuration. Figures 5 and 6 report the details of the recovery tests. A hot gun is used for heating but in future applications embedded heaters or solar radiation could be used.

Other SMPC prototypes from epoxy matrix were manufactured to study two example of self-deployable devices for de-orbiting systems: a composite cross without sail and a dual sail structure with composite frames and kapton sails [19, 20]. The dual sail system was made by two symmetrical sails that deploy on the opposite

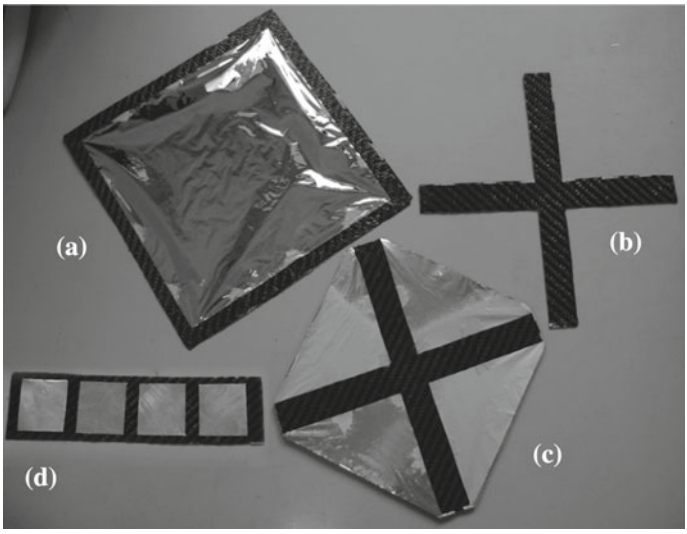

Fig. 3 Manufactured composite structures **a** prototype of solar sail; **b** self-deploying cross; **c** prototype of de-orbiting sail; **d** prototype of solar panel [19]. Copyright 2017. Reproduced with permission from Springer Nature

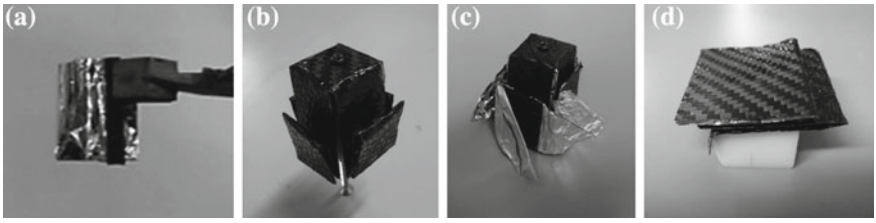

Fig. 4 Configuration of the composite structures after memorizing step: **a** solar sail, **b** self-deploying cross, **c** de-orbiting sail, **d** solar panel [19]. Copyright 2017. Reproduced with permission from Springer Nature

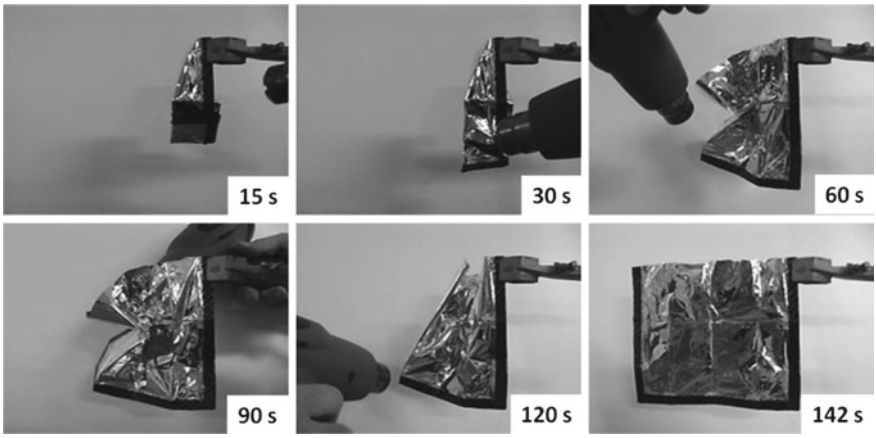

Fig. 5 Details of the prototype of the SMC frame recovery stage [19]. Copyright 2017. Reproduced with permission from Springer Nature

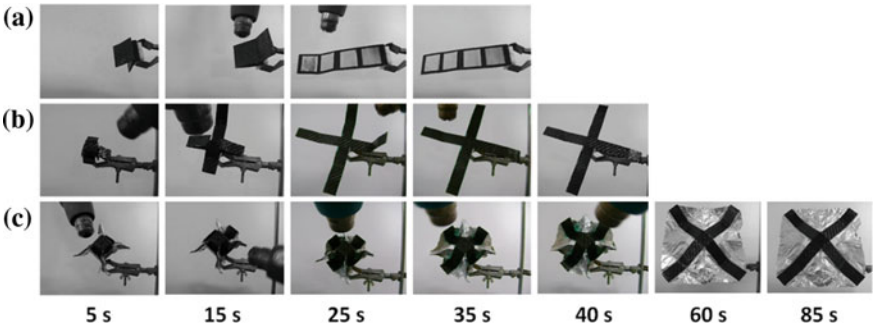

Fig. 6 Details of the recovery tests of **a** the panel, **b** the cross, **c** the cross with the sail [19]. Copyright 2017. Reproduced with permission from Springer Nature

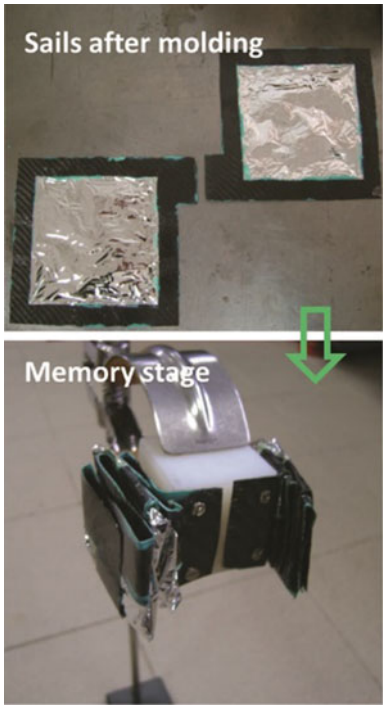

Fig. 7 Composite structures before and after the memory step [20]. Copyright 2016. Reproduced with permission from ASME

sides of a microsatellite. The results of the shape-memory tests are shown in Figs. 7 and 8.

The memory and recovery cycle results are very interesting, showing that such structures can successfully self-deploy. They follow the desired design constraints and are able to recover the original flatness without noticeable defects. The material, heating source, and configuration influence the time of deployment that can be tailored depending on the application.

A very innovative application of such SMPCs could be composite hands for space debris capture [19–21]. They could be manufactured in the closed-hand configuration, and subsequently opened in the phase of memorizing. In this case, composite hands recover the initial closed configuration by heating, and allow grabbing small objects. Figure 9 shows an example of composite hands during recovery stage in two different configurations (cubic and cylindrical).

The material used for the described prototypes has already tested in microgravity during the Russian BION-M1 mission of the Soyuz spacecraft (April 20, 2013). In that mission, for the first time, a shape-memory polymer composite (SMC) sheet was also tested together with prototypes of actuators made of SMP foams [29, 30]. Figure 10 shows the samples of the experiment, namely Ribes_Foam2. The view of one of them, the prototype of actuator, before and after the test in microgravity is also shown. The experiment has highlighted that the SMP and SMPC samples are

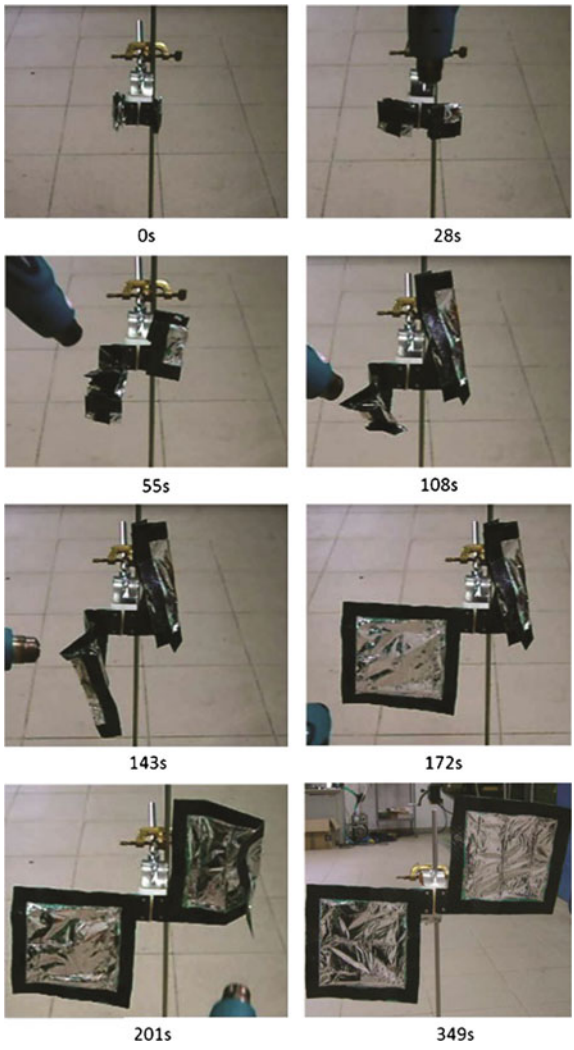

Fig. 8 Details of the shape recovery tests of the dual sail configuration [20]. Copyright 2016. Reproduced with permission from ASME

able to recover their shape in microgravity. In the case of small and lightweight parts, the effect of microgravity is surely negligible if compared with recovery forces but it influences the performances of heating devices. For this reason, it has to be taken into account for designing actuators or self-deployable structures for future space applications.

Furthermore, a low actuation rate of about 0.2 mm/min can be achieved by using such SMPs, and the resultant loading speed is about 0.1 N/mm, by using an SMP foam, size $14 \times 8 \times 8$ mm^3. These characteristics are very promising to design small-size actuators for self-deployable structures where other shape-memory materials (e.g., shape-memory alloys, SMA) cannot be used because they permit only

Fig. 9 Details of the shape-memory tests of the composite hands in cylindrical and cubic configuration [21]. Copyright 2016. Reproduced with permission from ASME

high actuation rate. Another possible application could be the fine regulation of the position of shields, mirrors, and other structures of satellites.

The SMP material used for the actuator has already tested in microgravity in a previous space mission in 2011 (experiment I-foam, NASA STS-134 mission) [31].

Currently, the other two new samples in SMPC are on orbit, outside the International Space Station. The NASA experiment is the MISSE-9 Polymers and Composites Experiment being flown on the MISSE-Flight Facility (Launch April 2, 2018). The duration of the mission is 1 year. The aim is to investigate the material behavior in the harsh space environment. High vacuum, ultra-high- or low-temperature cycle effect, ultraviolet (UV) radiation, atomic oxygen, cosmic ray are important factors to be considered when selecting structure materials for space.

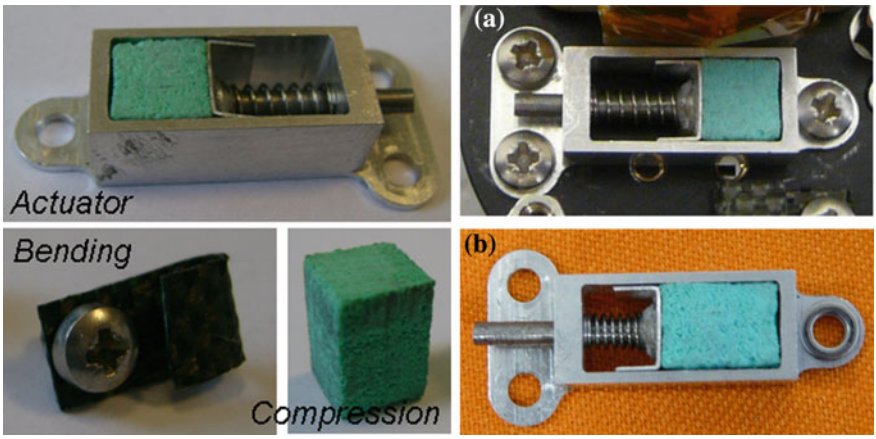

Fig. 10 On the left, the samples of the Ribes_Foam2 experiment; on the right, the prototype of actuator: **a** before and **b** after the microgravity experiment [29]

Therefore, the results of these experiments will be very useful for future applications of SMPCs in outer space.

However, there are some challenges to the applications of SMPC in aerospace, such as the limited types of high-temperature SMPC suitable for the harsh space environment.

Further applications of SMPs/SMPCs for aerospace are hinges, ground-based deployable mirrors, reflectors, and antennas [1, 11, 22]. For aerospace deployable devices, the change of structural configuration in-orbit is obtained through the use of a mechanical hinge, stored energy devices, or motor-driven tools. Complex assembling process, massive mechanisms, large volumes, and undesired effects during deployments are some drawbacks for such traditional deployments systems. On the contrary, using SMPs and their composites some of the abovementioned disadvantages can be overcome. Lan et al. investigated a carbon fiber-reinforced SMP for this application. The flexural deformation was the main mode of the deformation in the structures. The results are promising [32, 33].

SMPs are also suitable for the fabrication of ground-based mirrors. Such mirrors are generally thin, lightweight, and deployable. They can be manufactured by an SMP composite substrate and a coated reflective side of the composite reflector. The reflective surfaces are mainly composed of electroplated nickel (less than 30 μm thick) that provides high-quality reflectance. The substrate of the mirror can be deformed for packaging and then activated by an external power supply, for the shape recovery [1, 11].

Recently, SMPC have been conceived for the fabrication of the central part of large-aperture inflatable antenna, enabling a large deformation [1, 34]. Large apertures in space have applications for telecommunication, earth observation, and scientific missions. Shape adjustment and control of surfaces by the implementation of shape-memory materials and piezoelectric polymers has been evaluated. It has

been paid attention to the matching to the surface structural configurations and thermoelastic stability [34]. For example, in the case of precision system, to reduce manufacturing shape errors, compensation devices based on shape-memory polymers attached to the structure at proper positions could be used.

Expandable lunar habitat is another possible application. If space exploration is led for a long time, a special shelter or habitat is needed to maintain basic life and avoid damage from ultraviolet radiation [1]. SMP/SMPC is one of the advanced materials that can be packaged and stowed in a smaller volume and deployed using some stimuli when in space. For example, the ILC Dover Company has developed together with NASA Langley Research Center a kind of inflatable expandable lunar habitat; the framework of the structure is made of SMPCs, and the structure is self-deployable and has a high extensive area. In addition, the model was fabricated and the process for deploying of the structure was studied in on-ground experiment. The results show that the materials have good recovery properties. In addition, Cornerstone Research Group (CRG) has developed a self-constructing infrastructure for future missions to moon and Mars.

SMP and SMPC are also interesting for the future development of morphing structures [11, 28, 35]. Such structures have attracted the attention of many researchers and much effort in the aircraft technology development. In fact, they are very advantageous in lift-to-drag ratio and flight performance. Mission morphing requires large-scale shape change for adapting to different flight conditions.

As above mentioned, the interest in SMPs and SMPCs is mainly due to their lightweight, high strength–weight ratio, low density, low part count, simple design, good manufacturability, high shape deformability, easily tailorable glass transition temperature, and low cost.

An example of morphing concept of a variable camber wing was developed [11]. It consists of a flexible SMP skin, a metal sheet, and a honeycomb structure. Metal sheet is used to keep the surface smooth during the curvature changing, honeycomb provides distributed support to the flexible skin, and the flexible skin made of SPM is covered to create the smooth aerodynamic surface, as shown in [11].

4 Biomedical Applications

Recently, SMPs have generated great interest for biomedical applications like self-retractable and removable stents, drug delivery carriers, self-tightening sutures, fasteners, scaffolds for tissue engineering, self-expansion stents, endovascular clot removal, and orthodontic appliances.

Figure 11 shows the shape recovery test of a prototype of tracheal stent made of two-component polyurethane resin (MP3510, SMP technologies Inc.).

The main interest of SMPs is in their potential in minimally invasive surgery. In fact, a compacted device can be inserted into the body through a smaller incision, and subsequently deployed to its full shape once inside. Moreover, SMPs/SMPCs

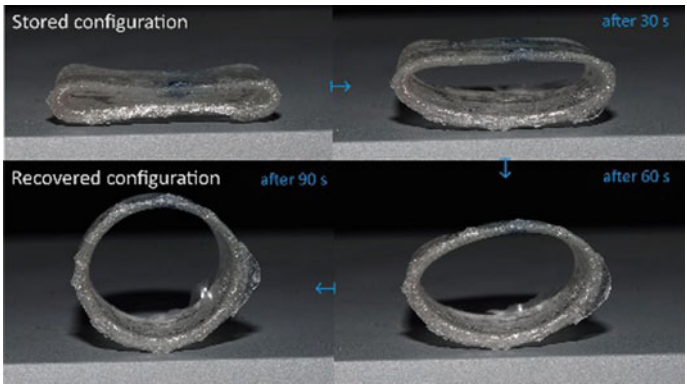

Fig. 11 Shape recovery test of prototype of tracheal stent

can provide structural support, exert stabilizing forces, elute therapeutic agents, and biodegrade [24].

Nevertheless, it is essential to consider the potentially harmful effects that these new materials could have when implanted in the body. For this reason, in vivo testing must be performed to evaluate the interaction of the smart material with the tissue [24].

Among different SMP materials, polyurethane (PU) SMP performs excellent biocompatibility, and can be used for different clinical devices when implanted in the human body.

In [36], biocompatible poly (propylene carbonate) (PPC)/polycaprolactone (PCL) shape-memory blends containing different components were fabricated through melt blending. These blends show distinct component-dependent shape-memory performance. The material had good blood compatibility, in vitro degradation, and drug release behavior, demonstrating its great potential for biomedical applications.

However, materials used in permanent biomedical products have to be also non-biodegradable in order to resist degradation by the body. They have to ensure that an extended period of functional use can be achieved. On the other hand, for products that are only required to serve a temporary function, the property of biodegradability is very useful. Biodegradable materials permit a temporary presence that eliminates the need for surgical removal after their functional time [37].

Biocompatibility and biodegradability are thus desirable properties of SMPs for biomedical applications. Biodegradable and bio-based polymers can meet this need and may replace the conventional SMPs [38, 39].

The rate at which biodegradation will occur should also be tailored to the best use of the product. The field of tissue engineering, for example, promotes the use of materials with controllable degradation rates in scaffold construction as this could permit the synchronization between scaffold degradation and natural tissue growth and replacement. Regulating the rate of biodegradation can also give better control in other SMP applications such as in drug delivery systems.

The biodegradable SMPs, reported so far are based on polyglycolide (PGA), poly(L-lactide) (PLLA), and polycaprolactone (PCL), which are well-known biodegradable polymers mostly used in the medical field [8]. The choice of shape-memory material will depend on the specific application.

The effectiveness of biodegradable SMP in wound closure has been recently investigated [8, 40]. A temporary shape is achieved by elongating the fiber under controlled stress. This suture can be applied on its temporary shape and when the temperature is above T_g, the suture shrink and then tighten the knot. Such sutures should be degradable and show gradual mass loss during degradation.

SMPs could also be useful for biodegradable stent with self-expandability [41].

In addition to biocompatibility and biodegradability, the texture of the material surface is of great interest for medical devices. Surface modification techniques for next-generation SMP stent devices was proposed [42]. These modification methods make the surfaces of these materials more compatible, depending on the application. In particular, the hemocompatibility of stent materials can be improved. Surface modification techniques include roughening, patterning, chemical modification, and surface modification for biomolecule and drug delivery.

Further interesting applications of SMPs/SMPCS in the biomedical field are the following.

The use of shape-memory polyurethane in orthodontic is investigated [43]. Shape-memory PU wire has shown strong potential as a novel orthodontic appliance with esthetically appealing appearance. In fact, the shape recovery force exerted by the wire is sufficient to correct misaligned teeth in orthodontic test.

The use of shape-memory effect in polymers is also proposed for cardiovascular stent intervention [8, 44]. This is proposed to reduce the catheter size for delivery and offers highly controlled and tailored deployment. The stent can be preprogrammed for activating at body temperature. The deployment is obtained without auxiliary devices.

The shape-memory properties of thermoplastic polyurethane allow designing new fully polymeric self-expandable stents used in constricted coronary blood vessel with the function of drug delivery. This can contribute to a significant reduction of restenosis and thrombosis. The use is not restricted to the cardial area, but may be applied in other organs too, e.g., trachea, esophagus, urethra, etc., when troubled by stenosis or tumors [45].

The combination of computer-aided design, computer-aided engineering, and additive manufacturing technologies can be studied and profitably applied to the development of interesting shape-memory polymer-based actuators. In this way, there is a special impact on the design and implementation stages [46].

An example of such an approach is reported in Fig. 12 for a “smart” annuloplasty ring based on shape-memory polymers oriented to the potential treatment of mitral valve insufficiency.

Finally, SMPs are also ideal candidate materials for devices to be used in minimally invasive procedures such as diagnostic devices, or sensors, tissue scaffolds for cell growth, artificial skin, or even as materials for 3D printing of biomedical devices. The development of new SMPs may affect more and more the biomedical field and

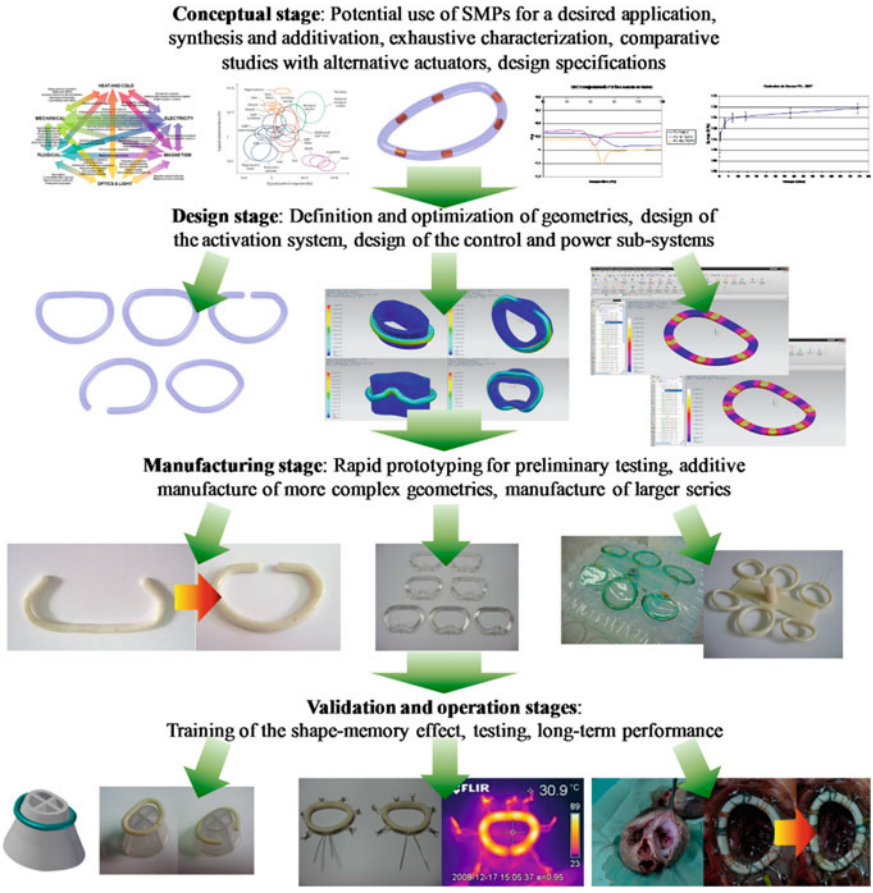

Fig. 12 Summary of the development process, supported by computer-aided engineering and additive manufacturing approaches, for a "smart" annuloplasty ring based on shape-memory polymers oriented to the potential treatment of mitral valve insufficiency [46]. Reproduced with permission from the author

open up new scenarios for designing novel bio-devices [37]. Further applications in the biomedical field can be found in [24–27].

5 Other Applications

The application of smart materials and SMP technology to the active disassembly of modern mobile phones is another interesting application. SMP made of PU was employed for this purpose [47, 48]. One of the most successful results in active disassembly times were the SME-SMP screws. They allow the most

successful self-disassembly of the Nokia 6110 mobile within 1.5 s. The mean time in disassembly of these devices was just over 8 s. By using these new smart material devices, it is possible to disassemble products at end of life (EoL). The disassembly is made at specific triggering temperatures. The technique is named as Active Disassembly using Smart Materials (ADSM), and has been successfully demonstrated on different mobile phones.

Another use of SMP in electronics is green electrophosphorescent organic light-emitting diodes (OLEDs) with inverted top-emitting structures. They are tested on biocompatible shape-memory polymer (SMP) substrates for wearable electronic applications [49], and combine the unique properties of SMP substrates with the light-emitting properties of OLEDs. For this reason, they are very interesting for new applications, including conformable smart skin devices, minimally invasive biomedical devices, and flexible lighting/display technologies.

SMPs have been also used in automobile engineering. Some interesting applications of SMPs include seat assemblies, reconfigurable storage bins, energy absorbing assemblies, tunable vehicle structures, hood assemblies, releasable fastener systems, airflow control devices, adaptive lens assemblies, and morphable automotive body molding [11]. The success for using SMPs are due to their shape-memory behavior, easy manufacturing, high-deformed strain, and low cost.

New interesting applications could come by shape-morphing composites with designed microarchitectures [35]. Lightweight, micro-architected composite SMPs may overcome the limitation in relatively small form factors of SMPs due to their low recovery stresses. Furthermore, they could combine functional properties (e.g., electrical conductivity) with shape-memory behavior. This is very challenging. Bio-based thermoset SMP composite inks are investigated. Figure 13 reports ink development and fabrication process for complex 3D architectures, 3d printed and origami structures.

Figure 14 shows an example of programmed stent and recovered stent in thermoset composite ink filled with carbon nanofibers CNF (5.6 vol% CNF).

This new approach has been named as “4D printing” because of the extra dimension of time (or shape change) that such programmable materials add to conventional 3D printing and origami process.

6 New Perspectives and Challenges

New perspectives and main challenges in using SMPs/SMPCs are summarized as follows.

In aerospace applications, the development of SMPs/SMPCs may be an enabling technology for building future spacecrafts components for long-term space flight, light actuators, and self-deployable structures. This could open new frontiers for space exploration. The challenge is mainly related to the manufacturing and testing in space of such structures and devices.

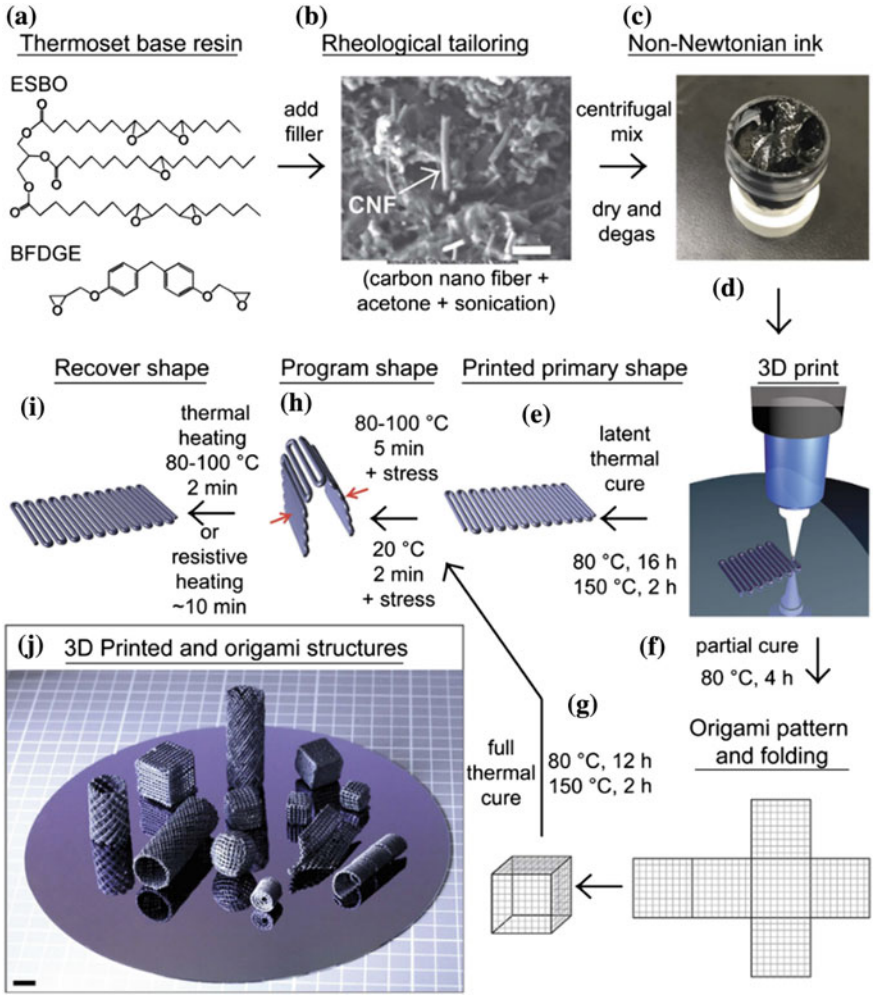

Fig. 13 Ink development and fabrication process for complex 3D architectures [35]

In biomedical applications, the main challenges concern the materials rate of degradation (enzymatic or hydrolytic), their degree of toxicity, mechanical strength, etc. Experimental tests in vitro and vivo will be fundamental for testing and subsequent applications.

Another attractive field is smart materials and structures obtained by three-dimensional manufacturing (3D printing). Some technological and design limitations remain unsolved such as limitation in the choice of usable polymers, multi-material components manufacturing, occurrence of microstructural defects, and material's real-time adapting. Therefore, a development in such an area is compulsory.

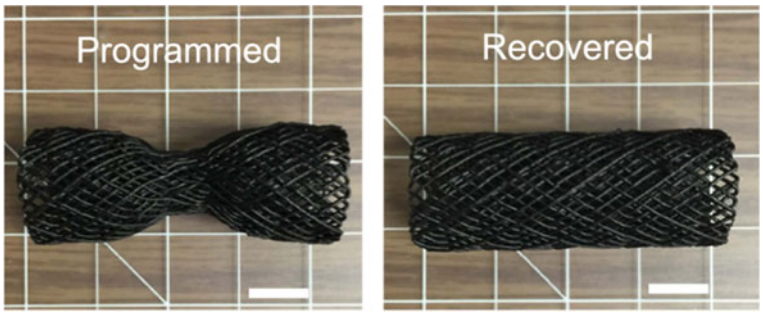

Fig. 14 Programmed stent and recovered stent (5.6 vol% CNF) [35]

The fabrication of nanocomposites with multistep responsive self-based capabilities and improved durability will further improve the performance in the field. The development of new polymers and polymer blends becomes necessary in order to make this. However, no polymer systems are commercially available at present.

The design and fabrication of self-cleaning, self-healing, and self-adapting SMPs materials is another interesting future challenge. In the last years, the interest in this topic is remarkable. These materials are suitable for the fabrication of load-bearing aircraft components, self-cleaning and light-guided windows, flexible solar modules (polymer solar cells), smart textiles, bionic robot, etc.

However, the direct transfer of results from the laboratory to the industrial scale is very difficult. The main problems are related to the complexity of the final shape-memory effect. This is affected by many factors such as the programming step and the triggering process parameters. In addition, a fast and flexible manufacturing process is needed.

7 Conclusions

SMPs and their blends and composites are new smart materials with many possible applications. Research works are focusing on design, evaluation, and manufacturing of SMP/SMPC components that can be used in different fields. More degrees-of-the freedom is available in handling such smart materials to meet the needs of a particular application. Their use is, therefore, challenging in the field of aerospace, biological medicine, automobile, microelectronics, smart textiles, and fabrics. The study and development of new higher performances materials, and the choice and optimization of manufacturing processes are surely the key to the success for future applications.

Joint research between different branches of science and engineering is surely required to obtain further advancements in SMP/SMPC technology. By using this approach, the transfer of research progress from laboratory to industry, and daily life will be possible.

References

1. Liu Y, Du H, Liu L, Leng J (2014) Shape memory polymers and their composites in aerospace applications: a review. Smart Mater Struct 23:023001 (22 pp)
2. Santo L (2016) Shape memory polymer foams. Prog Aerosp Sci 81:60–65
3. Lendlein A, Kelch S (2002) Shape-memory polymers. Angew Chem Int Edn 41:2034–2057
4. Meng H, Li G (2013) A review of stimuli-responsive shape memory polymer composites. Polymer 54:2199–2221
5. Hu J (2014) Shape memory polymers: fundamentals, advances and applications, chapter 4. Smithers Rapra Technology
6. Sun L, Huang WM, Ding Z, Zhao Y, Wang CC, Purnawali H, Tang C (2012) Stimulus-responsive shape memory materials: a review. Mater Des 33:577–640
7. Meng Q, Hu J (2009) A review of shape memory polymer composites and blends. Compos Part A 40:1661–1672
8. Ratna D, Karger-Kocsis J (2008) Recent advances in shape memory polymers and composites: a review. J Mater Sci 43:254–269
9. Behl M, Razzaq MY, Lendlein A (2010) Multifunctional shape-memory polymers. Adv Mater 22:3388–3410
10. Hagera MD, Bodea S, Weber C, Schubert US (2015) Shape memory polymers: past, present and future developments. Prog Polym Sci 49–50:3–33
11. Leng J, Lan X, Liu Y, Du S (2011) Shape-memory polymers and their composites: stimulus methods and applications. Prog Mater Sci 56:1077–1135
12. Karger-Kocsis J, Kéki S (2018) Review of progress in shape memory epoxies and their composites. Polymers 10:34
13. Zhang X, Geven MA, Grijpma DW, Peijs T, Gautrot JE (2017) Tunable and processable shape memory composites based on degradable polymers. Polymer 122:323–331
14. Hu J, Zhu Y, Huang H, Lu J (2012) Recent advances in shape-memory polymers: structure, mechanism, functionality, modelling and applications. Prog Polym Sci 37:1720–1763
15. Mu T, Liu L, Lan X, Liu Y, Leng J (2018) Shape memory polymers for composites. Compos Sci Technol 160:169–198
16. Barjibe RB, Kumar B (2015) Study on shape memory polymers and their applications. Int J Innov Eng Technol 5:3
17. Zhang X, Tang Z, Guo B (2016) Reversible plasticity shape memory polymers: key factors and applications. J Polym Sci Part B Polym Phys 54:1295–1299
18. Quadrini F, Santo L, Squeo EA (2012) Shape memory epoxy foams for space applications. Mater Lett 69:20–23
19. Santo L, Quadrini F (2017) Shape memory materials from epoxy matrix composites, smart polymer nanocomposites. Springer International Publishing AG
20. Santo L, Quadrini F, Bellisario D, Accettura AG (2016) Conceptual prototypes of composite structures for aerospace. In: Proceedings of the ASME 2016 international manufacturing science and engineering conference, MSEC2016, 27 June–1 July 2016, Blacksburg, Virginia, USA
21. Quadrini F, Tedde GM, Santo L (2015) Shape memory composite hands for space applications. In: ASME 2015 international manufacturing science and engineering conference, MSEC 2015 vol 1, Charlotte, United States, 8 June 2015 through 12 June 2015; Code 115672

22. Santo L, Quadrini F, Bellisario D (2016) Shape memory composite antennas for space applications. Mater Sci Eng 161
23. Santo L, Quadrini F, Accettura A, Villadei W (2014) Shape memory composites for self-deployable structures in aerospace applications. Procedia Eng 88:42–47
24. Yahia L (2015) Shape memory polymers for biomedical applications. In: Biomaterials, vol 97. Woodhead Publishing
25. Wang K, Strandman S, Zhu XX (2017) A mini review: shape memory polymers for biomedical applications. Front Chem Sci Eng 11(2):143–153
26. Wong Y, Kong J, Widjaja LK, Venkatraman SS (2014) Biomedical applications of shape memory polymers: how practically useful are they? Sci China Chem 57:1–15
27. Zare Y, Shabani I (2016) Polymer/metal nanocomposites for biomedical application. Mater Sci Eng C 60:195–203
28. Bashir M, Lee CF, Rajendran P (2017) Shape memory materials and their applications in aircraft morphing: an introspective study. J Eng Appl Sci 12
29. Santo L, Quadrini F, Villadei W, Mascetti G, Zolesi V (2015) Shape memory epoxy foams and composites: Ribes_foam2 experiment on spacecraft "Bion-m1" and future perspective. Procedia Eng 104:50–56
30. Santo L, Quadrini F, Ganga PL, Zolesi V (2015) Mission BION-M1: results of Ribes/Foam2 experiment on shape memory polymer foams and composites. Aerosp Sci Technol 40:109–114
31. Santo L, Quadrini F, Squeo EA, Dolce F, Mascetti G, Bertolotto D, Villadei W, Ganga PL, Zolesi V (2012) Behavior of shape memory epoxy foams in microgravity: experimental results of STS-134 mission. Microgravity Sci Technol 24:287–296
32. Lan X, Liu Y, Lv H, Wang X, Leng J, Du S (2009) Fiber reinforced shape-memory polymer composite and its application in a deployable hinge. Smart Mater Struct 18
33. Leng J (2013) Active moving polymers and multifunctional composites: shape the future structures. Adv Mater Res 745
34. Prowald J, Baier H (2013) Advances in deployable structures and surfaces for large apertures in space. Ceas Space J 5:89–115
35. Rodriguez JN, Zhu C, Duoss EB, Wilson TS, Spadaccini CM, Lewicki JP (2016) Shape-morphing composites with designed micro-architectures. Sci Rep
36. Zheng Y, Li Y, Hu X, Shen J, Guo S (2017) Biocompatible shape memory blend for self-expandable stents with potential biomedical applications. Appl Mater Interfaces 9:13988–13998
37. Qi Yu Chan B, Low ZWK, Heng SJW, Chan SY, Owh C, Loh XJ (2016) Recent advances in shape memory soft materials for biomedical applications. ACS Appl Mater Interfaces 8:10070–10087
38. Peterson GI, Dobrynin AV, Becker ML (2017) Biodegradable shape memory polymers in medicine. Adv Helathcare Mater 6
39. Zhang X, Tan BH, Li Z (2017) Biodegradable polyester shape memory polymers: Recent advances in design, material properties and applications. Mater Sci Eng C
40. Jing X, Mi HY, Huang HX, Turng LS (2016) Shape memory thermoplastic polyurethane (TPU)/poly(ε-caprolactone) (PCL) blends as self-knotting sutures. J Mech Behav Biomed Mater 64:94–103
41. Xue Liang, Dai Shiyao, Li Zhi (2010) Biodegradable shape-memory block co-polymers for fast self-expandable stents. Biomaterials 31:8132–8140
42. Govindarajan T, Shandas R (2014) A survey of surface modification techniques for next-generation in shape memory polymers stent devices. Polymers 6:2309–2331
43. Jung YC, Cho JW (2010) Application of shape memory polyurethane in orthodontic. J Mater Sci Mater Med 21:2881–2886
44. Yakackia CM, Shandasa R, Lanningb C, Recha B, Ecksteina A, Gall K (2007) Unconstrained recovery characterization of shape-memory polymer networks for cardiovascular applications. Biomaterials 28:2255–2263
45. Wache HM, Tartakowska DJ, Hentrich A, Wagner MH (2003) Development of a polymer stent with shape memory effect as a drug delivery system. J Mater Sci Mater Med 14:109–112

46. Lantada AD (2017) Systematic development strategy for smart devices based on shape-memory polymers. Polymers 9
47. Chiodo JD, Billett EH, Harison DJ. Active disassembly using shape memory polymers for the mobile phone industry
48. Kutz M (2007) Environmentally conscious manufacturing. In: Environmentally conscious engineering. Wiley
49. Gaj MP, Wei A, Hernandez CF, Zhang Y, Reit R, Voit W, Marder SR, Kippelen B (2015) Organic light-emitting diodes on shape memory polymer substrates for wearable electronics. Org Electron 25:151–155